polymers

Special Issue Reprint

Advances in Natural Polymers

Extraction Methods and Applications

Edited by
Cornelia Vasile, Gabriel Aguirre-Álvarez and Xiao-Feng Sun

mdpi.com/journal/polymers

MDPI

Advances in Natural Polymers: Extraction Methods and Applications

Advances in Natural Polymers: Extraction Methods and Applications

Editors

Cornelia Vasile
Gabriel Aguirre-Álvarez
Xiao-Feng Sun

MDPI

Basel • Beijing • Wuhan • Barcelona • Belgrade • Novi Sad • Cluj • Manchester

Editors

Cornelia Vasile
"P.Poni" Institute of
Macromolecular Chemistry of
the Romanian Academy
Iasi
Romania

Gabriel Aguirre-Álvarez
University Autonomous of
Hidalgo State
Pachuca
Mexico

Xiao-Feng Sun
Northwestern Polytechnical
University
Xi'an
China

Editorial Office
MDPI AG
Grosspeteranlage 5
4052 Basel, Switzerland

This is a reprint of articles from the Special Issue published online in the open access journal *Polymers* (ISSN 2073-4360) (available at: https://www.mdpi.com/journal/polymers/special_issues/natural_polym).

For citation purposes, cite each article independently as indicated on the article page online and as indicated below:

Lastname, A.A.; Lastname, B.B. Article Title. *Journal Name* **Year**, *Volume Number*, Page Range.

ISBN 978-3-7258-1671-2 (Hbk)
ISBN 978-3-7258-1672-9 (PDF)
doi.org/10.3390/books978-3-7258-1672-9

Contents

About the Editors

Cornelia Vasile

Dr. Cornelia Vasile is Senior Researcher at "P.Poni" Institute of Macromolecular Chemistry of the Romanian Academy, Physical Chemistry of Polymers Department, Iasi, Romania, Ass. Prof at Laval University, Quebec, Canada, and "Gh. Asachi" Technical University, Iasi. Her research interests are in the fields of polymeric (bionano)composites; biomaterials; smart polymers; biodegradation; polymer compatibility and biocompatibility; the kinetics and thermodynamics of polymeric systems; food packaging (active, bioactive, smart, (bio)degradable); drug delivery; the recovery of polymer wastes via destructive and non-destructive procedures; environmental pollution and protection.

Her research has received 12,096 citations and she has an h-index of 56.

Gabriel Aguirre-Álvarez

Gabriel Aguirre-Álvarez has been a full-time professor at the University Autonomous of Hidalgo State (UAEH), Mexico, since 1996. He is an agro-industrial engineer for the UAEH. In 2003, he was awarded with an MSc in Leather Technology from the University of Northampton, UK. Then, in 2009, Dr. Aguirre obtained his PhD in Food Sciences at the University of Nottingham, UK. His research is focused on the transformation of agri-food waste from agro-industrial processes. Some example areas of his research are as follows: the extraction and characterization of a wide range of biopolymers such as collagen, gelatin, hyaluronic acid, and lycopene for their application in the biomedical, pharmaceutical, cosmeceutical, and food industries; the preparation of films and coatings with antibacterial, antioxidant, water transport, and enhanced mechanical properties prepared from natural wastes.

Xiao-Feng Sun

Dr. Xiao-Feng Sun is a full-time associate professor at Northwestern Polytechnical University. He obtained his PhD degree at Bangor University of the United Kingdom in 2006, and then, as a research officer, he worked on an industrial-based project involving the use of a mixed culture of microbes to produce a specific synthon for the pharmaceutical industry. In 2007, he came back to China and focused his studies on environmental materials at Zhejiang University. Now, he works at Northwestern Polytechnical University, and he has published more than 100 papers which have been cited more than 6000 times by other scientists. His research concerns natural polymers and nanomaterials in the environmental protection and biomedical field.

Preface

The Reprint of Polymers titled "Advances in Natural Polymers: Extraction Methods and Applications" which belongs to the Polymer Applications section has a highly modern and interesting purpose because it publishes new developments/aspects of extraction techniques and applications of some natural polymers from various sources. It also explores the agro-waste or byproducts containing valuable natural components to be used as new sources of raw materials and active agents and to replace synthetic plastics known for their detrimental environmental and human health impacts. This collection of research papers and reviews is focused on green, eco-friendly, and easily scalable processes directed toward a sustainable and circular economy. Some research papers deal with new extraction procedures to obtain cellulose (A. C.Puițel et al., Integrated Hemicellulose Extraction and Papermaking Fiber Production from Agro-Waste Biomass and Optimization of Alkaline Extraction of Xylan-Based Hemicelluloses from Wheat Straws: Effects of Microwave, Ultrasound, and Freeze–Thaw Cycles) or lignin (C.Vasile and M. Baican Lignins as Promising Renewable Biopolymers and Bioactive Compounds for High-Performance Materials) and the recycling of biomass into high-value-added materials. Important developments in research and technology aiming to create a sustainable circular economy are also reported in the study of some proteins (D. Soto-Madrid et al., Structural and Physicochemical Characterization of Extracted Proteins Fractions from Chickpea (Cicer arietinum L.) as a Potential Food Ingredient to Replace Ovalbumin in Foams and Emulsions and different polysaccharides as chitosan; (M. Biernat et al., Effect of Selected Crosslinking and Stabilization Methods on the Properties of Porous Chitosan Composites Dedicated for Medical Applications), tea polysaccharides, (Q. Wang et al., Advances in the Utilization of Tea Polysaccharides: Preparation, Physicochemical Properties, and Health Benefits), and hyaluronan (R. Zhao In Vitro Fermentation of Hyaluronan with Different Molecular Weights by Human Gut Microbiota: Differential Effects on Gut Microbiota Structure and Metabolic Function), as well as how to reduce sugars in foods to obtain silver nanoparticles (R.M. El-Shishtawy et al., Novel and Facile Colorimetric Detection of Reducing Sugars in Foods via In Situ Formed Gelatin-Capped Silver Nanoparticles) through the valorization of some byproducts such as Nopal Mucilage (E.Herrera-Ibarraet al., Preparation of Surgical Thread from a Bioplastic Based on Nopal Mucilage) and milk whey hydrolysates (A, León-López et al., Milk Whey Hydrolysates as High Value-Added Natural Polymers: Functional Properties and Applications).

This Reprint is addressed to the experts interested in the large-scale development and valorization of different natural resources into high-value materials, engineers, researchers, and PhD students who may be performing their studies using the modern techniques described in the presented papers.

Cornelia Vasile, Gabriel Aguirre-Álvarez, and Xiao-Feng Sun
Editors

polymers

MDPI

Editorial

Advances in Natural Polymers: Extraction Methods and Applications

Cornelia Vasile [1,*], Gabriel Aguirre-Álvarez [2] and Xiao-Feng Sun [3]

[1] Physical Chemistry of Polymers Department, Petru Poni Institute of Macromolecular Chemistry, Romanian Academy, 41A Gr. Ghica Voda Alley, 700487 Iași, Romania
[2] Instituto de Ciencias Agropecuarias, Universidad Autónoma del Estado de Hidalgo, Av. Universidad Km 1, Rancho Universitario, Tulancingo 43600, Hidalgo, Mexico; aguirre@uaeh.edu.mx
[3] School of Chemistry and Chemical Engineering, Northwestern Polytechnical University, Xi'an 710129, China; xf001sn@nwpu.edu.cn
* Correspondence: cvasile@icmpp.ro

Biomass-based alternatives for the manufacturing of bioplastic materials are important aspects of a more sustainable future; their physicochemical properties need to be able to compete with the existing market to establish them as a viable alternative. This Special Issue, aims to present recent modern trends and scientific results on natural polymers. Natural polymers normally occur in nature and can be obtained from a wide variety of sources including plants, animals, and microorganisms. They present special characteristics such as high biodegradability, good biocompatibility, and external-stimuli responsiveness have been widely applied in various engineering fields, including food packaging and drug delivery, and they can be modified by physical and chemical methods to obtain multifunctional materials, etc.

The aim of the Special Issue entitled "Advances in Natural Polymers: Extraction—Methods and Applications" is to collect the latest original research studies on biomass and natural polymers, which are promising valuable sources for the creation of a sustainable and green circular economy, they are environmentally friendly, and also can facilitate the development of nanosized high-performance materials. Authors provided valuable contributions which collectively built a successful issue that will give to its readers an overview of the state-of-the-art activities and the future perspectives in this field.

The aim of this Special Issue is to advance our understanding of fundamental and technological aspects of the extraction of natural polymers and active compounds and their applications in various fields. Biomass has a complex chemical structure and a variety of bioactivities. Biomass valorization is a very interesting topic, because depending on its nature, cultivation conditions, and processing methods (including extraction), its composition, properties, and biological activities, such as anti-oxidative, hypoglycemic, hypolipidemic, immune regulation, and anti-tumor activities, are variable. This editorial provides brief overview on the recent developments in this field, the gaps in knowledge and how this Special Issue addressed those gaps, and it ends with a primary focus on the future research that should be considered. Submissions of original research articles or reviews from an extensive range of expertise in the wide-ranging field of natural polymers were both welcome. Natural polymers are mainly classified into the following groups: polysaccharides (cellulose, hemicelluloses, pectin, dextran, pullulan, starch, chitin, chitosan, alginate, hyaluronic acid, xanthan, guar gum, etc.), peptides/proteins (collagen, gelatin, casein, albumin, etc.) and polynucleotides (DNA and RNA), lignin, polyisoprenes, and polyesters. Natural polymers are gaining interest among the research community both as renewable sources, lack of toxicity, low cost, and bioactive compounds as attractive ingredients for the food industry (packaging, dietary supplements, food supplements, etc.), biomedicine, and cosmetics (skin repair and regeneration, bone tissue engineering,

Citation: Vasile, C.; Aguirre-Álvarez, G.; Sun, X.-F. Advances in Natural Polymers: Extraction Methods and Applications. *Polymers* **2024**, *16*, 1886. https://doi.org/10.3390/polym16131886

Received: 21 June 2024
Accepted: 25 June 2024
Published: 1 July 2024

moisture agents, greater cellular attachment and matrix deposition, mechanical stability, drug carriers in anticancer therapy, nanocarriers, high compatibility with the extracellular matrix, high bioavailability, safety, anti-inflammatory, antimicrobial and antioxidant activity, film formation, nutraceutical beverages, hydration of the skin, etc). [1–4].

This Reprint in *Polymers* which belongs to the Polymer Applications section, has a highly modern and interesting purpose because it contains publications regarding new aspects of progress/extraction and applications of some natural polymers from various sources. Also, agrowaste or byproducts containing valuable natural components have been used as new sources of raw materials and active agents to replace synthetic plastics known by their environmental and human health impacts. Both research papers and reviews are focused on green, eco-friendly, and easily scalable processes, with a view to facilitate a sustainable and circular economy. Some research papers deal with new extraction procedures to obtain celullose or lignin and the recycling of biomass into high-value-added materials, as well as important developments in research and technology, which have also been recorded via the study of some proteins and different polysaccharides such as chitosan, tea polysaccharides, hyaluronan, reducing sugars in foods to obtain silver nanoparticles and the valorization of some by-products such as Nopal Mucilage and milk whey hydrolysates.

This Reprint is addressed to experts in the large-scale development/valorization of different natural resources into high-value materials, engineers, researchers, and PhD students who may be performing their studies using the modern techniques used in the published papers.

Acknowledgments: The Guest Editors would like to acknowledge all authors and reviewers who contributed to the Special Issue and additionally thank the support team at MDPI for preparing the Special Issue.

Conflicts of Interest: The authors declare no conflicts of interest.

List of Contributions:

1. Puițel, A.C.; Balan, C.D.; Ailiesei, G.-L.; Drăgoi, E.N.; Nechita, M.T. Integrated Hemicellulose Extraction and Papermaking Fiber Production from Agro-Waste Biomass. *Polymers* **2023**, *15*, 4597. https://doi.org/10.3390/polym15234597.
2. Vasile, C.; Baican, M. Lignins as Promising Renewable Biopolymers and Bioactive Compounds for High-Performance Materials. *Polymers* **2023**, *15*, 3177. https://doi.org/10.3390/polym15153177.
3. Soto-Madrid, D.; Pérez, N.; Gutiérrez-Cutiño, M.; Matiacevich, S.; Zúñiga, R.N. Structural and Physicochemical Characterization of Extracted Proteins Fractions from Chickpea (*Cicer arietinum* L.) as a Potential Food Ingredient to Replace Ovalbumin in Foams and Emulsions. *Polymers* **2023**, *15*, 110. https://doi.org/10.3390/polym15010110.
4. Biernat, M.; Woźniak, A.; Chraniuk, M.; Panasiuk, M.; Tymowicz-Grzyb, P.; Pagacz, J.; Antosik, A.; Ciołek, L.; Gromadzka, B.; Jaegermann, Z. Effect of Selected Crosslinking and Stabilization Methods on the Properties of Porous Chitosan Composites Dedicated for Medical Applications. *Polymers* **2023**, *15*, 2507. https://doi.org/10.3390/polym15112507.
5. Wang, Q.; Yang, X.; Zhu, C.; Liu, G.; Sun, Y.; Qian, L. Advances in the Utilization of Tea Polysaccharides: Preparation, Physicochemical Properties, and Health Benefits. *Polymers* **2022**, *14*, 2775. https://doi.org/10.3390/polym14142775.
6. Zhao, R.; Zhang, C.; Yu, L.; Zhang, C.; Zhao, J.; Narbad, A.; Zhai, Q.; Tian, F. In Vitro Fermentation of Hyaluronan with Different Molecular Weights by Human Gut Microbiota: Differential Effects on Gut Microbiota Structure and Metabolic Function *Polymers* **2023**, *15*, 2103. https://doi.org/10.3390/polym15092103.
7. Herrera-Ibarra, E.; Salazar-Hernández, M.; Talavera-López, A.; Solis-Marcial, O.J.; Hernandez-Soto, R.; Ruelas-Leyva, J.P.; Hernández, J.A. Preparation of Surgical Thread from a Bioplastic Based on Nopal Mucilage. *Polymers* **2023**, *15*, 2112. https://doi.org/10.3390/polym15092112.
8. El-Shishtawy, R.M.; Al Angari, Y.M.; Alotaibi, M.M.; Almulaiky, Y.Q. Novel and Facile Colorimetric Detection of Reducing Sugars in Foods via In Situ Formed Gelatin-Capped Silver Nanoparticles. *Polymers* **2023**, *15*, 1086. https://doi.org/10.3390/polym15051086.

9. Puițel, A.C.; Suditu, G.D.; Drăgoi, E.N.; Danu, M.; Ailiesei, G.-L.; Balan, C.D.; Chicet, D.-L.; Nechita, M.T. Optimization of Alkaline Extraction of Xylan-Based Hemicelluloses from Wheat Straws: Effects of Microwave, Ultrasound, and Freeze–Thaw Cycles. *Polymers* **2023**, *15*, 1038. https://doi.org/10.3390/polym15041038.
10. León-López, A.; Pérez-Marroquín, X.A.; Estrada-Fernández, A.G.; Campos-Lozada, G.; Morales-Peñaloza, A.; Campos-Montiel, R.; Aguirre-Álvarez, G. Milk Whey Hydrolysates as High Value-Added Natural Polymers: Functional Properties and Applications. *Polymers* **2022**, *14*, 1258. https://doi.org/10.3390/polym14061258.

References

1. Jaiswal, A.K.; Prakash, B. Bioinformatics approaches: Elucidation of novel sites of action, toxicity prediction tool, and perception of bioactive compounds. In *Green Products in Food Safety*; Prakash, B., de São José, J.F.B., Eds.; Academic Press Elsevier Inc.: Cambridge, MA, USA, 2023; Chapter 11, pp. 309–327. [CrossRef]
2. Kurukavak, Ç.K.; Tok, M. Environmental Impact of Biobased Materials. In *Biobased Packaging Materials*; Ahmed, S., Ed.; Springer: Singapore, 2024. [CrossRef]
3. Wang, X.; Li, X.; Zhang, L.; An, L.; Guo, L.; Huang, L.; Gao, W. Recent progress in plant-derived polysaccharides with prebiotic potential for intestinal health by targeting gut microbiota: A review. *Crit. Rev. Food Sci. Nutr.* **2023**, 1–30. [CrossRef] [PubMed]
4. Zhan, K.; Ji, X.; Luo, L. Recent progress in research on Momordica charantia polysaccharides: Extraction, purification, structural characteristics and bioactivities. *Chem. Biol. Technol. Agric.* **2023**, *10*, 58. [CrossRef]

polymers

MDPI

Review

Milk Whey Hydrolysates as High Value-Added Natural Polymers: Functional Properties and Applications

Arely León-López [1], Xóchitl Alejandra Pérez-Marroquín [1], Ana Guadalupe Estrada-Fernández [2], Gieraldin Campos-Lozada [1], Alejandro Morales-Peñaloza [3], Rafael G. Campos-Montiel [1] and Gabriel Aguirre-Álvarez [1,4,*]

[1] Instituto de Ciencias Agropecuarias, Universidad Autónoma del Estado de Hidalgo, Av. Universidad Km 1, Tulancingo C.P. 43600, Hidalgo, Mexico; arely_leon@uaeh.edu.mx (A.L.-L.); pe409780@uaeh.edu.mx (X.A.P.-M.); ca409778@uaeh.edu.mx (G.C.-L.); rcampos@uaeh.edu.mx (R.G.C.-M.)
[2] Instituto Tecnológico Superior del Oriente del Estado de Hidalgo, Carretera Apan-Tepeapulco Km 3.5, Colonia Las Peñitas, Apan C.P. 43900, Hidalgo, Mexico; aestrada@itesa.edu.mx
[3] Escuela Superior de Apan, Universidad Autónoma del Estado de Hidalgo, Carretera Apan-Calpulalpan s/n, Colonia Chimalpa Tlalayote, Apan C.P. 43920, Hidalgo, Mexico; amorales@uaeh.edu.mx
[4] Uni-Collagen S.A. de C.V., Arnulfo González No. 203, El Paraíso, Tulancingo C.P. 43684, Hidalgo, Mexico
* Correspondence: aguirre@uaeh.edu.mx; Tel.: +52-775-145-9265

Abstract: There are two types of milk whey obtained from cheese manufacture: sweet and acid. It retains around 55% of the nutrients of the milk. Milk whey is considered as a waste, creating a critical pollution problem, because 9 L of whey are produced from every 10 L of milk. Some treatments such as hydrolysis by chemical, fermentation process, enzymatic action, and green technologies (ultrasound and thermal treatment) are successful in obtaining peptides from protein whey. Milk whey peptides possess excellent functional properties such as antihypertensive, antiviral, anticancer, immunity, and antioxidant, with benefits in the cardiovascular, digestive, endocrine, immune, and nervous system. This review presents an update of the applications of milk whey hydrolysates as a high value-added peptide based on their functional properties.

Keywords: milk whey; hydrolysates; immunity; antiviral; antihypertensive; natural polymer

Citation: León-López, A.; Pérez-Marroquín, X.A.; Estrada-Fernández, A.G.; Campos-Lozada, G.; Morales-Peñaloza, A.; Campos-Montiel, R.G.; Aguirre-Álvarez, G. Milk Whey Hydrolysates as High Value-Added Natural Polymers: Functional Properties and Applications. *Polymers* **2022**, *14*, 1258. https://doi.org/10.3390/polym14061258

Academic Editor: Xiao Hu

Received: 8 March 2022
Accepted: 18 March 2022
Published: 21 March 2022

1. Introduction

One of the most debated topics in food processing is the recycling of the by-products and their applications as a high value-added product. Milk whey represents a clear example of a by-product obtained from cheese production. This material can be considered as a contaminant and at the same time, the source of protein hydrolysates. Whey is a yellowish to greenish clear liquid obtained after milk coagulation during the cheese-making process. Whey represents about 85–95% of the volume of milk volume and contains over 55% of milk nutrients such as minerals, proteins, and lactose [1,2]. Sweet and acid whey are obtained when the coagulation of milk is carried out by enzymatic action (rennet) or the addition of acids posteriorly [3,4]. The most abundant nutrients in whey are: lactose, soluble proteins, lipids, and mineral salts (see Table 1). With the additional presence of some neutral salts such as NaCl, KCl, and calcium salts (primarily phosphate), among others. Aside from these nutrients, whey also contains lactic and citric acids, non-protein nitrogen compounds such as urea and uric acid, and B group vitamins [3,5].

Table 1. Comparison of sweet and acid whey components [6].

Characteristics	Sweet Whey	Acid Whey
pH	>5.6	<5.6
Water	93–94%	94–95%
Protein (g/L)	6–10	6–8
Lactose (g/L)	46–52	44–46
Minerals (g/L)	2.5–4.7	4.3–7.2
Obtained by	Enzymatic action	Organic acids

Whey is considered as a waste by-product from the production of cheese. The production of 1 kg of cheese generates approximately 9 kg of whey [7]. It is discarded without treatment to public sewage systems, creating a critical pollution problem. Unfortunately, only 50% of the whey produced globally is used to formulate products. Whey has been traditionally dumped into common water ducts or used to feed livestock. The treatment and re-use of whey is very important as it is one of the most polluting food by/co-product streams; its biochemical oxygen demand (BOD) is around 435,000 ppm and its chemical oxygen demand (COD) is 460,000 ppm [5,8]. Current environmental regulations are forcing cheese makers to treat whey before disposal. The continued growth of the cheese industry, the necessity for reduction in pollutants in the effluent, and the need to maximize returns on raw material have encouraged producers and researchers to seek new ways of using cheese whey with a great amount of research focused on converting this liability into an asset [7–11]. The protein content of whey is one of the main advantages of this by-product. It is known that diet is one of the factors that influence human health and the development of diseases. Proteins are important nutrients in foods that can be hydrolyzed into a wide range of peptides during gastrointestinal digestion. Some of these peptides share characteristics that act in the organism as hormones, neurotransmitters, or regulatory peptides [12]. The importance of whey protein peptides is associated with their functional properties. Some studies have demonstrated the action of these peptides as inhibitors of angiotensin converting enzyme (ACE) on the regulation of blood pressure and enhancement of the immune system. These hydrolysates also help to increase dopamine, improving memory in patients from the geriatric area. In the food industry, whey protein peptides present antimicrobial, antioxidant activities, and also emulsifying properties. All functional properties of whey protein hydrolysates are related to their molecular weight. These properties are in a latent state during the formation of the protein structure complex and is only activated when that structure is broken or hydrolyzed by different methods such as enzymatic action, chemical hydrolysis, and through the application of emerging technologies such as ultrasound and heat treatments [13–16]. The purpose of this review was to provide an overview of the current understanding of the different methods of extraction of whey protein hydrolysates and the benefits these proteins provide on the body as antiviral, anticancer, antioxidant, and immunological agents. Additionally, an updated overview of their application in different food matrices and improvement in techno-functional properties is described. To accomplish this goal, a scientific literature search was performed through several academic web sites that included Scopus, MDPI, Elsevier, Wiley, SciELO, Web of Science, PubMed, and Redalyc. The topics that we focused on were milk whey classification and composition, milk whey hydrolysates, technologies to obtain these hydrolysates including enzymatic, chemical, and green technologies and included both functional properties of milk whey hydrolysates (antioxidant, antimicrobial, antihypertensive, anticancer, etc.) and applications in food and supplements.

2. Intrinsic Properties and Composition of Milk Whey Native Proteins

Whey is regarded as a valuable source of numerous nutritional, functional, and bioactive compounds. Whey presents an elevated content of lactose and proteins that can be used to produce versatile health-oriented compounds [17]; it is also considered a valuable product because of its soluble proteins and high levels of amino acid, vitamins

B, lactose, and salt. Whey contains 55–75% and 40–70% of vitamin B6 and vitamin B12, respectively, and also thiamine, nicotinic acid, folic acid and ascorbic acid, riboflavin, and biotin. However, a major concentration of vitamin B12 is displaced in whey during enzymatic treatment compared to acid coagulation [18]. Whey proteins present a high content of essential and branched amino acids such as isoleucine, leucine, and valine. They play an important role as regulators of different metabolic functions, blood glucose homeostasis, and a balanced source of the sulfur-containing amino acids. Minerals such as calcium, magnesium, phosphorus, and trace amount of zinc are present in whey and can act as a base of electrolytes [19,20].

As can be seen in Table 2, whey contains several proteins providing specific functional, physiological, and nutraceutical characteristics, as described below [21,22].

Table 2. Protein composition of whey [21,22].

Protein	Content (g/L)
β-lactoglobulin	2.9
α-lactoalbumin	0.6
Inmunoglobulin	0.3
Serum albumin	0.6
Lactoferrin	0.1
Lactoperoxidase	0.03
Protease-peptone	1
Glycomacropeptide (GMP)	0.9

2.1. β-Lactoglobulin

β-Lactoglobulin is the main whey protein of the heat coagulable proteins representing approximately 50% of the total protein and approximately 10% of milk protein. Its molecular weight ranges from 8.36 kDa to 18.20 kDa. It occurs as a dimer of two identical subunits consisting of a sulfhydryl group and two disulfide bonds and composed of a 162 amino acid peptide chain. The solubility of this protein depends on pH and ionic strength. Heat denaturation occurs between 70–75 °C [23]. β-Lactoglobulin is not found in breast milk and is considered to be responsible for some allergic reactions in infants fed with cow milk products. For this reason, there are commercial products that imitate human milk based on whey [24,25]. Traditionally, β-lactoglobulin is separated by fractional precipitation with ammonium sulfate at pH with or without heating to cause the precipitation of all serum proteins other than β-lactoglobulin, which are characterized commonly by chromatographic methods such as ion exchange chromatography [26].

Functional activities of whey are related to its composition. Lactose promotes the absorption of magnesium and zinc and is considered better for diarrheal treatment. Additionally, whey proteins show important biological activity and unique functional properties that include high quality nutritional source of amino acids, anti-microbial activity, growth enhancement of beneficial microflora (*Bifidobacteria*), immune-enhancing properties, and the control of specific diseases including cancer and antitoxin activity [1,17,27,28].

The great nutritional value of whey enhances nutraceutical benefits, reducing atherosclerosis, obesity, diabetes, and cancer risk; also, the presence of sulfur amino acids in whey act as cancer prevention agents as forerunners to the strong intracellular cell reinforcement glutathione in one-carbon metabolism. Whey is used as a functional food because it can contribute to the regulation of body weight by providing satiety signals that affect both short-term and long-term food intake regulation [4,27,29,30].

Whey protein has been chosen as an ideal ingredient in diet aiming to prevent or ameliorate metabolic diseases such as obesity because it decreases appetite and increases satiety through several mechanisms such as the regulation of satiety hormones and alteration of hepatic gluconeogenesis [31,32]. Additionally, whey protein is an important component in optimizing body composition because it promotes muscle mass, muscular strength, and muscle hypertrophy in complement with resistance exercises. It induces protein synthesis

more efficiently compared to other protein sources due to its faster digestion. This feature leads to a more rapid increase in plasma amino acid levels, particularly in essential amino acids [33–36]. Furthermore, whey protein subfractions have specific anti-cancer effects because α-lactalbumin and lactoferrin hinder tumor pathways [37]. Whey acts positively in the body by improving the fast absorption of branched chain amino acids. Whey has demonstrated the ability to lower the blood pressure because of an angiotensin-converting enzyme inhibitory property and augmentation of nitric oxide-mediated vasodilation from the component of isoleucine–proline–alanine tripeptide. Furthermore, whey protein consumption can improve lipid metabolism by promoting lipoprotein lipase and inhibiting cholesterol absorption [38–40].

2.2. α-Lactoalbumin

α-Lactoalbumin represents 11% of total whey proteins. It has a high affinity to calcium and excellent source of essential amino acids mainly represented by tryptophan and cysteine. This protein can be considered as homologous to human α-lactoalbumin because it is 72% analogous in structure. The molecular weight of α-lactoalbumin is around 14 kDa. It has a compact globular structure with four disulfides and denatures at 63 °C, but returns to its natural state on cooling. Whey is an important source of bioactive peptides and essential amino acids including tryptophan, lysine, branched-chain amino acids, and sulfur-containing amino acids. All of them are vital for infant nutrition [41]. It is composed of 123 polypeptides that contain eight cysteine residues. α-lactoalbumin shows some other benefits such as incremental levels of tryptophan in plasma leading to better cognitive performance, good lipid oxidation, better absorption of minerals, antibacterial activity, immunomodulatory effects, and antitumor activity [23,42,43].

2.3. Immunoglobulins (Ig)

Immunoglobulins are the largest proteins in milk whey, representing 2% of the total protein in milk. These proteins are composed of three main classes: immunoglobulins IgG, IgA, and IgM. Each form has the same basic structure: two identical light chains of 23 kDa and two chains of 53 kDa. However, IgG is present in a monomeric form, IgA in dimers, and IgM in tetramers. Immunoglobulins are relatively stable to heat and have been incorporated as functional foods because they reduce the risk of gastrointestinal disorder [19,44]. Its main function is to encapsulate bacteria, neutralize toxins, and inactivate viruses. It can also promote gastric digestion, lower blood pressure by reducing cholesterol levels, and it is used in milk formulas for kids as substitutes for milk [23,42].

2.4. Bovine Serum Albumin (BSA)

Bovine serum albumin (BSA) represents approximately 5–6% of total milk proteins, and its molecular weight ranges from 66.2 to 66.5 kDa. It is composed of a single polypeptide chain that includes 583 amino acid residues. The cross-linked 17 disulfide bridges of cysteine (Cys) amino acid residues stabilize the structure. Its denaturation temperature is 4 °C. It is also a source of essential amino acids. BSA is able to bind a wide range of ligands including fatty acids, amino acids, drugs, and inorganic ions, and is deemed to be a primary carrier of endogenous and exogenous compounds in the circulatory system [45,46].

The functionality of these proteins has been reported as relevant for their human breast cancer cell inhibitory potential, opioid agonist activity, and antihypertensive property [47,48].

2.5. Lactoferrin

This is an iron-binding glycoprotein that belongs to the family of transfer proteins and is generally found in the exocrine secretions of mammalian milk, tears, mucus, and saliva [42,49]. It is a minor component in bovine milk with concentrations of 0.1–0.2 g/L, and has a molecular weight of 80 kDa with a high isoelectric point around 9.5–10. It is composed of a unique polypeptide chain of 700 amino acids; this chain can contain one or

two carbohydrate chains. This protein consists of a single polypeptide chain arranged in two highly homologous lobes linked by an a-helix structure. Each lobe contains a ferric iron-binding site. It has 16 intramolecular disulfide bonds but not a free sulfhydryl group [19]. Lactoferrin molecules are thermostable and resistant to acids at pH 4; they are also resistant to the action of trypsin and chymotrypsin but can be hydrolyzed with pepsin. Its ability to bind iron generates various biological functions such as the inhibition of bacteria and fungi growth, promoter of certain cell lines, prevention of lipid peroxidation, and good absorption of iron in the body. Its applications include health supplements, functional foods and beverages, infant formulas, cosmetics, and oral care products [47,50].

2.6. Lactoperoxidase

This is a glycoprotein present in the mammary, salivary, and lacrimal glands of mammals with a molecular weight of 78 kDa. This enzyme is a unique polypeptide chain with 612 amino acids. Lactoperoxidase is relativity stable to heat, it resists pasteurization treatment (72 °C, 15 s), and it can be inactivated at 78 °C. This glycoprotein can catalyze the oxidations of several substrates including fatty acids, aromatic amines, phenols, and aromatic acids [51]. Lactoperoxidase plays an important role in the protection of the lactating mammary gland and the intestinal tract of neonates against pathogenic microorganisms; it can also be used in combination with other materials for the production of films for food packaging. It is also involved in the degradation of certain carcinogens and in the protection of animal cells against peroxidative effects. All these functional properties allow this enzyme to be used in the food, cosmetics, pharmaceutical, and agricultural industries [52,53].

2.7. Protease–Peptone

This is defined as a heterogeneous mixture of whey proteins; it is thermostable and soluble at acid pH values. It can be separated by heat treatment and adjustment of the pH to 4.6. Proteose peptone 3 (PP3) represents the major factor of proteose peptone, it is a phosphorylated glycoprotein with low- molecular-weight fraction and surface-active property [47,54]. There is great interest in the food industry for protease–peptone because it has shown a good emulsifying activity in the oil-in-water emulsion model used in products with soya bean oil and ice cream. It presents excellent foam-forming properties [55,56] and is the fraction of the milk that remains soluble when the milk is heated at 95 °C for 20 min under acidic conditions. This protein acts as an immunomodulator, anti-bacterial, and also inhibits the activity of lipase [23,57].

2.8. Glycomacropeptide

Glycomacropeptide (GMP) is a peptide found in cheese whey, separated by the action of enzymatic action (rennin) on κ-casein proteins. It is the glycolyzed form of the casein macro peptide. The glycolmacropeptide is a soluble peptide of 64 amino acids with a molecular weight of 6.8 kDa. It contains variable amounts of oligosaccharides, mainly galactosamine, galactose, and sialic acid, is available as an ingredient for its application in food, beverages, cosmetics, functional and medicinal supplements, and is also associated with biological benefits and anti-infective and antioxidant activities [58,59].

Food supplementation with GMP exerts several health potentials because it acts as an immunomodulator and anti-inflammatory protein. It has a prebiotic effect on *Bifidobacterium* and *Lactobacillus* sp. It also enhances calcium absorption, improving bone health and inhibits the adhesion of several cariogenic bacteria including *Sobrinus*, *Sanguis,* and *Streptococcus mutans* [19,47,54].

3. Hydrolyzed Protein from Milk Whey as High Value-Added Compounds

The valorization of a waste product can be defined as a process that transforms waste through physical, thermal, chemical, or biological methods in order to create products that can be incorporated as part of the circular economy into production chains. Whey

valorization focuses mainly on the concentration and transformation of lactose, proteins, or any other nutrients into new value-added compounds [60,61]. Some value-added compounds from whey have been extracted from different biotechnological approaches such as enzymatic, microbial, thermal, galacto-oligosaccharide probiotics (GOS), lactose fatty acid esters, biocolorants, aroma compounds, and bacterial cellulose [62].

Galacto-oligosaccharides (GOS) are a well-known class of probiotics or substrates that are selectively utilized by host microorganisms, conferring a health benefit [63]. GOS have various benefits to human health including the selective stimulation of the beneficial intestinal bacteria growth, maintenance of the normal flora balance in the intestine, increased calcium absorption, and decreased serum cholesterol levels and cancer risks. The health-promoting effects of GOS include immunomodulation, lipid metabolism, mineral absorption, weight management, and obesity-related issues, among others [64–66].

Lactose fatty acid esters are odorless, non-toxic, and biodegradable compounds of high importance for the food, cosmetics, and pharmaceutical industries. Lactose fatty acid esters have been recognized for their superior properties as attractive substitutes of synthetic surfactants, excellent emulsifying and stability properties in food products. Additionally, they present antimicrobial activity against many foodborne pathogens as well as medicinal properties such as anticancer activity [67–69].

Carotenoids are one of the most important natural pigments and can usually be extracted from plants. However, cheese whey, or deproteinized cheese whey, has been used for the production of carotenoids by using various microorganisms (*Blakeslea trispora*, *Mucor azygosporus*, *Rhodotorula rubra*) for the fermentation of various carbon sources such as glucose, sucrose, and xylose. Carotenoids possess biological functions such as antioxidant activity, reduction in cardiovascular diseases, anti-diabetic, anti-cancer, and anti-inflammation activities. The interest in the carotenoids from whey focuses on the use of low-cost substrates to reduce the production costs [70–72]. Fermentation is also an alternative way for the production of natural aroma compounds from milk whey and involves the use of several yeast strains such as *Metschnikowia pulcherrima*, *Bacillus licheniformis*, *Wickerhamomyces pijperi*, and *Saccharomyces cerevisiae* [73–76].

Bacterial cellulose (BC) is a biopolymer with important physiochemical properties such as water holding capacity, hydrophilicity, high degree of polymerization, mechanical strength, crystallinity, and porosity. All these BC characteristics represent a wide range of potential applications starting from the food industry and biomedicine to electronics and cosmetics. Bacterial cellulose extracted from whey through enzymatic and acidic pretreatments can be considered as a cheaper growth medium for BC production due to the low-cost of raw materials as well as its enhanced BC yields [77], reducing environmental pollution from dairy waste. BC has been used as an edible antimicrobial food coating increasing shelf life as well as a healthy food supplement for patients with gastrointestinal disorders, obesity, cardiovascular diseases, and diabetes. BC is considered as a multifunctional food ingredient because it can be used to improve the rheology of foods as a fat replacer ingredient for the production of both low-calorie and low cholesterol food products [78,79].

4. Methods of Extraction of Whey Hydrolysates

Milk proteins have been considered as the most important source of bioactive peptides; after their ingestion, these peptides can positively influence the cardiovascular, digestive, endocrine, immune, and nervous systems. Peptides represent a functional food because they not only satisfy the nutritional needs, but also help to reduce the risk of health problems [80]. Whey represents 95% of milk weight so it is a good source of bioactive peptides that can be produced by hydrolysis by applying different methods: enzymatic action, chemical treatment (acid or alkaline), microbial fermentation with proteolytic bacteria, ultrasound, thermal process, and others (Figure 1) [81,82].

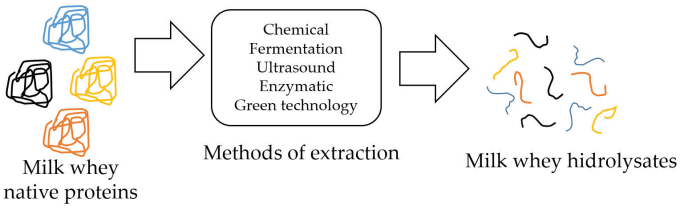

Figure 1. Different extraction methods of milk whey hydrolysates.

Hydrolysis of proteins by chemical processes using an alkaline or acidic media commonly using NaOH, KaOH, HCl at different concentrations is more difficult to control and generates hydrolysates with modified amino acids. Table 3 shows that chemical treatment presents several and important disadvantages: reduces nutritional quality, oxidizes cysteine and methionine, destroys some serine and threonine, and the conversion of glutamine and asparagine to glutamate and aspartate, respectively [83–85].

Fermentation of native whey proteins produces peptides or free amino acids valuable for their functional properties [86]. Many lactic acid bacteria (LAB) such as *Lactococcus lactis*, *Lactobacillus helveticus*, *Lactobacillus delbrueckii* ssp. *Bulgaricus*, *Bacillus* spp., and *Bifidobacterium* have proteolytic action in whey [87]. Fermentation has an advantage; hydrolysis is carried out by proteases of microorganisms, and thus, bioactive peptides can be purified without further hydrolysis. However, during fermentation, some of the peptides and/or amino acids released from the native proteins are used as a substrate for strain growth [17,83,88]. Another treatment to obtain hydrolysates from whey is high-energy power ultrasound. This method has been used successfully as it improves enzymatic hydrolysis, producing bioactive peptides. Ultrasound (>20 kHz) generates high temperature and pressure, causing physical and chemical changes at the molecular levels and consequently, better access of enzymes to hydrolysis sites [89,90]. The ultrasound method induces the unfolding of whey protein by high cavitation (20 kHz). This method also changes the secondary structure of proteins, decreasing the content of α-helices and increasing β-sheets and β-turn. Ultrasound treatment improves functional properties such as in vitro angiotensin converting enzyme inhibitor (ACE) and immunomodulatory activities [89,91,92]. The most common hydrolysis treatment is enzymatic; the functionality of these hydrolysates depends on different factors such as the type of enzyme, pH, temperature, time, and enzyme/substrate ratio [93,94]. Compared to chemical hydrolysis, enzymatic hydrolysis usually takes place under relatively mild operating conditions (temperature 20–70 °C, pH 6.0–8.0) [95]. The most widely used enzymes to produce whey hydrolysates are proteases and are capable of promoting specific and selective protein modifications. Trypsin is a commercial enzyme widely used for protein hydrolysis. This enzyme is highly active, has elevated cleavage specificity, and is very stable under different experimental conditions [93,96,97].

Not only are animal source enzymes used to obtain whey hydrolysates, some enzymes from plant sources such as papain have also been used [98–101]. Additionally, plant crude extracts were used for the hydrolysis of whey proteins, some examples are described as follows: extracts from Citrus aurantium flowers, trompillo (*Solanum elaeagnifolium*) berries, and melon (*Cucumis melo*) fruit [83,102]. However, enzymatic hydrolysis can modify the nutritional value of the hydrolysates and other properties such as solubility, emulsification, foaming, and gelation and bitter products [103].

Emerging technologies such as thermal treatments (>90°C), high hydrostatic pressure (100–1000 MPa), and even ultrasound can modify the characteristics of hydrolysates, creating a large number of hydrophobic groups, increasing antioxidant, ACE inhibitory, and immunomodulatory activities and also maintaining the original sensorial quality and nutrients [92,104,105].

These methods are environmentally-friendly (no generation of chemical waste) and are very promising because they increase the amount of whey hydrolysates, functional properties, and reduced time of hydrolysis [96,106–109].

Table 3. Advantages of different methods of the extraction of whey hydrolysates.

Methods of Extraction	General Characteristics	Advantages	References
Chemical	Difficult to control and generates hydrolysates with modified amino acids.	Easy access to reagents.	[83–85]
Fermentation	It involves some acid lactic bacteria (BAL), no need to use acid or alkaline media	Bioactive peptides obtained can be purified without further hydrolysis.	[17,88]
Ultrasound	>20 kHz induced the unfolding of whey protein by high cavitation	Improves the enzymatic hydrolysis producing bioactive peptides from proteins presents in whey.	[89–92]
Enzymatic	Takes place under relatively mild operating conditions	Not addition of chemical reagents, nutritional value is maintained, control of the process (time, temperature and pH), most common method.	[93–95,110]
Green technology	Can be thermal treatments and high hydrostatic	Reduce time of hydrolysis, no generation of chemical waste.	[96,106,107,109]

5. Functional Properties of Hydrolyzed Milk Whey Proteins

Milk whey biological functions are mainly related to the cardiovascular, digestive, endocrine, immune, and nervous systems. However, many of the bioactive peptides are encrypted in native whey protein, so in order to liberate these peptides, it is necessary to apply hydrolysis methods that generate milk whey hydrolysates. In recent years, milk whey hydrolysates have been studied due to their potential as a functional ingredient capable of producing beneficial effects on health such as immunity, antioxidant, anticancer, antiviral, and antihypertensive (Figure 2). At the same time, production of hydrolysates can be an interesting approach in adding value to whey protein, while at the same time protecting the environment from their pollutant effects [82,83,93,111].

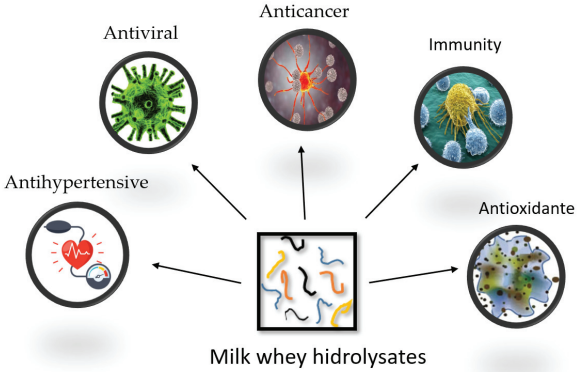

Figure 2. Functional properties of milk whey hydrolysates.

5.1. Antihypertensive

Management of hypertension is a multifactorial issue and must be accompanied by different prevention-oriented activities such as ACE-inhibitory drugs prescription, lifestyle changes including weight loss, quitting smoking, and reducing sodium and alcohol intake. Aside from these recommendations, milk-derived peptides obtained by fermentation have shown excellent ACE-inhibitory capacity, and thus a blood pressure-lowering effect [112].

Cardiovascular diseases are the main cause of death around the world. The renin–angiotensin system is the pathway that exerts control over blood pressure. The angiotensin converting enzyme (ACE) is responsible for altering blood pressure in the body. ACE is responsible for converting angiotensin I into angiotensin II, providing a vasoconstrictor effect [113,114]. The use of synthetic drugs to control these diseases causes several side effects such as cough, taste disturbance, and skin rash, among others. Therefore, an alternative for the prevention and/or treatment of arterial hypertension is the use of bioactive components obtained from natural sources (animal or vegetable) such as antihypertensive peptides [115–117].

Several studies have demonstrated the mechanism of action of peptides for ACE inhibition [118]. It can be described in two different points. First, by physiologic importance: oral administration of peptides reaches the bloodstream in an active form to exert their antihypertensive effect, since gastrointestinal digestion and transport are the main barriers to the bioavailability of peptides. Second, the digestion of peptides via gastrointestinal proteases could be used as a process for the production of peptides with ACE inhibitory capacity [116].

Miralles and co-workers [119] reported advances in the field of study of antihypertensive peptides. They concluded that food derived antihypertensive peptides represent a good source of functional agents in healthy diets. However, after oral intake, these peptides are hydrolyzed during digestion and absorption, rendering shorter peptide forms that have been revealed to exert a potent and more sustained antihypertensive effect. This peptide biotransformation is the reason why the technique in in vitro ACE-inhibitory activity is not sufficient to demonstrate their antihypertensive effect. Studies on whey peptides oriented to inhibit ACE activity are very scarce; this might be because the structure of β-lactoglobulin is resistant to digestive enzymes [120].

It is well-known that casein-derived tripeptides such as valyl-prolyl-proline (Val-Pro-Pro) and isoleucyl-prolyl-proline (Ile-Pro-Pro) present excellent antihypertensive properties as shown in vivo [121,122]. Additional benefits have also been reported such as when oral intakes of these bioactive tripeptides including fermented milk and casein hydrolysates attenuated atherosclerosis development in apolipoprotein E-deficient mice.

5.2. Antiviral

Peptides are considered as ideal alternatives for synthetic therapeutic agents. The mechanism of peptide action depends on their structure and can be enhanced by modification of the native form. The antiviral action of peptides can be generated through three mechanisms: (I) peptides that inhibit virus adhesion and cell membrane fusion; (II) peptides that disrupt viral envelope; and (III) peptides that inhibit virus replication by interacting with viral polymerase. Lactoferrin and its hydrolysates have antiviral multiactivity against virus-like adenovirus, poliovirus, rotavirus, hepatitis B virus, Zika, dengue virus, influenza virus A H1N1, and respiratory syncytial virus. The antiviral action depends on the time of incubation with the virus, the concentration of the hydrolysates, and the method of obtention. Hydrolysates, with a molecular weight under 10 kDa composed of basic, aliphatic and polar amino acids with an isoelectric point greater than 10, present excellent antiviral effect due to their capacity to form amphipathic structures. Their good efficacy, safe, selectivity, and predictable metabolism are the main strengths of peptides in drug production [123–127].

5.3. Anticancer

Food-derived protein hydrolysates or isolated peptides possess anticancer activities through various molecular mechanisms. This includes the stimulation of apoptosis, arrest of cell cycle profession, cell membrane damage, inhibition of cell adhesion, topoisomerases, modulation of immune response, and inhibition of intracellular signaling [128,129]. It has been reported that some predominant hydrophobic amino acids of peptides such as proline, leucine, glycine, alanine, and one or more residues of lysine, arginine, serine, threonine, and tyrosine play an essential role in anticancer activities [130]. The anticancer activity of peptides is based on their structural characteristics such as amino acid composition, sequence, and hydrophobicity. The lower the molecular weight of peptides, the greater the molecular mobility and diffusivity for interactions with cancer cell components and thus stronger anticancer activity. Peptides obtained from lactoferrin decreased metastasis and a significant delay in growing tumors [128,131,132].

5.4. Immunity

The mechanism of immunomodulatory activity occurs mainly through the activation of macrophages, stimulation of phagocytosis, increased leukocyte count, increased induction of immune modulators such as cytosines, immunoglobulins, stimulations of NK cells, stimulation effect on splenocytes, and activation of mitogen-activated protein kinase. This mechanism depends on the amino acid sequence, composition, length, and structure that peptides can modulate immune responses [128].

α-Lactoalbumin is a small protein composed of 123 amino acids and a molecular weight around 14 kDa [5,133]. Hydrolyzation of this protein provides an antihypertensive effect [134] as well as antimicrobial [135] and immunostimulatory properties [136]. Proteins function as antigens that present regions called epitopes, which are identified by antibodies and subsequently trigger an allergenic reaction [137–139].

Isothiocynates have been linked to health properties and result from the degradation of glucosinolates, which is found in plants such as cauliflower, broccoli, and cabbage [140–142].

Spötell et al. [143] carried out immunological staining in native untreated and benzyl isothiocyanate (BITC)-modified α-lactoalbumin performed directly on the plate after their separation using high performance chromatography-immunostaining (HPTLC-IS) analysis. They reported that the HPTLC immune staining procedure did not destroy the tertiary and secondary structure of the protein. The chemical modification of protein with BITC derived from structural changes of the protein molecule and influenced the increase in allergenicity.

5.5. Antioxidant

The antioxidant activity of peptide fragments has been investigated in different vegetable sources such as soy bean [144] and pea seed [145]. In beverages, the combination of nutritional properties of milk whey and banana passionfruit were reported to increase the antioxidant properties of the beverage due to the presence of phenolic compounds. The higher the content of pulp, the higher the antioxidant activity [146]. Additionally, healthy functional beverages based on whey milk added with soursop [147] and raspberry were reported to increase their antioxidant properties as well as antihypertensive activity [148].

6. Applications of Milk Whey Proteins Hydrolysates

Whey hydrolysates are commonly applied to a wide range of food applications (dairies, bakeries, meet products, beverages, food supplements or functional foods) due to their nutritional validity, functional activities, and cost effectiveness. Whey hydrolysates are also used to replace other proteins, improving the functional properties of many food products. Whey protein hydrolysates are important in food processing due to their technological properties including oil and water holding, emulsifying capacity, foam capacity, and solubility. They can promote the formation of volatile compounds in food products regardless of whether they are added in small quantities [149–152].

Whey-based beverages such as dairy, not dairy, fermented, or non-fermented show functional activity because of their highly nutritional and digestible properties associated with the presence of hydrolysates as well as their functional properties such as antioxidant, antimicrobial, antihypertensive, and others (see Table 4) [153,154].

Mann et al. [154] prepared a flavored milk beverage with the addition of whey hydrolysates and good antioxidant activity attributed to the existence of several peptides contained in it. Additionally, Arranz et al. [155] developed a whey protein-based beverage with the same characteristics and no effect on apparent viscosity and stability of the beverage. Ferreira et al. [148] prepared a whey-raspberry flavored beverage that presented antioxidant capacity and ACE inhibition. Some no dairy beverages have been developed with hydrolysates that very often contain citrus fruits (mainly orange, followed by lemon, rarely grapefruit) as well as mango, passionfruit, pear, apple, and strawberry. The addition of milk whey hydrolysates in these types of beverages increased sensory and physicochemical properties such as flavor, odor, low sedimentation, and storage stability [156–158]. The addition of milk whey hydrolysates with antioxidant and antimicrobial activities into a beverage appears to create an exciting link between food science and therapeutic nutrition [153]. However, the use of high amounts of hydrolysate could result in negative effects in appearance and aroma [152].

Several researchers have investigated the application of milk whey hydrolysates as a food supplement. These studies have demonstrated that consumption of whey hydrolysates and other sources of protein hydrolysates such as soy, casein, and wheat presented high protein synthesis in the body [159–161]. Fassina et al. [162] demonstrated that milk whey hydrolysates are an excellent source of nutritious and commercially available alternative food sources commonly used as a food supplement by athletes. This supplement provides them with essential amino acids and bioactive peptides. Lockwood et al. [163] concluded that whey protein supplementation increased muscle mass after eight weeks in college-aged males. Hansen and co-workers [164] demonstrated that consumption of whey protein hydrolysates before an exercise session, followed by ingestion of more protein hydrolysates plus carbohydrates for a training period of six weeks, improved specific mitochondrial protein adaptations compared to the intake of carbohydrates. Additionally, milk whey hydrolysate supplementation showed increments in muscle mass and strength over a 10-week experiment in older post-menopausal women [165]. Brown and colleagues [166] reported that milk whey supplementation improved the recovery of muscle function and flexibility, accelerating the repair of damaged skeletal muscle and thus its force generation capacity. The consumption of this type of supplementation may contribute to reduced immunosuppression and excessive inflammation, accelerating muscle function recovery after heavy training [162,167].

Table 4. Applications of MWH and functionality.

Product	Functionality	Reference
Flavored milk beverage	Antioxidant activity	[154]
Whey MWH food supplementation in post-menopausal women	Increase muscle mass and strength	[165]
Apple juice	Low sedimentation	[156]
Beverage enriched white flaxseed oil	Increased of flavor, odor	[157]
MWH food supplementation in college-aged males	Increase mixed muscle and protein synthesis	[163]
MWH food supplementation	Improved recovery of muscle function and flexibility	[166]
Whey-raspberry flavored beverage	Antioxidant capacity and ACE inhibition	[148]
MWH food supplementation in athletes	Excellent source of nutritious	[162]

Table 4. *Cont.*

Product	Functionality	Reference
Whey protein-based beverage	Antioxidant and antimicrobial activity, no affecting physicochemical properties	[155]
Protein supplementation	Increasing mixed muscle and protein synthesis and lean body mass	[164]

7. Future Considerations of Milk Whey Hydrolysates

The numerous treatments applied to whey proteins offer an opportunity for future researchers to modify their textural and structural properties, improving the functionality and obtention of low molecular weight hydrolysates. This includes enzymatic treatments, emerging technologies such as ultrasound, high pressure, and thermal processes. Although milk whey hydrolysates have been applied to a wide variety of food products oriented to human health, most of the reported experimental data have been documented through a series of studies based on in vitro models as well as animal systems. Scientists face challenges in the near future in the implementation of clinical trials in humans. Additionally, the commercialization of these natural polymers must comply with the health regulations of different regions. The claims related to health effects should be supported by scientific studies. Finally, the use of new enzyme selections with known specificity could offer new functionality and applications to hydrolyzed whey proteins, for example, in the fields of antigenic response, health maintenance, and healing.

8. Conclusions

Although considered as a waste product, the literature supports that milk whey has relevant nutritional and functional properties that make it suitable for use in the food industry. Whey presents an important content of proteins, group B vitamins, minerals, and lactose. These proteins can be hydrolyzed by different methods (enzymatic, with LAB, ultrasound, thermal process, and others) obtaining low molecular weight peptides. Several studies have shown that its consumption as a food supplement helps protein synthesis in the body and increases muscle mass. Furthermore, milk whey protein in its hydrolyzed form possesses functional properties such as antioxidants, antihypertensive, anticancer, antivirals, and immunomodulatory activity. The molecular weight and properties of whey hydrolysates depend on the hydrolysis method and can be used in different industries including functional foods. The applications of milk whey are not limited to the food industry; this review confirmed the wide range of uses and advantages of milk whey hydrolysates. Future investigations must be conducted under scientific methods, oriented toward human trials for the elucidation of their benefits on the human system.

Author Contributions: X.A.P.-M., A.G.E.-F., G.C.-L., A.M.-P. and R.G.C.-M. developed the concept for the review and co-wrote the manuscript. A.L.-L. and G.A.-Á. revised and edited the manuscript. All authors have read and agreed to the published version of the manuscript.

Funding: This review was funded by the National Council of Science and Technology (CONACYT), grant number 621400.

Conflicts of Interest: The authors declare no conflict of interest.

References

1. Kaminarides, S.; Zagari, H.; Zoidou, E. Effect of whey fat content on the properties and yields of whey cheese and serum. *J. Hell. Vet. Med. Soc.* **2020**, *71*, 2149–2156. [CrossRef]
2. Guo, M.; Wang, G. History of whey production and whey protein manufacturing. In *Whey Protein Production, Chemistry, Functionality, and Applications*; Guo, M., Ed.; John Wiley & Sons: Chichester, UK, 2019; pp. 1–12.
3. Abd AL-Razaq, A.H. Whey applications in plants. *Plant Arch.* **2019**, *19*, 45–48.

4. Shenana, M.; El-Alfy, M.; El-Nagar, G.; El-Barbary, A. Physico-chemical and functional properties of functional yoghurt made with different types of whey protein concentrates (Wpc). In Proceedings of the 5th International Conference on Biotechnology Applications in Agriculture (ICBAA), Hurghada, Egypt, 8–11 April 2020.
5. Smithers, G.W. Whey and whey proteins—From 'gutter-to-gold'. *Int. Dairy J.* **2008**, *18*, 695–704. [CrossRef]
6. Tunick, M.H. Whey protein production and utilization: A brief history. In *Whey Processing, Functionality and Health Benefits*; Onwulata, C.I., Huth, P.J., Eds.; Wiley-Blackwell: Ames, IA, USA, 2008; pp. 1–13.
7. Lee, H.; Song, M.; Hwang, S. Optimizing bioconversion of deproteinated cheese whey to mycelia of Ganoderma lucidum. *Process Biochem.* **2003**, *38*, 1685–1693. [CrossRef]
8. Khedkar, R.; Singh, K. Food industry waste: A panacea or pollution hazard? In *Paradigms in Pollution Prevention*; Springer: Berlin, Germany, 2018; pp. 35–47.
9. Arsić, S.; Bulatović, M.; Zarić, D.; Kokeza, G.; Subić, J.; Rakin, M. Functional fermented whey carrot beverage-qualitative, nutritive and techno-economic analysis. *Rom. Biotechnol. Lett.* **2018**, *23*, 13496–13504.
10. León-López, A.; Pérez-Marroquín, X.A.; Campos-Lozada, G.; Campos-Montiel, R.G.; Aguirre-Álvarez, G. Characterization of Whey-Based Fermented Beverages Supplemented with Hydrolyzed Collagen: Antioxidant Activity and Bioavailability. *Foods* **2020**, *9*, 1106. [CrossRef]
11. Prazeres, A.R.; Carvalho, F.; Rivas, J. Cheese whey management: A review. *J. Environ. Manag.* **2012**, *110*, 48–68. [CrossRef]
12. Hernández-Ledesma, B.; García-Nebot, M.J.; Fernández-Tomé, S.; Amigo, L.; Recio, I. Dairy protein hydrolysates: Peptides for health benefits. *Int. Dairy J.* **2014**, *38*, 82–100. [CrossRef]
13. Aoi, W.; Naito, Y.; Yoshikawa, T. Dietary exercise as a novel strategy for the prevention and treatment of metabolic syndrome: Effects on skeletal muscle function. *J. Nutr. Metab.* **2011**, *2011*, 676208. [CrossRef]
14. Dullius, A.; Fassina, P.; Giroldi, M.; Goettert, M.I.; Volken de Souza, C.F. A biotechnological approach for the production of branched chain amino acid containing bioactive peptides to improve human health: A review. *Food Res. Int.* **2020**, *131*, 109002. [CrossRef]
15. Heo, S.-Y.; Ko, S.-C.; Nam, S.Y.; Oh, J.; Kim, Y.-M.; Kim, J.-I.; Kim, N.; Yi, M.; Jung, W.-K. Fish bone peptide promotes osteogenic differentiation of MC3T3-E1 pre-osteoblasts through upregulation of MAPKs and Smad pathways activated BMP-2 receptor. *Cell Biochem. Funct.* **2018**, *36*, 137–146. [CrossRef]
16. Du, X.; Jing, H.; Wang, L.; Huang, X.; Wang, X.; Wang, H. Characterization of structure, physicochemical properties, and hypoglycemic activity of goat milk whey protein hydrolysate processed with different proteases. *LWT* **2022**, *159*, 113257. [CrossRef]
17. Kareb, O.; Aïder, M. Whey and its derivatives for probiotics, prebiotics, synbiotics, and functional foods: A critical review. *Probiotics Antimicrob. Proteins* **2019**, *11*, 348–369. [CrossRef] [PubMed]
18. Singh, S.; Khemariya, P.; Rai, A. Process optimization for the manufacture of lemon based beverage from hydrolyzed whey. *J. Food Sci. Technol.* **2014**, *51*, 691–699. [CrossRef]
19. Deeth, H.; Bansal, N. Chapter 1—Whey proteins: An overview. In *Whey Proteins*; Deeth, H.C., Bansal, N., Eds.; Academic Press: London, UK, 2019; pp. 1–50.
20. Kumar, R.; Chauhan, S.K.; Shinde, G.; Subramanian, V.; Nadanasabapathi, S. Whey Proteins: A potential ingredient for food industry—A review. *Asian J. Dairy Food Res.* **2018**, *37*, 283–290.
21. Fang, T.; Guo, M. Physicochemical, texture properties, and microstructure of yogurt using polymerized whey protein directly prepared from cheese whey as a thickening agent. *J. Dairy Sci.* **2019**, *102*, 7884–7894. [CrossRef] [PubMed]
22. Aguero, R.; Bringas, E.; San Roman, M.F.; Ortiz, I.; Ibanez, R. Membrane Processes for Whey Proteins Separation and Purification—A Review. *Curr. Org. Chem.* **2017**, *21*, 1740–1752. [CrossRef]
23. Yadav, J.S.S.; Yan, S.; Pilli, S.; Kumar, L.; Tyagi, R.D.; Surampalli, R.Y. Cheese whey: A potential resource to transform into bioprotein, functional/nutritional proteins and bioactive peptides. *Biotechnol. Adv.* **2015**, *33*, 756–774. [CrossRef]
24. Varlamova, E.G.; Zaripov, O.G. Beta–lactoglobulin–nutrition allergen and nanotransporter of different nature ligands therapy with therapeutic action. *Res. Vet. Sci.* **2020**, *133*, 17–25. [CrossRef]
25. Pali-Schöll, I.; Bianchini, R.; Afify, S.M.; Hofstetter, G.; Winkler, S.; Ahlers, S.; Altemeier, T.; Mayerhofer, H.; Hufnagl, K.; Korath, A.D. Secretory protein beta-lactoglobulin in cattle stable dust may contribute to the allergy-protective farm effect. *Clin. Transl. Allergy* **2022**, *12*, e12125. [CrossRef]
26. Schlatterer, B.; Baeker, R.; Schlatterer, K. Improved purification of β-lactoglobulin from acid whey by means of ceramic hydroxyapatite chromatography with sodium fluoride as a displacer. *J. Chromatogr. B* **2004**, *807*, 223–228. [CrossRef] [PubMed]
27. Macwan, S.R.; Dabhi, B.K.; Parmar, S.; Aparnathi, K. Whey and its utilization. *Int. J. Curr. Microbiol. Appl. Sci.* **2016**, *5*, 134–155. [CrossRef]
28. Panghal, A.; Patidar, R.; Jaglan, S.; Chhikara, N.; Khatkar, S.K.; Gat, Y.; Sindhu, N. Whey valorization: Current options and future scenario—A critical review. *Nutr. Food Sci.* **2018**, *48*, 520–535. [CrossRef]
29. Król, J.; Brodziak, A.; Zaborska, A.; Litwińczuk, Z. Comparison of whey proteins and lipophilic vitamins between four cow breeds maintained in intensive production system. *Mljekarstvo Dairy* **2017**, *67*, 17–24.
30. Narayanan, R. Health augmenting properties of whey. *Int. J. Curr. Microbiol. Appl. Sci.* **2013**, *2*, 152–154.

31. Boscaini, S.; Cabrera-Rubio, R.; Nychyk, O.; Speakman, J.R.; Cryan, J.F.; Cotter, P.D.; Nilaweera, K.N. Age and duration-dependent effects of whey protein on high-fat diet-induced changes in body weight, lipid metabolism, and gut microbiota in mice. *Physiol. Rep.* **2020**, *8*, e14523. [CrossRef]
32. Jakubowicz, D.; Wainstein, J.; Landau, Z.; Ahren, B.; Barnea, M.; Bar-Dayan, Y.; Froy, O. High-energy breakfast based on whey protein reduces body weight, postprandial glycemia and HbA1C in Type 2 diabetes. *J. Nutr. Biochem.* **2017**, *49*, 1–7. [CrossRef]
33. Cereda, E.; Turri, A.; Klersy, C.; Cappello, S.; Ferrari, A.; Filippi, A.R.; Brugnatelli, S.; Caraccia, M.; Chiellino, S.; Borioli, V. Whey protein isolate supplementation improves body composition, muscle strength, and treatment tolerance in malnourished advanced cancer patients undergoing chemotherapy. *Cancer Med.* **2019**, *8*, 6923–6932. [CrossRef]
34. Devries, M.C.; Phillips, S.M. Supplemental protein in support of muscle mass and health: Advantage whey. *J. Food Sci.* **2015**, *80*, A8–A15. [CrossRef]
35. Nabuco, H.C.; Tomeleri, C.M.; Sugihara Junior, P.; Fernandes, R.R.; Cavalcante, E.F.; Antunes, M.; Ribeiro, A.S.; Teixeira, D.C.; Silva, A.M.; Sardinha, L.B. Effects of whey protein supplementation pre-or post-resistance training on muscle mass, muscular strength, and functional capacity in pre-conditioned older women: A randomized clinical trial. *Nutrients* **2018**, *10*, 563. [CrossRef]
36. Smith, G.I.; Commean, P.K.; Reeds, D.N.; Klein, S.; Mittendorfer, B. Effect of protein supplementation during diet-induced weight loss on muscle mass and strength: A randomized controlled study. *Obesity* **2018**, *26*, 854–861. [CrossRef] [PubMed]
37. Teixeira, F.J.; Santos, H.O.; Howell, S.L.; Pimentel, G.D. Whey protein in cancer therapy: A narrative review. *Pharmacol. Res.* **2019**, *144*, 245–256. [CrossRef] [PubMed]
38. Lee, S.Y.; Hur, S.J. Antihypertensive peptides from animal products, marine organisms, and plants. *Food Chem.* **2017**, *228*, 506–517. [CrossRef] [PubMed]
39. Skrzypczak, K.; Fornal, E.; Waśko, A.; Gustaw, W. Effects of probiotic fermentation of selected milk and whey protein preparations on bioactive and technological properties. *Ital. J. Food Sci.* **2019**, *31*, 437–450.
40. Wirunsawanya, K.; Upala, S.; Jaruvongvanich, V.; Sanguankeo, A. Whey Protein Supplementation Improves Body Composition and Cardiovascular Risk Factors in Overweight and Obese Patients: A Systematic Review and Meta-Analysis. *J. Am. Coll. Nutr.* **2018**, *37*, 60–70. [CrossRef] [PubMed]
41. Layman, D.K.; Lönnerdal, B.; Fernstrom, J.D. Applications for α-lactalbumin in human nutrition. *Nutr. Rev.* **2018**, *76*, 444–460. [CrossRef]
42. Modler, W. Pioneer paper: Value-added components derived from whey. *Am. Dairy Sci. Assoc.* **2009**, *1*, 1–33.
43. Jiang, B.; Wang, L.; Na, J.; Zhang, X.; Yuan, Y.; Liu, C.; Feng, Z. Environmentally-friendly strategy for separation of α-lactalbumin from whey by aqueous two phase flotation. *Arab. J. Chem.* **2020**, *13*, 3391–3402. [CrossRef]
44. Heidebrecht, H.-J.; Kulozik, U. Fractionation of casein micelles and minor proteins by microfiltration in diafiltration mode. Study of the transmission and yield of the immunoglobulins IgG, IgA and IgM. *Int. Dairy J.* **2019**, *93*, 1–10. [CrossRef]
45. Jahanban-Esfahlan, A.; Ostadrahimi, A.; Jahanban-Esfahlan, R.; Roufegarinejad, L.; Tabibiazar, M.; Amarowicz, R. Recent developments in the detection of bovine serum albumin. *Int. J. Biol. Macromol.* **2019**, *138*, 602–617. [CrossRef]
46. Cheng, H.; Fang, Z.; Wusigale; Bakry, A.M.; Chen, Y.; Liang, L. Complexation of trans- and cis-resveratrol with bovine serum albumin, β-lactoglobulin or α-lactalbumin. *Food Hydrocoll.* **2018**, *81*, 242–252. [CrossRef]
47. Sharma, R. Chapter 17—Whey proteins in functional foods. In *Whey Proteins*; Deeth, H.C., Bansal, N., Eds.; Academic Press: London, UK, 2019; pp. 637–663.
48. Koh, B.-B.; Lee, E.-J.; Ramachandraiah, K.; Hong, G.-P. Characterization of bovine serum albumin hydrolysates prepared by subcritical water processing. *Food Chem.* **2019**, *278*, 203–207. [CrossRef] [PubMed]
49. Wang, B.; Timilsena, Y.P.; Blanch, E.; Adhikari, B. Characteristics of bovine lactoferrin powders produced through spray and freeze drying processes. *Int. J. Biol. Macromol.* **2017**, *95*, 985–994. [CrossRef]
50. Wang, Q.; Chen, G.Q.; Kentish, S.E. Isolation of lactoferrin and immunoglobulins from dairy whey by an electrodialysis with filtration membrane process. *Sep. Purif. Technol.* **2020**, *233*, 115987. [CrossRef]
51. Silva, E.; Oliveira, J.; Silva, Y.; Urbano, S.; Sales, D.; Moraes, E.; Rangel, A.; Anaya, K. Lactoperoxidase system in the dairy industry: Challenges and opportunities. *Czech J. Food Sci.* **2020**, *38*, 337–346. [CrossRef]
52. Urtasun, N.; Baieli, M.F.; Hirsch, D.B.; Martínez-Ceron, M.C.; Cascone, O.; Wolman, F.J. Lactoperoxidase purification from whey by using dye affinity chromatography. *Food Bioprod. Process.* **2017**, *103*, 58–65. [CrossRef]
53. Shokri, S.; Ehsani, A. Efficacy of whey protein coating incorporated with lactoperoxidase and α-tocopherol in shelf life extension of Pike-Perch fillets during refrigeration. *LWT Food Sci. Technol.* **2017**, *85*, 225–231. [CrossRef]
54. Mehra, R.; Kumar, H.; Kumar, N.; Ranvir, S.; Jana, A.; Buttar, H.S.; Telessy, I.G.; Awuchi, C.G.; Okpala, C.O.R.; Korzeniowska, M.; et al. Whey proteins processing and emergent derivatives: An insight perspective from constituents, bioactivities, functionalities to therapeutic applications. *J. Funct. Foods* **2021**, *87*, 104760. [CrossRef]
55. Hogenboom, J.A.; Rosi, V.; Monti, L. Effect of processing and storage conditions on the evolution of the proteose peptone content in pasteurized and extended shelf-life milk. *Sci. E Tec. Latt. Casearia* **2020**, *70*, 24–28. [CrossRef]
56. Innocente, N.; Biasutti, M.; Blecker, C. HPLC profile and dynamic surface properties of the proteose–peptone fraction from bovine milk and from whey protein concentrate. *Int. Dairy J.* **2011**, *21*, 222–228. [CrossRef]
57. Karamoko, G.; Renaville, R.; Blecker, C. Interfacial activities of milk total proteose-peptone: Contribution and miscibility of nonhydrophobic and hydrophobic fractions. *Int. Dairy J.* **2016**, *61*, 29–36. [CrossRef]

58. Chungchunlam, S.M.; Henare, S.J.; Ganesh, S.; Moughan, P.J. Effect of whey protein and glycomacropeptide on measures of satiety in normal-weight adult women. *Appetite* **2014**, *78*, 172–178. [CrossRef] [PubMed]
59. O'Riordan, N.; O'Callaghan, J.; Buttò, L.F.; Kilcoyne, M.; Joshi, L.; Hickey, R.M. Bovine glycomacropeptide promotes the growth of *Bifidobacterium longum* ssp. infantis and modulates its gene expression. *J. Dairy Sci.* **2018**, *101*, 6730–6741. [CrossRef] [PubMed]
60. Sebastián-Nicolás, J.L.; González-Olivares, L.G.; Vázquez-Rodríguez, G.A.; Lucho-Constatino, C.A.; Castañeda-Ovando, A.; Cruz-Guerrero, A.E. Valorization of whey using a biorefinery. *Biofuels Bioprod. Biorefin.* **2020**, *14*, 1010–1027. [CrossRef]
61. Valdez Castillo, M.; Laxman Pachapur, V.; Brar, S.K.; Naghdi, M.; Arriaga, S.; Ávalos Ramirez, A. Yeast-driven whey biorefining to produce value-added aroma, flavor, and antioxidant compounds: Technologies, challenges, and alternatives. *Crit. Rev. Biotechnol.* **2020**, *40*, 930–950. [CrossRef]
62. Lappa, I.K.; Papadaki, A.; Kachrimanidou, V.; Terpou, A.; Koulougliotis, D.; Eriotou, E.; Kopsahelis, N. Cheese Whey Processing: Integrated Biorefinery Concepts and Emerging Food Applications. *Foods* **2019**, *8*, 347. [CrossRef]
63. Gibson, G.R.; Hutkins, R.; Sanders, M.E.; Prescott, S.L.; Reimer, R.A.; Salminen, S.J.; Scott, K.; Stanton, C.; Swanson, K.S.; Cani, P.D.; et al. Expert consensus document: The International Sci. entific Association for Probiotics and Prebiotics (ISAPP) consensus statement on the definition and scope of prebiotics. *Nat. Rev. Gastroenterol. Hepatol.* **2017**, *14*, 491–502. [CrossRef]
64. Duan, F.; Zhao, R.; Yang, J.; Xiao, M.; Lu, L. Integrated Utilization of Dairy Whey in Probiotic β-Galactosidase Production and Enzymatic Synthesis of Galacto-Oligosaccharides. *Catalysts* **2021**, *11*, 658. [CrossRef]
65. Duncan, P.I.; Aitio, O.; Heiskanen, A.; Niemelä, R.; Saarinen, J.; Helin, J.; Porta, N.; Fiaux, M.; Moënnoz, D.; Golliard, M.; et al. Structure and Function of Bovine Whey Derived Oligosaccharides Showing Synbiotic Epithelial Barrier Protective Properties. *Nutrients* **2020**, *12*, 2007. [CrossRef]
66. Torres, D.P.M.; Gonçalves, M.d.P.F.; Teixeira, J.A.; Rodrigues, L.R. Galacto-Oligosaccharides: Production, Properties, Applications, and Significance as Prebiotics. *Compr. Rev. Food Sci. Food Saf.* **2010**, *9*, 438–454. [CrossRef]
67. Barba, F.J. An Integrated Approach for the Valorization of Cheese Whey. *Foods* **2021**, *10*, 564. [CrossRef] [PubMed]
68. Enayati, M.; Gong, Y.; Goddard, J.M.; Abbaspourrad, A. Synthesis and characterization of lactose fatty acid ester biosurfactants using free and immobilized lipases in organic solvents. *Food Chem* **2018**, *266*, 508–513. [CrossRef]
69. Staroń, J.; Dąbrowski, J.M.; Cichoń, E.; Guzik, M. Lactose esters: Synthesis and biotechnological applications. *Crit. Rev. Biotechnol.* **2018**, *38*, 245–258. [CrossRef] [PubMed]
70. Eggersdorfer, M.; Wyss, A. Carotenoids in human nutrition and health. *Arch. Biochem. Biophys.* **2018**, *652*, 18–26. [CrossRef] [PubMed]
71. Mapelli-Brahm, P.; Barba, F.J.; Remize, F.; Garcia, C.; Fessard, A.; Mousavi Khaneghah, A.; Santana, A.S.; Lorenzo, J.M.; Montesano, D.; Meléndez-Martínez, A.J. The impact of fermentation processes on the production, retention and bioavailability of carotenoids: An overview. *Trends Food Sci. Technol.* **2020**, *99*, 389–401. [CrossRef]
72. Mata-Gómez, L.C.; Montañez, J.C.; Méndez-Zavala, A.; Aguilar, C.N. Biotechnological production of carotenoids by yeasts: An overview. *Microb. Cell Factories* **2014**, *13*, 12. [CrossRef]
73. Chreptowicz, K.; Sternicka, M.K.; Kowalska, P.D.; Mierzejewska, J. Screening of yeasts for the production of 2-phenylethanol (rose aroma) in organic waste-based media. *Lett. Appl. Microbiol.* **2018**, *66*, 153–160. [CrossRef]
74. Izawa, N.; Kudo, M.; Nakamura, Y.; Mizukoshi, H.; Kitada, T.; Sone, T. Production of aroma compounds from whey using Wickerhamomyces pijperi. *AMB Express* **2015**, *5*, 23. [CrossRef]
75. Li, X.; Wang, D.; Cai, D.; Zhan, Y.; Wang, Q.; Chen, S. Identification and High-level Production of Pulcherrimin in Bacillus licheniformis DW2. *Appl. Biochem. Biotechnol.* **2017**, *183*, 1323–1335. [CrossRef]
76. Türkel, S.; Korukluoğlu, M.; Yavuz, M. Biocontrol Activity of the Local Strain of *Metschnikowia pulcherrima* on Different Postharvest Pathogens. *Biotechnol. Res. Int.* **2014**, *2014*, 397167. [CrossRef]
77. Kolesovs, S.; Semjonovs, P. Production of bacterial cellulose from whey—Current state and prospects. *Appl. Microbiol. Biotechnol.* **2020**, *104*, 7723–7730. [CrossRef] [PubMed]
78. Shi, Z.; Zhang, Y.; Phillips, G.O.; Yang, G. Utilization of bacterial cellulose in food. *Food Hydrocoll.* **2014**, *35*, 539–545. [CrossRef]
79. Azeredo, H.M.C.; Barud, H.; Farinas, C.S.; Vasconcellos, V.M.; Claro, A.M. Bacterial Cellulose as a Raw Material for Food and Food Packaging Applications. *Front. Sustain. Food Syst.* **2019**, *3*. [CrossRef]
80. Mann, B.; Athira, S.; Sharma, R.; Kumar, R.; Sarkar, P. Chapter 14—Bioactive Peptides from Whey Proteins. In *Whey Proteins*; Deeth, H.C., Bansal, N., Eds.; Academic Press: London, UK, 2019; pp. 519–547.
81. Ahmed, M.E.; Hamdy, A.M.; Hammam, A.R. Therapeutic Benefits and Applications of Whey Protein. *Int. J. Curr. Microbiol. App. Sci.* **2020**, *9*, 337–345. [CrossRef]
82. Dullius, A.; Goettert, M.I.; de Souza, C.F.V. Whey protein hydrolysates as a source of bioactive peptides for functional foods—Biotechnological facilitation of industrial scale-up. *J. Funct. Foods* **2018**, *42*, 58–74. [CrossRef]
83. Nasri, M. Chapter Four—Protein Hydrolysates and Biopeptides: Production, Biological Activities, and Applications in Foods and Health Benefits—A review. In *Advances in Food and Nutrition Research*; Toldrá, F., Ed.; Academic Press: London, UK, 2017; Volume 81, pp. 109–159.
84. Saadi, S.; Saari, N.; Anwar, F.; Abdul Hamid, A.; Ghazali, H.M. Recent advances in food biopeptides: Production, biological functionalities and therapeutic applications. *Biotechnol. Adv.* **2015**, *33*, 80–116. [CrossRef]
85. Tavano, O.L. Protein hydrolysis using proteases: An important tool for food biotechnology. *J. Mol. Catal. B Enzym.* **2013**, *90*, 1–11. [CrossRef]

86. Mayta-Apaza, A.C.; García-Cano, I.; Dabrowski, K.; Jiménez-Flores, R. Bacterial Diversity Analysis and Evaluation Proteins Hydrolysis During the Acid Whey and Fish Waste Fermentation. *Microorganisms* **2021**, *9*, 100. [CrossRef]
87. Marciniak, A.; Suwal, S.; Naderi, N.; Pouliot, Y.; Doyen, A. Enhancing enzymatic hydrolysis of food proteins and production of bioactive peptides using high hydrostatic pressure technology. *Trends Food Sci. Technol.* **2018**, *80*, 187–198. [CrossRef]
88. Daliri, E.B.-M.; Lee, B.H.; Park, B.-J.; Kim, S.-H.; Oh, D.-H. Antihypertensive peptides from whey proteins fermented by lactic acid bacteria. *Food Sci. Biotechnol.* **2018**, *27*, 1781–1789. [CrossRef]
89. Alizadeh, O.; Aliakbarlu, J. Effects of ultrasound and ohmic heating pretreatments on hydrolysis, antioxidant and antibacterial activities of whey protein concentrate and its fractions. *LWT* **2020**, *131*, 109913. [CrossRef]
90. Shen, X.; Shao, S.; Guo, M. Ultrasound-induced changes in physical and functional properties of whey proteins. *Int. J. Food Sci. Technol.* **2017**, *52*, 381–388. [CrossRef]
91. Lorenzetti, A.; Penha, F.M.; Cunha Petrus, J.C.; Rezzadori, K. Low purity enzymes and ultrasound pretreatment applied to partially hydrolyze whey protein. *Food Biosci.* **2020**, *38*, 100784. [CrossRef]
92. Wu, Q.; Zhang, X.; Jia, J.; Kuang, C.; Yang, H. Effect of ultrasonic pretreatment on whey protein hydrolysis by alcalase: Thermodynamic parameters, physicochemical properties and bioactivities. *Process Biochem.* **2018**, *67*, 46–54. [CrossRef]
93. Ballatore, M.B.; Bettiol, M.d.R.; Vanden Braber, N.L.; Aminahuel, C.A.; Rossi, Y.E.; Petroselli, G.; Erra-Balsells, R.; Cavaglieri, L.R.; Montenegro, M.A. Antioxidant and cytoprotective effect of peptides produced by hydrolysis of whey protein concentrate with trypsin. *Food Chem.* **2020**, *319*, 126472. [CrossRef]
94. Zhao, C.; Ashaolu, T.J. Bioactivity and safety of whey peptides. *LWT* **2020**, *134*, 109935. [CrossRef]
95. Sáez, L.; Murphy, E.; FitzGerald, R.J.; Kelly, P. Exploring the use of a modified High-Temperature, Short-Time Continuous Heat Exchanger with Extended Holding Time (HTST-EHT) for thermal inactivation of trypsin following selective enzymatic hydrolysis of the β-lactoglobulin fraction in whey protein isolate. *Foods* **2019**, *8*, 367.
96. Abadía-García, L.; Castaño-Tostado, E.; Ozimek, L.; Romero-Gómez, S.; Ozuna, C.; Amaya-Llano, S.L. Impact of ultrasound pretreatment on whey protein hydrolysis by vegetable proteases. *Innov. Food Sci. Emerg. Technol.* **2016**, *37*, 84–90. [CrossRef]
97. Olsen, J.V.; Ong, S.-E.; Mann, M. Trypsin Cleaves Exclusively C-terminal to Arginine and Lysine Residues. *Mol. Cell. Proteom.* **2004**, *3*, 608–614. [CrossRef]
98. Abdel-Hamid, M.; Goda, H.A.; De Gobba, C.; Jenssen, H.; Osman, A. Antibacterial activity of papain hydrolysed camel whey and its fractions. *Int. Dairy J.* **2016**, *61*, 91–98. [CrossRef]
99. Ambrosi, V.; Polenta, G.; Gonzalez, C.; Ferrari, G.; Maresca, P. High hydrostatic pressure assisted enzymatic hydrolysis of whey proteins. *Innov. Food Sci. Emerg. Technol.* **2016**, *38*, 294–301. [CrossRef]
100. Lestari, P. Antibacterial activity of hydrolysate protein from Etawa goat milk hydrolysed by crude extract bromelain. In *IOP Conference Series: Materials Science and Engineering*; IOP Publishing: Bristol, UK, 2019; p. 012111.
101. Silva, M.R.; Silvestre, M.P.; Silva, V.D.; Souza, M.W.; Lopes Junior, C.O.; Afonso, W.O.; Lana, F.C.; Rodrigues, D.F. Production of ACE-inhibitory whey protein concentrate hydrolysates: Use of pancreatin and papain. *Int. J. Food Prop.* **2014**, *17*, 1002–1012. [CrossRef]
102. Mazorra-Manzano, M.A.; Mora-Cortes, W.G.; Leandro-Roldan, M.M.; González-Velázquez, D.A.; Torres-Llanez, M.J.; Ramírez-Suarez, J.C.; González-Córdova, A.F.; Vallejo-Córdoba, B. Production of whey protein hydrolysates with angiotensin-converting enzyme-inhibitory activity using three new sources of plant proteases. *Biocatal. Agric. Biotechnol.* **2020**, *28*, 101724. [CrossRef]
103. Onwulata, C.; Huth, P. *Whey Processing, Functionality and Health Benefits*; John Wiley & Sons: Ames, IA, USA, 2009; Volume 82.
104. Liu, L.; Li, X.; Du, L.; Zhang, X.; Yang, W.; Zhang, H. Effect of ultrasound assisted heating on structure and antioxidant activity of whey protein peptide grafted with galactose. *LWT* **2019**, *109*, 130–136. [CrossRef]
105. Zhang, Q.; Chen, Q.-H.; He, G.-Q. Effect of ultrasonic-ionic liquid pretreatment on the hydrolysis degree and antigenicity of enzymatic hydrolysates from whey protein. *Ultrason. Sonochem.* **2020**, *63*, 104926. [CrossRef]
106. Cheison, S.C.; Leeb, E.; Toro-Sierra, J.; Kulozik, U. Influence of hydrolysis temperature and pH on the selective hydrolysis of whey proteins by trypsin and potential recovery of native alpha-lactalbumin. *Int. Dairy J.* **2011**, *21*, 166–171. [CrossRef]
107. Garcia-Mora, P.; Peñas, E.; Frias, J.; Gomez, R.; Martinez-Villaluenga, C. High-pressure improves enzymatic proteolysis and the release of peptides with angiotensin I converting enzyme inhibitory and antioxidant activities from lentil proteins. *Food Chem.* **2015**, *171*, 224–232. [CrossRef]
108. Kadam, S.U.; Tiwari, B.K.; Álvarez, C.; O'Donnell, C.P. Ultrasound applications for the extraction, identification and delivery of food proteins and bioactive peptides. *Trends Food Sci. Technol.* **2015**, *46*, 60–67. [CrossRef]
109. Ozuna, C.; Paniagua-Martínez, I.; Castaño-Tostado, E.; Ozimek, L.; Amaya-Llano, S.L. Innovative applications of high-intensity ultrasound in the development of functional food ingredients: Production of protein hydrolysates and bioactive peptides. *Food Res. Int.* **2015**, *77*, 685–696. [CrossRef]
110. Cheison, S.C.; Kulozik, U. Impact of the environmental conditions and substrate pre-treatment on whey protein hydrolysis: A review. *Crit. Rev. Food Sci. Nutr.* **2017**, *57*, 418–453. [CrossRef]
111. Anema, S.G. Chapter 9—The whey proteins in milk. In *Milk Proteins*, 3rd ed.; Boland, M., Singh, H., Eds.; Academic Press: Cambridge, MA, USA, 2020; pp. 325–384.
112. Bhat, Z.F.; Kumar, S.; Bhat, H.F. Antihypertensive peptides of animal origin: A review. *Crit. Rev. Food Sci. Nutr.* **2015**, *57*, 566–578. [CrossRef]

113. Cracowski, J.L.; Boutouyrie, P. Chapitre 1—Inhibiteurs du système rénine-angiotensine. In *Pharmacologie Cardiovasculaire et Respiratoire*; Bellien, J., Cracowski, J.-L., Eds.; Elsevier Masson: Paris, France, 2016; pp. 3–14.
114. Martínez-Medina, G.; Prado-Barragán, A.; Martínez-Hernández, J.; Ruíz, H.; Rodríguez, R.; Contreras-Esquivel, J.; Aguilar, C. Péptidos Bio-funcionales: Bioactividad, producción y aplicaciones. *Rev. Cient. Univ. Autón. Coahuila* **2019**, *13*, 1–7.
115. Herrera-Ponce, A.L.; Alarcón-Rojo, A.D.; Salmeron, I.; Rodríguez-Figueroa, J.C. Efectos fisiológicos de los péptidos bioactivos derivados de las proteínas del lactosuero en la salud: Una revisión. *Rev. Chil. Nutr.* **2019**, *46*, 205–214. [CrossRef]
116. Torruco-Uco, J.G.; Dominguez-Magaña, M.A.; Davila-Ortiz, G.; Martinez-Ayala, A.; Chel-Guerrero, L.A.; Betancur-Ancona, D.A. Antihypertensive peptides, an alternative for treatment of natural origin: A review. *Cienc. Tecnol. Aliment.* **2008**, *6*, 158–168. [CrossRef]
117. Fuentes-García, P. *Péptidos Bioactivos Derivados de la Leche de Bovino y Sus Efectos Fisiológicos en Humanos: Generalidades y Aspectos Moleculares*; CBG-IPN: Reynosa, Tamaulipas, Mexico, 2017; Volume 1, pp. 1–22.
118. Tovar-Jiménez, X.; Téllez-Jurado, A.; Gómez-Aldapa, C.A.; Mercado-Flores, Y.; Arana-Cuenca, A. Antioxidant and antihypertensive activity of bovine whey protein concentrate enzymatic hydrolysates. *Biotecnia* **2021**, *23*, 161–169. [CrossRef]
119. Miralles, B.; Amigo, L.; Recio, I. Critical Review and Perspectives on Food-Derived Antihypertensive Peptides. *J. Agric. Food Chem.* **2018**, *66*, 9384–9390. [CrossRef]
120. Hammam, A.; Tammam, A.; Elderwy, Y.; Hassan, A. Functional peptides in milk whey: An overview. *Assiut J. Agric. Sci.* **2017**, *48*, 77–91. [CrossRef]
121. Jahandideh, F.; Wu, J. Perspectives on the potential benefits of antihypertensive peptides towards metabolic syndrome. *Int. J. Mol. Sci.* **2020**, *21*, 2192. [CrossRef]
122. Beltrán-Barrientos, L.M.; Hernández-Mendoza, A.; Torres-Llanez, M.J.; González-Córdova, A.F.; Vallejo-Córdoba, B. Invited review: Fermented milk as antihypertensive functional food. *J. Dairy Sci.* **2016**, *99*, 4099–4110. [CrossRef]
123. Skalickova, S.; Heger, Z.; Krejcova, L.; Pekarik, V.; Bastl, K.; Janda, J.; Kostolansky, F.; Vareckova, E.; Zitka, O.; Adam, V.; et al. Perspective of Use of Antiviral Peptides against Influenza Virus. *Viruses* **2015**, *7*, 5428–5442. [CrossRef]
124. Ng, T.B.; Cheung, R.C.F.; Wong, J.H.; Wang, Y.; Ip, D.T.M.; Wan, D.C.C.; Xia, J. Antiviral activities of whey proteins. *Appl. Microbiol. Biotechnol.* **2015**, *99*, 6997–7008. [CrossRef]
125. Garg, L.; Kumar, K. Industrial applications of whey. *Pharma* **2021**, *2*, 387–390. [CrossRef]
126. Ashaolu, T.J.; Ashaolu, J.O. Bioactivity of Whey Peptides. *Int. J. Sci. Adv.* **2020**, *1*, 10–13. [CrossRef]
127. Sitohy, M.; Taha, S.; Osman, A.; Abdel-Hamid, M.; Hamed, A.; Abdelbacki, A. Antiviral action of native and methylated lactoferrin and β-Lactoglobulin against potato virus Y (PVY) infected into potato plants grown in an open field. *Antibiotics* **2020**, *9*, 430. [CrossRef] [PubMed]
128. Chalamaiah, M.; Yu, W.; Wu, J. Immunomodulatory and anticancer protein hydrolysates (peptides) from food proteins: A review. *Food Chem.* **2018**, *245*, 205–222. [CrossRef]
129. Umayaparvathi, S.; Meenakshi, S.; Vimalraj, V.; Arumugam, M.; Sivagami, G.; Balasubramanian, T. Antioxidant activity and anticancer effect of bioactive peptide from enzymatic hydrolysate of oyster (*Saccostrea cucullata*). *Biomed. Prev. Nutr.* **2014**, *4*, 343–353. [CrossRef]
130. Wang, Z.; Zhang, X. Isolation and identification of anti-proliferative peptides from Spirulina platensis using three-step hydrolysis. *J. Sci. Food Agric.* **2017**, *97*, 918–922. [CrossRef]
131. Kamal, H.; Jafar, S.; Mudgil, P.; Murali, C.; Amin, A.; Maqsood, S. Inhibitory properties of camel whey protein hydrolysates toward liver cancer cells, dipeptidyl peptidase-IV, and inflammation. *J. Dairy Sci.* **2018**, *101*, 8711–8720. [CrossRef]
132. Carrillo Pérez, C.; Cavia Camarero, M.d.M.; Alonso de la Torre, S. Antitumor effect of oleic acid; mechanisms of action. A review. *Nutr. Hosp.* **2012**, *27*, 1860–1865.
133. Permyakov, E.A.; Berliner, L.J. α-Lactalbumin: Structure and function. *FEBS Lett.* **2000**, *473*, 269–274. [CrossRef]
134. FitzGerald, R.J.; Murray, B.A.; Walsh, D.J. Hypotensive Peptides from Milk Proteins. *J. Nutr.* **2004**, *134*, 980S–988S. [CrossRef] [PubMed]
135. Pellegrini, A.; Thomas, U.; Bramaz, N.; Hunziker, P.; von Fellenberg, R. Isolation and identification of three bactericidal domains in the bovine α-lactalbumin molecule. *Biochim. Biophys. Acta Gen. Subj.* **1999**, *1426*, 439–448. [CrossRef]
136. Cross, M.L.; Gill, H.S. Immunomodulatory properties of milk. *Br. J. Nutr.* **2000**, *84* (Suppl. 1), S81–S89. [CrossRef] [PubMed]
137. Li, X.; Yuan, S.; Huang, M.; Gao, J.; Wu, Z.; Tong, P.; Yang, A.; Chen, H. Identification of IgE and IgG epitopes on native Bos d 4 allergen specific to allergic children. *Food Funct.* **2016**, *7*, 2996–3005. [CrossRef]
138. Willison, L.N.; Zhang, Q.; Su, M.; Teuber, S.S.; Sathe, S.K.; Roux, K.H. Conformational epitope mapping of Pru du 6, a major allergen from almond nut. *Mol. Immunol.* **2013**, *55*, 253–263. [CrossRef]
139. Pomés, A. Relevant B Cell Epitopes in Allergic Disease. *Int. Arch. Allergy Immunol.* **2010**, *152*, 1–11. [CrossRef]
140. Keppler, J.; Koudelka, T.; Palani, K.; Tholey, A.; Schwarz, K. Interaction of β-Lactoglobulin with Small Hydrophobic Ligands—Influence of Covalent AITC Modification on β-LG Tryptic Cleavage. *Food Biophys.* **2014**, *9*, 349–358. [CrossRef]
141. Keppler, J.K.; Martin, D.; Garamus, V.M.; Berton-Carabin, C.; Nipoti, E.; Coenye, T.; Schwarz, K. Functionality of whey proteins covalently modified by allyl isothiocyanate. Part 1 physicochemical and antibacterial properties of native and modified whey proteins at pH 2 to 7. *Food Hydrocoll.* **2017**, *65*, 130–143. [CrossRef]

142. Guzmán-Pérez, V.; Bumke-Vogt, C.; Schreiner, M.; Mewis, I.; Borchert, A.; Pfeiffer, A.F.H. Benzylglucosinolate Derived Isothiocyanate from Tropaeolum majus Reduces Gluconeogenic Gene and Protein Expression in Human Cells. *PLoS ONE* **2016**, *11*, e0162397. [CrossRef]
143. Spöttel, J.; Brockelt, J.; Badekow, S.; Rohn, S. Immunological Analysis of Isothiocyanate-Modified α-Lactalbumin Using High-Performance Thin Layer Chromatography. *Mol.* **2021**, *26*, 1842. [CrossRef]
144. Chen, H.-M.; Muramoto, K.; Yamauchi, F.; Fujimoto, K.; Nokihara, K. Antioxidative Properties of Histidine-Containing Peptides Designed from Peptide Fragments Found in the Digests of a Soybean Protein. *J. Agric. Food Chem.* **1998**, *46*, 49–53. [CrossRef] [PubMed]
145. Pownall, T.L.; Udenigwe, C.C.; Aluko, R.E. Amino Acid Composition and Antioxidant Properties of Pea Seed (*Pisum sativum* L.) Enzymatic Protein Hydrolysate Fractions. *J. Agric. Food Chem.* **2010**, *58*, 4712–4718. [CrossRef] [PubMed]
146. Vivas, Y.A.; Morales, A.J.; Otálvaro, Á.M. Aprovechamiento de lactosuero para el desarrollo de una bebida refrescante con antioxidantes naturales. Utilization of whey in the development of a refreshing beverage with natural antioxidants. *Aliment. Hoy* **2016**, *24*, 185–199.
147. Guimarães, J.T.; Silva, E.K.; Ranadheera, C.S.; Moraes, J.; Raices, R.S.L.; Silva, M.C.; Ferreira, M.S.; Freitas, M.Q.; Meireles, M.A.A.; Cruz, A.G. Effect of high-intensity ultrasound on the nutritional profile and volatile compounds of a prebiotic soursop whey beverage. *Ultrason. Sonochem.* **2019**, *55*, 157–164. [CrossRef]
148. Ferreira, M.V.S.; Cappato, L.P.; Silva, R.; Rocha, R.S.; Guimarães, J.T.; Balthazar, C.F.; Esmerino, E.A.; Freitas, M.Q.; Rodrigues, F.N.; Granato, D.; et al. Ohmic heating for processing of whey-raspberry flavored beverage. *Food Chem.* **2019**, *297*, 125018. [CrossRef] [PubMed]
149. Ozorio, L.; Silva, L.P.; Prates, M.V.; Bloch, C.; Takeiti, C.Y.; Gomes, D.M.; da Silva-Santos, J.E.; Deliza, R.; Brígida, A.I.S.; Furtado, A.; et al. Whey hydrolysate-based ingredient with dual functionality: From production to consumer's evaluation. *Food Res. Int.* **2019**, *122*, 123–128. [CrossRef]
150. Jeewanthi, R.K.C.; Lee, N.-K.; Paik, H.-D. Improved Functional Characteristics of Whey Protein Hydrolysates in Food Industry. *Korean J. Food Sci. Anim. Resour.* **2015**, *35*, 350–359. [CrossRef]
151. Skrzypczak, K.; Gustaw, W.; Fornal, E.; Kononiuk, A.; Michalak-Majewska, M.; Radzki, W.; Waśko, A. Functional and Technological Potential of Whey Protein Isolate in Production of Milk Beverages Fermented by New Strains of Lactobacillus helveticus. *Appl. Sci.* **2020**, *10*, 7089. [CrossRef]
152. Scalone, G.L.L.; Ioannidis, A.G.; Lamichhane, P.; Devlieghere, F.; De Kimpe, N.; Cadwallader, K.; De Meulenaer, B. Impact of whey protein hydrolysates on the formation of 2,5-dimethylpyrazine in baked food products. *Food Res. Int.* **2020**, *132*, 109089. [CrossRef]
153. Jrad, Z.; Oussaief, O.; Khorchani, T.; El-Hatmi, H. Microbial and enzymatic hydrolysis of dromedary whey proteins and caseins: Techno-functional, radical scavenging, antimicrobial properties and incorporation in beverage formulation. *J. Food Meas. Charact.* **2020**, *14*, 1–10. [CrossRef]
154. Mann, B.; Kumari, A.; Kumar, R.; Sharma, R.; Prajapati, K.; Mahboob, S.; Athira, S. Antioxidant activity of whey protein hydrolysates in milk beverage system. *J. Food Sci. Technol.* **2015**, *52*, 3235–3241. [CrossRef] [PubMed]
155. Arranz, E.; Corrochano, A.R.; Shanahan, C.; Villalva, M.; Jaime, L.; Santoyo, S.; Callanan, M.J.; Murphy, E.; Giblin, L. Antioxidant activity and characterization of whey protein-based beverages: Effect of shelf life and gastrointestinal transit on bioactivity. *Innov. Food Sci. Emerg. Technol.* **2019**, *57*, 102209. [CrossRef]
156. Goudarzi, M.; Madadlou, A.; Mousavi, M.E.; Emam-Djomeh, Z. Formulation of apple juice beverages containing whey protein isolate or whey protein hydrolysate based on sensory and physicochemical analysis. *Int. J. Dairy Technol.* **2015**, *68*, 70–78. [CrossRef]
157. Kabašinskienė, A.; Liutkevičius, A.; Sekmokienė, D.; Zaborskienė, G.; Šlapkauskaitė, J. Evaluation of the Physicochemical Parameters of Functional Whey Beverages. *Food Technol. Biotechnol.* **2015**, *53*, 110–115. [CrossRef]
158. Jelen, P. Whey-based functional beverages. In *Functional and Speciality Beverage Technology*; Paquin, P., Ed.; Woodhead Publishing Limited: Cambridge, UK, 2009; pp. 259–280.
159. Ali, A.; Lee, S.-J.; Rutherfurd-Markwick, K.J. Chapter 16—Sports and exercise supplements. In *Whey Proteins*; Deeth, H.C., Bansal, N., Eds.; Academic Press: London, UK, 2019; pp. 579–635.
160. Huecker, M.; Sarav, M.; Pearlman, M.; Laster, J. Protein Supplementation in Sport: Source, Timing, and Intended Benefits. *Curr. Nutr. Rep.* **2019**, *8*, 382–396. [CrossRef] [PubMed]
161. Kanda, A.; Nakayama, K.; Fukasawa, T.; Koga, J.; Kanegae, M.; Kawanaka, K.; Higuchi, M. Post-exercise whey protein hydrolysate supplementation induces a greater increase in muscle protein synthesis than its constituent amino acid content. *Br. J. Nutr.* **2013**, *110*, 981–987. [CrossRef]
162. Fassina, P.; Nunes, G.Q.; Adami, F.S.; Goettert, M.I.; Volken de Souza, C.F. Importance of Cheese Whey Processing: Supplements for Sports Activities—A Review. *Pol. J. Food Nutr. Sci.* **2019**, *69*, 83–99. [CrossRef]
163. Lockwood, C.M.; Roberts, M.D.; Dalbo, V.J.; Smith-Ryan, A.E.; Kendall, K.L.; Moon, J.R.; Stout, J.R. Effects of Hydrolyzed Whey versus Other Whey Protein Supplements on the Physiological Response to 8 Weeks of Resistance Exercise in College-Aged Males. *J. Am. Coll. Nutr.* **2017**, *36*, 16–27. [CrossRef]

164. Hansen, M.; Oxfeldt, M.; Larsen, A.E.; Thomsen, L.S.; Rokkedal-Lausch, T.; Christensen, B.; Rittig, N.; De Paoli, F.V.; Bangsbo, J.; Ørtenblad, N.; et al. Supplement with whey protein hydrolysate in contrast to carbohydrate supports mitochondrial adaptations in trained runners. *J. Int. Soc. Sports Nutr.* **2020**, *17*, 46. [CrossRef]
165. Weisgarber, K.D.; Candow, D.G.; Farthing, J.P. Whey protein and high-volume resistance training in postmenopausal women. *J. Nutr. Health Aging* **2015**, *19*, 511–517. [CrossRef]
166. Brown, M.A.; Stevenson, E.J.; Howatson, G. Whey protein hydrolysate supplementation accelerates recovery from exercise-induced muscle damage in females. *Appl. Physiol. Nutr. Metab.* **2018**, *43*, 324–330. [CrossRef] [PubMed]
167. Cruzat, V.F.; Krause, M.; Newsholme, P. Amino acid supplementation and impact on immune function in the context of exercise. *J. Int. Soc. Sports Nutr.* **2014**, *11*, 61. [CrossRef] [PubMed]

polymers

MDPI

Article

Integrated Hemicellulose Extraction and Papermaking Fiber Production from Agro-Waste Biomass

Adrian Cătălin Puițel [1], Cătălin Dumitrel Balan [1], Gabriela-Liliana Ailiesei [2], Elena Niculina Drăgoi [1] and Mircea Teodor Nechita [1,*]

[1] Faculty of Chemical Engineering and Environmental Protection "Cristofor Simionescu", "Gheorghe Asachi" Technical University Iasi, Bd. Prof. Dimitrie Mangeron, No. 73, 700050 Iasi, Romania; adrian-catalin.puitel@academic.tuiasi.ro (A.C.P.); catalin-dumitrel.balan@academic.tuiasi.ro (C.D.B.); elena-niculina.dragoi@academic.tuiasi.ro (E.N.D.)

[2] "Petru Poni" Institute of Macromolecular Chemistry, 41A Grigore Ghica Voda Alley, 700487 Iasi, Romania; gdarvaru@icmpp.ro

* Correspondence: mircea-teodor.nechita@academic.tuiasi.ro

Abstract: The present study deals with the valorization of corn stalks in an integrated processing strategy targeting two products: extracted hemicelluloses (HC) and papermaking fibers. Preliminary trials were conducted to assess the individual or the combined effects of biomass treatment on the quality of the obtained hemicelluloses and papermaking fibers. Depending on the hot alkaline extraction (HAE) conditions, the extracted HC had a xylan content between 44–63%. The xylan removal yield ranged between 19–35%. The recovery of HC from the extraction liquor and final black liquor was significantly affected by process conditions. The experimental approach continued with the study of HAE conditions on the obtained paper's mechanical properties. The optimization approach considered conserving paper strength properties while achieving an equilibrium with the highest possible HC extraction yield. The optimal values are sodium hydroxide concentration (1%), process time (33 min), and temperature (100 °C). The xylan content in the separated HC sample was ~55%. An extended extraction of HC from the resulting pulp under hot alkaline conditions with 5% NaOH was performed to prove the HC influence on paper strength. The xylan content in HC samples was 65%. The consequence of xylan content reduction in pulp leads to 30–50% mechanical strength loss.

Keywords: corn stalks; xylan HC; papermaking pulp; hot alkaline extraction; tensile index; burst index

Citation: Puițel, A.C.; Balan, C.D.; Ailiesei, G.-L.; Drăgoi, E.N.; Nechita, M.T. Integrated Hemicellulose Extraction and Papermaking Fiber Production from Agro-Waste Biomass. *Polymers* **2023**, *15*, 4597. https://doi.org/10.3390/polym15234597

Academic Editors: Mohammad L. Hassan and Bruno Medronho

Received: 26 October 2023
Revised: 24 November 2023
Accepted: 28 November 2023
Published: 1 December 2023

1. Introduction

Developed at the dawn of this century, the Circular Economy (CE) [1–3] and Zero Waste (ZW) [4–7] are two particularly attractive and popular management concepts that can be easily implemented in agriculture to complete the relatively "mature" concepts of Integrated Farming System (IFS) [8,9] and Integrated Crop Management (ICM) [10,11]. The conversion of agro-waste into value-added products meets the requirements of all of these management concepts. There are strong arguments that in the near future, this will be an environmentally friendly activity and a profitable business venture [12–14].

There is an inherent relationship between global population growth and food demand, and agriculture must develop to meet these needs. Although agricultural development does not necessarily imply an increase in agro-waste production, forecasting major agricultural products such as grains (maize, wheat, rice) indicates consistent growth. Consequently, various straws and stalks that are sought after as raw materials and primary resources will be readily available. Data Bridge Market Research shows that the wheat straw market was valued at USD 643.6 million in 2021 and is expected to reach USD 1330.24 million by 2029 [15]. The production of corn (maize) is even higher; according to Statista, the

worldwide production of grain in 2022/23 places corn first with an estimated production of 1151.36 million metric tonnes, followed by wheat with 783.8 and rice with 502.98 million metric tonnes [16]. In Europe, wheat comes first in 2023, with an estimated production of 143.2 million tonnes, and corn second with 64.5 million tonnes [17]. Romania ranks fourth among corn-producing countries in the European Union, trailing Ukraine, France, and Italy [18].

The corn agro-wastes are typically made up of leaves (20%), husks (8%), cobs (14%), stalks (42%), and other components (16%) [19]. The stalk is the main component of the corn plant, and this, along with the volume of corn produced, places corn stalks (CS) among the most prevalent agricultural waste worldwide. Following the various management recommendations (CE, ZW, IFS, ICM), many different initiatives were made to increase the value of this abundant and renewable agro-waste. The traditional "classic" valorization methods mostly recommended by ICM and IFS management strategies include the use of CS to prepare animal feed [20], as fuel [21], or as soil fertilizer [22]. The opportunities for CS valorization are expanded by the contemporary management strategies (CE, ZW). Nowadays, CS residues may be recycled to produce cellulose/epoxy resin composites [23], cellulose nanofibrils [24], cellulose composites [25], carbonaceous composite adsorbents [19], levulinic acid and biocarbon electrode material [26], second-generation bioethanol [27], biomethane [28], chemical pulp [29] and various biomaterials (plastics, hydrogels, fibers, composites) [30]. The use of agricultural waste biomass as fillers in different bio-composites [31], bio-plastics, tires [32], and other reinforced polymers [33,34] is one of the most promising directions to its conversion into value-added goods [34]. The CS fibers in particular were tested as fillers for various composite materials such as: tire rubber powder composite [35], polylactide composite [36], colorless and odorless bio-plastics [37] and other green composites [38]. Moreover, various integrated biorefinery processes were proposed to fully convert CS into value-added products [30,39,40]. A few examples include the coproduction of: saccharides, pulp, and lignosulfonate [41]; biodegradable film, bioethanol, and soda pulp [42]; fermented liquid feed and biologically modified biochar [43]; tissue paper and glucose [44]; hemicellulose and ethanol [45]; ethanol, furfural, and lignin [46]; ethanol and L-lactic acid [47]; hemicellulose, lignin, and activated carbon [48]; hemicellulose, lignin, cellulose (further processed to paper) [49]; cellulose, lignin, and xylose [50]; micro/nano-cellulose fibers, monosaccharides, and lignin fractions [51].

Such an ambitious level of corn stalk utilization (complete) to such a wide range of products necessitates a wide range of methods and/or combinations of methods. Some of the techniques are classic, e.g., alkaline extraction [52] or enzymatic hydrolysis [53–55], in some cases improved with complementary physicochemical pretreatments such as P-toluene sulfonic acid [54], mild alkaline presoaking (Na_2S) and Organosolv [55], ammonia [28] microwaves [53], ultrasound [51] and freeze/thaw cycles [28]. Combinations of processes are frequently used to fully transform corn stalks into finished goods or useful intermediates. To achieve the required yield and selectivity, most technological approaches necessitate the adjustment of specific parameters (e.g., treatment time, temperature, pH, solvent mixture) and process optimization. A few examples of technological processes include one-step aqueous formic acid fractionation [49]; two-stage fermentation (*S. cerevisiae* and *B. coagulans*) [47]; solvent extraction (toluene/ethanol) followed by $NaClO_2$/acetic acid delignification and NaOH pulping [24]; hot water, alkali (NaOH), and modified alkali (NaOH and $NaBH_4$) [42]; pre-hydrolysis (H_2SO_4) and alkaline sulfite cooking [41]; anaerobic fermentation (rumen inoculum) and pyrolysis [43]; hydrothermal pretreatment and batch acid hydrolysis [26]; peracetic acid and maleic acid pretreatment and enzymatic hydrolysis [50].

The current investigation focuses on coproducing hemicellulose polysaccharides and pulp using corn stalks as raw material. This study follows: (i) the identification of the appropriate coproduction process and (ii) the optimization of hemicellulose extraction through this process in a way that prevents the loss of specific paper qualities (tensile index and burst index). Screening trials were conducted in order to develop the optimal coproduction

procedure. Various sequences of hot water treatment (HWT), soda pulping (SP), and hot alkaline extraction (HAE) were tested during trials. Treatment time, temperature, and alkali concentration were the monitored process parameters during the trials and optimization stage. Hemicelluloses were separated and characterized after each technical stage. The controlled extraction of hemicelluloses aims at preserving the pulp and, consequently, paper mechanical characteristics—tensile and burst indexes. The novelty of the work is represented by the technical approach combined with the optimization technique that establishes a successful method for producing acceptable yields of hemicellulose and paper with satisfactory mechanical properties.

2. Materials and Methods

2.1. Materials

Corn stalks (a common Zea Mays hybrid) were provided free of charge by Romanian farmers. After harvesting, the CS were dried at room temperature to 8% humidity. The CS were then crushed and sieved to 0.2 mm particles per the standard chemical analysis technique. The CS were cut into 50 mm pieces for hemicelullose (HC) extraction and/or pulping studies.

All chemicals and reagents used are of analytical purity. Solutions of 99% purity of cellobiose, glucose, xylose, galactose, and arabinose, provided by Flucka, were used to obtain the calibration curves in the concentrations range of 0.1–1 g/L. Purified xylan extracted from beechwood was purchased from Sigma Aldrich (X4252 10G; St. Louis, MO, USA) and was used as reference material.

2.2. Equipment

2.2.1. Laboratory Reactor and Pulp Processing Equipment

The extraction and pulping experiments were conducted in a 10 L stainless steel laboratory rotating digester that was electrically heated and equipped with a temperature controller. The obtained pulps were refined at different revolutions in a Jokro mill, following the procedure described by Danielewicz et al. [56]. The refined and non-refined pulps were converted into paper sheets on a Rapid Koethen laboratory sheet former ISO 5269/2 [57]. The testing of the mechanical strength properties (tensile strength and burst strength) and necessary calculations were performed according to ISO 1924-2:2008 [58] and ISO 2758:2014 [59] using a Zwick Roell Z0.5 testing machine (ZwickRoell GmbH & Co. KG Headquarter, Ulm, Germany).

2.2.2. HPLC Analysis

A Shimadzu Nexera LC 40D liquid chromatography system equipped with a Shodex SP0810 column (300 × 8 mm, particle size 7 μm) heated at 65 °C was employed to perform the required HPLC analysis. The refractive index detector (Shimadzu RID 20A, Kyoto, Japan) was set at 40 °C. The flow rate of the mobile phase (ultrapure water) was 0.6 mL/minute. The injection volume was set between 20 to 40 μL to accommodate sugar concentrations. Each sample and standard solution (containing cellobiose, glucose, xylose, galactose, and arabinose of analytical grade) was filtered before injection using 0.2 μm syringe PTFE filters.

2.2.3. Spectroscopy

The FTIR spectra of selected hemicellulose samples were recorded by Agilent Cary 630 (Santa Clara, CA, USA) using the potassium bromide pellets technique on disks containing finely ground samples at 1% content.

The 1H NMR spectroscopy data were obtained by dissolving 16 mg of HC samples in 0.65 mL deuterated water and then pipetted into NMR tubes. Spectra were recorded on a Bruker Avance NEO 400 MHz spectrometer (Billerica, MA, USA), operating at 400.1 MHz for 1H nuclei, with a 5 mm four nuclei direct detection z-gradient probe using standard pulse sequences, as delivered by Bruker with TopSpin 4.0.8 spectrometer control and

processing software (version 4.0 8). Chemical shifts are reported in δ units (ppm) and were referenced to the residual solvent signal at 4.7 ppm. 128 scans were used for spectra registration.

2.2.4. Other Equipment

Sorvall GLC2 centrifuge equipped with an HL-4 rotor, CF value-2012, 3000 r.p.m. was used for precipitate separation (lignin, respectively HC).

Ubbelohde and capillary (glass with jacket, PSL-Rheotek type C) viscometers were used to determine the efflux time of pure solvent, HC, and cellulose solutions.

2.3. Experimental Approach

Screening trials (Figure 1) were utilized to determine the best strategy for achieving high extraction yields in HC and pulp, which was then used to manufacture paper with satisfactory mechanical qualities. The procedures used for HC extraction and pulp production were hot water treatment (HWT), soda pulping (SP), and hot alkaline extraction at low (HAE^{low}) and high (HAE^{high}) alkali charges. The selected sequence was further optimized considering time, temperature, and alkali concentration as process variables. The optimization goal was not to maximize the HC extraction yield but to produce an extraction yield that preserved the pulp qualities (including HC content) to prepare paper sheets with satisfactory mechanical properties (tensile and burst indexes).

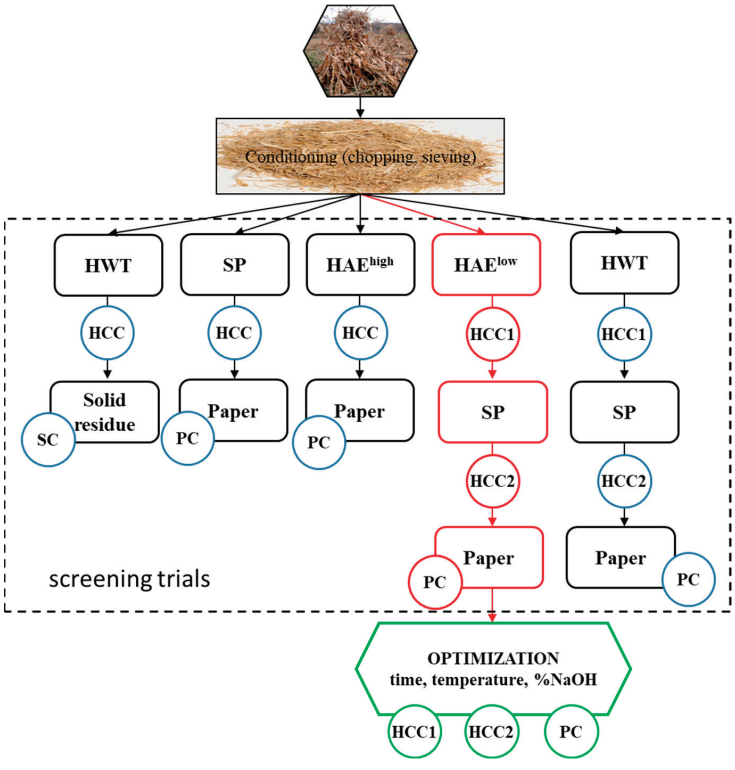

Figure 1. The experimental approach. (SC = solid residue characterization; PC = pulp and paper characterization; HCC = hemicellulose characterization; 1 = first extraction; 2 = second extraction).

All experiments were performed in triplicates unless otherwise stated by the mentioned standard methods. The accepted maximum relative standard deviation value was less than 5%.

The materials recovered from each experimental method (HWT, SP, or HAE), whether solid or liquid (extraction liquor, black liquor), were analyzed for HC, cellulose, and lignin content.

2.4. Extraction Methodology

2.4.1. HWT Treatment

Typical HWT experiments use 300 g of oven-dried (o.d.) corn stalks treated in the laboratory reactor at a solid-to-liquid ratio of 1:10. The treatment lasted 60 min at 100 °C. The heating time was 20 min. At the end of the HWT process, the resulting liquid phase was saved for further characterization and HC separation. The HWT-treated corn stalks were washed, dried to a suitable moisture content (8–10%), and then used for soda pulping. The material loss was determined gravimetrically.

2.4.2. Soda Pulping

The control soda pulping process (using untreated CS) was carried out in the same reactor (as HWT) under the following conditions: solid-to-liquid ratio of 1:20; heating time of 20 min; and cooking time of 30 min at 140 °C. The pressure during pulping was kept constant at 0.2 MPa. The active alkali charge was 12% expressed as NaOH units. The corresponding white liquor had a 0.6% NaOH concentration. The HWT followed by SP (Figure 1) treatments were performed in the same conditions as control pulping (SP). The obtained pulps were washed and used for further analysis and sheet formation. The solid yield was determined by gravimetric means.

The SP processes that followed HAE^{high} and HAE^{low} during trials were continued in the same reactor by increasing the temperature to 140 °C. The pulping stage was set for 30 min. After the pulping timer ran out, the heating was turned off, and the solid and liquid phases (black liquor) were separated and processed separately.

2.4.3. Hot Alkaline Extractions of Corn Stalks

In the trial phase of this study, the hot alkali extraction of hemicelluloses was performed using two different experimental approaches: high alkali charge (HAE^{high}) and low alkali charge (HAE^{low}). After that, an optimized approach was identified and conducted (HAE^{opt}).

HAE^{high} involves extracting hemicelluloses from corn stalks with solutions containing 5% NaOH and 3% NaOH, respectively. In both experiments, CS (200 g o.d.) were immersed in NaOH solutions at a solid-to-liquid ratio of 1:20. The reactor was closed and heated to 100 °C. The extraction time was set to 60 min. After the extraction, the liquid phase (HAE^{high} liquor) and the remaining solid material were separated, characterized, and/or further processed.

HAE^{low} was conducted for 60 min at 100 °C using a 0.6% NaOH solution. Following treatment, samples of HAE^{low} liquor were extracted for further hemicellulose separation.

HAE^{opt}—an extended hemicellulose extraction from pulp was performed at optimal process parameters. The following conditions were used for this hot caustic extraction (HCE): 5% NaOH concentration, solid-to-liquid ratio 1:10, temperature of 100 °C, and treatment time of 60 min. The recovered liquor was then processed for hemicellulose separation using the procedure described in Section 2.4.4.

2.4.4. Separation and Purification of HC from WHT, HAE, and SP Liquors

The ethanol precipitation method was used to separate hemicellulose from the liquors obtained during the experimental procedures. In brief, 50 mL liquor samples were neutralized to pH 4.5 with acetic acid. A first centrifugation stage was performed to remove the precipitated lignin. The supernatant was then mixed with 2 volumes of analytic purity ethanol (96%) and stored at −18 °C for 60 min. The precipitated HCs were separated by centrifugation at 3000 r.p.m. for 10 min. Next, two rounds of ethanol washing were performed. Following each washing, a 5-min centrifugation was carried out at 3000 r.p.m

to separate the solid from the ethanol. The crude HC samples were dried at 50 °C before further investigation.

2.5. Characterization Methods

2.5.1. CS, Treated CS, and Pulp Chemical Characterization

Several analytical procedures were used to determine the chemical composition of raw CS in terms of both major (polysaccharides and lignin) and minor components: ash–TAPPI T 211 om-02, 2002 [60]; hot water extractives—TAPPI T 207 om-88 [61]; organic solvent extractives T 204 cm-97 [62]; acetone extractives (AE)—TAPPI T280 pm-99 standard (2000) [63]. While acid-insoluble lignin (AIL) and acid-soluble lignin (ASL) were determined using the sulfuric acid two stages hydrolysis method specified by NREL/TP-510-42618 method [64], the major polysaccharide components (cellulose and hemicelluloses) of the biomass and the obtained papermaking fiber were determined following an adapted procedure of that described by Sluiter et al. [65]. The adaptation involved neutralizing the hydrolysate from a G3 crucible filter to pH 5.6 before HPLC analysis.

2.5.2. HC Characterization

The carbohydrates present in liquor samples were analyzed after they were treated with 4% sulfuric acid (60 min at 121 °C) according to NREL (LAP) TP-510-42623 [66]. Samples of 60 to 80 mg were suspended in 5 mL of 1 M NaOH and vigorously shaken for at least 30 min to facilitate dissolution. The complete hydrolysis was achieved by treating the samples with 4% sulfuric acid for 60 min at 121 °C. The acid treatment completes the hydrolysis of the polymeric carbohydrates extracted during HAE. Following hydrolysis, the samples were neutralized, and the concentration of monosaccharides was determined using HPLC.

2.5.3. HC Recovery Yield, Solid Extraction Yield

The glucan, xylan, and arabinan content of the liquor were added to determine the total amount of polysaccharides (PStot). The conversion of monomer concentrations to their corresponding polymer concentrations was realized considering the ratio between the molecular weight of the anhydro-sugar unit and sugar unit (162/180 = 0.9 for C6 sugars and 132/150 for C5 sugars).

The HC recovery yield (HCRY) was then calculated using Equation (1) as the ratio between the number of polysaccharides in recovered crude HC (o.d.) and the number of polysaccharides theoretically determined in either extraction or black liquor.

$$HCRY(\%) = \frac{\sum MS_i(\%) \cdot m_{HC}}{\sum C_{MS_i} \cdot V} \times 100 \quad (1)$$

where MS_i (%) is the content of individual polysaccharides (glucan, xilan, arabinan) content in the *HC* sample; m_{HC} is the mass of the *HC* sample, in g; C_{MSi} is the concentration of the individual sugar in the analyzed sample, in g/L; V is the volume of liquor sample, in L.

The solid extraction yield (SY, %) was calculated using Equation (2).

$$\text{SY } (\%) = \frac{m_f}{m_{i.}} \times 100, \quad (2)$$

where SY (%) represents the solid yield; m_i is the o.d. weight of the initial CS biomass; $m_{i.}$ is the o.d. weight of the CS after the treatment or treatment sequence.

2.5.4. Polymerization Degree (DP) of Obtained HC and Pulp

The degree of polymerization of HC was proven by using viscosity data as described in literature [67]. In brief, the samples were dissolved in a 0.04 M cupriethylenediamine

(CED) solution, and the intrinsic viscosity [η] was determined at 25 °C. The Staudinger–Mark–Houwink equation of xylan in CED is (Equation (3)) [67–69]:

$$[\eta] = 2.2 \times 10^{-2} \times DP^{0.72} \quad (3)$$

The obtained pulps' *DP* was established after determining the intrinsic viscosity (Equation (4)) in 0.5 M CED solution [70].

$$[\eta] = 2.28 \times DP^{0.76} \quad (4)$$

2.5.5. Pulp Refining and Laboratory Paper Strength

Following washing and refining (beating), the obtained pulps were transformed into paper sheets that were subjected to analysis of tensile strength (ISO 1924:2008) [58] and burst strength (ISO 2758:2014) [59].

2.5.6. The Severity Factor

The temperature and duration of extraction can be combined in a single parameter, the severity factor (*SF*), to reduce the total number of experiments. The *SF* is defined as the combination of extraction time and the temperature (Equation (5)) [71,72].

$$SF = \log_{10}(\tau \times e^{\frac{T-100}{14.75}}) \quad (5)$$

where τ is the processing time at selected temperature *T*.

2.6. Optimization Procedure

The results obtained in the trial phase indicate that the sequence HAElow–SP–Paper (Figure 1) generates the best equilibrium between HCRY and paper strength. Therefore, this sequence was selected for further optimization. Response surface methodology (RSM) was selected as an optimization procedure for modeling the HC extraction. The independent variable parameters and their variation range (Table 1) were chosen based on previous experience [52,73].

Table 1. Independent variables and their variation range for HAE_{low}.

Independent Variables	Units		Range		Symbol
			From	To	
Temperature	(°C)	X1	100	130	T
NaOH concentration	% wt.	X2	0.6	1.2	C_{NaOH}
Duration (time) of HAE	minutes	X3	30	90	t

The model dependent variables were: Y1—xylan content in the recovered hemicelluloses (XHC, %); Y2—xylan removed from corn stalk biomass XRCS, (%); Y3—tensile index of resulting paper sheets (TI, N·m/g); Y4—burst index of obtained paper sheets (BI, kPa·m^2/g). Experimental design and data processing were performed by using Stat-Ease Design-Expert Software (version 7). The experimental data were then used to reveal the equations describing the relationship between selected process parameters and model responses.

3. Results

3.1. Chemical Composition of CS and HWT CS Solid Residue

According to the literature analysis, a wide range of factors influence the chemical composition of CS (Table 2), including corn variety, precipitation/irrigation level, fertilization, harvesting period, harvesting equipment, and others. These factors affect not only the corn quality but also the HC, cellulose, lignin, and ash content of the CS (Table 2). A relatively mild treatment such as HWT only slightly affects the chemical composition of the

CS. Aside from xylan, which is partially extractable with hot water, the other polysaccharide content appears slightly increased due to CS weight loss after HWT treatment (Table 2). Kim and Lee also reported HWT selectivity for xylan extraction and glucan stability in such treatment [74].

Table 2. Chemical composition (% wt.) of corn stalks and HWT solid residue.

Material	Glucan	Xylan	Arabinan	PStot	AIL	ASL	AE	Ash	Ref.
CS	39.71	19.82	4.28	63.81	20.62	1.60	4.36	7.05	This work
HWT CS	47.68	16.44	5.43	69.55	23.59	1.37	n.d.	1.50	
CS	36.80	19.90	3.20	59.90	20.10		11.80	1.00	[75]
CS	34.40	15.88	n.d.	-	14.10	2.48	11.84	3.04	[76]
CS	36.80	21.70	2.60	61.10	17.20		n.d.	n.d.	[77]
CS	42.10	22.90	2.90	67.90	17.50	-	9.80	4.20	[78]

n.d. = not determined.

3.2. Solid Residue and Pulp Composition—Trial Results

The raw CS soda pulping process generates the maximum solid yield. This is most likely caused by the SP process's lower alkali charge than other treatment procedures/sequences. The HAE^{low}–SP treatment sequence comes in second place, with a slightly lower SY value (Table 3).

Table 3. Chemical composition (% wt.) of the obtained solid material—papermaking fibers (pulp).

Treatment Param.	Glucan	Xylan	Arabinan	SY (%)	AIL	ASL
HAE^{high}, 5%NaOH	63.58	12.75	5.67	33.60	6.80	0.75
HAE^{high}, 3%NaOH	64.50	13.90	6.55	35.50	8.80	0.95
SP, raw CS	68.70	18.9	2.74	48,30	9.95	1.05
HAE_{low}–SP	67.50	16.47	3.30	47.13	10.71	1.12
HWT–SP	66.04	19.40	2.72	46.65	11.99	1.22

The SY value, in conjunction with the polymerization degree (Table 4), directly impacts the paper's qualities in terms of the tensile and burst index values. The increase in C_{NaOH} (HAE^{high}, 3%NaOH; HAE^{high}, 5%NaOH) reduces both the HC and lignin content of the pulp and/or solid residue. The effects of light pretreatments (HAE^{low}, HWT) carried out before SP on the SY are minor (Table 3). Yet, the paper's resistance qualities are acceptable for the HAE^{low}–SP treatment sequence (Table 4).

Table 4. Polymerization degree and paper properties as a function of treatment sequence.

Treatment Param.	DP	TI, (N·m/g)	BI, (kPa·m^2/g)
HAEhigh, 5%NaOH	750	72.40	2.56
HAEhigh, 3%NaOH	880	62.90	3.62
SP, raw CS	1047	83.20	4.71
HAElow–SP	925	75.50	4.35
HWT–SP	830	70.40	3.11

3.3. Liquor's Chemical Composition (% wt.)—Trial Results

Samples of the liquid phase were collected after each individual and or sequential CS treatment. Black liquor (BL) refers to the liquid phase acquired after soda pulping, while extraction liquor (EL) refers to the liquid phase acquired after each primary treatment.

The amount of extracted xylan directly correlates with the NaOH concentration in the liquid; the higher the concentration, the higher the xylan content (Table 5). However, the cellulose produced under these circumstances (high alkali charge) has weaker resistance properties and lower DP than cellulose obtained at low alkali charge (HAE^{low}, EL). It is

worth noting that the DP increases as the NaOH concentration increases (Table 5). The EL produced in the absence of alkali (HWT) has a relatively low amount of xylan (7.7%) and a usually low amount of sugars, primarily glucan oligosaccharides residue. The EL produced at a low alkali charge (HAE^{low}) gives a satisfactory level of xylan extraction (49.06%) that can be further increased up to 61.82 by complementary SP treatment (HAE^{low}–SP). The chemical analysis of the reference material (xylan from beechwood) was also performed, and the results in terms of DP are very close to those obtained for the HAE^{low}–SP sequence (255 vs. 262).

Table 5. Chemical composition ((% wt.) of the hemicelluloses isolated from HAE extraction liquors and subsequent pulping black liquor.

Treatment Parameters	Glucan	Xylan	Arabinan	DP
HAE^{high}, 5%NaOH, EL	3.11	65.14	5.24	290
HAE^{high}, 3%NaOH, EL	2.85	62.47	8.95	285
SP, raw CS, BL	4.34	54.40	14.10	273
HAE^{low}, EL	4.80	49.06	17.93	320
HAE_{low}–SP, BL	5.70	61.82	14.51	262
HWT, EL	11.27	7.70	1.28	n.d.
HWT–SP, BL	3.35	57.20	12.24	230
X4252 10G	0.05	91.34	2.09	255

Since the sequence HAE^{low}–SP allows the simultaneous production of two commodities (paper pulp and HC–xylan) with good resistance properties (Table 4) and acceptable extraction yields (Table 5), this study was further focused on the optimization of this particular extraction procedure.

3.4. Optimization of HAE Parameters: Influence on HC Xylan Content, Xylan Removal Yields, and Pulp Properties

Table 6 shows experimental conditions (experiments programmed using the central composite design) and their associated results in terms of: (i) xylan content of crude o.d. hemicellulose samples recovered from extraction liquor (XHC); (ii) xylan extraction yield from the CS (XRCS). The XRCS (%) values were computed according to Equation (6); (iii) paper tensile index (N·m/g) and (iv) paper burst index (kPa·m^2/g) (obtained after beating at 1100 rpm)

$$\text{XRCS } (\%) = \frac{C_{xliq} \cdot V_{liq}}{X(\%) \cdot m_{CS}} \times 100 \quad (6)$$

where C_{xliq} is the concentration of xylan determined in the HAE liquor by HPLC in g/L; V_{liq} is the volume of the liquor existing in the reactor at a specific moment of the extraction, in L; X (%) is the xylan content of the *CS*; m_{CS} represents the o.d. weight of a working *CS* sample, usually 200 g.

Only two experiments (no. 11 and 21 from Table 6) resulted in HC with a xylan content greater than 60%. However, because the study's goal was not to achieve the highest HC extraction yields, but to generate an option that did not interfere significantly with paper strength properties, the extraction parameter values provided by the experiments discussed cannot be considered optimal.

The Equation (7) relates the independent variables: X_1, X_2, X_3 (Table 1) to system responses: Y_1—XHC (%); Y_2—XRCS (%); Y_3—TI, (N·m/g); and Y_4—BI (kPa·m^2/g). The terms β_0, β_i, β_{ij}, β_{ii} represent the equation constants. Table 7 presents the equation coefficients and statistical parameters.

$$Y_{1-4} = \beta_0 + \sum_{i=1}^{3} \beta_i X_i + \sum_{\substack{i=1 \\ j=1}}^{3} \beta_{ij} X_{ij} + \sum_{i=1}^{3} \beta_{ii} X_i^2 \quad (7)$$

Table 6. Experimental planning and experimental results.

Exp No.	T, (°C)	C_{NaOH}, (%)	T, (min)	XHC, (%)	XRCS, (%)	TI, (N·m/g)	BI, (kPa·m^2/g)
1	100	0.6	30	44.74	19.22	70.90	2.62
2	100	0.6	60	54.53	22.91	75.50	3.46
3	100	0.6	90	54.53	25.62	74.30	3.49
4	115	0.6	60	41.29	21.60	68.92	4.24
5	130	0.6	30	41.16	27.43	63.80	4.56
6	130	0.6	90	45.26	29.25	74.29	4.85
7	100	0.9	60	52.41	25.32	75.61	4.48
8	115	0.9	60	51.62	26.91	67.90	4.25
9	115	0.9	30	50.96	26.68	67.30	3.82
10	115	0.9	60	42.88	27.31	67.20	4.35
11	115	0.9	60	62.74	27.53	68.11	4.29
12	115	0.9	60	57.57	27.21	69.10	4.32
13	115	0.9	60	54.40	29.02	68.20	4.10
14	115	0.9	60	52.28	26.34	70.20	4.45
15	115	0.9	60	52.15	25.93	66.91	4.25
16	115	0.9	90	53.21	27.62	64.52	4.19
17	130	0.9	60	48.04	34.80	71.89	4.27
18	100	1.2	30	53.34	18.40	76.60	4.53
19	100	1.2	90	53.47	22.80	71.70	4.02
20	115	1.2	60	57.71	28.10	75.54	4.10
21	130	1.2	30	63.53	35.40	62.20	3.27
22	130	1.2	90	55.06	35.20	71.40	2.73

Table 7. Model equation coefficients (actual factors) and statistical parameters (Model p value < 0.05).

Y_i	β_0	X_1	X_2	X_3	X_1X_2	X_2X_3	X_1X_3	X_1^2	X_2^2	R^2	R^2_{adj}
Y_1	78.2	−0.511	−54.3	0.760	0.770	−0.00396	−0.309	-	-	0.918	0.87
Y_2	2.12	0.0306	−24.9	0.400	0.510	−0.0262	−0.0583	-	−13.8	0.915	0.872
Y_3	221	−4.31	245	3.59	−2.62	−0.0284	−4.85	0.0268	50.7	0.95	0.899
Y_4	−53.3	0.368	84.3	0.747	−0.729	−0.0064	−0.947	0.000847	−0.13	0.93	0.84

The evolution of XHC% and XHCS% as a function of temperature and NaOH concentration for constant time (30, 60, and 90 min) is shown in Figure 2. A first-order polynomial describes how the xylan content of the separated hemicelluloses depends on the process parameters. The simultaneous rise in temperature and C_{NaOH} caused a considerable increase in XHC. The XHC is barely impacted by lengthening the course of treatment.

A second-order polynomial equation describes the xylan removal from corn stalk biomass dependence on process parameters (Figure 2). It can be observed that the C_{NaOH} is the most important factor in the process, followed by temperature and time. The extraction yield can be increased by increasing C_{NaOH} and/or temperature. Extending the course of treatment has little effect on the XRCS.

Produced pulp paper sheets' TI is greatly affected by the sodium hydroxide content (Figure 3). TI increases with C_{NaOH} and decreases with increased treatment time. The combined action of sodium hydroxide and temperature has a positive effect; however, the cumulative interaction of C_{NaOH} and treatment time has a negative effect, decreasing TI. BI is negatively affected by the simultaneous increase in temperature and C_{NaOH} (Figure 3). Also, an increase in process time is accompanied by a BI decrease.

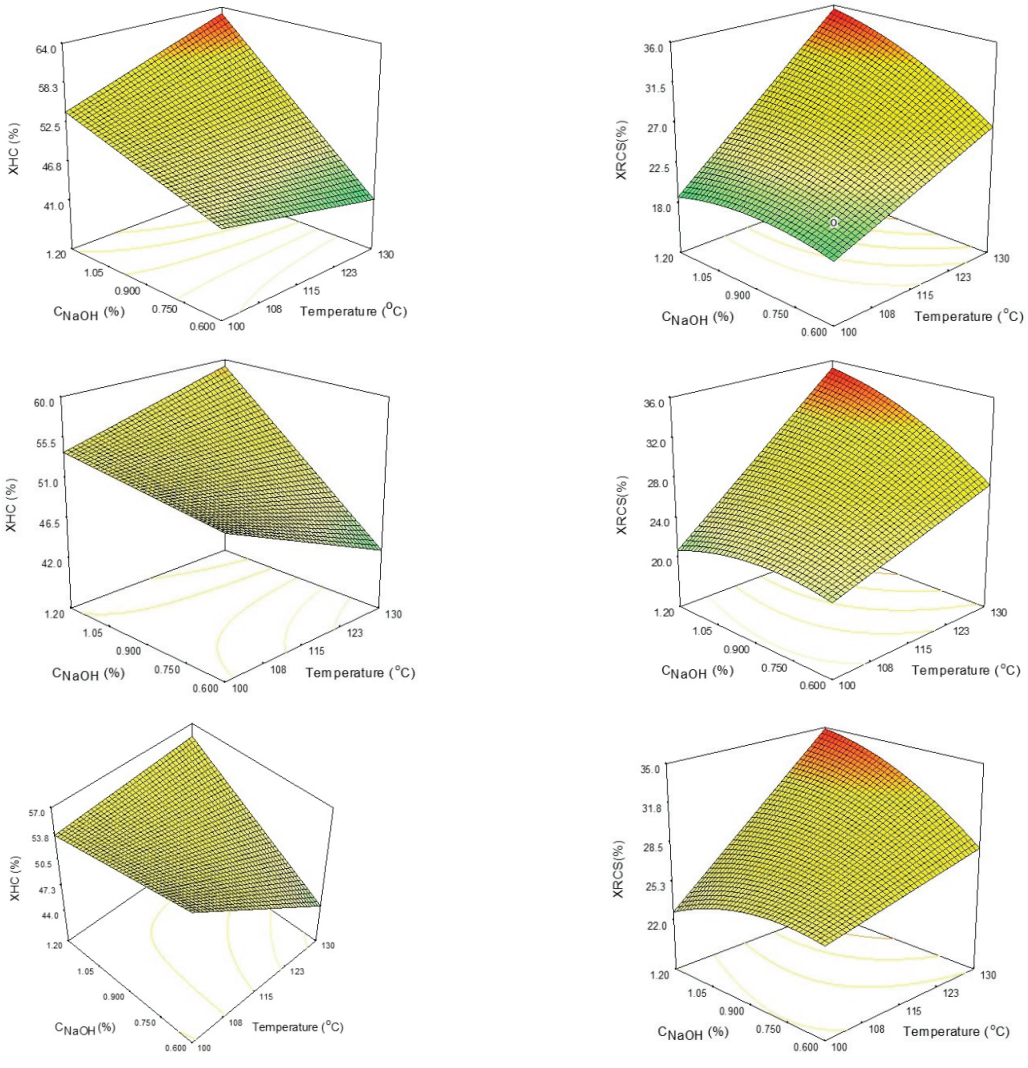

Figure 2. The influence of process parameters (temperature and C_{NaOH}) towards XHC% (**left column**) and XRCS% (**right column**) after 30 min (1st row), 60 min (2nd row), and 90 min (3rd row). The color ranges from green (low values) to yellow and orange (medium values) to red (high values).

The ANOVA analysis of the proposed models is presented in Tables S1–S4, which are included in the Supplementary Material.

The optimum hot alkaline extraction (HAE^{opt}) process parameters, considering maximizing HC extraction yield while maintaining the papermaking properties, are temperature = 100 °C; sodium hydroxide concentration = 1 percent (wt.); and extraction time = 33 min. Table 8 illustrates the experimental confirmation of the predicted values by the proposed mathematical model.

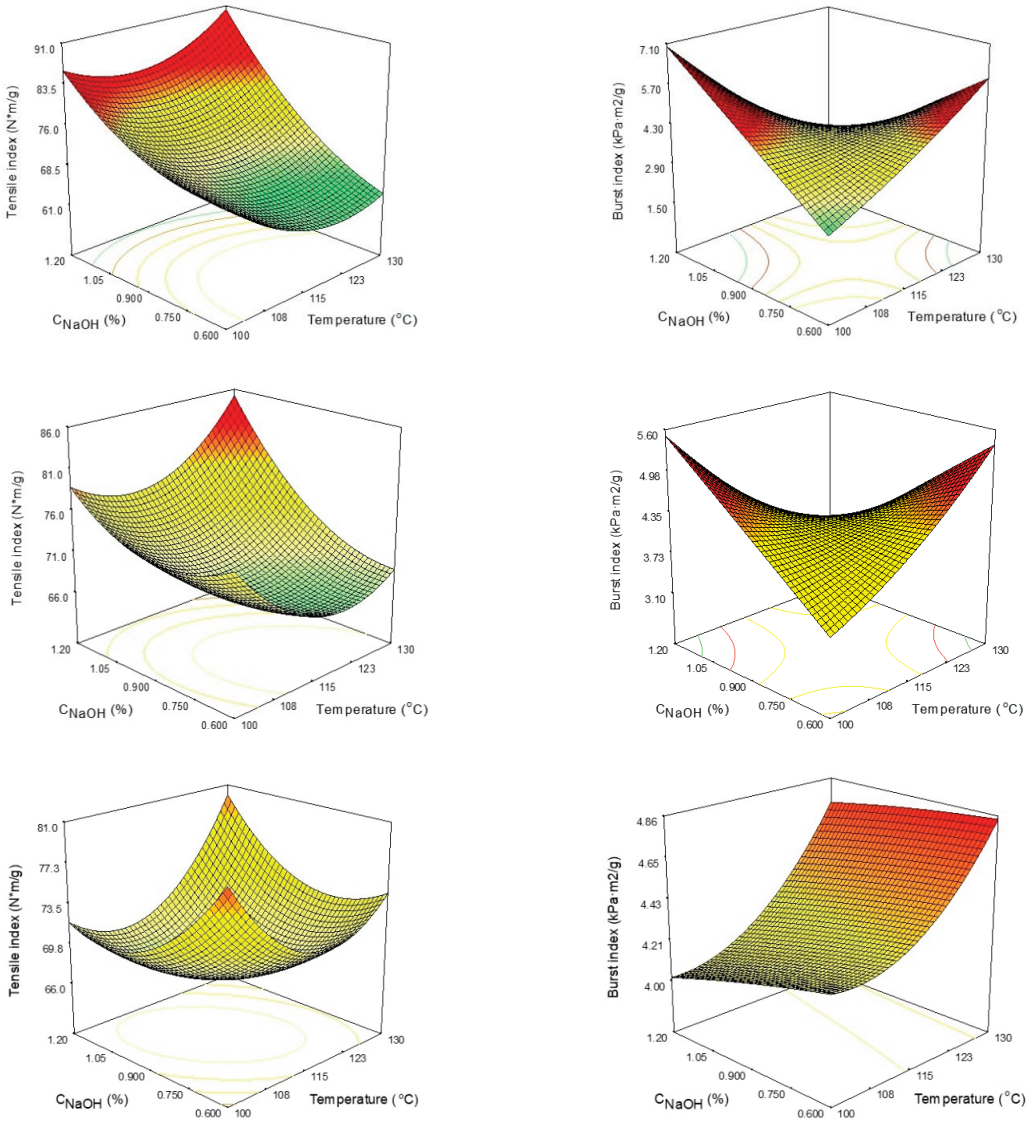

Figure 3. The influence of process parameters (temperature and C_{NaOH}) towards tensile index (**left column**) and burst index (**right column**) after 30 min (1st row), 60 min (2nd row), and 90 min (3rd row). The color ranges from green (low values) to yellow and orange (medium values) to red (high values).

Table 8. Model validation results.

System Responses	XHC (%)	XRCS (%)	TI (N·m/g)	BI (kPa·m^2/g)
Predicted values	51.67	21.77	78.50	4.54
Experimental values	54.64	20.54	80.10	4.33

3.5. Complementary Extraction Treatments—Hot Caustic Extraction: Influence of HC Content on Refinability and Strength Properties of Paper Sheets

This experimental phase aimed to determine the impact of HC refinability and refining degree on the paper's mechanical strength characteristics. Therefore, the results of the HAE^{opt} were further compared with a more aggressive extraction treatment, hot caustic extraction (HCE), expected to produce higher HC extraction yields (and, consequently, a pulp with lower HC content). To highlight the contribution of the HC content in pulp on the mechanical strength properties of paper, the TI and BI of the paper produced after HAE^{opt} and HCE treatments were compared. Based on the experimental results from the trial phase and optimization stage, the selected HCE process parameters were temperature = 100 °C, sodium hydroxide concentration = 5% (wt.), and extraction time = 60 min. The solid–liquid ratio was 1:20.

Table 9 shows the chemical contents of the pulps obtained after HAE^{opt} and HCE extractions. The HCE treatment reduced the amount of xylan by around 50%.

Table 9. Chemical composition of HAE^{opt} and HCE pulps.

Pulp Type	SY (%)	Glucan (%)	Xylan (%)	Arabinan (%)	AIL	ASL
HAE^{opt}	42.74	67.10	20.10	2.60	6.50	1.10
HCE	64.10	80.41	11.05	1.40	4.30	0.70

After obtaining the chemical composition, the obtained pulp was refined. Refining is recognized as a key unit process in the paper industry. It has a set of steps that are designed to realize the best papermaking properties: (i) fiber swelling; (ii) fibrillation (internal and external); (iii) formation of fines; and (iv) shortening of fibers [79–83]. Being one of the most energy-intensive processes, improved refinability means achieving a specific, optimal refining degree as fast as possible. Since xylan is the major HC constituent, the refining degree, the TI, and BI are further reported (Figures 4–6) as a function of xylan composition.

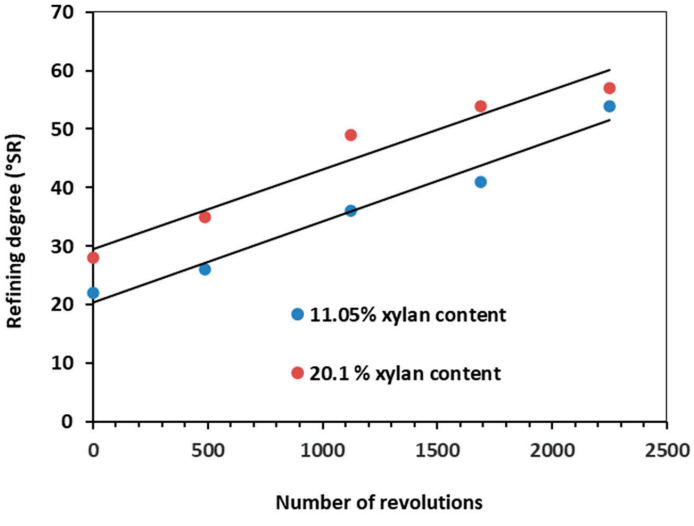

Figure 4. Evolution of the refining degree as a function of the refining input energy.

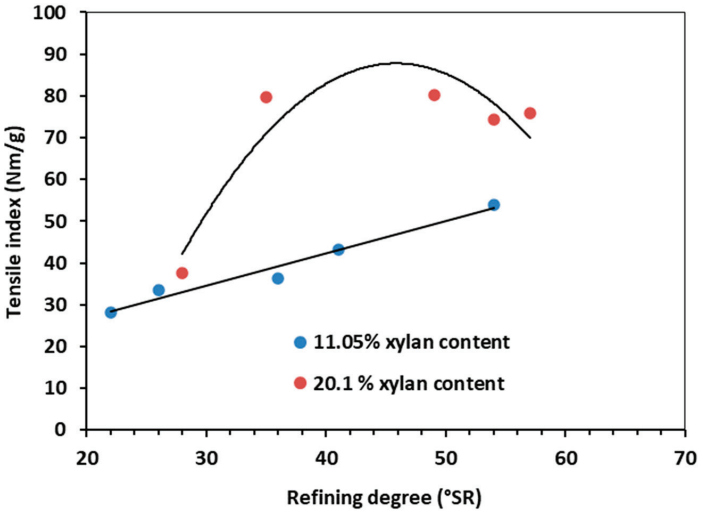

Figure 5. Tensile index vs. refining degree. Influence of HC (xylan) content.

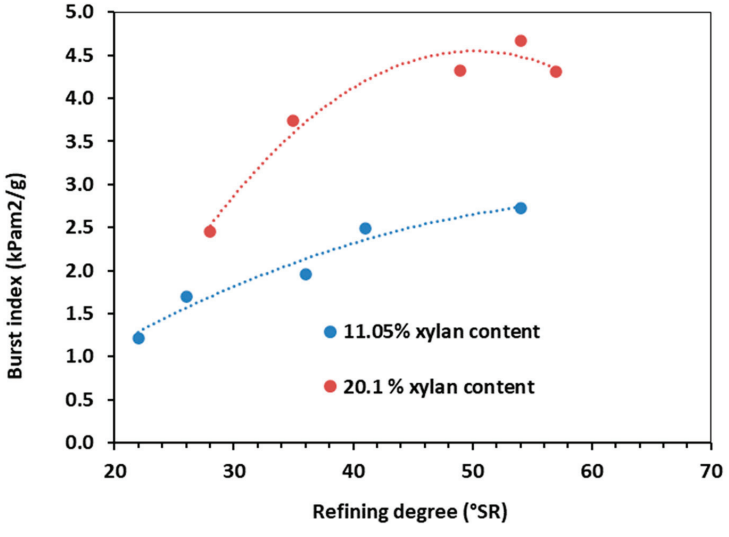

Figure 6. Burst index vs. refining degree. Influence of HC (xylan) content.

Figure 4 displays the evolution of refining degree as a function of beating intensity expressed as a total number of revolutions. It can be observed that the HAEopt pulp sample has a higher initial degree of refining, even in the unbeaten state. This may be explained by the increased swelling effect of acidic hemicellulosic groups [83].

The contribution of HC in enhanced fiber–fiber bonding and the diminished fiber swelling effect on HCE pulp samples may be responsible for the differences among the reported mechanical characteristics for the analyzed pulp samples in the unbeaten state [80]. Owing to its superior xylan content, the HAE^{opt} pulp showed a faster increase in refining degree than HCE pulp, supporting the existing literature [81].

The mechanical characteristics under investigation (TI, BI) exhibited similar evolutions in relation to refining degree (Figures 5 and 6). For HCE pulp (low xylan content), the TI-refining degree relationship is practically linear, whereas, for HCE^{opt}, the dependence

has a maximum point around 45 °SR (Figure 5). At this peak value, the TI of HAE^{opt} pulp is almost double in comparison with the HCE pulp. The BI showed a similar evolution. The BI-refining degree dependence is almost linear (Figure 6) for the HCE pulp, with a maximum value of ~50 °SR for the pulp with higher xylan content (HAE^{opt}).

The slight decrease in TI and BI for the HAE^{opt} pulp after reaching maximum values at ~45, ~50 °SR could be attributed to the shortening of fibers through cutting effects in the final refining stages [82]. Several explanations for the behavior of the investigated pulps also center on the combined impacts of HC concentration and refinement [79–83].

3.6. The Influence of Severity Factor on HC Chemical Composition and Recovery Yields

The SF quantifies the combined effect of time and temperature (Equation (5)), and it was introduced to compare pretreatment yields conducted using different conditions [84,85]. Such comparison is presented in Table 10, using samples recovered after various extraction procedures presented in this study. It is important to note that small variations in the SF value (from 2.12 to 2.65) might result in large variations in the HCRY (from 77.5% to 69.43%) for the same extraction process.

Table 10. Hemicellulose recovery yields and chemical composition (% wt.) as a function of severity factor.

Sample Source	SF	HCRY (%)	Glucan	Xylan	Arabinan	Pstot (%)
	2.12	77.50	3.23	54.28	4.12	61.63
HAE, 0.9% NaOH, EL	2.54	76.92	3.83	53.96	3.64	59.75
	2.65	69.43	3.47	52.29	3.45	59.21
	3.39	73.09	4.01	63.26	5.49	72.76
HAE, 0.9% NaOH, BL	3.45	72.82	3.69	68.97	5.60	78.25
	3.55	65.92	5.94	61.80	6.09	83.82
HAE^{opt}, EL	2.02	79.23	4.12	54.64	5.03	63.79
HAE^{opt}, BL	3.31	67.48	3.02	67.84	4.85	75.71
HCE, 5%NaOH, EL	2.12	72.34	7.22	65.07	2.37	74.66

The highest HCRY% value was obtained at the lowest SF, for the hot alkaline treatment from the extraction liquor. At the same value of SF (2.12), the total amount of extracted polysaccharides increased significantly (from 61.63% to 74.66%) when the NaOH concentration was increased from 0.9% to 5% (HAE vs. HCE). This aligns with earlier results made during the optimization phase, which indicated that the NaOH concentration is the process parameter with the most significant impact.

3.7. Characterization of HC Samples by FTIR and 1H-NMR Spectroscopy

All of the analyzed infrared spectra of the HC presented bands occurring at ~3400 cm^{-1} (Figure 7) that were assigned to the stretching vibrations of the O-H groups and also the band occurring at ~2950 cm^{-1} that is generally assigned to the -CH_2 antisymmetric stretching, while the band at 2850 cm^{-1} was a result of -CH_2 symmetric stretching—this portion of the spectra is not shown in the figure for a better view of the range 1600–400 cm^{-1}. All of the HC samples presented bands specific to polysaccharides: the band occurring at ~1630 cm−1 was assigned to the absorbed water [86]; The bands occurring ~1560 and ~1414 were assigned to glucuronic acid carboxylates [87]; the minor band occurring at about 1450 cm^{-1} in some samples could be assigned to the presence of the methyl groups; spectral peaks that are visible at ~1070 and ~1045 cm^{-1} of C-O stretching in the C-O-C ether linkages (the first is the inter sugar units and the second results from intra sugar (in alcoholic functional group). The peaks at ~898 cm^{-1} were attributed to the stretching vibration modes (both symmetric and antisymmetric) of C-O in the ether linkage and are considered specific to the β-1-4 bonds between xylose units of the xylan chain [88]. Other bands at lower wavenumbers, such as ~690 cm^{-1}, are attributed to the out-of-plane C-H deformations.

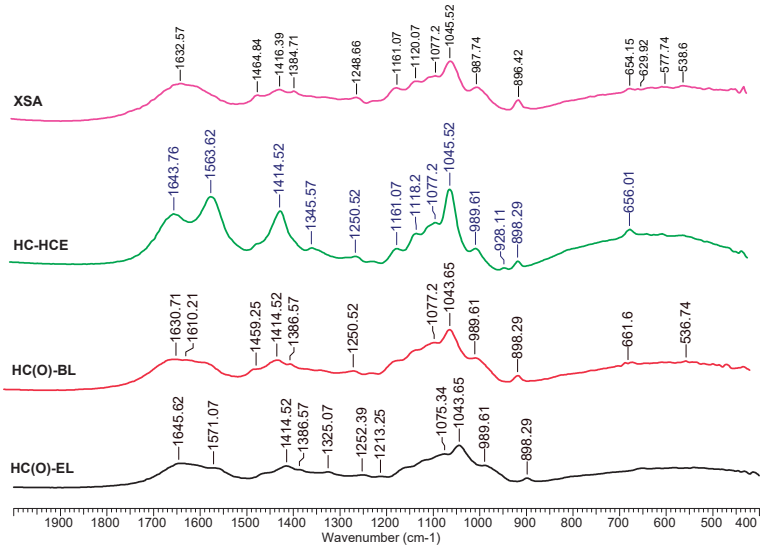

Figure 7. FTIR spectra of separated HC.

NMR spectroscopy was used to study the molecular structure of hemicelluloses. Figure 8 presents the proton NMR spectra of three samples of extracted HC and a commercial xylan sample (X4252 10G). The spectral pattern typical for the proton in HC has signals in the chemical shift region between 3.12–5.45 ppm due to xylose, arabinose, and glucuronic acid residues [89]. The main spectral characteristics of the analyzed HC samples and commercial xylan are shown in Table 11.

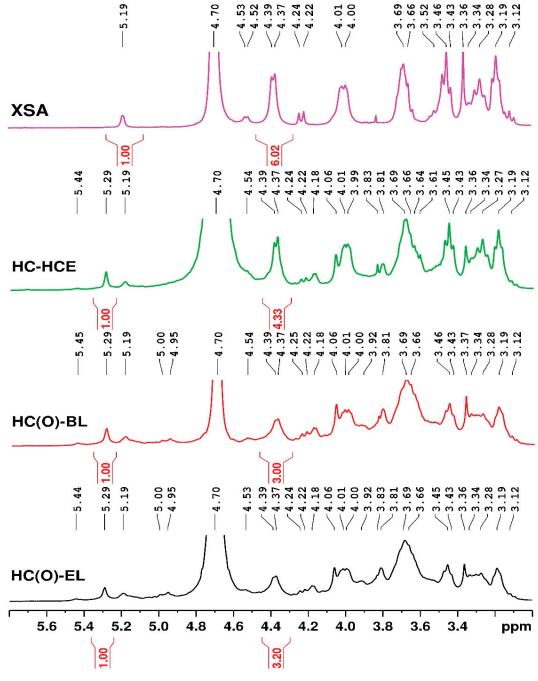

Figure 8. ^{1}H-NMR spectra of the separated hemicelluloses.

The protons from β-(1→4)-D-xylopyranose (β-D-Xylp or (X)) units have signals at 4.39 (H1), 4.01 (H5eq), 3.69 (H4), 3.45 (H3), 3.28 (H5ax) and 3.19 ppm (H2), being found in a significant amount. As shown in Figure 8, the HC samples have more signals in the range 4.9–5.5 ppm compared with the XSA spectrum. Thus, the signals at 5.44 (H1) and 3.34 (H3) ppm are due to the 2-α-L-arabinofuranosyl units (2-α-Araf) and the terminating xylopyranose units (Xylp) from β-Xylp-(1→2)-α-Araf-(1→3), respectively.

The sharp peaks at 5.29 ppm (H1), together with signals at 4.18 (H4), 4.06 (H2) and 3.83 ppm (H3) are attributed to α-L-arabinofuranosyl(1→3)-linkage with the mono-substituted β-D-Xylopyranose unit in the main chain (4-O-methyl glucuronic acid residue substituted xylose residues or (XG) [89], being in a significant proportion.

Peaks from 4.95–5.0 ppm and 4.53 ppm are attributed to H3 and H1 protons of 2-O-acetylated internal xylose residues (Xylp-3Ac). The signal at 5.19 ppm is assigned to the anomeric proton from 4-O-methyl-α-D-glucuronic acid (4-O-Me-α-D-GlcpA or (G)), together with the resonances at 4.2 (H5), 3.66 (H3), 3.43 (H2), 3.36 (-OCH_3) and 3.12 ppm (H4), all these signals being observed also in XSA spectrum. The ratio of xylose units (X) and 4-O-methyl glucuronic acid (G) was determined using the integration of the corresponding anomeric protons [90–92].

Table 11. Synthetic presentation of the 1H-NMR peak assignments.

Spectral Range/Chemical Shift	Assignment in Samples	Literature Data
non substituted xylose residues (X)	−4.39 ppm H1	4.4 [89]
	−3.19 ppm H2	3.21
	−3.28 ppm H5 axial	3.3
	−3.45 ppm H3	3.48
	−3.69 ppm H4	3.71
	−4.01 ppm H5 eq	4.03
4-O-methyl glucuronic acid residue substituted xylose residues (XG)	−5.29 ppm H1	5.31 [89]
	−4.06 ppm H2	4.08
	−3.83 ppm H3	3.83
	−4.18 ppm H4	4.2
4-O-methyl-glucuronic acid residue (G)	−3.36 ppm –OCH3	3.34 [93]
	−3.12 ppm H4	2.95 [94]
	−3.43 ppm H2	3.43 [95]
	−5.19 ppm H1	5.21 [89]
	−3.66 ppm H3	3.64 [95]
	−4.2 ppm H5	4.34/4.37 [95]

The different values of integrals for the range 4.2–4.4 ppm specific for the H1 XG signals reside in the HC extraction condition or source. In the case of the HC(O)-EL sample, a value of 3.2 was obtained. A smaller value is observable for the HC(O)-BL sample. This suggests a decrease in the number of 4-O-methyl glucuronic acid residue substituted anhydro-xylose residues as a result of the increase in the temperature (from 100 °C to 140 °C) in the reaction environment and intensification of the ether linkage cleavage in the alkaline pulping environment. The increase in C_{NaOH} from 1% to 5% causes liberation of different structure HC—this is why integral values for the H1 XG signals are increased in the sample denoted HC-HCE. The value of 6.0 of this integral obtained for the spectrum of beechwood xylan XSA suggests an even higher presence of XG groups in this sample, a feature which is common for hardwood hemicelluloses [96].

3.8. Comparison with Similar Studies

Several literature studies report similar attempts to produce both HC and/or HC derivatives and paper pulp with satisfactory mechanical properties starting from agro-wastes. Some focus on CS as raw material, but the extraction procedures differ from the current study. However, the results are promising regardless of the pretreatment and

extraction procedure used. The CS are an attractive raw material for the simultaneous production of HC and/or HC derivatives and paper pulp (Table 12).

Table 12. Comparison with similar studies *.

Raw Material	Extraction/Pretreatment	HC Derivatives	TI (N·M/G)	BI (kPa·m^2/g)	Ref.
CS	HAE	54.64% xylan	80.10	4.33	This work
CS	One-step formic acid	61.00% xylose	50.10	3.00	[49]
CS and kash	Soda-anthraquinone pulping	-	56.00	4.70	[97]
CS	Alkaline sulfite pulping	-	62.40	3.80	[98]
CS	Alkaline sulfite cooking	118.40 g xylose/kg CS	97.40	5.20	[41]
Corn cobs	Hydrothermal pretreatment	52.35% furfural	43.00	-	[99]
CS	Acid pre-impregnated steam explosion	acetone: 0.09 g/g, butanol: 0.18 g/g, ethanol: 0.04 g/g	24.00	0.99	[100]

* best results reported.

Our study's findings corroborate those of other authors who have noted a decline in paper quality in response to increasing extraction HC yields. Hot water extraction was utilized by Chen and colleagues [101] to extract sugars from CS, yielding a yield of xylose extraction of 70.2%; however, various paper quality indices, including brightness, BI, and breaking length, were negatively affected.

4. Conclusions

This work aimed to identify the best-suited strategy for the complete valorization of CS and focused on the optimum equilibrium between the amount of extracted HC and paper quality. To reach this objective, two different stages were applied (screening and optimization).

The screening phase revealed that conventional HAE at high alkali concentrations, which yields better results in terms of HC extraction but suffers from lowered pulp yield and papermaking properties, should not be considered as part of the pathway for the co-production of HC and papermaking pulp by using CS as raw material. The significant reduction in paper quality and DP directly results from the high C_{NaOH}. Therefore, lower alkali concentrations are recommended. The HWT treatment, although performed in relatively low severity, also inflicts significant mechanical strength losses. In this aspect, the preliminary HAE hemicellulose extraction using low alkali concentrations of liquors similar to those used in soda pulping situations seemed to show the promised result.

The RSM strategy showed the influence of the chosen factors: temperature, $C_{NaOH,}$ and time on the modeled system responses. Depending on the targeted yields' values, the model equation could be used to predict the system output under different circumstances. The resulting models were experimentally validated. A more aggressive extraction procedure (HCE) was used for comparison purposes, showing that a high HC extraction yield is detrimental to paper properties. The observed differences in pulp refinability and papermaking properties directly result from HC participation in refining stages and in developing sheet strength.

Supplementary Materials: The following supporting information can be downloaded at: https://www.mdpi.com/article/10.3390/polym15234597/s1,: Figure S1: Corn stalks chopped and shredded; Figure S2: The pulping reactor; Figure S3: Various stages of liquid phase processing; Figure S4: Hemicelluloses samples (before and after drying); Figure S5: Paper sheets and preliminary strength testing; Supplementary File S1: ANOVA; Supplementary File S2: 1H-NMR spectra; Supplementary File S3: FTIR data.

Author Contributions: Conceptualization, A.C.P. and M.T.N.; methodology, A.C.P.; software, A.C.P.; formal analysis, C.D.B. and G.-L.A.; investigation, A.C.P., C.D.B. and G.-L.A.; data curation, E.N.D.; writing—original draft preparation, A.C.P. and M.T.N.; writing—review and editing, A.C.P., E.N.D.

and M.T.N.; visualization, E.N.D.; funding acquisition, A.C.P. All authors have read and agreed to the published version of the manuscript.

Funding: This work was supported by a grant from the Ministry of Research, Innovation, and Digitization, CCCDI-UEFISCDI; project number PN-III-P2-2.1-PED-2021-3384, within PNCDI III.

Institutional Review Board Statement: Not applicable.

Data Availability Statement: Data will be available upon request.

Conflicts of Interest: The authors declare no conflict of interest.

References

1. Winans, K.; Kendall, A.; Deng, H. The history and current applications of the circular economy concept. *Renew. Sustain. Energy Rev.* **2017**, *68*, 825–833. [CrossRef]
2. Kirchherr, J.; Reike, D.; Hekkert, M. Conceptualizing the circular economy: An analysis of 114 definitions. *Resour. Conserv. Recycl.* **2017**, *127*, 221–232. [CrossRef]
3. Korhonen, J.; Honkasalo, A.; Seppälä, J. Circular Economy: The Concept and its Limitations. *Ecol. Econ.* **2018**, *143*, 37–46. [CrossRef]
4. Zaman, A.U. A comprehensive review of the development of zero waste management: Lessons learned and guidelines. *J. Clean. Prod.* **2015**, *91*, 12–25. [CrossRef]
5. Zaman, A.U.; Lehmann, S. Challenges and Opportunities in Transforming a City into a "Zero Waste City". *Challenges* **2011**, *2*, 73–93. [CrossRef]
6. Awasthi, A.K.; Cheela, V.R.S.; D'adamo, I.; Iacovidou, E.; Islam, M.R.; Johnson, M.; Miller, T.R.; Parajuly, K.; Parchomenko, A.; Radhakrishan, L.; et al. Zero waste approach towards a sustainable waste management. *Resour. Environ. Sustain.* **2021**, *3*, 100014. [CrossRef]
7. Pietzsch, N.; Ribeiro, J.L.D.; de Medeiros, J.F. Benefits, challenges and critical factors of success for Zero Waste: A systematic literature review. *Waste Manag.* **2017**, *67*, 324–353. [CrossRef]
8. Paramesh, V.; Ravisankar, N.; Behera, U.; Arunachalam, V.; Kumar, P.; Rajkumar, R.S.; Misra, S.D.; Kumar, R.M.; Prusty, A.K.; Jacob, D.; et al. Integrated farming system approaches to achieve food and nutritional security for enhancing profitability, employment, and climate resilience in India. *Food Energy Secur.* **2022**, *11*, e321. [CrossRef]
9. Babu, S.; Das, A.; Singh, R.; Mohapatra, K.P.; Kumar, S.; Rathore, S.S.; Yadav, S.K.; Yadav, P.; Ansari, M.A.; Panwar, A.S.; et al. Designing an energy efficient, economically feasible, and environmentally robust integrated farming system model for sustainable food production in the Indian Himalayas. *Sustain. Food Technol.* **2022**, *1*, 126–142. [CrossRef]
10. Meerman, F.; Van De Ven, G.W.J.; Van Keulen, H.; Breman, H. Integrated crop management: An approach to sustainable agricultural development. *Int. J. Pest Manag.* **1996**, *42*, 13–24. [CrossRef]
11. Leake, A. The development of integrated crop management in agricultural crops: Comparisons with conventional methods. *Pest Manag. Sci.* **2000**, *56*, 950–953. [CrossRef]
12. Cardoso Alves, S.; Díaz-Ruiz, E.; Lisboa, B.; Sharma, M.; Mussatto, S.I.; Thakur, V.K.; Kalaskar, D.M.; Gupta, V.K.; Chandel, A.K. Microbial meat: A sustainable vegan protein source produced from agri-waste to feed the world. *Food Res. Int.* **2023**, *166*, 112596. [CrossRef]
13. Donner, M.; de Vries, H. How to innovate business models for a circular bio-economy? *Bus. Strategy Environ.* **2021**, *30*, 1932–1947. [CrossRef]
14. Donner, M.; Verniquet, A.; Broeze, J.; Kayser, K.; De Vries, H. Critical success and risk factors for circular business models valorising agricultural waste and by-products. *Resour. Conserv. Recycl.* **2020**, *165*, 105236. [CrossRef]
15. Available online: https://www.databridgemarketresearch.com/reports/global-wheat-straw-market (accessed on 2 October 2023).
16. Available online: https://www.statista.com/statistics/263977/world-grain-production-by-type/ (accessed on 3 October 2023).
17. Available online: https://www.world-grain.com/articles/17875-eu-uk-grain-production-expected-to-increase-in-2023 (accessed on 2 October 2023).
18. Available online: https://www.mordorintelligence.com/industry-reports/europe-maize-market (accessed on 3 October 2023).
19. Ahmed, M.J.; Danish, M.; Anastopoulos, I.; Iwuozor, K.O. Recent progress on corn (*Zea mays* L.)-based materials as raw, chemically modified, carbonaceous, and composite adsorbents for aquatic pollutants: A review. *J. Anal. Appl. Pyrolysis* **2023**, *172*, 106004. [CrossRef]
20. Schmer, M.R.; Brown, R.M.; Jin, V.L.; Mitchell, R.B.; Redfearn, D.D. Corn Residue Use by Livestock in the United States. *Agric. Environ. Lett.* **2017**, *2*, 160043. [CrossRef]
21. Hu, J.; Lei, T.; Wang, Z.; Yan, X.; Shi, X.; Li, Z.; He, X.; Zhang, Q. Economic, environmental and social assessment of briquette fuel from agricultural residues in China—A study on flat die briquetting using corn stalk. *Energy* **2014**, *64*, 557–566. [CrossRef]
22. Wu, K.; Zhang, Z.; Feng, L.; Bai, W.; Feng, C.; Song, Y.; Gong, P.; Meng, Y.; Zhang, L. Effects of Corn Stalks and Urea on N_2O Production from Corn Field Soil. *Agronomy* **2021**, *11*, 2009. [CrossRef]

23. Lou, C.; Jiang, S.; Yan, A.; Zhou, Y.; Liu, Y.; Zhang, Y.; Kong, X. Self-extracted corn-stalk cellulose/epoxy resin composites. *Sci. Rep.* **2022**, *12*, 20968. [CrossRef]
24. Boufi, S.; Chaker, A. Easy production of cellulose nanofibrils from corn stalk by a conventional high speed blender. *Ind. Crop. Prod.* **2016**, *93*, 39–47. [CrossRef]
25. Li, B.; Liu, G.; Tang, X.; Zhang, H.; Gao, X. Facile preparation of all cellulose composite with excellent mechanical and antibacterial properties via partial dissolution of corn-stalk biomass. *Int. J. Biol. Macromol.* **2023**, *228*, 89–98. [CrossRef] [PubMed]
26. Thakkar, A.; Shell, K.M.; Bertosin, M.; Rodene, D.D.; Amar, V.; Bertucco, A.; Gupta, R.B.; Shende, R.; Kumar, S. Production of levulinic acid and biocarbon electrode material from corn stover through an integrated biorefinery process. *Fuel Process. Technol.* **2020**, *213*, 106644. [CrossRef]
27. Aghaei, S.; Alavijeh, M.K.; Shafiei, M.; Karimi, K. A comprehensive review on bioethanol production from corn stover: Worldwide potential, environmental importance, and perspectives. *Biomass Bioenergy* **2022**, *161*, 106447. [CrossRef]
28. Yuan, H.; Lan, Y.; Zhu, J.; Wachemo, A.C.; Li, X.; Yu, L. Effect on anaerobic digestion performance of corn stover by freezing–thawing with ammonia pretreatment. *Chin. J. Chem. Eng.* **2019**, *27*, 200–207. [CrossRef]
29. Hájková, K.; Jurczyková, T.; Filipi, M.; Bouček, J. Chemical pulp from corn stalks. *Biotechnol. Rep.* **2023**, *37*, e00786. [CrossRef] [PubMed]
30. Enawgaw, H.; Tesfaye, T.; Yilma, K.T.; Limeneh, D.Y. Multiple Utilization Ways of Corn By-Products for Biomaterial Production with Bio-Refinery Concept; a Review. *Mater. Circ. Econ.* **2023**, *5*, 7. [CrossRef]
31. Taurino, R.; Bondioli, F.; Messori, M. Use of different kinds of waste in the construction of new polymer composites: Review. *Mater. Today Sustain.* **2023**, *21*, 100298. [CrossRef]
32. Thomas, J.; Patil, R. The Road to Sustainable Tire Materials: Current State-of-the-Art and Future Prospectives. *Environ. Sci. Technol.* **2023**, *57*, 2209–2216. [CrossRef]
33. Mohammed, L.; Ansari, M.N.M.; Pua, G.; Jawaid, M.; Islam, M.S. A Review on Natural Fiber Reinforced Polymer Composite and Its Applications. *Int. J. Polym. Sci.* **2015**, *2015*, 243947. [CrossRef]
34. Dinu, R.; Bejenari, I.; Volf, I.; Mija, A. Vegetable Oil-Based Resins Reinforced with Spruce Bark Powder and with Its Hydrochar Lignocellulosic Biomass. *Appl. Sci.* **2021**, *11*, 10649. [CrossRef]
35. Hou, Y.; Wu, W. Derived from corn straw cellulose: Modified used tire rubber powder composites. *Cellulose* **2022**, *29*, 3935–3945. [CrossRef]
36. Łączny, D.; Macko, M.; Moraczewski, K.; Szczepański, Z.; Trafarski, A. Influence of the Size of the Fiber Filler of Corn Stalks in the Polylactide Matrix Composite on the Mechanical and Thermomechanical Properties. *Materials* **2021**, *14*, 7281. [CrossRef] [PubMed]
37. Li, R.; Zhu, X.; Peng, F.; Lu, F. Biodegradable, Colorless, and Odorless PLA/PBAT Bioplastics Incorporated with Corn Stover. *ACS Sustain. Chem. Eng.* **2023**, *11*, 8870–8883. [CrossRef]
38. Poudel, R.; Karak, N. Sustainable green composite of yam and agricultural waste corn stalk fiber with good mechanical, thermal, optical, aging performance and excellent biodegradability. *Compos. Sci. Technol.* **2023**, *244*, 110276. [CrossRef]
39. Zabed, H.M.; Akter, S.; Yun, J.; Zhang, G.; Zhao, M.; Mofijur, M.; Awasthi, M.K.; Kalam, M.A.; Ragauskas, A.; Qi, X. Towards the sustainable conversion of corn stover into bioenergy and bioproducts through biochemical route: Technical, economic and strategic perspectives. *J. Clean. Prod.* **2023**, *400*, 136699. [CrossRef]
40. Santana, Á.L.; Meireles, M.A.A. Valorization of Cereal Byproducts with Supercritical Technology: The Case of Corn. *Processes* **2023**, *11*, 289. [CrossRef]
41. Liang, J.; Li, Z.; Dai, S.; Tian, G.; Wang, Z. Production of hemicelluloses sugars, cellulose pulp, and lignosulfonate surfactant using corn stalk by prehydrolysis and alkaline sulfite cooking. *Ind. Crops Prod.* **2023**, *192*, 115880. [CrossRef]
42. Özyürek, Ö.; Çöpür, Y. Integrated biorefinery for production of biodegradable film, bioethanol, and soda pulp from corn stalks. *BioResources* **2023**, *18*, 2639–2656. [CrossRef]
43. Tao, Q.; Li, B.; Chen, Y.; Zhao, J.; Li, Q.; Chen, Y.; Peng, Q.; Yuan, S.; Li, H.; Huang, R.; et al. An integrated method to produce fermented liquid feed and biologically modified biochar as cadmium adsorbents using corn stalks. *Waste Manag.* **2021**, *127*, 112–120. [CrossRef]
44. Rahman, M.M.; Roy, A.; Nayeem, J.; Popy, R.S.; Ferdous, T.; Jahan, M.S. Tissue paper from corn stalk pulp in biorefinery concept. *Biomass Convers. Biorefinery* **2023**, 1–8. [CrossRef]
45. Huang, H.-J.; Ramaswamy, S.; Al-Dajani, W.W.; Tschirner, U. Process modeling and analysis of pulp mill-based integrated biorefinery with hemicellulose pre-extraction for ethanol production: A comparative study. *Bioresour. Technol.* **2010**, *101*, 624–631. [CrossRef] [PubMed]
46. Li, W.-C.; Zhang, S.-J.; Xu, T.; Sun, M.-Q.; Zhu, J.-Q.; Zhong, C.; Li, B.-Z.; Yuan, Y.-J. Fractionation of corn stover by two-step pretreatment for production of ethanol, furfural, and lignin. *Energy* **2020**, *195*, 117076. [CrossRef]
47. Wang, Y.; Liu, J.; Cai, D.; Zhao, G. Co-generation of ethanol and l-lactic acid from corn stalk under a hybrid process. *Biotechnol. Biofuels* **2018**, *11*, 331. [CrossRef] [PubMed]
48. Luo, Y.; Zhao, Z.; Jiang, B.; Wei, M.; Zhang, Z.; Zeng, L.; Clark, J.H.; Fan, J. An integrated process for the valorization of corn stover promoted by NaCl in a GVL/H_2O system. *Green Chem.* **2022**, *24*, 1515–1526. [CrossRef]
49. Zhong, X.; Yuan, R.; Zhang, B.; Wang, B.; Chu, Y.; Wang, Z. Full fractionation of cellulose, hemicellulose, and lignin in pith-leaf containing corn stover by one-step treatment using aqueous formic acid. *Ind. Crops Prod.* **2021**, *172*, 113962. [CrossRef]

50. Lyu, Q.; Chen, X.; Li, W.; Zhang, Y.; Xiao, A.; Chen, J.; Han, L.; Zhou, C.; Xiao, W. A multi-product strategy for the fractionation of corn stover based on peracetic acid and maleic acid processing. *J. Environ. Chem. Eng.* **2022**, *10*, 108764. [CrossRef]
51. Yang, S.; Chen, K.; Zhu, Z.; Guan, Q.; Zhou, H.; He, L. A green pretreatment approach of corn stalk wastes for obtaining micro/nano-cellulose fibers, monosaccharides and lignin fractions. *Renew Energy* **2022**, *194*, 746–759. [CrossRef]
52. Puițel, A.C.; Suditu, G.D.; Danu, M.; Ailiesei, G.-L.; Nechita, M.T. An Experimental Study on the Hot Alkali Extraction of Xylan-Based Hemicelluloses from Wheat Straw and Corn Stalks and Optimization Methods. *Polymers* **2022**, *14*, 1662. [CrossRef]
53. Hassan, A.A.; Hasanin, M.S.; Ismail, S.A. Enzymatic valorization of cellulosic and hemicellulosic-based biomasses via the production of antioxidant water-soluble hydrolyzate of maize stalks and the green bio-deinking of mixed office waste paper. *Biomass Convers. Biorefinery* **2023**, 1–16. [CrossRef]
54. An, S.; Li, W.; Xue, F.; Li, X.; Xia, Y.; Liu, Q.; Chen, L.; Jameel, H.; Chang, H.-M. Effect of removing hemicellulose and lignin synchronously under mild conditions on enzymatic hydrolysis of corn stover. *Fuel Process. Technol.* **2020**, *204*, 106407. [CrossRef]
55. Qing, Q.; Zhou, L.; Guo, Q.; Gao, X.; Zhang, Y.; He, Y.; Zhang, Y. Mild alkaline presoaking and organosolv pretreatment of corn stover and their impacts on corn stover composition, structure, and digestibility. *Bioresour. Technol.* **2017**, *233*, 284–290. [CrossRef] [PubMed]
56. Danielewicz, D.; Kmiotek, M.; Barbara Surma-Ślusarska, B. Comparison of Some Properties of Selected Non-Wood Plants and Wood Species and Unbleached Kraft Pulps from These Materials. *J. Nat. Fibers* **2019**, *18*, 1296–1306. [CrossRef]
57. *ISO 5269-2:2004*; Pulps—Preparation of Laboratory Sheets for Physical Testing—Part 2: Rapid-Köthen Method. ISO: Geneva, Switzerland, 2004.
58. *ISO 1924-2:2008*; Paper and Board—Determination of Tensile Properties—Part 2: Constant Rate of Elongation Method (20 mm/min). ISO: Geneva, Switzerland, 2008.
59. *ISO 2758:2014*; Paper—Determination of Bursting Strength. ISO: Geneva, Switzerland, 2014.
60. TAPPI. *T 211 om-02. Ash in Wood, Pulp, Paper and Paperboard: Combustion at 525 °C*; TAPPI: Atlanta, GA, USA, 2002; Volume 5.
61. TAPPI. *Water Solubility of Wood and Pulp*; TAPPI: Atlanta, GA, USA, 1988.
62. TAPPI. *T 204 cm-97, Solvent Extractives of Wood and Pulp*; TAPPI: Atlanta, GA, USA, 2007.
63. TAPPI. *Acetone Extractives of Wood and Pulp*; Technical Association of the Pulp and Paper Industry TAPPI Press: Atlanta, GA, USA, 2000.
64. Sluiter, A.; Hames, B.; Hyman, D.; Payne, C.; Ruiz, R.; Scarlata, C.; Sluiter, J.; Templeton, D.; Wolfe, J. Determination of total solids in biomass and total dissolved solids in liquid process samples. *Natl. Renew. Energy Lab.* **2008**, *9*, 1–6.
65. Sluiter, A.; Hames, B.; Ruiz, R.; Scarlata, C.; Sluiter, J.; Templeton, D.; Crocker, D. Determination of structural carbohydrates and lignin in biomass. *Gold. Natl. Renew. Energy Lab.* **2008**, *1617*, 1–16.
66. Sluiter, A.; Hames, B.; Ruiz, R.; Scarlata, C.; Sluiter, J.; Templeton, D. Determination of sugars, byproducts, and degradation products in liquid fraction process samples. *Gold. Natl. Renew. Energy Lab.* **2006**, *11*, 65–71.
67. Farhat, W.; Venditti, R.; Quick, A.; Taha, M.; Mignard, N.; Becquart, F.; Ayoub, A. Hemicellulose extraction and characterization for applications in paper coatings and adhesives. *Ind. Crops Prod.* **2017**, *107*, 370–377. [CrossRef]
68. Koshijima, T.; Timell, T.E.; Zinbo, M. The number-average molecular weight of native hardwood xylans. *J. Polym. Sci. Part C Polym. Symp.* **1965**, *11*, 265–279. [CrossRef]
69. Salam, A.; Pawlak, J.J.; Venditti, R.A.; El-Tahlawy, K. Incorporation of carboxyl groups into xylan for improved absorbency. *Cellulose* **2011**, *18*, 1033–1041. [CrossRef]
70. *ISO 5351:2010*; Cellulose in Dilute Solutions—Determination of Limiting Viscosity Number—Part 1: Method in Cupri-Ethylene-Diamine (CED) Solution. ISO: Geneva, Switzerland, 2010.
71. Ziegler-Devin, I.; Chrusciel, L.; Brosse, N. Steam Explosion Pretreatment of Lignocellulosic Biomass: A Mini-Review of Theorical and Experimental Approaches. *Front. Chem.* **2021**, *9*, 705358. [CrossRef]
72. Overend, R.P.; Chornet, E. Fractionation of lignocellulosics by steam-aqueous pretreatments. *Philos. Trans. R. Soc. Lond. Ser. A Math. Phys. Sci.* **1987**, *321*, 523–536. [CrossRef]
73. Puițel, A.C.; Suditu, G.D.; Drăgoi, E.N.; Danu, M.; Ailiesei, G.-L.; Balan, C.D.; Chicet, D.-L.; Nechita, M.T. Optimization of Alkaline Extraction of Xylan-Based Hemicelluloses from Wheat Straws: Effects of Microwave, Ultrasound, and Freeze–Thaw Cycles. *Polymers* **2023**, *15*, 1038. [CrossRef]
74. Kim, T.H.; Lee, Y. Fractionation of corn stover by hot-water and aqueous ammonia treatment. *Bioresour. Technol.* **2006**, *97*, 224–232. [CrossRef]
75. Cayetano, R.D.A.; Kim, T.H. Effects of Low Moisture Anhydrous Ammonia (LMAA) Pretreatment at Controlled Ammoniation Temperatures on Enzymatic Hydrolysis of Corn Stover. *Appl. Biochem. Biotechnol.* **2016**, *181*, 1257–1269. [CrossRef] [PubMed]
76. Wang, Z.; Dien, B.S.; Rausch, K.D.; Tumbleson, M.E.; Singh, V. Improving ethanol yields with deacetylated and two-stage pretreated corn stover and sugarcane bagasse by blending commercial xylose-fermenting and wild type Saccharomyces yeast. *Bioresour. Technol.* **2019**, *282*, 103–109. [CrossRef] [PubMed]
77. Zhu, Y.; Lee, Y.Y.; Elander, R.T. Optimization of Dilute-Acid Pretreatment of Corn Stover Using a High-Solids Percolation Reactor. *Appl. Biochem. Biotechnol.* **2005**, *124*, 1045–1054. [CrossRef]
78. Moniz, P.; Pereira, H.; Quilhó, T.; Carvalheiro, F. Characterisation and hydrothermal processing of corn straw towards the selective fractionation of hemicelluloses. *Ind. Crops Prod.* **2013**, *50*, 145–153. [CrossRef]

79. Bajpai, P. Chapter 1—Refining and Pulp Characterization. In *Biermann's Handbook of Pulp and Paper*, 3rd ed.; Bajpai, P., Ed.; Elsevier: Amsterdam, The Netherlands, 2018; pp. 1–34.
80. Pere, J.; Pääkkönen, E.; Ji, Y.; Retulainen, E.A. Influence of the Hemicellulose Content on the Fiber Properties, Strength, and Formability of Handsheets. *BioResources* **2018**, *14*, 13. [CrossRef]
81. Ban, W.; Chen, X.; Andrews, G.; Van Heiningen, A. Influence of hemicelluloses pre-extraction and re-adsorption on pulp physical strength. II. Beatability and strength study. *Cellul. Chem. Technol.* **2011**, *45*, 633.
82. Motamedian, H.R.; Halilovic, A.E.; Kulachenko, A. Mechanisms of strength and stiffness improvement of paper after PFI refining with a focus on the effect of fines. *Cellulose* **2019**, *26*, 4099–4124. [CrossRef]
83. Vainio, A.; Paulapuro, H. Interfiber bonding and fiber segment activation in paper. *BioResources* **2007**, *2*, 442–458. [CrossRef]
84. Pedersen, M.; Meyer, A.S. Lignocellulose pretreatment severity—Relating pH to biomatrix opening. *New Biotechnol.* **2010**, *27*, 739–750. [CrossRef]
85. Abouelela, A.R.; Nakasu, P.Y.S.; Hallett, J.P. Influence of Pretreatment Severity Factor and Hammett Acidity on Softwood Fractionation by an Acidic Protic Ionic Liquid. *ACS Sustain. Chem. Eng.* **2023**, *11*, 2404–2415. [CrossRef]
86. Butylina, S.; Koljonen, K.; Hiltunen, S.; Laatikainen, K. Study on spinnability of arabinoxylan extracted from barley husks. *Cellulose* **2022**, *29*, 1–17. [CrossRef]
87. Peng, F.; Jia, N.; Bian, J.; Peng, P.; Sun, R.; Liu, S. Isolation and fractionation of hemicelluloses from *Salix psammophila*. *Cellul. Chem. Technol.* **2012**, *46*, 177.
88. Kong, F.; Guo, Y.; Liu, Z.; Wang, S.; Lucia, L.A. Synthesis of Cationic Xylan Derivatives and Application as Strengthening Agents in Papermaking. *BioResources* **2018**, *13*, 2960–2976. [CrossRef]
89. Li, H.; Xue, Y.; Wu, J.; Wu, H.; Qin, G.; Li, C.; Ding, J.; Liu, J.; Gan, L.; Long, M. Enzymatic hydrolysis of hemicelluloses from Miscanthus to monosaccharides or xylo-oligosaccharides by recombinant hemicellulases. *Ind. Crops Prod.* **2016**, *79*, 170–179. [CrossRef]
90. Teleman, A.; Tenkanen, M.; Jacobs, A.; Dahlman, O. Characterization of O-acetyl-(4-O-methylglucurono)xylan isolated from birch and beech. *Carbohydr. Res.* **2002**, *337*, 373–377. [CrossRef]
91. Gonçalves, V.M.F.; Evtuguin, D.V.; Domingues, M.R.M. Structural characterization of the acetylated heteroxylan from the natural hybrid *Paulownia elongata/Paulownia fortunei*. *Carbohydr. Res.* **2008**, *343*, 256–266. [CrossRef]
92. Gufe, C.; Thantsha, M.S.; Malgas, S. Recovery of xylan from *Acacia mearnsii* using ultrasound-assisted alkaline extraction. *Biofuels Bioprod. Biorefining* **2023**, *17*, 976–987. [CrossRef]
93. Bian, J.; Peng, F.; Peng, X.-P.; Xu, F.; Sun, R.-C.; Kennedy, J.F. Isolation of hemicelluloses from sugarcane bagasse at different temperatures: Structure and properties. *Carbohydr. Polym.* **2012**, *88*, 638–645. [CrossRef]
94. Zhao, X.; Tong, T.; Li, H.; Lu, H.; Ren, J.; Zhang, A.; Deng, X.; Chen, X.; Wu, A.-M. Characterization of hemicelluloses from *Neolamarckia cadamba* (Rubiaceae) during xylogenesis. *Carbohydr. Polym.* **2017**, *156*, 333–339. [CrossRef]
95. Sharma, K.; Khaire, K.C.; Thakur, A.; Moholkar, V.S.; Goyal, A. Acacia Xylan as a Substitute for Commercially Available Xylan and Its Application in the Production of Xylooligosaccharides. *ACS Omega* **2020**, *5*, 13729–13738. [CrossRef] [PubMed]
96. Laine, C. *Structures of Hemicelluloses and Pectins in Wood and Pulp*; Helsinki University of Technology: Helsinki, Finland, 2005.
97. Jahan, M.S.; Rahman, M.M. Effect of pre-hydrolysis on the soda-anthraquinone pulping of corn stalks and *Saccharum spontaneum* (kash). *Carbohydr. Polym.* **2012**, *88*, 583–588. [CrossRef]
98. Latibari, A.J.; Hossein, M.A.; Hosseinpour, R. Application of alkaline sulfite pulping on corn stalks. *BioResources* **2010**, *6*, 48–58. [CrossRef]
99. Fan, Y.; Ji, H. Corncob Fractionations Toward Two Purposes: Furfural Production and Papermaking. *BioEnergy Res.* **2023**, 1–10. [CrossRef]
100. Xia, F.; Liu, H.; Lu, J.; Lv, Y.; Zhai, S.; An, Q.; Cheng, Y.; Wang, H. An integrated biorefinery process to produce butanol and pulp from corn straw. *Ind. Crops Prod.* **2019**, *140*, 111648. [CrossRef]
101. Chen, L.; Li, J.; Lu, M.; Guo, X.; Zhang, H.; Han, L. Integrated chemical and multi-scale structural analyses for the processes of acid pretreatment and enzymatic hydrolysis of corn stover. *Carbohydr. Polym.* **2016**, *141*, 1–9. [CrossRef]

polymers

MDPI

Article

Optimization of Alkaline Extraction of Xylan-Based Hemicelluloses from Wheat Straws: Effects of Microwave, Ultrasound, and Freeze–Thaw Cycles

Adrian Cătălin Puițel [1], Gabriel Dan Suditu [1], Elena Niculina Drăgoi [1], Maricel Danu [1,2], Gabriela-Liliana Ailiesei [2], Cătălin Dumitrel Balan [1], Daniela-Lucia Chicet [3] and Mircea Teodor Nechita [1,*]

[1] "Cristofor Simionescu" Faculty of Chemical Engineering and Environmental Protection, "Gheorghe Asachi" Technical University, Bd. Prof. Dimitrie Mangeron, No. 73, 700050 Iaşi, Romania
[2] "Petru Poni" Institute of Macromolecular Chemistry, 41A Grigore Ghica Voda Alley, 700487 Iași, Romania
[3] Faculty of Materials Science and Engineering, "Gheorghe Asachi" Technical University, Bd. Prof. Dimitrie Mangeron, No. 41, 700050 Iaşi, Romania
* Correspondence: mircea-teodor.nechita@academic.tuiasi.ro

Abstract: The alkaline extraction of hemicelluloses from a mixture of three varieties of wheat straw (containing 40.1% cellulose, 20.23% xylan, and 26.2% hemicellulose) was analyzed considering the following complementary pre-treatments: freeze–thaw cycles, microwaves, and ultrasounds. The two cycles freeze–thaw approach was selected based on simplicity and energy savings for further analysis and optimization. Experiments planned with Design Expert were performed. The regression model determined through the response surface methodology based on the severity factor (defined as a function of time and temperature) and alkali concentration as variables was then used to optimize the process in a multi-objective case considering the possibility of further use for pulping. To show the properties and chemical structure of the separated hemicelluloses, several analytical methods were used: high-performance chromatography (HPLC), Fourier-transformed infrared spectroscopy (FTIR), proton nuclear magnetic resonance spectroscopy (^{1}H-NMR), thermogravimetry and derivative thermogravimetry analysis (TG, DTG), and scanning electron microscopy (SEM). The verified experimental optimization result indicated the possibility of obtaining hemicelluloses material containing 3.40% glucan, 85.51% xylan, and 7.89% arabinan. The association of hot alkaline extraction with two freeze–thaw cycles allows the partial preservation of the hemicellulose polymeric structure.

Keywords: wheat straw; severity factor; response surface methodology; xylan; hemicellulose; extraction yields

Citation: Puițel, A.C.; Suditu, G.D.; Drăgoi, E.N.; Danu, M.; Ailiesei, G.-L.; Balan, C.D.; Chicet, D.-L.; Nechita, M.T. Optimization of Alkaline Extraction of Xylan-Based Hemicelluloses from Wheat Straws: Effects of Microwave, Ultrasound, and Freeze–Thaw Cycles. *Polymers* **2023**, *15*, 1038. https://doi.org/10.3390/polym15041038

Academic Editors: Sylvain Caillol and Luis Alves

Received: 30 January 2023
Revised: 17 February 2023
Accepted: 17 February 2023
Published: 19 February 2023

1. Introduction

Biomass is recognized as a sustainable, renewable, and virtually limitless resource. Therefore, biomass waste-to-energy valorization technologies are required [1–4]. Agricultural biomass waste is equally appealing [2,3] as a source of energy [5] and/or basic chemicals [6]. As a result, the biomass utilization pathway is critical for maximizing profits, while covering the energy sector and chemical demand [7].

Wheat straws (WS) are a significant component of agricultural waste biomass [8], available virtually worldwide in massive amounts and with multiple ways of valorization, [8–13] such as bioethanol [9,14], biofuels [13,15,16], packaging materials [17], fertilizers [15], sugars [18,19], and others. Each WS utilization pathway, as with biomass in general, corresponds to a specific technology, and each technology is based on a particular type of pretreatment [20,21]. Some sequences may be similar for many technologies (e.g., mechanical stages, such as chopping and sieving; washing; drying; mixing); however, others are particular and correspond to the final, desired product (e.g., sol-gel and carbonization to produce wheat straw-derived magnetic carbon foams [22]). The standard mechanical and

physical steps are usually followed by more aggressive physical, chemical, and biochemical pretreatments that are designed to (i) break down the covalent cross-linkages among lignin, cellulose, and hemicellulose; (ii) reduce the crystallinity of the cellulose in the cell walls of wheat straw [23,24]; and finally, (iii) separate the main components [21,25,26].

The separation of the three main constituents of lignocellulosic materials is generally recognized as the most challenging stage of the lignocellulosic biomass valorization process [27], regardless of the product sought or the technological sequence used [21,28,29]. Chemical pretreatments, such as acidic, alkaline, organic solvent, ionic liquid, ammonia, and ozone, can be used. Each extraction procedure affects the structure of the obtained material in a specific manner [21,25,29,30]. Recently, deep eutectic solvent-based methodologies attracted a lot of attention [31] for effective lignin extraction from various types of biomass, including wheat straw [32], bamboo [33], and *Triarrhena lutarioriparia* [34].

For example, if the lignocellulosic biomass is used as a feedstock for biofuel production lines, then the overall aim of such pretreatments would be a high removal rate of lignin, known for its inhibitory effect [35]. Consequently, the use of relatively harsh conditions for removing lignin is accompanied by removing hemicelluloses [36]. Alternatively, suppose the objective of the biomass processing technology includes the potential recovery of hemicelluloses and of the remaining cellulosic fibers material for the production of papermaking pulp. In that case, the pretreatment conditions must remain within a milder range to prevent excessive hemicellulose degradation and preserve a portion of them in the remaining pulp. This is due to the significance of hemicelluloses as paper-strength promoters [37–39].

Several benefits (efficient hemicellulose separation, effective removal of acetyl groups, mild reaction conditions, less sugar degradation, furan derivatives formation, and relatively low operation costs) [40,41] suggest that alkaline pretreatments are very effective for improving extraction yields in the case of biofuels' production processes [11,42–45]. However, to make the process economically viable, the selectivity must be increased, the pretreatment time reduced, and the chemicals recycled [41,45]. Furthermore, by separate usage or combining the alkaline treatment with physical techniques, such as microwave [46–49], ultrasound irradiation [18,19,41,49–51], or freeze–thaw (FT) cycles [44,47,52], the alkaline extraction can be improved even further taking into account the final objectives.

The current study aims to optimize the extraction and separation of hemicellulose from a highly available lignocellulosic crop residue biomass category—wheat straws (*Triticum aestivum* L.). Chemical characterization of the raw materials was performed on straws from three wheat varieties, which were mixed to simulate an authentic warehouse situation. Three types of hemicellulose alkaline extraction were performed in the screening phase of the study: (i) preceded by freeze–thaw cycles; (ii) ultrasound-assisted; and (iii) microwave-assisted. The best results were obtained for two freeze–thaw cycles, followed by alkaline extraction; thus, this strategy was chosen for further modeling and optimization. The selection of the wheat straw treatment sequence is justified by the possibility of industrializing the process and integrating it into an agri-waste fractionation facility that produces both xylan-based hemicelluloses and papermaking fibers.

The wheat-straw-separated hemicellulose's chemical structure was analyzed using high-performance chromatography (HPLC), Fourier-transformed infrared spectroscopy (FTIR), proton nuclear magnetic resonance spectroscopy (^{1}H-NMR), thermogravimetry, and derivative thermogravimetry analysis (TG, DTG). Based on the results, the purity and the content in terms of components such as xylan, arabinan, and glucan were established.

Response surface methodology (RSM) was used to model and optimize the selected extraction procedure. In addition, to reduce the total number of experiments, the temperature and extraction time have been combined in a single parameter, which will be further referred to as the severity factor [53].

The novelty of the current work is sustained by: (i) screening: trial analysis to determine the most effective complementary pretreatment for hemicellulose alkaline extraction (Section 3.2), taking into account the technical and economic advantages, and disadvantages of each tested combination (Section 3.6); (ii) experimental design (Section 3.3): the

experimental analysis of the selected procedure to unravel the influence of parameters on the process efficiency; and (iii) process optimization (Section 3.4): the identification of the optimal conditions that lead to a maximization of extraction considering different multi-objective criteria (simultaneous maximization of some outputs and minimization of others). To the best of the author's knowledge, such an approach for wheat straw alkaline extraction has never been reported.

2. Materials and Methods

2.1. Analysis Methodology and Equipment

The raw materials used in this study consisted of Otilia, Sorial, and Izvor wheat straw varieties collected from Romanian farmers. For further experimental work, equal portions of the straw were mixed to avoid differences in results obtained by individual processing of straws from the various mentioned varieties. This also helps find a situation closer to the reality of the industry when different types are collected in the same warehouse. Preliminary processing of the wheat straw included grinding and sieving. Classical analytical procedures were involved in establishing the chemical composition in terms of both significant (polysaccharides and lignin) and minor constituents: ash—TAPPI T 211 om-02 [54]; hot water extractives (denoted with HWT), which were determined by the TAPPI T 207 om-88 method [55]; and organic solvent extractives T 204 cm-97 [56]. This chemical characterization was performed for each wheat straw variety and its mixture. The NREL method [57,58] for cellulose determination involves hydrolysis to glucose in two steps of sample treatment: hydrolysis with sulfuric acid at 72% and post-hydrolysis after dilution with sulfuric acid at 4%. The acetone extractives (AE) were determined according to the ISO 14453:2014 procedure.

Acid-insoluble lignin (AIL) and acid-soluble lignin (ASL) were measured using the sulfuric acid two-stages hydrolysis method specified by the NREL/TP-510-42618 method [58]. In addition, the major polysaccharide components (cellulose and hemicelluloses) were determined following an adapted procedure to that described in [49].

The employed chromatography system—Agilent Infinity 1260 II—was equipped with Phenomenex Rezex RPM-Monosaccharide Pb^{+2} (8%) 300 × 7.8 mm, heated at 65 °C. The flow rate of the mobile phase (ultrapure water) had a value of 0.6 mL/min. The injection volume was set to 5 µL. Before injection, each sample and the standard solution were filtered using 0.2 µm syringe PTFE Roth filters. Calibration curves in the concentrations range of 0.05–0.3 g/L were plotted using solutions of 99% purity glucose, xylose, and arabinose (provided by Flucka). A Jasco V550 UV–Vis spectrometer was used to record the absorbance values at 205 nm [59].

2.2. Screening Phase for Extraction of Hemicellulose from Wheat Straw

An initial screening set of experiments was performed to establish the effect of individual pretreatments or alkaline extraction conditions on hemicelluloses' removal yields. This experimental stage included:

(i) trials on FT cycles. The freeze–thawing cycles were repeated up to four times to test their impact on the efficiency of the subsequent hot alkaline (HA) extraction stage. The freezing phase in the freeze–thaw cycle trials was performed by immersing 2 g of oven-dried straw in water in polypropylene sampling vessels. The samples were frozen in a conventional freezer (−22 °C) for 60 min. Then, they were removed from the fridge and left to thaw at room temperature. After defrosting, the samples were reinserted into the freezer to start a new cycle. The extraction yields were measured after a standalone FT cycle and for FT cycles followed by HA. The HA procedure is described in our previous work [40]. For the screening trials, a 5% sodium hydroxide (NaOH) solution was used as an extractive agent at a temperature of 90 °C and 40 min at a solid-to-liquid ratio of 1:30.

(ii) ultrasound treatment. The ultrasonic extraction experiments were realized using a custom-made ultra-sonication system with a generator and horn capable of supporting

50 W at 40 kHz for 10 min. In this case, the treatment was performed in an alkaline environment without supplementary heating.

(iii) extraction under microwave heating conditions. The microwave-assisted heating was performed in an alkaline solution using a 700 W commercially available home oven (Zanussi ZMC 19 MG, microwave frequency—2.45 GHz). This procedure was applied as a potential replacement for conventional heating employed in classic HA.

2.3. Experimental Design of Alkaline Extraction of Hemicelluloses from Freeze–Thaw Pretreated Wheat Straw

The RSM methodology with central composite design was used to model and optimize yields after the best extraction method was determined during the screening phase. The main parameters (Table 1) for modeling the extraction of hemicelluloses from the two preliminary freeze–thaw-cycles-treated wheat straw were: (i) the severity factor is defined as the combination of extraction time and the temperature, Equation (1) [53,60]; and (ii) NaOH concentration:

$$SF = \log_{10}\left(\tau * e^{\frac{T-100}{14.75}}\right) \quad (1)$$

where SF represents the severity factor; τ is the processing time at selected temperature T.

Table 1. Independent variables and variation range for hemicelluloses extraction from wheat straw.

Independent Variables	Units	Label	Range		Symbol
			From	To	
Severity factor	-	X1	1	3	SF
NaOH concentration	% wt.	X2	3	7	CNaOH

The analyzed dependent variables are: the total extraction yield (TY), the homoxylan extraction yield (XY), the total hemicellulose extracted yield (HCY), the acid-insoluble lignin removal yield (YAIL), and the acid-soluble lignin removal yield (YASL). Equations (2)–(6) indicate how the output was determined based on experimental data. Stat-Ease Design-Expert (version 7) was used for the experimental design and processing of the experiments;

$$\text{TY } (\%) = \frac{m_1 - m_2}{m_1} \times 100 \quad (2)$$

where TY (%) represents the total extraction yield; m_1 is the initial mass of the treated samples, oven dried; and m_2 is the mass of the solid residue remaining after the extractive treatment, oven dried;

$$\text{XY } (\%) = \frac{m_{X1} - m_{X2}}{m_{X1}} \times 100 \quad (3)$$

where XY (%) stands for the xylan extraction yield; m_{X1} is the absolute mass of the xylan in the raw material sample; and m_{X2} is the absolute mass of the xylan, determined after two-stage acid hydrolysis;

$$\text{HCY } (\%) = \frac{m_{AX1} - m_{AX2}}{m_{AX1}} \times 100 \quad (4)$$

where HCY (%) stands for the hemicellulose extraction yield; m_{AX1} is the absolute mass of the hemicellulose—arabinoxylan in the raw material sample; and m_{AX2} is the absolute mass of the hemicellulose—arabinoxylan, determined after two-stage acid hydrolysis;

$$YAIL\ (\%) = \frac{m_{AIL1} - m_{AIL2}}{m_{AIL1}} \times 100 \quad (5)$$

where *YAIL* (%) stands for the acid-insoluble lignin extraction yield; m_{AIL1} and m_{AIL2} are the absolute mass of the acid-insoluble lignin in the raw material and treated sample;

$$YASL\ (\%) = \frac{m_{ASL1} - m_{ASL2}}{m_{ASL1}} \times 100 \quad (6)$$

where Y_{ASL} (%) stands for the acid-soluble lignin extraction yield; m_{ASL1} and m_{ASL2} are the absolute mass of the acid-soluble lignin in the raw and treated sample, respectively. The NREL/TP-510-42618 method was used to determine m_{AIL1}, m_{AIL2}, m_{ASL1}, m_{ASL2} [58].

The plan consists of thirteen experiments, including five replications at the center point. The range of parameters included in the RSM analysis (Table 1) was determined based on a series of preliminary investigations and a previous study [40]. The experimental results were then utilized to generate regression models describing the interdependence between parameters and extraction yields.

After determining the regression models for each yield based on the experimental data, process optimization was performed, considering the maximization of the total extraction yield.

2.4. Separation and Characterization of Extracted Hemicelluloses

Separating hemicelluloses involves the preliminary lignin separation by acid precipitation at pH 5. The subsequent treatment of the supernatant with 96% ethanol leads to hemicellulose separation. The purity of the obtained hemicelluloses depends on the amount of lignin initially present in the alkaline extraction liquor, which depends on the extraction conditions. The increased extraction time, temperature, and sodium hydroxide concentration lead to higher amounts of lignin in the HA-produced liquor. At the same time, during the hemicellulose extraction process, lignin is degraded into soluble products at a pH below 5. This aspect leads to the co-precipitation of lignin with the hemicelluloses during the graded ethanol method used to separate hemicelluloses.

In the graded ethanol precipitation method, volumes of 100 mL samples of alkali extraction liquors were neutralized to pH 5.5 by using glacial acetic acid to precipitate and remove some of the lignin co-extracted. The resulting liquor was centrifugated at 3000 rpm for 15 min in a Sorvall GLC2 equipped with an HL-4 rotor (100-mL bucket). The remaining supernatant was mixed with 200 cm^3 of analytic purity ethanol (96%) and left to stand at 4 °C for 24 h. The precipitated hemicelluloses (HC) were separated by centrifugation for 15 min and double-washed with ethanol. Furthermore, the resulting HC samples were dried at 50 °C and prepared for HPLC analysis to determine the constituent monosaccharides residues. The HPLC system and analysis conditions were described in Section 2.1. The injection volume was increased to 20 µL to accommodate the concentration of sugars in the hemicelluloses derived hydrolysate. The exact procedure for wheat straw hemicelluloses processing before HPLC analysis was described in our previous work [40].

The FTIR spectra of the wheat straw extracted and separated hemicelluloses samples were recorded using potassium bromide disks containing finely ground samples at 1% content on an Agilent Cary 630 FTIR instrument (64 scans at 4 cm^{-1} resolution and 4000–400 cm^{-1}).

Samples of 30 mg of hemicelluloses dissolved in deuterated water and pipetted into NMR tubes were used for ^{1}H-NMR spectroscopy analysis. The spectra were recorded on a Bruker Avance NEO 400 MHz spectrometer, operating at 400.1 MHz for 1H nuclei, with a 5 mm four nuclei direct detection z-gradient probe using standard pulse sequences, as delivered by Bruker with TopSpin 4.0.8 spectrometer control and processing software. Chemical shifts are reported in δ units (ppm) and were referenced to the sodium 3-(trimethylsilyl)-(2,2,3,3-d4)-1-propionate (TSP) internal standard. For spectra registration, 128 scans were used.

Thermogravimetric analysis of hemicelluloses samples was carried out using a Toledo TGA/SDTA 851 instrument at a heating rate of 10 °C·min^{-1} and a nitrogen flow rate of 20 mL·min^{-1}, using a sample weight of 2–6 mg. Ceramic pans were used to heat the

samples from 25 °C to 800 °C. Mettler Stare SW 9.10 TGA/DTG software was used for data processing.

The surface morphology of the samples was studied with the help of a Vega-Tescan LMH II type scanning electron microscope, using a secondary electrons (SE) detector and an 8 kV filament voltage on a high-vacuum (HV) working module. First, the analyzed samples were taken in a dry state at the end of each extraction stage. Then, without further intervention, they were mounted directly on the holders using a double-copper adhesive strip.

3. Results and Discussion

3.1. Wheat Straw Chemical Composition

The main chemical components are cellulose, hemicelluloses, and lignin. Several methods of analysis were used (Section 2.1.) to estimate the amount of various constituents of the raw materials (Table 2). The total amount of hemicelluloses (xylan and arabinan) is denoted with HC. Table 2 is designed to compare the different types of constituents for the three varieties of wheat straw and their mixture (1:1:1), and the results do not represent the total chemical composition.

Table 2. Chemical composition of wheat straw varieties as raw materials in the study.

Variety	Cellulose % (Std)	Xylan % (Std)	HC % (Std)	AIL % (Std)	ASL % (Std)	AE % (Std)	HWT % (Std)	Ash % (Std)
Otilia	39.64 (0.98)	21.62 (1.14)	24.97 (0.38)	18.67 (1.12)	1.95 (0.12)	2.17 (0.03)	15.47 (0.02)	5.57 (0.06)
Sorial	39.73 (0.45)	18.79 (1.88)	26.01 (0.24)	15.8 (0.48)	2.45 (0.11)	4.09 (0.04)	18.08 (0.41)	6.44 (0.17)
Izvor	40.9 (0.59)	20.56 (1.37)	27.27 (0.31)	20.6 (0.11)	1.83 (0.16)	2.49 (0.05)	13.6 (0.5)	4.88 (0.14)
Mixture of WS (1:1:1)	40.1 (1.12)	20.23 (1.1)	26.2 (1.78)	16.36 (1.1)	1.48 (0.22)	2.91 (0.15)	15.66 (0.18)	5.61 (0.35)

Results presented as mean of triplicates; std represents the standard deviation.

There are minor differences (1% variation) in cellulose content between the different varieties, while for the hemicelluloses content, it ranged from 24.97% to 27.27%; and for acid-insoluble lignin values, from 15.8% to 20.6%.

AE were lower than 3% for Otilia and Izvor varieties, while for the Sorial variety, a value of 4% was recorded. This includes waxes, fats, resins, and sterols. The extraction was performed using acetone; thus, the current study-reported-data have smaller values than the standard ethanol–benzene mixture until recently [61,62]. The content of hot water extractives indicates the biomass's soluble organic materials (tannins, gums, soluble non-structural sugars, starch, and coloring substances) or inorganics, such as salts or nitrogenous material [63,64]; and the current obtained values are comparable to literature data [61].

The ash content is proportional to the amount of mineral substances present, and it is higher in non-wood biomass samples than in wood biomass samples. The experimental values obtained are consistent with those reported by other authors in similar studies [20].

3.2. Screening Phase for Extraction of Hemicellulose from Wheat Straw

The results displayed in Table 3 offer a comparative view of the proposed extractive treatment results. FT represents the freeze–thaw pretreatment stage; the number of cycles is given by the associated number (e.g., FT 2 indicates that the sample underwent two freeze–thaw cycles). HA 40-90 is the hot alkali extraction stage, where the former represents the time, while the latter represents the temperature, in Celsius degrees. US10-30 and US20-45 indicate ultra-sonication for 10 and 20 min at 30 °C and 45 °C, respectively. MW 10-100 represents microwave-assisted heating in an alkaline environment at 10 min and 100 °C.

Table 3. The effect of freeze–thawing cycles on the subsequent yields obtained in alkaline extraction.

Sample Treatment	TY (%)	XY (%)	HCY (%)	YAIL (%)	YASL (%)
HA 40-90	42.21	24.16	34.03	25.9	27.5
HA 40-100	44.2	36.1	35.8	32.08	35.1
FT2	7.50	3.72	3.08	2.68	0.89
US10-30	31.33	4.38	9.28	19.16	11.22
US20-45	34.40	21.67	21.96	24.85	18.9
MW 10-100	52.18	31.51	31.39	29.40	19.91
FT 1 HA 40-90	45.2	58.41	60.02	23.69	37.81
FT 2 HA 40-90	47.3	61.75	63.43	25.66	39.8
FT 3 HA 40-90	46.6	58.19	56.51	23.66	38.2
FT 4 HA 40-90	45.1	56.68	54.80	24.23	38.9

The data shows that the freeze–thawing cycles enhance the alkaline extraction process, while the microwave heating or ultrasound treatment acts as a standalone extraction process. Applying microwave heating or ultrasound irradiation in an alkaline solution (with the mechanisms detailed in Section 3.6.) has similar effects to classic HA. However, the yields strongly depend on the irradiation time and frequency. Both procedures reduce the treatment time; however, temperature control is difficult and specialized equipment is required, which limits its wide adaptation in various settings.

Freeze–thawing alone removes only a tiny amount of xylan and hemicelluloses, probably water-soluble fractions, together with some lignin. Regarding the number of freeze–thaw cycles, the most effective extraction occurred after two cycles. Considering the simplicity of the laboratory setup and its potential for up-scaling, the sequence consisting of two freeze–thaw cycles, followed by hot alkaline extraction (FT 2 HA) was chosen for modeling, optimization, and product characterization.

3.3. The Influence of Extraction Parameters

The central composite experimental design and results for FT 2 HA are displayed in Table 4. First- and second-order polynomial regression equations were used to fit the experimental data. The equations were simplified by removing some non-significant terms, while maintaining the model hierarchy. The proposed relationships between the extraction yields (total extraction yield, xylan extraction yield, total hemicelluloses removal and lignin removal, and parameters are shown in Equations (7)–(11) (all p-values were less than 0.05). The detailed ANOVA analysis and the statistical indicators for these models are presented in Tables S1–S5.

$$\text{TY } (\%) = -6.01X_1^2 + 0.267X_2^2 + 31.8X_1 - 0.676X_2 - 0.264X_1X_2 + 10.4; R^2 = 0.97 \quad (7)$$

$$XY\ (\%) = 21.4X_1 + 11.4X_2 - 2.08X_1X_2 - 30.5;\ R^2 = 0.95 \quad (8)$$

$$\text{HCY } (\%) = 15.9X_1 + 8.95X_2 - 1.1X_1X_2 - 17.5; R^2 = 0.94 \quad (9)$$

$$\text{YAIL } (\%) = 70.4 - 84.1X_1 + 3.11X_2 + 1.44X_1X_2 + 24X_1^2 - 0.267X_2^2; R^2 = 0.97 \quad (10)$$

$$\text{YASL } (\%) = -4.99X_1 - 0274X_2 + 2.01X_1X_2 + 27.2;\ R^2 = 0.89 \quad (11)$$

Figure 1 shows the tridimensional surface obtained for the total yield variation due to SF and sodium hydroxide concentration. Increasing both SF and CNaOH resulted in an increase of TY (%). At a constant value of 3% NaOH, a variation of 1 unity for SF leads to a nearly 27% rise in TY (%). The maximum value for the total extraction yield is obtained for an SF of 2.5. Over this value, TY (%) slightly decreases regardless of the alkali concentration, which can be explained by the NaOH consumption in concurrent reactions. To highlight the effect of CNaOH, the SF was held constant. At SF = 1, the increase of alkali concentration from 3 to 7 leads to a rise in TY (%) of 19.3%. The same rising trend is observed at higher SF values; however, the % is lower (12.1% for SF = 2 and 9.6% for SF = 3). Overall, SF has a higher impact on total extraction yield than CNaOH.

Table 4. Experimental results and conditions of hot alkaline extraction of wheat straw.

Exp.	SF	CNaOH (%)	TY (%)	XY (%)	HCY (%)	YAIL (%)	YASL (%)
1	1	3	34.86	15.24	19.24	19.67	28.42
2	2	3	49.79	34.75	34.87	13.65	24.66
3	3	3	49.58	50.15	48.28	56.05	28.77
4	1	7	41.60	52.57	50.72	27.55	32.19
5	2	7	56.01	63.84	61.70	26.24	45.89
6	3	7	54.21	70.84	70.98	75.46	48.56
7	1	5	40.22	49.65	49.06	38.59	31.44
8	3	5	51.43	55.60	57.23	60.21	44.86
9	2	5	49.76	48.44	46.98	20.97	36.30
10	2	5	50.55	54.32	52.23	21.03	34.93
11	2	5	49.73	49.68	42.46	20.77	39.04
12	2	5	50.36	45.11	47.10	25.94	35.62
113	2	5	50.22	49.18	48.45	19.67	36.30

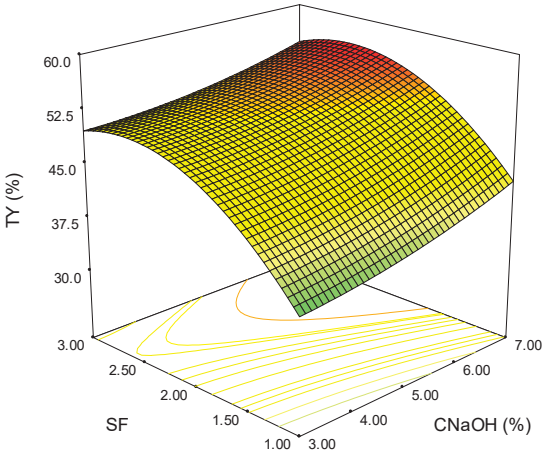

Figure 1. Variation of the total extraction yield as a function of severity factor and alkali concentration (the colours green-yellow-red indicate the shift from low to high values).

Figure 2 shows the response surface plot obtained for the homoxylan yield variation in relation to alkali concentration and severity factor. As can be observed, the maximum XY (%) value is obtained at SF = 3 and CNaOH = 7%. Distinctively from the TY (%) where the maximum was at SF = 2.5, indifferent of alkali concentration, in this case, both parameters have a significant influence on extraction yield. Due to the considerable impact of both parameters, the homoxylan yield does not reach a plateau as for TY (%). The total effect of the two parameters has a more substantial impact on XY (%) than either of them would have on their own.

Figure 3 shows the response surface of the model for the total hemicelluloses extraction yield. Similar behavior as in the case of XY (%) can be observed for HCY (%); the highest extraction yield being obtained at maximum values for SF and CNaOH. However, the individual influence of the considered variables is slightly different (indicated by the slopes of the surface in relation to each parameter).

Figure 4 displays the variation of YAIL (%) on the model parameters. At lower values of SF (interval 1–2), the variation has a non-linear trend; and the extraction efficiency is minimum, the increase of SF to 2 leading to a decrease in extraction yield (negative slope). On the other hand, the raise of SF to 3 leads to a rapid YAIL (%) increase (positive slope). Although the CNaOH has a low influence on the overall performance, the maximum YAIL (%) is reached at the highest alkali concentration (red-colored surface).

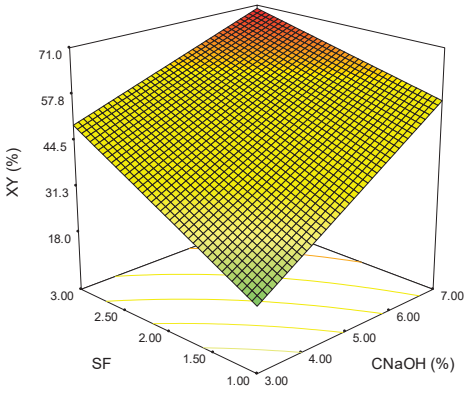

Figure 2. Variation of homoxylan extraction yield as a function of severity factor and alkali concentration (the colours green-yellow-red indicate the shift from low to high values).

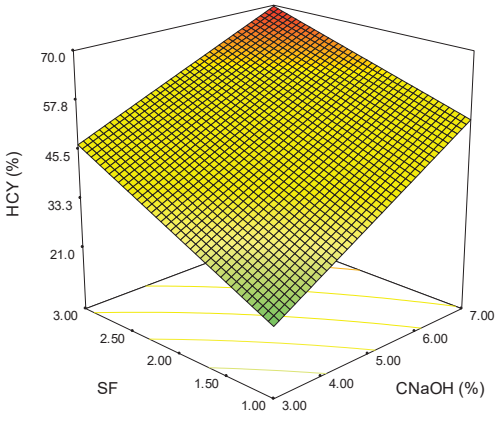

Figure 3. Variation of the total hemicelluloses extraction yield with severity factor and alkali concentration (the colours green-yellow-red indicate the shift from low to high values).

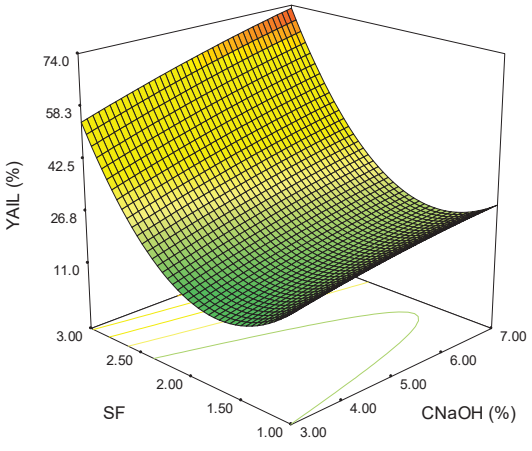

Figure 4. Variation of the acid-insoluble lignin removal yield on severity factor and alkali concentration (the colours green-yellow-red indicate the shift from low to high values).

The response surface plot for the variation of the acid-insoluble lignin removal yield is shown in Figure 5. In this case, it can be observed that the individual effects of SF and CNaOH are reduced in comparison with their combined effect. When SF = 2, YASL (%) ranges from 28.5% to 43.4% for the entire alkali concentration interval, while when CNaOH = 5, the acid-soluble lignin removal yield varies from 30.9% to 40.9% for the entire SF domain. The highest removal efficiency of the acid-soluble lignin is obtained for SF = 3 and CNaOH = 7.

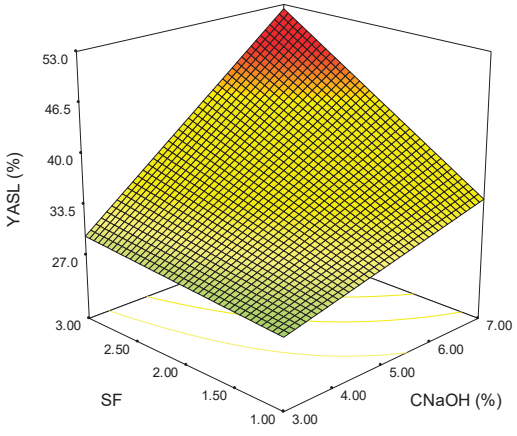

Figure 5. Variation of the acid-soluble lignin removal yield as a function of severity factor and alkali concentration (the colours green-yellow-red indicate the shift from low to high values).

Although the maximum extraction yields are obtained at the maximum values of SF and CNaOH for all the analyzed outputs, the shape of the surface plots suggests a linear dependence for homoxylan, hemicellulose, and the soluble acid lignin (Figures 2, 3 and 5). In contrast, for total extraction and acid-insoluble lignin (Figures 1 and 4), there is a non-linear dependence. This aspect can also be observed by analyzing the determined mathematical models and the ANOVA reports (Tables S1–S5).

3.4. Process Optimization

After determining the models and the impact of each individual parameter was analyzed, the process was optimized considering two cases: (i) the experimental limits (this will be further referred to as O1); and (ii) extrapolation for CNaOH to 9 % (this will be further referred as O2). In both cases, multiple objectives were considered in such a manner to obtain a maximum TY (%), XY (%), HCY (%), and a minimum YAIL (%) of YASL (%). In addition, the minimization of these two outputs was considered because higher amounts of lignin in alkaline extraction liquors hinder the hemicellulose-graded ethanol separation stage. The results obtained are presented in Table 5. For O1, a severity factor of 1.63 was identified. The experimental parameters were set at 100 °C and 43 min to obtain this value. For O2, the severity factor was 1.44, corresponding to 100 °C and 25 min.

Table 5. The optimized conditions of wheat straw hemicellulose extraction and obtained experimental results.

		TY (%)	XY (%)	HCY (%)	YAIL (%)	YASL (%)
O1	Predicted model parameters			CNaOH = 7%; SF = 1.63		
	Predicted results	51.56	59.97	57.07	21.58	39.60
	Experimental validation	49.94	62.56	61.25	20.72	38.63
O2	Predicted model parameters			CNaOH = 9%; SF = 1.44		
	Predicted result	55.9	67.71	63.69	24.10	23.62
	Experimental validation	50.34	52.20	52.05	19.64	19.70

As can be observed from Table 5, in the case of extrapolation (O2), the errors between the predicted and the experimental values are higher than for O1. This is because extrapolation has a higher uncertainty and assumes the same dynamic occurs as in the experimentally verified interval, which is not necessarily true for real-world processes.

3.5. Product Characterization

3.5.1. Component Identification

Table 6 indicates the main components of the hemicelluloses obtained through the experimental verification of the solutions provided by the optimization procedure. HC stands for hemicelluloses obtained from the wheat straw by alkaline extraction using optimized conditions and without performing the freeze–thaw cycles. The notations HC_O1 and HC_O2 were assigned for the hemicelluloses separated from alkaline extractive treatment liquor preceded by two freeze–thaw cycles for O1 and O2, respectively. As can be observed from Table 6, the freeze–thaw cycle seems to favor the xylan extraction yield versus the arabinan extraction yield.

Table 6. Main chemical components of hemicelluloses preparations isolated from wheat straw.

Sample	Glucan (%)	Xylan (%)	Arabinan (%)	Purity (%)
HC_C (control)	3.61	77.50	13.14	94.25
HC_O1	3.40	85.51	7.89	96.80
HC_O2	2.61	83.92	10.02	96.55

3.5.2. FTIR Analysis

The infrared spectra of wheat straw hemicellulose samples are presented in Figure 6. Figure S1 shows the complete spectra for the analyzed samples. The band occurring at ~1645 cm^{-1} was assigned to the absorbed water [64]. The absorptions at ~1550 cm^{-1} are probably caused by impurities such as co-separated lignin. Peaks shown at about 1460 cm^{-1} were assigned to the presence of the methyl groups. Peaks visible at ~1100 and ~1045 cm^{-1} result from C-O stretching in C-O-C ether linkages (the first is inter-sugar units; and the second is from intra-sugar, in the alcoholic functional group). The ~898 cm^{-1} peak is specific to β-1-4 bonds between xylose units of the xylan chain and is caused by the stretching vibration modes (both symmetric and antisymmetric) of C-O in this linkage [41].

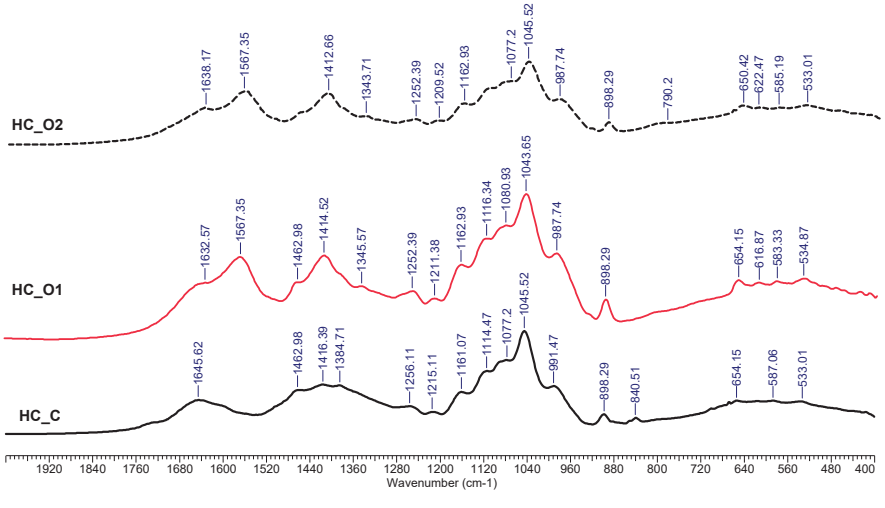

Figure 6. FTIR spectra of hemicelluloses separated from wheat straw by using different sequences.

Other bands at lower wavenumbers, such as ~690 cm^{-1}, were attributed to the CH deformations—out of the plane. Peaks at ~3400 cm^{-1}—stretching vibrations of O-H groups; the ~2950 cm^{-1} to -CH_2 antisymmetric stretching, while the 2850 cm^{-1} results from -CH_2 symmetric stretching.

3.5.3. ^{1}H-NMR Spectroscopy Analysis

Figure 7 shows the results obtained by ^{1}H-NMR spectroscopy. The displayed spectra include three regions: (i) the region of α-anomers in the range 5.5–4.9 ppm; (ii) β-anomers' region assigned in the interval 4.9–4.4 ppm; and (iii) the β-(1-4)-D-anhidroxylopyranose units heterocycle proton region 4.4–3.0 ppm [65]. The first region includes signals for α-L arafuranosyde residues assigned to the anomeric $H1_{Ara}$ at 5.4 ppm and for the $H4_{Ara}$ proton assigned at 4.3 ppm. The second region displays signals for non-substituted xylose units (4.49 ppm) and for glucuronic-acid-substituted β-xylose (4.64 ppm) [66–68]. For the third region, the assignment was considered as follows: $H2_{Ara}$—4.11 ppm; $H3_{Ara}$—3.75 ppm; $H5_{Ara}$—3.68 ppm for the α-L arafuranosyde residues (Ara); and $H5_{eq\ X}$—4.11 ppm, $H4_X$—3.80 ppm, $H3_X$—3.56 ppm, $H5_{ax}$—3.38 ppm, $H2_X$—3.30 ppm for the β-D-xylopyranoside residues (X).

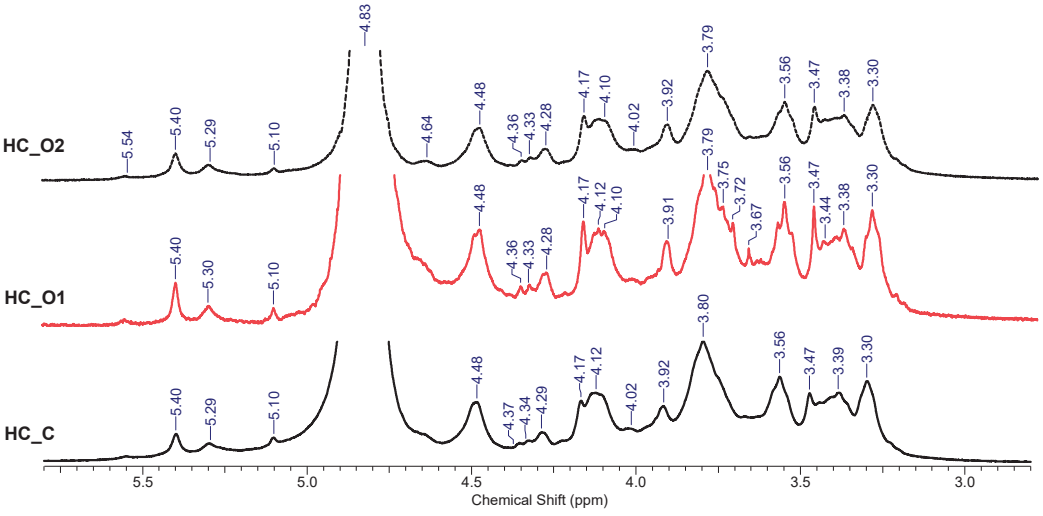

Figure 7. ^{1}H-NMR spectra of hemicelluloses separated from wheat straw.

3.5.4. Thermogravimetric Analysis

As Nurazzi et al. noted in their literature review on TG analysis of cellulose fiber and respective composites, hemicelluloses have typically lower decomposition temperatures than lignin [69]. Similar conclusions were previously highlighted by other authors, which showed that the biomass component decomposition temperatures increase in the order of hemicelluloses (max. weight loss 220–315 °C) < cellulose (max. weight loss 315–400 °C) < lignin (degradation extended up to 900 °C) [70].

Regarding the results obtained for the analyzed hemicelluloses, several phases are visible in the case of the mass variation graphs (Figure 8a,b). For the HC_C sample, the water removal (dehydration phase) occurs in two steps: one between 48 °C and 120 °C (mass removed yielded ~8.57%), and a short secondary step between 120 °C and 132 °C (with a DTG peak at 126 °C). Samples HC_O1 and HC_O2 displayed a single-step dehydration within the 50 °C to 101 °C range; and peaks on DTG curves occurring at 77 °C and 70 °C, respectively. The computed values of the mass loss were 15.8% for HC_O1 and 12.8% for HC_O2.

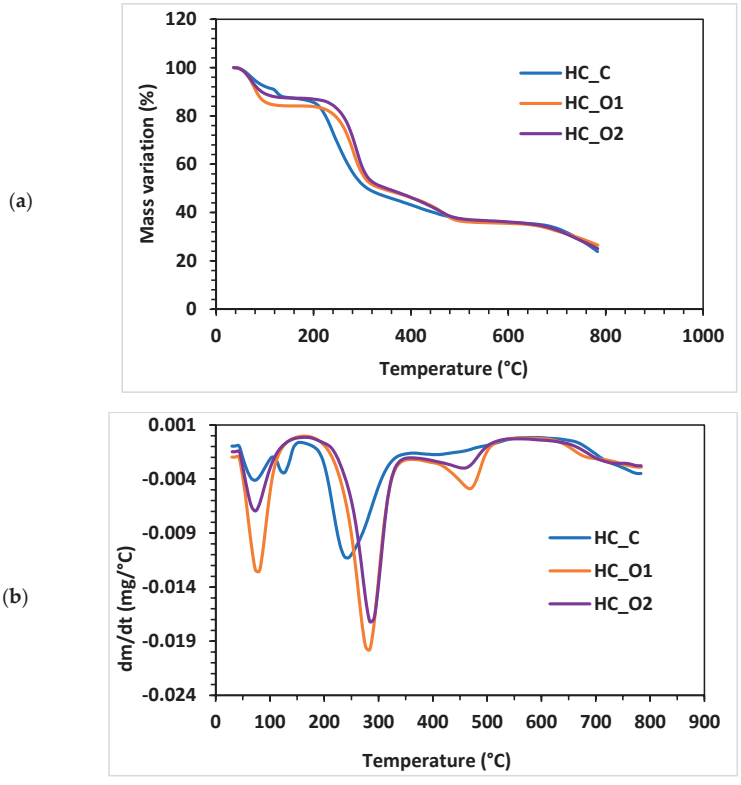

Figure 8. Thermogravimetric analysis: (**a**) mass-variation curves; (**b**) DTG curves.

The second stage of the thermo-gravimetric test corresponds to the polymeric chain degradation phase. For the HC_C sample, this occurs between 215 °C and 295 °C, with a mass loss of ~41% and a peak at 234 °C. HC_O1 and HC_O2 showed a degradation phase occurring in similar temperature ranges: (i) 248–303 °C for HC_O1 with a DTG peak observed at 283 °C, 37.6% mass loss; and (ii) 258–309 °C for HC_O2 with a peak at 290 °C and 39.3% mass loss. The higher temperatures of corresponding HC_O1 and HC_O2 peaks during the second stage compared with HC_C indicate their better thermal stability.

In the final stage of thermal decomposition, the oxidation of the remaining char occurs. The HC_C recorded range was 360–503 °C with a peak at 414 °C (~11% mass loss). The analysis of HC_O1 and HC_O2 revealed a similar interval of 360–490 °C with peaks at 490 °C (~12% mass loss).

Peng and Wu [71] proposed a mechanism for the breakdown of the hemicellulose polymer chain that involves dehydration, fragmentation of side chains, decarboxylation and decarbonylation, and charring. Carbon dioxide, acetic acid, and pentanal are the most widely encountered degradation products; and they are all released above 250 °C in varying amounts during the various stages of decomposition [71]. In the current work, the identified peaks are in accordance with literature data [69,71], and the hemicellulose samples showed thermal stabilities comparable with xylan-based polysaccharides [40,72–74].

3.6. Mechanism of Complementary Pretreatments and Comparison with Similar Studies

3.6.1. Freeze–Thaw Cycles

Freeze–thaw effects are of a mechanical nature, based on the water's property to expand volume when frozen. Ice formation may expand, distort, and finally disrupt biomass pores, hastening deterioration [75]. FT is considered a "green" procedure that

does not require chemicals or a lot of energy. Furthermore, FT cycles occur naturally in a variety of areas around the world without the need for energy [52]. Contrariwise, a significant amount of energy is required in other parts of the world to achieve and maintain the required temperature. Table 7 shows a comparative analysis of literature examples that investigated FT potential as a complementary pretreatment method. As can be observed, the results obtained in this study for two cycles of FT followed by alkaline extraction fit the trends presented in the literature. In addition, the proposed method has the benefit of a significantly reduced freezing time, which directly correlates with a reduction in energy consumption.

Table 7. Comparison of freeze–thaw enhancement of agro-waste biomass pretreatments.

Biomass Type	Extraction Procedure	No. of FT Cycles	Temperature (°C)	Freezing Time (h)	Reported Extraction Yields *	Reference No., Year
wheat straw	enzymatic hydrolysis	1	−10 −20 −40 −80	12, 24, 48, 96	57.06% cellulose, 70.66% hemicelluloses	[75], 2022
wheat straw	enzymatic hydrolysis	1	−20	48	75.95% cellulose and hemicelluloses	[52], 2012
wheat straw	enzymatic hydrolysis	2	−20	12	67% cellulose and hemicelluloses	[10], 2013
bamboo chips	alkaline extraction	1	−30	12	64.71% hemicelluloses	[76], 2021
bamboo chips	alkaline extraction	1	−20 −30 −40 −50 −60 −70	12	73.26% hemicelluloses	[77], 2022
wheat straw	FT standalone alkaline extraction FT + alkaline extraction	2	−22	1	3.8% hemicelluloses 34.03% hemicelluloses 63.43% hemicelluloses	this work, 2023

* Highest reported values.

3.6.2. Microwave Pretreatments

Unlike conventional ovens that transmit heat by conduction–convection mechanisms, exposure to a microwave field generates heat inside the material, the heat transfer and energy yield being significantly higher. Microwaves do not directly affect the molecular structure, and heat propagation is realized by two mechanisms: ionic conduction and dipole rotation [78]. During microwave pretreatments of lignocellulosic biomass, the structure of the biomass can be swelled and fractured due to microwave-generated oscillations: dipolar rotation and molecular collisions [79]. The presence of water speeds up heat transfer and improves the hydrolysis process. The "thermal" and/or "non-thermal" effects of MW are still under debate [46,80]. The main advantages of MW complementary treatments are: reduction in chemical consumption, energy, and reaction time [26,46,78]. However, there are a few drawbacks related to the unequal distribution of microwave power inside non-homogeneous materials that may generate hot spots (local overheating); the energy absorption depends upon the dielectric properties of the material [78]. Table 8 presents a comparative analysis of MW-assisted wheat straw alkaline extraction. The difference in efficiency between the reported data and the results obtained in this work is because no additional treatment was applied (HA), which indicates that MW can be used as a standalone extraction procedure. It is worth mentioning that the reported yield was obtained only after 10 min of MW.

Table 8. Comparison of MW-assisted wheat straw alkaline extraction.

Alkali Concentration Range (%wt)	Temperature Range (°C)	Time Range (Minutes)	Reported Yields *	Reference No., Year
0.5–2.5	120–200	5–25	69.48% of lignin solubilized	[79], 2019
1–5	60–140	5–80	90.66% purity of cellulose	[46], 2021
2–5	60–140	10–60	80% of hemicelluloses 90% of lignin	[81], 2012
5	100	10	31.39% hemicelluloses	this work, 2023

* Highest reported values.

3.6.3. Ultrasound Pretreatments

Ultrasound exposure can generate both physical and chemical effects. Cavitation phenomena (formation, growth, and implosive bubble collapse) produce huge temperatures and high pressures for extremely short periods [82]. The corresponding shock waves enhance energy and mass transfer. Acoustic cavitation at high frequencies generates highly reactive free radicals, such as hydroxyl, superoxide, or singlet oxygen [83]. The main features of US employment as complementary pretreatment are reducing processing time, lowering the temperature and pressure, and diminishing the amount of chemicals [41]. The main drawbacks of US-assisted pretreatments are related to the sonic field's uniformity and reduced possibilities of upscaling the procedure, caused by the transducers overheating [41,82]. Nevertheless, some modern ultrasound reactors equipped with multiple transducers can surpass these inconveniences [41,82]. Table 9 shows that US pretreatment alone has a reasonable extraction yield concerning the time used.

Table 9. Comparison of US-assisted wheat straw pretreatments.

Extraction Procedure	US Frequency (kHz)	Power (W)	Time, (Minutes)	Solvent	Reported Extraction Yields *	Reference No., Year
enzymatic hydrolysis	40 25	200 2000 3000	60, 120	water, diluted H_2SO_4, diluted NaOH	59.2% lignin removal	[41], 2022
organosolv	20	100	5, 10, 15, 20, 25, 30, 35	solution NaOH/methanol/water	78.5% lignin removal	[84], 2002
deep eutectic solvents	40	200	60, 120	acetic acid/glycerol/choline chloride γ-valerolactone/water	27% delignification	[85], 2018
ammonia	20	180, 270, 450, 540, 650	15, 30, 45, 60, 90	water	92% saccharification	[19], 2017
alkaline extraction	20	100	5, 10, 15, 20, 25, 30, 35	KOH	solubilization 91.6% hemicelluloses, 91.4% lignin	[86], 2005
standalone ultrasonic treatment	40	50	10 20	NaOH	9.28% hemicelluloses 21.96% hemicelluloses	this work, 2023

* Highest reported values.

3.6.4. SEM Analysis

The samples' surface morphology, studied at 200 × magnification and at a working distance of about 42 mm, are presented in Figure 9a–d. Figure 9a shows the secondary electrons image of wheat straw without any treatment. The damaging effect of alkali on the straw protective shell, exposing the inner fibers, is revealed in Figure 9b. Figure 9c demonstrates the disruptive effects of ice formation during freezing, as discussed in Section 3.6.1. Finally, the combination of freezing and alkali effects are displayed in Figure 9d, where it

can be observed that the fibers and cells are exposed and fractured. Since freezing causes mechanical damage, it sets the stage for alkaline action deep within the material.

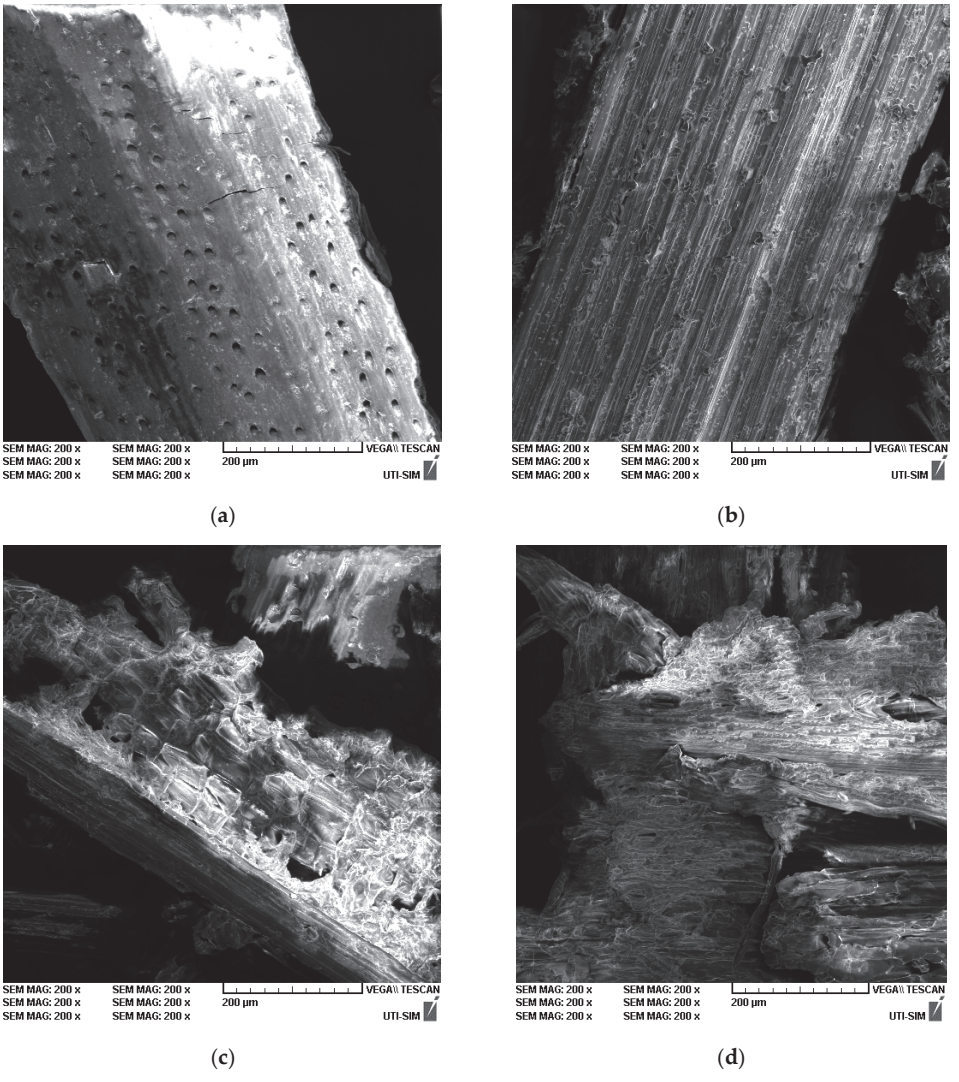

Figure 9. SEM images of wheat straw after various treatments: (**a**) wheat straw without any treatment; (**b**) wheat straw after alkali treatment; (**c**) wheat straw after the freeze–thaw cycle; (**d**) wheat straw after freeze–thaw and alkali treatment.

4. Conclusions

The performance of three complementary pretreatments: freeze–thaw cycles, ultrasound, and microwaves, was investigated in an experimental trial for the hot alkaline extraction of hemicelluloses from wheat straw. During trials, it was discovered that two freeze–thaw cycles are sufficient to achieve satisfactory extraction yields.

The severity factor and alkali concentration were subsequently considered variables in a multi-objective optimization study for two freeze–thaw cycles followed by hot alkaline extraction. The predicted values were experimentally validated: (i) considering an optimal

value within the range of process parameters; and (ii) considering an optimal value that extrapolates the process parameters. For the first case, the optimal conditions are represented by CNaOH = 7% and SF = 1.63. The hemicelluloses obtained in these conditions were then analyzed for purity (96.8%); and glucan (3.40%), xylan (85.51%), and arabinan (7.89%) content.

Although microwaves and ultrasounds outperformed the freeze–thaw procedure in terms of extraction yields, technical issues, such as temperature control, energy consumption, simplicity, the possibility of preserving the polymeric structure of the resulting materials, and upscaling perspectives, recommend the combination of classic hot alkaline extraction with freeze–thaw pretreatments for wheat straw processing.

Supplementary Materials: The following supporting information can be downloaded at: https://www.mdpi.com/article/10.3390/polym15041038/s1, Figure S1: Complete FTIR spectra of separated hemicelluloses; Table S1: ANOVA analysis results for the response model of the total extraction yield TY (%);Table S2 ANOVA analysis results for the response model of the xylan extraction yield XY (%); Table S3 ANOVA analysis results for the response model of the total hemicelluloses extraction yield HCY (%); Table S4 ANOVA analysis results for the response model of the acid insoluble lignin removal yield YAIL (%); Table S5 ANOVA analysis results for the response model of the acid soluble lignin removal yield YASL (%).

Author Contributions: Conceptualization and hemicelluloses extraction study, A.C.P. and G.D.S.; thermo-gravimetric analysis, M.D.; NMR spectroscopy, G.-L.A.; FTIR spectroscopy and HPLC analysis, A.C.P.; SEM analysis, D.-L.C.; sample preparation, C.D.B.; writing—review and editing, A.C.P., E.N.D. and M.T.N. All authors have read and agreed to the published version of the manuscript.

Funding: This work was supported by a grant from the Ministry of Research, Innovation, and Digitization, CCCDI-UEFISCDI; project number PN-III-P2-2.1-PED-2021-3384, within PNCDI III.

Institutional Review Board Statement: Not applicable.

Informed Consent Statement: Not applicable.

Data Availability Statement: The data supporting the reported results are presented in the manuscript.

Conflicts of Interest: The authors declare no conflict of interest. The funders had no role in the design of the study; in the collection, analyses, or interpretation of data; in the writing of the manuscript; or in the decision to publish the results.

References

1. Akbarian, A.; Andooz, A.; Kowsari, E.; Ramakrishna, S.; Asgari, S.; Cheshmeh, Z.A. Challenges and opportunities of lignocellulosic biomass gasification in the path of circular bioeconomy. *Bioresour. Technol.* **2022**, *362*, 127774. [CrossRef]
2. Gil, A. Challenges on waste-to-energy for the valorization of industrial wastes: Electricity, heat and cold, bioliquids and biofuels. *Environ. Nanotechnol. Monit. Manag.* **2022**, *17*, 100615. [CrossRef]
3. Babu, S.; Singh Rathore, S.; Singh, R.; Kumar, S.; Singh, V.K.; Yadav, S.K.; Yadav, V.; Raj, R.; Yadav, D.; Shekhawat, K.; et al. Exploring agricultural waste biomass for energy, food and feed production and pollution mitigation: A review. *Bioresour. Technol.* **2022**, *360*, 127566. [CrossRef]
4. Popp, J.; Kovács, S.; Oláh, J.; Divéki, Z.; Balázs, E. Bioeconomy: Biomass and biomass-based energy supply and demand. *New Biotechnol.* **2021**, *60*, 76–84. [CrossRef]
5. McKendry, P. Energy production from biomass (part 2): Conversion technologies. *Bioresour. Technol.* **2002**, *83*, 47–54. [CrossRef]
6. Gallezot, P. Conversion of biomass to selected chemical products. *Chem. Soc. Rev.* **2012**, *41*, 1538–1558. [CrossRef]
7. Qian, H.; Chen, W.; Zhu, W.; Liu, C.; Lu, X.; Guo, X.; Huang, D.; Liang, X.; Kontogeorgis, G.M. Simulation and evaluation of utilization pathways of biomasses based on thermodynamic data prediction. *Energy* **2019**, *173*, 610–625. [CrossRef]
8. Bian, H.; Yang, Y.; Tu, P.; Chen, J.Y. Value-Added Utilization of Wheat Straw: From Cellulose and Cellulose Nanofiber to All-Cellulose Nanocomposite Film. *Membranes* **2022**, *12*, 475. [CrossRef]
9. Talebnia, F.; Karakashev, D.; Angelidaki, I. Production of bioethanol from wheat straw: An overview on pretreatment, hydrolysis and fermentation. *Bioresour. Technol.* **2010**, *101*, 4744–4753. [CrossRef]
10. Wang, X.M.; Wang, L.J.; Yu, M.; Chen, H. Freeze-Thaw and Sulfuric Acid Pretreatment of Wheat Straw for Fermentable Sugar Release. *Adv. Mater. Res.* **2013**, *724–725*, 257–260. [CrossRef]
11. Rahmani, A.M.; Tyagi, V.K.; Gunjyal, N.; Kazmi, A.A.; Ojha, C.S.P.; Moustakas, K. Hydrothermal and thermal-alkali pretreatments of wheat straw: Co-digestion, substrate solubilization, biogas yield and kinetic study. *Environ. Res.* **2023**, *216*, 114436. [CrossRef]

12. Rodríguez-Sanz, A.; Fuciños, C.; Torrado, A.M.; Rúa, M.L. Extraction of the wheat straw hemicellulose fraction assisted by commercial endo-xylanases. Role of the accessory enzyme activities. *Ind. Crops Prod.* **2022**, *179*, 114655. [CrossRef]
13. Huang, L.-Z.; Ma, M.-G.; Ji, X.-X.; Choi, S.-E.; Si, C. Recent Developments and Applications of Hemicellulose From Wheat Straw: A Review. *Front. Bioeng. Biotechnol.* **2021**, *9*. [CrossRef]
14. Ingrao, C.; Matarazzo, A.; Gorjian, S.; Adamczyk, J.; Failla, S.; Primerano, P.; Huisingh, D. Wheat-straw derived bioethanol production: A review of Life Cycle Assessments. *Sci. Total Environ.* **2021**, *781*, 146751. [CrossRef]
15. Jaffar, M.; Pang, Y.; Yuan, H.; Zou, D.; Liu, Y.; Zhu, B.; Korai, R.M.; Li, X. Wheat straw pretreatment with KOH for enhancing biomethane production and fertilizer value in anaerobic digestion. *Chin. J. Chem. Eng.* **2016**, *24*, 404–409. [CrossRef]
16. Townsend, T.J.; Sparkes, D.L.; Ramsden, S.J.; Glithero, N.J.; Wilson, P. Wheat straw availability for bioenergy in England. *Energy Policy* **2018**, *122*, 349–357. [CrossRef]
17. Liu, Y.; Ahmed, S.; Sameen, D.E.; Wang, Y.; Lu, R.; Dai, J.; Li, S.; Qin, W. A review of cellulose and its derivatives in biopolymer-based for food packaging application. *Trends Food Sci. Technol.* **2021**, *112*, 532–546. [CrossRef]
18. Sui, Y.; Cui, Y.; Wang, Y.; Zeb, S.; Sun, G. A green and efficient way to improve sugar recovery of wheat straw by ultrasonic-assisted xylanase pretreatment. *Biomass Convers. Biorefin.* **2021**. [CrossRef]
19. Zhong, C.; Jia, H.; Wei, P. Enhanced saccharification of wheat straw with the application of ultrasonic-assisted quaternary ammonium hydroxide pretreatment. *Process Biochem.* **2017**, *53*, 180–187. [CrossRef]
20. Serna-Loaiza, S.; Adamcyk, J.; Beisl, S.; Miltner, M.; Friedl, A. Sequential Pretreatment of Wheat Straw: Liquid Hot Water Followed by Organosolv for the Production of Hemicellulosic Sugars, Lignin, and a Cellulose-Enriched Pulp. *Waste Biomass Valorization* **2022**, *13*, 4771–4784. [CrossRef]
21. Tian, S.-Q.; Zhao, R.-Y.; Chen, Z.-C. Review of the pretreatment and bioconversion of lignocellulosic biomass from wheat straw materials. *Renew. Sustain. Energy Rev.* **2018**, *91*, 483–489. [CrossRef]
22. Gou, G.; Meng, F.; Wang, H.; Jiang, M.; Wei, W.; Zhou, Z. Wheat straw-derived magnetic carbon foams: In-situ preparation and tunable high-performance microwave absorption. *Nano Res.* **2019**, *12*, 1423–1429. [CrossRef]
23. Liu, R.; Yu, H.; Huang, Y. Structure and morphology of cellulose in wheat straw. *Cellulose* **2005**, *12*, 25–34. [CrossRef]
24. Gao, C.; Yang, J.; Zhang, H.; Xiao, W.; Han, L. Quantitative and qualitative characterization of dual scale mechanical enhancement on cellulosic and crystalline-structural variation of NaOH treated wheat straw. *Bioresour. Technol.* **2020**, *312*, 123535. [CrossRef]
25. Gao, Y.; Guo, M.; Wang, D.; Zhao, D.; Wang, M. Advances in extraction, purification, structural characteristics and biological activities of hemicelluloses: A review. *Int. J. Biol. Macromol.* **2022**, *15*, 467–483. [CrossRef]
26. Mohammad Rahmani, A.; Gahlot, P.; Moustakas, K.; Kazmi, A.A.; Shekhar Prasad Ojha, C.; Tyagi, V.K. Pretreatment methods to enhance solubilization and anaerobic biodegradability of lignocellulosic biomass (wheat straw): Progress and challenges. *Fuel* **2022**, *319*, 123726. [CrossRef]
27. Huang, C.; Xu, C.; Meng, X.; Wang, L.; Zhou, X. Isolation, Modification, and Characterization of the Constituents (Cellulose, Hemicellulose, Lignin, et al.) in Biomass and Their Bio-Based Applications. *Front. Bioeng. Biotechnol.* **2022**, *10*, 866531. [CrossRef]
28. Goodman, B.A. Utilization of waste straw and husks from rice production: A review. *J. Bioresour. Bioprod.* **2020**, *5*, 143–162. [CrossRef]
29. Zhang, L.; Larsson, A.; Moldin, A.; Edlund, U. Comparison of lignin distribution, structure, and morphology in wheat straw and wood. *Ind. Crops Prod.* **2022**, *187*, 115432. [CrossRef]
30. Zheng, Q.; Zhou, T.; Wang, Y.; Cao, X.; Wu, S.; Zhao, M.; Wang, H.; Xu, M.; Zheng, B.; Zheng, J.; et al. Pretreatment of wheat straw leads to structural changes and improved enzymatic hydrolysis. *Sci. Rep.* **2018**, *8*, 1321. [CrossRef]
31. Chen, Z.; Wang, Y.; Cheng, H.; Zhou, H. Hemicellulose degradation: An overlooked issue in acidic deep eutectic solvents pretreatment of lignocellulosic biomass. *Ind. Crops Prod.* **2022**, *187*, 115335. [CrossRef]
32. Lou, R.; Zhang, X. Evaluation of pretreatment effect on lignin extraction from wheat straw by deep eutectic solvent. *Bioresour. Technol.* **2022**, *344*, 126174. [CrossRef]
33. Zhang, C.; Guo, K.-N.; Ma, C.-Y.; Bian, J.; Wen, J.-L.; Yuan, T.-Q. Assessing the availability of bamboo (Phyllostachys pubescens) fibers and parenchyma cells for producing lignin nanoparticles and fermentable sugars by rapid carboxylic acid-based deep eutectic solvents pretreatment. *Ind. Crops Prod.* **2023**, *193*, 116204. [CrossRef]
34. Yu, Y.; Wang, D.; Chen, L.; Qi, H.; Liu, A.; Deng, M.; Wu, X.; Wang, K. Recyclable choline chloride-based deep eutectic solvent pretreatment for accelerated enzymatic digestibility of Triarrhena lutarioriparia. *Ind. Crops Prod.* **2022**, *187*, 115542. [CrossRef]
35. Deng, Z.; Xia, A.; Liao, Q.; Zhu, X.; Huang, Y.; Fu, Q. Laccase pretreatment of wheat straw: Effects of the physicochemical characteristics and the kinetics of enzymatic hydrolysis. *Biotechnol. Biofuels* **2019**, *12*, 159. [CrossRef]
36. Tan, J.; Tiwari, S.K.; Ramakrishna, S. Single-Use Plastics in the Food Services Industry: Can It Be Sustainable? *Mater. Circ. Econ.* **2021**, *3*, 7. [CrossRef]
37. Sitch, D.A.; Marshall, H.B. The effect of hemicelluloses on the papermaking properties of white birch. *Can. J. Res.* **1950**, *28f*, 376–389. [CrossRef]
38. Fahmy, Y.; Fahmy, T.Y.; Mobarak, F.; El-Sakhawy, M.; Fadl, M. Agricultural residues (wastes) for manufacture of paper, board, and miscellaneous products: Background overview and future prospects. *Int. J. ChemTech Res.* **2017**, *10*, 424–448.
39. Lima, D.U.; Oliveira, R.C.; Buckeridge, M.S. Seed storage hemicelluloses as wet-end additives in papermaking. *Carbohydr. Polym.* **2003**, *52*, 367–373. [CrossRef]

40. Puițel, A.C.; Suditu, G.D.; Danu, M.; Ailiesei, G.-L.; Nechita, M.T. An Experimental Study on the Hot Alkali Extraction of Xylan-Based Hemicelluloses from Wheat Straw and Corn Stalks and Optimization Methods. *Polymers* **2022**, *14*, 1662. [CrossRef]
41. Calcio Gaudino, E.; Grillo, G.; Tabasso, S.; Stevanato, L.; Cravotto, G.; Marjamaa, K.; Pihlajaniemi, V.; Koivula, A.; Aro, N.; Uusitalo, J.; et al. Optimization of ultrasound pretreatment and enzymatic hydrolysis of wheat straw: From lab to semi-industrial scale. *J. Clean. Prod.* **2022**, *380*, 134897. [CrossRef]
42. Ouahabi, Y.R.; Bensadok, K.; Ouahabi, A. Optimization of the Biomethane Production Process by Anaerobic Digestion of Wheat Straw Using Chemical Pretreatments Coupled with Ultrasonic Disintegration. *Sustainability* **2021**, *13*, 7202. [CrossRef]
43. Liu, X.; Zicari, S.M.; Liu, G.; Li, Y.; Zhang, R. Improving the bioenergy production from wheat straw with alkaline pretreatment. *Biosyst. Eng.* **2015**, *140*, 59–66. [CrossRef]
44. Yang, C.; Qian, J.; Zhang, H. Cyclic Freeze-Thaw Treatment on Enzymatic Saccharification of Wheat Straw and its Synergism Effect with Alkali. *BioEnergy Res.* **2023**, 1–11. [CrossRef]
45. Xu, J.K.; Sun, R.C. Chapter 19 - Recent Advances in Alkaline Pretreatment of Lignocellulosic Biomass. In *Biomass Fractionation Technologies for a Lignocellulosic Feedstock Based Biorefinery*; Mussatto, S.I., Ed.; Elsevier: Amsterdam, The Netherlands, 2016; pp. 431–459.
46. Liu, Q.; He, W.-Q.; Aguedo, M.; Xia, X.; Bai, W.-B.; Dong, Y.-Y.; Song, J.-Q.; Richel, A.; Goffin, D. Microwave-assisted alkali hydrolysis for cellulose isolation from wheat straw: Influence of reaction conditions and non-thermal effects of microwave. *Carbohydr. Polym.* **2021**, *253*, 117170. [CrossRef]
47. Sasaki, C.; Sumitomo, Y.; Odashima, K.; Asada, C.; Nakamura, Y. Microwave-Assisted Hydrolysis of Cellulose in Towel and Wheat Straw Using Freeze-Thawing with NaOH. *Waste Biomass Valorization* **2021**, *12*, 3331–3339. [CrossRef]
48. Mikulski, D.; Kłosowski, G. Delignification efficiency of various types of biomass using microwave-assisted hydrotropic pretreatment. *Sci. Rep.* **2022**, *12*, 4561. [CrossRef]
49. Bussemaker, M.J.; Mu, X.; Zhang, D. Ultrasonic Pretreatment of Wheat Straw in Oxidative and Nonoxidative Conditions Aided with Microwave Heating. *Ind. Eng. Chem. Res.* **2013**, *52*, 12514–12522. [CrossRef]
50. Dedhia, B.S.; Csoka, L.; Rathod, V.K. Xylanase and Ultrasound Assisted Pulping of Wheat Straw. *Appl. Biochem. Biotechnol.* **2012**, *168*, 731–741. [CrossRef]
51. Korai, R.M.; Wachemo, A.C.; Yue, L.; Jaffar, M.; Li, Z.; Shahbaz, M.; Yuan, H.; Li, X. Effect of ultrasonic application during KOH pretreatment and anaerobic process on digestion performance of wheat straw. *RSC Adv.* **2020**, *10*, 9290–9298. [CrossRef]
52. Yu, M.; Wang, L.J.; Wang, X.M. Preliminary Study on Natural Freeze-Thaw Pretreatment of Wheat Straw. *Adv. Mater. Res.* **2012**, *550–553*, 472–475. [CrossRef]
53. Ziegler-Devin, I.; Chrusciel, L.; Brosse, N. Steam Explosion Pretreatment of Lignocellulosic Biomass: A Mini-Review of Theorical and Experimental Approaches. *Front. Chem.* **2021**, *9*. [CrossRef]
54. Technical Association of the Pulp and Paper Industry. *211 om-02. Ash in Wood, Pulp, Paper and Paperboard: Combustion at 525 °C*; TAPPI: Atlanta, GA, USA, 2002; Volume 5.
55. Technical Association of the Pulp and Paper Industry. *Water solubility of wood and pulp*; TAPPI: Atlanta, GA, USA, 1988.
56. Technical Association of the Pulp and Paper Industry. T 204 cm-97: Solvent extractives of wood and pulp. In *TAPPI Test Methods*; TAPPI: Atlanta, GA, USA, 1997.
57. Sluiter, A.; Hames, B.; Hyman, D.; Payne, C.; Ruiz, R.; Scarlata, C.; Sluiter, J.; Templeton, D.; Wolfe, J. Determination of total solids in biomass and total dissolved solids in liquid process samples. *Natl. Renew. Energy Lab.* **2008**, *9*, 1–6.
58. Sluiter, A.; Hames, B.; Ruiz, R.; Scarlata, C.; Sluiter, J.; Templeton, D.; Crocker, D. Determination of structural carbohydrates and lignin in biomass. *Lab. Anal. Proced.* **2008**, *1617*, 1–16.
59. Serna-Loaiza, S.; Zikeli, F.; Adamcyk, J.; Friedl, A. Towards a wheat straw biorefinery: Combination of Organosolv and Liquid Hot Water for the improved production of sugars from hemicellulose and lignin hydrolysis. *Bioresour. Technol. Rep.* **2021**, *14*, 100667. [CrossRef]
60. Overend, R.P.; Chornet, E. Fractionation of lignocellulosics by steam-aqueous pretreatments. *Philos. Trans. R. Soc. London. Ser. A Math. Phys. Sci.* **1987**, *321*, 523–536.
61. Sun, R.C.; Tompkinson, J. Comparative study of organic solvent and water-soluble lipophilic extractives from wheat straw I: Yield and chemical composition. *J. Wood Sci.* **2003**, *49*, 0047–0052. [CrossRef]
62. Lu, Y.-C.; Lu, Y.; Lu, Z.-L.; Wei, X.-Y. Detailed Componential Characterization of Extractable Species with Organic Solvents from Wheat Straw. *Int. J. Anal. Chem.* **2017**, *2017*, 7305682. [CrossRef]
63. Kuchelmeister, C.; Bauer, S. Rapid Small-Scale Determination of Extractives in Biomass. *BioEnergy Res.* **2015**, *8*, 68–76. [CrossRef]
64. Hickey, D.T.; Hayes, D.J.; Pembroke, J.T.; Ryan, M.P.; Leahy, J.J. The Importance of Extraction Protocol on the Analysis of Novel Waste Sources of Lignocellulosic Biomass. *Energies* **2021**, *14*, 6406. [CrossRef]
65. Wen, J.-L.; Xiao, L.-P.; Sun, Y.-C.; Sun, S.-N.; Xu, F.; Sun, R.-C.; Zhang, X.-L. Comparative study of alkali-soluble hemicelluloses isolated from bamboo (*Bambusa rigida*). *Carbohydr. Res.* **2011**, *346*, 111–120. [CrossRef]
66. Vincent, P.; Ham-Pichavant, F.; Michaud, C.; Mignani, G.; Mastroianni, S.; Cramail, H.; Grelier, S. Extraction and Characterization of Hemicelluloses from a Softwood Acid Sulfite Pulp. *Polymers* **2021**, *13*, 2044. [CrossRef]
67. Duan, J.; Karaaslan, M.A.; Cho, M.; Liu, L.-Y.; Johnson, A.M.; Renneckar, S. Investigation into electrospinning water-soluble xylan: Developing applications from highly absorbent and hydrophilic surfaces to carbonized fiber. *Cellulose* **2019**, *26*, 413–427. [CrossRef]

68. Peng, F.; Bian, J.; Peng, P.; Guan, Y.; Xu, F.; Sun, R.-C. Fractional separation and structural features of hemicelluloses from sweet sorghum leaves. *BioResources* **2012**, *7*, 4744–4759. [CrossRef]
69. Nurazzi, N.M.; Asyraf, M.R.M.; Rayung, M.; Norrrahim, M.N.F.; Shazleen, S.S.; Rani, M.S.A.; Shafi, A.R.; Aisyah, H.A.; Radzi, M.H.M.; Sabaruddin, F.A.; et al. Thermogravimetric Analysis Properties of Cellulosic Natural Fiber Polymer Composites: A Review on Influence of Chemical Treatments. *Polymers* **2021**, *13*, 2710. [CrossRef]
70. Lanjewar, R.; Thakur, L.; Parmar, H.; Verma, A.; Hinge, V. A Review on Physicochemical Characterization and Pyrolysis Kinetics of Biomass. *Int. J. Manag. Technol. Eng.* **2019**.
71. Peng, Y.; Wu, S. The structural and thermal characteristics of wheat straw hemicellulose. *J. Anal. Appl. Pyrolysis* **2010**, *88*, 134–139. [CrossRef]
72. Díez, D.; Urueña, A.; Piñero, R.; Barrio, A.; Tamminen, T. Determination of Hemicellulose, Cellulose, and Lignin Content in Different Types of Biomasses by Thermogravimetric Analysis and Pseudocomponent Kinetic Model (TGA-PKM Method). *Processes* **2020**, *8*, 1048. [CrossRef]
73. Werner, K.; Pommer, L.; Broström, M. Thermal decomposition of hemicelluloses. *J. Anal. Appl. Pyrolysis* **2014**, *110*, 130–137. [CrossRef]
74. Lazdovica, K.; Kampars, V.; Liepina, L.; Vilka, M. Comparative study on thermal pyrolysis of buckwheat and wheat straws by using TGA-FTIR and Py-GC/MS methods. *J. Anal. Appl. Pyrolysis* **2017**, *124*, 1–15. [CrossRef]
75. Sun, J.; Deng, Y.; Li, S.; Xu, W.; Liu, G. Enhanced efficiency of enzymatic hydrolysis of wheat straw via freeze–thaw pretreatment. *Environ. Sci. Pollut. Res.* **2022**, *29*, 56696–56704. [CrossRef]
76. Li, J.; Liu, Z.; Feng, C.; Liu, X.; Qin, F.; Liang, C.; Bian, H.; Qin, C.; Yao, S. Green, efficient extraction of bamboo hemicellulose using freeze-thaw assisted alkali treatment. *Bioresour. Technol.* **2021**, *333*, 125107. [CrossRef]
77. Zeng, F.; Wang, S.; Liang, J.; Cao, L.; Liu, X.; Qin, C.; Liang, C.; Si, C.; Yu, Z.; Yao, S. High-efficiency separation of hemicellulose from bamboo by one-step freeze–thaw-assisted alkali treatment. *Bioresour. Technol.* **2022**, *361*, 127735. [CrossRef]
78. Aguilar-Reynosa, A.; Romaní, A.; Rodríguez-Jasso, R.M.; Aguilar, C.N.; Garrote, G.; Ruiz, H.A. Microwave heating processing as alternative of pretreatment in second-generation biorefinery: An overview. *Energy Convers. Manag.* **2017**, *136*, 50–65. [CrossRef]
79. Tsegaye, B.; Balomajumder, C.; Roy, P. Optimization of microwave and NaOH pretreatments of wheat straw for enhancing biofuel yield. *Energy Convers. Manag.* **2019**, *186*, 82–92. [CrossRef]
80. Bichot, A.; Lerosty, M.; Radoiu, M.; Méchin, V.; Bernet, N.; Delgenès, J.-P.; García-Bernet, D. Decoupling thermal and non-thermal effects of the microwaves for lignocellulosic biomass pretreatment. *Energy Convers. Manag.* **2020**, *203*, 112220. [CrossRef]
81. Janker-Obermeier, I.; Sieber, V.; Faulstich, M.; Schieder, D. Solubilization of hemicellulose and lignin from wheat straw through microwave-assisted alkali treatment. *Ind. Crops Prod.* **2012**, *39*, 198–203. [CrossRef]
82. Iskalieva, A.; Yimmou, B.M.; Gogate, P.R.; Horvath, M.; Horvath, P.G.; Csoka, L. Cavitation assisted delignification of wheat straw: A review. *Ultrason. Sonochemistry* **2012**, *19*, 984–993. [CrossRef]
83. Calcio Gaudino, E.; Cravotto, G.; Manzoli, M.; Tabasso, S. Sono- and mechanochemical technologies in the catalytic conversion of biomass. *Chem. Soc. Rev.* **2021**, *50*, 1785–1812. [CrossRef]
84. Sun, R.; Sun, X.F.; Xu, X.P. Effect of ultrasound on the physicochemical properties of organosolv lignins from wheat straw. *J. Appl. Polym. Sci.* **2002**, *84*, 2512–2522. [CrossRef]
85. Calcio Gaudino, E.; Tabasso, S.; Grillo, G.; Cravotto, G.; Dreyer, T.; Schories, G.; Altenberg, S.; Jashina, L.; Telysheva, G. Wheat straw lignin extraction with bio-based solvents using enabling technologies. *Comptes Rendus Chim.* **2018**, *21*, 563–571. [CrossRef]
86. Sun, R.; Tomkinson, J. Separation and Characterization of Cellulose from Wheat Straw. *Sep. Sci. Technol.* **2005**, *39*, 391–411. [CrossRef]

polymers

MDPI

Article

Structural and Physicochemical Characterization of Extracted Proteins Fractions from Chickpea (*Cicer arietinum* L.) as a Potential Food Ingredient to Replace Ovalbumin in Foams and Emulsions

Daniela Soto-Madrid [1], Nicole Pérez [2], Marlen Gutiérrez-Cutiño [3,4], Silvia Matiacevich [1,*] and Rommy N. Zúñiga [2,*]

[1] Food Properties Research Group (INPROAL), Department of Food Science and Technology, Technological Faculty, Universidad de Santiago de Chile, Av. Ecuador 3769, Estación Central, Santiago 9170201, Chile
[2] Department of Biotechnology, Universidad Tecnológica Metropolitana, Las Palmeras 3360, Ñuñoa, Santiago 7800003, Chile
[3] Molecular Magnetism & Molecular Materials Laboratory (LM4), Department of Chemistry of Materials, Chemistry and Biology Faculty, Universidad de Santiago de Chile, Av. Lib. Bernardo O'Higgins 3363, Estación Central, Santiago 9170022, Chile
[4] Center for the Development of Nanoscience and Nanotechnology, CEDENNA, Santiago 9170022, Chile
* Correspondence: silvia.matiacevich@usach.cl (S.M.); rommy.zuniga@utem.cl (R.N.Z.)

Abstract: Chickpeas are the third most abundant legume crop worldwide, having a high protein content (14.9–24.6%) with interesting technological properties, thus representing a sustainable alternative to animal proteins. In this study, the surface and structural properties of total (TE) and sequential (ALB, GLO, and GLU) protein fractions isolated from defatted chickpea flour were evaluated and compared with an animal protein, ovalbumin (OVO). Differences in their physicochemical properties were evidenced when comparing TE with ALB, GLO, and GLU fractions. In addition, using a simple and low-cost extraction method it was obtained a high protein yield (82 ± 4%) with a significant content of essential and hydrophobic amino acids. Chickpea proteins presented improved interfacial and surface behavior compared to OVO, where GLO showed the most significant effects, correlated with its secondary structure and associated with its flexibility and higher surface hydrophobicity. Therefore, chickpea proteins have improved surface properties compared to OVO, evidencing their potential use as foam and/or emulsion stabilizers in food formulations for the replacement of animal proteins.

Keywords: plant proteins; chickpea; food ingredients; ovalbumin; total protein extraction

Citation: Soto-Madrid, D.; Pérez, N.; Gutiérrez-Cutiño, M.; Matiacevich, S.; Zúñiga, R.N. Structural and Physicochemical Characterization of Extracted Proteins Fractions from Chickpea (*Cicer arietinum* L.) as a Potential Food Ingredient to Replace Ovalbumin in Foams and Emulsions. *Polymers* **2023**, *15*, 110. https://doi.org/10.3390/polym15010110

Academic Editors: Cornelia Vasile, Gabriel Aguirre-Álvarez and Xiao-Feng Sun

Received: 2 November 2022
Revised: 1 December 2022
Accepted: 19 December 2022
Published: 27 December 2022

1. Introduction

In current times, the consumption of vegetable protein is increasing as consumers seek healthy and lower-cost alternatives to animal protein without compromising product quality, safety, and sustainability. This way, consumer groups, such as flexitarians, vegans, and vegetarians, opt for a diet rich in pulses such as beans, lentils, peas, and chickpeas. In addition, some consumers avoid common plant proteins, such as soy, due to their potential allergenicity and celiac disease or sensitivity [1]. Therefore, the technological development of protein concentrates and isolates derived from legumes, specifically from pulses, is an excellent alternative to meet current consumer demands. These proteins with high functionality could be required concerning stabilizing multiphasic systems, such as foams (e.g., whipped cream and ice cream) and emulsions (e.g., mayonnaise and dressing).

The use of proteins from pulses has grown considerably in the food industry due to their richness in essential amino acids (lysine, leucine, and arginine). Additionally, legumes are an economical protein source and have low water requirements for crops [2]. Therefore,

the future food market is focused on food security and the necessity for sustainable protein sources. The Food and Agriculture Organization (FAO) describes legumes as "nutritional seeds for a sustainable future" since crops, such as chickpeas, are resistant to drought and do not require intensive irrigation, becoming a sustainable protein source [3].

Chickpea is the third most abundant pulse crop worldwide, with a high protein content (14.9–24.6%) [4,5]. The literature has reported that chickpea seed proteins are composed of globulin (salt soluble; 56%), albumin (water-soluble; 12%), a prolamin (alcohol soluble; 2.8%), glutelin (acid/alkali-soluble; 18.1%), and residual proteins [4,6]. Compared to other legumes, chickpea proteins have a higher bioavailability [7]; for that, they could be an excellent potential alternative to animal proteins. Chickpea is currently used in the food industry to make bread, sandwiches, soups, pasta, crackers, cakes, beverages, mayonnaise-type dressing, and gluten-free pasta, among other foods [8,9].

The literature has reported three types of vegetable protein extraction techniques: (i) conventional extraction, based on organic and alkaline solvents; (ii) biochemical extraction, based on the use of enzymes and (iii) physical extraction, based on ultrasound, pulsed electric field, microwave or high pressure-assisted extraction [10]. Extraction based on protein solubility using Osborne's methodology and alkaline extraction is the most used extraction technique in the food industry to obtain protein concentrates and isolates [11–13]. It is due to the low cost of chemical products, the relative simplicity of the critical apparatus, and the use of environmentally friendly solvents.

Osborne's methodology sequentially extracts proteins based on their solubility and subsequent precipitation at the isoelectric point. Albumins are soluble in water; globulins are insoluble in water but soluble in dilute salt solutions; glutelins are insoluble in the above solutions but soluble in weak acid or basic solutions; and finally, prolamins are insoluble in the above solutions but soluble in alcohol/water mixtures [14]. This methodology was successfully used for the sequential extraction of proteins from rice, quinoa, and chickpeas [4,12,15].

Using isolated and/or protein fractions from pulses in food matrices depends on their composition and functional and structural properties [16,17]. However, the type and variety of legume seeds and the extraction methods can alter the protein composition in the final isolated or concentrated products [1,18]. Most studies on pulses protein isolates' structural and functional properties have yet to consider the role of the individual protein fractions (e.g., albumin, globulin, glutelin) compared to the total protein extracted. Chang et al. [17] evaluated the structural and functional properties of protein fractions such as globulin, legumin, and vicilin from green peas and chickpeas, observing differences in the functionality of the protein fractions. However, the authors did not consider the behavior of the total protein fraction. For that, evaluating the functional and structural properties of the total and each protein fraction is essential to provide knowledge to manufacture suitable pulse proteins according to the application area. Thus, it becomes a potential ingredient for the total or partial replacement of animal proteins.

In this study, chickpea proteins were compared to ovalbumin, an animal protein widely used as an emulsifying agent in the food industry, because of its intense surface activity and emulsion stabilization properties [19]. In addition, due to its high foaming property, it is used as a foaming agent to improve and maintain the quality (texture and volume) of aerated foods, such as cakes, cookies, dessert shells, and chocolate mousses [20]. However, it has disadvantages compared to vegetable protein due to the high cost, limited supply, and direct relationship to climate change [10]. For that, it is crucial to obtain alternative vegetable sources of proteins with functional properties similar to animal-origin proteins to replace them and develop appropriate technologies for their profitable extraction and incorporation as an ingredient in foods.

Today, the food industry calls for research and development in plant-derived protein as a versatile and inexpensive substitute for animal protein in the human diet. Therefore, this study aims to evaluate the surface and structural properties of protein fractions (by total and sequential extraction) isolated from defatted chickpea flour, compared to an

animal protein, ovalbumin, for its potential use as a food ingredient. For this purpose, extraction, fractionation, and physicochemical characterization were performed for each protein fraction to evaluate the quality of fraction proteins based on their amino acid profile and potential food application.

2. Materials and Methods

2.1. Samples

Chickpea flour (Extrumol, Santiago, Chile) was characterized by proximal composition (g/100 g): 8.4 ± 0.1 of moisture, 18.3 ± 0.3 of protein, 6.9 ± 0.1 of lipids, 2.9 ± 0.0 ash, 0.9 ± 0.0 crude fiber, and 62.6 ± 0.3 non-nitrogen extracts. This raw material was defatted before the protein extraction process.

Commercial ovalbumin (OVO) with a protein value of 38.2 ± 0.1 g/100 g was purchased from Cherry (Chile) for comparison as a control surface and structural properties.

Defatted chickpea flour: Hexane of analytical grade (Heyn, Santiago, Chile) was used to eliminate the lipid fraction from the chickpea flour by solvent extraction at a ratio of 1:3 weight: volume (flour:solvent) for 1 h under stirring at 200 rpm. Subsequently, the mixture was filtered and dried under an extractor hood at room temperature for 24 h. The defatting process of the chickpea flour was repeated twice, according to the methodology described by Karaca et al. [21]

2.2. Protein Extraction Processes from Defatted Chickpea Flour

2.2.1. Total Extraction (TE)

The total protein fraction (Figure 1) was obtained by isoelectric precipitation following the protocol of Chang et al. [22] with some modifications. For this, 20 g of defatted chickpea flour was mixed with 200 mL of NaOH 0.02% *w/v* (Heyn, Chile) at a pH of 11.5 and 400 µL of protease inhibitor (Sigma-Aldrich, Darmstadt, Germany), according to the methodology of Castellión et al. [12]. The mixture was stirred for 1 h with continuous stirring at a speed of 200 rpm (Boeco, model MSH 420, Hamburg, Germany). Then, the mixture was centrifuged at 4130× *g* for 10 min (Restek, model sep-3000, PA, USA), and a recycling process was carried out, where the sample was remixed with 200 mL of NaOH at 0.02% *w/v* for 1 h. The supernatant was filtered with the help of a vacuum pump (Rocker, model 300C, Kaohsiung, Taiwan). Subsequently, it adjusted the pH of the supernatant to 4.5 with 2 N HCl (isoelectric point of legumin proteins). The supernatant was centrifuged at 4130× *g* for 10 min, a process that was repeated twice, washing the pellet with purified water, and then resuspending it in purified water. The total protein obtained was stored at −80 °C in an ultra-freezer (Thermo Scientific, model 702, MA, USA) and then freeze-dried at −40 °C and 27 Pa (Virtis SP Scientific, Benchtop Pro 9L ES-55, PA, USA). After the freeze-drying process, the moisture and water activity of the TE sample were determined. Finally, the freeze-dried proteins were stored in desiccators until further analysis.

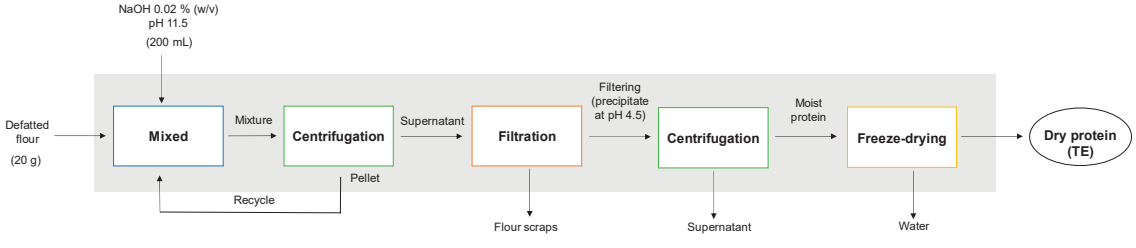

Figure 1. Flow chart describing the total extraction method of chickpea protein.

2.2.2. Sequential Extraction (SE) of Proteins from Chickpea Flour

Albumin (ALB), globulin (GLO), and glutelin (GLU) fractions were extracted sequentially according to the procedure of Chang et al. [4] with some modifications (Figure 2).

A sample of defatted chickpea flour (50 g) was mixed with purified water (200 mL) and 1 mL of protease inhibitor (Sigma-Aldrich, Darmstadt, Germany), according to the methodology of Castellión et al. [12]. The mixture was magnetic stirred (Boeco, model MSH 420, Hamburg, Germany) for 2 h and then centrifuged at 4130× *g* for 10 min (Restek, model Q-SEP 3000, PA, USA). The supernatant was filtered using Whatman N°1 paper and a vacuum pump (Rocker, model 300C, Kaohsiung, Taiwan), while the precipitate was reserved for GLO extraction (pellet 1). The filtered supernatant was precipitated at pH 4.1 with 1 M HCl, centrifuged at 4130× *g* for 10 min (Restek, model Q-SEP 3000, PA, USA), and subsequently freeze-dried (Virtis SP Scientific, Benchtop Pro 9L ES-55, PA, USA) obtaining the ALB fraction. Pellet 1 was mixed with 200 mL of a NaCl solution (5% *w*/*v*) and magnetically stirred for 2 h. It was centrifuged at 4130× *g* for 10 min, the supernatant was filtered in the same way as carried out previously, and the precipitate was reserved (pellet 2). The supernatant was precipitated at pH 4.3 with 1 M HCl, centrifuged again at 4130× *g* for 10 min, and the precipitate corresponding to the GLO fraction was also freeze-dried. Pellet 2 was mixed with 200 mL of a NaOH solution 0.1 M, stirred for 2 h, and centrifuged at 4130× *g* for 10 min. The supernatant was filtered and precipitated at pH 4.8 with 1 M HCl, centrifuged at 4130× *g* for 10 min, and freeze-dried, obtaining the GLU fraction. Finally, all the freeze-dried proteins (ALB, GLO, and GLU) were stored in desiccators until further analysis.

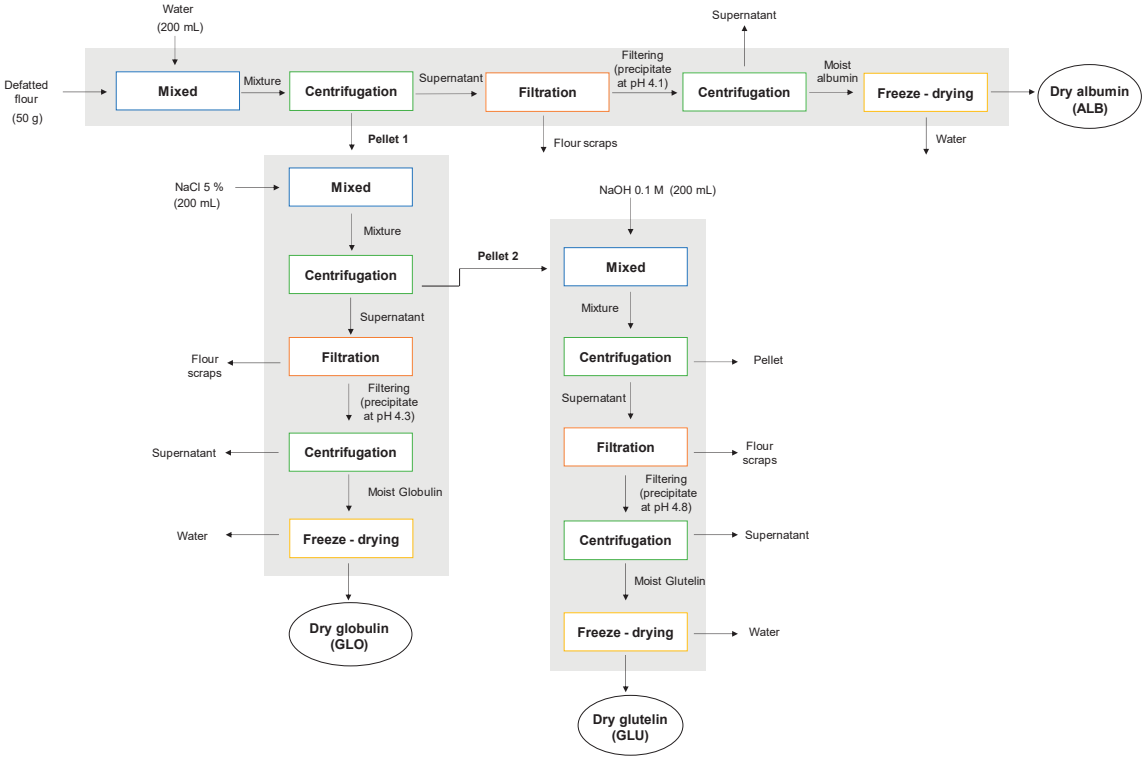

Figure 2. Flow chart describing the sequential extraction method of chickpea protein.

2.2.3. Moisture Content and Water Activity of Freeze-Dried Proteins

The moisture content of the freeze-dried proteins was determined gravimetrically by the difference in mass before and after drying the samples in an oven (Memmert, model WNB 22, Schwabach, Germany) at 105 °C until constant weight (AOAC, 1998). Results were expressed as dry basis percentage (% d.b; g water/100 g solids). The water activity

(a_w) was determined by automatic measuring equipment (Novasina, model Lab Start, Lachen, Switzerland) at 25 °C [23].

2.2.4. Protein Extraction Yield

The yield (Y) of the total and sequential extractions of chickpea proteins was estimated by a gravimetric method based on the initial protein mass and the mass of freeze-dried protein obtained after the extraction process, according to the following equation.

$$Y\ (\%) = \frac{\text{mass of freeze} - \text{dried protein (g)}}{\text{mass of protein in chickpea flour (g)}} \times 100\% \quad (1)$$

where the protein mass of the flour on a dry basis was 16.8 g/100 g of sample (corrected for moisture content), according to its proximal analysis.

2.3. Physicochemical Characterization of the Protein Fractions

2.3.1. Sodium Dodecyl Sulfate-Polyacrylamide Gel Electrophoresis (SDS-PAGE)

Electrophoresis was carried out according to the methodology described by Laemmli [24]. The molecular weight of the proteins was estimated using SDS-PAGE polyacrylamide gels (Bio-Rad, Mini-protein TGX 12% gel, CA, USA) compared to standard proteins (Precision Plus Protein Kaleidoscope Standards, Broad Range, Bio-Rad Laboratories Inc., CA, USA). Protein samples (0.3% w/w) were prepared by dissolving 50 µL of protein dispersion in 50 µL of a loading buffer (50 µL of β-mercaptoethanol (BME) per 950 µL 2X Laemmli sample buffer) (Bio-Rad Laboratories, Inc., CA, USA). The samples prepared in the previous step were heated at 95 °C for 5 min in a water bath for protein denaturation. Samples (20 µL) were loaded into each well. The electrophoretic migration was performed using refrigerated running buffer (1 L), which was prepared using 1X Tris-acetate-EDTA (TAE) buffer from 10X Tris R11 glycine/SDS buffer (Bio-Rad Laboratories Inc., CA, USA). This process was monitored at a constant current (100 V) for 1.5 h using a Mini-Protean Tetra Cell unit (Mini-PROTEAN® Tetra System, Bio-Rad Laboratories Inc., Richmond, CA, USA). The gel was stained with a Coomassie blue solution (Bio-Rad, Coomassie Brilliant Blue R-250, Bio-Rad Laboratories, Inc., CA, USA) for 12 h at room temperature. After the staining time, the solution was removed, and 200 mL of the destain solution I (10% acetic acid *v/v*, 50% methanol *v/v*) was added while gently stirring for 2 h. Then, it was removed, and 200 mL of the destain solution II (7% *v/v* acetic acid, 5% *v/v* methanol) was added and stirred for 12 h at room temperature. Finally, gels are stored in distilled water until digital images were taken. All reactive stains were of analytical grade (Heyn, Santiago, Chile).

2.3.2. Amino Acid Analysis by High-Performance Liquid Chromatography (HPLC)

The chickpea protein's amino acids were identified and quantified according to the methodology described by Janssen et al. [25]. Chickpea proteins (10 mg) were hydrolyzed with 300 µL of a 6 N HCl solution at 110 °C for 24 h. The hydrolyzate obtained was derivatized with 20 µL of phenylthiocyanate (10% *w/v*) to generate phenylthiocarbamyl amino acids, which were separated and quantified by HPLC at 254 nm. A liquid chromatograph (Waters 600 controller, MA, USA) with a diode array detector (Waters 996) and a Phenomenex (Los Angeles, CA, USA) RP18 column (150 mm × 4.6 mm, 5 µm) was used. The gradient separation was performed using two solvent solutions: Solution (A) composed by 94:6 *v/v* of 0.14 mol/L of HPLC-grade anhydrous sodium acetate (pH 5.9): HPLC-grade acetonitrile, and solution (B) by HPLC-grade acetonitrile: water (60:40 *v/v*) solution. The injection volume was 20 µL, the column temperature was 40 °C, and the analysis time was 30 min. The quantification of amino acids was carried out with external standards (Sigma-Aldrich, Darmstadt, Germany) and attributed to 17 amino acids previously described in chickpeas [26].

2.3.3. Zeta Potential of Protein Dispersions

The pH stability and isoelectric point determination were carried out through Zeta potential measurements (Zetasizer Nano Series, Nano ZS90, Malvern Instruments, UK). TE, ALB, GLO, and GLU dispersions (0.1% *w/v*) were prepared at the respective solubility solvent; with ultrapure water, 5% (*w/v*) 0.1 M NaCl and NaOH, respectively. pH values were adjusted in the range of 2 to 7, using NaOH or HCl (1 N). Samples of protein dispersions (1 mL) were placed in a cuvette with electrodes (Malvern Instruments, cell type DTS1070, UK), and Zeta potential was measured. Zeta potential versus pH was plotted to obtain the isoelectric point (IP), which is the point where the value of the net surface charge of proteins (and Zeta potential) is equal to zero, and +/−30 mV values are required for complete electrostatic stabilization [27].

2.4. Surface and Structural Properties of Protein Dispersion

2.4.1. Surface Hydrophobicity

Protein fractions were measured using 1-anilino naphthalene-8-sulfonic acid (ANS) as a fluorescence probe, as described by Kato & Nakai [28]. Samples were diluted between 0.002 and 0.01% (*w/v*) from a concentrated dispersion of proteins (TE, ALB, GLO, and GLU) at 0.1 (*w/v*). Four milliliters of diluted samples reacted with 20 μL of ANS solution (8×10^{-3} M). The fluorescence intensity was measured at the excitation wavelength of 365 nm and the emission wavelength of 484 nm on a fluorometer (Perkin Elmer, LS55, Massachusetts, UK). Fluorescence intensity and the corresponding concentration of protein were fitted using linear regression. The slope of the curve obtained was defined as the surface hydrophobicity index of the protein.

2.4.2. Dynamic Interfacial (DIT) and Surface Tension (DST) Measurements

Interfacial or surface tension changes between protein dispersions (TE, ALB, GLO, and GLU) were determined by an optical tensiometer (Ramé-Hart Inc., model 250-F4, Succasunna, NJ, USA). Commercial ovalbumin (OVO) was used as a control. All proteins were analyzed at a concentration of 0.1% (*w/v*), previously hydrated at 4 °C overnight, and, subsequently, the pH value was adjusted at 7 before measurements. Measurements were based on the pendant drop method using a lipid phase (sunflower oil) for DIT and air for DST. In this method, an axisymmetric drop of protein dispersion (8.5–10 μL) was delivered and allowed to stand at the tip of a steel needle inside a quartz cell with 30 mL of sunflower oil or air at 25 °C to achieve protein adsorption at the oil-water or air-water interface, respectively. For DIT measurements, commercial sunflower oil (Natura, Argentina) was purified by resin mixing (Florisil® 60-100 mesh, 46385, Sigma-Aldrich, Germany) at a 10:1 ratio for 4 h, according to the methodology of Bahtz et al. [29].

The Coupled Charged Device (CCD) camera of the optical tensiometer captured drop images at different time intervals. The interfacial or surface tension was calculated by analyzing the image profile of the drops stabilized by the surfactant dispersions using image analysis (Ramé-Hart Inc., DROPimage Advanced software, Succasunna, NJ, USA) and then by fitting the Laplace equation to the drop shape. To validate the DIT methodology, the interfacial tension of the sunflower oil/pure water system was the same as previously reported (26.6 ± 0.5 mN/m) for identical conditions [30]. For DST measurements, it corroborated that the surface tension of the pure water/air system was 72.8 ± 0.2 mN/m [31].

Results obtained from the DIT and DST measurements were interpreted in terms of interfacial pressure or surface pressure, respectively, which was defined as the decrease in interfacial or surface tension of a pure solvent caused by the addition of the protein:

$$\Pi = \tau - \tau_p \quad (2)$$

where Π is the interfacial or surface pressure of the protein dispersion (mN/m), τ is the interfacial tension of the oil-pure water system (26.6 mN/m), or the surface tension of the

air-pure water system (72.8 mN/m) at 25 °C, and τ_p is the interfacial or surface tension of the protein dispersion (mN/m) at the same temperature.

The evolution of interfacial or surface pressure was fitted to an empirical kinetic model based on the works of Azuara et al. [32] for the osmotic dehydration process and Moyano & Pedreschi [33] for oil absorption during deep-fat frying. A balance in terms of the interfacial or surface pressure at the interface is performed as follows.

$$\Pi = \Pi_0 + \Pi_{eq} - \Pi^* \quad (3)$$

where Π_0 is the interfacial or surface pressure at time zero (mN/m), Π_{eq} is the interfacial or surface pressure at the equilibrium (mN/m), and Π is the interfacial or surface pressure value needed to reach the equilibrium (mN/m). The limit conditions for interfacial or surface pressure are:

(i) At $t = 0 \rightarrow \Pi^* = \Pi_{eq}$ and $\Pi = \Pi_0$
(ii) At $t = \infty \rightarrow \Pi^* = \Pi_0$ and $\Pi = \Pi_{eq}$

It is assumed that changes in the ratio Π^*/Π are inversely proportional to protein adsorption time:

$$\frac{\Pi^*}{\Pi} = \frac{1}{k \times t} \quad (4)$$

Considering the above conditions, the empirical model proposed is:

$$\Pi = \frac{\Pi_{eq} \times k \times t}{1 + k \times t} + \Pi_0 \quad (5)$$

where k is the specific rate constant for protein adsorption to the interface (s^{-1}). Interfacial or surface pressure curves were fitted to the proposed model. The specific rate constant (k) and the interfacial or surface pressure at equilibrium (Π_{eq}) were obtained by employing nonlinear regression analysis performed with the Solver tool of Microsoft Excel, using as an objective function the minimization of the root mean square (RMS) equation.

$$\text{RMS}\ (\%) = \sqrt{\frac{1}{n} \times \sum \left(\frac{V_e - V_p}{V_p} \right)^2} \times 100\% \quad (6)$$

where n is the number of data points for each curve, V_e is the experimental value, and V_p is the predicted value by Equation (6).

2.4.3. Structural Characterization by Fourier Transform Infrared-Attenuated Total Reflectance (FTIR-ATR) Spectra Analysis

Chemical groups and bonding arrangement of components present in protein samples were determined by Fourier Transform Infrared-Attenuated Total Reflectance (FTIR -ATR), using a Jasco FTIR-4600 spectrophotometer equipped with an ATR PRO ONE (Jasco, Easton, MD, USA). Measurements were performed in a spectral range of 4000 to 400 cm^{-1} at a 4 cm^{-1} resolution and scan number 32. Fourier second derivative analysis was performed for the Amide I region (1700–1600 cm^{-1}) using the OriginPro 8.5 software (OriginLab, Northampton, MA, USA). Curve normalization was developed at the highest intensity peak and Gaussian peak fitting using OriginPro 8.5 software (OriginLab, Northampton, MA, USA). The percentages of the secondary structures were determined by integrating the areas of the fitted peaks. Intensity measurements were performed on the original and the second-derived spectra by calculating the height of the absorbance bands from their baseline. All chemical functional groups were identified using published reports [9,17,34].

2.5. Statistical Analysis

All experiments were run in triplicate. Data were reported as means with their corresponding standard deviation. ANOVA test, at a confidence level of 95%, was performed

to determine statistical differences using Statgraphics Centurion XVI® software (StatPoint Technologies Inc., VA, USA). Differences between samples were evaluated using multiple range tests, using the Least Significant Differences (LSD) multiple comparison method. The significance of the differences was determined at a 95% confidence level ($p < 0.05$).

3. Results and Discussion

3.1. Protein Extraction Processes

3.1.1. Effect of Process Parameters in Protein Fractions

Since lipids can interfere as a barrier to solvent penetration during protein extraction [11], a defatting procedure was previously applied to the flour. The initial lipid content of the flour was 6.9 g/100 g of wet basis sample (w.b.). The final lipid content of the defatted flour was 0.82 ± 0.01 g/100 g of sample (w.b.). Therefore, the defatted process was successful, and in this case, the lipid content was a process parameter not considered in the extraction process yield.

Moisture content and water activity (a_w) are relevant physical parameters to evaluate the freeze-drying process of protein extracts since moisture content and a_w influence their stability and safety during storage. Table 1 shows the moisture content of the extracted chickpea protein samples. All values were less than 4% w.b., which ensures stability while storing freeze-dried proteins, preventing particle agglomeration and caking [35]. All freeze-dried extracted protein samples (TE and SE) presented a_w values lower than 0.22 (Table 1), ensuring their preservation since most microorganisms grow at a_w values higher than 0.6 [36]. Therefore, the freeze-drying process of the TE, ALB, GLO, and GLU samples was optimal. Obtaining powdered protein extracts could allow their potential use as an ingredient in food applications, suggesting stable storage.

Table 1. Moisture content and a_w of lyophilized protein.

Sample	Moisture (%)	a_w
Total extraction	$3.65^{d} \pm 0.11$	$0.22^{c} \pm 0.030$
Albumin	$1.24^{a} \pm 0.03$	$0.05^{a} \pm 0.004$
Globulin	$1.91^{c} \pm 0.44$	$0.10^{ab} \pm 0.020$
Glutelin	$1.87^{bc} \pm 0.29$	$0.15^{b} \pm 0.004$

Different letters ($^{a, b, c, d}$) indicate significant differences ($p < 0.05$) between samples.

3.1.2. Protein Extraction Yield

Table 2 indicates no significant differences ($p \geq 0.05$) in the process yield for both extractions (TE and SE), which was 82 ± 3% (value obtained through the average of both extractions). These results were superior to those reported by [37], ranging between 50.3–69.1%, which depended on the chickpea variety (Kabuli and Desi) or protein extraction methodology. Sánchez-Vioque et al. [11] reported that protein recovery ranged from 62.1% to 65.9% for two protein isolates from ground Kabuli chickpea seeds. The differences in protein extraction yield values between authors can be attributed to raw materials, protein solubility, and processing times. However, the high value obtained in this study confirms this suitable methodology for TE.

Table 2. Protein extraction yield for total and sequential process extraction.

Sample	Yield Dry Weight (%)
Total extraction	$78.0^{c} \pm 1.0$
Total sequential extraction	$85.0^{c} \pm 5.7$
Albumin	$69.3^{b} \pm 4.4$
Globulin	$8.7^{a} \pm 1.0$
Glutelin	$7.1^{a} \pm 0.9$

Different letters ($^{a, b, c}$) indicate significant differences ($p < 0.05$) between samples.

In the SE (Table 2), ALB (64%) was the protein extracted with the highest proportion, followed by GLO (8%) and GLU (6.5%), obtaining a total protein extraction of 85 ± 6%. However, previous literature indicated that chickpea protein mainly comprises GLO (about 50%) [22,38,39]. In contrast, the highest percentage of ALB obtained (Table 2) could depend on the extraction conditions and physicochemical procedures used [40]. In this sense, Liu et al. [41] carried out ALB and GLO extractions from different chickpea varieties using solutions of water and salt (K_2SO_4 and NaCl). They obtained high concentrations of ALB (~60%) when using NaCl as an extraction solvent, similar to this study, because legumes are a source of minerals, especially a richer source of calcium and phosphorus than most cereals [2]. Therefore, the salts in the chickpea flour could convert the purified water used as the extraction medium into a very dilute saline solution, extracting significantly higher ALB and GLO content with distilled water.

3.2. Physicochemical Characterization of Total and Sequential Protein Extracted from Chickpea Flour

3.2.1. Electrophoretic Pattern of Chickpea Protein Fraction Evaluated by SDS-PAGE

SDS-PAGE was used to determine the molecular weight (Mw) of the subunits of the chickpea protein fractions. After electrophoresis of TE, ALB, GLO, and GLU proteins, multiple bands were observed and compared to a Mw standard (Figure 3 lane 1), ranging from approximately 97 to 12 kDa (Figure 3). These values agree with the characteristic band patterns of legumes reported by several authors [4,6,22], which indicates the high effectiveness of the protein extraction process from the chickpea flour.

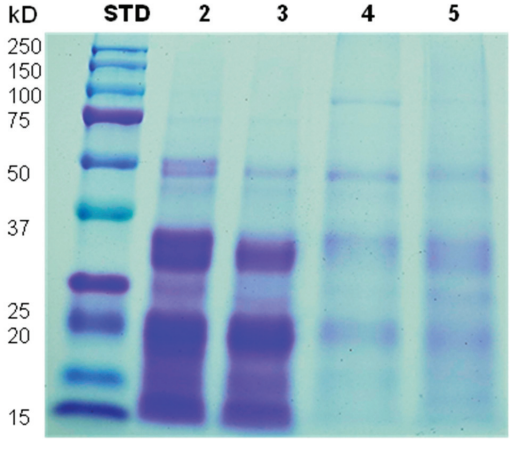

Figure 3. SDS-PAGE of chickpea protein isolates from sequential extractions and ovalbumin. STD: Standard protein markers; (2) Extraction total; (3) Albumin fraction; (4) Globulin fraction; (5) Glutelin fraction.

In Figure 3, the SDS-PAGE patterns of the TE (lane 2) and of the ALB fraction (lane 3) were very similar, observing the expected proteins for both fractions: legumin (11S), vicilin (7S) and albumin (2S) [4]. Legumin protein (α and β subunits) were slightly observed at ~46 kDa and ~25 kDa bands, respectively [4,11]. Furthermore, estimated molecular weights of ~49, ~35, ~33, ~19, and ~15 kD were identified as chickpea vicilin (7S) subunits reported by Chang et al. (2011). Finally, low molecular weight bands ~12 kD were attributed to albumin subunits (2S) [42]. These results indicate that the TE sample contains a high percentage of proteins extracted on the ALB fraction due to the similarity in the band pattern, which agrees with the extraction yield results (Table 2).

In the GLO fraction (Figure 3, lane 4), a ~98 kDa molecular weight (MW) band was identified, compared to the chickpea lipoxygenase, as Clemente et al. [43] reported.

However, a similar lighter band pattern was observed for GLO (lane 3) and GLU (lane 4) fractions, attributed to the chickpea 11S and 7S subunits.

Therefore, as expected, the pattern of bands for the TE corresponds to the mixture of the extracted proteins. The ALB, GLO, and GLU fractions present a similar pattern of bands but with low resolution compared to other legumin proteins [17].

3.2.2. Amino Acid Profile of Extracted Chickpea Proteins

Proteins are chains of amino acids linked by peptide bonds; these amino acids provide nutritional value and influence their structure and functionality. Table 3 shows the 17 amino acids detected by HPLC-DAD for each extraction sample from chickpea flour. The highest amino acids percentages in the TE, ALB, GLO, and GLU samples were glutamic acid, aspartic acid, and arginine, where the glutamic acid presented the highest proportion in all samples (TE: 14.5 ± 0.3; ALB: 11.5 ± 1.3; GLO: 8.3 ± 0.6, GLU: 9.7 ± 0.1 g/100 g protein). These results agree with Ghribi et al. [44] since, in chickpea protein isolates, glutamic acid showed the highest amount, varying from 15.04 to 19.23 g/100 g of protein. Furthermore, the total essential amino acids content was similar to that reported by Chang et al. [17] (~25 g/100 g protein).

Table 3. Amino acid profile of chickpea proteins.

Amino Acid	Total Extraction (g/100 g Protein)	Albumin (g/100 g Protein)	Globulin (g/100 g Protein)	Glutelin (g/100 g Protein)
Isoleucine	$2.95^{d} \pm 0.01$	$2.72^{c} \pm 0.07$	$2.23^{a} \pm 0.01$	$2.51^{b} \pm 0.01$
Leucine	$5.40^{d} \pm 0.08$	$4.99^{c} \pm 0.11$	$3.82^{a} \pm 0.07$	$4.55^{b} \pm 0.11$
Threonine	$2.54^{ab} \pm 0.04$	$2.44^{a} \pm 0.08$	$2.43^{a} \pm 0.05$	$2.83^{b} \pm 0.13$
Valine	$2.69^{b} \pm 0.09$	$2.62^{b} \pm 0.09$	$2.15^{a} \pm 0.08$	$2.56^{b} \pm 0.07$
Phenylalanine	$4.09^{c} \pm 0.05$	$3.30^{b} \pm 0.01$	$2.65^{a} \pm 0.00$	$3.27^{b} \pm 0.00$
Methionine	$0.88^{b} \pm 0.01$	$0.71^{a} \pm 0.02$	$0.70^{a} \pm 0.01$	$0.76^{ab} \pm 0.10$
Histidine	$1.51^{b} \pm 0.05$	$1.53^{b} \pm 0.08$	$1.04^{a} \pm 0.01$	$1.37^{b} \pm 0.16$
Lysine	$5.35^{b} \pm 0.23$	$3.83^{a} \pm 0.11$	$3.75^{a} \pm 0.20$	$4.02^{a} \pm 0.13$
Total essential amino acids	$25.4^{c} \pm 0.10$	$22.14^{b} \pm 0.69$	$18.76^{a} \pm 0.06$	$21.86^{b} \pm 0.46$
Essential amino acids (%)	$33.61^{a} \pm 0.26$	$32.85^{a} \pm 1.62$	$35.91^{b} \pm 0.05$	$35.92^{b} \pm 0.17$
Aspartic acid	$10.74^{c} \pm 0.46$	$10.00^{c} \pm 0.11$	$7.01^{a} \pm 0.04$	$7.86^{b} \pm 0.20$
Cysteine	$1.87^{b} \pm 0.27$	$1.27^{a} \pm 0.00$	$1.01^{a} \pm 0.05$	$1.35^{a} \pm 0.07$
Glutamic acid	$14.54^{c} \pm 0.33$	$11.51^{c} \pm 1.30$	$8.31^{a} \pm 0.57$	$9.74^{b} \pm 0.14$
Alanine	$3.20^{a} \pm 0.13$	$3.15^{a} \pm 0.10$	$2.92^{a} \pm 0.02$	$3.16^{a} \pm 0.06$
Serine	$4.63^{c} \pm 0.26$	$4.38^{bc} \pm 0.18$	$3.30^{a} \pm 0.08$	$3.96^{b} \pm 0.09$
Glycine	$3.07^{a} \pm 0.16$	$3.11^{a} \pm 0.18$	$2.26^{a} \pm 0.09$	$3.14^{a} \pm 0.03$
Tyrosine	$1.53^{a} \pm 0.13$	$1.22^{a} \pm 0.05$	$1.29^{a} \pm 0.05$	$1.56^{a} \pm 0.17$
Arginine	$7.46^{b} \pm 0.38$	$6.91^{b} \pm 0.02$	$4.42^{a} \pm 0.67$	$4.91^{a} \pm 0.13$
Proline	$3.14^{b} \pm 0.29$	$3.73^{c} \pm 0.07$	$2.61^{a} \pm 0.08$	$3.30^{bc} \pm 0.03$
Total non-essential amino acids	$50.17^{d} \pm 0.38$	$45.28^{a} \pm 1.93$	$33.48^{b} \pm 0.17$	$38.99^{c} \pm 0.53$
Non-essential amino acids (%)	$66.39^{b} \pm 0.26$	$67.17^{b} \pm 1.62$	$64.09^{a} \pm 0.05$	$64.08^{a} \pm 0.17$

Different letters ($^{a, b, c, d}$) indicate significant differences ($p < 0.05$) between samples.

The percentage of essential amino acids (EEA%) of the chickpea proteins detected was calculated (Sum of detected essential amino acids/total amino acids content × 100%). It did not determine the content of Tryptophan because it was hydrolyzed during the acid hydrolysis step of the methodology used. No significant differences were obtained between GLO and GLU samples (36.0 ± 0.1%) and between TE and ALB (33.5 ± 0.9%). It is essential to remark that the total essential amino acid determined for isolated chickpea after total and sequential fractions could reach the FAO/WHO [45] requirement for the essential amino acid for preschool children. Consequently, all protein fractions obtained in this study could be potentially applied to food matrices as a good source of quality proteins.

The amino acid profile of the extracted proteins shows significant differences ($p \leq 0.05$) related to hydrophobic amino acids quantity (TE: 25.4 ± 0.2; ALB: 24.33 ± 1.27;

GLO: 19.71 ± 0.03; GLU: 23.24 ± 0.42 g/100 g protein). The TE, ALB, and GLU samples presented the highest values, which shows their potential use as foam and/or emulsion stabilizers. The literature has indicated that globular proteins stabilize air/water interfaces in foams and oil/water interfaces in emulsions, where hydrophobic amino acids play a fundamental role [46,47].

Thus, the amino acid composition can affect the functional properties of proteins because it determines the ratio of hydrophilic and hydrophobic groups and the balance of positive, negative, and neutral groups, which affects their hydrophobicity at the surface and electrostatic interactions. The presence of charged patches along proteins and/or polyelectrolytes in the isolated fractions could also affect their stability [48]. These parameters must be considered when characterizing the protein's functional performance.

3.2.3. Zeta Potential of Extracted Chickpea Proteins

The measurement of the Zeta potential gives information on the dispersion stability. The highest Zeta potential of suspensions (more positive than +30 mV or negative than -30 mV) showed physical stability. It is due to charged particles repelling each other and overcoming the natural tendency to aggregate [27,49]. Figure 4 shows the Zeta potential of the protein fractions extracted from chickpea flour. The TE and ALB samples at pH 7 and 3 present the highest absolute values, respectively (TE: |36.4| ± 0.6 mV; |30.4| ± 1.4 mV and ALB: |30.0| ± 1.8 mV; |29.5| ± 1.4 mV), evidencing the stability of protein dispersions at this pH and may have a potential application in food matrices at neutral and acidic conditions.

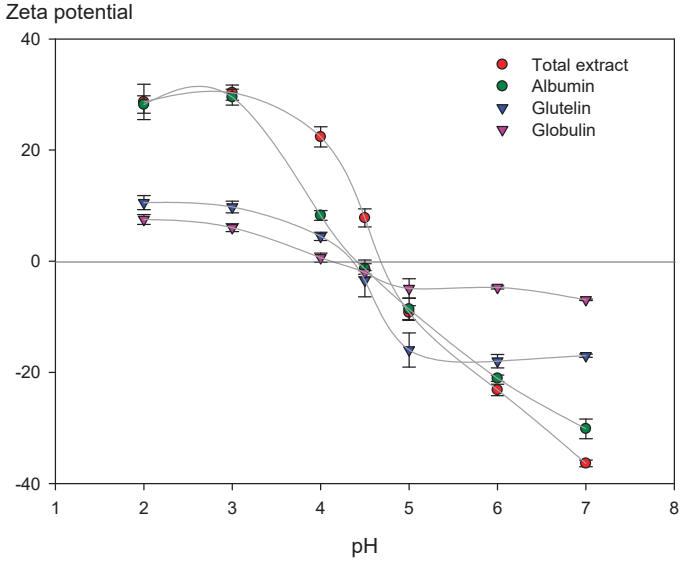

Figure 4. Zeta potential of proteins extracted from chickpea flour. Protein concentration 0.1% (*w/v*).

On the other hand, the GLO fraction presented the lowest Zeta potential range (+7 and –7 mV) for the range of pH studied, followed by the GLU fraction, where the literature has established that potentials between |5| and |15| are in the limiting flocculation region [27]. This low stability for GLO and GLU fraction was expected, considering that extraction solvents contained polyelectrolytes (NaCl and NaOH, respectively). Their presence could affect protein stability attributed to the protein-polyelectrolytes complex mechanism based on charge patch and charge regulation [48].

In parallel, Zeta potential results show an isoelectric point (IP) close to 4.5 for all proteins (Figure 4), which confirms the choice of a pH = 4.5 for protein precipitation

according to the method of extraction employed. This result also agrees with Vani & Zayas [50], who indicate that most vegetable proteins have an IP between 4.0–5.0. It is essential to consider that proteins could adsorb charges on their surfaces at their IP, even when their net charge is neutral. Second or higher-order electrostatic factors could also favor their adsorption/interaction and stability [48]. Based on the above, TE and ALB would potentially apply in food formulations with pHs higher or lower than the IP.

3.3. Surface and Structural Properties of Vegetable Protein Dispersion Compared to Animal Protein: Ovalbumin

3.3.1. Surface Hydrophobicity

Protein surface hydrophobicity characterizes the number of hydrophobic groups on the surface of protein molecules in contact with the polar water environment. It can affect many functional properties, such as emulsification, foaming, and gelation. It is an important index for the physical, chemical, and functional properties [51], which can also measure the degree of denaturation of proteins. This work compared the surface hydrophobicity of the extracted chickpea protein fractions with the food industry's most widely used animal protein: ovalbumin. This protein showed similar characteristics to chickpea proteins, such as a globular protein, high solubility in aqueous media, and isoelectric point at pH 4.6 [52]. The surface hydrophobicity was measured at pH = 7, considering potential applications in foods, due to the high stability in all fractions observed at neutral and acidic pH (Figure 4).

All the extracted proteins showed a higher surface hydrophobicity index than ovalbumin (OVO) (Figure 5). The index values for TE, ALB, GLO, and GLU were 3.7, 4.0, 5.7, and 2.2 times higher than OVO. The higher surface hydrophobicity of plant proteins was not expected because all fractions contain 11S subunits. Hexamers are hydrophobic and located within the macromolecular assembly of the legumin, while the less hydrophobic acid domains are located on the surface [53]. In this case, the balance of forces to maintain the legumin structural domains is disturbed, for example, by the dehydration step of the isolate preparation process, which modifies the final surface hydrophobicity of the protein. This was demonstrated, since the protein presented some degree of denaturation during the extraction process, which is corroborated by the SDS-PAGE (Figure 4, lane 4), where the 11S subunit showed a light pattern.

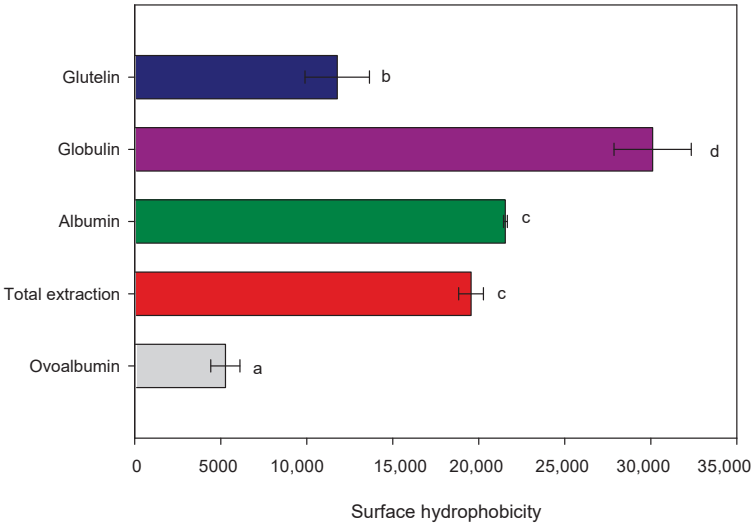

Figure 5. Surface hydrophobicity of proteins extracted from chickpea flour. Different letters (a–d) indicate significant differences ($p < 0.05$) between samples. Error bars indicate the mean and standard deviation of triplicates.

Figure 5 also indicated that GLO samples showed the highest surface hydrophobicity index (30,110 ± 2248 a.u.) compared to other fractions. It is important to note that surface hydrophobicity is a structure-related function. The above depends on the size and shape of the protein molecule, amino acid composition, sequence, and intra- e intermolecular cross-link [54,55]. So, in this case, it cannot be attributed to a high hydrophobic amino acid concentration (Table 3) and sequence, considering that no significant differences were observed between protein fractions. Although the GLO fraction is mainly composed of 11S protein, it is not enough to increase this parameter significantly. For that, the relationship between spatial conformations and surface hydrophobicity could be determined by FTIR as a shift in the wavelength of amide II, which is related to secondary structural conformation [56,57].

3.3.2. Dynamic Interfacial (DIT) and Surface Tension (DST)

Amphiphilic molecules, such as proteins, are recognized for their ability to reduce interfacial and surface tension between the dispersed and continuous phases, which is essential for stabilizing emulsions and foams. In recent decades, the literature has reported the wide use of partially hydrophobic molecules for the stabilization of foams and emulsions due to their ability to adsorb at air-liquid strongly and liquid-liquid interfaces to sterically hinder coarsening [58–60].

In this sense, the interfacial behavior of chickpea proteins (TE, ALB, GLO, and GLU) was evaluated in comparison with the animal protein OVO. The pendant drop method measured dynamic interfacial (DIT) and surface tension (DST). The results were expressed as interfacial and surface pressure and fitted to a kinetic model with excellent performance, with all RMS values $\leq$ 5.6% (Table 4). From this model, the specific rate constant for protein adsorption at the interface (k) and the equilibrium pressure (Π_{eq}) were obtained (Table 4).

Table 4. Comparison of the effect of surface and interfacial pressure of chickpea proteins concerning ovalbumin.

	Interfacial Pressure (mN/m)			**Surface Pressure (mN/m)**		
Sample	**k (s^{-1})**	**Π_{eq} (mN/m)**	**RMS (%)**	**k (s^{-1})**	**Π_{eq} (mN/m)**	**RMS (%)**
Ovalbumin	$0.0099^{c} \pm 0.0003$	$12.88^{a} \pm 0.23$	3.37	$0.0123^{d} \pm 0.0010$	$26.96^{a} \pm 0.59$	3.40
Total extraction	$0.0038^{ab} \pm 0.0006$	$15.97^{b} \pm 0.17$	5.60	$0.0040^{a} \pm 0.0001$	$31.46^{c} \pm 0.10$	3.87
Albumin	$0.0033^{a} \pm 0.0004$	$16.16^{b} \pm 0.15$	5.31	$0.0064^{bc} \pm 0.0009$	$29.12^{b} \pm 0.61$	2.75
Globulin	$0.0046^{b} \pm 0.0007$	$19.70^{c} \pm 0.27$	3.89	$0.0049^{ab} \pm 0.0006$	$32.01^{c} \pm 0.48$	3.32
Glutelin	$0.0029^{a} \pm 0.0002$	$18.12^{d} \pm 0.53$	1.17	$0.0071^{c} \pm 0.0009$	$34.29^{d} \pm 0.42$	1.83

Different letters ($^{a, b, c, d}$) indicate significant differences ($p < 0.05$) between samples.

The rate at which proteins are absorbed in an interface is essential during emulsions and foams' formation. Concerning the interfacial pressure (Table 4), all the chickpea proteins extracted in this work presented a lower absorption rate (k) than OVO. When analyzing Π_{eq}, GLO showed the highest value (19.70 ± 0.27 mN/m) (Figure 6b), indicating that this protein may have potential use in stabilizing emulsions. For surface pressure (Table 4), TE, ALB, GLO, and GLU fractions presented lower absorption rate values at the interface than OVO. The protein that showed the highest Π_{eq} value (34.29 ± 0.42 mN/m) (Table 4) was GLU fraction, which could positively affect foam stabilization. It can explain because chickpea proteins showed a rapid diffusion and absorption at the oil/water and air/water interface compared to OVO, followed by a slower stage in which the conformational rearrangement of the proteins occurs at the interface.

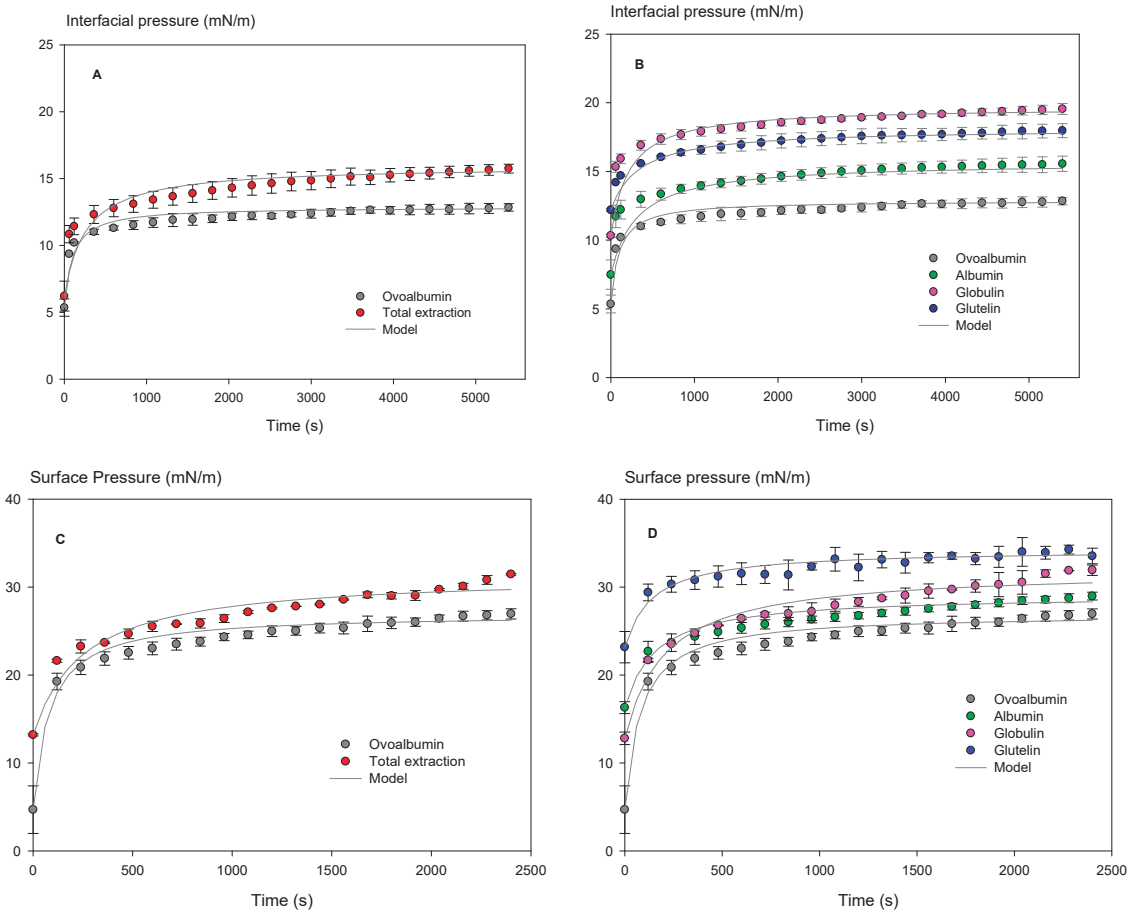

Figure 6. Changes in surface and interfacial pressure between protein dispersions extracted from chickpea flour and commercial ovalbumin. (**A**): Total extraction interfacial pressure concerning ovalbumin; (**B**): Interfacial pressure of albumin, globulin, and glutelin concerning ovalbumin; (**C**): Total extraction surface pressure concerning ovalbumin; (**D**): Surface pressure of albumin, globulin, and glutelin concerning ovalbumin. Protein concentration 0.1% (*w*/*v*), error bars indicate the mean and standard deviation of triplicates.

Molecular weight has been reported to influence the adsorption kinetics of amphiphilic molecules at the oil/water and air/water interface. Low molecular weight surfactants can diffuse faster and lower interfacial tension to a greater extent than high molecular weight surfactants. However, high molecular weight surfactants are more effective in forming a viscoelastic film surrounding oil droplets or gas bubbles, which favors the stabilization of emulsions and foams [61,62]. Those results agree with the results obtained in this study since the Mw profile of the OVO was in the range of 103 kD and 38 kDa (data not shown), values higher than the band profile for all chickpea proteins, which were concentrated between 49 and 12 kDa (Figure 3). Hence, TE, ALB, GLO, and GLU had a lower Mw than OVO. Therefore, chickpea proteins have improved surface and interfacial behavior compared to OVO, evidencing their potential as foam and emulsion stabilizers for proteins extracted (GLO and GLU) and may be a replacement alternative to animal protein.

3.3.3. Structural Properties: Secondary Structure Analysis

FTIR spectra of OVO, TE, ALB, GLO, and GLU proteins are shown in Figure 7a. A similar pattern was observed between samples, where the peak at 1050 cm^{-1} showed the OVO characteristic band corresponding to the sulfoxide (S=O) bond [63], having a significant intensity compared to plant proteins. All samples had a broad and robust peak between 3300–3500 cm^{-1} called amide A, representing the intermolecular H-bonded, O-H, and N-H stretching vibrations [64]. As expected in all the samples, FTIR showed two intense bands around ~1633 cm^{-1} and ~1520 cm^{-1} corresponding to the amide I (C=O stretching) and amide II (NH bending and CN stretching) regions of the proteins, respectively [6,65]. In addition, it also identified a band around ~1233 cm^{-1} corresponding to the amide III region (CN stretching, NH bending) [65].

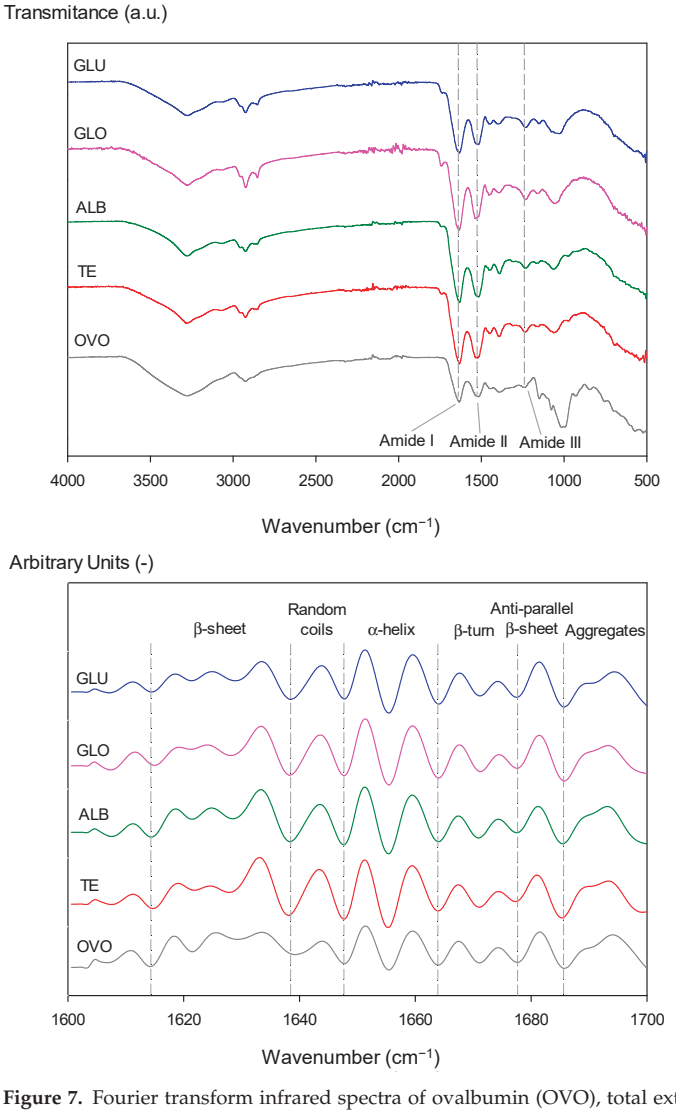

Figure 7. Fourier transform infrared spectra of ovalbumin (OVO), total extraction (TE), albumin (ALB), globulin (GLO), and glutelin (GLU). (**A**) Full spectra and (**B**) Second derivative spectrum.

The amide I absorption region in the infrared spectrum of a protein is helpful for secondary structure elucidation since the amide I band is the sum of overlapping component bands (α-helix, β-sheet, β-turn, and randomly coiled conformation). It is mainly related to the C=O stretching of the peptide bonds influenced by their various environments in the different kinds of secondary structures [65,66]. Therefore, knowing the secondary structural composition of the proteins analyzed (OVO, TE, ALB, GLO, and GLU) is relevant to understanding their behavior for technological applications. Previous studies have shown that the α–helix and β–sheet protein secondary structures are responsible for emulsion and foaming capacities [67].

It is important to note that a second derivative analysis is often performed before deconvolution to identify the peaks required for peak fitting. The current study's second derivative peaks were attributed to the secondary structure peak assignments (Figure 7b), following those reported by Chang et al. [17]. Normalization of the amide I region was also performed to obtain a good peak shape for peak fitting and comparison between samples, considering the highest intensity equal to 1. Later, it was deconvoluted using "Gaussian peak fitting". Each sample revealed 10 major Gaussian bands (Figure 7b) whose wavenumbers corresponded to β-sheet (~1620, ~1625, and ~1630 cm^{-1}), random coils (~1641 cm^{-1}), α-helix (~1651 and ~1659 cm^{-1}), β-turn (~1668 and 1675 cm^{-1}), anti-parallel β-sheet (~1681 cm^{-1}), and aggregates (~1692 cm^{-1}) [9,17,34]. For all samples, amide I peak deconvolution showed a secondary structure composition of β-sheet (~31%), followed by α-helix (~20%), β-turn (~18%), and anti-parallel β-sheet (~10%). These results were consistent with previous studies of chickpea protein [68]. Therefore, it is correct to compare animal and plant proteins used in this study due to their similar composition of structural conformation.

However, changes in peak area (1700–1600 cm^{-1}) were observed, which influenced the secondary structure of proteins. Generally, the α-helix and β-sheets are buried inside the polypeptide chains and utilize intermolecular hydrogen bonds between carbonyl oxygen (-CO) and amino hydrogen (-NH) to stabilize the secondary structures [67].

Meanwhile, β-turn and random coils originate from unfolding highly ordered protein structures and impart flexibility to proteins [69,70]. The ratio β-turn/random coil was higher in legumin protein fractions (1.8–2.0) compared to OVO (1.5), demonstrating that the extracted protein fractions could be more flexible than this animal protein. This behavior was previously report using the ability of ultrasound to convert random coil and β-turn into stable and orderly helical structures stabilized by hydrogen bonds but converted at different rates [71,72]. It is important to remark that cavitation-induced protein unfolding, and dissociation can coincide with aggregate formation [73]. The Amida I/Amida II ratio [67] indicated a shifted wavelength for all fractions compared to OVO (1.077), the highest shift for GLO of 1.067. Consequently, the most significant conformational changes in secondary structure protein were observed in the GLO fraction due to Amida II shift wavelength from 1516 (OVO) to 1530 cm^{-1} (GLO). This result confirms the highest surface hydrophobicity of this fraction.

On the other hand, when comparing the intensity results of secondary structure for α-helix, the samples TE, GLO, and GLU (20.3, 20.5, and 20.0%) present lower values than OVO (21.1%). It could be related to differences in the level of flexibility and functional properties [74,75]. Besides this, differences were observed in the intensity of the peak attributed to the β-sheet comparing OVO and TE. The intensity ratio between peaks at 1633 and 1624 cm^{-1} were 1.7 and 1.36–1.44 for OVO and TE and fractions, respectively, indicating significant differences between the conformational structure of the β-sheet of animal and plant proteins. Studies by Zhu et al. [74] and Yan et al. [75] indicated that a low content of α-helix provides high flexibility and good emulsifying and foaming properties in vegetable proteins such as soybean, where flexible proteins showed more robust surface activity than rigid ones. The above was related to the good results for interfacial pressure, surface pressure, and surface hydrophobicity that chickpea proteins presented compared to animal proteins. They significantly decreased the absorption rate at the oil-water and

air-water interface (Table 4) and showed higher values of surface hydrophobicity (Figure 5) than OVO.

The results could be explained by the high flexibility of the plant protein, which contributes to absorption at the oil-water or air-water interface for a stable interface layer. More high surface hydrophobicity contributes to the stability of foams and emulsions [74], which is correlated with the results obtained for GLO and TE in this study.

4. Conclusions

This study applied two extraction methodologies to obtain the total protein fraction (TE) and the individual fractions (ALB, GLO, and GLU) from defatted chickpea flour. It showed that simple and low-cost extraction methods (alkaline solubility and solvent solubility) could obtain a high protein yield with a significant contribution of essential and hydrophobic amino acids. When evaluating their physicochemical characteristics, a potential application of chickpea proteins in food formulations is for both acid and neutral pH, where its high stability was evidenced due to their high Z potential values under these conditions.

In this work, we observed differences in the physicochemical properties (yield, molecular weight, Z potential, and hydrophobic amino acids) of the total protein fraction compared to the individual fraction obtained. It was emphasized by analyzing its surface and structural properties compared to the food industry's most widely used animal protein. The correlation between the secondary structure of proteins concerning their functional properties (formation of foams and emulsions) was evidenced, which is crucial for the food industry when formulating products based on vegetable proteins in replacement of animal protein with functional features.

Chickpea proteins have improved surface properties compared to OVO, evidencing their potential use as foam and emulsion stabilizers. In addition, surface properties were related to the secondary structure of chickpea proteins and their flexibility. Although the best fraction for replacing OVO was the GLO fraction, the cost, yield, and time to obtain it are high. So, the TE fraction could be a better choice for industrial applications.

The food industry is increasingly interested in protein sources with good functional properties and less allergenicity. Therefore, based on our results, chickpea proteins could be a potential replacement alternative to the most widely used animal protein in the food industry, ovalbumin.

Author Contributions: Conceptualization, S.M., R.N.Z. and D.S.-M.; methodology, S.M., R.N.Z., N.P. and D.S.-M.; software, R.N.Z. and D.S.-M.; validation, S.M. and R.N.Z.; formal analysis, S.M., R.N.Z., N.P., M.G.-C. and D.S.-M.; investigation, S.M., R.N.Z. and D.S.-M.; resources, S.M., and R.N.Z..; data curation, S.M., R.N.Z., N.P. and D.S.-M.; writing—original draft preparation, D.S.-M.; writing—review and editing, S.M., R.N.Z., M.G.-C. and D.S.-M.; visualization, S.M. and R.N.Z.; supervision, S.M. and R.N.Z.; project administration, S.M. and R.N.Z.; funding acquisition, S.M., R.N.Z. and D.S.-M. All authors have read and agreed to the published version of the manuscript.

Funding: This research was funded by the University of Santiago de Chile, VRIDEI-DICYT Support C-Fondecyt 2022, grant number 5392208M_ACDicyt and Project FONDECYT, grant number 1201426. The APC was funded by CONICYT Ph.D. Grant 2019 No. 21190731.

Institutional Review Board Statement: Not applicable.

Informed Consent Statement: Not applicable.

Data Availability Statement: The data presented in this study are available on request from the corresponding author. The data are not publicly available due to it is part of Daniela Soto-Madrid Ph.D. thesis, which is not published yet.

Acknowledgments: The authors acknowledge that ANID Ph.D. Grant 2019 N° 21190731 and supported by a research grant 2022 of the Technological Faculty, USACH (Daniela Soto Madrid); Apoyo C-Fondecyt 2022 5392208M_ACDicyt (Silvia Matiacevich and Marlen Gutiérrez-Cutiño); Project FONDECYT 1201426 (Rommy N. Zúñiga).

Conflicts of Interest: The authors declare that there is no conflict of interest regarding the publication of this paper.

References

1. Ma, K.K.; Greis, M.; Lu, J.; Nolden, A.A.; McClements, D.J.; Kinchla, A.J. Functional Performance of Plant Proteins. *Foods* **2022**, *11*, 594. [CrossRef] [PubMed]
2. Iqbal, A.; Khalil, I.A.; Ateeq, N.; Khan, M.S. Nutritional quality of important food legumes. *Food Chem.* **2006**, *97*, 331–335. [CrossRef]
3. Kaur, R.; Prasad, K. Technological, processing and nutritional aspects of chickpea (*Cicer arietinum*)-A review. *Trends Food Sci. Technol.* **2021**, *109*, 448–463. [CrossRef]
4. Chang, Y.; Alli, I.; Konishi, Y.; Ziomek, E. Characterization of protein fractions from Chickpea (*Cicer arietinum* L.) and oat (*Avena sativa* L.) seeds using proteomic techniques. *Food Res. Int.* **2011**, *44*, 3094–3104. [CrossRef]
5. Glusac, J.; Isaschar-Ovdat, S.; Fishman, A. Transglutaminase modifies the physical stability and digestibility of chickpea protein-stabilized oil-in-water emulsions. *Food Chem.* **2020**, *315*, 126301. [CrossRef]
6. Xu, Y.; Obielodan, M.; Sismour, E.; Arnett, A.; Alzahrani, S.; Zhang, B. Physicochemical, functional, thermal and structural properties of isolated Kabuli chickpea proteins as affected by processing approaches. *Int. J. Food Sci. Technol.* **2017**, *52*, 1147–1154. [CrossRef]
7. Jukanti, A.K.; Gaur, P.M.; Gowda, C.L.; Chibbar, R.N. Nutritional quality and health benefits of chickpea (*Cicer arietinum* L.): A review. *Br. J. Nutr.* **2012**, *108*, S11–S26. [CrossRef]
8. Hall, C.; Hillen, C.; Garden Robinson, J. Composition, nutritional value, and health benefits of pulses. *Cereal Chem.* **2017**, *94*, 11–31. [CrossRef]
9. Shevkani, K.; Singh, N.; Chen, Y.; Kaur, A.; Yu, L. Pulse proteins: Secondary structure, functionality and applications. *J. Food Sci. Technol.* **2019**, *56*, 2787–2798. [CrossRef]
10. Kumar, M.; Tomar, M.; Potkule, J.; Verma, R.; Punia, S.; Mahapatra, A.; Belwal, T.; Dahuja, A.; Mukesh, J.; Joshi, S.; et al. Advances in the plant protein extraction: Mechanism and recommendations. *Food Hydrocoll.* **2021**, *115*, 106595. [CrossRef]
11. Sánchez-Vioque, R.; Clemente, A.; Vioque, J.; Bautista, J.; Millán, F. Protein isolates from chickpea (*Cicer arietinum* L.): Chemical composition, functional properties and protein characterization. *Food Chem.* **1999**, *64*, 237–243. [CrossRef]
12. Castellión, M.; Matiacevich, S.; Buera, P.; Maldonado, S. Protein deterioration and longevity of quinoa seeds during long-term storage. *Food Chem.* **2010**, *121*, 952–958. [CrossRef]
13. Yang, J.; Sagis, L.M. Interfacial behavior of plant proteins—Novel sources and extraction methods. *Curr. Opin. Colloid Interface Sci.* **2021**, *56*, 101499. [CrossRef]
14. Osborne, T.B. The vegetable proteins. In *Monographs in Biochemistry*; Longmans, Green and Company: London, UK, 1924.
15. Agboola, S.; Ng, D.; Mills, D. Characterisation and functional properties of Australian rice protein isolates. *J. Cereal Sci.* **2005**, *41*, 283–290. [CrossRef]
16. Singhal, A.; Karaca, A.C.; Tyler, R.; Nickerson, M. Pulse proteins: From processing to structure-function relationships. In *Grain Legumes*; Kumar Goyal, A., Ed.; IntechOpen: London, UK, 2016; Volume 3, pp. 55–78.
17. Chang, L.; Lan, Y.; Bandillo, N.; Ohm, J.B.; Chen, B.; Rao, J. Plant proteins from green pea and chickpea: Extraction, fractionation, structural characterization and functional properties. *Food Hydrocoll.* **2022**, *123*, 107165. [CrossRef]
18. Lam AC, Y.; Can Karaca, A.; Tyler, R.T.; Nickerson, M.T. Pea protein isolates: Structure, extraction, and functionality. *Food Rev. Int.* **2018**, *34*, 126–147. [CrossRef]
19. Thareja, P.; Saraswat, Y.C.; Oberoi, C. Ovalbumin-stabilized concentrated emulsion gels. *Bull. Mater. Sci.* **2020**, *43*, 194. [CrossRef]
20. Huang, T.; Tu, Z.C.; Wang, H.; Shangguan, X.; Zhang, L.; Niu, P.; Sha, X.M. Promotion of foam properties of egg white protein by subcritical water pre-treatment and fish scales gelatin. *Colloids Surf. A Physicochem. Eng. Asp.* **2017**, *512*, 171–177. [CrossRef]
21. Karaca, A.C.; Nickerson, M.; Low, N.H. Microcapsule production employing chickpea or lentil protein isolates and maltodextrin: Physicochemical properties and oxidative protection of encapsulated flaxseed oil. *Food Chemistry* **2013**, *139*, 448–457. [CrossRef]
22. Chang, Y.W.; Alli, I.; Molina, A.T.; Konishi, Y.; Boye, J.I. Isolation and characterization of chickpea (*Cicer arietinum* L.) seed protein fractions. *Food Bioprocess Technol.* **2012**, *5*, 618–625. [CrossRef]
23. AOAC. *Official Methods of Analysis*, 16th ed.; AOAC: Gaithersburg, MD, USA, 1998.
24. Laemmli, U.K. Cleavage of structural proteins during the assembly of the head of bacteriophage T4. *Nature* **1970**, *227*, 680–685. [CrossRef] [PubMed]
25. Janssen, P.S.; van Nispen, J.W.; Melgers, P.A.; Van den Bogaart HW, M.; Hamelinck RL, A.E.; Goverde, B.C. HPLC analysis of phenylthiocarbamyl (PTC) amino acids. I. Evaluation and optimization of the procedure. *Chromatographia* **1986**, *22*, 345–350. [CrossRef]
26. Espinosa-Ramírez, J.; Serna-Saldívar, S.O. Wet-milled chickpea coproduct as an alternative to obtain protein isolates. *LWT—Food Sci. Technol.* **2019**, *115*, 108468. [CrossRef]
27. Heurtault, B.; Saulnier, P.; Pech, B.; Proust, J.E.; Benoit, J.P. Physico-chemical stability of colloidal lipid particles. *Biomaterials* **2003**, *24*, 4283–4300. [CrossRef]
28. Kato, A.; Nakai, S. Hydrophobicity determined by a fluorescence probe method and its correlation with surface properties of proteins. *Biochim. et Biophys. Acta (BBA)-Protein Struct.* **1980**, *624*, 13–20. [CrossRef]

29. Bahtz, J.; Knorr, D.; Tedeschi, C.; Leser, M.E.; Valles-Pamies, B.; Miller, R. Adsorption of octanoic acid at the water/oil interface. *Colloids Surf. B Biointerfaces* **2009**, *74*, 492–497. [CrossRef] [PubMed]
30. Dapueto, N.; Troncoso, E.; Mella, C.; Zúñiga, R.N. The effect of denaturation degree of protein on the microstructure, rheology and physical stability of oil-in-water (O/W) emulsions stabilized by whey protein isolate. *J. Food Eng.* **2019**, *263*, 253–261. [CrossRef]
31. Zúñiga, R.N.; Skurtys, O.; Osorio, F.; Aguilera, J.M.; Pedreschi, F. Physical properties of emulsion-based hydroxypropyl methylcellulose films: Effect of their microstructure. *Carbohydr. Polym.* **2012**, *90*, 1147–1158. [CrossRef]
32. Azuara, E.; Cortes, R.; Garcia, H.S.; Beristain, C.I. Kinetic model for osmotic dehydration and its relationship with Fick's second law. *Int. J. Food Sci. Technol.* **1992**, *27*, 409–418. [CrossRef]
33. Moyano, P.C.; Pedreschi, F. Kinetics of oil uptake during frying of potato slices: Effect of pre-treatments. *LWT-Food Sci. Technol.* **2006**, *39*, 285–291. [CrossRef]
34. Lan, Y.; Xu, M.; Ohm, J.B.; Chen, B.; Rao, J. Solid dispersion-based spray-drying improves solubility and mitigates beany flavour of pea protein isolate. *Food Chem.* **2019**, *278*, 665–673. [CrossRef] [PubMed]
35. da Silva, F.C.; da Fonseca, C.R.; de Alencar, S.M.; Thomazini, M.; de Carvalho Balieiro, J.C.; Pittia, P.; Favaro-Trindade, C.S. Assessment of production efficiency, physicochemical properties and storage stability of spray-dried propolis, a natural food additive, using gum Arabic and OSA starch-based carrier systems. *Food Bioprod. Process.* **2013**, *91*, 28–36. [CrossRef]
36. Tang, J.; Yang, T. Dehydrated vegetables: Principles and systems. In *Handbook of Vegetable Preservation and Processing*, 2nd ed.; Hui, A.H., Ghazala, S., Graham, D.M., Murrell, K.D., Nip, W.K., Eds.; Marcel Dekker: New York, NY, USA, 2004; pp. 335–372.
37. Boye, J.I.; Aksay, S.; Roufik, S.; Ribéreau, S.; Mondor, M.; Farnworth, E.; Rajamohamed, S.H. Comparison of the functional properties of pea, chickpea and lentil protein concentrates processed using ultrafiltration and isoelectric precipitation techniques. *Food Res. Int.* **2010**, *43*, 537–546. [CrossRef]
38. Casey, R.; Domoney, C.; Smith, A.M. Peas: Genetics, molecular biology and biotechnology. In *Biochemistry and Molecular Biology of Seed Products*; Casey, R., Davies, D.R., Eds.; John Innes Institute: Norwich, UK, 1993; Volume 10, pp. 121–163.
39. Grasso, N.; Lynch, N.L.; Arendt, E.K.; O'Mahony, J.A. Chickpea protein ingredients: A review of composition, functionality, and applications. *Compr. Rev. Food Sci. Food Saf.* **2022**, *21*, 435–452. [CrossRef]
40. Franco, E.; Ferreira, R.B.; Teixeira, A.R. Utilization of an improved methodology to isolate *Lupinus albus* conglutins in the study of their sedimentation coefficients. *J. Agric. Food Chem.* **1997**, *45*, 3908–3913. [CrossRef]
41. Liu, L.H.; Hung, T.V.; Bennett, L. Extraction and characterization of chickpea (*Cicer arietinum*) albumin and globulin. *J. Food Sci.* **2008**, *73*, C299–C305. [CrossRef]
42. Vioque, J.; Sánchez-Vioque, R.; Clemente, A.; Pedroche, J.; Bautista, J.; Millán, F. Purification and partial characterization of chickpea 2S albumin. *J. Agric. Food Chem.* **1999**, *47*, 1405–1409. [CrossRef]
43. Clemente, A.; Vioque, J.; Sánchez-Vioque, R.; Pedroche, J.; Bautista, J.; Millán, F. Factors affecting the in vitro protein digestibility of chickpea albumins. *J. Sci. Food Agric.* **2000**, *80*, 79–84. [CrossRef]
44. Ghribi, A.M.; Gafsi, I.M.; Blecker, C.; Danthine, S.; Attia, H.; Besbes, S. Effect of drying methods on physicochemical and functional properties of chickpea protein concentrates. *J. Food Eng.* **2015**, *165*, 179–188. [CrossRef]
45. FAO/WHO. Protein quality evaluation. In *Report of Joint FAO/WHO Expert Consultation*; FAO/WHO: Bethesda, MD, USA; Rome, Italy, 1989.
46. Wilde, P.; Mackie, A.; Husband, F.; Gunning, P.; Morris, V. Proteins and emulsifiers at liquid interfaces. *Adv. Colloid Interface Sci.* **2004**, *108*, 63–71. [CrossRef]
47. Sagis, L.M.; Yang, J. Protein-stabilized interfaces in multiphase food: Comparing structure-function relations of plant-based and animal-based proteins. *Curr. Opin. Food Sci.* **2022**, *43*, 53–60. [CrossRef]
48. Lunkad, R.; Barroso da Silva, F.L.; Košovan, P. Both charge-regulation and charge-patch distribution can drive adsorption on the wrong side of the isoelectric point. *J. Am. Chem. Soc.* **2022**, *144*, 1813–1825. [CrossRef] [PubMed]
49. Salvia-Trujillo, L.; Rojas-Graü, M.A.; Soliva-Fortuny, R.; Martín-Belloso, O. Effect of processing parameters on physicochemical characteristics of microfluidized lemongrass essential oil-alginate nanoemulsions. *Food Hydrocoll.* **2013**, *30*, 401–407. [CrossRef]
50. Vani, B.; Zayas, J.F. Wheat germ protein flour solubility and water retention. *J. Food Sci.* **1995**, *60*, 845–848. [CrossRef]
51. Zhu, Z.; Mao, X.; Wu, Q.; Zhang, J.; Deng, X. Effects of oxidative modification of peroxyl radicals on the structure and foamability of chickpea protein isolates. *J. Food Sci.* **2021**, *86*, 824–833. [CrossRef] [PubMed]
52. Judge, R.A.; Johns, M.R.; White, E.T. Solubility of ovalbumin in ammonium sulfate solutions. *J. Chem. Eng. Data* **1996**, *41*, 422–424. [CrossRef]
53. Yust, M.M.; Pedroche, J.; Giron-Calle, J.; Alaiz, M.; Millán, F.; Vioque, J. Production of ace inhibitory peptides by digestion of chickpea legumin with alcalase. *Food Chem.* **2003**, *81*, 363–369. [CrossRef]
54. Aider, M.; Djenane, D.; Ounis, W.B. Amino acid composition, foaming, emulsifying properties and surface hydrophobicity of mustard protein isolate as affected by pH and NaCl. *Int. J. Food Sci. Technol.* **2012**, *47*, 1028–1036. [CrossRef]
55. Shen, L.; Tang, C.H. Microfluidization as a potential technique to modify surface properties of soy protein isolate. *Food Res. Int.* **2012**, *48*, 108–118. [CrossRef]
56. Vedantham, G.; Sparks, H.G.; Sane, S.U.; Tzannis, S.; Przybycien, T.M. A holistic approach for protein secondary structure estimation from infrared spectra in H_2O solutions. *Anal. Biochem.* **2000**, *285*, 33–49. [CrossRef]
57. Cai, S.; Singh, B.R. A distinct utility of the amide III infrared band for secondary structure estimation of aqueous protein solutions using partial least squares methods. *Biochemistry* **2004**, *43*, 2541–2549. [CrossRef] [PubMed]

58. Velikov, K.P.; Velev, O.D. Stabilization of thin films, foams, emulsions and bifluid gels with surface-active solid particles. In *Colloid Stability and Application in Pharmacy*, 1st ed.; Tadros, T., Ed.; Wiley-VCH Verlag GmbH & Co. KgaA: Weinheim, Germany, 2007; Volume 3, pp. 277–306.
59. Hunter, T.N.; Pugh, R.J.; Franks, G.V.; Jameson, G.J. The role of particles in stabilising foams and emulsions. *Adv. Colloid Interface Sci.* **2008**, *137*, 57–81. [CrossRef] [PubMed]
60. Horozov, T.S. Foams and foam films stabilised by solid particles. *Curr. Opin. Colloid Interface Sci.* **2008**, *13*, 134–140. [CrossRef]
61. Silva, H.D.; Cerqueira, M.A.; Vicente, A.A. Influence of surfactant and processing conditions in the stability of oil-in-water nanoemulsions. *J. Food Eng.* **2015**, *167*, 89–98. [CrossRef]
62. Deng, L. Current progress in the utilization of soy-based emulsifiers in food applications—A Review. *Foods* **2021**, *10*, 1354. [CrossRef]
63. Sigma-Aldrich. IR Spectrum Table by Frequency Range. 1924. Available online: https://www.sigmaaldrich.com/CL/es/technical-documents/technical-article/analytical-chemistry/photometry-and-reflectometry/ir-spectrum-table (accessed on 30 October 2022).
64. Kudre, T.G.; Benjakul, S.; Kishimura, H. Comparative study on chemical compositions and properties of protein isolates from mung bean, black bean, and Bambara groundnut. *J. Sci. Food Agric.* **2013**, *93*, 2429–2436. [CrossRef]
65. Kong, J.; Yu, S. Fourier transform infrared spectroscopic analysis of protein secondary structures. *Acta Biochim. et Biophys. Sin.* **2007**, *39*, 549–559. [CrossRef]
66. Schwinte, P.; Voegel, J.C.; Picart, C.; Haikel, Y.; Schaaf, P.; Szalontai, B. Stabilizing effects of various polyelectrolyte multilayer films on the structure of adsorbed/embedded fibrinogen Molecules: An ATR−FTIR Study. *J. Phys. Chem. B* **2001**, *105*, 11906–11916. [CrossRef]
67. de la Rosa-Millán, J.; Orona-Padilla, J.L.; Flores-Moreno, V.M.; Serna-Saldívar, S.O. Physicochemical, functional and ATR-FTIR molecular analysis of protein extracts derived from starchy pulses. *Int. J. Food Sci. Technol.* **2018**, *53*, 1414–1424. [CrossRef]
68. Carbonaro, M.; Maselli, P.; Nucara, A. Relationship between digestibility and secondary structure of raw and thermally treated legume proteins: A Fourier transform infrared (FT-IR) spectroscopic study. *Amino Acids* **2012**, *43*, 911–921. [CrossRef]
69. Chen, X.; Zhou, R.; Xu, X.; Zhou, G.; Liu, D. Structural modification by high-pressure homogenization for improved functional properties of freeze-dried myofibrillar proteins powder. *Food Res. Int.* **2017**, *100*, 193–200. [CrossRef] [PubMed]
70. Peng, H.; Chen, S.; Luo, M.; Ning, F.; Zhu, X.; Xiong, H. Preparation and self-assembly mechanism of Bovine Serum Albumin–Citrus peel pectin conjugated hydrogel: A potential delivery system for Vitamin C. *J. Agric. Food Chem.* **2016**, *64*, 7377–7384. [CrossRef] [PubMed]
71. Gülseren, İ.; Güzey, D.; Bruce, B.D.; Weiss, J. Structural and functional changes in ultrasonicated bovine serum albumin solutions. *Ultrason. Sonochem.* **2007**, *14*, 173–183. [CrossRef] [PubMed]
72. Li, W.; Li, S.; Hu, Y.; Zhou, M.; Wang, C.; Li, D.; Li, D. Impact of hot alkali modification conditions on secondary structure of peanut protein and embedding rate of curcumin. *Food Sci. Hum. Wellness* **2019**, *8*, 283–291. [CrossRef]
73. Asaithambi, N.; Singha, P.; Singh, S.K. Comparison of hydrodynamic and acoustic cavitation's effect on functional, rheological, and structural properties of egg white proteins. *Innov. Food Sci. Emerg. Technol.* **2022**, *82*, 103166. [CrossRef]
74. Zhu, Y.; Fu, S.; Wu, C.; Qi, B.; Teng, F.; Wang, Z.; Li, Y.; Jiang, L. The investigation of protein flexibility of various soybean cultivars in relation to physicochemical and conformational properties. *Food Hydrocoll.* **2020**, *103*, 105709. [CrossRef]
75. Yan, S.; Xu, J.; Zhang, S.; Li, Y. Effects of flexibility and surface hydrophobicity on emulsifying properties: Ultrasound-treated soybean protein isolate. *LWT—Food Sci. Technol.* **2021**, *142*, 110881. [CrossRef]

polymers

MDPI

Article

Effect of Selected Crosslinking and Stabilization Methods on the Properties of Porous Chitosan Composites Dedicated for Medical Applications

Monika Biernat [1,*], Anna Woźniak [1], Milena Chraniuk [2], Mirosława Panasiuk [2], Paulina Tymowicz-Grzyb [1], Joanna Pagacz [1], Agnieszka Antosik [1], Lidia Ciołek [1], Beata Gromadzka [2] and Zbigniew Jaegermann [1]

[1] Biomaterials Research Group, Łukasiewicz Research Network-Institute of Ceramics and Building Materials, Cementowa 8, 31-983 Kraków, Poland
[2] Department of In Vitro Studies, Institute of Biotechnology and Molecular Medicine, Kampinoska 25, 80-180 Gdańsk, Poland
* Correspondence: monika.biernat@icimb.lukasiewicz.gov.pl

Abstract: Chitosan is one of the most commonly employed natural polymers for biomedical applications. However, in order to obtain stable chitosan biomaterials with appropriate strength properties, it is necessary to subject it to crosslinking or stabilization. Composites based on chitosan and bioglass were prepared using the lyophilization method. In the experimental design, six different methods were used to obtain stable, porous chitosan/bioglass biocomposite materials. This study compared the crosslinking/stabilization of chitosan/bioglass composites with ethanol, thermal dehydration, sodium tripolyphosphate, vanillin, genipin, and sodium β-glycerophosphate. The physicochemical, mechanical, and biological properties of the obtained materials were compared. The results showed that all the selected crosslinking methods allow the production of stable, non-cytotoxic porous composites of chitosan/bioglass. The composite with genipin stood out with the best of the compared properties, taking into account biological and mechanical characteristics. The composite stabilized with ethanol is distinct in terms of its thermal properties and swelling stability, and it also promotes cell proliferation. Regarding the specific surface area, the highest value exposes the composite stabilized by the thermal dehydration method.

Keywords: chitosan; crosslinking; stabilization; porous composites; genipin; vanillin; TPP; BGP

Citation: Biernat, M.; Woźniak, A.; Chraniuk, M.; Panasiuk, M.; Tymowicz-Grzyb, P.; Pagacz, J.; Antosik, A.; Ciołek, L.; Gromadzka, B.; Jaegermann, Z. Effect of Selected Crosslinking and Stabilization Methods on the Properties of Porous Chitosan Composites Dedicated for Medical Applications. *Polymers* **2023**, *15*, 2507. https://doi.org/10.3390/polym15112507

Academic Editors: Cornelia Vasile, Gabriel Aguirre-Álvarez and Xiao-Feng Sun

Received: 27 April 2023
Revised: 24 May 2023
Accepted: 26 May 2023
Published: 29 May 2023

1. Introduction

The three most significant needs for biomaterials are biocompatibility, bioactivity, and simplicity of supply. The applicable standard [1] specifies the in vitro biocompatibility requirements that implant materials must meet. Porous implant materials for bone defect filling and bone tissue regeneration should also have optimum pore size, biodegradability, and strength qualities [2].

Chitosan is a naturally occurring polymer that has a broad application in tissue engineering and regenerative medicine [3–6]. It is biocompatible, biodegradable, and non-toxic. In addition, it has antimicrobial and osteoconductive properties, making it suitable for application in tissue engineering [7,8].

Due to their poor mechanical properties, chitosan-based scaffolds are usually applied in composites with ceramic particles such as hydroxyapatite or bioglass. Using such fillers also enables the production of reinforced and biologically active composites. In order to acquire the desired structure, chitosan biocomposites must be stabilized using a variety of techniques and crosslinking agents. Polymer crosslinking permits the enhancement of the biomaterial's mechanical properties and chemical resistance, as well as the acquisition of additional qualities such as elasticity, insolubility, and equilibrium swelling. Various

methods of chitosan crosslinking/stabilization are known from the literature and have been used depending on the form of biomaterial described [9]. Based on the literature review, it can be concluded that some crosslinking methods are dedicated directly to one selected structure of the chitosan-based biomaterial, while other structures can be obtained using two or more crosslinking methods.

For crosslinking/stabilizing chitosan porous structures in the form of scaffolds, genipin [10–13], L-aspartic acid [14,15], vanillin [16], sodium carbonate [17,18], sodium alginate [19], ethanol [17,19–22], thermal dehydration [23,24], and sodium tripolyphosphate [16,25,26] have been described previously. All these methods (except genipin) are inexpensive and simple and do not require the use of catalysts. However, methods using genipin or vanillin enable biomaterials with higher mechanical strength and better structural reproducibility than, for example, methods using sodium tripolyphosphate or disodium β-glycerophosphate. Some of the methods are able to stabilize chitosan scaffolds by crosslinking via covalent bounds (genipin, vanillin) or ionic bounds (tripolyphosphate or disodium β-glycerophosphate). Most of the crosslinking/stabilization methods of chitosan have been described in detail in the authors' previous review article [4].

Prior publications focused mostly on a detailed description of the features of chitosan biomaterials generated using a particular crosslinking/stabilization technique.

No studies that compare chitosan material in the form of a porous biocomposite with bioglass that were crosslinked/stabilized by the six methods described in this article have been found. The issue seems to be particularly interesting regarding the variety in the microstructure and physicochemical properties of biomaterials obtained by using different crosslinking methods, as well as the impact of the crosslinking compounds themselves on the biological properties of the obtained biomaterial.

Therefore, the authors of this paper undertook the effort of obtaining porous biocomposite scaffolds made of chitosan with a bioglass filler and crosslinking/stabilizing them using several methods.

The aim of the study was to compare the microstructure, physicochemical, and strength properties as well as the in vitro cytotoxicity of new porous composite scaffolds based on chitosan and bioglass. The structures of composites were chemically or physically stabilized using genipin, vanillin, disodium β-glycerophosphate, 5-hydrate sodium tripolyphosphate, ethanol and thermal dehydration. Considering the potential application in medicine, the researchers selected crosslinking/stabilization methods with zero or limited cytotoxicity.

The optimal crosslinking/stabilization techniques for porous composite scaffolds produced by lyophilization with chitosan and bioglass will be discussed here.

2. Materials and Methods

2.1. Materials

To obtain the chitosan/bioglass composites in this research work, chitoceutical chitosan 95/2000 (degree of deacetylation $\geq$92.6%) (HMC+-Heppe Medical Chitosan GmbH company, Halle, Germany) was used. As a composites filler, a bioglass (BG) synthesized by the sol-gel method from the system of 25% CaO-70% SiO_2-5% P_2O_5 (ŁUKASIEWICZ Research Network—Institute of Ceramics and Building Materials, Biomaterials Research Group, Warsaw, Poland) was used. The particle size range of the bioglass was in the range: d(0.1) 7.1 μm; d(0.5) 59.9 μm; d(0.9) 215 μm. As stabilizing and crosslinking agents, 99% vanillin (VAN) (Sigma-Aldrich, Steincheim, Germany), $\geq$99.9% genipin (GEN) (Pol-Aura, Olsztyn, Poland), 5-water disodium β-glycerophosphate (BGP) (Sigma-Aldrich, Steincheim, Germany), 5-hydrate sodium tripolyphosphate (TPP) (Sigma-Aldrich, Steincheim, Germany), and 96% ethanol (96%EtOH) (POCH, Gliwice, Poland) were used. In addition, 99.8% acetic acid (POCH, Gliwice, Poland), NaOH (Chempur, Piekary Śląskie, Poland), PBS (phosphate buffer) (Pol-Aura, Olsztyn, Poland), and deionized water were also used.

2.2. Preparation of Porous Chitosan Composites

Porous chitosan composites were obtained by the lyophilization process of stable dispersions of 2% wt. chitosan solution in acetic acid solution and the bioglass mixed in such amounts that the bioglass/polymer weight ratio was 1:1. The obtained dispersions underwent lyophilization process involving freezing and solvent sublimation for 28 h with the use of 1–16 BETA lyophilizer, Christ. The lyophilization process involved a preliminary stage with freezing dispersions to −35 °C; a main drying stage below the solidification point with decreased pressure to 0.06 MPa and sublimation of solvent; and a final drying phase performed through desorption with a pressure in lyophilizer chamber decreased to 0.005 MPa. The procedures used to obtain stable porous composites differed depending on the stabilization/crosslinking method according to descriptions below and as shown graphically in the Figure 1.

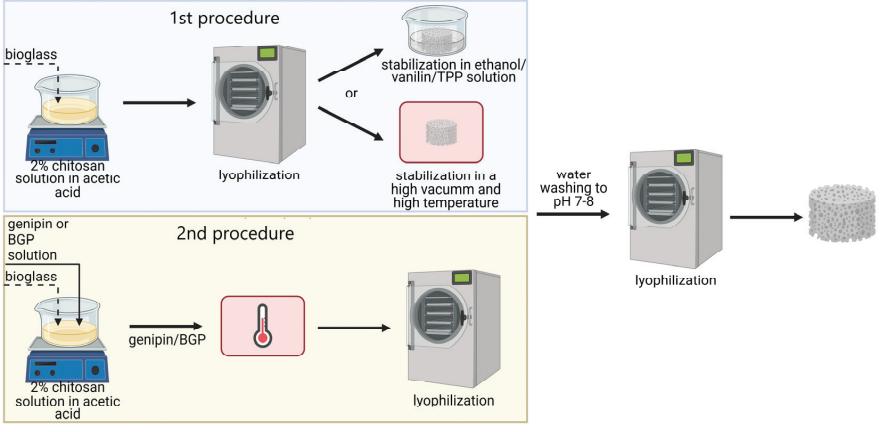

Figure 1. Procedures used to obtain stable porous composites with the use of different stabilization/crosslinking methods: 1st procedure—for composites stabilized by ethanol, vanillin, TPP, or thermal dehydration; 2nd procedure—for composites stabilized by genipin or BGP.

2.2.1. EtOH Stabilization

Freshly lyophilized samples of chitosan/bioglass composites prepared as above were subsequently immersed for 6 h in ethanol and then for 1 h in 0.1 M NaOH. Afterward, the samples were rinsed four times with distilled water, frozen to −35 °C, and again dried in the lyophilizer.

2.2.2. Temperature Stabilization

Freshly lyophilized samples of chitosan/bioglass composites prepared as described above were subsequently placed into a vacuum dryer in a temperature of 105 °C and a pressure of ~0.17 bar for 24 h. Afterward, the samples were rinsed four times with distilled water, frozen to −35 °C, and again dried in the lyophilizer.

2.2.3. TPP Stabilization/Crosslinking

Freshly lyophilized samples of chitosan/bioglass composites prepared as described above were subsequently immersed for 24 h in 0.1 M TPP solution in deionized water, and then the samples were rinsed four times with distilled water, frozen to −35 °C, and again dried in the lyophilizer.

2.2.4. Vanillin Stabilization/Crosslinking

Freshly lyophilized samples of chitosan/bioglass composites prepared as above were subsequently immersed for 24 h in 5 wt.% vanillin solution in ethanol, and then sam-

ples were rinsed four times with distilled water, frozen to −35 °C and again dried in the lyophilizer.

2.2.5. Genipin Stabilization/Crosslinking

Before the lyophilization process, 5 wt.% genipin solution in ethanol was added to the chitosan/bioglass dispersion, keeping the chitosan/genipin weight ratio of 1/0.04. The dispersion was mixed for 10 min (at a speed of about 200 rpm), placed in an incubator at the temperature of 40 °C for 5 h, and then frozen to −20 °C. The gelled dispersion was then lyophilized. Freshly lyophilized samples were rinsed four times with distilled water, frozen to −35 °C, and again dried in the lyophilizer.

2.2.6. BGP Stabilization/Crosslinking

Before the lyophilization process, chitosan/bioglass dispersion was placed in an ice bath, and 37.5 wt.% BGP solution in deionized water was added to the dispersion, keeping the chitosan/BGP weight ratio of 1:2. The dispersion was mixed for 20 min (at a speed of about 200 rpm), and then it was removed from the ice bath, placed in an incubator at the temperature of 40 °C for 5 h until gelled, and frozen to −20 °C. The frozen dispersions were then lyophilized. Freshly lyophilized samples were rinsed four times with distilled water, frozen to −35 °C, and again dried in the lyophilizer.

2.2.7. Sterilization

Prior to biological evaluation, all composites were sterilized by fast electron radiation at the Institute of Chemistry and Nuclear Technology (Warsaw, Poland). The set dose of radiation was 25 kGy, the speed of the transporter was 0.462 m/min, and the set current was 600 mA. This process was intended to destroy microbial contamination.

2.3. Methods

2.3.1. SEM Observations

Observation of the microstructure of the obtained composites was carried out using a Nova NanoSEM 200 emission scanning electron microscope, FEI. The samples were coated with conductive material (gold sputtering) before examination using a sputtering machine, Leica EM SCD500. The ETD detector was set at an accelerating voltage of 10 kV. The SEM method was used to determine the morphology of the samples.

2.3.2. ImageJ Analysis

This program was used to determine the average pore size in the resulting composites and to determine the pore size distribution in the samples. The values were determined from 300 pore measurements from SEM images (100 pores were measured in three ways—length, width, and oblique diameter). For TPP method, only 37 pores were measured in this way because of the undulating structure and its irregularity.

2.3.3. BET Analysis

The determination of the sample BET specific surface area was performed using a Gemini VII (2390t) analyzer from Micromeritics. The study included the determination of nine-point nitrogen adsorption and desorption isotherm points in the pressure range from 0.05–0.25 p/p°.

2.3.4. Pycnometric Density

The absolute density of prepared composite materials was examined by the pycnometric method using a helium pycnometer (Ultrapyc 1200e, Quantachrome, Boynton Beach, FL, USA,). Before measurements, samples were weighed and then put in the chamber. The analyses were carried out in the helium atmosphere, which allowed for

precise determination of the sample volume. Absolute density of sample was calculated using equation:

$$\rho = \frac{m}{V}$$

where: ρ—absolute density (g/cm^3), m—mass (g), and V—volume (cm^3) of the sample. Analysis was conducted with five replicates, with a mean and standard deviation reported.

2.3.5. Compressive Strength

The spatial porous composites were subjected to compressive strength testing on a Zwick Roell ProLine test machine with a 5 kN head mounted. The cylindrical molds were compressed by applying a load of 5 N and a compression strain rate of 0.6 mm/min, and the strength values were read at 50% strain of the mold. The number of trials for each type of composite was a minimum of 4, and then the mean value and the standard deviation were determined.

2.3.6. Swelling Test

The swelling capacity of the stable porous composites was evaluated by weighing the scaffolds before and after placing them in the PBS solution. The crosslinked/stabilized samples were weighed (w) and then incubated for two periods of time (1 day and 7 days). After this time, the samples were taken out of the PBS solution, and the liquid on the surface of the samples was removed with filter paper and weighed again (ws). The ratio of fluid absorption was determined as the ratio of weight increase (ws-w) relative to initial weight (w). Each value was calculated as the mean of 4 independent measurements.

2.3.7. Biological Assays

All biological assays in this study were performed as described previously [27,28]. Methods are described briefly below:

- Cell Culture. Immortalized human fetal osteoblastic cell line (hFOB 1.19 cells; ATCC nr CRL-11372, Rockville, MD, USA) was cultured in 1:1 mixture of Ham's F12 Medium and Dulbecco's Modified Eagle's Medium with 2.5 mM L-Glutamine (without phenol red; Thermo Fisher, Waltham, MA, USA). The medium was supplemented with 10 μg/mL of gentamicin and 0.25 μg/mL amphotericin B (Thermo Fisher, USA) and Fetal Bovine Serum (FBS; Thermo Fisher, USA) at final concentration of 10%. Cells were cultured at 34 °C and 5% CO_2.
- Extract preparation. Prior to the experiment, extracts from the chitosan/bioglass composites were prepared. For this purpose, the composites were placed into 24-well plates (Sarstedt, Germany) and incubated for 24 h in 1.5 mL culture medium at 34 °C and 5% CO_2.
- Indirect cytotoxicity testing. A total of 1 mL of composite extract or fresh medium (control cells) was added on hFOB cells seeded on 24-well plate a day prior. The plates were incubated for 48 h at 34 °C and 5% CO_2. Cell viability was determined by WST-1 test, and the cell cytotoxicity was measured by LDH cytotoxicity assay.
- Water Soluble Tetrazolium Salt-1 (WST-1) cell proliferation and mitochondrial activity assay. The proliferation of hFOB 1.19 cells was determined by using WST-1 assay kit (Abcam, Waltham, MA, USA) according to the supplier's protocol. Briefly, 40 μL of WST-1 reagent was added to the cells incubated with the extract of composites and incubated for 2 h in 34 °C and 5% CO_2. Conditioned media was collected from each well and transferred to 96-well flat bottom plate (Sarstedt, Germany). The optical density at 450 nm and 620 nm was measured using a plate reader Epoch (BioTek Instruments, Winooski, VT, USA). Untreated cells, blank medium, and control of the sterility of composites were included into each assay. Percentage of proliferation was calculated as follows: proliferation = (sample absorbance/control absorbance) × 100%.
- Lactate Dehydrogenase (LDH) cytotoxicity assay. The test was performed using a cytotoxicity detection kit (Roche Applied Science, Mannheim, Germany) according to

the supplier's protocol. Briefly, the dye solution was mixed with the catalyst solution and added to the samples (culture media from hFOB cells incubated with the extract of composites). After incubation in dark place, the optical density at 490 nm and 690 nm was measured using a plate reader Epoch (BioTek Instruments, USA).

As a positive control, cells treated with 1% Triton-X100 were used. Untreated cells, blank medium, and control of the sterility of composites were included in each assay.

Percentage of the cytotoxicity was calculated as follows:

$$\text{Cytotoxicity} = (\text{Sample absorbance} - \text{Control absorbance})/(\text{Positive control absorbance} - \text{Control absorbance}) \times 100\%$$

- Statistical analysis. GraphPad Prism (GraphPad Software, San Diego, CA, USA) was used to analyze and visualize the data. The normality of the results distribution could not be confirmed due to the small number of experimental samples. Thus, statistical calculations for various amounts of data obtained in the experiments were carried out using a mixed-effects model based on Restricted Maximum Likelihood (REML) calculations ($p = 0.05$). The Benjamini, Krieger, and Yekutieli multiple comparison test ($p = 0.05$) was then used to control the false discovery rate. The results of the experiments were compared for all composites in two data groups: cytotoxicity and proliferation.

3. Results and Discussion

3.1. Preparation Conditions of Stable Porous Chitosan/Bioglass Composites

Porous chitosan/bioglass composites were produced by the lyophilization process of stable dispersions chitosan solution and bioglass. The content of chitosan and bioglass in all composites defined as the chitosan/bioglass mass ratio was 1:1 and resulted from the authors' previous experiences [21,22]. With the ratio of components used, the composites were characterized by the highest rigidity and stability of the structure as well as open porosity with pores sizes, appropriated for cell migration and proliferation. All porous composites in this study were prepared under the same conditions of lyophilization, so that the differences in the properties of the obtained composites were related only to the stabilization method.

Six different stabilization methods were used to obtain stable porous chitosan/bioglass composite scaffolds. These methods were selected in such a way that the obtained materials did not show cytotoxicity. Namely, ethanol method stabilization, thermal method stabilization, and stabilization by crosslinking of chitosan chains with using genipin (GEN), vanillin (VAN), disodium β-glycerophosphate (BGP), 5-hydrate sodium tripolyphosphate (TPP) were used (Figure 2).

The stabilization/crosslinking processes were earlier optimized with respect to time, temperature and/or concentration of crosslinker. The optimization procedure followed the evaluation of the speed and efficiency of stabilization and the microstructure of the obtained scaffolds. The effectiveness of stabilization/crosslinking of chitosan materials was confirmed using FTIR spectroscopy and thermal analysis. The effective stabilization procedures (specified in Section 2) were used for preparation of composites for further characterization and comparison of the properties of porous materials obtained in various stabilization methods.

3.2. FTIR Studies on Stabilization/Crosslinking Process of Chitosan in Composites

The FTIR spectra of chitosan and stabilized chitosan bioglass composites are presented in Figure 3. The tested materials showed bands characteristic for chitosan, as well as crosslinking agents, which confirms the effectiveness of crosslinking in this research.

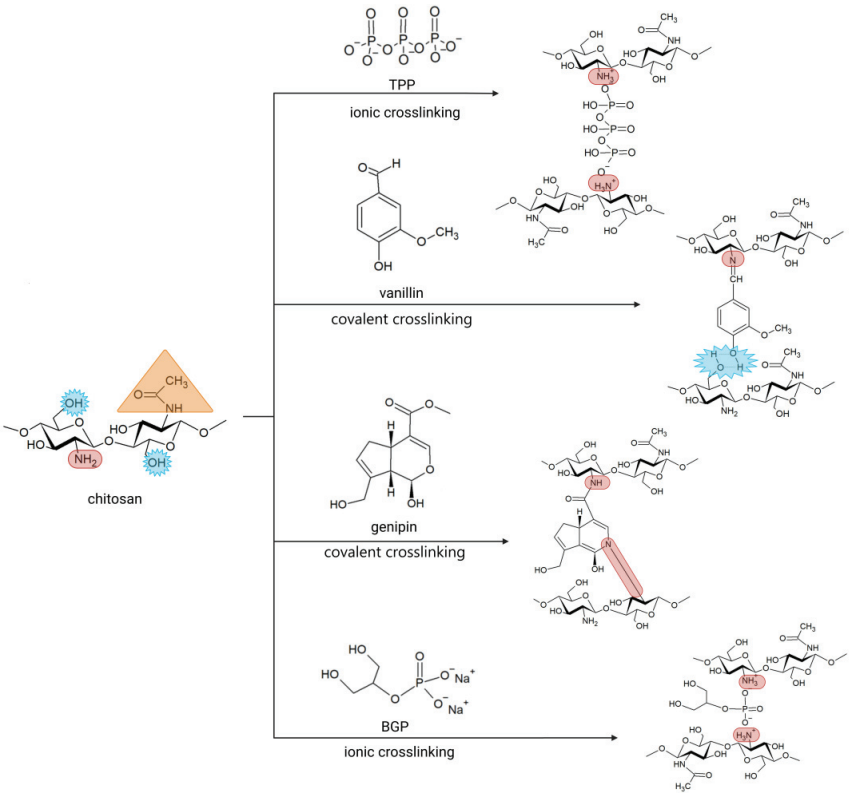

Figure 2. Chitosan crosslinking reaction scheme using genipin, vanillin, BGP, TPP.

Both for chitosan and its composites with the bioglass, the overlapping absorption bands of stretching vibrations of hydroxyl groups and amino groups (3550–3100 cm^{-1}) can be observed in the FTIR spectra [29,30]. The previous research reported that in this range of wavenumber, there is also a band attributed to water in silicate glass [31]. Additionally, other bands are observed, such as C–H stretching bands (2912 and 2865 cm^{-1}), carbonyl C=O stretching mode of amide group at 1644 cm^{-1} and 1583 cm^{-1}, and amine N–H bending vibrations possibly related to the following group (–NH–CO–CH_3) [13,30,32].

In the wavenumber range of 1463–1260 cm^{-1}, there are a number of signals related to vibrations in the (–CH_2–OH) group of chitosan, i.e., bending –OH, bending C–H, and stretching C–O [33]. Absorption bands at wavenumbers of 1150 cm^{-1}, 1068 cm^{-1}, and 1032 cm^{-1} can be assigned to the C–O–C asymmetric glycosidic bonds of chitosan [13,33]. The band at 895 cm^{-1} corresponds to the stretching vibrations of the glycosidic bonds, while the bands in the wavenumber region of 775–806 cm^{-1} are related to vibrations of Si–O–Si bonds in bioglass [34].

For composites stabilized with the use of ethanol (CHBG ETOH) and the thermal method (CHBG TEMP), the FTIR spectra show clearly outlined bands at 3371 cm^{-1} and 3321 cm^{-1} (stretching vibrations of O-H groups and NH_2 groups). A medium intense band at 3453 cm^{-1} can be associated with intramolecular hydrogen bonds [32,35], while the band at 3190 cm^{-1} is related to the stretching vibrations in O–H/N–H. Moreover, according to Shamekhi et al. [23], during the thermal stabilization of chitosan, the Millard reaction occurs, resulting in the formation of bonds between the amino and carbonyl groups, and this can be confirmed by the high intensity of the amide I and II bands at 1642 cm^{-1} and N-H bending at 1582 cm^{-1} in the spectrum of "CHBG TEMP". In addition, the difference

in relation to chitosan can be seen in the greater intensity of the C-H stretching vibration band (2909 cm^{-1}) and the C–C skeletal vibration band (997 cm^{-1}).

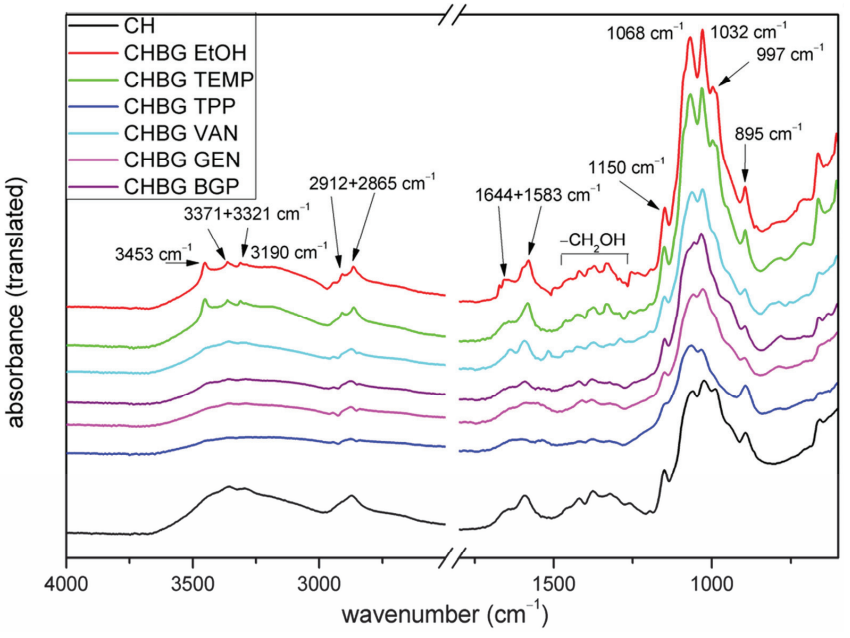

Figure 3. FTIR spectra of chitosan and chitosan bioglass composites stabilized with various methods and crosslinking agents.

For composites stabilized with genipin (CHBG GEN), the FTIR spectrum shows changes as compared to chitosan in the wavelength range of 1700 cm^{-1} to 1500 cm^{-1}. One can be seen the broadening of the band derived from the carbonyl (C=O stretching) group (1644 cm^{-1}) as the band is related to acetylated units of chitosan, and it is also related to the amide group formed by the reaction of chitosan with genipin [36]. At the same time, a broadening of the band at 1586 cm^{-1} originating from N-H bending at amide can be observed, which may result from the overlapping of a new band at 1558 cm^{-1} attributed to tertiary amine according to Figure 2.

In composites with vanillin (CHBG VAN), the main confirmation of crosslinking should be the appearance of absorption bands in the FTIR spectrum originating from the formation of Schiff-base bond as the reaction of chemical crosslinking of chitosan with vanillin is based on the Schiff reaction involving the amino groups of chitosan and the aldehyde group of vanillin [29]. The FTIR spectrum (Figure 3) shows a clear, intense sharp band at 1639 cm^{-1} corresponding to the stretching vibration of the imine linkage [29,37]. Crosslinking is also confirmed by the absorption band from intermolecular H-bonds formatted between vanillin and chitosan –OH group, according to Figure 2. This band is partially overlapped by absorption bands from stretching vibrations of –OH and $–NH_2$ groups (3600–3000 cm^{-1}).

On the other hand, crosslinking of chitosan composites with BGP (CHBG BGP) and TPP (CHBG TPP) may be a result of electrostatic interactions [25,30,38], as in the case of BGP the formation of hydrogen bonds [38,39]. In both cases, however, no clear bands for ionic bonds were observed in the FTIR spectrum compared to the spectrum of uncrosslinked chitosan, while the results of the mechanical strength of the composites shown in the next section of the paper clearly indicate effective stabilization. The interesting thing, however, are the differences observed in C–O stretching bands at 1060/1024/989 cm^{-1} visible for chitosan.

3.3. Thermal Analysis of Stabilized/Crosslinked Porous Chitosan/Bioglass Scaffolds

A thermal analysis of chitosan/bioglass composites stabilized by various agents provided information on their percentage weight losses with increasing temperature (Table 1). The solid residue amount at 900 °C was also determined. TG-DTG curves of the chitosan/bioglass composites stabilized with EtOH, TEMP, TPP, VAN, GEN, and BGP are shown in Figure 4.

Table 1. Results of TG/DTA analysis of chitosan/bioglass composites stabilized with various agents.

Sample	First Stage		Second Stage		Third Stage		Solid Residue after 900 °C (%)
	T (°C)	Weight Loss (%)	T (°C)	Weight Loss (%)	T (°C)	Weight Loss (%)	
CHBG EtOH	78	3.66	288	34.65	nd	17.39	44.28
CHBG TEMP	93	2.25	286/297	33.37	nd	18.30	46.07
CHBG TPP	91	4.73	253	22.61	~625	25.76	46.90
CHBG VAN	74/86	2.42	281	29.71	nd	15.16	52.68
CHBG GEN	78	4.08	276	26.38	nd	17.33	49.80
CHBG BGP	74/87	4.36	264/288	26.28	~626	28.96	40.40

nd—undetectable.

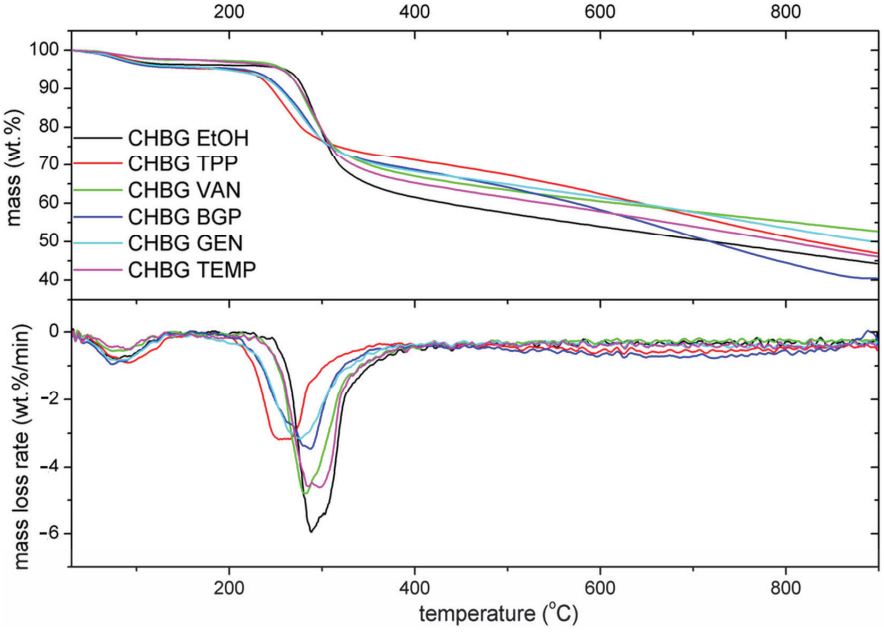

Figure 4. TG-DTG curves of the chitosan/bioglass composites stabilized with EtOH, TEMP, TPP, VAN, GEN, and BGP.

For all chitosan/bioglass crosslinked composites, three main steps on the TG curve can be observed, which is opposite to the observation made by Neto et al. [40] and Gültan et al. [17] in which stabilized chitosan decomposed in a two and single-stage process, respectively. The first stage on the TG curve is most probably related to the release of water from the composite's structure, while the next two correspond to the thermal degradation process. Above 400 °C, the slowest weight loss can be observed till the end of TG/DTA measurement, indicating the stepped process of material decomposition and carbonization.

The solid residue after the heating till 900 °C was in the range of 40.40–52.68 wt.% of the neat chitosan/bioglass composites.

The first stage of weight loss in our research occurs in the temperature range of 30–140 °C and is estimated at 2.4–4.08 wt.%. This effect is most probably related to the release of physically absorbed and loosely bonded water molecules, as chitosan is highly hygroscopic and can be easily hydrated [41]. According to Kittur et al. [42] the primary and supramolecular structure of polysaccharides affect their hydration ability, while Neto et al. [40] stated that the differences in the water loss may be related to the crosslinking of chitosan chains that causes physical and molecular changes in the structure. The moderately low weight loss in the first stage was observed for composites stabilized with TEMP, VAN, and EtOH, respectively. The stabilization of these composites occurs mainly through crosslinking associated with the formation of intermolecular hydrogen bonds. It can be stated that after crosslinking, the amount of free hydroxyl and amino groups in the composite decreases, and therefore, the capacity of hydration and water holding in the system is also reduced.

The thermal degradation of composites starts above 140 °C, and a clear step is observed in the temperature range of 140–384 °C, corresponding to the weight loss in the range of 24–35 wt.%. The second stage corresponds to the subsequent dehydration, as well as deacetylation and depolymerization of the polymer backbone [17]. From the DTG curves in the second stage of decomposition, it was observed that among the tested materials, the most thermally stable composites are CHBG EtOH and CHBG TEMP, while the least is composite stabilized with TPP. Two reasons may probably influence the obtained result. As the second stage of thermal decomposition is connected with dehydration, thermal stability can be related to the amount of bound water. The applied TPP and BGP crosslinking compounds in the form of 5-hydrates contain the most amount of water in their structure and result in the formation of composites with the lowest thermal stability. The second probable reason may be the fact that after an efficient stabilization within and between chitosan chains, connections are made due to various types of bonds (hydrogen, covalent, and ionic). According to the FTIR analysis, in the case of stabilization with ethanol, intermolecular hydrogen bonds between the hydroxyl groups as well as hydroxyl and amino groups of adjacent chitosan chains appear, while in the case of stabilization by thermal dehydration, both hydrogen and amide bonds appear. In the case of both of these methods, the decrease in the free volume of the system by the molecular rearrangement of polymer chains occurs during crosslinking, and as a result, the composites are characterized by the highest thermal stability. In the case of covalent crosslinking involving genipin and vanillin, molecules of crosslinking compounds are incorporated between the chitosan chains and also provide some thermal stability to the crosslinked composites, but lower than the hydrogen bonds of adjacent chitosan chains. The lowest stability is shown by ion-crosslinked composites with BGP and TPP. In this case, large molecules of crosslinking compounds separate the chitosan chains over a large distance, as a result of which no additional bonds are formed to strengthen the structure. As the second step of the thermal decomposition is also connected with depolymerization, we can conclude that in the thermal depolymerization process, the ionic bonds formed as a result of crosslinking with BGP and TPP are the first to break. The third weight loss occurs in a very wide range of temperatures above 400 °C and for almost all tested materials does not end at 900 °C when the TG/DTA measurement is finished, except for CHBG BGP material. The course of TG curves indicates that weight loss occurs continuously after exceeding the temperature of 400 °C and constitutes of several subsequent reactions, which are impossible to separate under this TG/DTA experimental method. The literature provides information that this stage is probably related to the evaporation of volatile compounds from the organic char (residual decomposition and evaporation of volatile by-products from the chitosan burn-off) [43].

3.4. Microstructure of the Obtained Composites

The porous structure of the composites discussed in this study was created at the stage of freeze-drying, during which the composite took the form of a scaffold with pores that could be a place for colonization, differentiation and proliferation of cells, transport of nutrients and, as a result, the growth of new tissue. The average pore size of the composites was from 40 μm (for CHBG TEMP and CHBG BGP) to 180 μm (for CHBG GEN) and was within the range considered optimal [44].The resulting pores were open and interconnected in almost all cases (Figure 5).

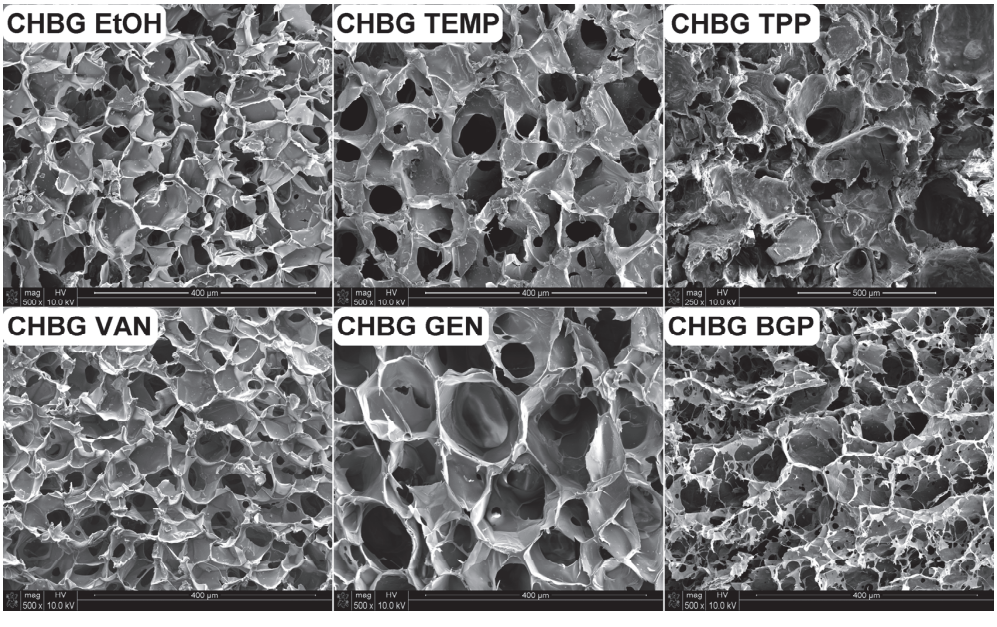

Figure 5. Microstructure of chitosan/bioglass composites stabilized or crosslinked by the use of various methods: ethanol (CHBG EtOH); thermal treatment (CHBG TEMP); sodium tripolyphosphate (CHBG TPP); vanillin (CHBG VAN); genipin (CHBG GEN); β-glycerophosphate pentahydrate (CHBG BGP).

It is known that the microstructure of chitosan/bioglass composites obtained in the lyophilization method depends on the conditions and course of the process itself, as well as the content and size of bioglass grains [21]. However, for the same amount and type of filler addition in different composites, the method of stabilizing the composite also significantly influences the microstructure.

In addition to SEM imaging, the average pore size was determined for the obtained porous structures (excluding the TPP composite—due to the uniqueness of the results) and an analysis of the pore size distribution was performed (Figure 6).

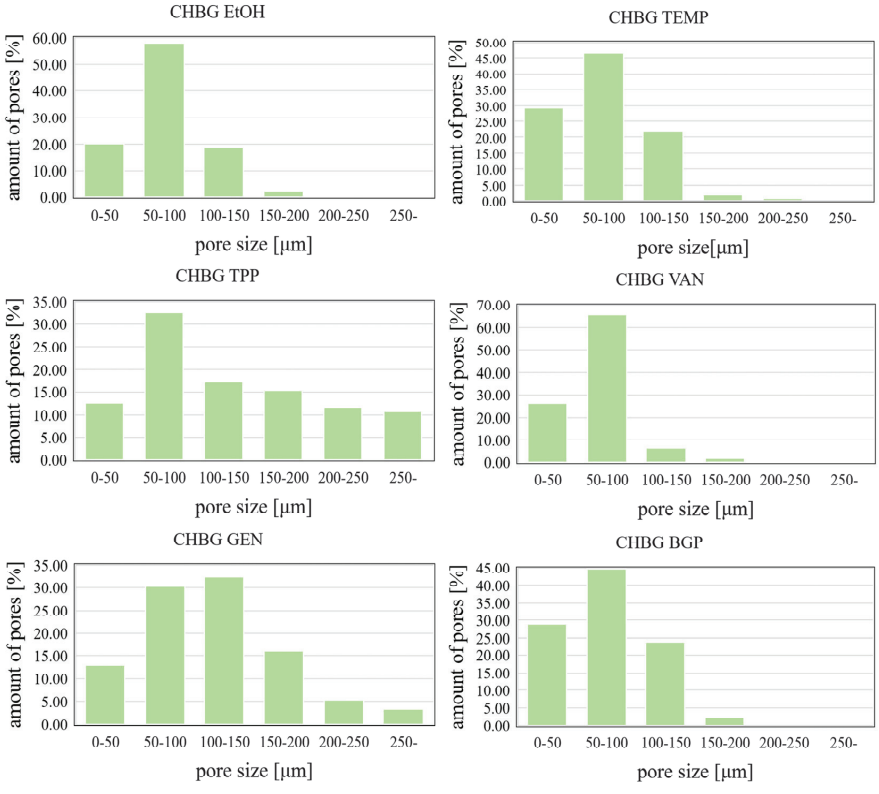

Figure 6. Pore size distributions in chitosan/bioglass composites crosslinked/stabilized by various methods.

The composites stabilized in our research with ethanol, the thermal method, and with the use of crosslinking compounds such as genipin and vanillin had a slightly folded structure, in which, however, individual pores could be clearly observed.

In the case of crosslinking with genipin, the obtained composites had the largest pores among the materials presented in this study (Table 2). On the other hand, the smallest pores had composites crosslinked with vanillin solution.

Table 2. Average pore sizes of the chitosan/bioglass composites crosslinked/stabilized by various methods.

	CHBG EtOH	**CHBG TEMP**	**CHBG TPP**	**CHBG VAN**	**CHBG GEN**	**CHBG BGP**
mean ± std. dev. [μm]	78.11 ± 32.84	74.76 ± 35.41	*	67.97 ± 25.80	116.35 ± 64.60	74.18 ± 35.17
min [μm]	15.07	12.90	18.87	16.66	13.89	10.29
max [μm]	184.11	216.7	520.99	174.9	450.36	192.56

* Structure too heterogeneous and shrunken to determine the average pore size.

It is known from the literature that high concentrations of the crosslinking agent result in the formation of small pores [45,46]. This relationship is confirmed in our research, taking into account the concentrations of genipin and vanillin used in this study and their content in relation to chitosan. As demonstrated by Gorczyca [10], in the case of crosslinking with genipin, it is possible to increase the pore size even with an increase in the concentration

of genipin. This may be due to the more favorable conditions for genipin ring-opening polymerization and its long-distance crosslinking [47].

Composites stabilized with ethanol, BGP, and the thermal method had pores almost 45% smaller than those crosslinked with genipin, and the structure of BGP stabilized composites was additionally disturbed and heterogeneous.

Crosslinking/stabilization using TPP solutions makes the structure very heterogeneous, and the pore sizes and their distribution based on SEM imaging are difficult to determine. Considering the SEM microphotographs, it was observed that the crosslinking/stabilization methods using BGP or TPP make the repeatability of the obtained structures low, and in the case of TPP, the structure is additionally corrugated (rough, not smooth) and shrunken. As shown in the literature [48], microfolding may be beneficial to cell adhesion, but it is negative due to the movement of fibroblasts.

The shrinkage caused by stabilization with the TPP solution can be seen at first glance when the samples are taken out of the solution in which they were immersed. The comparison of the size of composite shapes subjected to various stabilization/crosslinking methods is shown in Figure 7.

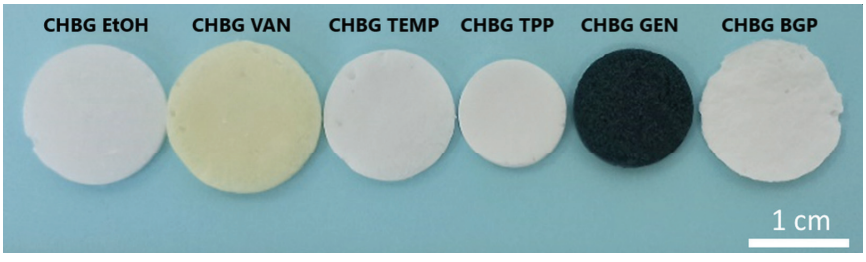

Figure 7. Shape and size of the chitosan/bioglass composites stabilized/crosslinked by various methods.

The obtained results for stabilization with the TPP solution are consistent with the literature data [25]. Additional studies of the authors on the stabilization of composites with the use of TPP solutions with a concentration below 0.1 M showed that the shapes shrink only slightly less, and they are also soluble in water, which indicates the lack of stabilization efficiency. The shapes, after stabilization with TPP solutions with a concentration above 0.1 M, underwent even greater shrinkage.

3.5. Density and Specific Surface Area

The density of the porous material is also related to the microstructure of composites. As a rule, the greater the number of smaller pores in the composite, the greater the density of the material due to the higher proportion of the material in a given volume. Such materials should consequently have the best strength properties. The density values determined by pycnometric method for the obtained composites are consistent with the above statement. The composite crosslinked with vanillin, which has the smallest pores, has the highest density, and the composite with the largest pores—crosslinked with genipin—has the lowest density (Figure 8). The obtained results are also confirmed by specific surface area tests.

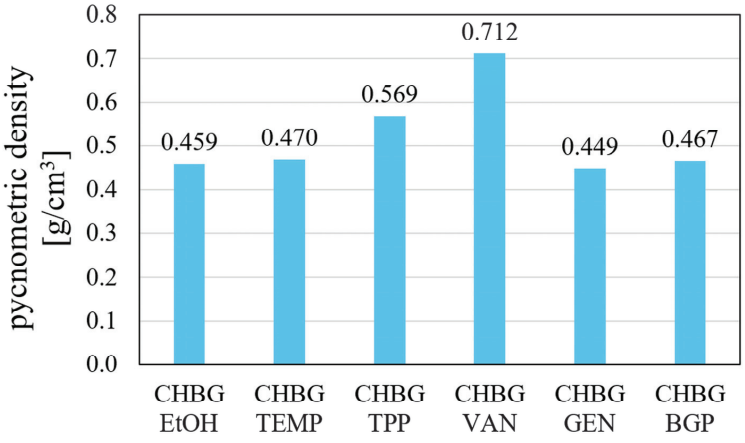

Figure 8. Pycnometric density values of porous chitosan composites stabilized with various methods.

In medical applications of porous composites for implantation, determination of the degree of surface development may also be extremely important in terms of implant morphology. The size of specific surface area may affect the amount of adsorption of active compounds on the implant's surface, such as drugs or active peptides, and thus, the possibility of using the composite as an active substance carrier [22,49]. The size of specific surface is alco crucial in the aspect of the release kinetics of active substances incorporated into the composite [50,51].

The results of the BET specific surface area (S_{BET}) for the obtained composites are shown in Figure 9.

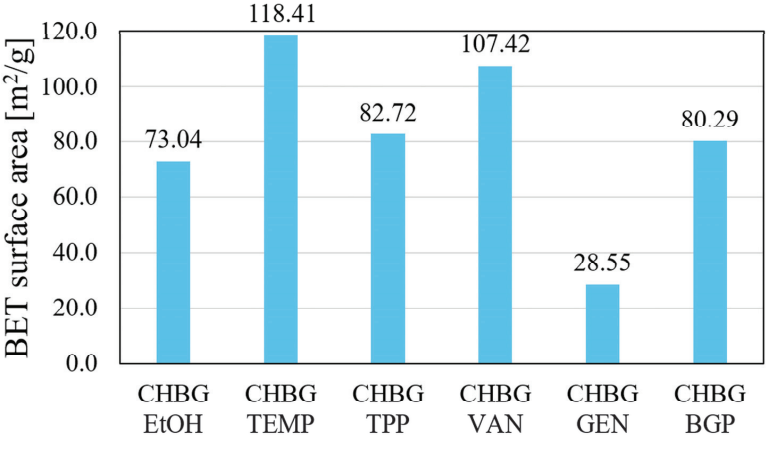

Figure 9. Specific surface area values (S_{BET}) of porous chitosan composites stabilized with various methods.

The specific surface area is equal to the sum of the external and internal surfaces. The external surface corresponds to the geometric surface of the material per gram. The internal surface consists of pore walls. Since, by definition, the pores must be open, the internal surface area value does not include the area of the closed pore walls. A large specific surface area indicates the presence of a large number of pores and thus a large surface area, while a low specific surface area is characteristic of materials with a smaller number of pores of larger dimensions.

Among the tested composites, the smallest specific surface area was shown by the genipin-crosslinked composite, which is consistent with the result of the pore size of this composite. As the pore size in individual composites decreases, they show higher S_{BET} values. The vanillin-crosslinked composite (with the smallest pore size) achieved an S_{BET} value of 107.42 m^2/g. The highest S_{BET} value was determined for the thermally stabilized composite, which, combined with the pore size results, may confirm that the largest number of pores remained open for this composite.

3.6. Compressive Strength

The mechanical properties of porous scaffolds are of great importance in the aspect of applications in tissue engineering due to the need for the structure to withstand stresses during in vitro culture and as in vivo implants. Mechanical properties also influence specific cell functions within modified tissues [52].

In the case of porous 3D composites, the determination of mechanical properties consists in examining their compressive strength. The compressive strengths in a wide range of strains from 1% to 50% were determined in the work (Table 3). To determine Young's modulus and to compare the obtained strength results, the values at strains in the yield range (10% of strain) on the compression curves were taken into account (Figure 10).

Table 3. The compressive strengths in a wide range of strains from 1% to 50% and Young's Modulus of chitosan/bioglass composites stabilized with various agents.

Sample	Stress at x% Strain ± Std. Dev. [MPa]					Young Modulus ± Std. Dev. (E_{mod}) [MPa]
	x = 1%	x = 5%	x = 10%	x = 20%	x = 50%	
CHBG EtOH	0.064 ± 0.006	0.121 ± 0.014	0.153 ± 0.018	0.182 ± 0.019	0.332 ± 0.027	3.046 ± 2.050
CHBG TEMP	0.060 ± 0.002	0.093 ± 0.009	0.116 ± 0.015	0.148 ± 0.018	0.299 ± 0.028	2.244 ± 1.561
CHBG TPP	0.143 ± 0.014	0.571 ± 0.116	0.860 ± 0.110	1.039 ± 0.117	1.781 ± 0.287	9.085 ± 3.494
CHBG VAN	0.052 ± 0.004	0.086 ± 0.013	0.106 ± 0.018	0.127 ± 0.019	0.228 ± 0.023	1.869 ± 0.998
CHBG GEN	0.148 ± 0.038	0.531 ± 0.195	0.764 ± 0.146	0.805 ± 0.115	0.910 ± 0.149	7.927 ± 2.665
CHBG BGP	0.075 ± 0.016	0.155 ± 0.046	0.215 ± 0.064	0.268 ± 0.070	0.348 ± 0.056	4.594 ± 1.710

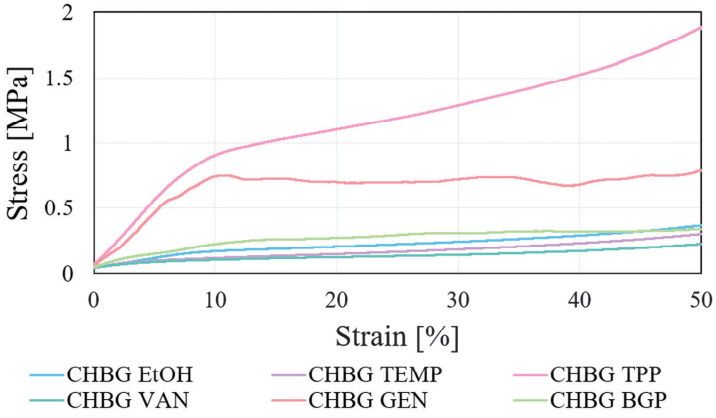

Figure 10. Compression curves of porous chitosan composites stabilized with various methods.

Figure 11 shows the results of compressive strength tests for the produced composites at 10% of strain values. As can be seen, depending on the method of crosslinking, the chitosan network can be strengthened to a greater or lesser extent. Regardless of the strain value at which the stress is determined, the composite stabilized with TPP has the highest strength (Table 3), which is justified by the microstructure obtained for this composite.

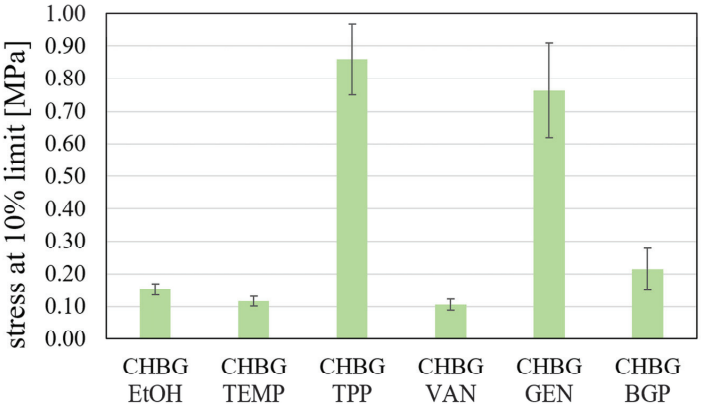

Figure 11. Compressive strength at 10% strain of porous chitosan composites stabilized with various methods.

The high shrinkage of the composite during its stabilization in the TPP solution and the large corrugation of the walls inside the composite structure (Figure 4) caused its strong hardening and strengthening, hence the high result of its stress.

In terms of microstructure, pore sizes also contribute to the strength properties of the composite. As a rule, the greater the pore sizes, the lower the mechanical strength. Our results of mechanical strength of the composite crosslinked with GEN, however, are in contradiction with this statement. Despite the fact that this composite showed the largest pore size, its compressive strength is at a high level and reaches a value of 0.76 MPa at 10% of strain. The reason for such strength of the composite with genipin may be the high crosslinking density. Gorczyca showed in his work [10] that the mechanical compressive strength of a genipin crosslinked chitosan composites increases with increasing degree of crosslinking of the chains with increasing amount of crosslinking agent. The author also demonstrated that in the case of crosslinking with genipin, it is possible to increase the pore size even with an increase in the concentration of genipin. The opposite observations were presented in the literature by Dimida [13], who showed that a double increase in the amount of genipin used to crosslink chitosan scaffolds resulted in imperceptible changes in the mechanical strength of the scaffolds. The author pointed out that the effect of the chemical crosslinking is negligible if compared to the macroscopic structure. However, Bi et al. [53] showed that the mechanical strength of the crosslinked porous scaffold is defined by the balance between the reduced mechanical strength due to the gradual increase in pore size and the increased mechanical strength due to the crosslinking reaction.

Compressive strengths for composites stabilized with EtOH, TEMP, VAN, and BGP were at a similar level and ranged from 0.10 MPa to 0.21 MPa at 10% of strain.

In the case of composite materials composed of a polymer matrix and ceramic particles, it is often also important to ensure adequate adhesion between the two phases. For this purpose, both surface adhesives as well as bonding methods between the organic and inorganic phases are used, e.g., in the case of class II polymer/bioglass hybrids. Such a solution, apart from improving the mechanical properties, ensures the connection of two phases and causes their simultaneous degradation in the composite during in vivo tests [7].

3.7. Swelling Capacity

An ideal scaffold for bone tissue engineering should also maintain sufficient mechanical strength as stability of the 3D structure during in vitro and in vivo growth and remodeling process. However, an implant placed in water or physiological fluids absorbs the fluid through adsorption processes, leading to swelling and changing dimensions.

The swelling ratio is an important factor used to assess the structural stability of a scaffold. Depending on the type of biomaterial and the pH of the incubation medium, the

degree of swelling may reach equilibrium at different times [54,55]. Since chitosan contains hydroxyl and amine groups, it is easily hydrated in water, which affects the shape and dimensions of the scaffold. Chitosan crosslinking may change the scaffold hydrophilicity and reduce the swelling coefficient, which in turn will contribute to maintaining the structural stability of the scaffold [56].

The results of the swelling ratio of the obtained composites during incubation in the PBS solution are presented in Figure 12. All composites considered in this study showed the highest swelling capacity within 1 day of incubation in PBS, and after 7 days, only small further changes in PBS absorption were observed. As can be seen in Figure 12, composites stabilized with TPP and GEN show the lowest swelling capacity. The reason for the obtained result was most likely the high crosslinking density of chitosan chains in these composites, as a result of which the polymer changed its hydrophilicity and became less absorbent. In addition, polymer chains with high crosslinking density do not have the possibility to move away from each other during immersion in PBS solution and do not swell. Slightly higher PBS absorption was shown by the BGP crosslinked composite, and the highest results were obtained for EtOH, TEMP, and VAN crosslinked composites. The results of the swelling test stay in agreement with the above-mentioned compressive strength values, as the highest values of strength for the TPP and GEN crosslinked composites can indicate the highest degree of stabilization by crosslinking.

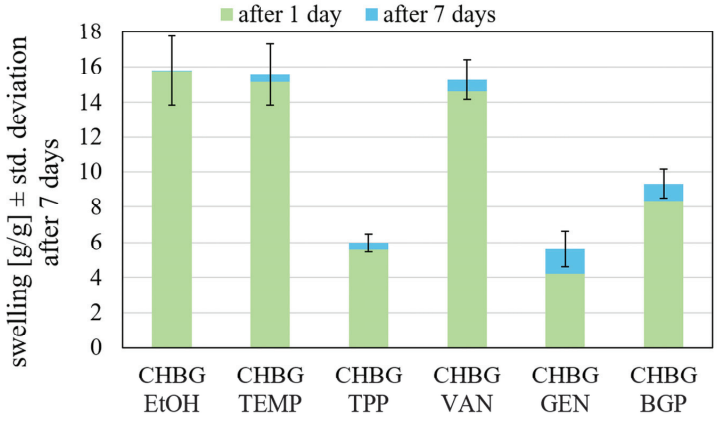

Figure 12. Swelling of composites depending on the stabilization method.

The swelling of implants, in turn, causes an increase in pore size. Larger pores can facilitate cell adhesion, proliferation (multiplication), and growth because they contribute to the penetration of cells deep into the internal structure of the scaffold. However, the swelling capacity must be controlled within a certain range because further fluid absorption can provide an increase in implant volume, which in turn can cause the scaffold to dislodge from the defect site [57,58]. Accordingly, the most stable and controlled swelling in our results is the ethanol stabilized composite, as it does not show changes in the swelling ratio after the first day of incubation.

3.8. Cell Cytotoxicity

The cytotoxic effect of the chitosan/bioglass composites' extracts (indirect method) on hFOB 1.19 cells was tested using the LDH test, which is based on the lactate dehydrogenase activity released from the cytoplasm into the environment through the damaged cell membrane.

Our results show that cytotoxicity of each tested composite extracts did not exceed 30% (Figure 13). According to ISO 10993-5, this value is considered to be the threshold value above which the material is considered toxic.

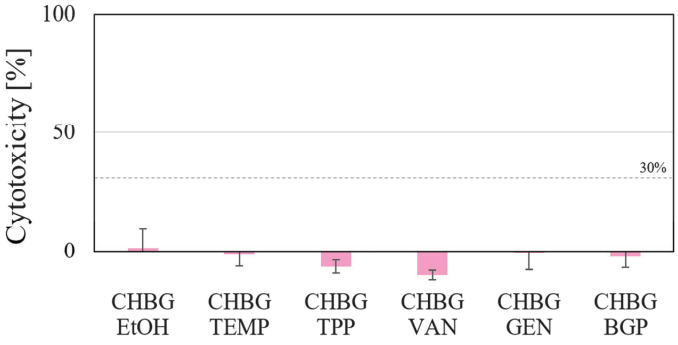

Figure 13. Cell cytotoxicity of hFOB 1.19 cells incubated with the extracts of porous chitosan composites stabilized with 6 different methods.

3.9. Cell Proliferation

The proliferation of cells incubated with the extracts of bioglass/chitosan composites' (indirect method) was measured using the WST-1 assay, which is based on mitochondrial activity. All results were calculated as a percentage of control cells (arbitrarily set as 100%). The analyses were performed according to ISO 10993-5:2009 guideline.

The obtained results showed that four of the tested composites did not decrease the cell proliferation below 90% (Figure 14). For the composite crosslinked with genipin, the largest proliferation value was obtained. The obtained result is in line with Gilarska et. all [59] observation that hydrogels with genipin can support the proliferation and adhesion of MG-63 cell line. Moreover, Mekhail et. all [60] observed that genipin in gels enhanced fibroblasts' attachment and cell viability was significantly improved after crosslinking with genipin, so finally, proliferation was enhanced up to five times. It is worth emphasizing, however, that for crosslinking with EtOH, TPP i BGP, the proliferation % of hFOB 1.19 cells is only several % lower, and it also exceeds 90%.

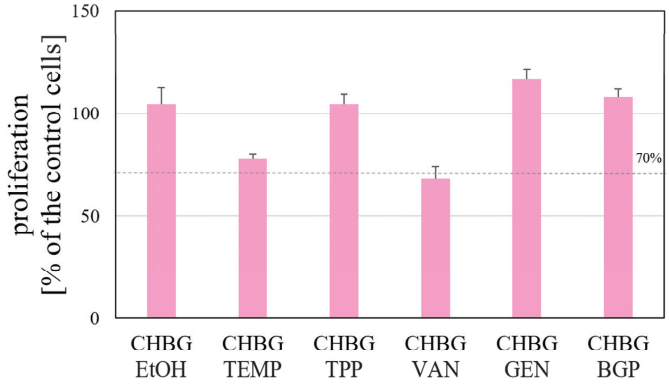

Figure 14. Proliferation of hFOB 1.19 cells incubated with the extracts of porous chitosan composites stabilized with six different methods.

Considering the largest pore sizes in the composite crosslinked with genipin, it can be expected that the proliferation of cells in direct contact with this composite during implantation will also be at the highest level. Szustakiewicz et. all [61] stated that the larger pores, the higher viability/metabolic activity of hFOB 1.19 osteoblasts and that foams with large pores promoted the adhesion and penetration of osteoblasts to the surface of the biomaterial is more effective than for the scaffolds with smaller pores.

3.10. Pre-Summary

In order to compare the crosslinking methods used, the authors performed a simple summary of the studies performed on a scale of 0–5 (where 5 was the most favorable results and 0 was the least favorable, without specifying validity of the test). The summarized results are shown in Table 4:

Table 4. Comparing the cross-linking methods used by simply scoring the most favorable and least favorable methods. In particular, for the TGA category: 5 points for the sample with the greatest thermal stability; for the microstructure category: 5 points for the sample with the largest average pore size; for the pycnometric density category: 5 points for the sample with the lowest pycnometric density; for the BET surface area category: 5 points for the sample with the lowest BET surface area; for the compressive strength category: 5 points for the sample with the highest compressive strength; for the swelling category: 5 points for the sample with the lowest swelling; for the stability category: 5 points for the sample with the least change in swelling after 7 days; for the cytotoxicity category: 5 points for the sample with the lowest cytotoxicity; and for the proliferation category: 5 points for the sample with the highest proliferation.

Sample/Category	CHBG EtOH	CHBG TEMP	CHBG TPP	CHBG VAN	CHBG GEN	CHBG BGP
TGA	5	4	0	3	2	1
Microstructure	4	3	0	1	5	2
Pycnometric density	4	2	1	0	5	3
BET Surface area	4	0	2	1	5	3
Compressive strength	2	1	5	0	4	3
Swelling	0	1	4	2	5	3
Stability	5	3	4	2	0	1
Cytotoxicity	0	2	4	5	1	3
Proliferation	3	1	2	0	5	4
Total	27	17	22	14	32	23

According to the scores resulting from our study, the methods from most favorable to least favorable for a specific tests category are arranged as follows:

for TGA category EtOH > TEMP > VAN > GEN > BGP > TPP;
for microstructure category GEN > EtOH > TEMP > BGP > VAN > TPP;
for pycnometric density category GEN > EtOH > BGP > TEMP > TPP > VAN;
for BET surface area category GEN > EtOH > BGP > TPP > VAN > TEMP;
for compressive strength category TPP > GEN > BGP > EtOH > TEMP > VAN;
for swelling category GEN > TPP > BGP > VAN > TEMP > EtOH;
for stability category EtOH > TPP > TEMP > VAN > BGP > GEN;
for cytotoxicity category VAN > TPP > BGP > TEMP > GEN > EtOH;
for proliferation category GEN > BGP > EtOH > TPP > TEMP > VAN.

In total the comparison is GEN > EtOH > BGP > TPP > TEMP > VAN. Of course, readers should not forget in this case the possible disadvantage of the method with genipin, which is the black-blue color of the composites.

4. Conclusions

In this study, we compare the physicochemical, microstructural and strength properties as well as in vitro cytotoxicity of new porous chitosan/bioglass composite scaffolds. For comparative studies, we used six different strategies for crosslinking/stabilizing composites using: genipin, vanillin, disodium β-glycerophosphate, 5-hydrate sodium tripolyphosphate, ethanol, and thermal dehydration.

The effectiveness of each crosslinking method was confirmed by FTIR spectroscopy.

The thermal analysis of the composites showed that the most thermally stable are the composites stabilized with ethanol (TDTG02 in 288 °C) and thermal dehydration (TDTG in 286/297 °C), and the least stable is composite stabilized with TPP (TDTG in 253 °C).

All the crosslinking methods used allowed to obtain stable porous structures of chitosan/bioglass composites. Microstructural studies of the composites showed that the composite crosslinked with genipin had the largest (average pore size is 116.35 ± 64.60 μm) and at the same time the best-developed pores, while the smallest pores were found in the composite crosslinked with vanillin (average pore size is 67.97 ± 25.80 μm). Two of the obtained composites (CHBG TPP, CHBG BGP) had a very irregular structure with inhomogeneous porosity, which may be a serious limitation in future applications. Moreover, the genipin crosslinked composite had a characteristic dark blue color, which also may not be visually favorable for implantation. The composite with the smallest pores was characterized by the highest density and almost largest specific surface area, but unexpectedly showed the lowest mechanical compressive strength.

Among the obtained composites, the composite with the smallest specific surface area (CHBG GEN, S_{BET} = 28.55 m^2/g) had the best compressive strength (stress at 10% strain limit = 0.764 ± 0.146 [MPa]).

Composites crosslinked with genipin and TPP showed the lowest swelling coefficient, but the most stable in terms of swelling is the composite crosslinked with ETOH.

All crosslinking methods allowed to obtain non-cytotoxic for hFOB 1.19 cells composites that met the requirements of the PN EN ISO 10993-5 standard. Cell proliferation exceeded 90% for four obtained composites: CHBG GEN, CHBG BGP, CHBG EtOH, CHBG, TPP and was the highest for the genipin-crosslinked composite.

The obtained test results allowed for the comparison of the crosslinking strategies suitable for the design of particular biomaterials. Based only on the data in this article, the arrangement of methods from most favorable to least favorable are arranged as follows: GEN > EtOH > BGP > TPP > TEMP > VAN. However, it should be remembered that this comparison does not reflect the entire scale of complexity of various technological and application limitations. There is also no doubt that in terms of future applications, it would be necessary to choose a material that would meet the current requirements in terms of a given feature, or choose the golden mean, depending on the current needs in a given application.

Author Contributions: M.B.: Conceptualization, Supervision, Methodology, Investigation, Writing—original draft, Writing—review & editing A.W.: Investigation, Methodology, Graphical visualization, Writing—original draft, Writing—review and editing, M.C.: Methodology, Investigation, Writing—original draft, M.P.: Investigation, P.T.-G.: Investigation, J.P.—Investigation, A.A.: Investigation, L.C.: Investigation, B.G.: Investigation, Z.J.: Project administration. All authors have read and agreed to the published version of the manuscript.

Funding: This research was funded by The National Centre for Research and Development, Poland, grant No. TECHMATSTRATEG2/406384/7/NCBR/2019.

Institutional Review Board Statement: Not applicable.

Data Availability Statement: The data generated during this study are available at ŁUKASIEWICZ Research Network Institute of Ceramics and Building Materials, Center of Ceramic and Concrete in Warsaw, Biomaterials Research Group, Postępu 9, Warsaw, 02-676, Poland, and biological data are available at Department of In Vitro Studies, Institute of Biotechnology and Molecular Medicine, Kampinoska 25, 80-180 Gdańsk, Poland, and are available from the corresponding author upon request.

Conflicts of Interest: The authors declare no conflict of interest.

References

1. *ISO/EN10993-5, ISO 10993-5*; Biological Evaluation of Medical Devices—Part 5: Tests for Cytotoxicity: In Vitro Methods. International Organization for Standardization: Geneve, Switzerland, 2009.
2. Li, Y.; Sun, S.; Gao, P.; Zhang, M.; Fan, C.; Lu, Q.; Li, C.; Chen, C.; Lin, B.; Jiang, Y. A tough chitosan-alginate porous hydrogel prepared by simple foaming method. *J. Solid State Chem.* **2021**, *294*, 121797. [CrossRef]
3. Abdellatif, A.A.; Mohammed, A.M.; Saleem, I.; Alsharidah, M.; Al Rugaie, O.; Ahmed, F.; Osman, S.K. Smart Injectable Chitosan Hydrogels Loaded with 5-Fluorouracil for the Treatment of Breast Cancer. *Pharmaceutics* **2022**, *14*, 661. [CrossRef] [PubMed]
4. Setiyorini, Y.; Anggraeni, A.; Pintowantoro, S. In-Vivo study of nano chitosan as therapeutic agent for toxic metal implant. *Results Eng.* **2022**, *13*, 100352. [CrossRef]
5. Xue, Y.; Zhang, J.; Chen, X.; Zhang, J.; Chen, G.; Zhang, K.; Lin, J.; Guo, C.; Liu, J. Trigger-Detachable Hydrogel Adhesives for Bioelectronic Interfaces. *Adv. Funct. Mater.* **2021**, *31*, 2106446. [CrossRef]
6. Ahmad, U.; Sohail, M.; Ahmad, M.; Minhas, M.U.; Khan, S.; Hussain, Z.; Kousar, M.; Mohsin, S.; Abbasi, M.; Shah, S.A.; et al. Chitosan based thermosensitive injectable hydrogels for controlled delivery of loxoprofen: Development, characterization and in-vivo evaluation. *Int. J. Biol. Macromol.* **2019**, *129*, 233–245. [CrossRef]
7. Vukajlovic, D.; Parker, J.; Bretcanu, O.; Novakovic, K. Chitosan based polymer/bioglass composites for tissue engineering applications. *Mater. Sci. Eng. C* **2019**, *96*, 955–967. [CrossRef]
8. Khoshakhlagh, P.; Rabiee, S.M.; Kiaee, G.; Heidari, P.; Miri, A.K.; Moradi, R.; Moztarzadeh, F.; Ravarian, R. Development and characterization of a bioglass/chitosan composite as an injectable bone substitute. *Carbohydr. Polym.* **2017**, *157*, 1261–1271. [CrossRef]
9. Woźniak, A.; Biernat, M. Methods for crosslinking and stabilization of chitosan structures for potential medical applications. *J. Bioact. Compat. Polym.* **2022**, *37*, 151–167. [CrossRef]
10. Gorczyca, G.; Tylingo, R.; Szweda, P.; Augustin, E.; Sadowska, M.; Milewski, S. Preparation and characterization of genipin cross-linked porous chitosan–collagen–gelatin scaffolds using chitosan–CO_2 solution. *Carbohydr. Polym.* **2014**, *102*, 901–911. [CrossRef]
11. Szweda, P.; Gorczyca, G.; Tylingo, R.; Kurlenda, J.; Kwiecinski, J.; Milewski, S. Chitosan–protein scaffolds loaded with lysostaphin as potential antistaphylococcal wound dressing materials. *J. Appl. Microbiol.* **2014**, *117*, 634–642. [CrossRef]
12. Gorczyca, G. Preparation and Characterization of Novel Chitosan-Collagen-Gelatin Biomaterials with Antimicrobial Activity. Ph.D. thesis, Gdańsk University of Technology, Gdańsk, Poland, 2015.
13. Dimida, S.; Barca, A.; Cancelli, N.; De Benedictis, V.; Raucci, M.G.; Demitri, C. Effects of genipin concentration on cross-linked chitosan scaffolds for bone tissue engineering: Structural characterization and evidence of biocompatibility features. *Int. J. Polym. Sci.* **2017**, *2017*, 8410750. [CrossRef]
14. Radwan-Pragłowska, J.; Piątkowski, M.; Janus, Ł.; Bogdał, D.; Matysek, D.; Čablik, V. Microwave-assisted synthesis and characterization of antibacterial O-crosslinked chitosan hydrogels doped with TiO_2 nanoparticles for skin regeneration. *Int. J. Polym. Mater. Polym. Biomater.* **2019**, *68*, 881–890. [CrossRef]
15. Radwan-Pragłowska, J.; Piątkowski, M.; Kitala, D.; Janus, Ł.; Klama-Baryła, A.; Łabuś, W.; Tomanek, E.; Glik, J.; Matysek, D.; Bogdał, D.; et al. Microwave-assisted synthesis and characterization of bioactive chitosan scaffolds doped with Au nanoparticles for mesenchymal stem cells culture. *Int. J. Polym. Mater. Polym. Biomater.* **2019**, *68*, 351–359. [CrossRef]
16. Hunger, M.; Domalik-Pyzik, P.; Reczyńska, K.; Chłopek, J. Double crosslinking of chitosan/vanillin hydrogels as a basis for mechanically strong gradient scaffolds for tissue engineering. *Eng. Biomater.* **2020**, *23*, 155.
17. Gültan, T.; Bektaş Tercan, Ş.; Çetin Altındal, D.; Gümüşderelioğlu, M. Synergistic effect of fabrication and stabilization methods on physicochemical and biological properties of chitosan scaffolds. *Int. J. Polym. Mater. Polym. Biomater.* **2021**, *70*, 371–382. [CrossRef]
18. Jana, S.; Florczyk, S.J.; Leung, M.; Zhang, M. High-strength pristine porous chitosan scaffolds for tissue engineering. *J. Mater. Chem.* **2012**, *22*, 6291–6299. [CrossRef]
19. TIğlI, R.S.; Gumüşderelioğlu, M. Evaluation of alginate-chitosan semi IPNs as cartilage scaffolds. *J. Mater. Sci. Mater. Med.* **2009**, *20*, 699–709. [CrossRef]
20. Madihally, S.V.; Matthew, H.W.T. Porous chitosan scaffolds for tissue engineering. *Biomaterials* **1999**, *20*, 1133–1142. [CrossRef]
21. Ciołek, L.; Biernat, M.; Jaegermann, Z.; Tymowicz-Grzyb, P.; Taźbierski, P.; Jastrzębska, A.; Olszyna, A. Controlling the microstructure of lyophilized porous biocomposites by the addition of ZnO-doped bioglass. *Int. J. Appl. Ceram. Technol.* **2017**, *14*, 1107–1116. [CrossRef]
22. Biernat, M.; Ciołek, L.; Dzierżyńska, M.; Oziębło, A.; Sawicka, J.; Deptuła, M.; Bauer, M.; Kamysz, W.; Pikuła, M.; Jaegermann, Z.; et al. Porous chitosan/ZnO-doped bioglass composites as carriers of bioactive peptides. *Int. J. Appl. Ceram. Technol.* **2020**, *17*, 2807–2816. [CrossRef]
23. Shamekhi, M.A.; Rabiee, A.; Mirzadeh, H.; Mahdavi, H.; Mohebbi-Kalhori, D.; Eslaminejad, M.B. Fabrication and characterization of hydrothermal cross-linked chitosan porous scaffolds for cartilage tissue engineering applications. *Mater. Sci. Eng. C* **2017**, *80*, 532–542. [CrossRef] [PubMed]
24. Tangsadthakun, C.; Kanokpanont, S.; Sanchavanakit, N.; Banaprasert, T.; Damrongsakkul, S. Properties of collagen/chitosan scaffolds for skin tissue engineering. *J. Met. Mater. Miner.* **2006**, *16*, 37–44.

25. Goh, C.Y.; Lim, S.S.; Tshai, K.Y.; El Azab, A.W.Z.Z.; Loh, H.S. Fabrication and in vitro biocompatibility of sodium tripolyphosphate-crosslinked chitosan–hydroxyapatite scaffolds for bone regeneration. *J. Mater. Sci.* **2019**, *54*, 3403–3420. [CrossRef]
26. Shavandi, A.; Bekhit, A.E.D.A.; Ali, M.A.; Sun, Z.; Gould, M. Development and characterization of hydroxyapatite/β-TCP/chitosan composites for tissue engineering applications. *Mater. Sci. Eng. C* **2015**, *56*, 481–493. [CrossRef] [PubMed]
27. Chraniuk, M.; Panasiuk, M.; Hovhannisyan, L.; Żołędowska, S.; Nidzworski, D.; Ciołek, L.; Woźniak, A.; Kubiś, A.; Karska, N.; Jaegermann, Z.; et al. Assessment of the Toxicity of Biocompatible Materials Supporting Bone Regeneration: Impact of the Type of Assay and Used Controls. *Toxics* **2022**, *10*, 20. [CrossRef]
28. Chraniuk, M.; Panasiuk, M.; Hovhannisyan, L.; Żołędowska, S.; Nidzworski, D.; Ciołek, L.; Woźniak, A.; Jaegermann, Z.; Biernat, M.; Gromadzka, B. The Preliminary Assessment of New Biomaterials Necessitates a Comparison of Direct and Indirect Cytotoxicity Methodological Approaches. *Polymers* **2022**, *14*, 4522. [CrossRef]
29. Xu, C.; Zhan, W.; Tang, X.; Mo, F.; Fu, L.; Lin, B. Self-healing chitosan/vanillin hydrogels based on Schiff-base bond/hydrogen bond hybrid linkages. *Polym. Test.* **2018**, *66*, 155–163. [CrossRef]
30. Skwarczynska, A.; Kaminska, M.; Owczarz, P.; Bartoszek, N.; Walkowiak, B.; Modrzejewska, Z. The structural (FTIR, XRD, and XPS) and biological studies of thermosensitive chitosan chloride gels with β-glycerophosphate disodium. *J. Appl. Polym. Sci.* **2018**, *135*, 46459. [CrossRef]
31. Efimov, A.M.; Pogareva, V.G. IR absorption spectra of vitreous silica and silicate glasses: The nature of bands in the 1300 to 5000 cm^{-1} region. *Chem. Geol.* **2006**, *229*, 198–217. [CrossRef]
32. Manimohan, M.; Pugalmani, S.; Ravichandran, K.; Sithique, M.A. Synthesis and characterisation of novel Cu(ii)-anchored biopolymer complexes as reusable materials for the photocatalytic degradation of methylene blue. *RSC Adv.* **2020**, *10*, 18259–18279. [CrossRef]
33. Modrzejewska, Z.; Skwarczyńska, A.; Douglas, T.E.L.; Biniaś, D.; Maniukiewicz, W.; Sielski, J. Structure of chitosan gels mineralized by sorption. *J. Mol. Struct.* **2015**, *1098*, 101–109. [CrossRef]
34. Caridade, S.G.; Merino, E.G.; Alves, N.M.; de Zea Bermudez, V.; Boccaccini, A.R.; Mano, J.F. Chitosan membranes containing micro or nano-size bioactive glass particles: Evolution of biomineralization followed by in situ dynamic mechanical analysis. *J. Mech. Behav. Biomed. Mater.* **2013**, *20*, 173–183. [CrossRef] [PubMed]
35. Kumirska, J.; Czerwicka, M.; Kaczyński, Z.; Bychowska, A.; Brzozowski, K.; Thöming, J.; Stepnowski, P. Application of spectroscopic methods for structural analysis of chitin and chitosan. *Mar. Drugs* **2010**, *8*, 1567–1636. [CrossRef] [PubMed]
36. Pozzo, L.D.Y.; da Conceição, T.F.; Spinelli, A.; Scharnagl, N.; Pires, A.T.N. Chitosan coatings crosslinked with genipin for corrosion protection of AZ31 magnesium alloy sheets. *Carbohydr. Polym.* **2018**, *181*, 71–77. [CrossRef]
37. Marin, L.; Ailincai, D.; Mares, M.; Paslaru, E.; Cristea, M.; Nica, V.; Simionescu, B.C. Imino-chitosan biopolymeric films. Obtaining, self-assembling, surface and antimicrobial properties. *Carbohydr. Polym.* **2015**, *117*, 762–770. [CrossRef]
38. Chenite, A.; Buschmann, M.; Wang, D.; Chaput, C.; Kandani, N. Rheological characterisation of thermogelling chitosan/glycerol-phosphate solutions. *Carbohydr. Polym.* **2001**, *46*, 39–47. [CrossRef]
39. Qiu, X.; Yang, Y.; Wang, L.; Lu, S.; Shao, Z.; Chen, X. Synergistic interactions during thermosensitive chitosan-β-glycerophosphate hydrogel formation. *RSC Adv.* **2011**, *1*, 282–289. [CrossRef]
40. Neto, C.G.T.; Giacometti, J.A.; Job, A.E.; Ferreira, F.C.; Fonseca, J.L.C.; Pereira, M.R. Thermal analysis of chitosan based networks. *Carbohydr. Polym.* **2005**, *62*, 97–103. [CrossRef]
41. Prashanth, K.V.H.; Kittur, F.S.; Tharanathan, R.N. Solid state structure of chitosan prepared under different N-deacetylating conditions. *Carbohydr. Polym.* **2002**, *50*, 27–33. [CrossRef]
42. Kittur, F.S.; Prashanth, K.V.H.; Sankar, K.U.; Tharanathan, R.N. Characterization of chitin, chitosan and their carboxymethyl derivatives by differential scanning calorimetry. *Carbohydr. Polym.* **2002**, *49*, 185–193. [CrossRef]
43. Faqhiri, H.; Hannula, M.; Kellomäki, M.; Calejo, M.T.; Massera, J. Effect of melt-derived bioactive glass particles on the properties of chitosan scaffolds. *J. Funct. Biomater.* **2019**, *10*, 38. [CrossRef]
44. Kim, B.S.; Park, I.K.; Hoshiba, T.; Jiang, H.L.; Choi, Y.J.; Akaike, T.; Cho, C.S. Design of artificial extracellular matrices for tissue engineering. *Prog. Polym. Sci.* **2011**, *36*, 238–268. [CrossRef]
45. Yan, L.P.; Wang, Y.J.; Ren, L.; Wu, G.; Caridade, S.G.; Fan, J.B.; Wang, L.Y.; Ji, P.H.; Oliveira, J.M.; Oliveira, J.T.; et al. Genipin-cross-linked collagen/chitosan biomimetic scaffolds for articular cartilage tissue engineering applications. *J. Biomed. Mater. Res. Part A* **2010**, *95*, 465–475. [CrossRef]
46. Chen, H.; Ouyang, W.; Martoni, C.; Prakash, S. Genipin cross-linked polymeric alginate-chitosan microcapsules for oral delivery: In-vitro analysis. *Int. J. Polym. Sci.* **2009**, *2009*, 617184. [CrossRef]
47. Mu, C.; Zhang, K.; Lin, W.; Li, D. Ring-opening polymerization of genipin and its long-range crosslinking effect on collagen hydrogel. *J. Biomed. Mater. Res. Part A* **2013**, *101*, 385–393. [CrossRef] [PubMed]
48. Radwan-Pragłowska, J.; Piątkowski, M.; Janus, Ł.; Bogdał, D.; Matysek, D.; Cablik, V. Microwave-assisted synthesis and characterization of antioxidant chitosan-based aerogels for biomedical applications. *Int. J. Polym. Anal. Charact.* **2018**, *23*, 721–729. [CrossRef]
49. Palomino-Durand, C.; Lopez, M.; Marchandise, P.; Martel, B.; Blanchemain, N.; Chai, F. Chitosan/polycyclodextrin (CHT/PCD)-based sponges delivering VEGF to enhance angiogenesis for bone regeneration. *Pharmaceutics* **2020**, *12*, 784. [CrossRef]
50. Kierys, A.; Zaleski, R.; Grochowicz, M.; Gorgol, M.; Sienkiewicz, A. Polymer–mesoporous silica composites for drug release systems. *Microporous Mesoporous Mater.* **2020**, *294*, 109881. [CrossRef]

51. Pawar, V.; Bulbake, U.; Khan, W.; Srivastava, R. Chitosan sponges as a sustained release carrier system for the prophylaxis of orthopedic implant-associated infections. *Int. J. Biol. Macromol.* **2019**, *134*, 100–112. [CrossRef]
52. Huang, Y.; Onyeri, S.; Siewe, M.; Moshfeghian, A.; Madihally, S.V. In vitro characterization of chitosan–gelatin scaffolds for tissue engineering. *Biomaterials* **2005**, *26*, 7616–7627. [CrossRef]
53. Bi, L.; Cao, Z.; Hu, Y.; Song, Y.; Yu, L.; Yang, B.; Mu, J.; Huang, Z.; Han, Y. Effects of different cross-linking conditions on the properties of genipin-cross-linked chitosan/collagen scaffolds for cartilage tissue engineering. *J. Mater. Sci. Mater. Med.* **2011**, *22*, 51–62. [CrossRef] [PubMed]
54. Chen, X.; Zhang, J.; Chen, G.; Xue, Y.; Zhang, J.; Liang, X.; Lei, I.M.; Lin, J.; Xu, B.B.; Liu, J. Hydrogel Bioadhesives with Extreme Acid-Tolerance for Gastric Perforation Repairing. *Adv. Funct. Mater.* **2022**, *32*, 2202285. [CrossRef]
55. Veiga, I.G.; Moraes, Â.M. Study of the swelling and stability properties of chitosan-xanthan membranes. *J. Appl. Polym. Sci.* **2012**, *124* (Suppl. 1), E154–E160. [CrossRef]
56. Yuan, Y.; Chesnutt, B.M.; Utturkar, G.; Haggard, W.O.; Yang, Y.; Ong, J.L.; Bumgardner, J.D. The effect of cross-linking of chitosan microspheres with genipin on protein release. *Carbohydr. Polym.* **2007**, *68*, 561–567. [CrossRef]
57. Saravanan, S.; Vimalraj, S.; Thanikaivelan, P.; Banudevi, S.; Manivasagam, G. A review on injectable chitosan/beta glycerophosphate hydrogels for bone tissue regeneration. *Int. J. Biol. Macromol.* **2019**, *121*, 38–54. [CrossRef]
58. Yang, J.; Long, T.; He, N.F.; Guo, Y.P.; Zhu, Z.A.; Ke, Q.F. Fabrication of a chitosan/bioglass three-dimensional porous scaffold for bone tissue engineering applications. *J. Mater. Chem. B* **2014**, *2*, 6611–6618. [CrossRef]
59. Gilarska, A.; Lewandowska-Łańcucka, J.; Horak, W.; Nowakowska, M. Collagen/chitosan/hyaluronic acid—Based injectable hydrogels for tissue engineering applications—Design, physicochemical and biological characterization. *Colloids Surf. B Biointerfaces* **2018**, *170*, 152–162. [CrossRef]
60. Mekhail, M.; Jahan, K.; Tabrizian, M. Genipin-crosslinked chitosan/poly-l-lysine gels promote fibroblast adhesion and proliferation. *Carbohydr. Polym.* **2014**, *108*, 91–98. [CrossRef]
61. Szustakiewicz, K.; Włodarczyk, M.; Gazińska, M.; Rudnicka, K.; Płociński, P.; Szymczyk-ziółkowska, P.; Ziółkowski, G.; Biernat, M.; Sieja, K.; Grzymajło, M.; et al. The effect of pore size distribution and l-lysine modified apatite whiskers (Hap) on osteoblasts response in plla/hap foam scaffolds obtained in the thermally induced phase separation process. *Int. J. Mol. Sci.* **2021**, *22*, 3607. [CrossRef]

polymers

MDPI

Review

Advances in the Utilization of Tea Polysaccharides: Preparation, Physicochemical Properties, and Health Benefits

Qian Wang [1,†], Xiaoyan Yang [2,†], Changwei Zhu [1], Guodong Liu [1], Yujun Sun [1,*] and Lisheng Qian [1,*]

[1] College of Life and Health Sciences, Anhui Science and Technology University, Chuzhou 233100, China; qianwang420@163.com (Q.W.); zhucw@ahstu.edu.cn (C.Z.); liugd@ahstu.edu.cn (G.L.)
[2] College of Agriculture, Anhui Science and Technology University, Chuzhou 233100, China; yangxiaoyan8166@163.com
* Correspondence: sunyujun208@163.com (Y.S.); qlsfy@163.com (L.Q.)
† These authors contributed equally to this work.

Abstract: Tea polysaccharide (TPS) is the second most abundant ingredient in tea following tea polyphenols. As a complex polysaccharide, TPS has a complex chemical structure and a variety of bioactivities, such as anti-oxidation, hypoglycemia, hypolipidemic, immune regulation, and anti-tumor. Additionally, it shows excellent development and application prospects in food, cosmetics, and medical and health care products. However, numerous studies have shown that the bioactivity of TPS is closely related to its sources, processing methods, and extraction methods. Therefore, the authors of this paper reviewed the relevant recent research and conducted a comprehensive and systematic review of the extraction methods, physicochemical properties, and bioactivities of TPS to strengthen the understanding and exploration of the bioactivities of TPS. This review provides a reference for preparing and developing functional TPS products.

Keywords: tea; polysaccharides; extraction method; chemical composition; bioactivity; gut microbiota

Citation: Wang, Q.; Yang, X.; Zhu, C.; Liu, G.; Sun, Y.; Qian, L. Advances in the Utilization of Tea Polysaccharides: Preparation, Physicochemical Properties, and Health Benefits. *Polymers* **2022**, *14*, 2775. https://doi.org/10.3390/polym14142775

Academic Editors: Cornelia Vasile, Gabriel Aguirre-Álvarez and Xiao-Feng Sun

Received: 17 June 2022
Accepted: 5 July 2022
Published: 6 July 2022

1. Introduction

As a traditional drink, tea has been cultivated and consumed for thousands of years, and it is deeply loved by consumers from many countries, such as China, Japan, and South Korea. Tea not only creates a lot of wealth but also generates tea culture and tea ceremony [1]. As a result, tea has become one of the most popular beverages in the world after water [2–4].

The unprecedented popularity of tea is due not only to its unique aroma and taste but also to the health benefits of drinking it. The primary bioactivities of tea, including anti-oxidation, hypoglycemic, antibacterial, hypolipidemic, and anti-cancer activities, have been studied and explored. Tea has also been broadly utilized in the food, medical, and health care industries [5,6]. Tea's biological and pharmacological activities are mainly attributed to the diversity of its chemical components. The chemical features of tea mainly include tea polyphenols (TPPs), tea polysaccharides (TPSs), tea proteins, catechins, theanine, and inorganic elements [4]. Tea polyphenols have long received attention for their excellent antioxidant properties for which accumulating evidence has been presented [7]. Modern pharmacological studies have shown that TPS, an important bioactive component along with TPP, is also the main tea compound that helps lower blood glucose and lipids, resist oxidation, and enhance the body's immune function [8–10]. It also has excellent potential for development and application in the cosmetic industry [11]. In general, the content of TPS decreases with increases in tea quality or grade [12]. Wang et al., reported that the TPS content in low-grade tea was twice that of high-grade tea [13]. Therefore, using low-grade tea as a raw material to extract TPS is conducive to the full utilization of tea resources and has important implication for preventing diseases and promoting human health.

Therefore, the authors of this paper conducted a detailed comparison and summary of the current research on tea polysaccharide's extraction, preliminary physicochemical properties, and in vitro and in vivo bioactivities in order to provide new insights for the better utilization and development of TPS or TPS-related functional foods.

2. TPS Extraction

Tea leaves, flowers, and seeds are the three primary sources of TPS extraction materials. The current production process of TPS mainly includes hot water extraction, ultrasonic-assisted extraction, microwave-assisted extraction, and enzymolysis extraction (Table 1). Its conventional preparation process is shown in Figure 1.

Table 1. Comparison of extraction methods of tea polysaccharide (TPS).

Extraction Method	TPS Origin	Extraction Step	Ref
Hot water extraction	Green tea leaves and flowers	Pre-extraction with 95% ethanol at 40 °C for 2 h, repeated three times; a water bath extraction at 60 °C for 2 h, repeated 3 times	[14]
	Fuan Baicha and Pingyang Tezaocha	Extraction at 80 °C for 1.5 h, repeated two times	[15]
	Fuzhuan tea	2 h extraction time, 1:20 solid–liquid ratio, and 95 °C extraction temperature; repeated three times	[10]
	White tea	8 min extraction time, 54.1 °C extraction temperature, 12.48 L/g material–water ratio; repeated four times	[16]
	Green tea	Heating in a water bath at 90 °C for 2 h with continuous stirring	[17]
	Green tea	Pre-extraction with absolute ethanol for 24 h and extraction with deionized water at 60 °C for 90 min	[18]
	Chin brick tea	80% ethanol pretreatment and continuous stirring with distilled water (1:20, w/v) at 90 °C for 2 h	[19]
	Liupao tea	80% ethanol pretreatment for 24 h and extraction with deionized water at 70 °C for 2 h; repeated three times	[20]
	Tea flowers	Extraction at 90 °C for 1 h (2 times)	[21]
	Green tea	80% ethanol pretreatment at 70 °C for 1.5 h, extraction with ethanol at 40 °C for 3 h	[22]
	Green tea	Pretreatment with two times volume of 95% ethanol at 50 °C for 4 h, 1:8 solid–liquid ratio, and extraction with stirring at 50 °C for 120 min	[23]
	Green tea	Pretreatment with 95% alcohol (1:5, w/v) for 2 h, extraction in hot water (1:10, w/v) at 80 °C; repeated 3 times for 1 h each time	[24]
	Green tea	95% ethanol (1:6, w/v) pretreatment at 60 °C for 4 h and extraction with distilled water (1:10, w/v) at 80 °C for 4 h; repeated 3 times	[25]
	Keemun black tea	Pretreatment with 95% ethanol (1:6, w/v) at 80 °C for 2 h and immersed in distilled water (1:10, w/v) at 80 °C for 4 h; repeated four times	[26]
Ultrasonic-assisted extraction	Low-grade green tea	80 °C extraction temperature, 60 min extraction time, 400 W ultrasonic power, and 22 mL:g liquid–solid ratio	[27]
	Coarse tea	Pretreatment in an ultrasonic bath (50 °C, 200 W) for 30 min followed by extraction in a water bath for 90 min; repeated three times	[23]
	Green tea flowers	Ultrasonic power (25 °C, 100, 150, 200, 250, and 300 W) extraction for 5 min; repeated 2 times	[21]
	Yellow tea	95% ethanol pretreatment for 6 h, 90 °C water bath extraction for 55 min (repeated twice), and sonication (20 kHz, 500 W) for 55 min	[21]

Table 1. *Cont.*

Extraction Method	TPS Origin	Extraction Step	Ref
Microwave-assisted extraction	Green, black, and oolong teas	1:20 solid/liquid ratio, 200–230 °C extraction temperature, and 2 min extraction time	[28]
	Green tea flowers	Extraction at controlled microwave power for 5 min followed by extraction with distilled water for 5 min at the same microwave power	[21]
	Green tea	Extraction in a 600 W microwave apparatus for 30 min, followed by stirring in a water bath for 90 min; repeated three times	[29]
Enzymolysis extraction	Green tea	Extraction at 100 °C for 3 h and aqueous extraction with pectinase and tannase at 35 °C for 2 h	[30]
	Green tea	Extraction with complex enzymes (cellulase:pectinase:glucanase = 1:1:2) at 50 °C for 30 min, boiling at 90 °C for 10 min, and then extraction in a water bath at 50 °C for 80 min	[29]
	Green tea leaves and flowers	95% ethanol pretreatment at 40 °C for 2 h (repeated 3 times), treatment with 0.5% (m/v) pentosan complex enzyme solution (45 °C, pH 5.5) for 2 h, and extraction in 45 °C water bath for 2 h	[14]
	Green tea	Heating in a water bath at 90 °C for 2–4 h, repeated twice; incubating with 0.5% pectinase (260,001 PGU/mL, *v*/*w*) at 40 °C for 30 min; and heating at 90 °C for 1 h to inactivate the enzyme	[31]
Hydro/solvothermal extraction	Chinese tea Zhongcha 108	Extraction at 120 °C for 1 h	[1]
Alkali-assisted extraction	Fuzhuan brick tea	Extraction with 0.1 M NaOH solution (pH = 10.0) at 60 °C, repeated 3 times	[32]
Supercritical fluid extraction	Green tea	380 μm particle size, 20% absolute ethanol, 35 MPa extraction pressure, 45 °C extraction temperature, and 2 h extraction time	[33]
Anionic reverse micelle extraction	Green tea	pH = 4.6, 0.06 M guanidine hydrochloride, 7% methanol, and 0.05 M NaCl; forward extraction	[34]

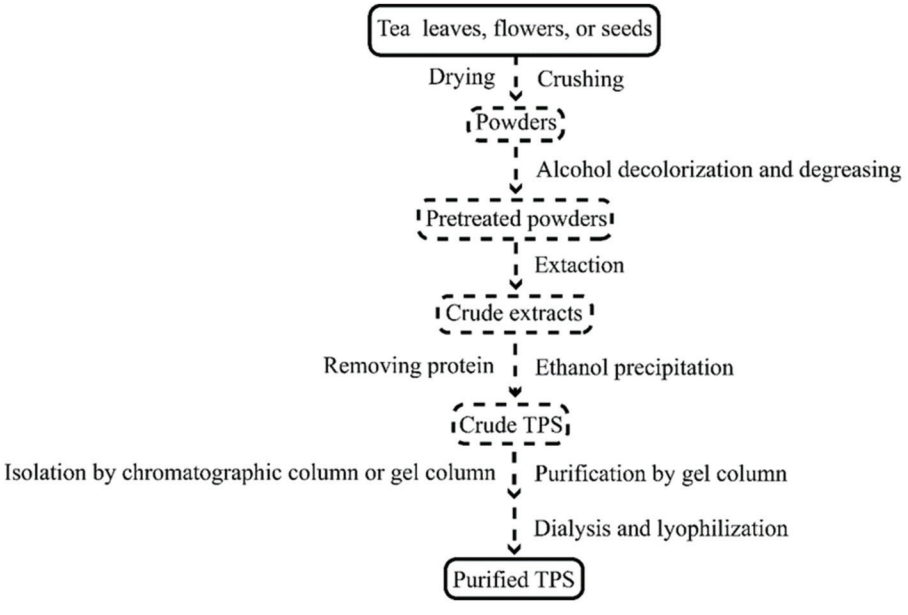

Figure 1. The conventional process of TPS preparation.

2.1. Hot Water Extraction

Most bioactive polysaccharides are polar, so polar solvents such as hot water or alkaline solutions are usually used for polysaccharide extraction [33]. Hot water extraction is a classic method widely used to prepare polysaccharides in food, medicine, and other industries [34]. Chen et al., used water bath heating (70 °C, 60 min) to extract three kinds of crude TPSs from black, oolong, and green tea leaves [35]. Xu et al., prepared TPS from Pu-erh tea three times for 180 min in hot water at 70 °C [36]. Fan et al., extracted TPS twice in Fuan Baicha and Pingyang Tezaocha by adding double-distilled water and heating in a water bath at 80 °C for 1.5 h [37]. Zhu et al., used the response surface methodology to explore the extraction process of Fuzhuan tea crude polysaccharide (CDTPS) and found that the optimal extraction conditions (repeated four times) were as follows: an extraction time of 2 h, a solid–liquid ratio of 1:20, and an extraction temperature of 95 °C. Under these conditions, the yield of CDTPS was 6.07% [10]. The response surface methodology used by Jin et al., predicted the optimal extraction conditions of TPS via repetition four times in white tea: the optimal extraction time was 97.8 min, the extraction temperature was 54.1 °C, and the material–water ratio was 12.48 L/g [14]. Wang et al., pretreated dried green tea leaves and flowers in 95% ethanol and 40 °C for 2 h, then repeated the process three times to remove pigments and other substances. Then, 2 L of distilled water was added to the filtered tea samples for extraction in a water bath at 60 °C for 2 h. After filtration, 2.5 L of distilled water was added, and the hot water extraction was repeated again (60 °C, 2 h) [38]. Similarly, Cai et al., pretreated green tea leaves with absolute ethanol for 24 h to remove some small-molecular pigments and polyphenols, and then they dried the tea samples with deionized water for 90 min at 60 °C [16]. Li et al., also pretreated Chin brick tea powder with 80% ethanol, centrifuged it, and then continuously stirred it with distilled water (1:20, *w*/*v*) for 2 h at 90 °C to extract TPS [17]. Qin et al., pretreated Liupao tea samples with 80% ethanol for 24 h. After filtration and drying, the samples were extracted with deionized water at 70 °C for 2 h, and the process was repeated three times [18]. Wei et al., performed the hot water extraction of dried tea flower polysaccharides (TFPSs) and then extracted TFPSs twice with distilled water (1 h each). They found that the yield of TFPS increased with the extraction temperature, and 90 °C was the optimal extraction temperature for TFPS. The yield at this condition was close to 35% [19]. Though hot water extraction is a commonly used method for TPS extraction, conventional hot water extraction has disadvantages such as a low extraction efficiency, long extraction time, and high extraction temperature, all of which limit its availability [33,39]. For example, Wang et al., further compared the yields of hot water extraction, boiling water extraction, and enzymolysis extraction for TFPS, and they found that the yield of TFPS obtained with enzymolysis extraction was the highest (2.01%), followed by boiling water extraction (1.91%) and finally hot water extraction (1.83%) [20]. Zhu et al., compared the yields of crude green tea polysaccharides (CTPSs) under hot water extraction (WE), enzymatic extraction (EE), microwave-assisted extraction (MAE) and ultrasonic-assisted extraction (UAE), and they found that the four yields of CTPS under these extraction methods were 3.98%, 4.17%, 4.31%, and 4.52%, respectively [21]. Numerous studies have verified that although hot water extraction has strong practicability, its obtained TPS yield is relatively low and easily leads to the unnecessary waste of raw materials. Therefore, many researchers have also improved the technology on the basis of hot water extraction and developed other auxiliary extraction methods, such as ultrasonic-assisted extraction, microwave-assisted extraction, and enzyme-assisted extraction, to improve the extraction efficiency of TPS [40].

2.2. Ultrasonic-Assisted Extraction (UAE)

UAE can accelerate the rupture of plant cell walls by the high-speed movement of molecules in samples caused by high-frequency ultrasonic vibration, thereby dissolving and releasing intracellular substances. Karadag et al., used UAE to extract low-grade green tea polysaccharides (GTPSs) and then reported the optimal extraction parameters through response surface optimization as follows: 80 °C for extraction temperature, 60 min for

extraction time, 400 W for ultrasonic power, and 22 mL/g for liquid–solid ratio. Under these conditions, the yield of GTPS was 4.65%, which was higher than that of the hot water extraction method (1.83%) without ultrasound [25]. In addition, they also found that the Mw of GTPS obtained with ultrasonic-assisted extraction was lower, which may have been due to the partial degradation of TPS caused by the ultrasonic process. Zhu et al., prepared TPS from coarse green tea leaves, placing the tea leaves in an ultrasonic bath (50 °C, 200 W) for pretreatment for 30 min and then performing extraction in a water bath for 90 min. The TPS yield obtained with this method was higher than other tested methods [21]. To explore the effects of ultrasound on the structure and activity of yellow tea polysaccharide (YTPS), Wang et al., treated a YTPS fraction obtained after hot water extraction and deproteinization with ultrasound (20 kHz, 500 W) for 55 min. The results showed that ultrasonic treatment basically did not change the main chemical composition of YTPS but did cause it to degrade [26]. Wei et al., mixed dried green tea flower blocks with distilled water and extracted them for 5 min at 25 °C under ultrasonic powers of 100, 150, 200, 250, and 300 W. This process was repeated twice to obtain crude TFPS [19]. Overall, the UAE method has the advantages of saved time, simple operation, experimental safety, low cost, and high extraction rate. Still, it may degrade soluble TPS and affect its bioactivity.

2.3. Microwave-Assisted Extraction (MAE)

Recently, microwave-assisted extraction (MAE) technology has become widely used to analyze and extract active components in plants. MAE is a new extraction technology that uses high-frequency electromagnetic waves (0.3–300 GHZ) with strong penetrability and heating effect to extract active plant components. High-energy microwaves can penetrate solvents and plant cell walls, transfer energy to the cytoplasm, and interact with polar components to generate heat, which increases the temperature and pressure inside cells. When the pressure reaches a certain level, the cell wall expands and ruptures, releasing intracellular polysaccharides and other substances [41]. Shuntaro et al., used MAE technology to extract TPS from tea residues (green tea, black tea, and oolong tea). When the extraction conditions were a solid/liquid ratio of 1:20, an extraction temperature of 200–230 °C, and an extraction time of 2 min, the yield of tea residue TPS was 40–50% [27]. Wei et al., used MAE equipment to extract TFPS twice, for 5 min each time. They found that the yield of TFPS changed irregularly with the increase in microwave power. In addition, with increases in microwave power, the content of neutral sugars in TFPS increased while the content of acidic sugars increased and then decreased [19]. Li et al., used a 600 W microwave instrument to extract coarse green tea crude TPS (CTPS), and the extraction process was repeated three times. After extraction with MAE, the content of soluble protein in CTPS was the highest of all tested methods, reaching 5.93%. Furthermore, they found that MAE treatment had little effect on CTPS chains with high Mw but resulted in the drastic degradation of small-Mw CTPS. According to related reports, small-Mw polysaccharides tend to have better bioactivities than their high-Mw counterparts [42]. The subsequent in vitro activity test of CTPS prepared by the MAE method by Zhu et al., also confirmed this conclusion [21]. Compared to other extraction methods, the MAE method has the advantages of high extraction efficiency, high purity, non-degradable active ingredients, convenient operation, saved time, and environmental friendliness. It is a "green extraction process", which has made it popular. Although MAE has favorable prospects in TPS extraction, it also has disadvantages such as complex extract components, difficult separation and purification in the later stages, and the necessity of polar solvents [43]. Therefore, in addition to the basic closed and open systems, several improved microwave extraction technologies, such as vacuum microwave-assisted extraction, nitrogen-protected microwave-assisted extraction, ultrasonic microwave-assisted extraction, and dynamic microwave-assisted extraction, have been developed [41].

2.4. Enzymolysis Extraction

The enzymolysis method refers to the destruction of plant cell walls with enzymatic hydrolysis. The cell wall is decomposed into small molecular substances readily soluble in the extraction solvent, thereby accelerating the dissolution of active ingredients. The yield of TPS extracted with enzymatic hydrolysis is usually higher and the effect of mixed enzymes is better than that of a single enzyme. However, the enzyme's activity is easily affected by the reaction temperature, pH, and concentration, so the requirements for experimental conditions and costs are usually higher. Baik et al., investigated the effect of the simultaneous treatment of pectinase and tannase on TPS extraction from green tea. They found that the concurrent treatment of the two enzymes was an effective method for TPS extraction and could significantly improve TPS's free radical scavenging activity [28]. Chang et al., used pectinase-assisted extraction to obtain green tea TPS, and the primary extraction process was as follows: the ground tea powder was heated in a water bath at 90 °C for 2–4 h, 0.5% pectinase (260,001 PGU/mL, *v*/*w*) was added and incubated at 40 °C for 30 min, and then the enzyme was inactivated by heating at 90 °C for 1 h. The prepared TPS presented excellent immune stimulation and protection against immune cells [30]. In addition to bioactivity, yield is also a concern for enzymolysis extraction. Zhu et al., used mixed enzymes (cellulase:pectinase:glucanase = 1:1:2) for crude green tea polysaccharide (CTPS) extraction at 50 °C (30 min), followed by boiling to inactivate the enzyme (10 min) and extracting in a water bath at 50 °C for 80 min. The whole process was repeated three times. The CTPS obtained with this method had a high total sugar content (71.83%), which could mainly be attributed to the gentle and efficient destruction of the cell walls by mixed enzymes [21,44]. Wang et al., used a 0.5% (m/v) pentosan complex enzyme solution (45 °C, pH 5.5) to extract TPS from green tea leaves and flowers pretreated with 95% ethanol for 2 h. After filtration, the same extraction process at the same temperature was repeated. The yields of two TPSs obtained with this method were 4.08% and 6.88%, respectively, which were much higher than those obtained with hot water extraction under the same conditions (1.28% and 2.93%, respectively) [38]. Compared to the conventional solvent extraction method, the enzymolysis extraction method has the advantages of a high extraction efficiency, strong specificity, and high extraction rate. In addition, it can reduce the environmental pollution caused by using a large amount of solvent and thus has broad application prospects. However, since the price of the enzyme is relatively high and its activity is affected by various factors, the extraction conditions for enzymolysis extraction must be strictly controlled to effectively obtain a higher extraction rate.

2.5. Other Extraction Methods

Some new methods for TPS extraction in addition to the above-mentioned common extraction methods have also been reported. For example, Xu et al., optimized extraction conditions using a hydro/solvothermal method. They used high temperature and pressure (120 °C, 0.1 MPa) to infiltrate water into the tea leaves of Zhongcha 108 to destroy the cell structure, thereby separating TPS [1]. The extraction rate of crude polysaccharides obtained with this method was 4.7%, which was much higher than that of TPS obtained with ordinary hot water extraction, such as Ziyang green tea (3.46%) [22], Huangshan Maofeng tea (2.3%) [23], and Keemun black tea (3.2%) [24]. Sun et al., used alkali-assisted extraction to extract Fuzhuan brick tea polysaccharide (FBTPS); the extraction conditions were a 60 °C extraction temperature and a 0.1 mol/L NaOH solution (pH = 10.0). Compared to hot water extraction, the yield of FBTPS by alkaline extraction was found to have a greater impact on the monosaccharide composition and yield [30]. In addition, emerging extraction technology supercritical fluid extraction (SFE) has also been used to extract polysaccharides in recent years. Many researchers have used SFE to extract various plant-derived polysaccharides, though there are still few applications of this process for TPS extraction. Chen et al., extracted TPS with a CO_2-based SFE method, and they determined the optimum parameters of this method in TPS extraction as a particle size of 380 μm, 20% absolute ethanol, an extraction pressure of 35 MPa, an extraction temperature of 45 °C,

an extraction time of 2 h, which enabled a TPS extraction rate of up to 92.5%. Moreover, the TPS obtained with this method was significantly bioactive [31]. Although the SFE method is impressive, manageable, efficient, and environmentally-friendly, it is still not as common as other extraction methods in practical applications due to its expensive and time-consuming equipment. In addition, Li et al., found that extraction via a anionic reverse micelle system exhibited the advantages of a fast mass transfer, high selectivity, and low cost [32]. In short, various auxiliary methods for TPS extraction are able to improve the bioactivity of polysaccharides, shorten extraction times, and improve extraction yields.

3. Preliminary Physicochemical Properties of TPS

3.1. Monosaccharide Composition

The monosaccharide composition of TPS is usually analyzed using gas chromatography (GC) and GC mass spectrometry (GC–MS) after the hydrolysis of glycosidic bonds with trifluoroacetic acid and derivatization with acetic anhydride [45]. It has been reported that TPS is formed by linking 2–10 monosaccharides in different arrangements with glycosidic bonds (Table 2). Zhu et al., detected and compared the monosaccharide compositions of CTPS obtained with four different extraction methods (WE, UAE, MAE, and EE) [21]. The results showed that the monosaccharide compositions of the four CTPS were the same. They all contained rhamnose (Rha), arabinose (Ara), galactose (Gal), glucose (Glc), xylose (Xyl), mannose (Man), fucose (Fuc), and galacturonic acid (GalA); the molar ratio of Glc was the highest at 29.22%, 36.05%, 31.09%, and 44.24%, respectively, for WE, UAE, MAE, and EE. These results were the same as those of Wang et al., [46], indicating that although different extraction techniques can affect the composition of monosaccharides, Glc in CTPS may be the main monosaccharide component [21]. Zhu et al., also obtained two homogeneous TPSs (ASe-TPS2 and NSe-TPS2) from natural selenium-enriched and artificial selenium-enriched green teas, respectively, with uronic acid contents as high as 65.45% and 69.98%, respectively, confirming that they were typical acidic polysaccharides [47]. Further monosaccharide composition analysis by ion chromatography (IC) showed that ASe-TPS2 mainly contained Rha, Ara, Glc, Xyl, and GalA with a molar ratio of 1.93: 7.05: 1.00: 1.05: 26.12, respectively, while NSe-TPS2 was mainly composed of Ara, Gal, glucuronic acid (GlcA), and GalA at a molar ratio of 0.59: 1.00: 0.49: 1.24, respectively. These results suggest that different selenium-enriched methods may also lead to differences in the monosaccharide composition of TPS, and differences in uronic acid content may affect its chemical properties or bioactivity. Wang et al., also used the IC method to detect the purified components of selenium-enriched green tea polysaccharides (Se-TPS1, Se-TPS2, and Se-TPS3). They found that the three purified components were also acidic polysaccharides [48], and though their monosaccharide composition was the same as that of NSe-TPS2, their molar ratios were different. Yang et al., extracted crude tea polysaccharide (CTPS) and two fractions, TPS-1 and TPS-2, from Qingzhuan brick tea. TPS-2, with the lowest uronic acid content (24.45 mg/g), showed stronger ferric ion-reducing antioxidant power (FRAP) and in vitro scavenging capability against 1,1-diphenyl-2-picrylhydrazyl (DPPH) and 2,2-azino-bis(3-ethylbenzothiazoline-6-sulphonic acid) ABTS radicals [49]. According to related reports, a large amount of uronic acid in polysaccharides may lead to a stronger ABTS free radical scavenging capability [50], whereas the monosaccharide composition of TPS may have a huge impact on its FRAP properties [51]. The crude Fuzhuan brick tea polysaccharide (FBTPS) obtained with the hot water extraction method (1:10, w/v; 70 °C) by Chen et al., contained 37.78% uronic acid content, and its monosaccharide composition comprised D-ribose (Rib) (1.69 mol%), Man (3.66 mol%), Ara (11.83 mol%), Rha (12.11 mol%), Gal (19.15 mol%), Glc (21.97 mol%), GlcA (1.41 mol%), and GalA (28.17 mol%) [52]. Wang et al., further purified FBTPS and found that FBTPS-3 was the main component of FBTPS (the yield was 37.7%), and its monosaccharide composition included Man, Rha, GalA, Gal, and Ara at a molar ratio of 8.7: 15.5: 42.2: 19.7: 13.9, respectively [53]. Among them, the high GalA composition of FBTPS-3 corresponded to its high uronic acid content (40.4%), indicating that FBTPS-3 is an acidic polysaccharide. Ke et al., obtained crude green tea

polysaccharide (CGPS) by extraction with boiling water at 100 °C and then further purified it to obtain homogeneous GTP consisting only of Glc [54]. Li et al., also used boiling water to extract Yingshan Cloud Mist green tea polysaccharide (GTPS) [55], a neutral polysaccharide composed of Rha, Ara, Xyl, Man, Glc, and Gal at a molar ratio of 11.4: 26.1: 1.9: 3.0: 30.7: 26.8, respectively. Although there was no uronic acid in the studied GTPS, it also had certain in vitro anti-radical activity, which may have been related to its high Glc and Gal contents. Gu et al., isolated and purified two selenium-enriched polysaccharides, SeTPS-1 and SeTPS-2, from green tea crude leaves by extraction at high temperature and high pressure (150 °C, 6 MPa) [56]. Component content and monosaccharide detection showed that their selenium contents were 23.50 μg/g and 13.47 μg/g, respectively. SeTPS-1 did not contain any uronic acid, and its monosaccharide composition mainly comprised Glc and Gal with a molar ratio of 80.1:2.3, respectively. The uronic acid content in SeTPS-2 was found to be 15.77%, and its monosaccharide composition mainly comprised Glc and Gal with a molar ratio of 80.1:2.3, respectively. Importantly, SeTPS-2 had stronger antioxidant capacity in vitro, which may have been related to its rich uronic acid content. Wang et al., analyzed the monosaccharide composition of yellow tea polysaccharide (YTPS) before and after sonication by HPLC and found that sonication did not change its monosaccharide composition but did have a slight effect on the molar ratio. Both YTPSs mainly consisted of Rha, with small amounts of Man, Rib, GlcA, Gal, and Ara [26]. Chen et al., explored the effect of an ultra-high pressure (200–600 MPa, 25 °C) treatment on the monosaccharide composition of large-leaf yellow tea polysaccharide (LYTP) [57]. LYTP was mainly composed of Ara, Gal, GalA, Rha, Glc, GlcA, and Man. After ultra-high pressure treatment, the content of GlcA in LYTP significantly increased and the contents of Ara, Gal, and GlcA significantly decreased. The shear force generated by ultra-high pressure was able to break the glycosidic bonds connecting Ara, Gal, and GlcA in the main chain or side chain, thereby promoting TPS degradation. However, fragments linked by a large amount of GalA were more stable, thus increasing the proportion of GalA [58]. In addition, numerous studies have shown that acidic polysaccharides generally have high bioactivity [59,60].

Table 2. Monosaccharide composition of different TPSs.

TPS Origin	Monosaccharide Composition and Molar Ratio	Ref
Green tea	WE, Rha: Ara: Gal: Glc: Xyl: Man: Fru: GalA = 4.11: 9.96: 28.05: 29.22: 3.46: 4.62: 4.14: 16.43, respectively; UAE, 2.27: 9.22: 27.54: 36.05: 5.38: 4.75: 6.72: 8.07, respectively; MAE, 4.03: 11.84: 27.06: 31.09: 3.64: 6.17: 6.84: 9.33, respectively; EE, 5.40: 8.86: 12.32: 44.24: 3.15: 4.38: 11.78: 9.87, respectively	[21]
Green tea	Ara: Xyl: Fuc: Glc: Gal = 6.49: 2.60: 6.53: 43.27: 41.11, respectively;	[46]
Natural and artificial selenium-enriched green teas	ASe-TPS2, Rha: Ara: Glc: Xyl: GalA = 1.93: 7.05: 1.00: 1.05: 26.12, respectively; NSe-TPS2, Ara: Gal: GluA: GalA = 0.59: 1.00: 0.49: 1.24, respectively	[47]
Selenium-enriched green tea	Se-TPS1, Fuc: Rha: Ara: Gal: Glc: GlcA: GalA = 0.07: 0.21: 0.58: 1.00: 0.47: 0.17: 1.75, respectively; Se-TPS2, Fuc: Rha: Ara: Gal: Glc: GlcA: GalA = 0.07: 0.28: 0.59: 1.00: 0.10: 0.49: 1.24, respectively; Se-TPS3, Fuc: Rha: Ara: Gal: Glc: GlcA: GalA = 0.07: 0.38: 0.72: 1.00: 0.30: 0.19: 0.88, respectively	[48]

Table 2. *Cont.*

TPS Origin	Monosaccharide Composition and Molar Ratio	Ref
Fuzhuan brick tea	FBTPS, Rib: Man: Ara: Rha: Gal: Glc: GlcA: GalA = 1.69: 3.66: 11.83: 12.11: 19.15: 21.97: 1.41: 28.17, respectively	[52]
Fuzhuan brick tea	FBTPS-3, Man: Rha: GalA: Gal: Ara = 8.7: 15.5: 42.2: 19.7: 13.9, respectively	[53]
Green tea	GTP consisting only of Glc	[54]
Yingshan Cloud Mist green tea	GTPS, Rha: Ara: Xyl: Man: Glc: and Gal = 11.4: 26.1: 1.9: 3.0: 30.7: 26.8, respectively	[55]
Selenium-enriched green tea	SeTPS-1, Glc: Gal = 80.1: 2.3; SeTPS-2, Glc: Gal = 80.1: 2.3, respectively	[56]
Yellow tea	YTPS-N, Man: Rib: Rha: GlcA: GalA: Glc: Gal: Ara = 1.65: 1: 10.95: 1.06: 2.03: 5.49: 3.50: 4.02; YTPS-U, 1.72: 1: 11.05: 1.09: 2.13: 5.36: 3.62: 4.17, respectively	[26]
Large-leaf yellow tea	LYTP, Ara: Gal: GalA: Rha: Glc: GlcA: Man	[57]

3.2. Molecular Weight (Mw)

Mw is one of the most important physical properties of polysaccharides. Numerous studies have shown that Mw is not only an essential indicator for judging the chemical properties of polysaccharides but may also affect their bioactivity. The Mw size of TPS is closely related to the type of tea and the purification process [61,62]. In most studies, gel permeation chromatography (GPC), gel filtration chromatography (GFC), and multi-angle laser light scattering (MLLS) detection methods have been employed to determine the Mw of TPS [45]. Zhu et al., used high-performance gel permeation chromatography (HPGPC) to determine the Mw of crude TPS obtained with four different extraction methods (WE, UAE, MAE, and EE) [21]. The results showed that the Mw of WE-CTPS was mainly distributed at 2558 kDa, accounting for 59.46% of the area. However, the Mw distribution curves of UAY-CTPS and EE-CTPS shifted to the right, the number of peaks at 1000 kDa and 3000 Da significantly increased, and the Mw of UAE-CTPS was smaller than that of EE-CTPS. In addition, MAE treatment resulted in the vigorous degradation of small-Mw TPS but had little effect on high-Mw TPS chains. MAE treatment will damage the cell structure and accelerate the collision between small molecules, easily leading to the fragmentation of small-Mw polysaccharides [63]. In addition, polysaccharides with smaller Mw values may find it relatively easier to enter the cell interior to escape the stress of the immune system, thus showing better bioactivity than large-Mw polysaccharides [42]. Another study by Zhu et al., also proved this conclusion by detecting the in vitro inhibitory activities of α-glucosidase and α-amylase on four CTPSs [21]. In their other study, it was found that different selenization methods also affected the Mw of Se-TPS. Among them, the Se-TPS obtained with the natural Se-enriched method had a higher Mw of 244.32 kDa than that of NSe-TPS2 (6.73 kDa) [47]. The Mw of three purified selenium-enriched green tea polysaccharide fractions (Se-TPS1, Se-TPS2, and Se-TPS3) obtained under WE (70 °C) were tested by Wang et al., Under WE at 90 °C, Se-TPS1 and Se-TPS2 (as homogeneous polysaccharides,) had lower Mw values of 110 kDa and 240 kDa, respectively, compared to NSe-TPS2. At the same time, Se-TPS3 was found to be a polysaccharide polymer with an Mw range of 250–920 kDa [48]. Chen et al., conducted a study on the digestion of TPS in the gastrointestinal tract, and they found that the initial Mw of FBTPS was 828×10^3 g/mol and that the Mw of FBTPS did not change after the "digestion" treatment of in vitro digestive juice. However, after being acted on by microorganisms in the large intestine, FBTPS's Mw decreased with the prolongation of treatment time [52]. Wang et al., found similar results when exploring the purified components of FBTPS with an Mw of 741 kDa [53]. Li et al., obtained GTPS with an Mw of 96.9 kDa by boiling water extraction, and they found that GTPS showed better in vitro antioxidant activities in a dose-dependent

manner [55]. Previous studies have shown that polysaccharides' antioxidant activity is related to their Mw and that the Mw is mainly distributed between 10 and 1000 kDa [64]. Sun et al., found various antioxidant activities of green tea TPSs (TPS1, TPS2, and TPS3) with different Mw values (8.16, 4.82, and 2.31 kDa, respectively); TPS2, with a medium Mw, had the strongest hydroxyl-radical, ABTS free radical, and hydroxyl-radical scavenging capabilities [65]. Compared to those with smaller Mw values, large-Mw TPSs were found to have tighter spatial structures, resulting in fewer active groups being exposed to the outside and weakening their capacity to terminate free radical chain reactions [66,67]. Zhao et al., obtained similar results and found that the cellular repair capacity of TPSs was positively correlated with their antioxidant activity [67]. Gu et al., separated and purified two Se-enriched polysaccharides, SeTPS-1 and SeTPS-2, under high-temperature and high-pressure conditions, resulting in Mw values of 17 and 13 kDa, respectively. SeTPS-2 had a stronger antioxidant capacity in vitro, which may have been related to its lower Mw content [68]. By sonicating YTPS, Wang et al., found that the Mw of YTPS-3 purified with 30% ethanol decreased from 37.7 to 15.1 kDa, proving that ultrasonic irradiation promotes the fragmentation of polysaccharides and results in a decrease in Mw [69]. The YTPS after ultrasound showed more substantial antioxidant capacity than pre-ultrasound YTPS, further confirming that a low Mw could promote antioxidant capacity, which may be attributed to the larger surface area and number of reaction sites of degraded YTPS [26]. Chen et al., found that UHP treatment significantly reduced the Mw of large leaf yellow tea TPS [70], and turbulent flow and high shear forces formed during UHP processing may cause cell deformation or even rupture and lead to fragmentation and degradation of polysaccharides [57,71].

3.3. Solubility

Since TPS contains a large number of polar groups [47,72], it has a strong affinity for water molecules, which allows it to restrict the flow of water. The hydrophilicity of TPS is related to its Mw. The smaller-Mw and less-branched chains of TPS have higher water solubility. Usually, proper heating would promote the dissolution of polysaccharides. Zhu et al., compared the solubility of coarse green tea polysaccharide (CTPS) obtained with different extraction methods. They found that the time for a complete dissolution of CTPS decreased with increasing temperature. At the same temperature, the dissolution time of CTPS obtained with hot water extraction was always the longest [21]. In addition, they also investigated the solubility of TPSs (DTPS-1, DTPS-2, DTPS-3, DTPS-4, DTPS-5, and DTPS-6) from dark tea, and the time for the complete dissolution of DTPS was also negatively correlated with the heating time. When the temperature exceeded 80 °C, the solubility of different DTPSs was almost the same. Additionally, at the same temperature, the dissolution time of DTPS-3 was always the shortest, probably because its structure was more fragmented and then increased the surface area for its reaction [10].

3.4. Viscosity

Due to the particularity of the solubility of polysaccharides, polysaccharides have high viscosity in aqueous solutions and even form gels [73]. The principle is that polysaccharide molecules exist in the form of random coils in solution, and their tightness is related to the composition of monosaccharides and their connection form [74]. When polysaccharide molecules are stirred and rotated in the solution, they need to occupy a large space. At the same time, the collision probability between polysaccharide molecules is elevated and the friction force is enhanced, thus generating a higher viscosity [74]. Due to their specific structural compositions, different polysaccharides produce a high viscosity even at low concentrations. Generally, the viscosity of polysaccharide molecules is not only related to the composition and connection form of monosaccharides but also their Mw. Wang et al., performed intrinsic viscosity analysis on four purified fractions of oolong tea polysaccharides (OTPSs) with different Mw values: OTPS1 (>80 kDa), OTPS2 (30–80 kDa), OTPS3 (10–30 kDa), and OTPS4 (<10 kDa) [75]. The intrinsic viscosities of the four OTPS com-

ponents were 239.56, 162.63, 7.75, and 2.57 mL/g, respectively, which indicated that their intrinsic viscosities increased with relative decreases in Mw. Xu et al., isolated and purified six TPS components with different Mw values from green, oolong, and black teas, and then they performed an intrinsic viscosity analysis [76]. The Mw values of GTPS1, OTPS1, and BTPS1 were less than 80 kDa, while the Mw values of GTPS2, OTPS2, and BTPS2 were greater than 80 kDa. Their intrinsic viscosities were 53.96 mL/g, 60.28, 60.29, 106.95, 106.76, and 104.67 mL/g, respectively. The intrinsic viscosity of TPS1s was found to be lower than that of TPS2s, which may have been related to the decrease in Mw.

3.5. Emulsifying and Stability

Emulsifiers are a crucial material in the production of food, cosmetics, and pharmaceuticals. Emulsifiers contain hydrophilic and hydrophobic regions and are rapidly adsorbed at the oil–water interface, stabilizing emulsion through steric hindrance or electrostatic interactions [77]. Currently, the most commonly used emulsifiers are mainly chemically synthesized ones, such as fatty acid monoglycerides, Tween-80, and sucrose esters [78]. With consumers' increasing pursuit of "green products and healthy life", the development of natural emulsifiers has received great attention [79]. Polysaccharide-based emulsifiers are some of the most commonly used natural emulsifiers in the food industry [49]. The emulsification of polysaccharides improves with increases in solution viscosity, but viscosity is not the main factor affecting emulsification [80]. The Mw of polysaccharides is related to the viscosity, interfacial activity, and hydrophobic groups of polysaccharide solutions. Thus, the Mw of polysaccharides may also affect their emulsification. Studies have shown that increases in Mw can increase polysaccharides' steric hindrance, prevent droplets' aggregation and flocculation, and improve emulsification [81]. The effects of chemical modification on the Mw of polysaccharides can be divided into two types: when the alkyl chain is short and the degree of substitution is low, the degradation of polysaccharides is dominant and the Mw is reduced; when the alkyl chain is long and the degree of substitution is high, the Mw and hydrophobicity of the polysaccharide are increased, resulting in a reduction in the particle size of the emulsion and an improvement of the emulsification [82]. The Mw of acetylated pectin polysaccharides was found to first decrease and then increase with the rise in substitution degree, and the viscosity was found to first decrease and then increase with the rise in substitution degree [83]. At this time, the emulsifying properties are improved, so the degree of substitution can increase the emulsifying properties of the polysaccharide. The stability of an emulsified polysaccharide solution is also closely related to the structure of the polysaccharide molecule itself. Uncharged linear polysaccharides can be combined with hydrogen bonds after forming a colloidal solution. With extensions of time, the degree of association becomes stronger and precipitation or molecular crystallization will occur under the action of gravity. Branched polysaccharide colloids also become unstable due to molecular aggregation, though at a slower rate. In addition, charged polysaccharide colloids have higher stability due to the repulsion of the same charge between molecules. In addition, the protein–polysaccharide conjugate formed by the distribution of the protein part along the polysaccharide chain combines the characteristics of proteins and polysaccharides, which is also beneficial to improving emulsification and stability to a certain extent [84]. In a report by Chen et al., an alkali-extracted tea polysaccharide conjugate (TPC-A) was used to stabilize oil-in-water emulsions, and TPC-A was shown to have a favorable protective effect on catechins and could be used as a natural emulsifier [85]. Li et al., also obtained a TPS conjugate with good emulsifying properties and excellent antioxidant activity from Chin brick tea [86]. The effects of a certain degree of heat treatment on the physicochemical and functional properties of TPC were also investigated. The heat treatment of TPC (TPC-3d) at 110 °C for three days significantly improved its emulsification activity and stability but did not affect its antioxidant activity [45]. Chen et al., studied the emulsifying properties and emulsifying stability of polysaccharide conjugates (TPC-C) from Chin-Brick Tea. They found that TPC-C had no effect on the dynamic interfacial tension and particle size formation of emulsions or storage, and it showed excellent potential

as a natural emulsifier in terms of stability; the TPS part mainly provided pH stability for the TPC-C stabilized emulsion [87]. In another study, Chen et al., extracted a TPS conjugate (gTPC) from low-grade green tea and obtained two purified components: gTPC-1 and gTPC-2 [88]. The high-Mw gTPC-1 fraction exhibited a higher emulsion stability than the low-Mw gTPC-2, which may be attributed to differences in polysaccharide chain length and conformation in the conjugates. Compared to the lower-Mw polysaccharides, higher-Mw polysaccharides were able to more efficiently coat the droplet surface. At the same time, the high-Mw polysaccharide conjugates improved the emulsion's salt and thermal stability, which may have been due to the capability of high-Mw polysaccharides to form thicker charged coatings, causing an increased steric hindrance between droplets and a greater electrostatic repulsion compared to low-Mw polysaccharides [89,90].

4. In Vitro Bioactivity of TPS

As a bioactive polysaccharide, TPS has been reported to show favorable performance in various in vitro activity evaluation models (Figure 2).

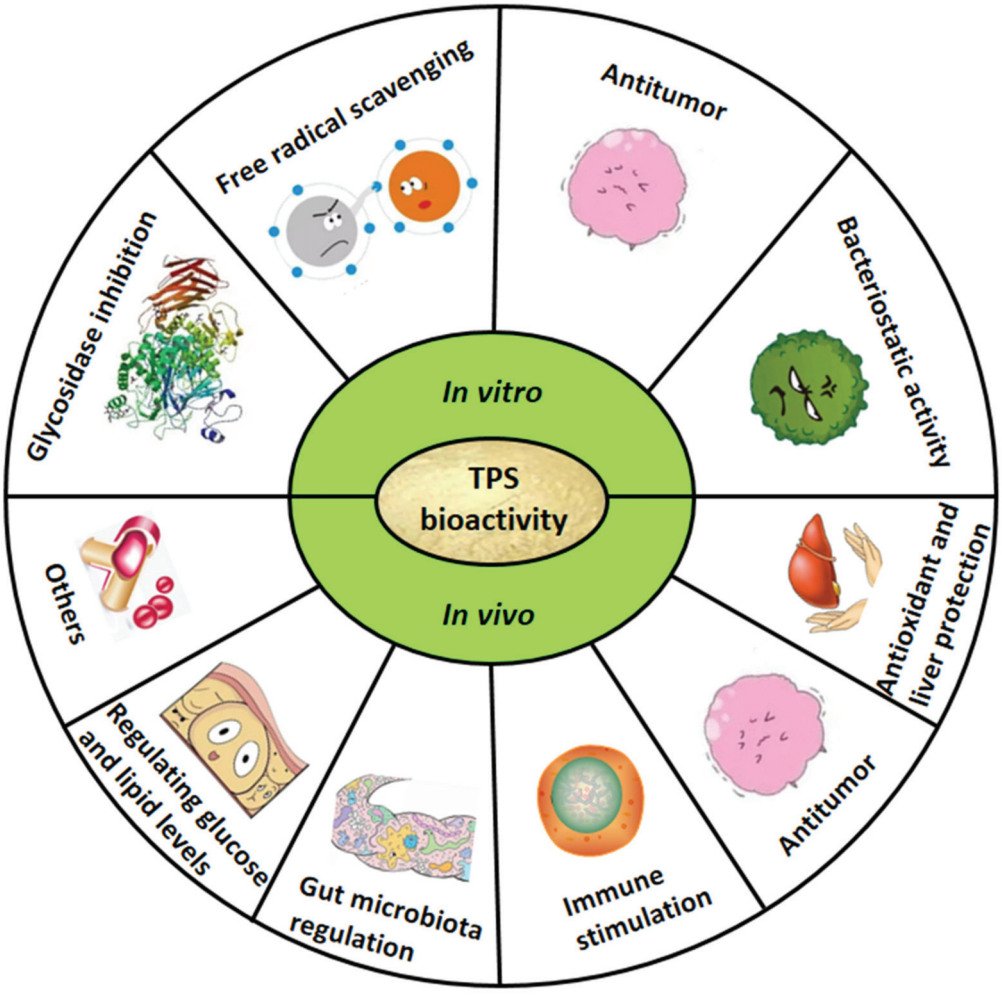

Figure 2. In vitro and in vivo bioactivities of TPS.

4.1. Glycosidase Inhibition

Alpha-glucosidase is an essential enzyme in carbohydrate digestion. In a regular diet, starch is first cleaved into oligosaccharides by α-amylase. The oligosaccharides are hydrolyzed by α-glucosidase to release glucose, which is absorbed into the blood by intestinal epithelial cells. Thus, the inhibition of α-glucosidase, an enzyme that has been proposed as a therapeutic target for regulating postprandial hyperglycemia, prevents excess glucose absorption in the small intestine and controls postprandial hyperglycemia [91]. Acarbose can inhibit alpha-glucosidase and prevent elevated postprandial blood glucose levels, and it is widely used in treating patients with type 2 diabetes. However, synthetic chemicals have various side effects, such as flatulence and diarrhea [92]. Therefore, natural α-glucosidase inhibitors without side effects have attracted more and more attention. Chen et al., isolated three TPS fractions—GTPS, OTPS, and BTPS—from green, oolong, and black tea, respectively, and then compared their in vitro α-glucosidase inhibitory activities [35]. Among them, BTPS could inhibit α-glucosidase activity in dose-dependent manner (14.3–91% with an increase from 25 to 200 μg/mL), whereas the inhibitory activities of GTPS and OTPS on α-glucosidase were lower. This may have been due to differences in the conformation and composition of polysaccharides, which lead to differential interactions between aminoglycosides and the hydrophobic pockets of enzymes. Xu et al., prepared crude TPSs of GTPS, OTPS and BTPS according to the same method as above, and they further performed ultrafiltration to obtain six TPS components: GTPS1 (<80 kDa), GTPS2 (>80 kDa), OTPS1 (<80 kDa), OTPS2 (>80 kDa), BTPS1 (<80 kDa), and BTPS2 (>80 kDa). BTPS1, BTPS2, OTPS1, and OTPS2 were found to have a dose-dependent inhibitory effect on α-glucosidase activity, and BTPS1 exhibited the most robust α-glucosidase inhibitory activity. Additionally, the inhibitory activities of GTPS1 and GTPS2 against α-glucosidase were weaker than those of other TPS fractions, results consistent with those of Chen et al., In addition to the type of tea, the degree of fermentation of tea can also affect its glycosidase inhibitory activity. The aging (light fermentation) process was found to significantly enhance the antioxidant and α-glucosidase inhibitory activities of Pu-erh TPS [76]. Xu et al., extracted three TPSs (PTPS-1, PTPS-3, and PTPS-5) from Pu-erh tea with different fermentation years (first, third, and fifth) and then tested their α-glucosidase inhibitory activity [36]. Based on EC50 (concentration for 50% of maximal effect), PTPS-5 inhibited α-glucosidase at least 3 times more than the positive drug (acarbose), PTPS-3 inhibited α-glucosidase comparably to acarbose, and the inhibition of PTPS-1 was the weakest. These results suggest that the aging time of Pu-erh tea TPSs may be positively correlated with the inhibitory effect of PTPS on α-glucosidase. Notably, processing technology also plays a significant role in the inhibition of glycosidase activity by TPS. Wei et al., investigated the effects of different extraction methods, including WE, UAE, and MAE, on the bioactivity of TFPS [93]. TFPS extracted with the UAE and MAE methods had almost no inhibitory activity on β-glucosidase, while the TFPS extracted with the TWE method had little inhibitory activity on β-glucosidase. The inhibitory activity of glucosidase (83.3% inhibition rate) for TFBS extracted with WE was significantly higher than that of TPS from tea leaves. At the same time, Wang et al., compared the effects of different drying methods on the bioactivity of TPS. They found that the TPS obtained with freeze drying (TPS-F) had 92.8% and 82.75% inhibition rates of α-amylase and α-glucosidase, respectively. Its inhibitory activity was significantly more substantial than that of TPS obtained with vacuum drying (TPS-V) and spray drying (TPS-S) [94]. In addition, the species of TPS may also affect its glycosidase inhibitory activity. Wang et al., isolated the acidic TPS fraction (TP-1) from Maofeng tea via acid extraction, and its inhibitory activities (IC50, the half-maximal inhibitory concentration) against α-glucosidase and α-amylase were 394.3 and 90.1 μg/mL, respectively [95]. Recently, a study by Zhu et al., showed that the inhibition of α-glucosidase and α-amylase activities by coarse green tea TPS might be related to the Mw of TPS [21]. They pointed out that the Mw of TPS was negatively correlated with the inhibition of glycosidase activity. Accordingly, they also found that the inhibitory activity of dark tea TPS on glycosidase may have a significant positive correlation with its uronic acid content [10]. Further reports

by Fan et al., showed that higher purities of TPS led to weaker inhibitory activities on α-glucosidase and α-amylase [96].

4.2. Free Radical Scavenging

Oxidative stress caused by the transition of oxygen-derived free radicals is an important cause of the occurrence and development of many diseases, such as cancer, hypoglycemia, atherosclerosis, and rheumatoid arthritis, as well as degenerative diseases related to aging [97]. The free radical scavenging activity of TPS has also been widely reported. Chen et al., compared the in vitro free radical inhibitory activities of GTPS, OTPS, and BTPS from green, oolong, and black teas [35]. They found that the three TPSs showed significant antioxidant activities on DPPH free radicals, hydroxyl radicals, and lipid peroxidation ($p < 0.05$). Among them, the scavenging effects of GTPS and BTPS were better than that of OTPS, and GTPS showed the strongest lipid peroxidation inhibitory activity (IC50 = 75 μg/mL). Sun et al., extracted a water-soluble polysaccharide (KBTP) from Keemun black tea and evaluated its in vitro antioxidant capacity. The KBTP showed strong DPPH free radical scavenging, superoxide anion-radical scavenging, and iron-reduction capacity in a dose-dependent manner, though with lower values than the positive control benzyl alcohol (BHT) [24]. Xiao et al., investigated and compared the DPPH free radical scavenging activity of four corresponding crude tea polysaccharides—XTPS, TTPS, CTPS, and HTPS—prepared from four types of expired tea leaves on the market—Xihu Longjing, Huizhoulvcha, Chawentianxia, and Anxi Tieguanyin, respectively [13]. The scavenging activities of the four TPSs against DPPH showed a similar effect. In the concentration range of 25–200 g/mL, the scavenging effects of the four TPSs were enhanced with the increase in the concentration, but all were lower than that of Vc. Among them, the content of polyphenols in CTPS was relatively low (6.53%), but its DPPH free radical scavenging activity was similar to that of TTPS, indicating that the main antioxidants in CTPS are polysaccharides. Xu et al., prepared crude tea flower polysaccharides (TFPS) and obtained three purified components: TFPS-1, TFPS-2, and TFPS-3 [98]. In vitro antioxidant testing revealed that all TFPS samples had appreciable scavenging activities of DPPH, superoxide anion, and superoxide anion free radicals in a concentration-dependent manner. Among them, TFPS-1 had the strongest in vitro antioxidant capacity. Xu et al., compared the free radical scavenging capability of six TPS samples (GTPS1, GTPS2, OTPS1, OTPS2, BTPS1, and BTPS2), and they found that the fermentation process and the Mw of TPS had significant impacts on the DPPH free radical scavenging [76]. Another study by Xu et al., indicated that PTPS-5, with the highest studied proportion of low-Mw polysaccharides, had the strongest free radical scavenging capability [99]. Likewise, Sun et al., showed that a green tea TPS fraction with a moderate Mw exhibited the strongest in vitro free radical scavenging activity and reducing power of studied fractions [65]. Thus, the Mw of TPS may play an important role in its antioxidant activity, and low-Mw TPSs generally exhibit higher radical scavenging capacities [97]. In addition, the hydroxyl groups in polysaccharides are also an important factor affecting their free radical scavenging activity [100]. Other studies have shown that the content of uronic acid is closely related to the antioxidant activity of TPS [10,101]. In addition, changes in the spatial structure of TPS caused by ultrasound can also enhance its scavenging activity to DPPH, superoxide, and hydroxyl radicals [26].

4.3. Antitumor Activity

In recent years, TPS has received extensive attention due to its broad therapeutic properties and relatively low toxicity to normal cells, and it is expected to become an alternative or adjunct to traditional anticancer drugs [102]. Liu et al., isolated and purified a water-soluble homogeneous polysaccharide (DTP-1) from dark brick tea, and then they evaluated the cytotoxic activity of DTP-1 on cancer cells and normal cells in vitro [103]. The results showed that DTP-1 had significant in vitro anti-tumor effects, especially on A549 and SMMC7721 cells, and the inhibitory effect of DTP-1 on cancer cell proliferation was positively correlated with its dose. In addition, DTP-1 could effectively inhibit the

proliferation of cancer cells, induce apoptosis, and inhibit migration. At the same time, it hardly affected the growth and viability of normal cells. Wang et al., isolated a selenium-enriched TPS (Se-ZYTP) from Ziyang selenium-enriched green tea and investigated its in vitro antitumor activity against human osteosarcoma cells (U-2 OS). Both MTT and lactate dehydrogenase (LTH) assays demonstrated that Se-ZYTP could significantly inhibit the proliferation of U-2 OS cells in a concentration-dependent manner [104]. Zhou et al., extracted a green tea polysaccharide (GTPS) from crude green tea and tested its inhibitory effect on the viability of colon cancer cells (CT26). The results showed that the inhibitory effect of GTPS on CT26 cells was concentration-dependent and time-dependent. At the highest concentration (800 μg/mL), the anticancer effect of GTPS was stronger than that of the positive control Lentinus edodes (LNT). Additionally, GTPS was not toxic to normal rat intestinal epithelial cells. This study also showed that GTPS intervention significantly up-regulated signal transduction pathways related to apoptosis, lysosomes, mitochondria, and cell death, suggesting that GTPS might target lysosomes and activate caspase $-9/-3$-inducing apoptosis of CT26 cells, thereby exerting anti-cancer effects [105]. In addition, Xu et al., conducted an anticancer evaluation on tea flower polysaccharide (TFPS) and its purified fractions (TFPS-1, TFPS-2, and TFPS-3). They found that these samples could significantly inhibit human gastric cancer cells (BGC-823) in a concentration- and time-dependent manner. Among them, TFPS-1 and TFPS-3 exhibited higher in vitro antitumor activities than TFPS-2, possibly due to their differences in monosaccharide composition, sulfate content, and antioxidant activity [98]. Yang et al., investigated the effect and possible mechanism of green tea polysaccharide (GTP) in anti-prostate cancer (PC). They found that GTP could promote PC cell apoptosis by increasing Bcl2-associated X protein (Bax)/B-cell lymphoma-2 (Bcl-2) ratio and caspase-3 protein expression while decreasing *micro RNA-93* (*miR-93)* expression. Of these, *miR-93* might be a key target of GTP in PC treatment [54].

4.4. Bacteriostatic Activity

The human body has a diverse microflora that contain more cells than the body, and these microbiotas are mainly composed of bacteria. The ordinary microbial communities in the respiratory tract, gastrointestinal tract, and skin interact with the human body's innate immunity. These microbial communities also produce metabolites that serve as essential nutrients for human cells and play a protective role by inhibiting pathogenic bacteria [106]. There is growing evidence that interactions between humans and their symbiotic flora may play an essential role in human health. However, bacterial attachment to human epithelial cells may also lead to skin infections, inflammation, and some pathogenic diseases [107]. For example, *Helicobacter pylori* is a micro-aerophilic Gram-negative bacterium that exclusively colonizes the gastric mucosa of humans and primates, causing chronic active or type B gastritis, duodenal ulcers, gastric cancer, and mucosal-associated lymphoid tumors [108]. *Propionibacterium acnes* (*P. acnes*) is an anaerobic Gram-positive bacterium that is common in microscopic studies of adult skin and predisposes one to the formation of human cutaneous acne [109]. *Staphylococcus aureus* is an aerobic Gram-positive bacteria that mainly hides on the skin and mucous membrane surfaces, resulting in atopic dermatitis [110]. In addition to being a healthy drink, tea has been regarded as an anti-cancer and antibacterial herb since ancient times. As an essential active ingredient in tea, TPS has also been reported to show favorable antibacterial activity. Lee et al., obtained an acidic TPS (ATPS) from green tea and analyzed its anti-adhesion effect against pathogenic bacteria (*Staphylococcus aureus*, *P. acnes*, and *Helicobacter pylori*) [111]. The results showed that ATPS had a significant inhibitory effect on pathogenic bacteria-mediated hemagglutination, with a minimum inhibitory concentration of between 0.01 and 0.1 mg/L. In addition, ATPs had no inhibitory effect on beneficial commensal bacteria such as *Staphylococcus epidermidis*, *Escherichia coli*, and *Lactobacillus acidophilus*, suggesting that ATPs could be applied as selective natural antiadhesive polymers to some pathogenic bacteria. However, there have been few reports on the significant bacteriostatic activity of TPS, and more studies are needed to support this evidence of this property.

5. In Vivo Bioactivity of TPS

In addition to the presented in vitro bioactivities, TPS also showed favorable in vivo bioactivities (Table 3 and Figure 2), and its potential regulatory mechanism is presented in Figure 3.

Table 3. In vivo bioactivity of different TPSs.

Bioactivity	TPS Origin	Regulatory Mechanism	Ref
Antioxidant and hepatoprotective activity	Ziyang green tea	Ameliorating high-fructose diet-induced pancreatic β-cell damage and inhibiting hepatic steatosis and oxidative damage	[112]
	Ziyang green tea	Mediating antioxidant and free radical scavenging, thereby effectively preventing liver damage	[113]
	Green tea	Promoting superoxide dismutase (SOD), catalase (CAT), and glutathione peroxidase (GPx) activity in blood, liver, and heart	[114]
	Huangshan Maofeng	Inhibiting lipid peroxidation while promoting the body's antioxidant activity to protect the liver	[23]
	Longjing 43 tea flower	Inhibiting the elevation of serum aspartate aminotransferase (AST) and alanine aminotransferase (ALT) levels, reducing the formation of malondialdehyde (MDA), and simultaneously enhancing the activities of SOD and GPx to reduce liver damage	[98]
	Keemun black tea	Improving the enzymatic and non-enzymatic antioxidant defense system to protect the liver, thereby effectively alleviating the production of free radicals in the body and inhibiting lipid peroxidation in liver tissue	[24]
Antitumor activity	Dark brick tea	Inhibiting cancer cell proliferation and migration and inducing cancer cell apoptosis	[103]
	Ziyang green tea	Inhibiting the proliferation of human osteosarcoma cells (U-2 OS)	[104]
	Green tea	Targeting lysosomes and activated caspase-9/-3 via the lysosome-mitochondrial pathway to induce apoptosis in colon cancer cells (CT26)	[105]
	Tea flowers	Inhibiting the proliferative activity of human gastric cancer cells (BGC-823)	[98]
	Green tea	Increasing the levels of SOD, CAT, and GPx while inhibiting lipid peroxidation and pro-inflammatory cytokine levels from attenuating oxidative damage and inflammatory responses	[115]
	Ziyang green tea	Inhibiting the proliferation of osteosarcoma cells in vitro and the growth of tumor volume and tumor weight in vivo	[104]
	Green and black teas	Inhibiting pulmonary neutrophil recruitment and oxidative tissue damage, resulting in higher anti-inflammatory effects and resistance to murine sepsis	[116]
	Oolong tea	Inhibiting tumor growth, reducing liver toxicity and nephrotoxicity, stimulating the body's antioxidant activity and immune function, and finally achieving an anti-liver cancer effect	[75]
	Green tea	Increasing the Bcl2-associated X protein (Bax)/B-cell lymphoma-2 (Bcl-2) ratio, elevating caspase-3 protein expression, and decreasing miR-93 expression in prostate cancer cells	[54]
Immunostimulatory activity	Green tea	Activating the TLR7 receptor and enhancing the macrophage activity	[117]
	Green tea	Improving the serum IgG level, thymus index, macrophage activity, and lymphocyte transformation rate in broilers, as well as increasing the serum antioxidant enzyme activity	[118]

Table 3. *Cont.*

Bioactivity	TPS Origin	Regulatory Mechanism	Ref
	Selenium-enriched green tea	Enhancing the regulatory mechanism involved in free radical scavenging, synergistically improving immune function, and reducing oxidative stress	[9]
	Green tea	Enhancing the body's cellular immunity and humoral immunity	[119]
	Fuzhuan brick tea	In vitro: promoting the in vitro proliferation activity and phagocytic capability of macrophages and enhancing the activity of acid phosphatase; in vivo: promoting the release of tumor necrosis factor (TNF-α), interleukin-1β (IL-1β), and nitric oxide (NO) and then inhibiting decreases in thymus/spleen index and colon rupture	[30]
	Selenium-enriched green tea	Improving the spleen and thymus index, promoting the lymphocyte proliferation and NK cell activity in the spleen, promoting the CD4 T cell proliferation, and reducing oxidative stress	[9]
Gut microbiota modulating activity	Fuzhuan brick tea	Reducing the disease activity index (DAI) in mice with enteritis, alleviating the colonic tissue damage and inflammation, and simultaneously promoting the proliferation of beneficial gut microbiota and the increase in short-chain fatty acids (SCFAs)	[120]
	Wuyi rock tea	Improving gut microbiota composition and microbial structural dysbiosis in type 2 diabetic rats	[121]
	Fuzhuan brick tea	Promoting the secretion and mRNA expression of mucin 2, occludin, and zonula occludens 1 (ZO-1); altering gut microbiota composition; and stimulating the proliferation of beneficial bacteria and production of SCFAs	[30]
	Fuzhuan brick tea	Increasing the phylogenetic diversity of the gut microbiota, suppressing the increase in the relative abundance of pathogenic bacteria, and altering key OUTs associated with metabolic syndrome	[8]
	Fuzhuan brick tea	Altering the gut morphology and ZO-1 expression, increasing the relative abundance of Muribaculaceae, and decreasing the relative abundance of *Lachnospiraceae*, *Helicobacteraceae*, and *Clostridaceae*	[122]
	Tea flowers	Protecting the intestinal barrier function and promoting the increase in the number of beneficial microorganisms and their metabolites, thereby maintaining intestinal health and improving adaptive intestinal immunity	[123]
Glucose and lipid metabolism-regulating activity	Pu-erh tea	Inhibiting intestinal alpha-glucosidase activity	[36]
	Green, oolong, and black teas	Enhancing in vitro free radical scavenging activity and α-glucosidase inhibition in skeletal muscle cells	[76]
	Tea flowers	Protecting cell membranes from peroxidative damage and reducing oxidative stress	[124]
	Pu-erh tea	Inhibiting the intestinal alpha-glucosidase activity	[125]
	Green tea	Adjusting body weight, reducing serum triglyceride (TG) and leptin (LT) levels, inhibiting fatty acid absorption, improving anti-inflammatory activity, and treating obesity	[126]
	Black tea	Inhibiting the formation and accumulation of fat, promoting the decomposition of fat, and promoting the expression of essential genes involved in fat metabolism	[127]
	Oolong tea	Decreasing serum LT levels in obese rats, improving blood lipids and antioxidant levels, and affecting lipid metabolism pathways	[128]
	Fenggang zinc selenium tea	Improving oxidative stress, inhibiting lipid peroxidation, and enhancing liver protection	[129]
Anticoagulant activity	Green tea	Inhibiting the intrinsic and common coagulation pathways of fibrinogen-to-fibrin conversion without inhibiting the extrinsic pathway	[16]

Table 3. *Cont.*

Bioactivity	TPS Origin	Regulatory Mechanism	Ref
Bacteriostatic activity	Green tea	Destroying the cell wall of *Escherichia coli* and increasing the permeability of the cell membrane and the content of intracellular ROS	[130]
Anti-fatigue activity	Ziyang green tea	Preventing lipid peroxidation by modification of GPx activity	[22]
Skincare activity	Green tea	Promoting skin's moisturization and enhancing fibroblast proliferation capability	[11]

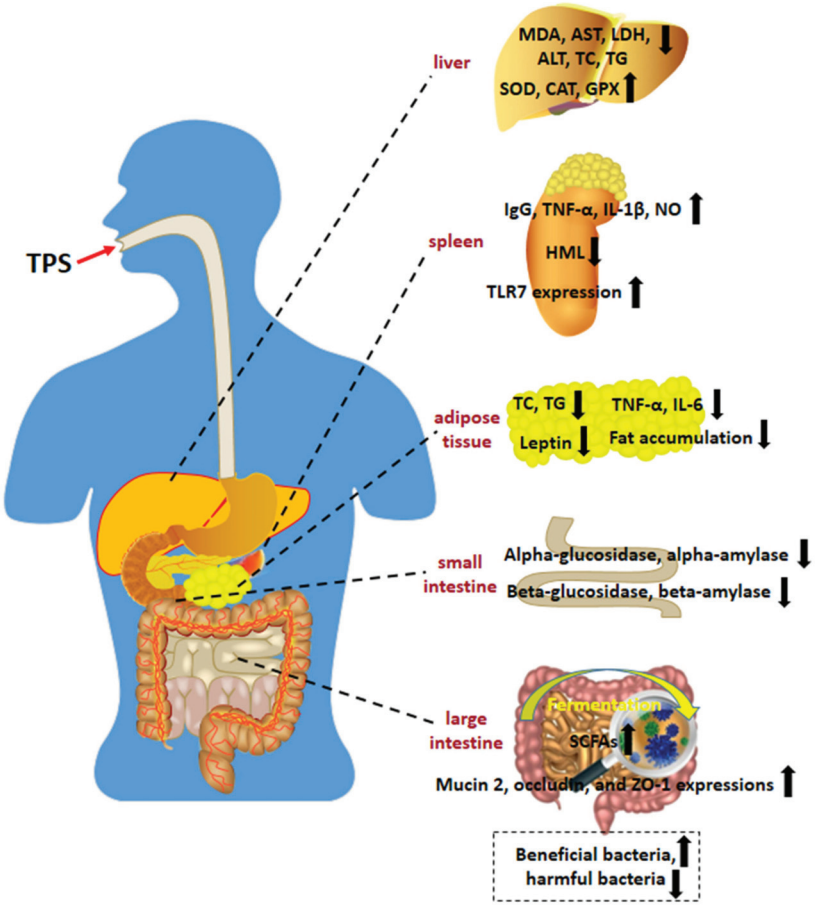

Figure 3. A potential mechanism by which TPS exerts its in vivo bioactivity.

5.1. Antioxidant and Hepatoprotective Activity

Oxidative stress has been reported to be associated with many diseases, such as cancer, Alzheimer's disease, nephritis, arteriosclerosis, and diabetes, due to the overproduction of oxygen free radicals [4]. The liver is a vital detoxification organ in the human body and plays a key role in the metabolism of various endogenous and exogenous harmful substances [3]. Many in vivo studies in mouse models for the antioxidant and liver-protective effects of TPS have been reported. Ren et al., fed healthy male Kunming mice with 20% fructose water for eight weeks and then provided different concentrations of Ziyang selenium-enriched green TPS (Se-TPS) for eight weeks. Se-TPS was shown to be able to

significantly attenuate hepatic steatosis and oxidative stress injury in mice [112], and Se-TPS could substantially attenuate hepatic steatosis and oxidative stress injury in mice [112]. Wang et al., explored the hepatoprotective effect of Ziyang tea polysaccharide (ZTPS) on CCl_4-induced oxidative liver injury in mice [113]. They found that the administration of ZTPS (100, 200, and 400 mg/kg) to mice prior to CCl_4 treatment significantly inhibited CCl_4-induced elevations in liver MDA levels, AST, lactate dehydrogenase (LDH), and serum ALT. In addition, ZTPS-treated mice exhibited regular SOD and glutathione peroxidase (GPx) activities compared to a CCl_4-induced group. Sun et al., studied the antioxidant activity of TPS in exhaustive exercise mice. They found that MDA levels in the heart, liver, and plasma were reduced after 30 days of TPS treatment compared to a control group [131]. Lu et al., investigated the antioxidant and hepatoprotective effects of Huangshan Maofeng acid polysaccharide (HMTPS) on CCl_4-induced oxidative liver injury in mice [23]. The results showed that HMTPS could significantly regulate the serum markers of triglyceride (TG), total cholesterol (TC), aspartate aminotransferase (AST), and alanine aminotransferase (ALT) in mice with liver injury induced by CCl_4. In addition, HMTPS could significantly increase the antioxidant levels of SOD and hepatic glutathione and could reduce the formation of the hepatic lipid peroxidation products 15-F2t isoprostanes and MDA. Similarly, a study by Xu et al., indicated that TFPS could significantly reduce the serum levels of ALT and AST in mice with CCl_4-induced hepatotoxicity in a dose-dependent manner while considerably reducing the level of MDA in the liver and enhancing antioxidant enzyme activity (SOD and GPx) [98]. Sun et al., reported that Keemun black tea polysaccharide (KBTP) intervention in mice prior to CCl_4 injection significantly prevented CCl_4-induced elevations in serum ALT, AST, TG, TC, and MDA levels [24]. Compared to CCl_4-induced liver injury mice, KBTP-pretreated mice exhibited better liver body indexes and higher GSH and SOD activities. Accumulating evidence has revealed that TPS can reduce oxidative stress in the body and may be a potent antioxidant in medicines and functional foods. However, some researchers hold the opposite view on the antioxidant activity of TPS. Wang et al., separated TPS components from a crude TPS extract and then compared their DPPH free radical scavenging, reducing power, and hydroxyl radical scavenging activities. They found that the purified TPS had almost no antioxidant activity and that the primary antioxidants in crude TPS may be polyphenols [132]. Importantly, single TPS fractions should be isolated and purified to test their antioxidant and hepatoprotective effects individually, which would help clarify TPS's main antioxidant and hepatoprotective components and help improve TPS preparation.

5.2. Antitumor Activity

In cellular models, TPS has been reported to play an essential role in tumor and cancer prevention. Several experiments in mouse models have also been investigated to analyze the antitumor activity of TPS. Pharmacological experiments in mice with gastric cancer showed that TPS could increase the serum levels of interleukin-2 (IL-2), interleukin-4 (IL-4), interleukin-10 (IL-10), Immunoglobulin M (IgM), Immunoglobulin M (IgG), and Immunoglobulin A (IgA) in mice and reduce the level of MDA in gastric tissue and the levels of interleukin-6 (IL-6) and TNF-α in serum, which suggests that TPS might be a potential modulator in the intervention of gastric cancer [132]. Another study by Wang et al., showed that Se-ZYTP could significantly reduce tumor volume and weight in U-2 OS-xenograft model mice [104]. Scoparo et al., found that two TPS interventions from green and black tea significantly reduced mortality in septic mice (40% and 25%, respectively), as well as reduced neutrophil entry into the lungs and tissue damage, which may have been due to the difference in uronic acid content in TPSs [116]. In addition to the solid anticancer activity of TPS in experimental animals, studies have shown that other tea-active substances can have synergistic effects when combined with TPS. Combining polysaccharides with other substances could bring several advantages, such as enhanced lethality, reduced toxicity, increased solubility, and reduced drug resistance and immunogenicity [133]. Wang et al., found that the co-administration of oolong tea TPS and polyphenols had a synergistic effect

on inhibiting the proliferation and growth of liver tumors of mice, and the antioxidant and immune levels of mice were shown to be significantly increased [75].

5.3. Immunostimulatory Activity

The immune system plays a vital role in defending against pathogen invasion and maintaining human health. Generally speaking, polysaccharides mainly regulate the body's immunity through two pathways: one is to kill pathogens directly, and the other is to enhance the immune system by improving the activity of macrophages and T lymphocytes [134]. Immunostimulatory activity is one of the most remarkable biological functions of natural polysaccharides, and it is related to their active role as a critical basis for antitumor effects [39,135]. Numerous studies have demonstrated the potential regulatory impacts of TPS on immune system stimulation and activation. Monobe et al., investigated the phagocytic activity of macrophages after crude TPS treatment [118]. They found that crude TPS enhanced macrophage activity by stimulating Toll-like receptor 7 (TLR7) and that immature (not fermented by microorganisms) TPS had higher immunostimulatory activity than mature TPS. In addition, studies have found that high-Mw TPS had a stronger immunostimulatory activity than low-Mw TPS. Hu et al., explored the effect of TPS on the immunostimulatory activity of broilers, and they discovered that TPS could significantly increase the serum IgG level; thymus index; serum CAT, GPx, and SOD activities; macrophage activity; and lymphocyte transformation rate in broilers [118]. Yuan et al., studied the synergistic effects of selenium-enriched green tea polysaccharide (Se-TPS) and Huo-ji polysaccharide (HJP) on immune stimulation [9]. The results showed that they could enhance the body's free radical scavenging ability, improve immune function, and reduce oxidative stress, thereby exhibiting solid immunostimulatory activity. Sun et al., found that two Fuzhuan tea TPSs obtained with hot water and alkali-assisted extraction could promote the proliferation and phagocytosis of macrophages and enhance the activity of their signaling enzymes (acid phosphatase) [31]. In addition, they both showed the positive regulation of cyclophosphamide (CTX)-induced immunosuppression in mice by promoting TNF-α, IL-1β, NO release, inhibiting thymus/spleen index reduction, and inhibiting colon fragmentation. Similar results were reported by Yuan et al. [9]. In addition, chemical modification was found to affect the immune activation of TPS. Glycosidase-modified green tea polysaccharide (ETPS) has been reported to significantly increase NK cell activity and serum hemolysin (HML) levels, delay ear swelling, and increase peritoneal macrophage index, peritoneal macrophage phagocytosis, and splenic phagocytosis [119].

5.4. Gut Microbiota-Modulating Activity

The structure and homeostasis of the gut microbiome (GM) are closely related to human health, so the GM is known as the "second genome" of the human body [136]. Recently, it has been increasingly recognized that GM composition and homeostasis are disease modifiers, fundamental components of immunity, and functional entities for metabolism, and an imbalanced GM may contribute to various intestinal diseases [137]. The distribution of the GM in the human body can be modulated by diet, which can influence the composition of the GM by altering the gut environment (e.g., pH) or the activity of certain microbial enzymes [138–140]. After GM fermentation, dietary products can regulate certain life activities through the metabolic cycle [141]. Generally, TPSs cannot be degraded or absorbed in the upper gastrointestinal tract, as they mainly metabolized and utilized by the GM in the ileum or colon. Not only does TPS affect the structure and diversity of the GM, but its metabolites in the gut, such as SCFAs (especially acetate, propionate, and butyrate), can also have beneficial effects on gut health [142]. Yang et al., used 16S rDNA amplicon sequencing and metabolomics to analyze the protective effect of Fuzhuan brick tea polysaccharide (FBTP) on dextran sulfate sodium (DSS)-induced ulcerative colitis (UC) in mice [143]. The results showed that the oral administration of FBTP reduced the disease activity index (DAI), prevented colon shortening, and alleviated colon tissue damage and inflammation in UC mice. Furthermore, FBTP intervention also promoted the proliferation of beneficial micro-

biota (such as *Lactobacillus* and *Akkermansia*) and significant increases in SCFAs, especially butyrate content in the cecum. Butyrate, a type of SCFA, has anti-inflammatory properties and can be absorbed by colon cells as an energy source [144]. This report suggests that FBTP may exert its anti-inflammatory effects by producing SCFAs while improving UC by promoting beneficial bacterial abundance to repair the intestinal epithelial barrier and reduce immune stress [120]. In addition, FBTP intervention was shown to improve tryptophan metabolism in the gut [143]. Tryptophan can be decomposed into indole derivatives by the gut microbiota, which further activates the immune system and ultimately affects the integrity of the intestinal barrier in mice [145]. Wu et al., found that acid TPS from Wuyi rock tea could significantly alter the composition of intestinal flora and improve the dysbiosis of microbial structure in type 2 diabetic rats [121]. Sun et al., reported that the early intake of FBTPs was beneficial to the secretion and mRNA expression of mucin 2, occludin, and ZO-1, thereby preventing and relieving CTX-induced intestinal mucosal damage and protecting intestinal barrier function. In addition, FBTP could improve gut microbiota composition and then promote the proliferation of beneficial bacteria (especially *Lactobacillus*) and the production of SCFAs [31]. Bai et al., established a mouse model of immunosuppression induced by cyclophosphamide and explored the regulatory effect of FBTPS on its immune function and gut microbiota [122]. They found that crude and pure FBTPS could improve the immune organ index, immune cytokines, and immunoglobulin A levels in mice to play an immunoregulatory role. In addition, intestinal injury was ameliorated by improving intestinal morphology and ZO-1 expression. Additionally, they modulated the gut microbiota structure by increasing the relative abundance of Muribaculaceae and decreasing the abundance of *Lachnospiraceae*, *Helicobacteraceae*, and *Clostridaceae*. Chen et al., also used FBTPS as a raw material to study the effect of FBTPS on metabolic syndrome (MS) and gut microbiota dysbiosis in high-fat diet (HFD)-fed mice. The results showed that FBTPS treatment could increase the phylogenetic diversity of the HFD-induced microbiota and significantly inhibit the HFD-induced increase in the relative abundance of pathogenic bacteria such as *Erysipelotrichaceae*, *Coriobacteriaceae*, and *Streptococcaceae*. In addition, FBTPS may also play a key role in the prevention of MS by significantly affecting 44 key OUTs that are negatively or positively correlated with MS [8]. A study by Chen et al., showed that the long-term intake of Longjing tea flower polysaccharide (TFPS) is beneficial to the protection of the intestinal barrier and could promote increases in the number of beneficial microorganisms and their metabolites, thereby maintaining intestinal health [123].

5.5. Glucose and Lipid Metabolism-Regulating Activity

Diabetes mellitus (DM) and obesity caused by long-term glucose and lipid metabolism disorders are the two most common and complex metabolic diseases, and their morbidity, chronic course, and disabling complications are increasing [3]. Controlling postprandial blood glucose and inhibiting oxidative stress are considered effective methods for treating diabetes [4]. One treatment for reducing postprandial hyperglycemia is to delay glucose absorption by inhibiting carbohydrate hydrolase enzymes in the digestive organs, such as alpha-amylase and alpha-glucosidase [146]. In China and Japan, coarse tea was used to treat diabetes, and its hypoglycemic activity increased with increasing TPS content in coarse tea [147]. Studies have shown that the hypoglycemic effect of polysaccharides can mainly be implemented through oral or injection therapy. When polysaccharides are administered via injection, they can directly act on target cells through blood circulation; when polysaccharides are orally administered, they usually enter the intestine directly to be decomposed and absorbed due to the high Mw of polysaccharides, thereby exerting indirect hypoglycemic effects [76]. Many studies has revealed the hypoglycemic activity of TPS. Xu et al., extracted TPSs (PTPS-1, PTPS-3, and PTPS-5) from Pu-erh tea with different fermentation years and then compared their effects on postprandial blood glucose in alloxan-induced diabetic mice [36]. The results showed that all PTPSs significantly inhibited postprandial blood glucose in diabetic mice ($p < 0.05$). PTPS-5, with the most prolonged fermentation period, had the strongest inhibitory effect on postprandial hyperglycemia in

diabetic mice, and it had no significant difference with acarbose ($p > 0.05$). Similar results were also reported by Deng et al., [125]. In addition, Wei et al., found that TFPS could effectively reduce alloxan-induced hyperglycemia in Sprague-Dawley (SD) rats, maybe due to the superior hydrogen-donating capability of TFPS, which can protect cell membranes from peroxidative damage and alleviate oxidative stress [124]. Altogether, the possible mechanisms of the antidiabetic activity of TPS include: (1) preventing the hydrolysis and absorption of carbohydrates by inhibiting the activity of digestive enzymes in the digestive tract; (2) regulating the structure and diversity of gut microbiota, thereby affecting the types and levels of its metabolites and then regulating intestinal homeostasis and body inflammation; (3) affecting the interaction of the "gut–liver axis", thereby promoting glucose and lipid metabolism and improving insulin resistance; (4) improving β-cell dysfunction and promoting insulin secretion; and (5) improving oxidative stress and oxidative damage [148,149].

The weight loss and lipid-lowering activities of TPS have also been widely reported. Xu et al., investigated the effects of TPS, caffeine, polyphenols, and the TPS–polyphenol complex in green tea on high-fat diet-fed rats. The results showed that TPS and polyphenols presented apparent blocking effects on fat accumulation and weight gain, and they could inhibit the absorption of fatty acids, reduce serum leptin and blood lipid levels, and reduce the protein expressions of IL-6 and TNF-α. Additionally, a synergistic effect of TPS and polyphenols in lipid-lowering activity was also observed [126]. The weight loss mechanisms of black tea TPS and polyphenols were investigated in male, obese, Sprague-Dawley rats. The results showed that black tea TPS and polyphenols could increase fecal fatty acid content and reduce body weight, adipocyte size, visceral fat weight, and Lee's index, thereby achieving weight loss. In addition, the black tea TPS also promoted the expression of multiple genes involved in fat metabolism (such as *Aqp1*, *Ugt2b*, and *Gck*), exerting an obesity-suppressing effect [127]. Wu et al., found that oolong tea TPS could effectively reduce serum leptin and lipid levels in obese rats. In addition, it could also inhibit obesity through the effects of pathways affecting fatty acid biosynthesis, steroid hormone biosynthesis, unsaturated fatty acid biosynthesis, glycerolipid metabolism, and glycerophospholipid metabolism [128]. Mao et al., studied the hypolipidemic effect of Chinese Liupao dark tea polysaccharides (CLTPS). It was found that the body weight gain of the high-fat diet-induced rats was significantly inhibited after four weeks of CLTPS intervention [150]. Additionally, the rats' serum lipid levels, lipid oxidation, and antioxidant enzyme activities were greatly improved in a dose-dependent manner. Accordingly, CLTPS was shown to be able promote the bile acid synthesis pathway and cholesterol catabolism to further prevent atherosclerosis.

5.6. Others

In addition to the above-mentioned activities, there have also been some reports on the excellent regulation of TPS in anticoagulant, antibacterial, antifatigue, and skincare activities. Cardiovascular diseases, including cerebral/pulmonary thrombosis and stroke, have recently become the leading causes of death in patients [151]. Of the mentioned activities, anticoagulants can effectively prevent thrombus formation by inhibiting physiological coagulation [134]. Cai et al., investigated the anticoagulant effect of purified fractions of green tea TPS (TPS-1, TPS-2, TPS-3, and TPS-4). It was found that the heterogeneous acidic polysaccharide TPS-4 could exert anticoagulant activity by significantly inhibiting the endogenous and common coagulation pathways of fibrinogen-to-fibrin conversion [16]. Regarding the bacteriostatic activity of polysaccharides, previous reports have shown that polysaccharides have anti-biofilm properties and that they might also inhibit bacterial growth by blocking the input of nutrients [152]. Cai et al., found that green tea polysaccharide conjugate (gTPC) had an antibacterial effect on *Escherichia coli* (*E. coli*) [130]. The morphology of *E. coli* cells treated with gTPC was found to be significantly changed, and some of the *E. coli* cell walls had cytoplasmic leakage due to rupture. At the same time, the permeability of the cell membrane was increased, and the level of intracellular ROS was

also significantly increased. A further study revealed that the destruction of the cell wall may be the critical mechanism for gTPC to exert its antibacterial effect. The anti-fatigue activity of Ziyang selenium-enriched green tea (Se-TP) was investigated by Chi et al., [22], who found that Se-TP treatment could prolong the fatigue time of fatigue model mice; reduce serum urea, blood lactate, and lactic dehydrogenase levels; and increase the antioxidant capacity. The anti-fatigue effect of Se-TP may be achieved through enhancing GPx activity to effectively inhibit lipid peroxidation. The appearance of the skin can often provide a rough estimate of a person's age and health [153]. Water retention is an essential function of skincare cosmetics, and the skin's moisturizing tissue is damaged with age and exposure to the external environment. Furthermore, ultraviolet (UV)-induced photoaging is the primary factor of the numerous external factors that promote skin aging. Wei et al., studied the protective effects of TPS and TPP on the skin from four perspectives: water absorption and retention, sun protection, the promotion of fibroblast proliferation, and tyrosinase inhibition [153]. The results showed that both TPS and polyphenols had positive skin protective capabilities; TPS (with higher purity) had better hygroscopicity and moisturizing properties, as well as the capacity to promote the proliferation of fibroblasts, whereas TPP could strongly absorb UV-A and UV-B, thereby better reducing ultraviolet damage to the skin. Accordingly, it also showed potent tyrosinase inhibition. However, further human clinical validation is still required.

6. Conclusions and Prospects

As an essential ingredient in tea, TPS has attracted more and more attention due to its excellent bioactivity and great development potential. The authors of this review fully discussed the extraction process, preliminary physicochemical properties, and bioactivities of TPS. Among the preparation methods of TPS, hot water extraction is the most widely reported, but the yield of polysaccharides obtained with this method is low. Therefore, the development of other auxiliary methods combined with hot water extraction can significantly improve the yield of TPS. For the preparation of TPS, the extraction and isolation of active TPS with high purity, maximum extraction yield, and complete structure is a major future focus because the functional food and pharmaceutical industries require simpler, more efficient, and cheaper methods for the large-scale production of high quality TPS. The analysis of physicochemical properties showed that the physicochemical properties of TPS, especially the uronic acid content, molecular weight, and monosaccharide composition, had significant effects on its bioactivity. Thus, more research on the physicochemical properties of TPS (especially regarding the availability of its bioactivities) is needed to broaden its biological applications. Over the past decade, the potential application of TPS in functional foods or medicines has attracted increasing attention due to its excellent bioactivities such as biodegradability, nontoxicity, and biocompatibility. TPS has shown its inherent advantages in intervening in the formation and development of metabolic diseases, anti-tumor activities, and skincare activities. The current study shows that TPS has many excellent bioactivities, but its bioactivity is likely to be significantly affected by the origin of its tea, the variety of its tea trees, its tea-making process, and its extraction method. Therefore, the specific effects of TPS preparation and source on its bioactivity need comprehensive research. In addition, the underlying mechanism of how TPS exerts its favorable bioactivity is unclear. Many reports have revealed that TPS likely acts as a prebiotic, exerting its health care activities through direct interactions with the gut microbiota and indirect effects by affecting the "gut–liver axis" or "gut–pancreas axis". However, this area still needs further exploration, as all current work is based on cell models or rodent models. Whether a similar function will be observed after human intervention remains unknown. Therefore, clinical trials should be carried out to further evaluate the bioactivity and mechanism of TPS on the basis of animal experiments. It is believed that either the exploration mechanism of its population cohort or the specific exploration of its application scope and conditions will become a hot spot in future work on TPS.

Author Contributions: Software, G.L.; validation, C.Z.; writing—original draft preparation, Q.W. and X.Y.; writing—review and editing, Q.W. and X.Y.; visualization, Y.S.; supervision, Y.S. and L.Q.; project administration, L.Q.; funding acquisition, L.Q. All authors have read and agreed to the published version of the manuscript.

Funding: This research was funded by the Open Fund Project of Key Laboratory of Tea Plant Biology and Tea Processing of Ministry of Agriculture (LTBB20140401), Talent introduction project of Anhui University of Science and Technology (NXYJ201801).

Institutional Review Board Statement: Not applicable.

Informed Consent Statement: Not applicable.

Data Availability Statement: Not applicable.

Conflicts of Interest: The authors declare no conflict of interest.

References

1. Gao, Y.; Zhou, Y.; Zhang, Q.; Zhang, K.; Peng, P.; Chen, L.; Xiao, B. Hydrothermal extraction, structural characterization, and inhibition HeLa cells proliferation of functional polysaccharides from Chinese tea Zhongcha 108. *J. Funct. Foods* **2017**, *39*, 1–8. [CrossRef]
2. Ye, X.; Tang, X.; Li, F.; Zhu, J.; Wu, M.; Wei, X.; Wang, Y. Green and Oolong Tea Extracts with Different Phytochemical Compositions Prevent Hypertension and Modulate the Intestinal Flora in a High-Salt Diet Fed Wistar Rats. *Front. Nutr.* **2022**, *9*, 892801. [CrossRef] [PubMed]
3. Zhu, J.; Wu, M.; Zhou, H.; Cheng, L.; Wei, X.; Wang, Y. Liubao brick tea activates the PI3K-Akt signaling pathway to lower blood glucose, metabolic disorders and insulin resistance via altering the intestinal flora. *Food Res. Int.* **2021**, *148*, 110594. [CrossRef] [PubMed]
4. Zhu, J.; Yu, C.; Zhou, H.; Wei, X.; Wang, Y. Comparative evaluation for phytochemical composition and regulation of blood glucose, hepatic oxidative stress and insulin resistance in mice and HepG2 models of four typical Chinese dark teas. *J. Sci. Food Agric.* **2021**, *101*, 6563–6577. [CrossRef]
5. Ding, Y.; Pu, L.; Kan, J. Hypolipidemic effects of lipid-lowering granulated tea preparation from Monascus -fermented grains (adlay and barley bran) mixed with lotus leaves on Sprague–Dawley rats fed a high-fat diet. *J. Funct. Foods* **2017**, *32*, 80–89. [CrossRef]
6. Orem, A.; Alasalvar, C.; Kural, B.V.; Yaman, S.; Orem, C.; Karadag, A.; Pelvan, E.; Zawistowski, J. Cardio-protective effects of phytosterol-enriched functional black tea in mild hypercholesterolemia subjects. *J. Funct. Foods* **2017**, *31*, 311–319. [CrossRef]
7. Khan, N.; Mukhtar, H. Tea Polyphenols in Promotion of Human Health. *Nutrients* **2018**, *11*, 39. [CrossRef]
8. Chen, G.; Xie, M.; Wan, P.; Chen, D.; Dai, Z.; Ye, H.; Hu, B.; Zeng, X.; Liu, Z. Fuzhuan Brick Tea Polysaccharides Attenuate Metabolic Syndrome in High-Fat Diet Induced Mice in Association with Modulation in the Gut Microbiota. *J. Agric. Food Chem.* **2018**, *66*, 2783–2795. [CrossRef]
9. Yuan, C.; Li, Z.; Peng, F.; Xiao, F.; Ren, D.; Xue, H.; Chen, T.; Mushtaq, G.; Kamal, M.A. Combination of selenium-enriched green tea polysaccharides and Huo-ji polysaccharides synergistically enhances antioxidant and immune activity in mice. *J. Sci. Food Agric.* **2015**, *95*, 3211–3217. [CrossRef]
10. Zhu, J.; Zhou, H.; Zhang, J.; Li, F.; Wei, K.; Wei, X.; Wang, Y. Valorization of polysaccharides obtained from dark tea: Preparation, physicochemical, antioxidant, and hypoglycemic properties. *Foods* **2021**, *10*, 2276. [CrossRef]
11. Wei, X.; Liu, Y.; Xiao, J.; Wang, Y. Protective effects of tea polysaccharides and polyphenols on skin. *J. Agric. Food Chem.* **2009**, *57*, 7757–7762. [CrossRef]
12. Wang, Y.; Wei, X.; Jin, Z. Structure analysis of an acidic polysaccharide isolated from green tea. *Nat. Prod. Res.* **2009**, *23*, 678–687. [CrossRef]
13. Xiao, J.; Huo, J.; Jiang, H.; Yang, F. Chemical compositions and bioactivities of crude polysaccharides from tea leaves beyond their useful date. *Int. J. Biol. Macromol.* **2011**, *49*, 1143–1151. [CrossRef]
14. Jin, F.; He, J.; Jia, L.-Y.; Tu, Y.-Y. Optimizing conditions for the extraction of polysaccharides of white tea. *Biotechnol. Biotechnol. Equip.* **2015**, *29*, 921–925. [CrossRef]
15. Chen, X.; Zhi, L.; Yang, Y.; Rui, Z.; Yin, J.; Jiang, Y.; Wan, H. Suppression of diabetes in non-obese diabetic (NOD) mice by oral administration of water-soluble and alkali-soluble polysaccharide conjugates prepared from green tea. *Carbohydr. Polym.* **2010**, *82*, 28–33. [CrossRef]
16. Cai, W.; Xie, L.; Chen, Y.; Zhang, H. Purification, characterization and anticoagulant activity of the polysaccharides from green tea. *Carbohydr. Polym.* **2013**, *92*, 1086–1090. [CrossRef]
17. Li, Q.; Shi, J.; Li, J.; Liu, L.; Zhao, T.; McClements, D.J.; Fu, Y.; Wu, Z.; Duan, M.; Chen, X. Influence of thermal treatment on the physicochemical and functional properties of tea polysaccharide conjugates. *LWT-Food Sci. Technol.* **2021**, *150*, 111967. [CrossRef]
18. Qin, H.; Huang, L.; Teng, J.; Wei, B.; Xia, N.; Ye, Y. Purification, characterization, and bioactivity of Liupao tea polysaccharides before and after fermentation. *Food Chem.* **2021**, *353*, 129419. [CrossRef]

19. Wei, X.; Chen, M.; Xiao, J.; Ying, L.; Lan, Y.; Zhang, H.; Wang, Y. Composition and bioactivity of tea flower polysaccharides obtained by different methods. *Carbohydr. Polym.* **2010**, *79*, 418–422. [CrossRef]
20. Wang, Y.; Peng, Y.; Wei, X.; Yang, Z.; Xiao, J.; Jin, Z. Sulfation of tea polysaccharides: Synthesis, characterization and hypoglycemic activity. *Int. J. Biol. Macromol.* **2010**, *46*, 270–274. [CrossRef]
21. Zhu, J.; Chen, Z.; Zhou, H.; Yu, C.; Han, Z.; Shao, S.; Hu, X.; Wei, X.; Wang, Y. Effects of extraction methods on physicochemical properties and hypoglycemic activities of polysaccharides from coarse green tea. *Glycoconj. J.* **2020**, *37*, 241–250. [CrossRef]
22. Chi, A.; Li, H.; Kang, C.; Guo, H.; Wang, Y.; Guo, F.; Tang, L. Anti-fatigue activity of a novel polysaccharide conjugates from Ziyang green tea. *Int. J. Biol. Macromol.* **2015**, *80*, 566–572. [CrossRef]
23. Lu, X.; Zhao, Y.; Sun, Y.; Yang, S.; Yang, X. Characterisation of polysaccharides from green tea of Huangshan Maofeng with antioxidant and hepatoprotective effects. *Food Chem.* **2013**, *141*, 3415–3423. [CrossRef]
24. Sun, Y.; Yang, X.; Lu, X.; Wang, D.; Zhao, Y. Protective effects of Keemun black tea polysaccharides on acute carbon tetrachloride-caused oxidative hepatotoxicity in mice. *Food Chem. Toxicol.* **2013**, *58*, 184–192. [CrossRef]
25. Karadag, A.; Pelvan, E.; Dogan, K.; Celik, N.; Ozturk, D.; Akaln, K.; Alasalvar, C. Optimisation of green tea polysaccharides by ultrasound-assisted extraction and their in vitro antidiabetic activities. *Qual. Assur. Saf. Crops Foods* **2019**, *11*, 479–490. [CrossRef]
26. Wang, H.; Chen, J.; Ren, P.; Zhang, Y.; Omondi Onyango, S. Ultrasound irradiation alters the spatial structure and improves the antioxidant activity of the yellow tea polysaccharide. *Ultrason. Sonochem.* **2021**, *70*, 105355. [CrossRef]
27. Tsubaki, S.; Iida, H.; Sakamoto, M.; Azuma, J. Microwave heating of tea residue yields polysaccharides, polyphenols, and plant biopolyester. *J. Agric. Food Chem.* **2008**, *56*, 11293–11299. [CrossRef]
28. Baik, J.H.; Shin, K.S.; Park, Y.; Yu, K.W.; Suh, H.J.; Choi, H.S. Biotransformation of catechin and extraction of active polysaccharide from green tea leaves via simultaneous treatment with tannase and pectinase. *J. Sci. Food Agric.* **2015**, *95*, 2337–2344. [CrossRef]
29. Chang, B.Y.; Kim, T.Y.; Kim, S.Y. Polysaccharides from pectinase digests of green tea enhances host immune defence through toll-like receptor 4. *Food Agric. Immunol.* **2018**, *29*, 870–885. [CrossRef]
30. Sun, Y.; Wang, F.; Liu, Y.; An, Y.; Chang, D.; Wang, J.; Xia, F.; Liu, N.; Chen, X.; Cao, Y. Comparison of water- and alkali-extracted polysaccharides from Fuzhuan brick tea and their immunomodulatory effects in vitro and in vivo. *Food Funct.* **2022**, *13*, 806–824. [CrossRef]
31. Chen, M.; Xiong, L.Y. Supercritical extraction technology in tea polysaccharide extracting application. *Adv. Mater. Res.* **2012**, *347–353*, 1683–1688. [CrossRef]
32. Li, S.; Cao, X. Extraction of tea polysaccharides (TPS) using anionic reverse micellar system. *Sep. Purif. Technol.* **2014**, *122*, 306–314. [CrossRef]
33. Shashidhar, G.M.; Giridhar, P.; Manohar, B. Functional polysaccharides from medicinal mushroom Cordyceps sinensis as a potent food supplement: Extraction, characterization and therapeutic potentials—A systematic review. *RSC Adv.* **2015**, *5*, 16050–16066. [CrossRef]
34. Jin, M.; Zhao, K.; Huang, Q.; Xu, C.; Shang, P. Isolation, structure and bioactivities of the polysaccharides from *Angelica sinensis* (Oliv.) Diels: A review. *Carbohydr. Polym.* **2012**, *89*, 713–722. [CrossRef] [PubMed]
35. Chen, H.; Qu, Z.; Fu, L.; Dong, P.; Zhang, X. Physicochemical properties and antioxidant capacity of 3 polysaccharides from green tea, oolong tea, and black tea. *J. Food Sci.* **2009**, *74*, 469–474. [CrossRef]
36. Xu, P.; Wu, J.; Zhang, Y.; Chen, H.; Wang, Y. Physicochemical characterization of puerh tea polysaccharides and their antioxidant and α-glycosidase inhibition. *J. Funct. Foods* **2014**, *6*, 545–554. [CrossRef]
37. Fan, M.; Sun, X.; Qian, Y.; Xu, Y.; Wang, D.; Cao, Y. Effects of metal ions in tea polysaccharides on their in vitro antioxidant activity and hypoglycemic activity. *Int. J. Biol. Macromol.* **2018**, *113*, 418–426. [CrossRef]
38. Wang, Y.; Yang, Z.; Wei, X. Sugar compositions, α-glucosidase inhibitory and amylase inhibitory activities of polysaccharides from leaves and flowers of *Camellia sinensis* obtained by different extraction methods. *Int. J. Biol. Macromol.* **2010**, *47*, 534–539. [CrossRef]
39. Yan, J.K.; Wang, W.Q.; Wu, J.Y. Recent advances in Cordyceps sinensis polysaccharides: Mycelial fermentation, isolation, structure, and bioactivities: A review. *J. Funct. Foods* **2014**, *6*, 33–47. [CrossRef]
40. Chen, G.; Yuan, Q.; Saeeduddin, M.; Ou, S.; Zeng, X.; Ye, H. Recent advances in tea polysaccharides: Extraction, purification, physicochemical characterization and bioactivities. *Carbohydr. Polym.* **2016**, *153*, 663–678. [CrossRef]
41. Chan, C.H.; Yusoff, R.; Ngoh, G.C.; Kung, F.W. Microwave-assisted extractions of active ingredients from plants. *J. Chromatogr. A* **2011**, *1218*, 6213–6225. [CrossRef]
42. Li, X.; Wang, L. Effect of extraction method on structure and antioxidant activity of *Hohenbuehelia serotina* polysaccharides. *Int. J. Biol. Macromol.* **2016**, *83*, 270–276. [CrossRef]
43. Dean, J.R.; Xiong, G. Extraction of organic pollutants from environmental matrices: Selection of extraction technique. *TrAC Trends Anal. Chem.* **2000**, *19*, 553–564. [CrossRef]
44. Nadar, S.S.; Rao, P.; Rathod, V.K. Enzyme assisted extraction of biomolecules as an approach to novel extraction technology: A review. *Food Res. Int.* **2018**, *108*, 309–330. [CrossRef]
45. Hu, T.; Wu, P.; Zhan, J.; Wang, W.; Shen, J.; Ho, C.T.; Li, S. Influencing factors on the physicochemical characteristics of tea polysaccharides. *Molecules* **2021**, *26*, 3457. [CrossRef]
46. Wang, D.F.; Wang, C.H.; Jun, L.L.; Guiwen, Z.Z. Components and activity of polysaccharides from coarse tea. *J. Agric. Food Chem.* **2001**, *49*, 507–510. [CrossRef]

47. Zhu, J.; Chen, Z.; Chen, L.; Yu, C.; Wang, H.; Wei, X.; Wang, Y. Comparison and structural characterization of polysaccharides from natural and artificial Se-enriched green tea. *Int. J. Biol. Macromol.* **2019**, *130*, 388–398. [CrossRef]
48. Wang, Y.; Li, Y.; Liu, Y.; Chen, X.; Wei, X. Extraction, characterization and antioxidant activities of Se-enriched tea polysaccharides. *Int. J. Biol. Macromol.* **2015**, *77*, 76–84. [CrossRef]
49. Yang, X.; Huang, M.; Qin, C.; Lv, B.; Mao, Q.; Liu, Z. Structural characterization and evaluation of the antioxidant activities of polysaccharides extracted from Qingzhuan brick tea. *Int. J. Biol. Macromol.* **2017**, *101*, 768–775. [CrossRef]
50. Liu, Y.; Zhang, B.; Ibrahim, S.A.; Gao, S.S.; Yang, H.; Huang, W. Purification, characterization and antioxidant activity of polysaccharides from *Flammulina velutipes* residue. *Carbohydr. Polym.* **2016**, *145*, 71–77. [CrossRef]
51. Nie, S.P.; Xie, M.Y. A review on the isolation and structure of tea polysaccharides and their bioactivities. *Food Hydrocoll.* **2011**, *25*, 144–149. [CrossRef]
52. Chen, G.; Xie, M.; Wan, P.; Chen, D.; Ye, H.; Chen, L.; Zeng, X.; Liu, Z. Digestion under saliva, simulated gastric and small intestinal conditions and fermentation in vitro by human intestinal microbiota of polysaccharides from Fuzhuan brick tea. *Food Chem.* **2018**, *244*, 331–339. [CrossRef]
53. Wang, M.; Chen, G.; Chen, D.; Ye, H.; Sun, Y.; Zeng, X.; Liu, Z. Purified fraction of polysaccharides from Fuzhuan brick tea modulates the composition and metabolism of gut microbiota in anaerobic fermentation in vitro. *Int. J. Biol. Macromol.* **2019**, *140*, 858–870. [CrossRef]
54. Yang, K.; Gao, Z.Y.; Li, T.Q.; Song, W.; Xiao, W.; Zheng, J.; Chen, H.; Chen, G.H.; Zou, H.Y. Anti-tumor activity and the mechanism of a green tea (*Camellia sinensis*) polysaccharide on prostate cancer. *Int. J. Biol. Macromol.* **2019**, *122*, 95–103. [CrossRef]
55. Li, X.; Chen, S.; Li, J.E.; Wang, N.; Liu, X.; An, Q.; Ye, X.M.; Zhao, Z.T.; Zhao, M.; Han, Y.; et al. Chemical Composition and Antioxidant Activities of Polysaccharides from Yingshan Cloud Mist Tea. *Oxid. Med. Cell. Longev.* **2019**, *2019*, 1915967. [CrossRef]
56. Luo, A.; He, X.; Zhou, S.; Fan, Y.; Luo, A.; Chun, Z. Purification, composition analysis and antioxidant activity of the polysaccharides from *Dendrobium nobile* Lindl. *Carbohydr. Polym.* **2010**, *79*, 1014–1019. [CrossRef]
57. Shpigelman, A.; Kyomugasho, C.; Christiaens, S.; Loey, A.; Hendrickx, M.E. The effect of high pressure homogenization on pectin: Importance of pectin source and pH. *Food Hydrocoll.* **2015**, *43*, 189–198. [CrossRef]
58. Cui, R.; Zhu, F. Ultrasound modified polysaccharides: A review of structure, physicochemical properties, biological activities and food applications. *Trends Food Sci. Technol.* **2021**, *107*, 491–508. [CrossRef]
59. Yang, Y.; Qiu, Z.; Li, L.; Vidyarthi, S.K.; Zheng, Z.; Zhang, R. Structural characterization and antioxidant activities of one neutral polysaccharide and three acid polysaccharides from *Ziziphus jujuba* cv. Hamidazao: A comparison. *Carbohydr. Polym.* **2021**, *261*, 117879. [CrossRef] [PubMed]
60. Li, X.; Lu, Y.; Zhang, W.; Yuan, S.; Zhou, L.; Wang, L.; Ding, Q.; Wang, D.; Yang, W.; Cai, Z.; et al. Antioxidant capacity and cytotoxicity of sulfated polysaccharide TLH-3 from *Tricholoma lobayense*. *Int. J. Biol. Macromol.* **2016**, *82*, 913–919. [CrossRef] [PubMed]
61. Zhang, X.; Chen, H.; Zhang, N.; Chen, S.; Zhang, Y. Extrusion treatment for improved physicochemical and antioxidant properties of highmolecular weight polysaccharides isolated from coarse tea. *Food Res. Int.* **2012**, *136*, 735–741.
62. Zhao, Z.Y.; Huangfu, L.T.; Dong, L.L.; Liu, S.L. Functional groups and antioxidant activities of polysaccharides from five categories of tea. *Ind. Crop Prod.* **2014**, *58*, 31–35. [CrossRef]
63. Zhu, Z.Y.; Dong, F.; Liu, X.; Lv, Q.; Liu, F.; Chen, L.; Wang, T.; Wang, Z.; Zhang, Y. Effects of extraction methods on the yield, chemical structure and anti-tumor activity of polysaccharides from *Cordyceps gunnii* mycelia. *Carbohydr. Polym.* **2016**, *140*, 461–471. [CrossRef]
64. Liu, Y.; Zhou, Y.; Liu, M.; Wang, Q.; Li, Y. Extraction optimization, characterization, antioxidant and immunomodulatory activities of a novel polysaccharide from the wild mushroom *Paxillus involutus*. *Int. J. Biol. Macromol.* **2018**, *112*, 326–332. [CrossRef]
65. Sun, X.Y.; Wang, J.M.; Ouyang, J.M.; Kuang, L. Antioxidant Activities and Repair Effects on Oxidatively Damaged HK-2 Cells of Tea Polysaccharides with Different Molecular Weights. *Oxid. Med. Cell. Longev.* **2018**, *2018*, 5297539. [CrossRef]
66. Sheng, J.; Sun, Y. Antioxidant properties of different molecular weight polysaccharides from *Athyrium multidentatum* (Doll.) Ching. *Carbohydr. Polym.* **2014**, *108*, 41–45. [CrossRef]
67. Huang, S.Q.; Ding, S.; Fan, L. Antioxidant activities of five polysaccharides from *Inonotus obliquus*. *Int. J. Biol. Macromol.* **2012**, *50*, 1183–1187. [CrossRef]
68. Gu, Y.; Qiu, Y.; Wei, X.; Li, Z.; Hu, Z.; Gu, Y.; Zhao, Y.; Wang, Y.; Yue, T.; Yuan, Y. Characterization of selenium-containing polysaccharides isolated from selenium-enriched tea and its bioactivities. *Food Chem.* **2020**, *316*, 126371. [CrossRef]
69. Kardos, N.; Luche, J.L. Sonochemistry of carbohydrate compounds. *Carbohydr. Res.* **2001**, *332*, 115–131. [CrossRef]
70. Chen, H.; Huang, Y.; Zhou, C.; Xu, T.; Chen, X.; Wu, Q.; Zhang, K.; Li, Y.; Li, D.; Chen, Y. Effects of ultra-high pressure treatment on structure and bioactivity of polysaccharides from large leaf yellow tea. *Food Chem.* **2022**, *387*, 132862. [CrossRef]
71. Liu, C.M.; Liang, R.H.; Dai, T.T.; Ye, J.P.; Zeng, Z.C.; Luo, S.J.; Chen, J. Effect of dynamic high pressure microfluidization modified insoluble dietary fiber on gelatinization and rheology of rice starch. *Food Hydrocoll.* **2016**, *57*, 55–61. [CrossRef]
72. Zhu, J.; Yu, C.; Han, Z.; Chen, Z.; Wei, X.; Wang, Y. Comparative analysis of existence form for selenium and structural characteristics in artificial selenium-enriched and synthetic selenized green tea polysaccharides. *Int. J. Biol. Macromol.* **2020**, *154*, 1408–1418. [CrossRef]
73. Ren, Y.; Xiao, W.; Rong, L.; Han, X.; Shen, M.; Liu, W.; Luo, Y.; Xie, J. The role of alkali in sweet potato starch-*Mesona chinensis* Benth polysaccharide gels: Gelation, rheological and structural properties. *Int. J. Biol. Macromol.* **2021**, *170*, 366–374. [CrossRef]

74. Junker, F.; Michalski, K.; Guthausen, G.; Bunzel, M. Characterization of covalent, feruloylated polysaccharide gels by pulsed field gradient-stimulated echo (PFG-STE)-NMR. *Carbohydr. Polym.* **2021**, *267*, 118232. [CrossRef]
75. Wang, J.; Liu, W.; Chen, Z.; Chen, H. Physicochemical characterization of the oolong tea polysaccharides with high molecular weight and their synergistic effects in combination with polyphenols on hepatocellular carcinoma. *Biomed. Pharmacother.* **2017**, *90*, 160–170. [CrossRef]
76. Xu, L.; Chen, Y.; Chen, Z.; Gao, X.; Wang, C.; Panichayupakaranant, P.; Chen, H. Ultrafiltration isolation, physicochemical characterization, and antidiabetic activities analysis of polysaccharides from green tea, oolong tea, and black tea. *J. Food Sci.* **2020**, *85*, 4025–4032. [CrossRef]
77. Tcholakova, S.; Denkov, N.D.; Ivanov, I.B.; Campbell, B. Coalescence stability of emulsions containing globular milk proteins. *Adv. Colloid Interface Sci.* **2006**, *123–126*, 259–293. [CrossRef] [PubMed]
78. McClements, D.J.; Gumus, C.E. Natural emulsifiers—Biosurfactants, phospholipids, biopolymers, and colloidal particles: Molecular and physicochemical basis of functional performance. *Adv. Colloid Interface Sci.* **2016**, *234*, 3–26. [CrossRef]
79. Wang, F.C.; Marangoni, A.G. Advances in the application of food emulsifier α-gel phases: Saturated monoglycerides, polyglycerol fatty acid esters, and their derivatives. *J. Colloid Interface Sci.* **2016**, *483*, 394–403. [CrossRef]
80. Desplanques, S.; Renou, F.; Grisel, M.; Malhiac, C. Impact of chemical composition of xanthan and acacia gums on the emulsification and stability of oil-in-water emulsions. *Food Hydrocoll.* **2012**, *27*, 401–410. [CrossRef]
81. Dickinson, E. Hydrocolloids at interfaces and the influence on the properties of dispersed systems. *Food Hydrocoll.* **2003**, *17*, 25–39. [CrossRef]
82. Liu, C.M.; Guo, X.J.; Liang, R.H.; Liu, W.; Chen, J. Alkylated pectin: Molecular characterization, conformational change and gel property. *Food Hydrocoll.* **2017**, *69*, 341–349. [CrossRef]
83. Li, J.; Hu, X.; Li, X.; Ma, Z. Effects of acetylation on the emulsifying properties of Artemisia sphaerocephala Krasch. polysaccharide. *Carbohydr. Polym.* **2016**, *144*, 531–540. [CrossRef]
84. Han, L.; Hu, B.; Ma, R.; Gao, Z.; Nishinari, K.; Phillips, G.O.; Yang, J.; Fang, Y. Effect of arabinogalactan protein complex content on emulsification performance of gum arabic. *Carbohydr. Polym.* **2019**, *224*, 115170. [CrossRef]
85. Chen, X.; Han, Y.; Meng, H.; Li, W.; Zhang, Y. Characteristics of the emulsion stabilized by polysaccharide conjugates alkali-extracted from green tea residue and its protective effect on catechins. *Ind. Crop Prod.* **2019**, *140*, 111611. [CrossRef]
86. Li, Q.; Shi, J.; Du, X.; McClements, D.J.; Chen, X.; Duan, M.; Liu, L.; Li, J.; Shao, Y.; Cheng, Y. Polysaccharide conjugates from Chin brick tea (*Camellia sinensis*) improve the physicochemical stability and bioaccessibility of β-carotene in oil-in-water nanoemulsions. *Food Chem.* **2021**, *357*, 129714. [CrossRef]
87. Chen, X.; Zhang, Y.; Han, Y.; Li, Q.; Wu, L.; Zhang, J.; Zhong, X.; Xie, J.; Shao, S.; Zhang, Y.; et al. Emulsifying Properties of Polysaccharide Conjugates Prepared from Chin-Brick Tea. *J. Agric. Food Chem.* **2019**, *67*, 10165–10173. [CrossRef]
88. Shi, F.; Tian, X.; McClements, D.J.; Chang, Y.; Shen, J.; Xue, C. Influence of molecular weight of an anionic marine polysaccharide (sulfated fucan) on the stability and digestibility of multilayer emulsions: Establishment of structure-function relationships. *Food Hydrocoll.* **2021**, *113*, 106418. [CrossRef]
89. Benjamin, O.; Silcock, P.; Leus, M.; Everett, D.W. Multilayer emulsions as delivery systems for controlled release of volatile compounds using pH and salt triggers. *Food Hydrocoll.* **2012**, *27*, 109–118. [CrossRef]
90. Fazaeli, M.; Emam-Djomeh, Z.; Omid, M.; Kalbasi-Ashtari, A. Prediction of the physicochemical properties of spray-dried black mulberry (*Morus nigra*) juice using artificial neural networks. *Food Bioprocess Technol.* **2013**, *6*, 585–590. [CrossRef]
91. Di Stefano, E.; Oliviero, T.; Udenigwe, C.C. Functional significance and structure–activity relationship of food-derived α-glucosidase inhibitors. *Curr. Opin. Food Sci.* **2018**, *20*, 7–12. [CrossRef]
92. Fujisawa, T.; Ikegami, H.; Inoue, K.; Kawabata, Y.; Ogihara, T. Effect of two alpha-glucosidase inhibitors, voglibose and acarbose, on postprandial hyperglycemia correlates with subjective abdominal symptoms. *Metabolism* **2005**, *54*, 387–390. [CrossRef]
93. Yang, E.; Cho, J.Y.; Sohn, U.D.; Kim, I.K. Calcium sensitization induced by sodium fluoride in permeabilized rat mesenteric arteries. *Korean J. Physiol. Pharmacol.* **2010**, *14*, 51–57. [CrossRef]
94. Wang, Y.; Liu, Y.; Huo, J.; Zhaoa, X.; Zheng, J.; Wei, X. Effect of different drying methods on chemical composition and bioactivity of tea polysaccharides. *Int. J. Biol. Macromol.* **2013**, *62*, 714–719. [CrossRef] [PubMed]
95. Wang, X.F.; Zhang, N.N.; Zhang, H.Y.; Liu, Y.; Lu, Y.M.; Xia, T.; Chen, Y. Characterization, antioxidant and hypoglycemic activities of an acid-extracted tea polysaccharide. *Int. J. Polym. Anal. Charact.* **2022**, *27*, 195–204. [CrossRef]
96. Fan, M.; Zhu, J.; Qian, Y.; Yue, W.; Xu, Y.; Zhang, D.; Yang, Y.; Gao, X.; He, H.; Wang, D. Effect of purity of tea polysaccharides on its antioxidant and hypoglycemic activities. *J. Food Biochem.* **2020**, *44*, 13277. [CrossRef] [PubMed]
97. Wang, Z.; Luo, D. Antioxidant activities of different fractions of polysaccharide purified from *Gynostemma pentaphyllum* Makino. *Carbohydr. Polym.* **2007**, *68*, 54–58. [CrossRef]
98. Xu, R.; Ye, H.; Sun, Y.; Tu, Y.; Zeng, X. Preparation, preliminary characterization, antioxidant, hepatoprotective and antitumor activities of polysaccharides from the flower of tea plant (*Camellia sinensis*). *Food Chem. Toxicol.* **2012**, *50*, 2473–2480. [CrossRef]
99. Chen, H.; Zhang, M.; Qu, Z.; Xie, B. Antioxidant activities of different fractions of polysaccharide conjugates from green tea (*Camellia Sinensis*). *Food Chem.* **2008**, *106*, 559–563. [CrossRef]
100. Tian, L.; Yan, Z.; Chao, G.; Yang, X. A comparative study on the antioxidant activities of an acidic polysaccharide and various solvent extracts derived from herbal *Houttuynia cordata*. *Carbohydr. Polym.* **2011**, *83*, 537–544. [CrossRef]

101. Chen, H.; Zhang, M.; Xie, B. Quantification of uronic acids in tea polysaccharide conjugates and their antioxidant properties. *J. Agric. Food Chem.* **2004**, *52*, 3333–3336. [CrossRef]
102. Fan, Y.; Zhou, X.; Huang, G. Preparation, structure, and properties of tea polysaccharide. *Chem. Biol. Drug Des.* **2022**, *99*, 75–82. [CrossRef]
103. Liu, M.; Gong, Z.; Liu, H.; Wang, J.; Wang, D.; Yang, Y.; Zhong, S. Structural characterization and anti-tumor activity in vitro of a water-soluble polysaccharide from dark brick tea. *Int. J. Biol. Macromol.* **2022**, *205*, 615–625. [CrossRef]
104. Wang, Y.; Chen, J.; Zhang, D.; Zhang, Y.; Wen, Y.; Li, L.; Zheng, L. Tumoricidal effects of a selenium (Se)-polysaccharide from Ziyang green tea on human osteosarcoma U-2 OS cells. *Carbohydr. Polym.* **2013**, *98*, 1186–1190. [CrossRef]
105. Zhou, Y.; Zhou, X.; Hong, T.; Qi, W.; Zhang, K.; Geng, F.; Nie, S. Lysosome-mediated mitochondrial apoptosis induced by tea polysaccharides promotes colon cancer cell death. *Food Funct.* **2021**, *12*, 10524–10537. [CrossRef]
106. Marco, M.L. Defining how microorganisms benefit human health. *Microb. Biotechnol.* **2021**, *14*, 35–40. [CrossRef]
107. Nunes, S.C.; Serpa, J. Recycling the Interspecific Relations with Epithelial Cells: Bacteria and Cancer Metabolic Symbiosis. *Adv. Exp. Med. Biol.* **2020**, *1219*, 77–91.
108. Gravina, A.G.; Zagari, R.M.; De Musis, C.; Romano, L.; Loguercio, C.; Romano, M. Helicobacter pylori and extragastric diseases: A review. *World J. Gastroenterol.* **2018**, *24*, 3204–3221. [CrossRef]
109. Dréno, B.; Pécastaings, S.; Corvec, S.; Veraldi, S.; Khammari, A.; Roques, C. Cutibacterium acnes (*Propionibacterium acnes*) and acne vulgaris: A brief look at the latest updates. *J. Eur. Acad. Dermatol. Venereol.* **2018**, *32* (Suppl. 2), 5–14. [CrossRef]
110. Parlet, C.P.; Brown, M.M.; Horswill, A.R. Commensal Staphylococci Influence *Staphylococcus aureus* Skin Colonization and Disease. *Trends Microbiol.* **2019**, *27*, 497–507.
111. Lee, J.H.; Shim, J.S.; Lee, J.S.; Kim, J.K.; Yang, I.S.; Chung, M.S.; Kim, K.H. Inhibition of pathogenic bacterial adhesion by acidic polysaccharide from green tea (*Camellia sinensis*). *J. Agric. Food Chem.* **2006**, *54*, 8717–8723. [CrossRef]
112. Ren, D.; Hu, Y.; Luo, Y.; Yang, X. Selenium-containing polysaccharides from Ziyang green tea ameliorate high-fructose diet induced insulin resistance and hepatic oxidative stress in mice. *Food Funct.* **2015**, *6*, 3342–3350. [CrossRef]
113. Wang, D.; Zhao, Y.; Sun, Y.; Yang, X. Protective effects of Ziyang tea polysaccharides on CCl4-induced oxidative liver damage in mice. *Food Chem.* **2014**, *143*, 371–378. [CrossRef]
114. Dabrowski, J.M.; Urbanska, K.; Arnaut, L.G.; Pereira, M.M.; Abreu, A.R.; Simoes, S.; Stochel, G. Biodistribution and photodynamic efficacy of a water-soluble, stable, halogenated bacteriochlorin against melanoma. *ChemMedChem* **2011**, *6*, 465–475. [CrossRef] [PubMed]
115. Yang, J.; Chen, B.; Gu, Y. Pharmacological evaluation of tea polysaccharides with antioxidant activity in gastric cancer mice. *Carbohydr. Polym.* **2012**, *90*, 943–947. [CrossRef] [PubMed]
116. Cts, A.; Lmds, A.; Ydra, B.; Nd, A.; Smmp, A.; Gls, A.; Pajg, A.; Mi, A. Polysaccharides from green and black teas and their protective effect against murine sepsis. *Food Res. Int.* **2013**, *53*, 780–785.
117. Monobe, M.; Ema, K.; Tokuda, Y.; Maeda-Yamamoto, M. Enhancement of the phagocytic activity of macrophage-like cells with a crude polysaccharide derived from green tea (*Camellia sinensis*) extract. *J. Agric. Chem. Soc. Jpn.* **2010**, *74*, 1306–1308. [CrossRef] [PubMed]
118. Hu, Z.Z.; Jin, G.M.; Wang, L.K.; Yang, J.F. Effect of tea polysaccharides on immune functions and antioxdative activity in broilers. *J. Tea Sci.* **2005**, *25*, 61–64.
119. Yu, Z.; Shi, Y.T.; Ni, D.J. Effect of enzymatic modification green tea polysaccharide on immune function of the immunosuppressant mice. *J. Tea Sci.* **2010**, *30* (Suppl. 1), 567–572.
120. Tang, C.; Ding, R.; Sun, J.; Liu, J.; Kan, J.; Jin, C. The impacts of natural polysaccharides on intestinal microbiota and immune responses—A review. *Food Funct.* **2019**, *10*, 2290–2312. [CrossRef]
121. Wu, Z.; Zeng, W.; Zhang, X.; Yang, J. Characterization of acidic tea polysaccharides from yellow leaves of Wuyi Rock Tea and their hypoglycemic activity via intestinal flora regulation in rats. *Foods* **2022**, *11*, 617. [CrossRef]
122. Bai, Y.; Zeng, Z.; Xie, Z.; Chen, G.; Chen, D.; Sun, Y.; Zeng, X.; Liu, Z. Effects of polysaccharides from Fuzhuan brick tea on immune function and gut microbiota of cyclophosphamide-treated mice. *J. Nutr. Biochem.* **2022**, *101*, 108947. [CrossRef]
123. Chen, D.; Ding, Y.; Ye, H.; Sun, Y.; Zeng, X. Effect of long-term consumption of tea (*Camellia sinensis* L.) flower polysaccharides on maintaining intestinal health in BALB/c mice. *J. Food Sci.* **2020**, *85*, 1948–1955. [CrossRef]
124. Wei, X.; Cai, X.; Xiong, S.; Wang, Y. Hypoglycemic effect of oral crude tea flower polysaccharides on alloxan modeling Sprague-Dawley rats and the possible mechanism. *CyTA-J. Food* **2012**, *10*, 325–332. [CrossRef]
125. Deng, Y.T.; Lin-Shiau, S.Y.; Shyur, L.F.; Lin, J.K. Pu-erh tea polysaccharides decrease blood sugar by inhibition of α-glucosidase activity in vitro and in mice. *Food Funct.* **2015**, *6*, 1539–1546. [CrossRef]
126. Xu, Y.; Zhang, M.; Wu, T.; Dai, S.; Xu, J.; Zhou, Z. The anti-obesity effect of green tea polysaccharides, polyphenols and caffeine in rats fed with a high-fat diet. *Food Funct.* **2015**, *6*, 297–304. [CrossRef]
127. Wu, T.; Guo, Y.; Liu, R.; Wang, K.; Zhang, M. Black tea polyphenols and polysaccharides improve body composition, increase fecal fatty acid, and regulate fat metabolism in high-fat diet-induced obese rats. *Food Funct.* **2016**, *7*, 2469–2478. [CrossRef]
128. Wu, T.; Xu, J.; Chen, Y.; Liu, R.; Zhang, M. Oolong tea polysaccharide and polyphenols prevent obesity development in Sprague-Dawley rats. *Food Nutr. Res.* **2018**, *62*, 10. [CrossRef]
129. Yu, J.; Yang, J.; Li, M.; Yang, X.; Wang, P.; Xu, J. Protective effects of Chinese Fenggang zinc selenium tea on metabolic syndrome in high-sucrose-high-fat diet-induced obese rats. *Sci. Rep.* **2018**, *8*, 3528. [CrossRef]

130. Zhou, Y.; Yao, Q.; Zhang, T.; Chen, X.; Cheng, Y. Antibacterial activity and mechanism of green tea polysaccharide conjugates against *Escherichia coli*. *Ind. Crop Prod.* **2020**, *152*, 112464. [CrossRef]
131. Sun, H. Evaluation of antioxidant activity of polysaccharides isolated from *Camellia sinensis* (tea) in exhausting training mice. *J. Med. Plant Res.* **2011**, *5*, 791–795.
132. Wang, Y.; Zhao, Y.; Andrae-Marobela, K.; Okatch, H.; Xiao, J. Tea polysaccharides as food antioxidants: An old woman's tale? *Food Chem.* **2013**, *138*, 1923–1927. [CrossRef]
133. Williams, S.N.; Shih, H.; Guenette, D.K.; Brackney, W.; Denison, M.S.; Pickwell, G.V.; Quattrochi, L.C. Comparative studies on the effects of green tea extracts and individual tea catechins on human CYP1A gene expression. *Chem. Biol. Interact.* **2000**, *128*, 211–229. [CrossRef]
134. Wang, Z.; Xie, J.; Shen, M.; Nie, S.; Xie, M. Sulfated modification of polysaccharides: Synthesis, characterization and bioactivities. *Trends Food Sci. Technol.* **2018**, *74*, 147–157. [CrossRef]
135. Ferreira, S.S.; Passos, C.P.; Madureira, P.; Vilanova, M.; Coimbra, M.A. Structure-function relationships of immunostimulatory polysaccharides: A review. *Carbohydr. Polym.* **2015**, *132*, 378–396. [CrossRef]
136. Qin, J.; Li, R.; Raes, J.; Arumugam, M.; Burgdorf, K.S.; Manichanh, C.; Nielsen, T.; Pons, N.; Levenez, F.; Yamada, T.; et al. A human gut microbial gene catalogue established by metagenomic sequencing. *Nature* **2010**, *464*, 59–65. [CrossRef]
137. Gomaa, E.Z. Human gut microbiota/microbiome in health and diseases: A review. *Antonie Van Leeuwenhoek* **2020**, *113*, 2019–2040. [CrossRef]
138. Bibbò, S.; Ianiro, G.; Giorgio, V.; Scaldaferri, F.; Masucci, L.; Gasbarrini, A.; Cammarota, G. The role of diet on gut microbiota composition. *Eur. Rev. Med. Pharmacol. Sci.* **2016**, *20*, 4742–4749.
139. Sandhu, K.V.; Sherwin, E.; Schellekens, H.; Stanton, C.; Dinan, T.G.; Cryan, J.F. Feeding the microbiota-gut-brain axis: Diet, microbiome, and neuropsychiatry. *Transl. Res.* **2017**, *179*, 223–244. [CrossRef]
140. Thursby, E.; Juge, N. Introduction to the human gut microbiota. *Biochem. J.* **2017**, *474*, 1823–1836. [CrossRef]
141. Fraga, C.G.; Croft, K.D.; Kennedy, D.O.; Tomás-Barberán, F.A. The effects of polyphenols and other bioactives on human health. *Food Funct.* **2019**, *10*, 514–528. [CrossRef]
142. Macfarlane, G.T.; Macfarlane, S. Bacteria, colonic fermentation, and gastrointestinal health. *J. AOAC Int.* **2012**, *95*, 50–60. [CrossRef]
143. Yang, W.; Ren, D.; Zhao, Y.; Liu, L.; Yang, X. Fuzhuan Brick Tea Polysaccharide Improved Ulcerative Colitis in Association with Gut Microbiota-Derived Tryptophan Metabolism. *J. Agric. Food Chem.* **2021**, *69*, 8448–8459. [CrossRef]
144. Louis, P.; Flint, H.J. Diversity, metabolism and microbial ecology of butyrate-producing bacteria from the human large intestine. *FEMS Microbiol. Lett.* **2009**, *294*, 1–8. [CrossRef]
145. Li, X.; Zhang, Z.H.; Zabed, H.M.; Yun, J.; Zhang, G.; Qi, X. An insight into the roles of dietary tryptophan and its metabolites in intestinal inflammation and inflammatory bowel disease. *Mol. Nutr. Food Res.* **2021**, *65*, 2000461. [CrossRef]
146. Kim, Y.M.; Wang, M.H.; Rhee, H.I. A novel alpha-glucosidase inhibitor from pine bark. *Carbohydr. Res.* **2004**, *339*, 715–717. [CrossRef]
147. Chen, H.; Min, Z.; Xie, B. Components and antioxidant activity of polysaccharide conjugate from green tea. *Food Chem.* **2005**, *90*, 17–21. [CrossRef]
148. Chen, G.; Chen, R.; Chen, D.; Ye, H.; Hu, B.; Zeng, X.; Liu, Z. Tea polysaccharides as potential therapeutic options for metabolic diseases. *J. Agric. Food Chem.* **2019**, *67*, 5350–5360. [CrossRef]
149. Li, S.; Chen, H.; Wang, J.; Wang, X.; Hu, B.; Lv, F. Involvement of the PI3K/Akt signal pathway in the hypoglycemic effects of tea polysaccharides on diabetic mice. *Int. J. Biol. Macromol.* **2015**, *81*, 967–974. [CrossRef]
150. Mao, Y.; Wei, B.; Teng, J.; Xia, N.; Zhao, M.; Huang, L.; Ye, Y. Polysaccharides from Chinese Liupao dark tea and their protective effect against hyperlipidemia. *Int. J. Food Sci. Technol.* **2018**, *53*, 599–607. [CrossRef]
151. Liu, Y.; Tang, Q.; Duan, X.; Tang, T.; Ke, Y.; Zhang, L.; Li, C.; Liu, A.; Su, Z.; Hu, B. Antioxidant and anticoagulant activities of mycelia polysaccharides from *Catathelasma ventricosum* after sulfated modification. *Ind. Crop Prod.* **2018**, *112*, 53–60. [CrossRef]
152. Feng, Y.; Li, W.; Wu, X.; Liang, H.; Ma, S. Rapid and efficient microwave-assisted sulfate modification of lentinan and its antioxidant and antiproliferative activities in vitro. *Carbohydr. Polym.* **2010**, *82*, 605–612. [CrossRef]
153. Bowe, W.; Patel, N.B.; Logan, A.C. Acne vulgaris, probiotics and the gut-brain-skin axis: From anecdote to translational medicine. *Benef. Microbes* **2014**, *5*, 185–199. [CrossRef]

polymers

MDPI

Article

In Vitro Fermentation of Hyaluronan with Different Molecular Weights by Human Gut Microbiota: Differential Effects on Gut Microbiota Structure and Metabolic Function

Ruohan Zhao [1,2], Chuan Zhang [1,2], Leilei Yu [1,2,*], Chengcheng Zhang [1,2], Jianxin Zhao [1,2], Arjan Narbad [3,4], Qixiao Zhai [1,2] and Fengwei Tian [1,2,*]

[1] State Key Laboratory of Food Science and Technology, Jiangnan University, Wuxi 214122, China
[2] School of Food Science and Technology, Jiangnan University, Wuxi 214122, China
[3] International Joint Research Laboratory for Probiotics, Jiangnan University, Wuxi 214122, China
[4] Gut Health and Microbiome Institute Strategic Programme, Quadram Institute Bioscience, Norwich NR4 7UA, UK
* Correspondence: edyulei@126.com (L.Y.); fwtian@jiangnan.edu.cn (F.T.); Tel./Fax: +86-510-85912155 (F.T.)

Abstract: Hyaluronan (HA) has various biological functions and is used extensively as a dietary supplement. Previous studies have shown that the probiotic effects of polysaccharides are closely associated with their molecular properties. The intestinal microbiota has been demonstrated to degrade HA; however, the regulatory effects of different molecular weights (MW) of HA on gut microbiota and metabolites are unknown. In the present study, we performed *in vitro* fermentation of human-derived feces for three MWs of HA (HA1, 32.3 kDa; HA2, 411 kDa; and HA3, 1510 kDa) to investigate the differences in the fermentation properties of HA with different MWs. We found that gut microbiota can utilize all HAs and, consequently, produce large amounts of short-chain fatty acids (SCFAs). In addition, we showed that all three HA MWs promoted the growth of *Bacteroides*, *Parabacteroides*, and *Faecalibacterium*, with HA1 being more effective at promoting the growth of *Bacteroides*. HAs have various regulatory effects on the structure and metabolites of the gut microbiota. Spearman's correlation analysis revealed that alterations in gut microbiota and their metabolites were significantly correlated with changes in metabolic markers. For instance, HA1 enriched α-eleostearic acid and DL-3-aminoisobutyric acid by regulating the abundance of *Bacteroides*, and HA3 enriched Thymidin by regulating *Faecalibacterium*. Collectively, the fermentation properties of HA vary across MW, and our results provide insights into the potential association between the MW of HA and its fermentation characteristics by the gut microbiota. These findings provide insights into the influence of the gut microbiota and HAs on the health of the host.

Keywords: hyaluronan; molecular weight; *in vitro* fermentation; gut microbiota; metabolomics

Citation: Zhao, R.; Zhang, C.; Yu, L.; Zhang, C.; Zhao, J.; Narbad, A.; Zhai, Q.; Tian, F. *In Vitro* Fermentation of Hyaluronan with Different Molecular Weights by Human Gut Microbiota: Differential Effects on Gut Microbiota Structure and Metabolic Function. *Polymers* **2023**, *15*, 2103. https://doi.org/10.3390/polym15092103

Academic Editors: Cornelia Vasile, Gabriel Aguirre-Álvarez and Xiao-Feng Sun

Received: 19 March 2023
Revised: 20 April 2023
Accepted: 25 April 2023
Published: 28 April 2023

1. Introduction

Hyaluronan (HA), an endogenous linear glycosaminoglycan, consists of repeating disaccharide units composed of N-acetyl-glucosamine and β-glucuronic acid [1]. HA is a high-molecular-weight (HMW) polymer found in synovial fluid and the extracellular matrix of several tissues [2]. Despite its simple chemical composition, HA plays important roles in tissue remodeling, inflammation, and cancer formation and has been extensively applied in medicine, food, and healthcare [3]. A growing body of evidence has shown that the biological activity of HA is intricately linked to its molecular weight (MW) [4]. HMW-HA (MW $\geq$ 100 kDa) has good viscoelasticity, moisturizing properties, and promotes wound healing [5]. In contrast, low-molecular-weight HA (LMW-HA) (1–100 kDa) is more readily absorbed by the host than HMW-HA and plays a significant role in the formation of HA cross-linking products and chronic wound healing [6]. In addition, HA oligosaccharides play a crucial role in promoting fibroblast proliferation, inflammatory mediator expression,

and tumor growth inhibition [7]. Recent studies have shown that HA has the potential to modulate intestinal barrier function. Multiple MWs of HA have been shown to alleviate dextran sodium sulfate (DSS)-induced colitis [8,9].

Orally administered HA can be degraded into oligosaccharides by the gut microbiota [10] and the genus-level relative abundance of *Bifidobacterium*, *Faecalibacterium*, *Dialister*, and *Bacteroides* can be modulated by HA fermentation [11]. The effect of HA as a popular dietary supplement on the composition of the gut microbiota, as well as degradation and metabolism of HA by the gut microbiota, has become an important topic. The gut microbiota is a highly complex microbial community and it can affect host health, including obesity, metabolic syndrome, and cardiovascular disease, which are associated with alterations in the gut microbiota. Oral administration of HA can improve resistance to pathogenic bacterial infections and inhibit DSS-induced intestinal inflammation in mice by regulating the structure and composition of the gut microbiota, promoting the abundance of *Akkermansia muciniphila*, and increasing short-chain fatty acid (SCFA) levels [12]. These results suggest that oral administration of HA may directly interact with the gut microbiota, increasing the abundance of beneficial bacteria such as *Bifidobacterium* and *Akkermansia muciniphila*, promoting the production of SCFAs, maintaining intestinal homeostasis, and indicating that HA has the potential to be developed as a novel prebiotic. However, the interactions between the gut microbiota and different MWs of HA are still poorly understood, severely hindering the development of HA. Polysaccharides' biological activity is strongly related to their MW; for example, LMW blackberry polysaccharides are more easily degraded and used by the gut microbiota [13]. Therefore, it is important to determine the fermentation characteristics of HA with different MWs during intestinal digestion.

In this study, we investigated the fermentability characteristics and prebiotic functions of HA with different MWs in six healthy gut microbiota using *in vitro* fermentation. To examine HA degradation, we assessed HA consumption and the amounts of SCFAs. In addition, we applied untargeted metabolomics in combination with 16S rRNA gene high-throughput sequencing to investigate the impact of the three MWs of HA on the modulation of the gut microbiota during metabolism. In conclusion, we investigated whether there are differences in the effect of different MWs of HA on the structure and metabolites of the gut microbiota by *in vitro* fermentation. This information is useful for understanding the relationship between MW and function of polysaccharides and provides guidance for potential prebiotic applications of HA with different molecular weights.

2. Materials and Methods

2.1. Materials

Hyaluronan (HA1, 32.3 kDa; HA2, 411 kDa; and HA3, 1510 kDa) was generously provided by Topscience Biotech Co., Ltd. (Shandong, China). Standard SCFA reagents were sourced from the China National Medicines Corporation Ltd. (Beijing, China). Ultrapure water was used in all the experiments. The organic reagents were purchased from Thermo Fisher Scientific (Waltham, MA, USA).

2.2. Sample Preparation for Stool

Fresh fecal samples were collected from six individuals (three from women and three from men, ages: 22–30 years, BMI: 18.5–24), who had not been prescribed antibiotics or probiotics for at least 3 months and without digestive disease. The study protocol was approved by the Medical Ethics Committee of the Affiliated Hospital of Jiangnan University (approval number: JNU20220901IRB07). All participants provided informed consent before participation. The information on volunteers were shown in Table 1.

Immediately after collection, each fresh fecal sample was homogenized at a ratio of 1:7 (*m*/*v*) in 100 mM sterile phosphate-buffered saline (PBS; 0.1% cysteine, pH 7.4). Sieves (0.4 mm) were used to filter the combinations, and the resulting suspension was transferred to an anaerobic incubator (Whitley DG250 Anaerobic Workstation, Bradford, West Yorkshire, UK) for fermentation.

Table 1. Information on volunteers.

Volunteers	Gender	Age	BMI
A	Female	24	21.5
B	Female	26	22.7
C	Female	25	20.2
D	Male	24	21.8
E	Male	30	21.8
F	Male	22	23.2

2.3. In Vitro Fermentation

The fermentation process simulated the fermentation of HA in the colon [14]. A commonly used gut microbiota medium was used as the *in vitro* fermentation medium. However, instead of glucose, 5 g/L HA was used as the carbon source [15]. The medium was autoclaved and placed in an anaerobic incubator to maintain an anaerobic state. The 10 mL fermentation culture medium was inoculated with 2 mL stool suspension, and the mixture was then anaerobically maintained at 37 °C. Parallel tests were performed in triplicate. The fermentation broth was collected at 0, 24, and 48 h for subsequent assays.

2.4. HA Degradation Analysis

Supernatant of the fermentation broth after being centrifuged at 4 °C (12,000× *g* for 10 min) was used to analysis the degradation of HA. The HA concentration was measured using the carbazole-sulfuric acid method, with glucuronic acid serving as the reference standard [16]. Parallel tests were performed in triplicate. The results are expressed as the average quantity of HA remaining during fermentation versus the control at 0 h.

2.5. SCFAs

The concentration of SCFAs was determined using gas chromatography-mass spectrometry (GC-MS) [17]. After centrifugation at 4 °C (12,000× *g* for 10 min), 500 μL of sample supernatant was acidified by adding 20 μL of 10% H_2SO_4. Anhydrous ether (1 mL) was added and the mixture was centrifuged at 4 °C (18,000× *g* for 15 min). The resultant supernatant was combined with anhydrous sodium sulfate (0.25 g), left to stand for 30 min, and centrifuged at 4 °C (18,000× *g* for 15 min). Finally, the upper layer was transferred to a gas-phase vial for GC-MS analysis (QP2010 Ultra, SHIMADZU, Kyoto, Japan). Extracts were measured using a Rtx-Wax capillary column with 0.89 mL/min of helium as the carrier gas. The initial oven temperature was 100°C, while the input temperature was 240 °C. Following injection, the oven temperature climbed to 140°C at a rate of 7.50 °C/min, then to 200 °C at a rate of 60 °C/min for three minutes. The following parameters were programmed into the mass spectrometer: temperature of the ion source: 220 °C; temperature of the interface: 250 °C; solvent delay: 2.5 min; m/z scan range: 2 to 100 [18].

2.6. Gut Microbiota Analysis

The fecal samples were centrifuged at 4 °C (12,000× *g* for 10 min) to remove the supernatant. The FastDNA SPIN kit for feces was used to extract bacterial DNA from the sediments. The V3-V4 gene section of 16s rRNA was amplified using the universal primers 341F and 806R. The quality of the extracted DNA was assessed by agarose gel electrophoresis. Following gel detection using the kit (Biomiga, San Diego, CA, USA), the PCR products were recovered. Genomic DNA was accurately quantified using a Nano Photometer N60 Touch [19]. The Illumina MiSeq platform was used for the paired-end sequencing of purified and merged amplicon libraries.

2.7. Untargeted Metabolomics Analysis

Culture media were centrifuged at 4 °C (10,000× *g* for 5 min) and 0.1 mL of the resulting supernatants was added to 0.4 mL of organic liquid chilled at −20 °C (methanol: acetonitrile = 1:1). To precipitate the proteins, the mixture was vortexed vigorously, soni-

cated in an ice bath for 10 min, and then stored at −20 °C for 1 h. After the proteins were precipitated, the samples were centrifuged at 4 °C (15,000× *g* for 15 min). The supernatant was then transferred to a new 1.5 mL centrifuge tube and dried using a rotary evaporator. The dried samples were re-solubilized in 200 μL of solvent (water: acetonitrile = 1:1) and vortexed. After another centrifugation under the same conditions, the supernatant was filtered through a 0.22-μm filter membrane into an injection bottle. To generate quality control (QC) samples, identical volumes of samples were transferred to fresh injection vials and thoroughly blended. An Atlantis Hilic Silica (3.0 μm, 100 × 2.1 mm) was used as sapartation column. The MS was operated in the ESI ionization mode and scanned from 70 to 1050 with a resolution of 70,000. The mobile phases were as follows: Positive mode, consisting of 10 mM ammonium acetate (0.1% formic acid) and ACN:H_2O at a ratio of 95:5 for phase A and 50:50 for phase B; Negative mode,10 mM ammonium acetate and ACN:H_2O at a ratio of 95:5 (pH 9.0 with ammonia) for phase A and 50:50 (pH 9.0 with ammonia) for phase B. Compound Discovery 3.1 (Thermo Fisher Scientific, Waltham, MA, USA) was used to analyze raw data files.

2.8. Statistical Analysis

All tests were performed in triplicate and data are expressed as mean ± standard deviation (SD). Statistical significance was set at $p < 0.05$ was determined with analysis of variance (ANOVA) tests followed by Tukey's multiple cormparisons test. Data were analyzed using GraphPad Prism software (version 9.0).

3. Results

3.1. Degradation of HA

HA is a new food ingredient that is widely used in the health food industry [20]. However, the poor absorption of HA by oral administration means that its bioavailability is low [21]. HA has previously been shown to not be degraded by gastrointestinal enzymes but can be degraded by the gut microbiota [10]. In the present study, we measured the pH of the fermentation supernatant and determined the HA utilization curve for each sample using the carbazole-sulfuric acid method. There were no significant differences in pH or HA utilization among the fermentation samples of the three sugars. After 24 h of fermentation, the pH values of all samples were at their lowest (Figure 1A) and gradually increased over time. Figure 1B shows the changes in the total HA concentration in the culture media during *in vitro* fecal fermentation. Relative HA content was determined after 24 and 48 h of fermentation. After 24 h, the HA utilization of all three sugars exceeded 85%, and the utilization of HA3 exceeded 90%. After 48 h, HA utilization by the three sugars reached >90%. The six stool samples showed strong HA degradation at all three MWs, as most of the HA was utilized during the first 24 h. This is consistent with the trend of pH change during fermentation. In addition, the amount of HA utilization increased as the MW increased, and we hypothesized that the gut microbiota in the collected stool samples preferred to utilize HMW-HA.

3.2. SCFAs Production during Fermentation

SCFAs are fatty acids with fewer than six carbons in their aliphatic tails, and the three most abundant carbons in the intestine are acetate (C2), propionate (C3), and butyrate (C4) [22]. SCFAs are produced by the anaerobic intestinal microbiota by saccharolytic fermentation of complex carbohydrates (for example, dietary fiber, resistant starch, and inulin) that cannot be digested and absorbed by the small intestine [23]. Figure 1C,D show the SCFA variables every 24 h during the fermentation process. The total SCFAs concentration increased substantially after 24 h of fermentation, with an increase of 30–40 mM. By 48 h of fermentation, only HA2 produced a significant amount of SCFAs, which was much less than the 24 h yield. From 24 to 48 h, the production of SCFAs decreased, as most of the HA was utilized in the first 24 h. This is consistent with the trend of HA utilization during fermentation. The main components of SCFAs produced by the anaerobic fermentation

of HA *in vitro* include acetate, propionate, and butyrate. During fermentation for 24 h, HA1 produced significantly ($p < 0.05$) higher levels of acetate and propionate than HA2, whereas there was no significant difference in the level of butyrate among the three HA MWs. Studies have shown that SCFAs can maintain intestinal homeostasis, prevent obesity, and ameliorate colitis and diabetes [24–26]. Oral acetate improves glucose tolerance [27], whereas butyrate and propionate could prevent diet-induced obesity and regulate intestinal hormones [28]. In summary, all three MWs of HA promoted the production of SCFAs, and the effect of MW was mainly reflected in the levels of acetate and propionate. Small-molecular-weight HA produced comparable or slightly more SCFAs than larger molecules, which is consistent with previously reported results [29].

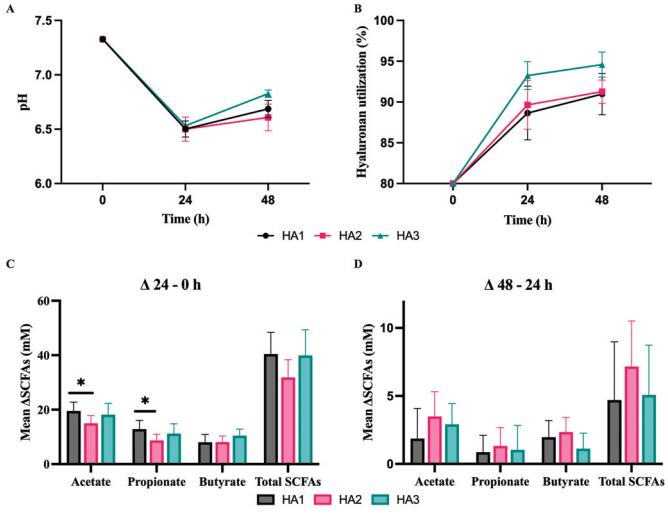

Figure 1. Human feces microbiota fermentation and degradation of HAs *in vitro*. (**A**) pH fluctuations in fermentation medium. (**B**) HAs utilization during fermentation. (**C**) Changes in the SCFAs concentration by HAs fermentation 24 h compared to that at 0 h. (**D**) Changes in the SCFAs concentration by HAs fermentation 48 h compared to that at 24 h. Significant differences were marked based on the *p*-value (* $p < 0.05$).

3.3. Changes in Microbial by Fermentation of HA

Human microbiota comprises trillions of microorganisms, with bacteria being the most abundant [30]. The gut microbiota is significantly associated with numerous physiological processes in the host, such as intestinal epithelium and immune system homeostasis [31,32]. It affects the metabolic system and may influence the liver, inflammation, and the cardiovascular system [33]. The consumption of specific dietary components, such as polysaccharides, can serve as a means to modulate the microbial community's structure and metabolic activity, thereby maintaining intestinal homeostasis [34]. High-throughput 16S rRNA gene sequencing technology was employed to analyze the microbiota structure of fecal samples both pre- and post-fermentation to investigate the interaction between different MWs of HA and the gut microbiota. As most of the HA was degraded at 24 h, the microbiome profiles at 24 h of fermentation were assessed. The Chao1 and Shannon indices were used to estimate community diversity. After 24 h of fermentation, the alpha diversities of HA1, HA2, and HA3 were not significantly different from that of the control group (Figure 2A). Cluster analysis based on evolutionary trees and non-metric multidimensional scaling (NMDS) were used to analyze global structural alterations in the intestinal microbiota before and post-24 h of HA fermentation (Figure 2B,C). Figure 2C shows an obvious taxonomic difference in the microbiota between HAs and control groups

at the genus level. In each individual, a distinct separation was observed between HA1, HA2, and HA3. However, due to inter-individual variation in the quantity and diversity of the gut microbiota, no significant differences were observed between HA1, HA2, and HA3. In addition, the distance between the control and HA1 groups was greater, indicating that HA1 significantly influenced the intestinal microbiota.

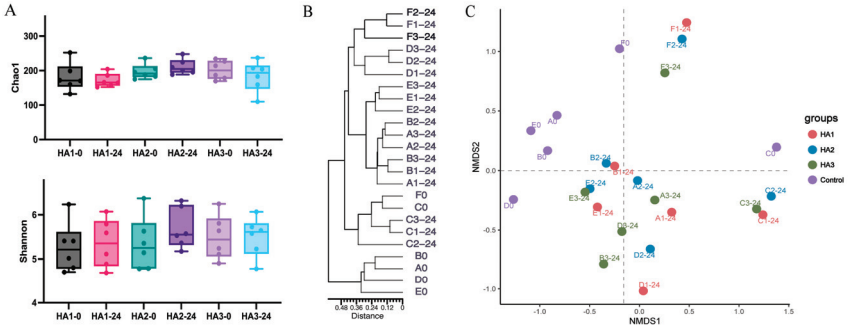

Figure 2. Analysis of microbial diversity in samples following HAs fermentation (**A**) Alpha-diversity analysis, (Chao1 and Shannon indexes). (**B**) Clustering analysis of gut microbiota. (**C**) NMDS.

Alterations in the gut microbiota were examined at the genus level following HA fermentation (Figure 2C). At the genus level, the fermentation of HA of all MWs led to an increase in the abundance of *Bacteroidetes*, *Faecalibacterium* and *Parabacteroides*. Previous studies have shown a consistent conclusion; Pan et al. [11] found that fermentation with 1.3 MDa HA increased the frequency of *Bacteroides* and *Faecalibacterium*. These discrepancies may be due to variations in the composition of the medium and gut microbiota used. In addition, it can be concluded from Figure 3C that HA1, HA2, and HA3 are more prominent in promoting the growth of *Bacteroides*, *Parabacteroides*, and *Faecalibacterium* respectively after 24 h fermentation. It has been reported that *Bacteroides* is known to produce acetate and propionate, and *Faecalibacterium* is butyrate producing bacteria [35–38]. This could explain the differences in the SCFA levels between HA1, HA2, and HA3 after 24 h of fermentation. In addition, structural differences in the gut microbiota of HA1, HA2, and HA3 at the genus level are shown in Figure S1, and 15 differential genera were identified. These findings indicate that the intestinal microbiota is capable of fermenting HA with different MWs. Different MW of HA have various regulatory effects on the structure of the microbiota.

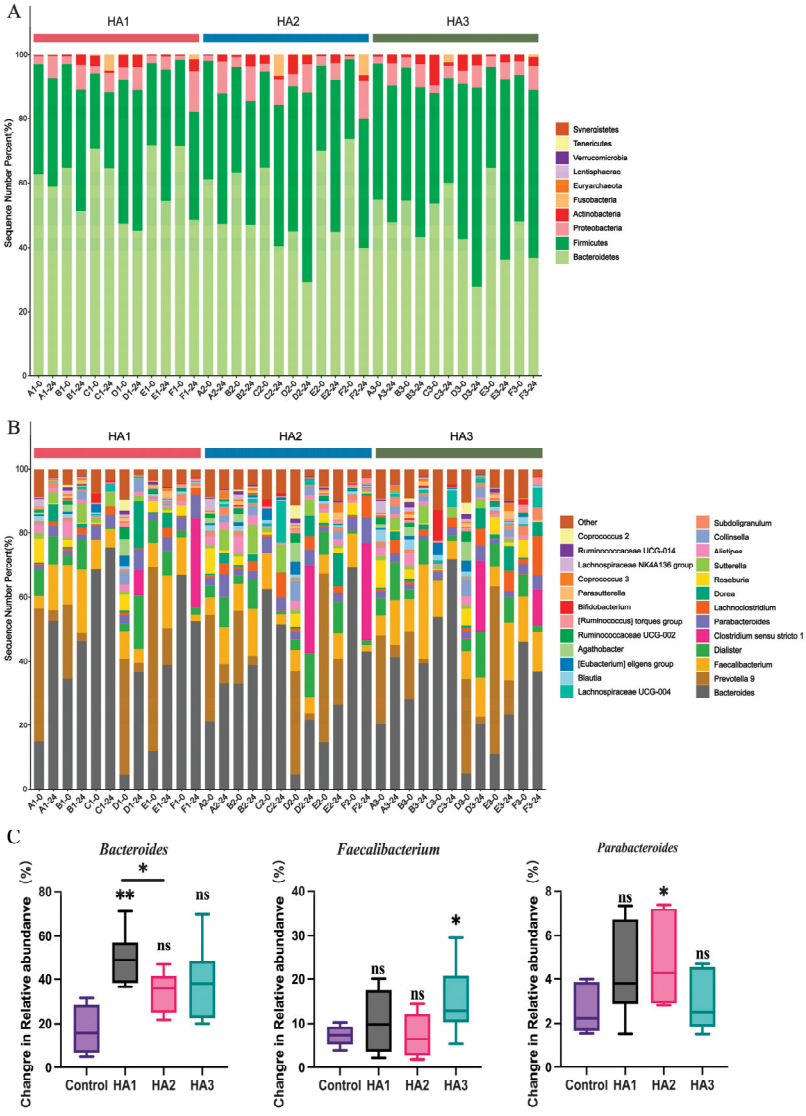

Figure 3. Reaction of the gut microbiota following HA fermentation. Bacterial taxonomic profiling of gut bacteria at the phylum (**A**) and genus (**B**). Change in relative abundance of (**C**) *Bacteroidetes*, *Faecalibacterium*, and *Parabacteroides* by HA fermentation after 24 h compared to after 0 h. Significant differences were marked based on the *p*-value (* $p < 0.05$, ** $p < 0.01$). "ns" means "no significant differences".

3.4. Changes in the Fecal Metabolism

Metabolomics is the analysis of small molecular intermediates and end products in biological samples that provide a valuable characterization of the biological profile and reflect the metabolism of the colony [39]. In this study, untargeted metabolomics of the fermentation broth supernatant was used to investigate the modulatory effects of the three MWs of HA on the metabolite profiles of the intestinal microbiota. The metabolite profiles were evaluated after 24 h of fermentation, and 146 active substance peaks were

detected. In addition, the similarity of the principal components and overall metabolic differences between the sets of samples were examined using principal component analysis (PCA; Figure 4A) and orthogonal partial least squares discriminant analysis (OPLS-DA; Figure 4C). The PCA score plot showed that the QC group clustered together, signifying consistent instrument performance and minimal reliable data errors, whereas the HA1, HA2, and HA3 groups showed significant differences. This result further demonstrates that different MWs of HA have various modulatory effects on microbiota composition as well as the profiles of microbiota metabolites. The accuracy of the prediction was 0.645 (Q2), which satisfied the requirements for a precise prediction. (Figure 4B). Similar studies demonstrated that different MWs of guar gum have different abilities to regulate bile acid levels in the cecum [40].

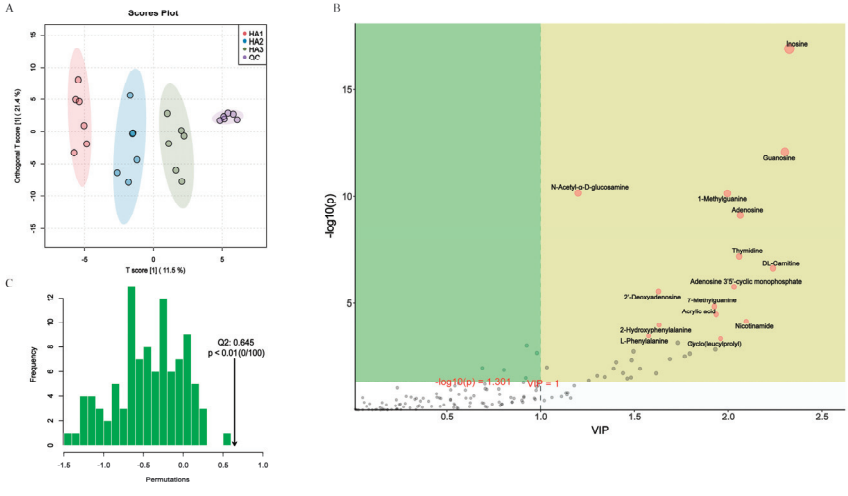

Figure 4. Alterations in metabolism caused by HAs fermentation. (**A**) PCA. (**B**) OPLS-DA. (**C**) OPLS-DA score plot.

Molecular properties of polysaccharides affect microbiota metabolism. Thus, there is the potential for different MWs of HA to target the modulation of the intestinal microbiota metabolome. By further screening the matches based on the VIP values obtained from OPLS-DA (red dots indicate VIP > 1), the metabolites with VIP > 1 were selected as potential biomarkers (Figure 4B). Overall, 38 variables were identified as biomarkers (Table S1), which serve as characteristic biomarkers with high intragroup confidence. Metabolomic analysis, as shown in Figure 5A, revealed that HA1 increased the content of N-acetyl-α-D-glucosamine, citric acid, 5-aminovaleric acid, Cyclo(leucylprolyl), linoleic acid, N,N-dimethyl-9H-purin-6-amine, 2′-deoxyadenosine, N-acetylanthranilic acid, cyclo(phenylalanyl-prolyl), acrylic acid, adenosine, guanine, N-Butyl-N′-(2-phenoxyphenyl)urea, DL-3-aminoisobutyric acid, and α-eleostearic acid. HA2 increased the content of 5-aminovaleric acid, cyclo(leucylprolyl), 2-hydroxyphenylalanine, taurochenodeoxycholic acid, and adenosine 3′5′-cyclic monophosphate. HA3 increased the content of N6-Me-Adenosine.

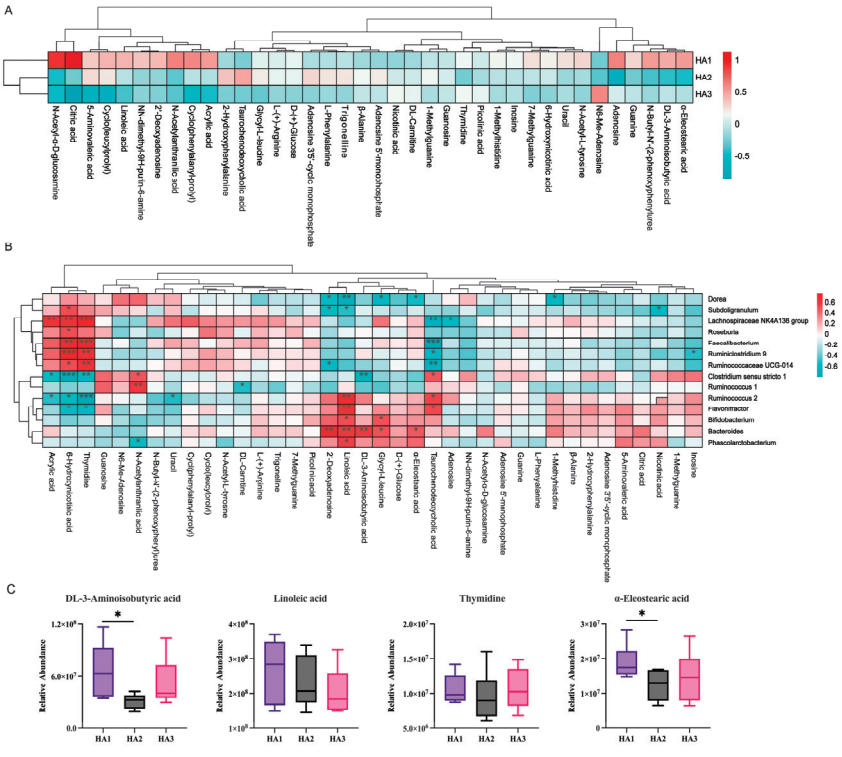

Figure 5. (**A**) Heat map of differential metabolite clustering among the groups after HAs fermentation. (**B**) Correlation analysis between the altered gut microbiota and metabolites. (**C**) Relative abundance of DL-3-aminoisobutyric acid, linoleic acid, thymidine, and α-eleostearic acid after 24 h of HA fermentation. Significant differences were marked based on the *p*-value (* $p < 0.05$, ** $p < 0.01$, *** $p < 0.001$.).

3.5. Association of Gut Microbiota and Metabolites

The influence of the gut microbiota on the host is intricately linked to the microbial metabolic axis. Previous studies have shown that *Poria cocos* oligosaccharides ameliorate the development of glucolipid metabolism disorders in HFD-fed mice, and correlation analyses have demonstrated that changes in the gut microbiota and metabolites induced by *Poria cocos* oligosaccharides are significantly associated with changes in metabolic markers [41]. To elucidate the link between microbes and metabolites, Spearman's correlation analysis was performed on the significantly altered microbiota taxa and metabolites after the fermentation of the three HAs. The correlation analysis of the 15 gut bacteria that differed in the three HAs with 38 altered metabolites is shown in Figure 5B. The α-eleostearic acid, DL-3-aminoisobutyric acid, and linoleic acid levels were strongly positively correlated with the abundance of *Bacteroides*, and Thymidine levels were strongly positively correlated with the abundance of *Faecalibacterium*. The levels of α-eleostearic acid and DL-3-aminoisobutyric acid were significantly higher in HA1 than in HA2, providing further evidence that the levels of these metabolites corresponded to the abundance of *Bacteroides* in the samples (Figure 5C). The present study suggests that HA of different MWs can further influence bacterial community metabolites by affecting the structure of intestinal colonies. Meanwhile, DL-3-aminoisobutyric acid can reduce liver inflammation in obese mice and hepatocyte apoptosis in diabetic mice [42,43], and can function as a protective metabolite in the intestine to alleviate Clostridium difficile infection in mice [44]. α-eleostearic acid reduces the severity of mice with inflammatory bowel disease by stimulating the peroxi-

some proliferator-activated receptor-γ [45]. Chrysanthemum polysaccharides and luteolin ameliorate colitis in rats by modulating linoleic acid and purine metabolism [46,47].

A recent study showed that HA (34 KDa) induces alterations in the intestinal microbiome and protects mice from *Citrobacter rodentium* infection and intestinal inflammation [12]. We speculate this MW of HA attenuates intestinal inflammation in pathogenic and chemically induced intestinal mucosal injury by modulating the levels of DL-3-aminoisobutyric acid as well as α-eleostearic acid in intestinal colony metabolites. Studies have also reported that the therapeutic effects of chitosans on ulcerative colitis vary by MW [48], as they exhibit variations in antioxidant, anti-inflammatory, immunoglobulin modulation, and intestinal microbiota regulation. In conclusion, HA of different MWs can target the regulation of intestinal microbiota and metabolites, and differences in MW may cause different therapeutic effects in diseases such as colitis. These findings shed light on the effects of MW on the prebiotic potential of HA *in vitro* and contribute to its future use as a functional food. The conclusions of this study are based on an *in vitro* fermentation system, which is farthest from physiological conditions and needs to be further validated by clinical trials.

4. Conclusions

In conclusion, an *in vitro* fermentation procedure was used to investigate the interaction between HA of different MWs and the intestinal microbiota. These findings suggest that, under anaerobic conditions in the colon, HMW-HA is more readily degraded by the gut microbiota, whereas LMW-HA produces a higher amount of SCFA. Different MWs of HA were fermented by the microbiota in human feces and differed in their effects on the microbiota, metabolites, and metabolic pathways. HA1 can increase the abundance of α-eleostearic acid and DL-3-aminoisobutyric acid promoting the growth of *Bacteroides*, and HA3 can increase the level of Thymidin by promoting the growth of *Faecalibacterium*. Differences in fermentation properties due to MW confer more possibilities for the development of HA products. Our research provides the scientific basis for the targeted regulation of gut microbiota by oral HA. In addition, oral HA1 as well as HA3 may have the potential to attenuates intestinal inflammation, which would facilitate the development of new therapies for many critical diseases with broad and important public health implications.

Supplementary Materials: The following supporting information can be downloaded at: https://www.mdpi.com/article/10.3390/polym15092103/s1, Figure S1: Using the random forest method, the highest contributing features of gut microbiota were selected; Table S1: Totally 38 metabolites were identified as biomarkers with large between-group differences, which represent characteristic biomarkers with high intra-group confidence.

Author Contributions: Data curation, R.Z. and C.Z. (Chuan Zhang); Formal analysis, R.Z.; Funding acquisition, L.Y. and F.T.; Investigation, R.Z. and C.Z. (Chuan Zhang); Methodology, R.Z. and C.Z. (Chuan Zhang); Project administration, J.Z.; Resources, L.Y. and F.T.; Supervision, J.Z.; Validation, C.Z. (Chengcheng Zhang); Visualization, A.N.; Writing—original draft, R.Z.; Writing—review & editing, Q.Z. All authors have read and agreed to the published version of the manuscript.

Funding: This work was supported by the Natural Science Foundation of Jiangsu Province [BK20220155, BE2021623]; National Natural Science Foundation of China [32001665, U1903205]; the Key Scientific and Technological Research Projects in the Key Areas of the Xinjiang Production and Construction Corps [2018AB010]; and Collaborative innovation center of food safety and quality control in Jiangsu Province.

Institutional Review Board Statement: The study protocol was approved by the Medical Ethics Committee of the Affiliated Hospital of Jiangnan University (approval number: JNU20220901IRB07).

Conflicts of Interest: The authors declare no conflict of interest.

References

1. Laurent, T.C.; Fraser, J.R. Hyaluronan. *FASEB J.* **1992**, *6*, 2397–2404. [CrossRef] [PubMed]
2. Laurent, T.C.; Laurent, U.B.; Fraser, J.R. The Structure and Function of Hyaluronan: An Overview. *Immunol. Cell Biol.* **1996**, *74*, A1–A7. [CrossRef] [PubMed]

3. Qiu, Y.; Ma, Y.; Huang, Y.; Li, S.; Xu, H.; Su, E. Current Advances in the Biosynthesis of Hyaluronic Acid with Variable Molecular Weights. *Carbohydr. Polym.* **2021**, *269*, 118320. [CrossRef]
4. Yao, Z.-Y.; Qin, J.; Gong, J.-S.; Ye, Y.-H.; Qian, J.-Y.; Li, H.; Xu, Z.-H.; Shi, J.-S. Versatile Strategies for Bioproduction of Hyaluronic Acid Driven by Synthetic Biology. *Carbohydr. Polym.* **2021**, *264*, 118015. [CrossRef] [PubMed]
5. Stern, R.; Asari, A.A.; Sugahara, K.N. Hyaluronan Fragments: An Information-Rich System. *Eur. J. Cell Biol.* **2006**, *85*, 699–715. [CrossRef]
6. Ke, C.; Wang, D.; Sun, Y.; Qiao, D.; Ye, H.; Zeng, X. Immunostimulatory and Antiangiogenic Activities of Low Molecular Weight Hyaluronic Acid. *Food Chem. Toxicol.* **2013**, *58*, 401–407. [CrossRef]
7. Boltje, T.J.; Buskas, T.; Boons, G.-J. Opportunities and Challenges in Synthetic Oligosaccharide and Glycoconjugate Research. *Nat. Chem.* **2009**, *1*, 611–622. [CrossRef]
8. Kessler, S.P.; Obery, D.R.; Nickerson, K.P.; Petrey, A.C.; McDonald, C.; de la Motte, C.A. Multifunctional Role of 35 Kilodalton Hyaluronan in Promoting Defense of the Intestinal Epithelium. *J. Histochem. Cytochem.* **2018**, *66*, 273–287. [CrossRef]
9. Zheng, L.; Riehl, T.E.; Stenson, W.F. Regulation of Colonic Epithelial Repair in Mice by Toll-Like Receptors and Hyaluronic Acid. *Gastroenterology* **2009**, *137*, 2041–2051. [CrossRef]
10. Kimura, M.; Maeshima, T.; Kubota, T.; Kurihara, H.; Masuda, Y.; Nomura, Y. Absorption of Orally Administered Hyaluronan. *J. Med. Food* **2016**, *19*, 1172–1179. [CrossRef]
11. Pan, L.; Ai, X.; Fu, T.; Ren, L.; Shang, Q.; Li, G.; Yu, G. *In Vitro* Fermentation of Hyaluronan by Human Gut Microbiota: Changes in Microbiota Community and Potential Degradation Mechanism. *Carbohydr. Polym.* **2021**, *269*, 118313. [CrossRef] [PubMed]
12. Mao, T.; Su, C.-W.; Ji, Q.; Chen, C.-Y.; Wang, R.; Vijaya Kumar, D.; Lan, J.; Jiao, L.; Shi, H.N. Hyaluronan-Induced Alterations of the Gut Microbiome Protects Mice against Citrobacter Rodentium Infection and Intestinal Inflammation. *Gut Microbes* **2021**, *13*, 1972757. [CrossRef] [PubMed]
13. Dou, Z.; Chen, C.; Fu, X. Digestive Property and Bioactivity of Blackberry Polysaccharides with Different Molecular Weights. *J. Agric. Food Chem.* **2019**, *67*, 12428–12440. [CrossRef] [PubMed]
14. Zhang, C.; Yu, L.; Zhai, Q.; Zhao, R.; Zhao, J.; Zhang, H.; Chen, W.; Tian, F. *In Vitro* Fermentation of Heparin by the Human Gut Microbiota: Changes in the Microbiota Community and Metabolic Functions. *Food Chem.* **2023**, *406*, 135010. [CrossRef]
15. Goodman, A.L.; Kallstrom, G.; Faith, J.J.; Reyes, A.; Moore, A.; Dantas, G.; Gordon, J.I. Extensive Personal Human Gut Microbiota Culture Collections Characterized and Manipulated in Gnotobiotic Mice. *Proc. Natl. Acad. Sci. USA* **2011**, *108*, 6252–6257. [CrossRef] [PubMed]
16. Bitter, T.; Muir, H.M. A Modified Uronic Acid Carbazole Reaction. *Anal. Biochem.* **1962**, *4*, 330–334. [CrossRef]
17. Tian, P.; Wang, G.; Zhao, J.; Zhang, H.; Chen, W. Bifidobacterium with the Role of 5-Hydroxytryptophan Synthesis Regulation Alleviates the Symptom of Depression and Related Microbiota Dysbiosis. *J. Nutr. Biochem.* **2019**, *66*, 43–51. [CrossRef]
18. Wang, B.; Kong, Q.; Li, X.; Zhao, J.; Zhang, H.; Chen, W.; Wang, G. A High-Fat Diet Increases Gut Microbiota Biodiversity and Energy Expenditure Due to Nutrient Difference. *Nutrients* **2020**, *12*, 3197. [CrossRef]
19. Li, D.; Feng, Y.; Tian, M.; Ji, J.; Hu, X.; Chen, F. Gut Microbiota-Derived Inosine from Dietary Barley Leaf Supplementation Attenuates Colitis through PPARγ Signaling Activation. *Microbiome* **2021**, *9*, 83. [CrossRef]
20. Kawada, C.; Yoshida, T.; Yoshida, H.; Matsuoka, R.; Sakamoto, W.; Odanaka, W.; Sato, T.; Yamasaki, T.; Kanemitsu, T.; Masuda, Y.; et al. Ingested Hyaluronan Moisturizes Dry Skin. *Nutr. J.* **2014**, *13*, 70. [CrossRef]
21. Oe, M.; Tashiro, T.; Yoshida, H.; Nishiyama, H.; Masuda, Y.; Maruyama, K.; Koikeda, T.; Maruya, R.; Fukui, N. Oral Hyaluronan Relieves Knee Pain: A Review. *Nutr. J.* **2016**, *15*, 11. [CrossRef] [PubMed]
22. Van der Hee, B.; Wells, J.M. Microbial Regulation of Host Physiology by Short-Chain Fatty Acids. *Trends Microbiol.* **2021**, *29*, 700–712. [CrossRef] [PubMed]
23. Nogal, A.; Valdes, A.M.; Menni, C. The Role of Short-Chain Fatty Acids in the Interplay between Gut Microbiota and Diet in Cardio-Metabolic Health. *Gut Microbes* **2021**, *13*, 1897212. [CrossRef] [PubMed]
24. Singh, N.; Gurav, A.; Sivaprakasam, S.; Brady, E.; Padia, R.; Shi, H.; Thangaraju, M.; Prasad, P.D.; Manicassamy, S.; Munn, D.H.; et al. Activation of Gpr109a, Receptor for Niacin and the Commensal Metabolite Butyrate, Suppresses Colonic Inflammation and Carcinogenesis. *Immunity* **2014**, *40*, 128–139. [CrossRef]
25. Canfora, E.E.; Jocken, J.W.; Blaak, E.E. Short-Chain Fatty Acids in Control of Body Weight and Insulin Sensitivity. *Nat. Rev. Endocrinol.* **2015**, *11*, 577–591. [CrossRef]
26. Bajic, D.; Niemann, A.; Hillmer, A.-K.; Mejias-Luque, R.; Bluemel, S.; Docampo, M.; Funk, M.C.; Tonin, E.; Boutros, M.; Schnabl, B.; et al. Gut Microbiota-Derived Propionate Regulates the Expression of Reg3 Mucosal Lectins and Ameliorates Experimental Colitis in Mice. *J. Crohn's Colitis* **2020**, *14*, 1462–1472. [CrossRef]
27. Yamashita, H.; Fujisawa, K.; Ito, E.; Idei, S.; Kawaguchi, N.; Kimoto, M.; Hiemori, M.; Tsuji, H. Improvement of Obesity and Glucose Tolerance by Acetate in Type 2 Diabetic Otsuka Long-Evans Tokushima Fatty (OLETF) Rats. *Biosci. Biotechnol. Biochem.* **2007**, *71*, 1236–1243. [CrossRef]
28. Lin, H.V.; Frassetto, A.; Kowalik, E.J.; Nawrocki, A.R.; Lu, M.M.; Kosinski, J.R.; Hubert, J.A.; Szeto, D.; Yao, X.; Forrest, G.; et al. Butyrate and Propionate Protect against Diet-Induced Obesity and Regulate Gut Hormones via Free Fatty Acid Receptor 3-Independent Mechanisms. *PLoS ONE* **2012**, *7*, e35240. [CrossRef]
29. Zhao, Y.; Bi, J.; Yi, J.; Wu, X.; Ma, Y.; Li, R. Pectin and Homogalacturonan with Small Molecular Mass Modulate Microbial Community and Generate High SCFAs via *in Vitro* Gut Fermentation. *Carbohydr. Polym.* **2021**, *269*, 118326. [CrossRef]

30. Marchesi, J.R.; Adams, D.H.; Fava, F.; Hermes, G.D.A.; Hirschfield, G.M.; Hold, G.; Quraishi, M.N.; Kinross, J.; Smidt, H.; Tuohy, K.M.; et al. The Gut Microbiota and Host Health: A New Clinical Frontier. *Gut* **2016**, *65*, 330–339. [CrossRef]
31. Clemente, J.C.; Ursell, L.K.; Parfrey, L.W.; Knight, R. The Impact of the Gut Microbiota on Human Health: An Integrative View. *Cell* **2012**, *148*, 1258–1270. [CrossRef] [PubMed]
32. Kau, A.L.; Ahern, P.P.; Griffin, N.W.; Goodman, A.L.; Gordon, J.I. Human Nutrition, the Gut Microbiome and the Immune System. *Nature* **2011**, *474*, 327–336. [CrossRef] [PubMed]
33. Lynch, S.V.; Pedersen, O. The Human Intestinal Microbiome in Health and Disease. *N. Engl. J. Med.* **2016**, *375*, 2369–2379. [CrossRef] [PubMed]
34. Chengxiao, Y.; Dongmei, W.; Kai, Z.; Hou, L.; Xiao, H.; Ding, T.; Liu, D.; Ye, X.; Linhardt, R.J.; Chen, S. Challenges of Pectic Polysaccharides as a Prebiotic from the Perspective of Fermentation Characteristics and Anti-Colitis Activity. *Carbohydr. Polym.* **2021**, *270*, 118377. [CrossRef] [PubMed]
35. Valles-Colomer, M.; Falony, G.; Darzi, Y.; Tigchelaar, E.F.; Wang, J.; Tito, R.Y.; Schiweck, C.; Kurilshikov, A.; Joossens, M.; Wijmenga, C.; et al. The Neuroactive Potential of the Human Gut Microbiota in Quality of Life and Depression. *Nat. Microbiol.* **2019**, *4*, 623–632. [CrossRef]
36. Tomioka, S.; Seki, N.; Sugiura, Y.; Akiyama, M.; Uchiyama, J.; Yamaguchi, G.; Yakabe, K.; Ejima, R.; Hattori, K.; Kimizuka, T.; et al. Cooperative Action of Gut-Microbiota-Accessible Carbohydrates Improves Host Metabolic Function. *Cell Rep.* **2022**, *40*, 111087. [CrossRef]
37. Aoki, R.; Onuki, M.; Hattori, K.; Ito, M.; Yamada, T.; Kamikado, K.; Kim, Y.-G.; Nakamoto, N.; Kimura, I.; Clarke, J.M.; et al. Commensal Microbe-Derived Acetate Suppresses NAFLD/NASH Development via Hepatic FFAR2 Signalling in Mice. *Microbiome* **2021**, *9*, 188. [CrossRef]
38. Lei, Y.; Tang, L.; Liu, S.; Hu, S.; Wu, L.; Liu, Y.; Yang, M.; Huang, S.; Tang, X.; Tang, T.; et al. Parabacteroides Produces Acetate to Alleviate Heparanase-Exacerbated Acute Pancreatitis through Reducing Neutrophil Infiltration. *Microbiome* **2021**, *9*, 115. [CrossRef]
39. Fu, Y.-P.; Peng, X.; Zhang, C.-W.; Jiang, Q.-X.; Li, C.-Y.; Paulsen, B.S.; Rise, F.; Huang, C.; Feng, B.; Li, L.-X.; et al. Salvia Miltiorrhiza Polysaccharide and Its Related Metabolite 5-Methoxyindole-3-Carboxaldehyde Ameliorate Experimental Colitis by Regulating Nrf2/Keap1 Signaling Pathway. *Carbohydr. Polym.* **2023**, *306*, 120626. [CrossRef]
40. Ghaffarzadegan, T.; Marungruang, N.; Fåk, F.; Nyman, M. Molecular Properties of Guar Gum and Pectin Modify Cecal Bile Acids, Microbiota, and Plasma Lipopolysaccharide-Binding Protein in Rats. *PLoS ONE* **2016**, *11*, e0157427. [CrossRef]
41. Regulation of Gut Microbiota and Intestinal Metabolites by Poria Cocos Oligosaccharides Improves Glycolipid Metabolism Disturbance in High-Fat Diet-Fed Mice—PubMed. Available online: https://pubmed.ncbi.nlm.nih.gov/35472435/ (accessed on 5 March 2023).
42. Shi, C.-X.; Zhao, M.-X.; Shu, X.-D.; Xiong, X.-Q.; Wang, J.-J.; Gao, X.-Y.; Chen, Q.; Li, Y.-H.; Kang, Y.-M.; Zhu, G.-Q. β-Aminoisobutyric Acid Attenuates Hepatic Endoplasmic Reticulum Stress and Glucose/Lipid Metabolic Disturbance in Mice with Type 2 Diabetes. *Sci. Rep.* **2016**, *6*, 21924. [CrossRef] [PubMed]
43. Begriche, K.; Massart, J.; Abbey-Toby, A.; Igoudjil, A.; Lettéron, P.; Fromenty, B. β-Aminoisobutyric Acid Prevents Diet-Induced Obesity in Mice with Partial Leptin Deficiency. *Obesity* **2008**, *16*, 2053–2067. [CrossRef] [PubMed]
44. Wang, J.; Ghali, S.; Xu, C.; Mussatto, C.C.; Ortiz, C.; Lee, E.C.; Tran, D.H.; Jacobs, J.P.; Lagishetty, V.; Faull, K.F.; et al. Ceragenin CSA13 Reduces Clostridium Difficile Infection in Mice by Modulating the Intestinal Microbiome and Metabolites. *Gastroenterology* **2018**, *154*, 1737–1750. [CrossRef] [PubMed]
45. Lewis, S.N.; Brannan, L.; Guri, A.J.; Lu, P.; Hontecillas, R.; Bassaganya-Riera, J.; Bevan, D.R. Dietary α-Eleostearic Acid Ameliorates Experimental Inflammatory Bowel Disease in Mice by Activating Peroxisome Proliferator-Activated Receptor-γ. *PLoS ONE* **2011**, *6*, e24031. [CrossRef]
46. Tao, J.-H.; Duan, J.-A.; Zhang, W.; Jiang, S.; Guo, J.-M.; Wei, D.-D. Polysaccharides From *Chrysanthemum Morifolium* Ramat Ameliorate Colitis Rats via Regulation of the Metabolic Profiling and NF-κ B/TLR4 and IL-6/JAK2/STAT3 Signaling Pathways. *Front. Pharmacol.* **2018**, *9*, 746. [CrossRef]
47. Li, B.; Du, P.; Du, Y.; Zhao, D.; Cai, Y.; Yang, Q.; Guo, Z. Luteolin Alleviates Inflammation and Modulates Gut Microbiota in Ulcerative Colitis Rats. *Life Sci.* **2021**, *269*, 119008. [CrossRef]
48. Niu, W.; Dong, Y.; Fu, Z.; Lv, J.; Wang, L.; Zhang, Z.; Huo, J.; Ju, J. Effects of Molecular Weight of Chitosan on Anti-Inflammatory Activity and Modulation of Intestinal Microflora in an Ulcerative Colitis Model. *Int. J. Biol. Macromol.* **2021**, *193*, 1927–1936. [CrossRef]

polymers

MDPI

Article

Preparation of Surgical Thread from a Bioplastic Based on Nopal Mucilage

Evelyn Herrera-Ibarra [1], Mercedes Salazar-Hernández [2], Alfonso Talavera-López [3], O. J. Solis-Marcial [4], Rosa Hernandez-Soto [1], Jose P. Ruelas-Leyva [5,*] and José A. Hernández [1,*]

[1] UPIIG, del Instituto Politécnico Nacional, Guanajuato 36275, Mexico; eherrerai1601@alumno.ipn.mx (E.H.-I.); rohernandezs@ipn.mx (R.H.-S.)
[2] Departamento de Ingeniería en Minas, Metalurgia y Geología, División de Ingenierías, Universidad de Guanajuato, Guanajuato 36025, Mexico; merce@ugto.mx
[3] Unidad Académica de Ciencias Químicas, Campus UAZ siglo XXI, Universidad Autónoma de Zacatecas, Zacatecas 98160, Mexico; talavera@uaz.edu.mx
[4] UPIIZ, del Instituto Politécnico Nacional, Zacatecas 98160, Mexico; ojsolis@ipn.mx
[5] Facultad de Ciencias Químico-Biológicas, Universidad Autónoma de Sinaloa, Ciudad Universitaria, Culiacán 80030, Mexico
* Correspondence: jose.ruelas@uas.edu.mx (J.P.R.-L.); jahernandezma@ipn.mx (J.A.H.)

Abstract: Currently, natural materials represent a sustainable option for the manufacture of biopolymers with numerous industrial applications and characteristics comparable with synthetic materials. Nopal mucilage (NM) is an excellent natural resource for the synthesis of bioplastics (BPs). In the present research, the fabrication of biopolymers by using NM is addressed. Changes in the plasticizer (sorbitol and cellulose) concentration, in addition to the implementation of two sources of starch (corn starch (CS) and potato starch (PS)) to obtain the surgical thread, were analyzed. The NM extracted was close to 14% with ethanol. During the characterization of the extract, properties such as moisture, humidity, viscosity, and functional groups, among others, were determined. In the CS and PS analysis, different structures of the polymeric chains were observed. BP degradation with different solvents was performed. Additionally, the addition of sorbitol and cellulose for the BP mixtures presenting the highest resistance to solvent degradation and less solubility to water was conducted. The obtained thread had a uniform diameter, good elasticity, and low capillarity compared to other prototypes reported in the literature.

Keywords: biopolymer; degradation; mucilage; bioplastic; surgical thread; solvents

Citation: Herrera-Ibarra, E.; Salazar-Hernández, M.; Talavera-López, A.; Solis-Marcial, O.J.; Hernandez-Soto, R.; Ruelas-Leyva, J.P.; Hernández, J.A. Preparation of Surgical Thread from a Bioplastic Based on Nopal Mucilage. *Polymers* **2023**, *15*, 2112. https://doi.org/10.3390/polym15092112

Academic Editors: Cornelia Vasile, Gabriel Aguirre-Álvarez and Xiao-Feng Sun

Received: 16 March 2023
Revised: 23 April 2023
Accepted: 25 April 2023
Published: 28 April 2023

1. Introduction

The environmental damage derived from anthropogenic activity has accelerated the change in the planet's climate, and the use of fossil hydrocarbons contributes significantly to this process since they produce greenhouse gases [1,2]. The manufacture of synthetic materials (mainly polymers) from oil refining represents a large part of the products used in homes, industries, shops, and medicines, among other applications [2–4]. These plastics cause serious damage to the environment because they are mainly non-reusable products, generating large amounts of solid waste which require decades to degrade [1,2]. Due to this situation, in recent years there has been an increased interest in polymers obtained from renewable sources with features similar to synthetic plastics, giving rise to the development of BPs [3,5]. These BPs are biocompatible, biodegradable, non-toxic, and recycle organic matter from agricultural waste, animals, microorganisms, and plants. Therefore, they are considered cheap, sustainable, and widely available materials [1,2,5]. These advantages allow their use in different industries such as food, medicine, and agriculture, among others [2,3,5]. In the medical industry, BPs are widely used to pack and control the supply of medicine, fixation equipment, adhesion, and biomedical polymers

used for suture wounds, cuts, tissue engineering, etc. [3,5,6]. Biomedical polymers are products employed to reproduce the function of living tissues in biological systems in a safe, mechanically functional, and physiologically acceptable way [7]. They are implanted in the body (temporarily or permanently), and they try to restore the existing defect by activating tissue regeneration, decreasing the probability of infection, and minimizing patient discomfort [7,8]. In the case of sutures, many factors must be considered, such as the required tension and the biological reaction to the material that occurs in sutures based on synthetic polymers. Furthermore, natural polymers such as starch and cellulose fulfill these characteristics to achieve a natural thread useful in suture wounds [5,9]. For manufacturing surgical threads, the source of the biopolymer and plasticizers conferring the appropriate properties for a particular application has to be analyzed [10–13]. Glycerol is a plasticizer in the manufacture of starch films preventing cracking during handling and storage; moreover, it has a good sorption capacity due to water permeability. Therefore, adding glycerol as a plasticizer is essential to improve the toughness of the films [12]. On the other hand, sorbitol is a polyalcohol employed as a plasticizer because it confers better elasticity and resistance to films compared to glycerol [13]. Cellulose is a polysaccharide composed of D-glucose units and is the main component of various plants such as cotton and flax. Cellulose derivatives have several applications due to their mechanical properties and biocompatibility; in addition, cellulose is considered a non-harmful component of the environment. These features are why cellulose fibers have stood out in tissue reconstruction and regenerative medicine [11].

For the manufacture of biopolymers, fibrous polysaccharide materials are preferred. There has been an increasing interest in the nopal, a fruit tree in the arid and semi-arid zones of Mexico, with physiological and morphological characteristics that allow its adaptation to extreme temperature and water scarcity [14–17]. Nopal leaves excrete mucilage, a highly branched fibrous polysaccharide, whose molecular weight is around 13×10^6 g/mol [18–20]. It is a complex carbohydrate since it contains approximately 35–40% arabinose, 20–25% galactose and xylose, and 7–8% rhamnose and galacturonic acid [21–25]. The proportion of these monomers in their composition changes depending on factors such as variety, age, environmental conditions, and structure (fruit, shell, or cladode) used for extraction [22,23]. Nonetheless, mucilage is considered a residue commonly discarded by consumers [8,14,18].

In this work, thread for medical applications was obtained by the mixture of NM, potato starch, and glycerol as a base to form molecular networks. Modifications in the proportion of the components in this mixture led to changes in viscosity, elasticity, hardness, resistance, texture, tension, water retention, and degradation in different solvents of the thread. Additionally, its physical properties (diameter, malleability, and color) changed. Moreover, the effect of adding sorbitol and cellulose as a plasticizer on the properties of the thread was studied.

2. Materials and Methods

2.1. Reagents and Nopal Harvest

All chemicals used were analytical grade. Two different potato starches (PSs) were employed, one from Sigma Aldrich (St. Louis, MO, USA) (CAS: 9005-25-8) and the other one from Baker Analyzed (CAS: 9005-84-9). Sorbitol ($C_6H_{14}O_6$) and cellulose were purchased from Merc (100%, CAS: 50-70-4) and J.T. Baker (DEAE, CAS: 9004-34-6), respectively. The water used for the preparation of all the solutions was deionized. The cladodes (leaves) of nopal (*Opuntia ficus indica*) were collected from a producing area in Silao city, Guanajuato, Mexico, at an altitude of 1780 m above sea level with two types of a sub-humid temperate climate with summer rains and semi-dry. Through the PlantNet identifica®, PlantSnap®, and PictureThis® applications, which are databases of images and plant data, it was identified whether the nopal collected belonged to the species *Opuntia ficus indica*.

2.2. Nopal Mucilage (NM) Extraction

For the NM extraction, the nopal should be two years old because the tissue contains a considerable amount of mucilage [17–19,24]. The collected cladodes were brushed to remove spines, washed, and disinfected by immersing in 10% (*v*/*v*) sodium hypochlorite (NaClO) solution for 10 min. The cuticle and epidermis were subsequently removed [18,19]. The remaining material was cut into cubes, submerged in deionized water with a ratio of 1:7 (*wt*/*v*) for 48 h, and was stored in a refrigerator (Thermo Scientific (Waltham, MA, USA) FRGL 1204V) at a temperature of 4 °C. Subsequently, the mixture was crushed in an industrial blender (Tapisa 12 L) and then sieved through filter no. 16 (1.18 mm stainless steel mesh) to remove the rest of the plant tissue. Small plant debris was removed from the viscous fluid with a vacuum pump (THOMAS QR-0080), and then this fluid was heated in a water bath (Julabo Ecotemp TW20) at 80 °C for 1 h. Next, the viscous liquid was allowed to cool at room temperature, followed by the addition of ethyl alcohol (J.T. Baker, ≥96%) in a 1:2 (*v*/*v*) ratio. The resulting solution was heated at 80 °C for 1 h. Finally, the mixture was centrifuged (HERMLE Z383K) for 20 min at 2240 rpm to extract the sediment corresponding to the mucilage [18,19,25]. The efficiency of the extracted NM was calculated with an equation based on the recovered weight of mucilage as follows:

$$R_{NM} = \frac{W_{MO}}{W_P} \times 100 \quad (1)$$

where R_{NM} is NM efficiency (%), W_{MO} is the mucilage weight (g), and W_P is the initial nopal weight (g).

2.3. Starch Extraction from Corn Grains

In the CS extraction, 250 g of corn grains were dried, grounded, and immersed in a 0.1 M NaOH solution for 18 h. Afterward, the mixture was poured and mixed in an industrial blender (Tapisa 12 L) and sieved (0.15 mm) to separate big particles from the solution. These big particles were washed several times with deionized water until the washing water remained crystalline. The solution and the washed particles were centrifuged (HERMLE Z383K) for 30 min at 5000 rpm to discard the supernatant. In the solid phase, there was a gray coloration in the upper zone, indicative of proteins, lipids, and small CS granules. In the lower region, it had a white coloration, allegedly by the presence of starch [23,24]. The obtained starch was submerged in a 0.1 M HCl solution until reaching a pH of 6.5 to neutralize the NaOH in CS. Subsequently, the CS was washed with deionized water to remove the remaining HCl. Then, the solution was centrifuged again under the above-mentioned conditions. Finally, it was filtered with a vacuum pump (THOMAS QR-0080) and dried in a forced convection oven (Shel Lab CE5F) at 45 °C for 24 h, for later storage until needed.

2.4. Bioplastics (BPs) Elaboration

The extracted NM was slowly poured into deionized water at 25 °C with vigorous stirring for 24 h and then heated at 35 °C for 12 h. Immediately after, each component (NM, glycerol, CS, and water) was added to the mixture (350 mL) while maintaining the glycerol (0.5 mL) and CS (1 g) constant and modifying the proportions of water, as indicated in Table 1. In each experiment, the solution was heated to 90 °C for 30 min and homogenized for 10 min. After this time, the mixtures were cooled to 25 °C, and the pH was adjusted (between 4.5 and 7.5) with 0.1 M citric acid ($C_6H_8O_7$) [26]. The BP obtained was poured into Petri dishes and placed in a forced convection oven (Shel Lab CE5F) at 40 ± 2 °C for approximately 24 h to reduce the humidity of the mixtures. Following this, resistance tests of the BP (0.2 g) were carried out using 10 mL of different solvents (water, ethyl alcohol, acetone, HCl (0.1 M) and CH_3COOH (0.1 M)) by observing the BP solubility in each of the solvents for 12 h.

Table 1. Mixtures employed to generate the BP.

Experiment	Mucilage (mg)	H_2O (mL)
1	1.05	10
2	1.03	20
3	1.04	30
4	1.01	5
5	1.02	15
6	1.53	30
7	1.51	10

To perform the experiments of BP solubility in water, first, the material was cut into 4 cm^2 squares, dried at 100 °C for 24 h, and weighed. Subsequently, the samples were immersed in 100 mL of deionized water for 24 h. Finally, the remaining films were recovered by filtration and dried (100 °C in an oven for 24 h) to determine the non-solubilized dry mass. The solubility percentage was obtained with the following equation [10,26,27]:

$$\text{Solubility } (\%) = \frac{W_{ds} - W_{df}}{W_{ds}} \times 100 \quad (2)$$

where W_{ds} and W_{df} are the initial and final dry weight (g) of the bioplastic, respectively.

2.5. Surgical Thread (ST) Preparation

To the bioplastic with the highest resistance to solvent degradation, sorbitol and cellulose with different concentrations were added. The amounts of plasticizers and starch are shown in Table 2. Finally, this mixture is placed in a syringe (Plastipak 10 mL pharmaceutical grade syringe and hypodermic nursing needle) to produce the thread [5,11,27,28].

Table 2. Components and proportions employed during the preparation of surgical thread.

Starch	Sorbitol (mg)	Cellulose (mg)
Corn (CS)	10	10 50 100
	20	10 20 50 100
	30	10 20 50 100
Potato of Sigma Aldrich (SAPS)	10	10 50 100
	20	10 20 50 100
	30	10 20 50 100

Table 2. *Cont.*

Starch	Sorbitol (mg)	Cellulose (mg)
Potato of Baker Analyzed (BAPS)	10	10
		50
		100
	20	10
		20
		50
		100
	30	10
		20
		50
		100

2.6. Characterization of Nopal Mucilage and Bioplastic Additives

Attenuated total reflectance-Fourier transform spectroscopy (ATR-FTIR) analyses on NM, CS, SAPS, and BAPS were conducted in a Thermo Scientific Nicolet iS10 analyzer; 32 scans were obtained with a resolution of 4 cm^{-1} over the wavenumber range of 4000–400 cm^{-1}. X-ray diffraction (XRD) patterns were obtained in a diffractometer (Ultima IV Rigaku). Scanning electron microscopy images and X-ray energy dispersion spectroscopy (SEM-EDS) were obtained in a JOEL spectrometer (6510 pus). Adsorption spectra in the UV-Vis region (1100–200 nm) were performed in a UV-Vis-NIR (Near IR) spectrophotometer (Cary 5000 Varian). Textural properties of the different starches were determined using the BET equation (Micromeritics Tristar II plus). The apparent viscosity of NM was measured by a digital Brookfield Viscometer (Generic DH-DJ-8S Model). The mechanical properties of the selected bioplastics were determined using a Texture Analyzer (Shimadzu EZ-LX Short Model). The diameter of the obtained thread was measured with a Digital Vernier (Mitutoyo 150 mm 500-196-20 model).

3. Results and Discussion

3.1. Nopal Mucilage (NM) Extraction

The cladodes of the nopal were cleaned, disinfected, cut into small cubes, and placed in distilled water (1 g/1 mL ratio), and then the solution was crushed, sifted, and filtered. The solid was suspended with ethyl alcohol (ratio 1:2 v/v). Figure 1a shows the mixture of NM and ethanol, which was centrifuged to separate the supernatant and then dried (Figure 1b), obtaining a yield of 11.1%.

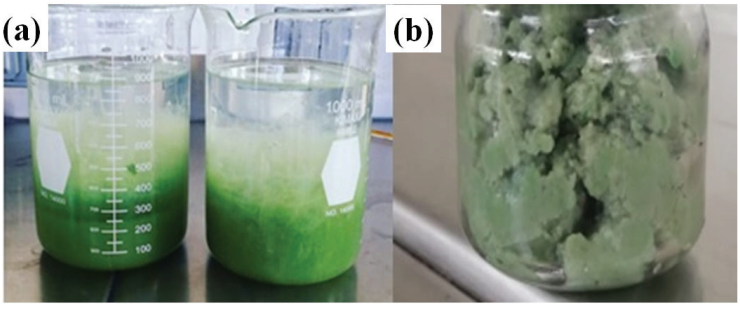

Figure 1. Images of the mucilage extraction: (**a**) ethanol blended with NM and (**b**) sediment.

The NM yield can be affected by different variables, including temperature, washing, solvent, and the age of the nopal [12,19]. The yield of NM in this work was ~62%, a value higher than reports in the literature [12] due to cleaning, washing, cutting the nopal into cubes at a pH of 4.45, and NM separation after the addition of ethanol. These modifications

were crucial to increase the yield. It is worth mentioning that it was not required to dry the precipitate obtained because the aqueous solution of NM can be directly used. In the particular case of the use of solvents for the precipitation of NM, yields between 18.8 and 20.9% have been reported using isopropanol (1:4, *v*/*v* ratio) and ethanol (1:3, *v*/*v* ratio) [17]. In comparison, the results of the present study are slightly higher than those reported in the literature [12].

The apparent viscosity obtained for the NM in this study was 55.2 mPa·s at a pH of 5.8. In the literature [29,30], a direct relationship between the pH value and the viscosity of the extract is mentioned, in which increasing the pH increases the viscosity value. A liquid with this behavior is considered a non-Newtonian fluid with characteristics of a pseudoplastic fluid [29,30].

3.2. Characterization of the NM and Starch

The textural properties of the NM extracted had a surface area of 1.76 m^2/g, with a pore volume and diameter of 0.0081 cm^3/g and 5.79 nm, respectively, characteristic of a mesoporous structure [31]. These properties are comparable with those reported by Abdullah et al. [32]. Figure 2 shows the ATR-FTIR spectrum of the NM, where the bands observed at 3400 cm^{-1} are attributed to the stretching vibration of the hydroxyl groups (O–H) while at 2925 and 1642 cm^{-1} they are assigned to the symmetric stretching vibrations of the –CH group and polysaccharide molecules, respectively [18,19]. The shoulder at 2870 cm^{-1} is attributed to the symmetric extension vibration of the –CH groups. The band at 1414 cm^{-1} corresponds to the carboxylic acid and peptide bond with the vibrations of deformation C–H and deformation N–H bonds of NM [18,19]. The bands at 1242, 1038, and 890 cm^{-1} are related to the functional groups of polysaccharides and are known as the NM fingerprint [14,15]. The structure (Figure 2), morphology (Figure 3), and surface area of the NM allowed an excellent interaction with the plasticizers and starch, a requirement for the manufacture of the surgical thread [18,19].

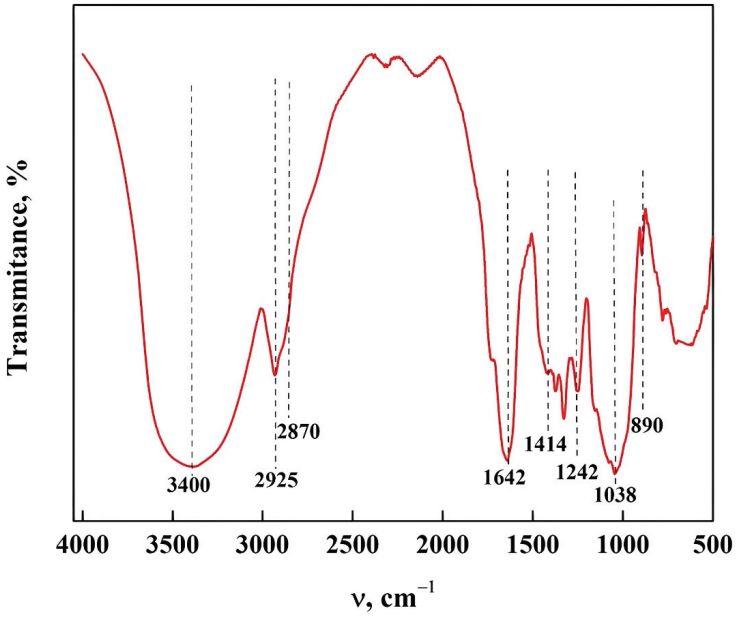

Figure 2. Characterization of NM by ATR-FTIR.

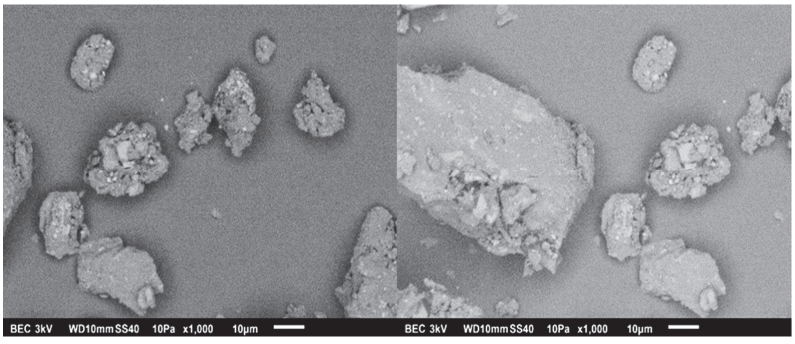

Figure 3. SEM images of NM.

The ATR-FTIR characterization of SAPS and CS can be seen in Figure 4. For the PS, the bands appearing at 3575 and 3215 cm^{-1} correspond to the stretching vibrations of the hydroxyl group (–OH); meanwhile, the band at 2935 cm^{-1} is attributed to the stretching vibrations of C–H bonds. The signal at 1660 cm^{-1} is assigned to the extension vibrations of C=O, and the band at 1467 cm^{-1} is due to the extensional vibration of N–H bonds. The bands at 1364 and 1161 cm^{-1} appear due to symmetric C–H bending and asymmetric C–O–C extension, respectively. The signals at 1082 and 982 cm^{-1} are related to the stretching vibrations of C–O–C bonds. The bands at 925, 862, and 769 cm^{-1} are generated by the vibrations of the carbohydrate ring in the C–O–C bond [32,33]. In the case of CS, the bands at 3400 cm^{-1} correspond to the extension vibration of the hydroxyl group (–OH), while the signal at 2935 cm^{-1} is attributed to the extension of C–H bonds. The band at 1655 cm^{-1} is associated with OH groups. The bands at 1460 and 1421 cm^{-1} are consistent with the deformation and symmetric scissoring of CH_2, respectively. The signals at 1360 and 1168 cm^{-1} are assigned to the symmetric bending of C–H and the asymmetric extension vibration of C–O–C. At the bands at 1075 and 991 cm^{-1}, the stretching vibrations of C–O are observed; and at 928, 856, and 762 cm^{-1}, the carbohydrate ring vibrations due to the C–O–C bonds appear in the spectra [33].

The micrographs of CS and SAPS are shown in Figure 5. Predominantly, polygonal spherical morphology with a size > 5 μm is observed for the CS. An ellipsoidal oval shape with a size > 20 μm is observed for PS. The shape and size of the starch particles are directly dependent on amylopectin. In the case of CS, there are small starch granules, which allows the structure to have short chains with several ramifications, while for the PS, its chains are long with few ramifications due to its larger granules [23,34]. These characteristics are important because they transcend the physical–chemical, functional, and nutritional properties. For example, there is better digestibility in CS since the size of the granules is related to the viscosity; with smaller granules, there is a lower viscosity. Therefore, the small CS granules are digested at a higher speed when compared to the PS granules [23,33,35].

In Figure 6, the diffractograms of CS and PS are shown. The CS has a type A pattern, and the PS is consistent with a type B pattern. In the diffraction patterns of CS (Figure 6b), there are peaks at 15.2°, 17.4°, 18.0°, 19.9° and 26.7°, characteristic of a crystalline structure of double helixes forming a cell monoclinic unitary type [23,27,33,36,37]. The peaks between 15.0° and 23.0° are related to the amylose content and the degree of crystallinity of the starch granules [23,27,33,36,37]. For the PS diffractogram (Figure 6a), peaks at 5.7°, 15.2°, 17.1°, 19.9°, 22.2°, and 24.1° appear and are characteristic of this tuber indicative of a hexagonal symmetry due to the hydrated double helix of amylopectin [33,36]. The peak at 5.7° suggests a more hydrated and open structure of the polymorphism type [23,27,33,36,37]. In addition, PS has semicrystalline starch granules because a part of the structure consists of amylopectin, and the other part is related to the amorphous crystalline structure of starch (between 25° and 35°) [33,36].

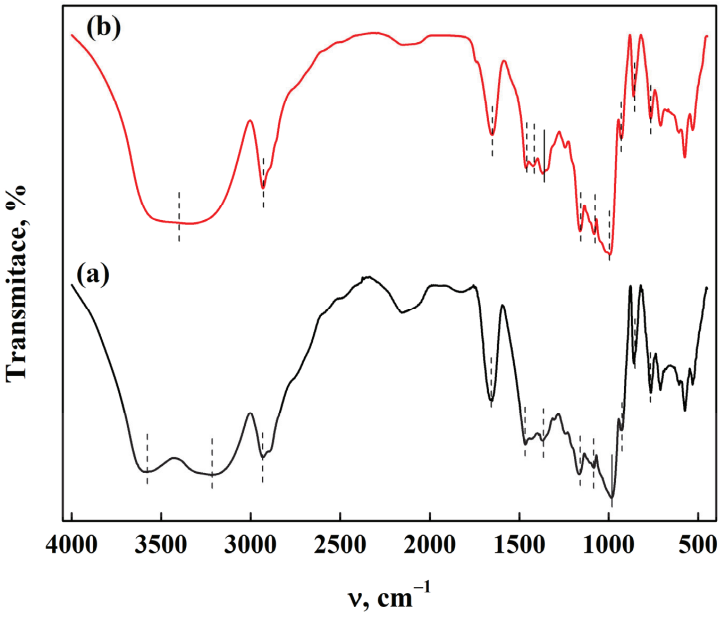

Figure 4. ATR-FTIR characterization of starch from (**a**) potato and (**b**) corn.

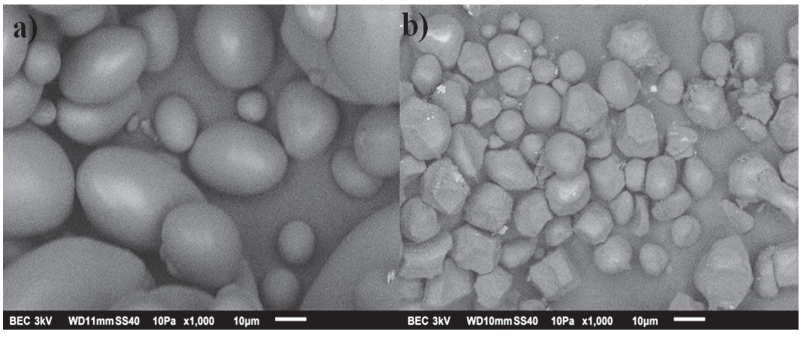

Figure 5. SEM images of starch from (**a**) potato and (**b**) corn.

PS and CS have similarities and differences in their structure, observed by ATR-FTIR, SEM, and XRD analysis. This characterization allowed the selection of starch to obtain a BP with better features [10–13]. Based on this analysis, the most suitable choice is CS to elaborate the BP with the designated plasticizers (glycerol, cellulose, and sorbitol).

3.3. Manufacture of the Bioplastics (BPs)

For the elaboration of the bioplastic from the NM, CS was added in the proportions shown in Table 1. The resulting bioplastics from these combinations can be seen in Figure 7. In experiments 1, 2, and 4, the bioplastics are almost transparent with a weak adhesion and brittle texture. In test 7, a high presence of humidity caused less malleability and resistance to the tension of the bioplastic. In test 6, the bioplastic presented good hardness, rigidity, resistance, and low malleability, which are not desired features for a bioplastic [2,3,5,28,34]. The properties of the BP discussed so far are not the most appropriate complicating its implementation in the medical industry, specifically in the case of threads for medical use. Furthermore, the BP obtained in experiments 3 (E3) and 5 (E5) had the appropriate malleability, adhesion, and elasticity. These characteristics are essential when the bioplastic is considered for surgical thread use [2,3,5,28].

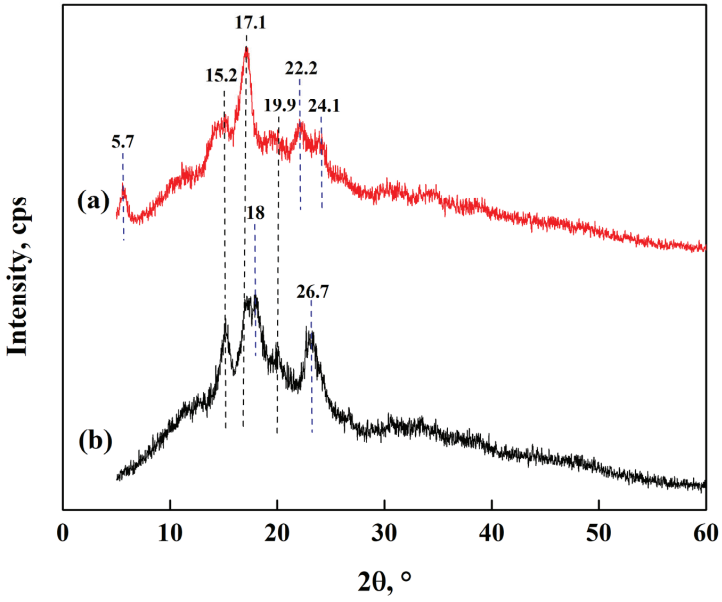

Figure 6. XRD patterns of starch from (**a**) potato and (**b**) corn.

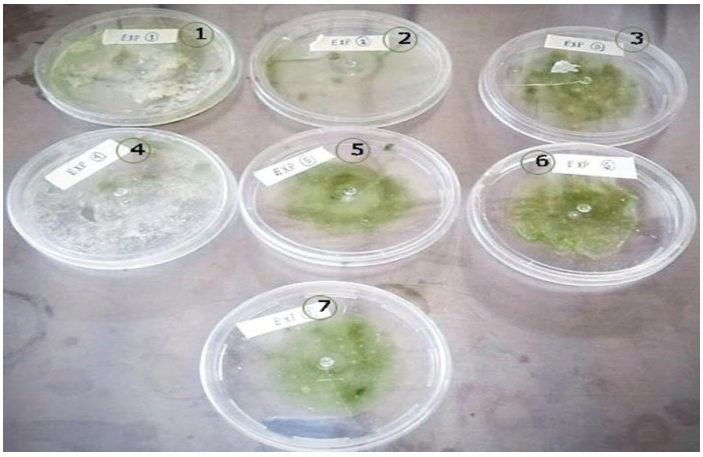

Figure 7. Images of the BP prepared with NM, CS, and glycerol at different proportions and dried at 40 °C for 24 h. The label number corresponds to the experiment number in Table 1.

The bioplastics with unfavorable characteristics for surgical thread manufacture are due to the hydrophilic nature of the starch-containing films, which causes a fragile appearance due to weak intermolecular forces [27,38]. In the elaboration of the polymeric films from NM, glycerol, and starch, as the concentration of the plasticizer rose, the solubility of the biofilm increased. According to the properties required for a surgical thread mentioned in the literature, the bioplastics E3 and E5 had the best characteristics; nonetheless, the thermoplastic properties of the CS and NM film still need to be improved to obtain a more appropriate BP for its application in wound suturing [2,3,5,28,35]. Thus, a plasticizer was added to promote molecular disruption or interruption, triggering film flexibility by reducing the internal hydrogen bonds in the polymer chains while increasing the space between the molecules [27,39].

3.4. Analysis of Solubility in Solvents

The mechanical resistance of bioplastics is studied by analyzing the polymeric degradation of the material by processes including hydrolytic agents [3,40,41]. Here, the decomposition of the polymer chains of the bioplastics was examined by hydrolysis of the amide bonds. To accomplish this, the resulting bioplastics of experiments 3 and 5 (E3 and E5) were placed in contact with different solvents (Figure 8) at room temperature for 12 h. With this, the mechanical behavior was investigated.

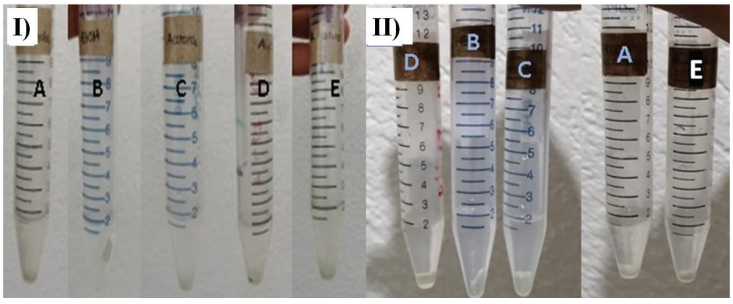

Figure 8. Tests conducted to explore the solubility of the biofilm, (**I**) E3 and (**II**) E5 after 12 h of contact with different solvents at 25 °C. Solvents: (**A**) distilled water, (**B**) ethyl alcohol, (**C**) acetone, (**D**) hydrochloric acid, and (**E**) acetic acid.

Table 3 contains the results of the solubility of the biofilm. The manufactured bioplastics E3 (B1) and E5 (B2) had high resistance to solubility in ethyl alcohol; on the other hand, the bioplastic was dissolved entirely in acetic acid. With these results, it is possible to mention that the biofilm solubility increases as follows: ethyl alcohol > acetone > hydrochloric acid > water > acetic acid. The depolymerization occurring in the biofilms was due to the hydrolysis reaction (breaking of hydrogen bonds) between the polar groups of the amide ester or urethane bonds of the polymer chains [4,40–43].

Table 3. Comparison of the bioplastic solubility with different solvents.

Solvent	Solubility	
	B1	**B2**
(**A**) Distilled water	Completely soluble	Completely soluble
(**B**) Ethyl alcohol	Insoluble	Insoluble
(**C**) Acetone	Slightly soluble	Slightly soluble
(**D**) Hydrochloric acid (0.1 M)	Completely soluble	Slightly soluble
(**E**) Acetic acid (0.1 M)	Highly soluble	Highly soluble

To know which of the two bioplastics is a better choice during the elaboration of surgical thread, measurements of water solubility were conducted. The bioplastic solubility with water is an important property to measure in biodegradable films since some applications of these materials require the preservation of the integrity and resistance to corrosion. The percentage of water solubility for each bioplastic is listed in Table 4. A lower solubility was observed in B2 with water and solvents (except for acetic acid); therefore, it is considered suitable for surgical thread applications.

When comparing our bioplastics solubility results in water, the literature has reported similar values (between 23.20 and 33.37%) with different starch sources. Several studies have reported the water solubility of bioplastics containing glycerol and starch of different origins, such as cassava, wheat, potato, corn, and yam, with solubility values of 24%, 30.2–33.2%, 33.88%, 34.37%, and 32%, respectively. In other studies, the obtained bioplastics used sorbitol and starch extracted from sugar palm, mango, and rice seeds, obtaining a solubility of 31.56 to

37.05%, 29.12 to 37.05%, and 24.70 to 31.60%, correspondingly [4,10,40–43]. The presence of sorbitol as a plasticizer in the bioplastic increases the solubility and diffusion in water because it changes the mobility chain and makes the polymeric matrix more flexible [4]. Hence, the solubility of the bioplastic containing glycerol, sorbitol, starch, and NM obtained in this study presents a suitable solubility for consideration in thread manufacture for medical applications.

Table 4. Experimental results of water solubility of the manufactured bioplastics.

Bioplastic	Initial Weight (g)	Initial Dry Weight (W_{ds}; g)	Final Dry Weight (W_{df}; g)	Solubility (%)
B1	0.367	0.347	0.110	68.30
B2	0.253	0.170	0.118	30.59

3.5. Mechanical Properties of Bioplastics

The analysis of the breaking or bending stress (σi) and Young's modulus (Ei) performed on B1 and B2 is shown in Table 5. It was observed that B2 has a bending greater than B1. This indicates that there are structural changes in bioplastics due to the formation of agglomerates between the protein and amylase/pectin, which can decrease the plasticization of the biopolymer and reduce the mechanical resistance of the material [44]. It was also observed that the bending of the bioplastic depends directly on the pressure applied to the material. The results of the Young's modulus of the bioplastics (Table 5) indicate that B2 has a greater capacity to resist the stresses that can deform it, which would prevent it from breaking when handled. Bioplastics obtained with materials of natural origin with glycerol and starch have been reported in the literature, where it is mentioned that this behavior may be due to the adherence of the materials that make up the bioplastic due to its manufacturing process that favors its mechanical resistance [43,45,46]. Based on the results obtained from the bioplastic prototypes obtained, B2 is the best option to produce the thread because it presents greater resistance to traction, tension, and bending, and it must have a lower solubility in water.

Table 5. Mechanical properties of bioplastics.

Bioplastic	σ_F, MPa	E_F, MPa	σ_T, MPa	E_T, MPa
B1	2.71	278.4	1.87	340.1
B2	4.12	333.2	3.97	373.2

3.6. Preparation of BP with Starch from Different Sources

Another relevant factor in the manufacture of surgical thread is the origin of the starch, the basis of the bioplastic, given that this source determines the size and shape of the granules, originating modifications of some functional and nutritional properties [19,36]. Figure 9 shows the resulting bioplastics made with starch from different sources of origin. The bioplastic with the best perceptible physical properties was prepared with CS, followed by SAPS. This behavior is due to the shape of the starch granules, which depends directly on the structure of the amylopectin ramification since amylopectin can have long chains with few branches (large granules) and short chains with several branches (small granules) [23,34]. There are reports in the literature stating that corn starch granules have a smaller size than potato starch (ratio 1:4); in addition, the shape of the granules is very different since corn has a polygonal shape and potato starch a spherical oval shape [23].

The plasticizer can be related to structural modifications of the resulting network between the starch and NM. The films become denser when the plasticizer concentration is decreased [4,27]. Lower plasticizer concentration hinders the movement of the polymeric chains, increasing the solubility of the biofilm. Glycerol has been used as a plasticizer for starch biofilms due to its compatibility with amylose, improving the mechanical properties of the biofilm by directly interfering with the ordering of amylose. This arrangement

reduces intermolecular forces [4,27,41–43] due to the hydroxyl groups (–OH) in its structure, allowing glycerol to join through hydrogen bonds with the starch chains, completing their order and avoiding the fragility of the biofilm [42]. During the synthesis of BP, the most commonly used plasticizer is glycerol [4,27,39]; however, with sorbitol, better mechanical resistance to the obtained film is conferred since its moisture content is lower compared with the formed films with glycerol [42]. In the elaboration of BP with sorbitol, an increase in the resistance of the biomaterial is found when mechanical stress is applied, suggesting that sorbitol concentration in the bioplastic should be high to obtain a thread for medical applications [4,27,42].

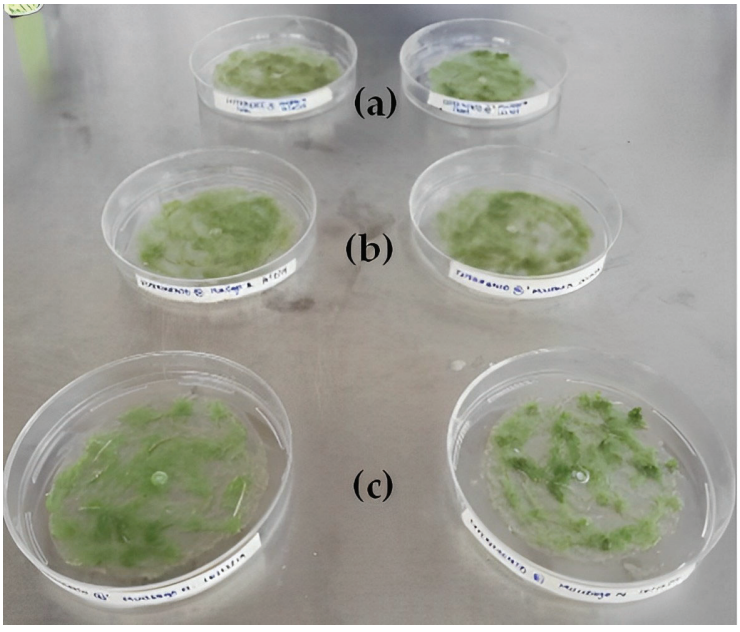

Figure 9. Bioplastic production using different starch sources (**a**) SAPS, (**b**) CS, and (**c**) BAPS.

3.7. Preparation of Surgical Thread with Different Plasticizers

The manufacture of thread with the proposed methodology (Table 2) resulted in materials with different characteristics. In the resulting prototypes with SAPS, the materials contained high humidity and viscosity. The excessive water in these materials was hard to remove by drying (at low or high temperatures) or increasing the evaporation time; hence, the materials were discarded. The thread prototypes made from the bioplastic with CS, sorbitol, and different cellulose concentrations (Figure 10a) showed greater tensile strength and consistency (1) when adding the same amount of sorbitol to the mixture (0.58 wt%). In another prototype (2), where the amount of cellulose was increased (0.97 wt%) while maintaining the sorbitol amount in the mixture, the threads had greater flexibility and moisture. For the last prototype (3), the amount of cellulose was 1.93 wt% (twice as much as prototype 2), and these threads were more rigid; nevertheless, the tensile strength diminished. These results suggest that with an increment in cellulose concentration of the mixture, the resulting material is more flexible and humid. However, if the cellulose concentration is higher than 0.97 wt%, resistance to mechanical stress is lost, and the thread becomes hard.

The prototypes made without sorbitol (Figure 10b) and different cellulose concentrations (1.93 wt%, 2.90 wt%, and 3.89 wt%) with CS presented different characteristics in terms of cellulose content since there is better consistency and resistance to tension in the prototype thread (1). In the other prototype (3), the cellulose concentration varied from 1.93 wt% to 2.9 wt%, and better texture and malleability were observed. Finally, when

the cellulose concentration was 3.89 wt%, the thread prototype (2) presented fragility in its structure. Based on the USP classification, which is based on suture diameter, knot security, and the nature of the suture material structure, among other properties, threads manufactured with different concentrations of sorbitol and cellulose can be considered suture material, suture USP 4 (diameter between 0.7 and 0.79 mm) [45–47].

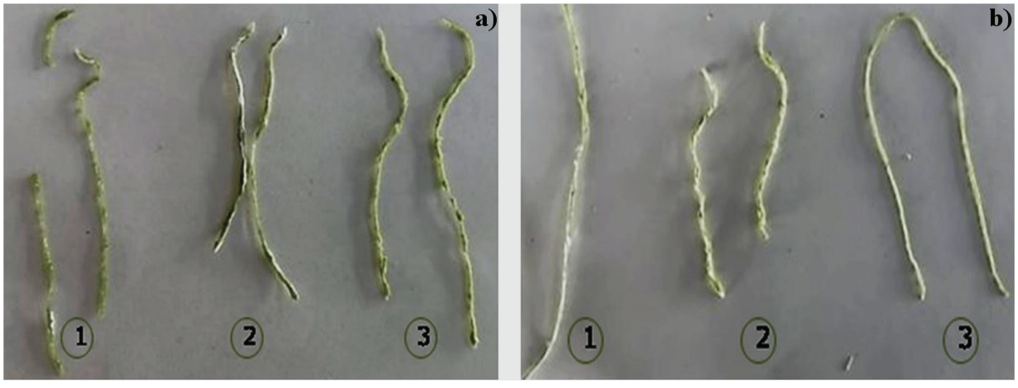

Figure 10. Manufacture threads with CS and cellulose: (**a**) with sorbitol and (**b**) without sorbitol. (1) Cellulose 0.58 wt%, (2) Cellulose 0.97 wt% and (3) Cellulose 1.93 wt%.

Based on the results, the thread prototypes require the presence of sorbitol and cellulose. Nevertheless, after a given value of cellulose concentration, it should not be increased since the flexibility, hardness, and solubility become inadequate. Therefore, the cellulose in the threads should be less than 0.58 wt%. Another three prototypes were manufactured (Figure 11) with CS, 0.58 wt% of sorbitol, and three concentrations of cellulose (0.19 wt%, 0.29 wt%, and 0.39 wt%). By modifying the cellulose concentration, the characteristics of the threads changed. With a higher cellulose concentration, excellent consistency, texture, malleability, and tensile strength were obtained (1). Decreasing the cellulose concentration by half, the thread presented greater flexibility with good elongation capacity (2). When having a concentration greater than 50% of the initial, a thread with greater rigidity, low malleability, and little resistance to the tension was obtained.

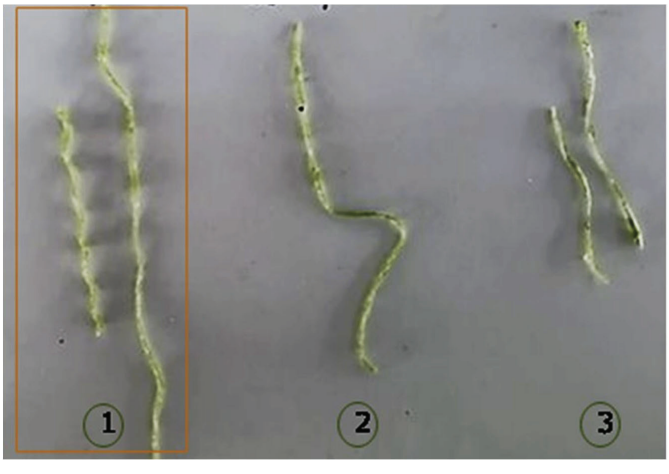

Figure 11. Manufacture of thread with sorbitol, cellulose, and CS. (1) Cellulose 0.19 wt%, (2) Cellulose 0.29 wt% and (3) Cellulose 0.39 wt%. The best thread is marked in the square.

The thread prototypes that presented the best physical properties and good mechanical characteristics were obtained with 5.03 wt% corn starch, 19.34 wt% mucilage, 0.58 wt% sorbitol, 0.97 wt% cellulose, and 9.67 wt% glycerol in 64.41 wt% in water. Moreover, the thread formed a monofilament suture; having multifilament saturation in the thread is not desired due to the passage of microorganisms being favored [3,42]. Moreover, a monofilament suture benefits the healing process of wounds by having less rigidity and fragility, avoiding loss of tension, and being an absorbable biological thread; these are necessary features in medical applications [3,39,42,43]. The selected surgical thread prototype complies with most of the characteristics mentioned, except for good tensile strength or toughness. To avoid this, sorbitol and cellulose were employed as a plasticizer in the surgical thread synthesis.

Currently, natural cellulose fibers are mainly used for internal gastric sutures. They are characterized by gaining tensile strength when wet, losing between 50% of their tensile strength at six months, and retaining between 30 wt% and 40 wt% at two years [5,42]. Moreover, biological characteristics such as bacterial adherence and tissue reaction, or histocompatibility, were considered for the selection of biopolymers and type of thread [3, 34,35]; considering that the bioplastic obtained for the elaboration of the thread is of organic origin (NM), it is expected that it will not have an adverse reaction in the patient [3,34,35].

The physicochemical, functional, and rheological differences between cereal and fruit starches (in this research cereal starch was employed) are due to their different size, shape, and crystalline arrangement, the reason for which they can have diverse applications. Cereal starch presents a better alternative to making bioplastics or solid materials, while fruit starch works better for making gels or emulsifiers. Regarding the prototype thread and the possibility for biomedical use (suture thread), there is still a need to improve the tensile strength or use some class of coating (wax or paraffin) to prevent the tendency to desquamation (release of suture particles in the wound), or adding chitin, since it contributes with advantages for healing wounds (accelerated healing).

4. Conclusions

In this study, the extraction of NM was carried out using ethyl alcohol as a solvent; the experimental conditions allowed us to obtain a 50% higher yield than the yields reported in the literature. The bioplastics obtained were based on NM, CS, and glycerol as the plasticizer. The variation in concentration of NM and CS resulted in eight prototypes. From these, B1 and B2 have the appropriate characteristics for consideration in surgical thread manufacture. The resistance to solvents and solubility with water of these biopolymeric films (B1 and B2) were also analyzed, showing a lower degradation and solubility for B2 when compared to B1. Therefore, the concentrations of the base reagents (starch, glycerol, and mucilage) were similar to B2, and the incorporation of cellulose and sorbitol was studied for surgical thread synthesis. The thread prototype that presented the best physical properties (tensile strength and flexibility for good handling) was obtained using 5.03 wt% corn starch, 19.34 wt% mucilage, 0.58 wt% sorbitol, 0.97 wt% cellulose, and 9.67 wt% glycerol in 64.41 wt% distilled water. Compared to other prototypes reported in the literature, a surgical thread with uniform diameter, good elasticity, and low capillarity was obtained. In addition, the fact that its components are inert materials reduces the probability of an allergic reaction by the patient. These results indicate that it is possible to perform in vitro and in vivo tests with the obtained thread to evaluate its biocompatibility and viability in medical applications.

Author Contributions: Conceptualization, writing—original draft preparation, E.H.-I. and J.A.H.; methodology, O.J.S.-M. and J.A.H.; formal analysis, J.A.H., J.P.R.-L., O.J.S.-M. and M.S.-H.; investigation, J.A.H., A.T.-L. and J.P.R.-L.; writing—review and editing, R.H.-S. All authors have read and agreed to the published version of the manuscript.

Funding: This research was funded by Secretaría de Investigación y Posgrado, Instituto Polo (project SIP: 20210475) of the Instituto Politécnico Nacional (IPN).

Institutional Review Board Statement: Not applicable.

Data Availability Statement: The data presented in this study are available on request from the corresponding author.

Acknowledgments: The researchers want to thank UPIIG-IPN and Laboratorio de Investigación y Caracterización de Minerales y Materiales (LICAMM UG).

Conflicts of Interest: The authors declare no conflict of interest.

Sample Availability: Samples of the materials are not available from the authors.

References

1. Dassanayake, R.S.; Acharya, S.; Abidi, N. Biopolymer-based materials from polysaccharides: Properties, processing, characterization and sorption applications. In *Advanced Sorption Process Applications*; Edebali, E., Ed.; IntechOpen: England, UK, 2019; pp. 1–25. [CrossRef]
2. Ferreira-Filipe, D.A.; Paço, A.; Duarte, A.C.; Rocha-Santos, T.; Patrício Silva, A.L. Are Biobased Plastics Green Alternatives?—A Critical Review. *Int. J. Environ. Res. Public Health* **2021**, *18*, 7729. [CrossRef] [PubMed]
3. Tajirian, A.; Goldberg, D. A Review of sutures and other skin closure materials. *J. Cosmet. Laser Ther.* **2010**, *12*, 296–302. [CrossRef] [PubMed]
4. Nawab, A.; Alam, F.; Hasnain, A. Biodegradable film from mango kernel starch: Effect of plasticizers on the physical, barrier, and mechanical properties. *Starch* **2016**, *68*, 919–928. [CrossRef]
5. Baranwal, J.; Barse, B.; Fais, A.; Delogu, G.L.; Kumar, A. Biopolymer: A Sustainable Material for Food and Medical Applications. *Polymers* **2022**, *14*, 983. [CrossRef] [PubMed]
6. Marques, A.P.; Reis, R.L.; Hunt, J.A. The biocompatibility of novel starch-based polymers and composites: In vitro studies. *Biomaterials* **2002**, *23*, 1471–1478. [CrossRef]
7. Olmo, N.; Martin, A.I.; Salinas, A.J.; Turnay, J.; Vallet-Regi, M.; Lizarbe, M.A. Bioactive sol-gel glasses with and without a hydroxycarbonate apatite layer as substrates for osteoblast cell adhesion and proliferation. *Biomaterials* **2003**, *24*, 3383–3393. [CrossRef]
8. Rossi, M.; Taboada-Liceaga, H.A.; Garcia-Mazcorro, J.F.; Gill, S.; Amieva-Balmori, M.; Hernández-Ramírez, G.A.; Whelan, K.; Remes-Troche, J.M. Fibre from nopal cactus (*Opuntia ficus-indica*) improves symptoms in irritable bowel syndrome in the short term: A pilot randomised-controlled trial. *Proc. Nutr. Soc.* **2020**, *79*, E13. [CrossRef]
9. Lee, C.H.; Singla, A.; Lee, Y. Biomedical applications of collagen. *Int. J. Pharm.* **2001**, *221*, 1–22. [CrossRef]
10. Farahnaky, A.; Saberi, B.; Majzoo, M. Bieffect of glycerol on physical and mechanical properties of wheat starch edible films. *J. Text. Stud.* **2013**, *44*, 176–186. [CrossRef]
11. Luangapai, F.; Peanparkdee, M.; Iwamoto, S. Biopolymer films for food industries: Properties, applications, and future aspects based on chitosan. *Rev. Agric. Sci.* **2019**, *7*, 59–67. [CrossRef]
12. Yadav, P.; Yadav, H.; Shah, V.G.; Shah, G.; Dhaka, G. Biomedical biopolymers, their origin and evolution in biomedical sciences: A systematic review. *J. Clin. Diag. Res.* **2015**, *9*, ZE21–ZE25. [CrossRef]
13. Habig McHugh, T.; Krochta, J.M. Sorbitol- vs Glycerol-Plasticized Whey Protein Edible Films: Integrated Oxygen Permeability and Tensile Property Evaluation. *J. Agric. Food Chem.* **1994**, *42*, 841–845. [CrossRef]
14. Delgado Hernández, J.L.A.; Jaquelina González Castañeda, J. El nopal de verdura en Guanajuato. Caso cooperativa pronopval scl. Valtierrilla, Salamanca, Gto. *Rev. Mex. Agronegoc.* **2005**, *IX*, 450–462.
15. Espino-Díaz, M.; Ornelas-Paz, J.; Martínez-Téllez, M.; Santillán, C.; Barbosa-Cánovas, G.; Zamudio-Flores, P.B.; Olivas, G.I. Development and Characterization of Edible Films Based on Mucilage of *Opuntia ficus-indica* (L.). *J. Food Sci.* **2010**, *75*, 347–352. [CrossRef]
16. Pires, C.; Ramos, C.; Teixeira, G.; Batista, I.; Mendes, R.; Nunes, L.; Marques, A. Characterization of biodegradable films prepared with hake proteins and thyme oil. *J. Food Eng.* **2011**, *105*, 422–428. [CrossRef]
17. Sepúlveda, E.; Sáenz, C.; Aliaga, E.; Aceituno, C. Extraction and characterization of mucilage in *Opuntia* spp. *J. Arid Environ.* **2007**, *68*, 534–545. [CrossRef]
18. Rivera-Cañón, A.F.; Hernández-Carrillo, C.G.; Gómez-Cuaspud, J.A. Evaluation of physicochemical properties of Nopal (*Opuntia ficus-Indica*) as bio coagulant-flocculant for water treatment. *IOP J. Phys. Conf. Ser.* **2021**, *2046*, 012057. [CrossRef]
19. Hernández-Carrillo, C.G.; Gómez-Cuaspud, J.A.; Martínez-Suarez, C.E. Compositional, thermal and microstructural characterizatiof the Nopal (*Opuntia ficus indica*), for addition in commercial cement mixtures. *IOP J. Phys. Conf. Ser.* **2017**, *935*, 012045. [CrossRef]
20. Pascoe-Ortiz, S. Mezcla y Proceso, Para Elaborar un Material Plástico Biodegradable. IMPI Patente WO 2016/093685, 16 June 2016.
21. Velasco-Aquino, A.A.; Espuna-Mujica, J.A.; Perez-Sanchez, J.F.; Zuñiga-Leal, C.; Palacio-Perez, A.; Suarez-Dominguez, E.J. Compressed earth block reinforced with coconut fibers and stabilized with aloe vera and lime. *J. Eng. Des. Technol.* **2021**, *19*, 795–807. [CrossRef]
22. Amari, A.; Alalwan, B.; Eldirderi, M.M.; Mnif, W.; Rebah, F.B. Cactus material-based adsorbents for the removal of heavy metals and dyes: A review. *Mater. Res. Express* **2020**, *7*, 012002. [CrossRef]

23. Aquilina, A.; Borg, R.P.; Buhagiar, J. The application of Natural Organic Additives in Concrete: *Opuntia ficus-indica*. *IOP Conf. Ser. Mater. Sci. Eng.* **2018**, *442*, 012016. [CrossRef]
24. Casarrubias-Castillo, M.G.; Méndez-Montealvo, G.; Rodriguez-Ambriz, S.L.; Sánchez-Rivera, M.M.; Bello-Pérez, L.A. Structural and Rheological differences between fruit and cereal starches. *Agrociencias* **2012**, *46*, 455–466.
25. Del Valle, V.; Hernández, P.; Guarda, A.; Galotto, M. Development of a cactusmucilage edible coating (*Opuntia ficus indica*) and its application to extend strawberry (*Fragaria ananassa*) shelf-life. *Food Chem.* **2005**, *91*, 751–756. [CrossRef]
26. León-Martínez, F.M.; Rodríguez-Ramírez, J.; Medina-Torres, L.L.; Méndez Lagunas, L.L.; Bernad-Bernad, M.J. Effects of drying conditions on the rheological properties of reconstituted mucilage solutions (*Opuntia ficus-indica*). *Carbohydr. Polym.* **2011**, *84*, 439–445. [CrossRef]
27. Salinas-Salazar, V.M.; Trejo-Márquez, M.A.; Lira-Vargas, A. Propiedades físicas, mecánicas y de barrera de películas comestibles a base de mucílago de Nopal como alternativa para la aplicación en frutos. *Rev. Iberoam. Tecnol. Postcosecha* **2015**, *16*, 193–198.
28. Ballesteros-Mártinez, L.; Pérez-Cervera, C.; Andrade-Pizarro, R. Effect of glycerol and sorbitol concentrations on mechanical, optical, and barrier properties of sweet potato starch film. *NFS J.* **2020**, *20*, 1–9. [CrossRef]
29. Vargas, L.; Figueroa, G.A.; Méndez, C.H.H.; Nieto, A.P.; Vieyra, M.I.G.; Núñez, J.R.R. Propiedades físicas del mucílago de nopal. *Acta Univ.* **2016**, *26*, 8–11. [CrossRef]
30. Naod, G.; Tsige, G.M. Comparative physico-chemical characterization of the mucilages of the two cactus pears (*Opuntia* spp.) obtained from Mekelled northern, Ethiopia. *J. Biomater. Nanobiotechnol.* **2012**, *3*, 79–86. [CrossRef]
31. Joaquín-Medina, E.; Patiño-Saldivar, L.; Ardilas, A.A.A.; Salazar-Hernández, M.; Hernández, J.A. Bioadsorption of methyl orange and methylene blue contained in water using as bioadsorbent natural brushite (nDCPD). *Tecnol. Cienc. Agua* **2021**, *12*, 304–357. [CrossRef]
32. Abdullah, A.H.D.; Chalimah, S.; Primadona, I.; Hanantyo, M.G.H. Physical and chemical properties of corn, cassava, and potato starchs. *IOP Conf. Ser. Earth Environ. Sci.* **2018**, *160*, 012003. [CrossRef]
33. Rodríguez-Pineda, L.M.; Muñoz-Prieto, E.J.; Rius-Alonso, C.A.; Palacios-Alquisira, J. Preparation and Characterization of Potato Starch Microparticles with Acrylamide by Microwave Radiation. *Cienc. Desarro.* **2018**, *9*, 149–159. [CrossRef]
34. Jane, J.; Chen, Y.Y.; Lee, L.F.; McPherson, A.E.; Wong, K.S.; Radosavljevic, M.; Kasemsuwan, T. Effects of Amylopectin Branch Chain Length and Amylose Content on the Gelatinization and Pasting Properties of Starch. *Cereal Chem.* **1999**, *76*, 629–637. [CrossRef]
35. Dong, S.; Fang, G.; Luo, Z.; Gao, Q. Effect of granule size on the structure and digestibility of jackfruit seed starch. *Food Hydrocoll.* **2021**, *120*, 106964. [CrossRef]
36. Hernando-Pardo, O.C.; Castañeda, J.C.; Ortiz, C.A. Caracterización estructural y térmica de almidones provenientes de diferentes variedades de papa. *Acta Agronómi.* **2013**, *62*, 289–295.
37. Agama-Acevedo, E.; Ottenhof, M.-A.; Farhat, I.A.; Paredes-López, O.; Ortíz-Cereceres, J.; Bello-Pérez, L.A. Isolation and characterization of starch from pigmented maizes. *Agrociencia* **2005**, *39*, 419–429.
38. Lourdin, D.; Della Valle, G.; Colonna, P. Influence of amylase content on starch films and foams. *Carbohydr. Polym.* **1995**, *27*, 261–270. [CrossRef]
39. Mali, S.; Sakanaka, L.S.; Yamashita, F.; Grossmann, M.V.E. Water sorption and mechanical properties of cassava starch films and their relation to plasticizing effect. *Carbohydr. Polym.* **2005**, *60*, 283–289. [CrossRef]
40. Bastioli, C. Starch-polymer composites. In *Degradable Polymers*; Scott, G., Ed.; Springer: Dordrecht, The Netherlands, 2002. [CrossRef]
41. Vieira, M.G.A.; da Silva, M.A.; dos Santos, L.O.; Beppu, M.M. Natural-based plasticizers and biopolymer films: A review. *Eur. Polym. J.* **2011**, *47*, 254–263. [CrossRef]
42. Gacen, J.; Cayuela, D. Solubilidad diferencial de las fibras químicas de celulosa. *Rev. Química Ind. Téxt.* **2010**, *199*, 8–12.
43. Navia-Porras, D.P.; Bejarano-Arana, N. Evaluation of physical properties of thermopressing bioplastics made from cassava flour. *Biotecnol. Sect. Agropecu. Agroind.* **2014**, *12*, 40–48.
44. González, J.; Partal, P.; García, M.; Gallegos, C. Effect of processing on the viscoelastic, tensile and optical properties of albumen/starch-based bioplastics. *Carbohydr. Polym.* **2011**, *84*, 308–315. [CrossRef]
45. Luo, X.; Li, J.; Lin, X. Effect of gelatinization and additives on morphology and thermal behavior of corn starch/PVA blend films. *Carbohydr. Polym.* **2012**, *90*, 1595–1600. [CrossRef] [PubMed]
46. Smeak, D.D. Chapter 1: Selection and use of currently available suture materials and needles. In *Current Techniques in Small Animal Surgery*, 5th ed.; Bojrab, M.J., Ed.; Teton NewMedia: Philadelphia, PA, USA, 2014; pp. 1–11.
47. Chu, C.C. Chapter 19: Textile-based biomaterials for surgical applications. In *Polymeric Biomaterials*, 2nd ed.; Dumitriu, S., Ed.; CRC Press: New York, NY, USA, 2001; pp. 1–54.

polymers

MDPI

Article

Novel and Facile Colorimetric Detection of Reducing Sugars in Foods via In Situ Formed Gelatin-Capped Silver Nanoparticles

Reda M. El-Shishtawy [1,*], Yasser M. Al Angari [1], Maha M. Alotaibi [1] and Yaaser Q. Almulaiky [2]

[1] Chemistry Department, Faculty of Science, King Abdulaziz University, Jeddah 21589, Saudi Arabia
[2] Department of Chemistry, College of Science and Arts at Khulis, University of Jeddah, Jeddah 21921, Saudi Arabia
* Correspondence: relshishtawy@kau.edu.sa or elshishtawy@hotmail.com

Abstract: The evolution of green technology for the simple and ecological formation of silver nanoparticles (AgNPs) inspired the present work for simple and efficient detection of reducing sugars (RS) in foods. The proposed method relies on gelatin as the capping and stabilizing agent and the analyte (RS) as the reducing agent. This work may attract significant attention, especially in the industry, for testing the sugar content using gelatin-capped silver nanoparticles as it not only detects the sugar in food, but also determines the content (%), which could be an alternative technique to the conventionally used DNS colorimetric method. For this purpose, a certain amount of maltose was mixed with a gelatin-silver nitrate. Different conditions that may affect the color changes at 434 nm owing to the in situ formed AgNPs, such as gelatin-silver nitrate ratio, PH, time, and temperature, have been investigated. The 1:3 mg/mg ratio of gelatin-silver nitrate dissolved in 10 mL distilled water was most effective in color formation. The development of AgNPs color increases within 8–10 min at PH 8.5 as the selected optimum value and at the optimum temperature of 90 °C for the evolution of the gelatin-silver reagent's redox reaction. The gelatin-silver reagent showed a fast response (less than 10 min) with a detection limit for maltose at 46.67 μM. In addition, the selectivity of maltose was checked in the presence of starch and after its hydrolysis with α-amylase. Compared with the conventionally used dinitrosalicylic acid (DNS) colorimetric method, the proposed method could be applied to commercial fresh apple juice, watermelon, and honey to prove its viability for detecting RS in fruits; the total reducing sugar content was 287, 165, and 751 mg/g, respectively.

Keywords: reducing sugar; spectrophotometry; gelatin-AgNPs; DNS; maltose; glucose

Citation: El-Shishtawy, R.M.; Al Angari, Y.M.; Alotaibi, M.M.; Almulaiky, Y.Q. Novel and Facile Colorimetric Detection of Reducing Sugars in Foods via In Situ Formed Gelatin-Capped Silver Nanoparticles. *Polymers* **2023**, *15*, 1086. https://doi.org/10.3390/polym15051086

Academic Editors: Cornelia Vasile, Gabriel Aguirre-Álvarez and Xiao-Feng Sun

Received: 31 December 2022
Revised: 19 February 2023
Accepted: 20 February 2023
Published: 21 February 2023

1. Introduction

Carbohydrases (glycoside hydrolases or *O*-glycosidases) are a significant class of enzymes that hydrolyze polysaccharides and low-molecular-weight glycosides. They belong to the hydrolase family of enzymes. Amylase, cellulases, xylanases, mannanases, pectinases, chitinases, and other carbohydrases are categorized according to their selectivity toward natural glycoside substrates. In biotechnology, many carbohydrates have found extensive applications [1]. The majority of carbohydrase activity measurement techniques depend on the examination of reducing sugars (RS) generated as a result of the enzymatic cleavage of a glycosidic bond between two carbohydrates or between a carbohydrate and a noncarbohydrate component [2,3]. In addition to performing particular roles in vital processes, carbohydrates are significant macronutrients that function as a primary source of energy in human nutrition [4]. Deoxyribose and ribose in nucleic acids structure, lactose in milk, and galactose in some oils are a few examples. The four categories of carbohydrates are monosaccharides, disaccharides, oligosaccharides, and polysaccharides. Free-form monosaccharides and disaccharides are commonly referred to as sugars, and depending on how they react chemically, they can be divided into reducing and non-reducing sugars [5]. Sugars are a marker for several nutritional qualities, including flavor, naturalness, and taste [6]. Reducing sugar is essential for biological samples, such as tissue,

blood, plasma, and serum. European law regulates the sugar level of some products and beverages [7]. Since sugars are known to be crucial in developing severe diseases (such as obesity and diabetes), determining their identity is a complex analytical challenge. Sugar measurement is required in several intricate biological systems and food and beverage matrices. Soft drinks with added sugar should be given extra attention because they are the primary source of calories in the American diet and raise the risk of obesity [8]. Advanced analytical methods for determining carbohydrate concentrations have been developed as a result of the wide variety of carbohydrates present in these areas, including capillary electrophoresis [9], chromatography [10], infrared (IR) spectroscopy [11], nuclear magnetic resonance (NMR) spectroscopy [12], and light scattering detection [13]. These techniques demand a substantial financial investment, sophisticated analytical abilities, and effort. The colorimetric method, based on a redox reaction in which a reducing sugar acts as the reductant and the reagent as the oxidant leading to the production of color that could be measured by the spectrophotometric method, is one of the most flexible, reasonably simple, and affordable methods for determining reducing sugar. Different techniques for evaluating RS have been used in carbohydrate activity estimations. The Somogyi–Nelson [2], phenol-sulfuric acid [14], anthrone-sulfuric acid [15], Fehling [16], and dinitrosalicylic acid (DNS) [17] methods were evaluated for the determination of RS. The Fehling approach involves several analysis steps (including precipitation and titration). The phenol–sulfuric acid method has a variety of significant limitations. Multiple health risks are associated with phenol employed in this approach. The prolonged or repeated inhalation of phenol fumes brings on lung edema. Long-term phenol exposure seriously impacts the central nervous system [18]. The Nelson–Somogyi assay and the 3,5-dinitrosalicylic acid (DNS) assay described are the most popular methods used by many researchers. Although the DNS assay is known to be approximately 10 times less sensitive than the Nelson–Somogyi assay and it does not provide stoichiometric data with oligosaccharides, giving significantly higher values of RS than the actual number of hemiacetals reducing groups [19–21], it has been recommended by the International Union of Pure and Applied Chemistry (IUPAC) commission on biotechnology for measuring standard cellulase activities against filter paper and carboxymethylcellulose (CMC) [22]. Our goal was to develop a visible spectrophotometric method for quantifying RS with high sensitivity. We have developed a new and simple method for determining reducing sugar. Gelatin-silver reagent was found to be suitable for the determination of reducing sugar. In previous literature, gelatin-silver nanoparticles were utilized for several purposes. Gelatin-silver nanoparticles were used as antimicrobial composite films [23], and gelatin-silver nanoparticles coating for polycaprolactone was used for wound healing [24]. Composite films made of chitosan/gelatin-silver nanoparticles were used in biodegradable food packaging [25]. Gelatin, an abundant biopolymer, is both biocompatible and biodegradable. It can be extracted from animal tissues such as muscle, bone, and skin. Gelatin is widely employed in pharmaceutical, cosmetics, food, and medical applications due to its natural abundance and inherent biodegradability in physiological conditions [26]. The most common nanoparticles used in food and other industries are silver nanoparticles. A nanoparticle is described as a tiny item or particle that behaves as a whole unit in terms of its transport and properties. Nanotechnology makes use of the fact that when the size of a solid material shrinks, its surface area grows, enhancing its reactivity and quantum-related phenomena. Nanomaterials' physical and chemical characteristics can change dramatically from those of the same substance in its bulk size [27]. Consumer products, food technology, textiles/fabrics, and the medical industries are all interested in silver NP due to its chemical and biological qualities. Silver NP also has special optical and physical characteristics that are not found in bulk silver and are said to offer a lot of potential in medicinal applications [27]. Generally, the formation of nanoparticles such as AgNPs has been made possible ecologically using reducing sugars such as glucose [28–32]. As a capping agent, gelatin in the presence of glucose was used for the green preparation of AgNPs [33]. The appearance of visible color due to the surface plasmon resonance (SPR) of

nanoparticles has caught the attention of many researchers. The AgNPs SPR appear around 400 nm and, thus, could be applied as an analytical tool for detecting grallic acid [34], o-phenylenediamine [35], formaldehyde [36], and RS using Tollens' reagent [37]. Gold nanoparticles were also used for the determination of RS [38].

Given the benefits that AgNPs provide, such as their high SPR across a broad spectrum [39], low cost, and environmentally friendly production, it was intended in this work to exploit the SPR of AgNPs that can be formed via a redox process with RS for its detection in the presence of gelatin as a capping agent for the in situ formed AgNPs.

2. Experimental

2.1. Materials

Silver nitrate, gelatin, maltose, starch, tris(hydroxymethyl)aminomethane, nitric acid, α-amylase from porcine pancreas, and 3,5-dinitrosalicylic acid (DNS) were purchased from Sigma-Aldrich (Saint Louis, MO, USA) and then used as obtained. Watermelon, apple, and honey juice samples were purchased from local market, Jeddah, KSA.

2.2. Effect of Gelatin-Silver Reagent Ratio

To determine the gelatin-silver nitrate ratio for effective color formation, the gelatin-silver nitrate reagent was prepared in 10 mL distilled water at a ratio weight by weight (for example, 100 mg/100 mg for 1:1 ratio) 1:1, 2:1, 1:3, 1:2, and 2:2. The conditions at which the best chemical treatment yield obtained was 1:3 gelatin-silver nitrate. A 1 mL of reaction mixture contained 250 μL maltose (0.1 mM), 250 μL Tris–HNO_3 buffer PH 8.5 (0.2 M) (prepared by 0.2 M of tris(hydroxymethyl)aminomethane then adjust PH by dilute HNO_3 to the appropriate PH), and 500 μL gelatin-silver reagent. The reaction mixture was incubated for 10 min at 90 °C in a boiling water bath before cooling then the absorbance was recorded at 434 nm. The recorded optical density (OD) at 434 nm was used to determine the relative OD (%).

$$\text{Relative OD (\%)} = (OD_x/OD_{max}) \times 100 \quad (1)$$

where OD_{max} is the maximum OD and OD_x is OD for a sample with OD less than the maximum OD.

2.3. Effect of Time

To determine the effect of time on the evolution of color, a 1 mL of reaction mixture contained 250 μL maltose (0.1 mM), 250 μL of 0.2 M Tris–HNO_3 buffer PH 8.5, and 500 μL gelatin-silver reagent (1:3). The reaction mixture was incubated for different times (2–20 min) at 90 °C in a boiling water bath then cooled to room temperature to measure the absorbance at 434 nm. The recorded OD was used to determine the relative OD (%).

2.4. Effect of PH on the Silver-Gelatin Reagent

The following buffers were used to determine the optimal PH, 50 mM Tris–HNO_3 (PH 6.0–8.5). A 1 mL of reaction mixture contained 250 μL maltose (0.1 mM), 250 μL of different Tris–HNO_3 buffers (0.2 M), and 500 μL gelatin-silver reagent (1:3). The reaction mixture was incubated for 10 min at 90 °C in a boiling water bath before cooling then the absorbance was recorded at 434 nm. The recorded OD at 434 nm was used to determine the relative OD (%).

2.5. Effect of Temperature

Different scales (30–90 °C) were applied to the reaction mixture containing 250 μL maltose (0.1 mM), temperature 250 μL of different Tris–HNO_3 buffers, and 500 μL gelatin-silver reagent (1:3) to assess the impact of temperature on the gelatin-silver reagent. The reaction mixture was incubated for 10 min at different temperature scales in a boiling water

bath before cooling then the absorbance was recorded at 434 nm. The recorded OD at 434 nm was used to determine the relative OD (%).

2.6. Maltose Selectivity

The gelatin-silver method was validated as selective toward reducing sugar as follows; in the Eppendorf tube, 185 µL of maltose (0.1 mM) was added to 185 µL of starch (1%) and 125 µL of Tris-HNO_3 buffer (0.2 M, PH 8.5). In another tube, 185 µL of maltose (0.1 mM) was added to 190 µL distilled water and 125 µL Tris-HNO_3 buffer. The third tube contained 185 µL of starch (1%), 190 µL distilled water, and 125 µL Tris-HNO_3 buffer. A volume of 500 µL of gelatin-silver reagent (1:3) was added to all tubes. It was then incubated for 10 min at 90 °C in a boiling water bath and then cooled to room temperature to measure the absorbance at 434 nm.

2.7. Hydrolysis of Starch with α-Amylase

The hydrolysis of starch was carried out using α-amylase to ascertain the impact of gelatin-silver reagent on the reducing sugar content generated by carbohydrase enzymes. Thus, in the Eppendorf tube, 10 units of α-amylase were incubated for 30 min with 0.06, 1.25, and 1.9% starch (1 mL prepared in 50 mM Tris–HNO_3 buffers, PH 7.0) at 37 °C. After that, 1 mL of gelatin-silver reagent (1:3) was added and heat for 10 min at 90 °C to help develop the color. After cooling, the absorbance was recorded at 434 nm. One unit of α-amylase activity was defined as the amount of enzyme producing 1 µmol reducing sugar as maltose per min under the standard assay conditions [17].

2.8. Effect of Maltose Concentration and Detection Limit

Different concentrations of maltose (0.2–1.2 mM) were applied, and OD values were recorded following the reaction condition described above. A sample of different concentrations of maltose, 0.2 M Tris–HNO_3 buffer PH 8.5, and 500 µL gelatin-silver reagent (1:3) was incubated for 10 min at 90 °C in a boiling water bath before cooling. Then the absorbance was recorded at 434 nm ten times to determine the standard deviation from which and the linear relation of maltose concentration versus OD, the limit of detection (LOD), was obtained.

2.9. Real Samples Analysis

Watermelon, apple, and honey juice samples were used as models to determine the effect of gelatin-silver reagent on reducing sugar content in some food samples. The watermelon, apple, and honey samples were supplied from a local market in Jeddah. The fruit of the watermelon and apple were rinsed, skinned, and eliminated waste. One gram of watermelon and apple flesh was crushed separately on a glass grater. The watermelon and apple juices were extracted from the pulps by centrifugation at 6000 rpm for 5 min and filtering using a PTFE filter with a pore size of 0.45 µm. The honey sample was generated by weighing 1.0 g of honey, homogenizing it with distilled water, and then diluting it to 100 mL with distilled water. Reducing sugar was determined as follows: 250 µL of each sample was mixed with 250 µL of different Tris–HNO_3 buffers (0.2 M, PH 8.5) and 500 µL gelatin-silver reagent (1:3). The reaction mixture was incubated for 10 min at 90 °C in a boiling water bath before cooling then the absorbance was recorded at 434 nm. A standard curve of maltose concentrations was used to determine the total reducing sugar contents. The total reducing sugar contents were recorded as mg maltose Eq. g^{-1} of the studied sample.

DNS reagent was utilized to determine each sample's total reducing sugar contents and compare it with our method. DNS reagent was prepared according to the Miller method [17] as follows: 20 g of potassium sodium tartrate was dissolved in 20 mL distilled water and stirred to totally dissolved, then sodium hydroxide (1 g, 20 mL) was added, followed by 1 g of 3,5-dinitrosalicylic acid prepared in 60 mL of distilled water. While the solution was mixed by magnetic stirrer with a hot plate at 90–95 °C, 50 mg of sodium sulfide was added followed 200 mg of phenol. After the components were dissolved entirely, the final solution

was filtered with filter paper, then transferred the solution in dark glass bottles and stored at ambient temperature. Reducing sugar was determined according to DNS reagent: 250 μL of each sample was mixed with 250 μL of different Tris–HCl buffers (0.2 M, PH 7.0) and 500 μL DNS reagent. The reaction mixture was incubated for 10 min at 95 °C in a boiling water bath before cooling then the absorbance was recorded at 560 nm. A standard maltose concentration curve was used to determine the total reducing sugar contents.

3. Results and Discussion

3.1. Gelatin-Silver Method Optimization

The proposed method for RS detection was optimized, considering some crucial factors, including gelatin-silver nitrate ratio, time, PH, temperature, and color formation. Maltose was selected as a representative RS for the method optimization. Figure 1 shows the effect of the gelatin-silver ratio on the developed optical density (OD) value that was measured at the SPR of the in situ formed AgNPs. As shown in the figure, the ratio 1:3 w/w of gelatin-silver nitrate ratio was most effective in color formation owing to the in situ AgNPs. The inset color image reveals the intensity of the SPR color of AgNPs.

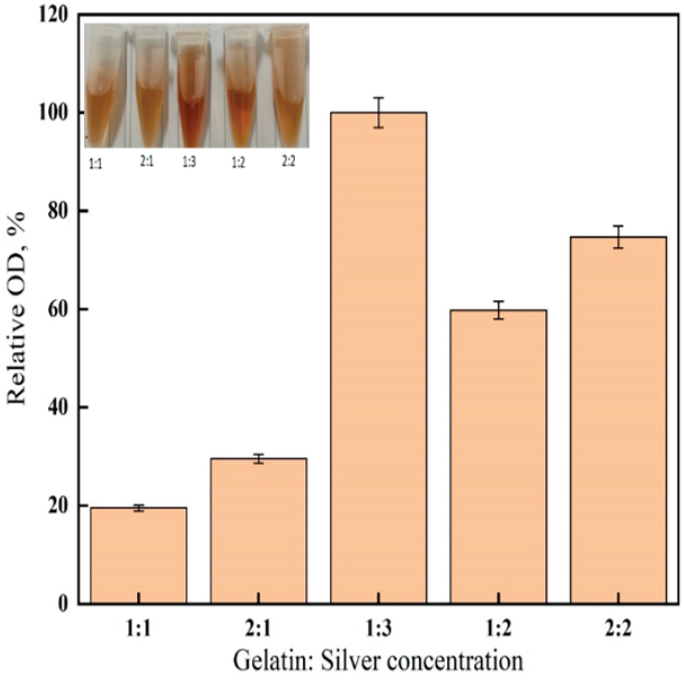

Figure 1. Effect of gelatin- silver reagent ratio on the color evolution. Conditions: A 1 mL of the reaction mixture contained 250 μL maltose (0.1 mM), 250 μL Tris–HNO_3 buffer PH 8.5 (0.2 M), 500 μL gelatin-silver reagent (1:1, 2:1, 1:3, 1:2, and 2:2), incubated for 10 min at 90 °C, cooling read absorbance at 434 nm. Each point represents the mean of three experiments ± SE.

The UV-visible spectrum of the in situ-formed AgNPs is shown in Figure 2. The SPR peak is displayed at 434 nm to confirm the formation of AgNPs due to the occurrence of a redox reaction between silver nitrate and maltose-reducing sugar. The successful appearance of stable color due to gelatin-capped AgNPs confirms their formation in agreement with other similar green syntheses of AgNPs [33].

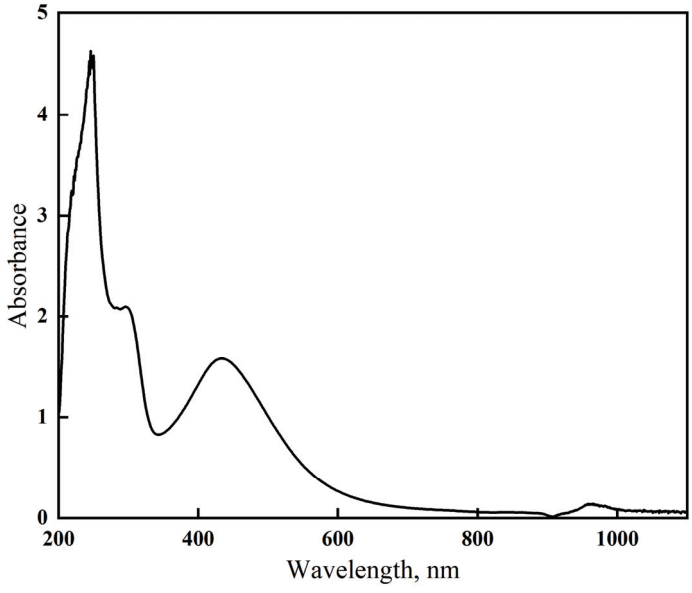

Figure 2. Wavelength of AgNPs produced after gelatin-silver reagent (1:3) react with maltose. Conditions: A 1 mL of the reaction mixture contained 250 μL maltose (0.1 mM), 250 μL Tris–HNO_3 buffer PH (0.2 M), 500 μL gelatin-silver reagent (1:3), incubated for 10 min at 90 °C.

The effect of time on the evolution of color was monitored spectrophotometrically at the SPR peak. As shown in Figure 3, the development of AgNPs color increases by time up to 8–10 min above, after which there was no further increase, indicating fast response for RS detection in about 10 min. In addition, the OD values remain the same over the studied time, indicating the stability of the in situ-formed AgNPs. Therefore, compared with the conventional DNS method [17], the short-time response and the stability of AgNPs suggest the suitability of the gelatin-silver method for detecting RS.

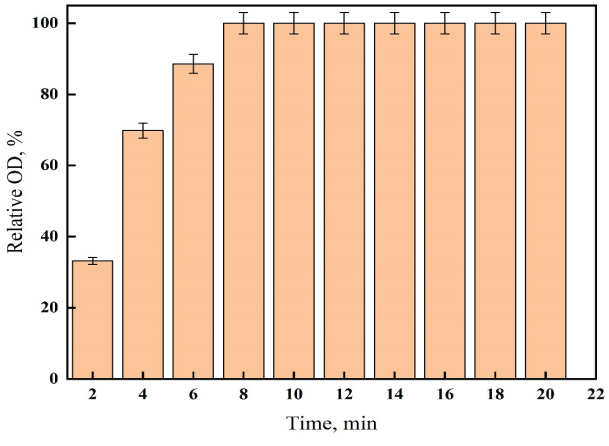

Figure 3. Effect of time on the color evolution of gelatin-silver reagent. Conditions: A 1 mL of the reaction mixture contained 250 μL maltose (0.1 mM), 250 μL of 0.2 M Tris–HNO_3 buffer PH 8.5, 500 μL gelatin-silver reagent (1:3), incubated for different times at 90 °C in a boiling water bath, cooling, recorded the absorbance at 434 nm. Each point represents the mean of three experiments ± SE.

The PH of the reaction mixture was varied to obtain the optimum PH. As shown in Figure 4, the formation of AgNPs needs a slightly alkaline medium to form the intensive color of AgNPs. The inset color image reveals the color-PH dependent on the SPR color of AgNPs. The results agree with our previous studies and those found in literature [28,29,37]. Subsequently, PH 8.5 was selected as the optimum value of the gelatin-silver reagent. This alkaline PH is favorable for reducing silver nitrate with RS by enhancing the addition of water molecules on the carbonyl groups, as shown in Scheme 1.

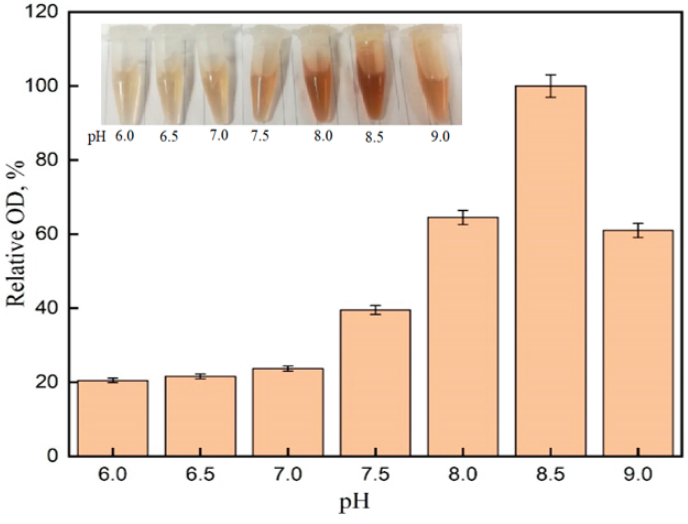

Figure 4. Effect of PH on the color evolution of the gelatin-silver reagent. Conditions: A 1 mL of the reaction mixture contained 250 μL maltose (0.1 mM), 250 μL Tris–HNO_3 buffer with deferent PH (0.2 M), 500 μL gelatin-silver reagent (1:3), incubated for 10 min at 90 °C, cooling read absorbance at 434 nm. Each point represents the mean of three experiments ± SE.

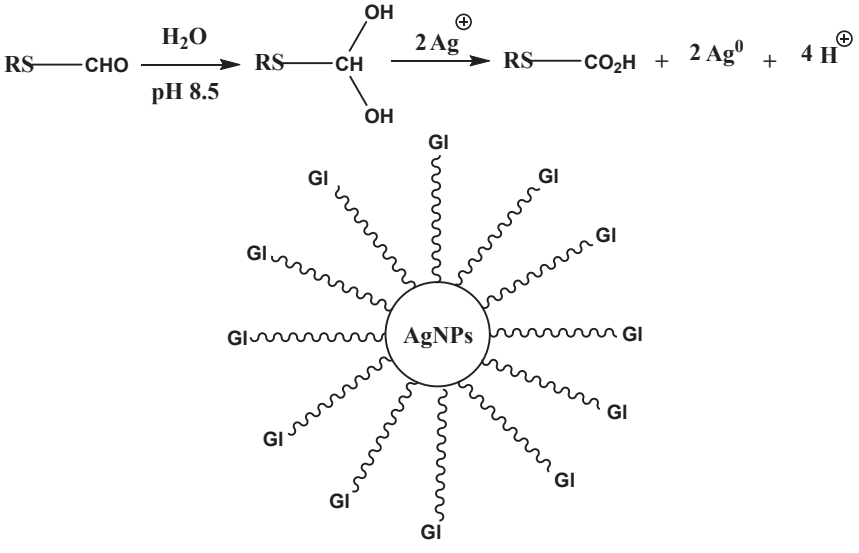

Scheme 1. Possible mechanism for the formation of gelatin (Gl) stabilized AgNPs.

The impact of temperature on AgNPs' color is depicted in Figure 5. Therefore, the detection of RS works well at a temperature close to 90 °C. As a result, 90 °C was used to conduct the gelatin-silver reagent's redox reaction.

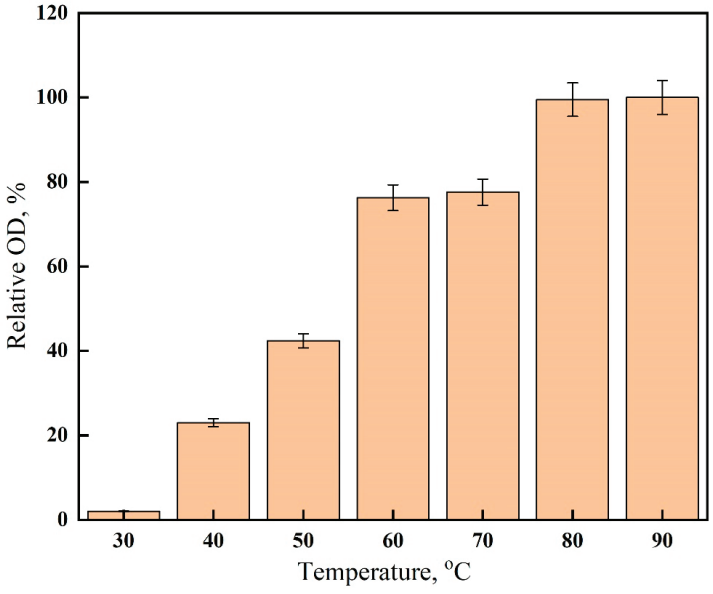

Figure 5. Effect of temperature on the color evolution of gelatin-silver reagent. Conditions: A 1 mL of the reaction mixture contained 250 μL maltose (0.1 mM), 250 μL of 0.2 M Tris–HNO_3 buffer PH 8.5, 500 μL gelatin-silver reagent (1:3), incubated at different temperature, cooling, recorded the absorbance at 434 nm. Each point represents the mean of three experiments ± SE.

3.2. Possible Mechanism for Gelatin-Capped AgNPs

The presence of the aldehyde-containing compound in an aqueous alkaline medium may lead to the addition of water molecules on the carbonyl group and, subsequently, the formation of an oxysilver complex that ultimately converted to silver nanoparticles and carboxylic-containing compound via a redox reaction. The presence of gelatin help stabilizes the nanoparticles, as shown in Scheme 1.

3.3. Maltose Selectivity and Starch Hydrolysis

Three samples were tested to validate whether the gelatin-silver method is selective toward RS. The first sample was maltose, the second was a mixture of maltose and starch, and the third was starch only. To these samples, gelatin-silver reagent, as described in the experimental section, was mixed, and the evolution of the color was tracked. Figure 6 shows the OD values of the samples, and the inset shows an image of their colors. It is indicated that the reagent is selective toward maltose-reducing sugar but not starch.

Furthermore, starch hydrolysis was made using α-amylase, and the RS obtained was detected by gelatin-silver reagent, as shown in Figure 7. It is shown that the higher the content of starch, the higher the activity of the α-amylase in increasing the production of RS, as evidenced spectrophotometrically by the gelatin-silver reagent.

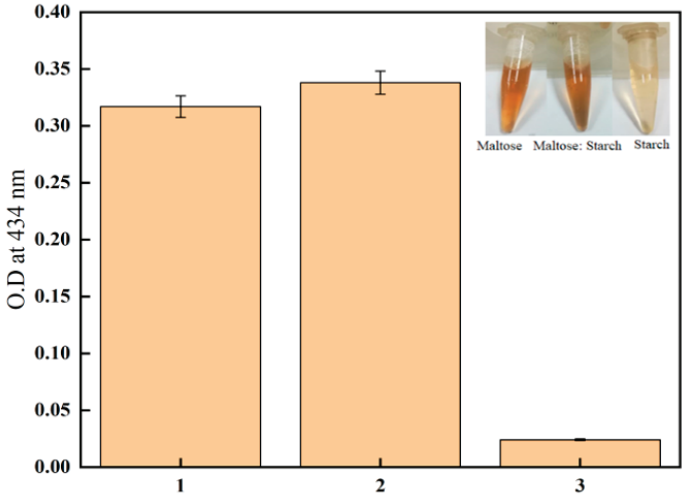

Figure 6. Selectivity for gelatin-silver reagent (1) maltose; (2) maltose: starch; (3) starch. Conditions: A 1 mL of the reaction mixture in sample 1 contained 185 μL of maltose (0.1 mM),190 μL distilled water, 125 μL of Tris-HNO_3 (0.2 M, PH 8.5); sample 2 contained 185 μL of maltose (0.1 mM), 185 μL of starch (1%), 125 μL of Tris-HNO_3 (0.2 M, PH 8.5); sample 3 contained 185 μL of starch (1%), 190 μL distilled water, 125 μL Tris-HNO_3 (0.2 M, PH 8.5); all samples incubated for 10 min at 90 °C, cooling read absorbance at 434 nm. Each point represents the mean of three experiments ± SE.

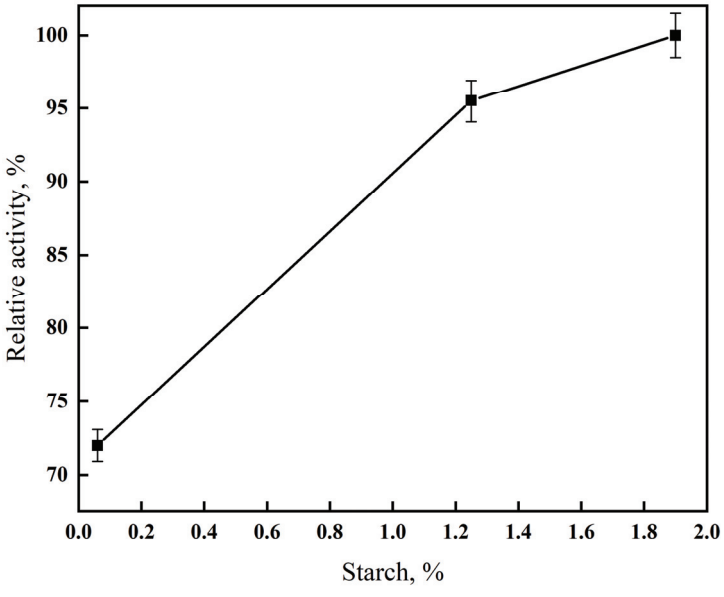

Figure 7. Reduced sugar produced after starch hydrolysis by α-amylase. Conditions: A 1 mL of reaction mixture contained different concentrations of starch (0.06, 1.25, and 1.9%), Tris–HNO_3 buffers, PH 7.0, incubates at 37 °C, 1 mL of gelatin-silver reagent (1:3), heated for 10 min at 90 °C, recorded absorbance at 434 nm. Each point represents the mean of three experiments ± SE.

3.4. Limit of Detection of Maltose

The following equation calculated the limit of detection (LOD); LOD = 3.3 σ/S (40 and elsewhere), where σ is the standard deviation of 10 repeated readings of the measured optical density at 434 nm for a selected sample and S is the slope of the calibration curve (Figure 8) of maltose concentration versus OD values. The LOD obtained is LOD = 46.67 μM. Table 1 shows a comparative LOD limit of reported reagents with the present work. Gelatin-silver reagent reveals higher sensitivity than the conventional time-consuming DNS method. As we know, DNS methods are multistep and complicated processes that take more than 1 h. [17].

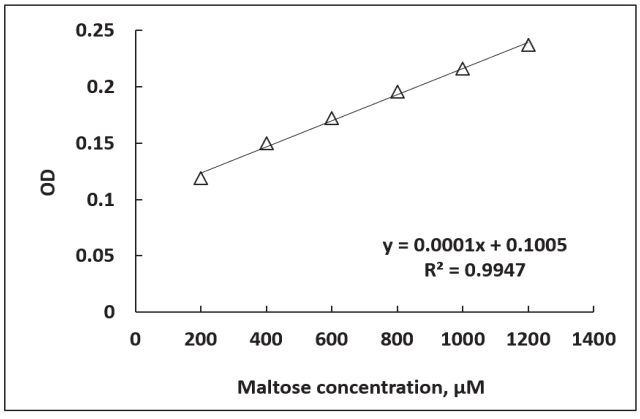

Figure 8. Calibration curve of maltose concentration versus OD. Conditions: See the conditions under Figure 5 using different concentrations of maltose.

Table 1. Comparative LOD of reducing sugar with other reported work.

Reference	Method	Analyte	LOD
[17,40]	DNS	Glucose	80 μM
[37]	Tollens' Reagent	Glucose	40 nM
[41]	DNS	Honey	83.3 μM
[40]	Alkaline Cu(II)-Nc	Glucose	0.6 μM
[42]	Electrochemical Biosensor	Maltose	100 μM
[43]	Benedict's reagent	Maltose	96.49 μM
[17]	DNS	Maltose	80 μM
This work	Gelatin-silver	Maltose	46.67 μM

3.5. Real Samples Analysis

Real sample analysis was made for selected commercial samples, namely, honey, watermelon, and fresh apple juice. The total reducing sugars were determined by the conventional DNS method and the developed gelatin-silver method. Table 2 shows that the gelatin-silver method produced similar analysis data made by the DNS method to suggest its viability for food industries.

Table 2. Total reducing sugar content (as mg maltose Eq. g^{-1}) of studied samples. Each point represents the mean of three experiments ± SE.

	mg Maltose Eq. g^{-1}	
Sample	**Gelatin-Silver Reagent**	**DNS**
Fresh apple juice	287 ± 1.05	284 ± 0.84
Watermelon	165 ± 0.95	169 ± 0.76
Honey	751 ± 1.12	723 ± 0.92

4. Conclusions

This work is devoted to developing a method for measuring reducing sugars using nanoparticles based on silver nitrate and gelatin. The developed approach was improved by considering many essential aspects, including the amount of reagent, reaction interval, PH, temperature, and the gelatin-silver reagent's selectivity for starch and maltose. For optimization studies, maltose was selected as the representative reducing sugar. The gelatin-silver reagent showed a fast response (less than 10 min) with a detection limit for maltose at 46.67 μM more sensitive than DNS conventional method. Gelatin-silver nitrate in a ratio of 1:3 w/w produced the best results for color formation. The development of AgNPs color increases within 8–10 min at PH 8.5 as the selected optimum value and at the optimum temperature of 90 °C for the evolution of the gelatin-silver reagent's redox reaction. In addition, the selectivity of maltose was checked in the presence of starch and after its hydrolysis with α-amylase. Compared with the conventionally used DNS colorimetric method, the proposed method could be applied to commercial fresh apple juice, watermelon, and honey to prove its viability for detecting reducing sugar in food products. The present work explored a viable method for determining the reducing sugar in food industries. Furthermore, the color-based AgNPs would inspire future success in exploiting other colorful nanomaterials to detect reducing sugars.

Author Contributions: Conceptualization, R.M.E.-S.; methodology, R.M.E.-S. and Y.Q.A.; validation, R.M.E.-S. and Y.Q.A.; investigation, R.M.E.-S., Y.Q.A., M.M.A. and Y.M.A.A.; resources, R.M.E.-S., Y.M.A.A. and M.M.A.; data curation, R.M.E.-S. and Y.Q.A.; writing—review and editing, R.M.E.-S., Y.M.A.A., M.M.A. and Y.Q.A.; visualization, Y.Q.A.; supervision, R.M.E.-S., Y.M.A.A. and M.M.A.; funding acquisition, R.M.E.-S. All authors have read and agreed to the published version of the manuscript.

Funding: This research work was funded by Institutional Fund Projects under grant no (IFPRC-110-130-2020).

Institutional Review Board Statement: Not applicable.

Data Availability Statement: All data are presented in the article.

Acknowledgments: This research work was funded by Institutional Fund Projects under grant no (IFPRC-110-130-2020). Therefore, authors gratefully acknowledge technical and financial support from the Ministry of Education and King Abdulaziz University, Jeddah, Saudi Arabia.

Conflicts of Interest: The authors declare no conflict of interest.

References

1. Uhlig, H. (Ed.) . *Industrial Enzymes and Their Applications*; John Wiley & Sons: Hoboken, NJ, USA, 1998.
2. Nelson, N. A photometric adaptation of the Somogyi method for the determination of glucose. *J. Biol. Chem.* **1944**, *153*, 375–380. [CrossRef]
3. Waffenschmidt, S.; Jaenicke, L. Assay of reducing sugars in the nanomole range with 2,2-bicinchoninate. *Anal. Biochem.* **1987**, *165*, 337–340. [CrossRef] [PubMed]
4. Gropper, S.S.; Smith, J.L. *Advanced Nutrition and Human Metabolism*; Wadsworth Cengage Learning: Belmont, CA, USA, 2012.
5. Cummings, J.H.; Stephen, A.M. Carbohydrate terminology and classification. *Eur. J. Clin. Nutr.* **2007**, *61*, 5–18. [CrossRef] [PubMed]
6. Gomis, D.B.; Tamayo, D.M.; Alonso, J.M. Determination of monosaccharides in cider by reversed-phase liquid chromatography. *Anal. Chim. Acta* **2001**, *436*, 173–180. [CrossRef]
7. Neeley, W.E. Simple Automated Determination of Serum or Plasma Glucose by a Hexokinase/Glucose-6-Phosphate Dehydrogenase. *Method Clin. Chem.* **1972**, *18*, 509–515. [CrossRef]
8. Apovian, C.M. Sugar-sweetened soft drinks, obesity, and type 2 diabetes. *JAMA* **2004**, *292*, 978–979. [CrossRef]
9. Cortacero-Ramirez, S.; Segura-Carretero, A.; Cruces-Blanco, C.; de Castro, M.; Fernandez-Gutierrez, A. Analysis of carbohydrates in beverages by cap-illary electrophoresis with precolumn derivatization and UV detection. *Food Chem.* **2004**, *87*, 471–476. [CrossRef]
10. Mason, B.S.; Slover, H.T. Gas-chromatographic method for the deter-mination of sugars in foods. *J. Agric. Food Chem.* **1971**, *19*, 551–554. [CrossRef]
11. Wang, Z.; Liu, X.; Li, R.; Chang, X.; Jing, R. Development of near-infrared reflectance spectroscopy models for quantitative determination ofwater-soluble carbohydrate content in wheat stem and glume. *Anal. Lett.* **2011**, *44*, 2478–2490. [CrossRef]

12. Duquesnoy, E.; Castola, V.; Casanova, J. Identification and quantitative determination of carbohydrates in ethanolic extracts of two conifers using C-13NMR spectroscopy. *Carbohydr. Res.* **2008**, *343*, 893–902. [CrossRef]
13. Zhang, M.-L.; Sheng, G.-P.; Yu, H.-Q. Determination of proteins and carbohydrates in the effluents from wastewater treatment bioreactors usingresonance light-scattering method. *Water Res.* **2008**, *42*, 3464–3472. [CrossRef] [PubMed]
14. Nielsen, S.S. Phenol-sulfuric acid method for total carbohydrates. In *Food Analysis Laboratory Manual*; Springer: Boston, MA, USA, 2010; pp. 47–53.
15. Somani, B.L.; Khanade, J.; Sinha, R. A modified anthrone-sulfuric acid method for the determination of fructose in the presence of certain proteins. *Anal. Biochem.* **1987**, *167*, 327–330. [CrossRef] [PubMed]
16. *AOAC Official Methods of Analysis*; Association of Official Analytical Chemists: Washington, DC, USA, 1995.
17. Miller, G.L. Use of dinitrosalicylic acid reagent for determination of reducing sugar. *Anal. Chem.* **1959**, *31*, 426–428. [CrossRef]
18. Michalowicz, J.; Duda, W. Phenols—Sources and toxicity. *Pol. J. Environ. Stud.* **2007**, *16*, 347–362.
19. Robyt, J.F.; Whelan, W.J. Reducing value methods for maltodextrins. I. Chain-length dependence of alkaline 3,5-dinitrosalicylate and chain-length independence of alkaline copper. *Anal. Biochem.* **1972**, *45*, 510–516. [CrossRef] [PubMed]
20. Lindner, W.A.; Dennison, C.; Quicke, G.V. Pitfalls in the assay of carboxymethylcellulase activity. *Biotechnol. Bioeng.* **1983**, *2*, 377–385. [CrossRef]
21. Breuil, C.; Saddler, J.N. Comparison of the 3,5-dinitrosalicylic acid and Nelson-Somogyi methods of assaying for reducing sugars and determining cellulase activity. *Enzym. Microb. Technol.* **1985**, *7*, 327–332. [CrossRef]
22. Ghose, T.K. Measurement of cellulase activities. *Pure Appl. Chem.* **1987**, *2*, 257–268. [CrossRef]
23. Kanmani, P.; Rhim, J.W. Physicochemical properties of gelatin/silver nanoparticle antimicrobial composite films. *Food Chem.* **2014**, *148*, 162–169. [CrossRef]
24. Thanh, N.T.; Hieu, M.H.; Phuong, N.T.M.; Thuan, T.D.B.; Thu, H.N.T.; Do Minh, T.; Thi, H.N. Optimization and characterization of electrospun polycaprolactone coated with gelatin-silver nanoparticles for wound healing application. *Mater. Sci. Eng. C* **2018**, *91*, 318–329. [CrossRef]
25. Ediyilyam, S.; George, B.; Shankar, S.S.; Dennis, T.T.; Wacławek, S.; Černík, M.; Padil, V.V. Chitosan/gelatin/silver nanoparticles composites films for biodegradable food packaging applications. *Polymers* **2021**, *13*, 1680. [CrossRef]
26. Jeong, L.; Park, W.H. Preparation and characterization of gelatin nanofibers containing silver nanoparticles. *Int. J. Mol. Sci.* **2014**, *15*, 6857–6879. [CrossRef]
27. Biswas, P.K.; Dey, S. Effects and applications of silver nanoparticles in different fields. *Int. J. Rec. Sci. Res.* **2015**, *28*, 5880–5884.
28. El-Shishtawy, R.M.; Asiri, A.M.; Al-Otaibi, M.M. Synthesis and spectroscopic studies of stable aqueous dispersion of silver nanoparticles. *Spectrochim. Acta A Mol. Biomol. Spectrosc.* **2011**, *79*, 1505–1510. [CrossRef] [PubMed]
29. El-Shishtawy, R.M.; Asiri, A.M.; Abdelwahed, N.A.M.; Al-Otaibi, M.M. In situ production of silver nanoparticle on cotton fabric and its antimicrobial evaluation. *Cellulose* **2011**, *18*, 75–82. [CrossRef]
30. Al-Bar, O.A.M.; El-Shishtawy, R.M.; Mohamed, S.A. Immobilization of camel liver catalase on nanosilver-coated cotton fabric. *Catalysts* **2021**, *11*, 900. [CrossRef]
31. Al-Zahrani, F.A.M.; AL-Zahrani, N.A.; Al-Ghamdi, S.N.; Lin, L.; Salem, S.S.; El-Shishtawy, R.M. Synthesis of Ag/Fe_2O_3 nanocomposite from essential oil of ginger via green method and its bactericidal activity. *Biomass Convers. Biorefin.* **2022**, 1–9. [CrossRef]
32. Al-Zahrani, F.A.M.; Salem, S.S.; Al-Ghamdi, H.A.; Nhari, L.M.; Lin, L.; El-Shishtawy, R.M. Green Synthesis and Antibacterial Activity of Ag/Fe_2O_3 Nanocomposite Using Buddleja lindleyana Extract. *Bioengineering* **2022**, *9*, 452. [CrossRef]
33. Darroudi, M.; Ahmad, M.B.; Abdullah, A.H.; Ibrahim, N.A. Green synthesis and characterization of gelatin-based and sugar-reduced silver nanoparticles. *Int. J. Nanomed.* **2011**, *6*, 569–574. [CrossRef]
34. Wang, H.; Chen, D.; Wei, Y.; Chang, Y.; Zhao, J. A simple and sensitive assay of gallic acid based on localized surface plasmon resonance light scattering of silver nanoparticles through modified Tollens process. *Anal. Sci.* **2011**, *27*, 937–941. [CrossRef]
35. Li, N.; Gu, Y.; Gao, M.; Wang, Z.; Xiao, D.; Li, Y.; Lin, R.; He, H. Colorimetric determination of o-phenylenediamine in water samples based on the formation of silver nanoparticles as a colorimetric probe. *Spectrochim. Acta Part A* **2015**, *140*, 328–333. [CrossRef] [PubMed]
36. Chaiendoo, K.; Sooksin, S.; Kulchat, S.; Promarak, V.; Tuntulani, T.; Ngeontae, W. A new formaldehyde sensor from silver nanoclusters modified Tollens' reagent. *Food Chem.* **2018**, *255*, 41–48. [CrossRef] [PubMed]
37. Durmazel, S.; Üzer, A.; Erbil, B.; Sayln, B.; Apak, R. Silver Nanoparticle Formation-Based Colorimetric Determination of Reducing Sugars in Food Extracts via Tollens' Reagent. *ACS Omega* **2019**, *4*, 7596–7604. [CrossRef]
38. Palazzo, G.; Facchini, L.; Mallardi, A. Colorimetric detection of sugars based on gold nanoparticle formation. *Sens. Actuators B* **2012**, *161*, 366–371. [CrossRef]
39. Evanoff, D.D., Jr.; Chumanov, G. Synthesis and optical properties of silver nanoparticles and arrays. *ChemPhysChem* **2005**, *6*, 1221–1231. [CrossRef] [PubMed]
40. Başkan, K.S.; Tütem, E.; Akyüz, E.; Özen, S.; Apak, R. Spectrophotometric total reducing sugars assay based on cupric reduction. *Talanta* **2016**, *147*, 162–168. [CrossRef] [PubMed]
41. Negrulescu, A.; Patrulea, V.; Mincea, M.M.; Ionascu, C.; Vlad-Oros, B.A.; Ostafe, V. Adapting the reducing sugars method with dinitrosalicylic acid to microtiter plates and microwave heating. *J. Braz. Chem. Soc.* **2012**, *23*, 2176–2182. [CrossRef]

42. Liu, A.; Lang, Q.; Liang, B.; Shi, J. Sensitive detection of maltose and glucose based on dual enzyme-displayed bacteria electrochemical biosensor. *Biosens. Bioelectron.* **2017**, *87*, 25–30. [CrossRef] [PubMed]
43. Hernández-López, A.; Felix, D.A.S.; Sierra, Z.Z.; Bravo, I.G.; Dinkova, T.D.; Alejandre, A.X.A. Quantification of Reducing Sugars Based on the Qualitative Technique of Benedict. *ACS Omega* **2020**, *5*, 32403–32410. [CrossRef]

polymers

MDPI

Review

Lignins as Promising Renewable Biopolymers and Bioactive Compounds for High-Performance Materials

Cornelia Vasile [1,*,†] and Mihaela Baican [2,†]

[1] Romanian Academy, "P. Poni" Institute of Macromolecular Chemistry, Physical Chemistry of Polymers Department 41A Grigore Ghica Voda Alley, RO700487 Iași, Romania
[2] "Grigore T. Popa" Medicine and Pharmacy University, Faculty of Pharmacy, Pharmaceutical Sciences I Department, Laboratory of Pharmaceutical Physics, 16 University Street, RO700115 Iași, Romania; m_pascu2000@yahoo.com
* Correspondence: cvasile@icmpp.ro
† These authors contributed equally to this work.

Abstract: The recycling of biomass into high-value-added materials requires important developments in research and technology to create a sustainable circular economy. Lignin, as a component of biomass, is a multipurpose aromatic polymer with a significant potential to be used as a renewable bioresource in many fields in which it acts both as promising biopolymer and bioactive compound. This comprehensive review gives brief insights into the recent research and technological trends on the potential of lignin development and utilization. It is divided into ten main sections, starting with an outlook on its diversity; main properties and possibilities to be used as a raw material for fuels, aromatic chemicals, plastics, or thermoset substitutes; and new developments in the use of lignin as a bioactive compound and in nanoparticles, hydrogels, 3D-printing-based lignin biomaterials, new sustainable biomaterials, and energy production and storage. In each section are presented recent developments in the preparation of lignin-based biomaterials, especially the green approaches to obtaining nanoparticles, hydrogels, and multifunctional materials as blends and bio(nano)composites; most suitable lignin type for each category of the envisaged products; main properties of the obtained lignin-based materials, etc. Different application categories of lignin within various sectors, which could provide completely sustainable energy conversion, such as in agriculture and environment protection, food packaging, biomedicine, and cosmetics, are also described. The medical and therapeutic potential of lignin-derived materials is evidenced in applications such as antimicrobial, antiviral, and antitumor agents; carriers for drug delivery systems with controlled/targeting drug release; tissue engineering and wound healing; and coatings, natural sunscreen, and surfactants. Lignin is mainly used for fuel, and, recently, studies highlighted more sustainable bioenergy production technologies, such as the supercapacitor electrode, photocatalysts, and photovoltaics.

Keywords: lignin; raw material; bioactive compound; nanoparticles; nanofibers; hydrogels; green composites; applications

Citation: Vasile, C.; Baican, M. Lignins as Promising Renewable Biopolymers and Bioactive Compounds for High-Performance Materials. *Polymers* **2023**, *15*, 3177. https://doi.org/10.3390/polym15153177

Academic Editor: Luis Alves

Received: 26 June 2023
Revised: 16 July 2023
Accepted: 17 July 2023
Published: 26 July 2023

1. Introduction

At present, in all countries, priority is given to the good quality of the environment and its preservation. Because of the exhaustion of fossil product resources, both research and industry units search for environmentally friendly materials manufactured independently on petroleum products, which means, in other words, the development of new biomaterials for the possible replacement of existing products, like conventional plastics. New materials will be developed by combined green chemistry and engineering technology [1]. Nowadays, bioplastics represent annually only around one percent of the total plastic produced, but it is expected that the demand for bioplastics will increase [2–4]. As a consequence, numerous studies have been conducted to develop natural alternatives, starting from biodegradable,

renewable resources, which are safer and cleaner for the environment, as precursor materials instead of petroleum and also using innovative technological approaches developed to control pollution [5].

The biomass of living organisms in the global biosphere is expressed in gigatons of carbon, with 1 Gt C = 10^{15} g of carbon [6]. Plant biomass as a renewable resource constitutes ~80% of the 550 GtC of total biomass, as an abundant available resource in the biosphere [6]. The biomass distribution on Earth indicates that the dominant kingdom primarily comprises terrestrial plants with ≈450 Gt C; animals with 2 Gt C are mainly from the seas and oceans, while bacteria (≈70 Gt C) and archaea, as microorganisms that define the limits of life on Earth, (≈7 Gt C), are predominantly located in deep subsurface environments. The terrestrial biomass is about two orders of magnitude higher than the aquatic biomass and it contains more consumers than producers [7,8]. The enormous potential of biomass as a petroleum alternative is exemplified by its availability as in the United States alone; it accounts for ~1 billion tons/year of dry biomass [9]. Thus, the demand for development of environmentally friendly and sustainable production/consumption/waste management systems for both plastics and biodegradable materials has changed in recent years because of modifications in consumer habits; preferences for single-use products, fresh food, and ready-to-eat packed food; awareness of the need for a healthy life and environment; and the growing need for fabricating packaging, medical devices, healthcare products, and others in a more environmentally friendly way. Biomass-based materials are extensively studied, with recent research being focused on them because they present biodegradability, compostability, low carbon footprint, and recyclability and appropriate physical, mechanical, and barrier properties [10].

Plant lignocellulosic biomass is one of the most abundant raw materials and sustainable resources in the world, with a production rate of 2×10^{11} tons/year. Lignocellulosic biomass (LCB), a complex heterogeneous mixture comprising carbohydrate polymers, namely cellulose (40–45% w/w) and hemicellulose (25–35% w/w) and lignin (15–30 wt%), includes agricultural residues, energy crops (temperate grasses), and wood residues. Its abundance in nature could potentially solve the problem of the rapidly depleting resources if it is used as renewable resource or valorized to higher value materials. LCB is by far the largest proportion of the natural material available on terrestrial earth for sustainable production of energy and chemicals. Global demand for biofuels is set to grow by 41 billion liters, or 28%, over 2021–2026 [11–13]. Conventionally, they are used in second-generation biofuel plants, for production of ethanol, diesel, methane, etc. The Energy Security and Independence Act of 2007 called for the annual production of nearly 80 billion L of second-generation biofuels by 2022, which implies roughly 62 million tons of lignin byproduct.

Lignin, an organic polymer is potentially an import market product as a raw material for chemicals and life science industries. Lignin, the second-most abundant renewable biopolymer on Earth, is one of the largest natural renewable sources of aromatic structures and the second-largest renewable source of carbon, with a heating value similar to carbon. Its aromatic compounds have multiple special chemical properties and show important bioactive effects. Some studies on the energy need in bioethanol plants show that the energy content of lignin is higher than the need for ethanol production; this will always lead to an energy excess which can be used for other purposes like external uses or as a chemical raw material. A computer simulation has been developed to evaluate the efficiency of lignin separation from lignocellulosic raw materials, like straw and spruce, for bioethanol production and purposes other than energy [14].

Lignin exhibits impressive properties, including good mechanical and physicochemical properties, low weight, antioxidant and antimicrobial properties, and excellent thermal stability, and it can undergo a range of modifications to tailor or impart special characteristics, such as improved compatibility and processability, that explain the interest in extending its applicability in various domains. Since lignin has intra- and intermolecular hydrogen linkages, it exhibits thermoplastic properties at low temperatures, being useful for lignin-derived biobased polymers and film materials, and can also serve as a thermoset

at high temperatures (T > 200 °C) because of its substantial crosslinking. At elevated temperatures, significant degradation could arise [15]. Therefore, lignin possesses huge potential for the production of a variety of materials because of its high carbon content, low cost, and bio-renewability [16]. It can be considered an excellent alternative for developing novel green functional and sustainable materials as plastic substitutes, considering its availability, excellent environmental friendliness, ecological adaptability, degradability, reinforcing ability, etc. The interest in lignin from the scientific and industrial communities increased over the last decade because of the growing concern over climate change and the need to decrease industrial pollution [17]. Therefore, lignin is a viable alternative to fossil nonrenewable resources for energy, chemicals, polymers, and various materials [18–20].

The main technical lignin resources are pulp and paper mills and emerging cellulosic biorefineries, as well as agricultural and forestry residues. The annual production of industrial lignin is approximately 1.8×10^9–2×10^{10} tons, which is mainly obtained as a byproduct from the pulp or paper industry and emerging cellulosic biorefineries, while a cellulosic ethanol plant can generate 100,000–200,000 tons lignin/year [21]. Presently, only ~2% of lignin as a byproduct is recovered, while 98% is burned for energy or dumped in landfills, this alternative creating a major disposal issue [22]. Lignin as a byproduct of pulp and paper production processes is available commercially. The major fraction of lignin is used in boilers to generate steam and satisfy the heating requirements of the biomass processing plants (thermal recycling) and recover inorganics. The small fraction of lignin (~2%) is used for manufacturing of vanillin, dispersants, animal feed, cement fillers, carbon fibers, agglomerates, adhesives, renewable materials, etc. Therefore, it is still underutilized. Biorefineries generate green energy through well-established processes such as fermentation of corn, sugar cane, and wheat to obtain bioethanol, and also biodiesel can be produced by the transesterification of rapeseed and soybean oil. The sustainability of these processes is debatable because the utilization of the edible crops competes with food production. To avoid a potential increase in food price and deforestation, a new generation of biorefineries is being developed by utilizing nonedible lignocellulosic biomass. There are several types of technical lignins, such as kraft lignin, lignosulfonate, alkali lignin, acid hydrolysis, steam explosion lignin, and organosolv lignin (see below). Recently, new treatments have been applied, such as steam-assisted or solvent-assisted biomass fractionation, which produce lignins for targeted applications. Annually, lignin production with the kraft process, with approximately 130–170 kton, produces the largest amount of lignin compared to other production processes.

Lignin valorization involves both the use and application of the whole polymer and the exploration of low-molecular-weight oligomers [23–28].

Lignin applications in the field of polymer materials started in 2010 and include the use of lignins as dispersants, phenolic resins, components of thermoplastics, polyurethane (PUR) foams, epoxy resins, and asphalt or concrete modifiers [29], where lignin could act as a superplasticizer. Lignin as a dispersant improves viscosity and fluidity of bioasphalt, concrete, drilling mud for oil recovery, and dyes for textile and agricultural chemicals [30]. Modified lignins are used as concrete modifiers as lignin-derived plasticizers [31].

Lignins provide a physical-strength-forming water-conducting vascular network and protect plants against attacking organisms and insects. Lignin also acts as a natural additive/bioactive compound. The role of natural additives and other components with a concentration smaller than 15% raises interest because they assure quality and functionality of many products. Their role in various materials as natural additives, including lignin and lignans, is to improve physicochemical properties: mechanical, barrier, sealing, optical, biodegradability, hydrophobicity, sensory, etc. Bioactive compounds (BCs) or "active ingredients" used in many advanced materials for food packaging, medical devices, cosmetics, etc., induce desired functionalities such as antimicrobial, antifungal, and antioxidant activities. Bioactive compounds can be used as antimicrobial agents to inhibit the harmful activity of bacteria, fungi, and viruses, being very interesting not only in terms of their biological activities but also for their biocompatibility, renewability, and biodegradability,

etc. Active compounds are very important in tailoring the advanced polymeric material properties, assuring their applications in many fields especially if they are used with a corresponding concentration and they show a modulated controlled release. They can be developed and implemented in industries as adhesives, biosurfactants, antimicrobial agents in packaging and textiles, antioxidants, adhesives, anticorrosion agents, carbon fiber or carbon black, cosmetics, reinforcing agents, hydrogels, phenolic resin, flame retardants, polyurethane, foam composites, compatibilizers, and new biomedical materials. Functionalities of lignin and its derivatives include binding, dispersing, crystal growth modification, emulsion stabilization, antioxidant and antimicrobial activities, UV-absorbing capabilities, biocompatibility, and low cytotoxicity, confirming its role as a bioactive compound. Soda lignin plays a significant role in antifungal and antibacterial activity since it contains various functional groups, i.e., carboxylic acid and hydroxyl groups [32]. In new bioasphalts, a part of bitumen is replaced by renewable resources as demonstrated in a study in the Netherlands, where 50% bitumen was replaced by three lignins, namely soda, kraft and hydrolysis, with the technology being in TRL5-7 stage [33]. Many applications are in the development stage; therefore, the studies are still in the patent stage.

Applications have been found for nanostructures based on natural biopolymers including lignin in multiple fields, including bioactive/smart packaging, cosmetics, medical fields, pharmaceutics, drug delivery systems, textiles, food, adhesives, plastics, paper, and the environment [34].

Lignin-based biomaterial delivery systems, consisting of microparticles, nanoparticles, hydrogel, bio(nano)composites, and blends, offer the possibility to improve the efficiency of drug delivery, as they protect drugs from degradation, increase their absorption and transport, and, in the case of tailor-designed nanoparticles, favor targeting [35–38]. Therefore, lignin is a multipurpose/multifunctional raw material with important roles/applications in the various fields.

The review papers published in this field are related to such applications as production of chemicals and fuels [7,9]; lignocellulosic bioethanol plants [14]; lignin biopolymers [18–20,23]; agricultural applications of lignin [25]; bio-oil, bio-binder, and bio-asphalt materials [30]; valorization in medicine, cosmetics, and environmental remediation [35]; food packaging [36]; and r additives [39]. This review highlights the recent developments in lignin use, both as a raw material and bioactive compound in new types of high-performance materials, emphasizing on the multiple applications of lignins and their role in sustainable development to evidence their role as promising renewable biopolymer sources and bioactive compounds. It is divided into ten main sections, starting with an outlook on lignin diversity; main properties and possibilities to be used as a raw material for fuels, aromatic chemicals, plastics, or thermoset substitutes; and new developments in the use of lignin as a bioactive compound and in nanoparticles, hydrogels, 3D-printing-based lignin biomaterials, new sustainable biomaterials, and energy production and storage. In each section are presented recent developments in the preparation of lignin-based materials, especially the green approaches to obtaining nanoparticles, hydrogels, and multifunctional materials as blends and bio(nano)composites, by selecting the most suitable lignin type for each category of the envisaged products/applications and the main properties of the obtained newly developed lignin-based materials, etc. Different application categories of lignin within various sectors, which could provide completely sustainable energy conversion, such as in agriculture and environment protection, food packaging, biomedicine, and cosmetics, are described. The medical and therapeutic potential of lignin-derived materials is evidenced in applications such as antimicrobial, antiviral, and antitumor agents; carriers for drug delivery systems with controlled/targeting drug release; tissue engineering and wound healing; and coatings, natural sunscreen, and surfactants. Lignin is mainly used for fuel, and, recently, studies highlighted more sustainable bioenergy production technologies, such as the supercapacitor electrode, photocatalysts, and photovoltaics.

2. Lignin Structure and Properties

Lignin is a three-dimensional, amorphous, randomly crosslinked network consisting of both aliphatic and aromatic components of methoxylated and hydroxylated phenylpropanoid units, the main ones being p-hydroxyphenyl (H), guaiacyl (G), and syringyl (S) units, derived from p-coumaryl, coniferyl, and sinapyl alcoholic precursors, respectively (Figure 1). Lignin deconstruction results in these three major aromatic motifs, as fundamental monolignols of lignin. Their composition and properties depend on different extraction processes as well as the deconstruction method and source [39]. These three units are repeatedly linked by various chemical bonds, such as β-O-4, 4-O-5, β-5, β-1, β-β, 5-5, spirodienone, and dibenzodioxocin [40].

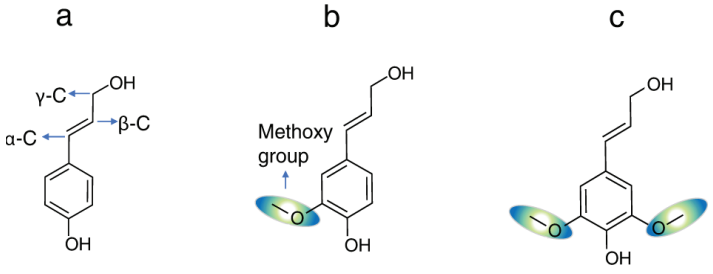

Figure 1. Primary monomer units used for lignin sequence generation: (**a**) p-coumaryl alcohol or H monomer, (**b**) coniferyl alcohol or G monomer and (**c**) syringyl alcohol or S monomer.

Based on the different number of the main lignin units, wood can be classified into three groups, namely softwood, with a high preponderance of guaiacyl lignin (G); hardwood, with a certain composition of G and syringyl units (S) and a very small proportion of p-coumaryl alcohol or p-hydroxyphenyl units (H); and herbaceous, containing mainly G units and a smaller proportion of H units [41].

2.1. Analytics and Structure

Lignin must be analyzed to identify its composition and molecular constitution, to determine the proportions of its main building blocks (guaiacyl, syringyl, and p-hydroxyphenyl), and, based on these possible reaction strategies, to utilize some chemical/biological pretreatments and to achieve a final conversion to useful desired compounds [42]. All protocols for lignin characterization have been summarized by the International Lignin Institute (ILI) and have been reviewed during July 2009 and updated in 2023 [43]. Each type of lignin should be characterized from structural and morphological perspectives and with respect to various properties to evidence its particularities required to define the application domain [44–48]. Pyrolysis–gas chromatography/mass spectroscopy (Py-GC/MS) provides a "structural fingerprint" of H-, G-, and S-substituted phenols as constituents of lignin. Lignin with a large number of G units has a more condensed structure because the aromatic C5 position is available for coupling, resulting in strong C-C bonds, while S-units are mainly linked by more labile ether bonds at C4 positions of aromatic rings. The average molecular weight of lignin and its distribution affects biomass recalcitrance, lignin valorization and mechanical properties, and melt viscosity, etc. It is determined by gel-permeation chromatography (GPC) or size-exclusion chromatography. Spectroscopic methods are used to assess the detailed structure of polymers [46]. Thermal behavior of lignin as a special biopolymer indicates that Tg of lignin varies with water content and varies between 95 and 162 °C depending on lignin type and applied pretreatment [49,50]. Thermal decomposition temperature depends on the heating rate and atmosphere. Lignin decomposition begins at about 280 °C with a maximum rate occurring between 350 and 450 °C and the completion of the reaction at 450 °C and 500 °C [51].

Natural polyphenols, such as lignins, lignans, and tannins, represent important structural materials in the support tissues of plants and valuable products of secondary plant metabolism that have a fundamental role in different stages of plant life.

Lignans are compounds with a 2,3-dibenzyl-butane structure. Lignans possess a steroid-like chemical structure, being defined as phytoestrogens. They are minor constituents of many plants, including higher plants (gymnosperms and angiosperms), such as whole grains, legumes, vegetables, and seeds, with the highest concentrations of lignans found in flax seed [52,53], where they form the building blocks for the formation of lignin (as distinguished from lignans) found in the plant cell wall. The bioactive properties of lignans as human health-promoting molecules include a lowered risk of heart disease, menopausal symptoms, osteoporosis, and breast cancer.

2.2. Technical Lignins

Cellulose/lignin is obtained from wood and non-wood plants as lignocellulosic biomasses, lignin being the second-most abundant biopolymer of terrestrial biomass. Lignin is an important source for biobased products; its valorization can also contribute to reducing greenhouse gas (GHG) emissions. As already mentioned, pulp and paper mills and second-generation biorefineries produce large quantities of low-value technical lignin as a byproduct.

Several physical, chemical, and physicochemical fractionation methods of lignins from LCB have been developed. The commonly used lignin extraction processes are the kraft process (kraft lignin or alkali lignin), sulfite process (lignosulfonates), and organosolv process (organosolv lignin), while for medical uses the enzymatic hydrolysis process (hydrolytic lignin) is preferred. Each method alters the chemical structure and molar mass of native lignin in a different way, thus conferring different characteristics that result in various levels of performance as a substrate for chemical/biochemical transformations. Technical lignins have particular chemical structures with respect to their functional groups and properties, and therefore they differ by structure, composition, molecular weight, water solubility, and purity, with covalently bonded sugars residues or sulfur, degree of condensation, and content of functional groups, such as –OH aliphatic or aromatic, methoxyl, and carboxyl groups (Table 1).

The difference between technical lignins is the uniqueness of the functional groups present in each of them [57]. Differences in molecular structure are also found in lignins resulting/extracted from different sources (plant family and species, their culture conditions, part of plant, age, climate, etc.) and extraction procedures [58,59], as evidenced for kraft lignin and lignosulfonates in Figure 2. They can contain different amounts of carboxyl, carbonyl, phenolic, and aliphatic hydroxyl groups. The properties and main applications vary with lignin type; soda lignin possesses superior mechanical properties, being suitable for the production of phenolics, animal nutrition, dispersants, and polymer synthesis, while organosolv lignin exhibits improved water retention ability and is sulfur-free, also being of high purity, quality, and chemical reactivity, which makes it ideal for direct use or upgradation into high-value chemicals. Lignosulfonates are randomly branched polyaromatic polyelectrolytes that are water-soluble and exhibit surfactant-like behavior. They are mostly used as emulsifiers, antistatic agents, dispersants, and in the electronics sector.

Following the sulfite pulping process, where sulfite base can differ (e.g., Na, Ca, NH_4^+, Mg) and aqueous SO_2 (pH 1–2) is used for delignification of the lignocellulosic biomass, the differences include changes in molecular weight, solubility, variations in aromatic content, and the presence of impurities, ash, and sulfur. Lignosulfonate has mostly been used in manufacturing wearable electronics mainly due to high methoxy and carbonyl groups on the lignin backbone. Lignosulfonate has been produced at a rate of 1 million tons/year.

In soda and alkali lignin, sulfur is absent, but the content of methoxy groups is very high at 10–19%, enabling their use in the synthesis of phenolic resins and making it possible to obtain bioplastics and biocomposites. Compared with kraft and lignosulfonate, organosolv lignin is more hydrophobic and has a low glass transition, being considered a

high-value biochemical for obtaining elastomers, polyesters, polyurethanes, carbon fibers, binders, and coating resins. The kraft method is recognized as the primary source of commercial-grade lignin [57].

Recently developed processes to separate kraft lignin are LignoBoost (1997), Domtar (2003), and LignoForce (2008). Soda and alkali lignins were obtained by GreenValue SA, India, in 2003 and by North Lignin Chemical in 2010. In 2019, in Limeira, São Paulo, Suzano began a pioneering initiative in lignin and its derivatives—ECOLIG0 as the first plant for lignin derived from 100% certified Eucalyptus planted and grown from selected clones and harvested in Brazil with a production capacity of 20,000 tons/year. The LignoBoost plant for lignin separation is now operational in Stora Enso's Sunila mill, Finland, separating lignin from black liquor by treating the black liquor with carbon dioxide and a strong acid. This lignin extraction process replaces a large amount of natural gas with dried lignin, so the carbon dioxide emissions are reduced. The LignoBoost plant is the second commercial-scale manufacturing center in the world. Lignin powder can be used as a raw material, or it can be converted into other materials and products.

Acid-hydrolyzed lignin has a wide molecular weight and high methoxy group content, being suitable for synthesis of various types of polymers. Avantium (NL, 2000) and ST1 (FI, 1995) produced such lignin. New producers of organosolv lignins are Biomass Industrial Company CIMV, France (2006); the Fibria/Lignol Pilot plant 2010; Fortum/Chempolis (FI) 2009; and Frauhofer LEUNA Park (DE). Steam explosion lignin resembles native lignin due to mild extraction conditions being preferred in the phenolic resin synthesis [56].

Table 1. Characteristics of technical lignins adapted from [54–56].

Characteristic/ Technical Lignin	Soda and Alkali Lignin	Kraft Lignin	Acid Hydrolysis/ Enzymatic Lignin	Organosolv Lignin	Lignosulfonates	Ionic Liquid Lignin	Steam Explosion Lignin
Lignin separation	For non-woody biomass; 13–16% NaOH 140–170 °C	Na_2S and NaOH 150–180 °C Thermo-chemical conversion of black liquor-small alkali soluble fragments	Diluted or concentrated acids as H_2SO_4, HCl, HNO_3, H_3PO_4, maleic acid	Hydrothermal treatment of biomass with water and organic solvent	SO_2 and water at 140–160 °C and carbonates and hydroxide salts	Ionic liquid	Mild hydrolysis; steam at high T temperature and pressure
Ash, %	0.7–2.3	0.5–3.0	1.0–3.0	1.7	4.0–8.0	0.6–2.0	5–8
Moisture content, %	2.5–5.0	3.0–6.0	4.0–9.0	7.5	5.8	-	
Carbohydrates, %	1.5–3.0	1.0–2.3	10.0–22.4	1–3	-	0.1	2.5–4
Acid soluble lignin, %	1.0–11	1–4.9	2.9	1.9	-	-	
Nitrogen, %	0.2–1.0	0.05	0.5–1.4	0–0.3	0.02	-	
Sulphur, %	0	1.0–3.0	0–1.0	0	3.5–8.0	1.5/	0–0.5
Phenolic hydroxyls, %	2.9–5.1	2.6–5	3–9	3.7–3.4	2–2.5	4.5–7	
Acids, %	5.4–13.6	4.1–6	6–10	7–8	4.6	1.0–5	
Methoxy, %	10–19	11–14	−19	−15	9	−13	
Purity	Moderate–High	High	Moderate–Low	High	Low–moderate	Moderate–Low	
Molecular weight, Mw	1000–3000 (up to 15,000)	1500–5000 (up to 25,000)	5000–10,000	500–5000	1000–50,000 (up to 150,000)	≈~2000	3500–15,000
Polydispersity	2.5–3.5	2.5–3.5	4.0–11.0	1.5–4.2	7.0	-	

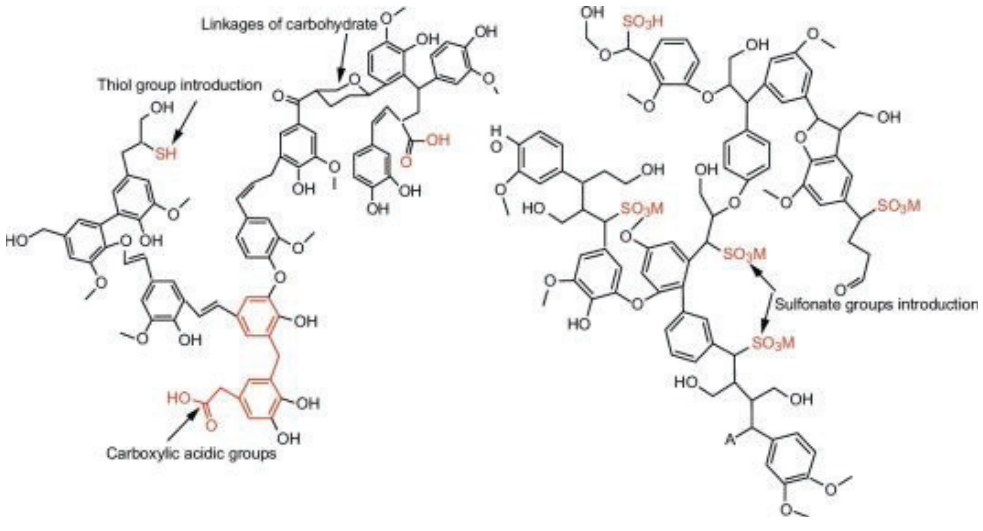

Figure 2. Structures of kraft pine lignin (**A**) and lignosulfonate lignin (**B**) [56].

Networking groups of scientists and experts devoted to lignin valorization for large/industrial application of materials containing lignin, production of chemicals, etc. have been assembled, such as the International Lignin Institute (1991, Lausanne, Switzerland), Lignin Club Ecosystem, LignoCOST, LIGNOVAL, and Wageningen UR Lignin Platform.

2.3. Other Sources of Lignin

Agricultural waste contains approximately 80 wt% of lignocellulosic materials. It includes straw, husk, stalks, stover, and cobs as the largest known sources of wasted lignin. As recent preoccupations have shifted toward greener solutions, agricultural crop residues have been considered highly valuable as bioenergy and biorefinery materials [60,61]. The extraction of lignin is one of the major barriers in the reclamation and reuse of lignin from waste. The following principles have been considered: (1) make full use of the lignin from the waste source, (2) effectively avoid the loss of carbon, and (3) decrease the impact on the environment caused during combustion. Natural resources, such as plants, animals, and the aquatic medium, are envisaged, but if huge quantities are used, competition with the food industry will result. To avoid this competition and to direct main activities toward sustainability and environment protection, the valorization of byproducts and biowastes is exploited. Valorization of the residual products or byproducts and biowaste as sources of biopolymers and BC is a feasible strategy for ecofriendly, biobased, good-performance materials and could be an important solution enabling a transition from a polluting, fuel-based to a circular, biobased economy. Food-grade and suitable materials acting as matrices in various materials and ingredients are abundant in biowastes and byproducts. Better-controlled composition and properties of the obtained products is necessary.

3. Biobased Products from Lignin

Lignin can be a matrix and/or additive in various fields. Common uses of lignin-based compounds are as flame retardants, wood adhesives, flocculants, lubricants, dispersant media, prebiotics, animal feed supplements, food additives, natural antioxidants and antimicrobial agents, reinforcement for polymers, components in biocomposite/nanocomposites materials, adsorbents for heavy metals and toxic organic compounds from the environment, biobased thermoplastics, platform chemicals, BTX, hydrocarbons, carbon fibers, aromatic

monomers, renewable chemicals, smart materials, biofuels, and battery electrode fuels, including production of carbon materials and energy storage materials. The vast recent research developments in the application of lignin consist of creating lignin nanoparticles, hydrogels, and lignin for 3D printing, biocomposites, surfactants, electrodes for energy storage devices, and chemical deconstruction of lignin for the production of platform chemicals. As final polymeric compounds, phenolic resins and polyurethanes have already been mentioned. For specific uses, certain qualities/characteristics of lignin are required. A low content of inorganic and hemicellulose moieties is preferable for lignin-based fuels. High S lignin content is desirable for lignin as a food additive and in food applications due to higher hydroxyl substitution in the lignin units. Low molecular weight and high presence of carboxyl (C=O) and alkyl hydroxyl (OH–) groups are suitable properties for lubricants in polyethyleneglycol. For the production of aromatic compounds, a low degree of condensation (or a high degree of hydration) is necessary [62]. The utilization of low-quality/high-quantity lignin (e.g., kraft lignin) to produce high-added value compounds is achieved via two methods: by deconstruction (sometimes named depolymerization) into smaller fragments and specific chemical modification/functionalization. Valorization of lignin as a raw material to obtain oils or fine chemicals by deconstruction involves several routes of reactions/techniques, such as [63] thermochemical/pyrolytic methods; direct liquefaction at elevated temperatures [64] producing complex product mixtures; base/acid-catalyzed techniques such as reductive, oxidative, and solvolytic chemical modifications occurring in organic solvents in the presence of acids, bases, metals, or ionic liquids [65]; and biological or enzymatic degradation [66]. All of these methods should be followed by upgrading [67].

However, the valorization of lignin to high-performance and cost-competitive materials remains a challenge. It has been demonstrated that the biopolymers better adhere to "green design" principles in comparison to petroleum counterparts, but their properties rank below those of several common petrochemical plastics (e.g., polyolefins) with respect to environmental impact considering a full life-cycle analysis [68]. Moreover, lignin valorization has encountered a series of constraints related to heterogeneous polymeric nature/composition, intrinsic recalcitrance, strong smell, dark color, some problems encountered in lignocellulose fractionation, recalcitrance to depolymerization/deconstruction, and a complex mixture of aromatic compounds resulting during degradation, etc. However, lignin-based compounds are excellent candidates for greenhouse gas diminution in comparison to many petroleum-based chemicals [69,70]. Selected criteria to assess the sustainability of lignin valorization by applying such techniques include waste generation, atom and energy efficiency, usage of safer solvents, biocatalytic methodology, environmental factor (E factor), and atom economy. The greenness evaluation provides a quantitative base for strategic decisions. It was concluded that future collaboration between industry, academia, and policy regulators is needed to assess optimal processing and manufacturing routes of lignin-based polymers and to realize the potential of lignin in this regard. A suitable valorization of lignin waste streams from the pulp and paper industry and biorefinery processes could be a crucial step for the development of a circular sustainable economy.

3.1. Aromatic Chemicals

There are many opportunities for producing fine chemicals and pharmaceuticals from biomass. Due to the high content of aromatics, lignin is a prospective natural source to produce a range of aromatic chemicals, such as phenol, guaiacol (1-hydroxy-2-methoxybenzene), and vanillin (4-hydroxy-3-methoxybenzaldehyde). The difficulties in lignin use to obtain aromatic chemicals or building blocks chemicals mainly derive from its complex variability in chemical composition, molecular weight, and impurities, depending both on natural source and methods used in biorefineries/separation. Lignin as a feedstock for producing fuels, chemicals, and other materials is already an advanced-stage process. Technical lignins result in large quantities as low-cost industrial resources directed to obtain renewable aromatic chemicals. The conversion routes of technical lignins and other LCBs to

biobased aromatics are (non-catalytic) lignin pyrolysis, direct hydrodeoxygenation, and hydrothermal upgrading. The products generated are mixed oxygenated aromatic monomers, light organics, heavy organics, and biochar. Hydrodeoxygenation was found to be the most promising [71] because of the highest return on investment. Hydrothermal liquefaction of lignin occurring in near-critical water conditions produces a bio-oil that is suitable for co-feeding into a petroleum refinery hydrotreatment unit to obtain water-soluble organics, gaseous products, and char. Lignin decomposes into phenolic compounds as the main products when the process is conducted under high-temperature and supercritical water conditions, which may be followed by liquid–liquid extraction and hydrotreatment to produce benzene, toluene, ethylbenzene, and xylenes (BTEX) compounds..Coproduction of BTEX and biofuel did not reduce the biofuel cost. Lower bio-oil oxygen content and decreased capital and operating costs are necessary to make hydrothermal liquefaction-based fuels competitive with fossil fuel-based options [72,73]. At low temperatures (<300 °C), methoxyphenols are the most commonly obtained monomers, whereas, when the reaction is developed at high temperatures (T > 300 °C), catechol and alkylcatechols are the main products [74,75].

Oxidative depolymerization using heterogeneous catalysts is a viable upgrading option to produce aromatic monomers. Base-catalyzed depolymerization/deconstruction is extensively studied because of its simplicity and efficiency. It has been established that the cleavage of ether bond of lignin leads to phenolic oil generation, but unstable reaction intermediates participate in repolymerization reactions through reformation of carbon–carbon bonds.

Production of *Benzene*, *Toluene*, *and Xylenes (BTX*) from lignin, as coproducts of biorefining, started in 1970, and an increasing interest still exists, as evidenced by the high number of publications and patents [76–78]. The processes applied to low-quality lignins are hydrothermal liquefaction operating in critical water conditions, fast pyrolysis (T > 600 °C), catalytic fast pyrolysis from agroindustrial biomass blended with PVC, and the use of NaZSM-5 and HZSM-5 as catalysts [79]. Reductive catalytic fractionation generates phenolic fractions, which, via deoxygenation, lead to specific chemicals such as BTX. Catalytic fast pyrolysis of biomass indicates that oxygen-containing compounds decreased, whereas aromatics increased, and, at the same time, the increase in the formation of mono-aromatics and reduction in polyaromatic hydrocarbons occurred. All mentioned technologies are in R&D stages, and many improvements are still being studied. Olive pomace and almond shell valorization through this process is inexpensive. BTX yield varies between 10 and 30%. BTX are used to obtain both polymers and other chemicals with a wide range of applications, such as healthcare and pharmaceutics, the automotive industry (parts of cars), packaging, electronics, textiles, sport, and construction. Benzene is used to obtain polystyrene (PS) and toluene for polyurethanes and as an additive in gasoline and para-xylene for production of polyethyleneterephthalate (PET) and polyamides, etc. The increasing use of biobased BTX is expected to open new market opportunities, and their quantity will increase in the next 10 years by 50%, reaching 220 million tons in 2030 (in accordance with EC directives).

3.2. Phenolic Compounds

Catalytic reductive deconstruction of lignin is a promising and effective method for valorization to obtain phenolic monomers [80,81]. As an example, liquefaction/fragmentation of lignin using biochar-derived, activated-carbon-supported metal catalysts as bimetallic catalyst Ni-Co/AC (5 to 20 wt %), and various solvents (water, ethanol, methanol) was tested for alkali lignin at 260 to 300 °C for a 15 min reaction time. The process, using an ethanol solvent system at 280 °C, gave the highest bio-oil yield (72.0 wt %) [82]. In the liquefaction/fragmentation of lignin using chloride (MClx) and Pd/C, biochar-derived, activated-carbon-supported catalysts produced a phenolic monomer (namely 85.6% lignin liquefaction with 35.4% phenolic monomer yield [83]) and vanillin (34.8%) [82].

Phenolic compounds are known as natural compounds with several beneficial biological effects, such as antioxidant and anti-carcinogenic activities. Their antioxidant activity is dependent on their structure, as it is affected by the reduction in or inhibition of free radicals via transfer of a hydrogen atom (hydrogen atom transfer—HAT) from their hydroxyl group or by single-electron transfer (SET). The reaction of a phenolic compound with a peroxyl radical (ROO•) involves the transfer of the hydrogen cation from the phenol to the radical, forming a transition state of a H-O bond [84]. Phenolic compounds are useful for various industrial applications, such as in foods, cosmetics, and pharmaceutics. The major drawbacks are their low bioavailability and pH, temperature, and light. Nanotechnology and lipidic encapsulation systems are alternatives to overcome these limitations, to protect molecules from external factors, and to improve their bioavailability. The loading of polyphenols into lipid nanocarriers (NCs) is an efficient way to increase their bioavailability, for reducing degradation, and protecting antioxidant activity of the polyphenols [85,86].

Because of the multiple possibilities in conduction biorefinery and lignin valorization, the simulation of biorefinery processes for the design of manufacturing processes to obtain value-added chemicals from lignocellulosic resources has been conducted, involving phenols from lignin [87], biochemicals [88], and eugenol and phenolic products [89].

Due to the complex structure of lignin, it cannot be degraded by commonly known degradation methods. Specific microorganisms, such as bacteria and certain fungi such as wood-rotting *Basidiomycetes* fungi can degrade lignin by producing enzymes both in the presence and absence of oxygen; under this effect, lignin can be broken down into simpler compounds and used as a carbon source for growth. The main microbial degraders of lignin are white-, brown-, and soft-rot fungi and soil fungi, which produce several extracellular enzymes, such as laccases, lignin peroxidases (LiP), manganese-dependent superoxide dismutase peroxidase (MnP), dye-decolorizing peroxidase (DyP) multicopper oxidase, and polyphenol oxidoreductases and versatile peroxidase, which are effective for lignin degradation via the generation of free radicals. The lignolitic enzymes from bacteria and fungi are useful in delignification of biomass and depolymerization of lignin [90]. Similarly, white-rot fungi such as *Ceriporiopsis subvermispora*, *Phlebiopsis gigantea*, and *Coriolus hirsutus* are used in the biological pulping process. *Phanerochaete chrysosporium* a lignin-degrading fungus produces various oxidoreductive enzymes, including lignin peroxidase (LiP) and manganese peroxidase (MnP). Bacteria lignin and lignin-derived aromatic compounds are transformed into valuable products such as vanillin; monolignols; pyrogallol; lipids; furfural, cis,cis-muconate; pyruvate; lactate; succinate; polyhydroxyalkanoate, ferulate; pyridine-2,4-dicarboxylic acid; and pyridine-2,5-dicarboxylic acid [91]. However, lignin valorization using the microbial approach is still not feasible at an industrial scale, and many studies are necessary to understand the biochemical mechanisms.

Phenols are important precursors for a range of pharmaceuticals, herbicides, plastics, epoxy- and polyurethane resins, and various cosmetics. Organosolv depolymerization is considered the most feasible solution to increase yield in catechol derivatives for direct depolymerization processes resulting from the liquors. Catechol is a model compound for solid fuels, as is present in biomass tar and tobacco smoke, and its chemical structure is related to those of lignin and brown coal.

3.3. Vanillin

Vanillin is a mono-aromatic compound used as a food-flavoring agent in pharmaceuticals and in the fragrance industry. It is extracted from vanilla beans, but its consumption exceeds that of the vanilla resulting from this procedure. Therefore, synthetic methods have been developed. However, the need for alternatives to non-renewable raw materials used in these syntheses has encouraged research on the use of renewable feedstocks for vanillin production. The production of vanillin on an industrial scale occurs via the oxidative depolymerization of lignin derived from the pulp and paper industry and was commenced in 1937 by the Salvo Chemical Corporation. Lignin extracted by sulfite pulping was used, but this production ceased due to a decrease in the number of sulfite pulping facilities,

and the kraft pulping process was implemented. Vanillin has increasingly been produced from the cheap petrochemical guaiacol, and its production now covers about 85% of the vanillin demand. Oxidative lignin depolymerization using oxygen as the oxidizing agent in alkaline media enables the selective production of aromatic aldehydes (i.e., vanillin and syringaldehyde), and their respective acids acetovanillone and acetosyringone as oxidation products in low yields have been produced [92]. The presence of the catalyst and solvent increased the cleavage of β-O-4 bonds, resulting in increased selectivity toward vanillin (32.3–36.2%). Kraft lignin undergoes sequential solvent fractionation using acetone aqueous mixtures. The obtained lignin fractions exhibit specific structural characteristics and low content of impurities [93]. Developing an efficient and environmentally friendly separation process is one of the most important tasks toward the industrial application of lignin-derived aromatics. The Norwegian company Borregaard has produced vanillin from lignin extracted by the lignosulfonate pulping process for more than 50 years together with other lignin-based high-performance chemicals. Stable and robust catalytic systems for oxidative lignin conversion should be developed.

3.4. Adipic Acid from Lignin

The conversion of lignin residue to adipic acid occurs via its base-catalyzed depolymerization to low-molecular-weight fragments, followed by microbial conversion of these to cis,cis-muconic acid by genetically engineered *Pseudomonas putida* separation, and purification of the muconic acid and catalytic upgrading to adipic acid are necessary as final steps [94].

3.5. Carbon Fibers

Lignin-derived carbon materials, such as carbon fibers, carbon mats, activated carbons, carbon films, and templated carbon, can be obtained. Lignin from a lignocellulosic biorefinery is an ideal potential precursor of carbon fibers (CFs). Its application in this direction offers some advantages such as abundant reserves, renewable and high carbon content, and low associated environmental impact, and could have a substantial impact if some important processing and quality hurdles can be overcome [95].

Heterogeneity and purity of lignin are critical challenges in carbon fiber production. The first step in lignin-derived carbon fiber production consists of lignin being processed into fibers. Lignin-based fibers are prepared by melt spinning, wet-spinning solvent-swollen gel, solution spinning, and electrospinning [96], followed by thermal stabilization and carbonization. Spinning temperature (100–230 °C) varies with lignin type, glass transition temperature, and melt viscosity. Nanofibers result from electrospinning [97]. Such nanofibers are used in batteries, supercapacitors, fuel cells, structural composites, and filtration devices. During thermal stabilization, dehydration, CO and CO_2 elimination, additional crosslinking, and other reactions take place; thus, the oxygen, hydrogen, and nitrogen are eliminated by evolution of the HCN, H_2O, CH_4, O_2, H_2, CO, and NH_3. Carbonization occurs at $T \approx 2000$ °C in an inert atmosphere. By variation of the heating rate, it is possible to control the brittleness and the morphology of the carbon fibers. Lignin-based carbon fibers are composed of >98% graphene carbon in highly ordered structure, but their mechanical strength is low due to impurities and low molecular weight of lignin, as in the case of kraft lignin [98,99].

Lignin-based CF quality could be profitable only for lightweight vehicles and in association with biorefinery developments. To achieve this, improvements in lignin quality, such as chemical modification; increased purity; blending of various types of lignin or with polymers such as PET, PEO, PP, PLA, and phenolic resins; and addition of chlorinated PVC and diisocyanate, should be carried out. In this direction, there have been reported studies on phenolated hardwood, acetylated softwood kraft lignin, pyrolytic lignin, organosolv hardwood, etc. In Europe, Research Institutes of Sweden, in collaboration with other research organizations and industries, have made an important contribution with a proposal

of a plant with 50,000 t capacity [100], while in the USA, Oak Ridge National Laboratory and Michigan State University has also made an important contribution in this field.

3.6. Biochar

Biochar has been produced from LCB and technically hydrolyzed lignin as a byproduct through pyrolysis (T = 500–700 °C) or hydrothermal carbonization (T = 180–300 °C). During heating at high temperatures, the functional groups are gradually lost, resulting in materials with polycyclic aromatic structures and a high condensation degree. The second step of the process is physical and/or chemical activation at high temperatures [101].

Biochar characteristics correspond to a solid biofuel with reduced H and O amounts, while N and S contents are below the detection limit. The biochar obtained at 600 and 700 °C has a good quality, and it behaves as a microporous adsorbent, being suitable for selective adsorption; primary, secondary, and tertiary wastewater treatment; as a catalyst; etc. [102].

4. New Developments in Lignin Use as Raw Material for Some Polymeric Materials

Borregaard (Norway) is the world's leading producer of lignin-based biopolymers as green alternatives to synthetic polymers from wood derived from sustainably managed forests. These environmentally friendly products can be used in a range of industrial applications and markets. They are nontoxic with a documented, favorable environmental footprint and are based on a sustainable raw material and thus do not compete with food production [103,104].

The chemical and structural recalcitrance of lignin, especially technical lignin, limits processability and chemical reactivity. Deconstruction of lignin is one route to obtaining aromatic building blocks as, oligomeric fragments for the synthesis of new polymers. The resultant products contain several functional reactive alkenes, aldehydes, and phenolic residues that provide sites for chemical modifications to impart polymerizability. The crude lignin, lignin-derived oils, or depolymerized lignins of reduced molecular weights and improved reactivity have been used to produce lignin-based phenolic resins/adhesives, polyphenolic/polyurethane foams, and epoxy resins and others.

4.1. Phenolic Resins

The phenolic structure of lignin is exploited to obtain phenol–formaldehyde resins, which are mainly used as wood adhesives, but a pretreatment should be applied to increase its reactivity toward formaldehyde. The replacement ratio of phenol with lignin should be less than 50 wt%. Purified organosolv lignin and softwood lignin are recommended [105]. Lignin reactivity in condensation reactions can be increased by methyllation, phenolation as well as enzymatically (in the presence of laccase and oxidase) [106] and thermochemically by mild hydrogenolysis or pyrolysis [107]. Costs and non-recyclability of enzymes are limiting factors. A report published in 2018 indicated a TRL = 8 level for biobased phenolic resin production, with many patents registered in China.

4.2. Polyurethanes

In order to develop high-performance polyurethane (PUR) materials containing lignin, it was used not only as macromonomer to substitute petroleum-based polyols but also as blending filler for the PUR industry. Applied pretreatments involve both extraction of lignin fractions with various solvents and chemical modifications, e.g., depolymerization/deconstruction/liquefaction, hydroxyalkylation, dealkylation, and esterification, which are performed to obtain a more reactive lignin suitable for synthesis of PUR products. Lignin/PUR blends were also prepared to enhance properties of PUR. A higher bio-substitution (20–25 wt %) lignin ratio demonstrated the potential industrial application of lignin for high-value-added sustainable PUR materials [108] such as PUR foams containing lignin, which are already on the market. Developments required in the use of lignin in PUR production and materials are depolymerization and fractionation of lignin into well-

defined oligomonomers, avoiding chemical modifications, improved dissolution of lignin into polyols, and modulation of the properties of flexible PUR foams obtained by green synthesis from liquefied lignin, which should be achieved using the most efficient chain extenders. Applications have been found for PUR foams in packaging of furniture and for the interior parts of car seats [109]. Increasing lignin reactivity via its prefunctionalization with isocyanates is sometimes necessary [110]. Researchers and the industry should pay attention to life-cycle assessment (LCA) studies and technical–economic assessments [111].

Lettner et al. [112] studied the use of kraft lignin in phenol–formaldehyde (PF) resins for wood-based panels and in PUR foams. The importance of reactivity and constant quality of lignin as a raw material was evidenced.

4.3. Epoxy Thermosets

Different procedures have been used to obtain high-performance epoxy thermosets from biomass. The depolymerization products of lignins resulting from the mixtures of both softwood and hardwood were subjected to Dakin oxidation in order to increase their phenolic functionality, and then they were glycidylated to obtain mixtures of epoxy monomers. Biobased epoxy thermosets were conveniently prepared from these epoxy monomer mixtures. They displayed outstanding thermomechanical properties, and, at the same time, environmentally damaging purification steps are avoided [113]. In other studies, oxirane moieties were introduced to the refined fractions, resulting in lignin epoxides that were crosslinked with polyether diamines (Mn = 2000 and 400) to obtain lignin-based epoxy resins [114]. Liu et al. [115] prepared series of high-performance epoxy thermosets via the reaction of epichlorohydrin with lignin oligomers blended with renewable epoxied cardanol glycidyl ether and then cured with methyltetrahydrophthalic anhydride.

In conclusion, at present, kraft lignin and other types of lignin resulting from biorefineries with unique structures and properties can be considered as raw materials for at least eight types of products, three with polymeric structures, namely carbon fibers, polyurethane foams, and phenol–formaldehyde resins, and five, chemicals, specifically vanillin, aromatic monomers, phenols, eugenol, adipic acid, and also fuels.

5. New Developments in the Use of Lignin as a Bioactive Compound

5.1. Antioxidant, Antimicrobial, Antifungal, Antiviral, Antitumoral, and Drug Carrier Activities

Because of their particular characteristics, lignins are used in pharmaceutic, medical, and cosmetics applications as bioactive agents. The medical or therapeutic potential of lignin-derived materials, such as antimicrobial, antiviral, and antitumor compounds, in controlled drug delivery [116], tissue engineering, and gene therapy has been studied [116,117], and the effect of the lignin type on the properties of the obtained materials was demonstrated [118–120].

Lignin obtained from agricultural/forestry residues or paper-pulping wastewater is rich in aromatic structures and a potential natural antioxidant. The lignin structure offers different functional groups along a phenol ether backbone that render it predisposed for: (i) functionalization with surface-active groups; (ii) confer to them an amphiphilic character; (iii) phenolic groups that allow them to undergo interactions such as π–anion and π–hydrogen/hydroxyl; (iv) phenolic groups that are susceptible to oxidation; therefore, lignins act as natural antioxidants [121–123]. Lignins exhibit comparable/higher radical scavenging ability compared to synthesized commercial antioxidants [124,125], being promising renewable alternatives. Preparation of lignin nanoparticles and of the chemically modified compounds are efficient procedures to improve the antioxidant activity, due to the increase in the free phenolic hydroxyl content and to the decreasing bond dissociation enthalpy. The reaction mechanism explaining antioxidant activity is based on SET and HAT reactions occurring together; usually. The HAT reaction is quite rapid (seconds to minutes), while SET reaction takes longer. The phenolic hydroxyl content and the mechanical properties of lignin-containing composites are negatively correlated with variation of the molecular weight. Lignins as natural phenols offer interesting properties,

such as enhanced mechanical, antibacterial, antioxidant, antiviral, and anti-inflammatory properties; UV-shielding activities; and steady biocompatibility. Studies on lignin-based composites in biomedical, cosmetic and cosmeceutical applications have been focused on their use in sunscreen, antiaging formulations, and as an excipient for the production of conventional tablets.

Antimicrobial properties of lignin must be explored more through extensive research to provide a replacement for the current, toxic antimicrobial products. There are several studies related to antimicrobial activity of lignin and materials containing it [126,127]. Both scavenging activity and antimicrobial activity are dependent on the biomass source and extraction procedure, showing the following trend: organosolv of softwood > kraft of softwood > organosolv of grass. The antibacterial performance depends on the type of lignin, the bacterial strain, and the testing conditions. Kraft lignin isolated from corn efficiently inactivated *Listeria monocytogenes* and *Staphylococcus aureus* but not Gram-negative bacteria or bacteriophages, while kraft lignin extracted from eucalyptus inactivated both Gram-positive bacteria, such as *Bacillus cereus*, *Staphylococcus aureus*, and *Pseudomonas aeruginosa*, and Gram-negative bacteria, such as *Escherichia coli* and *Salmonella enteritidis* [128]. Lignins and lignin-containing films showed high antimicrobial activities against Gram-positive and Gram-negative bacteria at 35 °C and at lower temperatures (0–7 °C). The antimicrobial activity of lignins also depends on the solvent polarity (as shown for ethanol, acetone, and DMSO). Storage led to an increase in the antimicrobial activity against *S. aureus* due to the degradation of lignin over time. Purification of kraft lignin has a negative effect on the antimicrobial activity, while storage has a positive effect. Lignin incorporated into complex systems, as in the case of lignin around silver nanoparticle (AgNP) cores, showed an excellent antibacterial performance against *Staphylococcus aureus* and *Escherichia coli*, while Ag^+ had no environmentally adverse effects [129,130].

Antifungal activity also depends on lignin type and processing conditions. It has been found that antifungal activity against *Aspergillus Niger* was the best for kraft lignin extracted from eucalyptus, which exhibited better antifungal performance with respect to that of the spruce lignin extracted via organosolv [131]. Lignin–carbohydrate complexes extracted from biomass via different methods, such as acidolysis, fractionation, and enzymatic hydrolysis, efficiently inactivated the *Encephalomyocarditis* virus and herpes simplex virus (HSV) [132,133]. Lignosulfonate, with a structural similarity to heparan sulfate, has antiviral activity against HSV and human immunodeficiency virus (HIV) [134].

Porous structure of materials influences their geometry, density, high surface area, permeability, water solubility, and adsorption ability, features required for medical applications, especially for controlled drug delivery systems, wound dressing, and tissue engineering. Such characteristics are also possessed by many lignin-based/containing biomaterials [38,135]. The chemical features of the oligomers and polymers of monolignol C9-building blocks of lignins can be exploited in the pharmaceutical sector mainly as a material for matrices and carriers for drug delivery, such as acetylsalicylic acid or paracetamol [136]. Lignin, chemically derived carboxylated lignin and lignin-based materials increased the release efficiency compared to controls while protecting the active compounds [137]. However, some cases present challenges. As an example, the kraft process involves high temperatures and harsh chemicals, leading to irreversible damage to the reduction of ether bond linkages, mainly β-O-4 bonds, and highly condensed lignin. Therefore, some processed lignins and technical lignins.are less chemically reactive and more cytotoxic compared to native lignin In such cases, it is important to evaluate the biocompatibility of each type of lignin [138].

Lignins are able to encapsulate either hydrophobic [139] or hydrophilic drugs [140]. Lignin copolymers as multi-arm carriers with antioxidant lignin core and poly(glycidyl methacrylate-co-poly(ethylene glycol) methacrylate) derivative arms are highly efficient in gene delivery [141].

5.2. Lignin Chemical Modification

Lignin chemical modification generates a number of functional lignin-based polymers, which integrate both the intrinsic features of lignin and the additional properties of the grafted/modified polymers. Some techniques have been reported for lignin functionalization, such as methoxy group substitution, phenolation, demethylation, ring-opening, dehydration polymerization, condensation polymerization, crosslinking, solvolysis, and combinations thereof. Lignin derivatives and copolymers mainly deriving from chemical processes at hydroxyl groups present in their structure (including acetylation, esterification, hydroxymethylation alkylation, methylation, and phenolation arylation, epoxidation, etherification, and amination) via copolymerization, such as silylation and grafting, or physical methods (irradiation, freeze-drying, sorption, changes in surface properties of lignin by cold plasma, electron beams, etc.) are also utilized to induce enhancements in green polymer composites as advanced and sustainable materials because they offer better miscibility with other polymeric matrices, leading to improved performance of lignin/polymer composites.

Stimuli-responsive materials. pH-sensitive lignin-based materials have attracted great interest in various fields, such as biomass refining, pharmaceuticals, and detecting techniques. The pH-sensitive mechanism of the smart materials is dependent on the hydroxyl or carboxyl content in the lignin structure. A novel pH-sensitive material was obtained by incorporation of ester bonds between lignin and 8-hydroxyquinoline (8HQ). The pH sensitivity and the sustained amount of 8HQ released under alkaline conditions (pH = 8) was higher than that under acidic conditions (pH = 3 and 5) [142]. Alkali lignin, as an ionotropic crosslinker, has been used to obtain chitosan–alkali lignin thermo-responsive hydrogels [143] for wound-dressing applications.

5.3. Lignin Use in Agriculture

Lignin can be transformed into agrochemicals such as fertilizers, pesticides, liquid plastic films, feed, soil improver, and plant growth regulator [144] and can be utilized in the cultivation of edible fungi. Ammonia-oxidized lignin nitrogen fertilizer, lignin urea, and lignin sulfonate nitrogen fertilizer have the characteristics of slow nutrient release and leaching loss when irrigating crops are small. They can also reduce the number of required fertilization periods, which greatly reduces water pollution. Lignin is very attractive for the production of agrochemicals with improved efficiency in slowing or controlling nutrient/fertilizer release into the soil upon the biodegradation of lignin due to its biocompatibility, wide availability at low cost, and many reactive groups that allow the chemical binding of a wide number of nutrient-containing groups. The hydroxyl, carboxyl group, methyl oxygen base, and carbonyl active groups with others in the lignin structure can combine with a variety of heavy metal ions (ferrous ions, Zn^{2+}, Ca^{2+}, Mg^{2+}, $Cu^{+1;+2}$, etc.) and chelating micro-materials to in the preparation of controlled-release fertilizers [145,146]. Lignin from the pulp and paper industry or agricultural waste can be chelated to achieve microfertilizers with reduced cost and good biological reaction activity. Lignin-chelated micro-fertilizer has a slow release, low cost, good stability, and high biological activity.

Lignin-based slow/controlled-release fertilizers can be obtained using three main approaches, namely (i) chemical modification of lignin constituting the nutrient, (ii) use of lignin as a coating for the active ingredient, or (iii) application of lignin as a chelating agent for trace element release [145,147–149]. Nitrogen-containing groups attached to lignin via ammoxidation (a process for the production of nitriles using ammonia and oxygen) and Mannich reactions are used, but both methods use toxic chemicals. The main limitation of the coating is the uneven surface and presented cracks; therefore, the nutrient release is less controllable than in the products prepared via chemical modification. Therefore, there are needed improvements to optimize the coating process. In valorization processes, the production of lignin-derived humic substances is also an attractive direction. To convert lignin into humic-like materials, alkaline aerobic oxidation, alkaline oxidative digestion, and oxidative ammonolysis of lignin are applied. The obtained humic substances are

useful in soil enrichment, fertilizers, wastewater treatment, water decontamination, and medicine [150,151].

The use of commonly known agrochemicals increases the agricultural productivity, but they have negative impacts on the environment. The administration of fertilizers and pesticides in cultivated areas is achieved by spraying of these compounds over large areas, but the changes in weather patterns and geographical shifts make it more difficult to cultivate crops in many regions of the world. More sustainable methods to manage fertilizers and pesticides in fields should be elaborated. The encapsulation of agrochemicals to develop more sustainable formulations, such as nanofertilizers, nanoherbicides, and nanopesticides, which provide the sustained release of active compounds, is needed. Nanoencapsulation reduces the rate of dissolution of the agrochemicals and allows their slow, sustained release [152–155]. For grapevines and other woody plants, sicknesses such as Esca sickness, caused by fungi, bacteria, and viruses, are a global challenge that increasingly leads to economic losses. Presently, there is no efficient fungicide with systemic action against Esca. Worldwide damage by Esca is estimated to be USD 1.5 billion and is expected to further increase in the coming years, due to climate change and the connected increasing stress on plants. Lignilabs GmbH in Mainz (Germany) has developed a platform technology that can encapsulate various substances into lignin nano- and microparticles. Polymer additives/3D printing technology has been used for treating Esca sickness. An aqueous suspension of lignin carriers (hollow nanospheres) filled with an adapted fungicide is directly injected into the plant, which allows for treatment of the sickness at the place of its origin. The product with the commercial name ESCApe acts instantaneously against Esca fungi, and it preventively acts on healthy vines to prevent the disease. ESCApe is active against a large spectrum of wood-destroying fungi and can potentially be used against pathogens on fruit trees, shrubs, ornamental plants, or in the forest. ESCApe suspension is injected in minimal dosage (0.8 mL) into a drill hole (Ø 6 mm, 35 mm long) oblique to the vine trunk. Once the injected product is distributed in the plant vessels, the lignin is degraded by the enzymes produced by the fungus, which liberates the pesticides. The fungus therefore destroys itself through its enzymes. In addition to the instantaneous treatment effect, the length of preventive action is 3 to 5 years. Due to lignin and its unique properties applied, the production and the application of ESCApe are completely sustainable as well as user- and environmentally friendly.

6. Lignin Nanoparticles

Cellulose and lignin of lignocellulosic biomass are widely explored for the formation of several nano-ranged particles [156]. The emerging applications of nano-based cellulose and lignins have been explored in different sectors, including the biomedical and environmental fields [157]. There are some difficulties in obtaining certain types of lignin nanoparticles (LNPs) because the lignin structure is of an aromatic material with multiple phenolic rings. Nowadays, these difficulties have been overcome, and many types of nanosized lignins are produced, such as irregular nanoparticles, nanospheres and hollow nanospheres, hollow nanotubes, and nanofibers.

The preparation of lignin-based nanoparticles (LNPs) transforms unordered and complicated lignin materials into ordered nanoparticles with uniform size and morphology and excellent properties such as controlled structures and sizes, better miscibility with polymers, and improved antioxidant activity. LNPs are obtained by different methods, such as self-assembly; solvent exchange; acid precipitation; polymerization; ultrasonication, such as from empty fruit bunches of oil palms [158,159]; crosslinking; electrospinning; and CO_2 use as a non-solvent. In the self-assembly process, an ordered or organized morphology results because of some specific intermolecular noncovalent interactions such as hydrophobic, electrostatic, hydrogen-bonding, and Van der Waals interactions in the absence of any external factor. LNPs are obtained by solvent exchange following dissolution (in tetrahydrofuran, dioxane, dimethyl sulfoxide, acetone, ethanol changed by water); precipitation; ultrasonication; oil-in-water emulsions, which are used for microcapsules (0.3–1.4 μm);

preparation by ultrastirring when lignin micro- and nanocapsules are obtained; or by electrospinning of softwood organosolv in the presence of 2 wt % $FeCl_3$ [160,161]. Hollow lignin-based nanospheres of a diameter around 200 nm were produced. Firstly, lignin was dissolved in tetrahydrofuran (THF), and then water was added under very specific conditions. Such LNPs have been loaded with an anticancer drug, which was successfully released under controlled conditions. Lignin has no cytotoxicity and shows better biocompatibility than many other possible carriers. To fix the anticancer drug inside the lignin spheres, β-cyclodextrin was grafted on the lignin, prior to the formation of the nanospheres. Hydrolysis lignin, kraft/alkali lignin, lignosulfonate, enzymatic hydrolysis lignin, and organosolv lignin can be used for LNP preparation. The β-Cyclodextrin-modified LHNPs exhibited a good sustained-release capability for the antitumor hydroxycamptothecin (HCPT) drug [162]. Modified lignin has an improved network structure and increased specific surface area and porosity. The obtained hollow nanoparticles encapsulate and load the drugs via self-assembly. The irregular lignin-based particles are ordered into the colloidal spheres (r = 110 nm) by dissolving acetylated lignin in THF followed by gradual addition of water [163]. Various combinations of different types of lignin, such as enzymatic hydrolysis lignin, kraft/alkali lignin [164–167], lignosulfonate [168,169], and organosolv lignin [170,171], and chemical modification of lignin or solvent/non-solvent systems have been used by several authors [172–174]. Utilization of the hazardous and expensive chemical reagents, such as acetyl bromide, cyclohexane, dioxane, $NaNO_2$, maleic anhydride, THF, and acetone or processes involving complicated chemical modification reactions should be avoided.

6.1. Green Approaches to Preparing LNPs and Their Properties

The traditional manufacturing techniques of LNP preparation are costly and often toxic and with a high impact on the environment. Ecological approaches, which are simple and safe, have been developed for the synthesis of LNPs [175]. Green approaches to preparing LNPs include non-solvent nanoprecipitation and ultrasonication [176]. A very simple approach for producing LNPs with wide suitability and high efficiency consists of their processing in aqueous sodium p-toluenesulfonate (pTsONa) solution (APS-LNPs) at different pHs, at room temperature, without any other modifications. This method was applied to various types of lignin [177]. The hydrodynamic diameter of the LNPs varied with lignin type and decreased with the increase in COOH content at an initial processing pH < 7. Their zeta potentials decreased from −22.6 mV to −35.2 mV. LNPs from various production techniques show a specific variation of the minimum cytotoxic concentration (MCC) with solution concentration. In cytotoxic testing of LNPs using the Cell-Counting Kit-8 (CCK-8) assay, standard mouse fibroblasts, namely NIH-3T3 cells, were used. The obtained cell viabilities were over 90% when the concentrations were less than 800, 500, and 200 μg/mL sodium p-toluenesulfonate (pTsONa) solution (APS-LNPs) and THF/ethanol/water–LNPs respectively. Therefore, LNPs prepared using APS are less cytotoxic than many other nanomaterials.

LNPs have been obtained with high yield; therefore, a scale-up production of this procedure is promising. The properties of the LNPs depend on the synergistic behavior of the entrapped pTsONa and the intrinsic phenolic OH and COOH groups of the LNPs. Drug-loaded LNPs can be simultaneously prepared. Three types of technical lignins, namely BLN birch lignin (hardwood, BB), alkali Protobind 1000 (grass, PB), and kraft LignoBoost (softwood, LB), have been compared in an LNP preparation study utilizing non/anti-solvent precipitation, using as the lignin solvent 70% aqueous ethanol, acetone/water (3:1) and NaOH and water/aqueous HCl as the non-solvent. The acetone/water (3:1) system was found to be the most effective because it allowed production of small, spherical, homogeneous, and monodisperse LNPs with a negative surface charge and smooth surfaces [178]. Another simple and sustainable synthesis approach to obtaining LNPs was developed using a recycled γ-valerolactone (GVL)/water binary solvent through nanoprecipitation (dropping or dialysis) of the lignin solution. The highest yield of LNPs reached 90%.

Their diameter was ca. 250 nm, and their zeta potential was −40 mV. LNPs showed good dispersibility and stability in water. LNPs can be used to stabilize essential oils and to promote their growth inhibition activity against microbes; therefore, they exhibit enhanced antimicrobial activity [179].

6.2. Lignin Nanoparticle Applications

LNPs showed superior antibacterial and antioxidant/UV barrier properties. Lignin-based hollow nanoparticles are considered suitable for many applications both as additives in polymers and in therapies. There are various fields for industrial applications of LNPs, such as in drug delivery carriers, UV absorbents, hybrid nanocomposites, antioxidant and antibacterial agents, adsorbents for heavy metal ions and dyes, and anticorrosion agents' nanofillers [180]. Entrapment, encapsulation, adsorption, and covalent binding are common methods for loading active compounds into lignin materials. LNPs as drug delivery nanosystems are capable of loading both hydrophobic and hydrophilic drugs for targeted cancer and tumor treatments [181], including poorly soluble curcumin, hydrophobic coumarin-6 [182,183], bioactive molecules of resveratrol, hexadecane, sorafenib (SFN), benzazulene, capecitabine [37,165,166], hydrophilic rhodamine 6G, and doxorubicin hydrochloride (DOX) [160,165]. LNPs form through the supramolecular assembly of poorly water-soluble molecules via electric interactions with aromatic rings. Most of the substances that have been successfully entrapped in lignin NPs to date are poorly water-soluble, low-molecular-weight compounds, such as antibodies and enzymes.

pH-responsive lignin-based nanocapsules have been obtained by interfacial miniemulsion polymerization. Sodium lignosulfonate grafting with allyl groups takes place via etherification. An oil-in-water miniemulsion system has been prepared through ultrasonication and dispersion and has been used for a thiolene radical reaction with lignin-based coumarin-6 [168]. Curcumin, a polyphenolic natural compound, can be delivered by LNPs obtained by modified phase separation [168]. Curcumin was used as a lipophilic drug model, as its poor solubility and low oral bioavailability limit its therapeutic efficacy. The average particle diameter of curcumin-loaded LNPs was 104 nm, and the encapsulation efficiency was 92%. They also showed enhanced protection of the entrapped curcumin under storage conditions and are also stable in simulated gastric fluid and slow release under intestinal conditions. In vivo pharmacokinetics tests demonstrated that the LNP system increased by ten-fold the bioavailability of curcumin in comparison to common administration. Temperature and pH at which the entrapped drug is released are other important parameters for drug delivery systems [171]. They are extensively studied, especially as drug and gene delivery systems and in cancer therapy [175,181,183].

The antioxidant and UV protection properties of nanosized lignin have been utilized in the food, pharmaceutical, and cosmetic industries [184,185] (Table 2). Two sets of nanocellulose-based cryogels that differ in their overall surface charge density have been prepared by freeze-drying, namely those containing anionic LNPs anchored to cationic cellulose nanofibrils (cCNFs) and or cationic LNPs (cLNPs) that are combined with anionic TEMPO-oxidized CNFs (TCNFs) [186]. LNPs acted as crosslinkers and affected rheological and water holding capacity as well as the firmness of the cryogels. The cryogels are pH dependent, regenerable, and reusable, being suitable for cationic, anionic, and neutral aromatic pharmaceuticals and adsorption of the anionic aromatic pharmaceutical diclofenac of the aromatic cationic metoprolol and tramadol and of neutral aromatic carbamazepine. As crosslinking agents, the LNPs or cLNPs affected the rheological behavior of the cryogels. Reusable adsorbents, such as macroporous cryogels resulting from anchoring lignin nanoparticles (LNPs) to the nanocellulose network via electrostatic attraction, have been developed. They are useful for simultaneously removing pharmaceuticals of varying chemical structure and properties from polluted media [186].

Essential-oil-loaded LNPs showed interesting antifungal activity against both white-rot fungi and brown-rot fungi [187]. Cumulative release profiles of EOs vary with the EO type and lignin concentration in loaded LNPs, as shown in Figure 3, while minimal

inhibitory concentration (MIC) also depends on fungus type (*T. versicolor*, *G. trabeum*, *P. ostreatus*, and *P. monticola*), ranging from 0.05 mg/mL (*P. monticola*) up to 0.60 mg/mL (*P. ostreatus*).

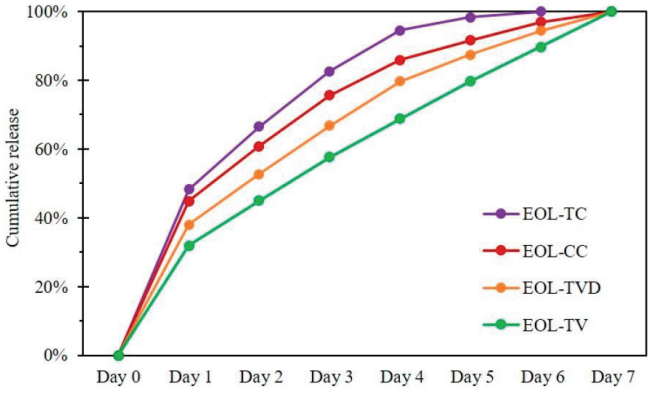

Figure 3. Cumulative release profiles of essential oils from LNPs containing C. *capitatus* (EOL-CC), T. *capitatus* (EOL-TC), T. *vulgaris Demeter* (EOL-TVD), and T. *vulgaris* (EOL-TV) oils (reprinted from [187]).

Antibacterial and adhesive hydrogels, such as core-shell nanoparticles and Ag-LNPs, embedded into pectin/acrylic acid polymeric networks have been obtained [188].

Softwood lignin nanoparticles (SLNs) are promising alternative bio-additives for enhancing PLLA crystallizability toward the development of fully biobased and biodegradable plastics [189].

Lignin macromolecules have been in situ modified by mild ozone oxidation without significant degradation of carbohydrate polymers (i.e., cellulose and hemicellulose) in lignocellulose nanofibrils [161]. The interfacial hydrogen-bond energy was improved, and, by molecular dynamics simulation, the deformation process of lignocellulose nanopaper was validated. Lignin acts as a functional component in the lignocellulose nanopaper matrix, but the interfacial hydrogen-bonding among lignocellulose nanofibrils is diminished, and mechanical performance is decreased. Ozone oxidation of 40 min leads to changes in the carboxyl content onto nanofibers, so that the zeta potential values, the crystallinity index, and the degree of polymerization were reduced, while the lignocellulosic structures were preserved. The kappa number decreased from 78.9 to 68.3, while the whiteness of the lignocellulose nanopaper increased from 15.2 to 38.8. The ozone preferentially oxidized chromophoric structures of lignin. Lignin-modified lignocellulose nanopaper preserved its water and thermal stability, mechanical properties, and optical performance. The developed lignocellulose nanopaper is a multifunctional and flexible material used in electronic applications. Multifunctional ozone oxidation substrate was printable and highly compatible with conductive materials (as silver), providing an eco-friendly alternative to conventional substrate materials (e.g., Mylar film and polyimide).

6.3. Lignin Nanofibers

Nanofibrous networks that closely resemble the native extracellular matrix (ECM) for new drug delivery systems and other biomedical applications have been developed by electrospinning [190]. They offer a high surface area, high porosity, pore interconnectivity, resistance to agglomeration, and high drug loading and encapsulation capacity, etc., properties that make them excellent candidates for drug delivery. A wide variety of bioactive compounds or therapeutic agents can be incorporated within the fibrous meshes [191]. Heterogeneous chemical composition, complex branched structure, and low molecular weight are challenges to electrospinning pure lignin. Pure lignin nanofibers were obtained using a

coaxial electrospinning technique via the optimization of the electrospinning parameters or using suitable solvents [160,192]. The spinnability of lignin is improved by its combination with various hydrophilic or hydrophobic polymers, such as PLA [193], polycaprolactone (PCL) [194], polyvinyl acetate (PVA) [195], and polyhydroxybutyrate (PHB) [196].

Abudula et al. used coaxial electrospinning to encapsulate chitin/lignin gels with polycaprolactone (PCL) for fibrous scaffolds with controlled drug release ability [197]. The minimum fiber diameter, porosity, biodegradation, optimum pore size, tensile strength, and Young's modulus were improved by lignin (10 wt%) addition.

Antioxidant PLA/lignin nanofibrous scaffolds have been applied for cartilage tissue engineering and osteoarthritis treatment. It has also been suggested that the scaffolds can be used in many other biomedical applications, including delivery of various bioactive molecules, UV filtration, and consumer care [198].

Table 2. Lignin nanoparticles (LNs) and electrospun-based lignin biomaterial properties and applications (recent studies).

LNPs and Other Components	Properties and Applications	Refs
Lignin nanoparticles (LNPs)/starch	Green nanofiller in starch-based biocomposites; strong interfacial hydrogen bonding; enhanced mechanical properties, thermal stability, antioxidant activity, and good (UV) irradiation shielding performance; applications such as delayed oxidative deterioration of soybean oil/advanced food packaging	[199]
Lignin nanoparticles obtained by a acidolysis process from corn lignin/polyurethane, polyethylene glycol and diisocyanates	LNPs as crosslinking agent in polyurethane nanocomposites. Composites with hydrophobic, UV resistant and dielectric properties, enhanced tensile strength; good reprocessability	[200]
0.5 wt% lignin and nanolignin in poly(lactic acid) composites synthesized by in situ reactive processing as melt mixing and ring-opening polymerization (ROP)	Reactive processing produced nanolignin-containing composites with superior crystallization, mechanical, and antioxidant properties. LNPs act as a macroinitiator in the ROP of lactide, resulting in PLA-grafted nanolignin particles, improved dispersion and the formation of interfacial covalent bonds facilitated by LNPs	[201]
Lignin-based nano-micelles using the "grafting-from" method	pH-sensitive, biocompatible, suitable for oral drug delivery	[202]
Nanolignin/chitin nanofibrils and complexes loaded with active molecules, such as vitamin E, sodium ascorbyl phosphate, lutein, nicotinamide, and glycyrrhetinic acid	Spray-drying method; nanostructured chitin; Functional agents in skin regeneration and antimicrobial, anti-inflammatory, and antioxidant activities; cytocompatibility in skin regeneration.	[203]
PCL coated with chitin–lignin gel; shell/core fiber, coaxial electrospinning; electrospun PCL/lignin, initial blending	Methylene blue, penicillin/streptomycin; sustainable drug release; wound dressing; fibrous scaffolds; MTT tissue engineering	[197,204]
LNP/PVA/PVP electrospinning. Initial blending	Paclitaxel local anticancer therapy	[205]
AgNP-loaded electrospun PVA/lignin nanofibers	Membrane filtration, antimicrobial fabrics, and wound dressing	[206]
Lignin/cellulose acetate/N-vanillidene-phenylthiazole copper (Il) complexes, nanofibrous materials	Antimicrobial for hygienic applications	[207]

Electrospinning is generally used to fabricate 2D dense fibrous scaffolds with limited cell infiltration. By coupling electrospinning with other advanced manufacturing techniques (e.g., 3D printing and cryogelation), the nanofibers will be more efficient for drug delivery applications [208,209]. Lignin and LNPs are biodegradable and offer good performance and special properties, but their utilization in the medical fields is still very low. It is expected that the surface modifications with various functional groups will

increase their application in medicine, especially in drug delivery. The development of alternative preparation methods for LNPs, nanocomposites, and hybrid materials with low cost, biocompatibility, and sustainable surface modification, that are eco-friendly and easier for large-scale production, is necessary, especially for medical applications.

Developments in lignin valorization also involve important applications, such as lignin-based hydrogels, three-dimensional printing materials, electrospun scaffolds, surfactants, electrodes, and production of fine chemicals.

7. Lignin-Based Hydrogels

A drastic increase in the number of published articles, 336 (1990–2022) in the field of lignin hydrogels, suggests the importance of this research area [38,210] or future development, with 55 publications on lignin in drug delivery in 2022 and with most of them being focused on LNPs [211]. A major prerequisite for lignin with respect to synthesizing hydrogels is the abundance of phenolic OH groups in the lignin backbone which can crosslink with COOH groups of the co-joining monomer. The highest concentration of phenolic OH groups is found in kraft lignin, followed by organosolv and soda lignin. In terms of mechanical properties, soda lignin-based hydrogel is superior, since strong crosslinks will result in improved elastic nature. Organosolv-based hydrogel may be the best choice, while superior mechanical properties will necessitate the use of soda lignin-based hydrogels.

The three-dimensional network of hydrogels can be easily adjusted by the degree of crosslinking to achieve the desired physical properties, elastic modulus, and gelation time suitable for in situ use degradation rate, so they can act as indicators. The increase in the crosslinking degree leads to inferior water swelling capability. Thus, shape and flexibility can conform to the target tissue, and the degradation period can be tuned to follow the progress of tissue regeneration [212]. The biodegradability of the natural polymers and their non-inflammatory effect and nontoxicity of these degradation products suggest that these types of materials are suitable for being used in tissue regeneration. Nanogels obtained from natural polymers have become very important in many scientific and industrial domains, due to a series of interesting properties, such as their large surface area, significant swelling, high ability for loading active substances, and flexibility. The design and the production of nontoxic, biocompatible, and biodegradable micro/nanocarriers, demonstrated their suitability and feasibility for biomedical applications, such as drug delivery, tissue engineering, and bioimaging [213,214]. Controlled hydrogels or highly functional hydrogels are used in drug or bioactive substance delivery systems as well as other clinical applications.

Due to its well-known properties (i.e., biodegradability, biocompatibility, low-toxicity, antioxidant, and antimicrobial properties), lignin is often used as an important component of hydrogels. Furthermore, lignin-containing hydrogels are more environmentally friendly when compared to synthetic hydrogels. Because the high diversity of their functional groups, lignin-based hydrogels can be loaded and can deliver a large number of both hydrophilic and hydrophobic therapeutic agents, such as small molecules, nanoparticles, proteins, enzymes, and nucleic acids.

Different innovative physical, chemical, and biological processes have been elaborated to obtain lignin-based hydrogels [215].

Physical hydrogels are formed by intermolecular interactions, including self-assembly through hydrogen bonds and electrostatic, hydrophobic, and van der Waals interactions. Lignin-based macroporous hydrogels are obtained using either salt leaching or gas foaming methods, but from these processes byproducts with high toxicity can result, and the synthesis is a multi-step procedure with a high cost. Cryogels show major advantages over hydrogels prepared by classical methods because they have a highly interconnected pore network structure coupled with macro-sized pores [216]. The walls of the cryogels can be highly crosslinked and dense, and they act as depots for drug storage and improve mechanical properties, suggesting their potential use as scaffolds and in sustaining injectability and shape memory. Two distinct cryogelation procedures may be employed:

(i) the freeze-drying approach with multiple freeze-drying cycles using traditional lignin hydrogel precursors, where each freezing cycle generates additional hydrogen/electrostatic bonds and strengthens the polymer network, and (ii) the freeze-thawing approach occurring in a frozen solvent via a single-step cryopolymerization step resulting in the polymer network [217]. Frozen aqueous solvent, such as porogen, induces the appearance of large pores following ice thawing [218]. The properties of products obtained by cryogelation, such as the size and the shape of the pores, their interconnectivity, and also the ability of drug adsorption, vary with lignin sources along with possible modification, temperature, and polymer concentration [219].

The polar sites on the lignin backbone can be involved in physical crosslinking with hydrophilic polymers by H-bonding (such as polyurethanes and lignin–chitosan–polyvinyl alcohol (PVA) composite hydrogel) [135,220]. Such hydrogels are obtained using several methods, such as heating in an oven for short periods of time when the crosslinking is hypothesized to be uniform, microwave irradiation, use of ultrasound, and reactive extrusion. All these techniques can be considered as green because they use no or few toxic solvents [221,222].

Chemical hydrogels are synthesized using crosslinking agents. Covalent crosslinking includes the use of carbodiimide compounds (e.g., 1-ethyl-3-(3-dimethylaminopropyl) carbodiimide/N-hydroxysuccinimide (EDC/NHS), and glutaraldehyde (GA)), radical polymerization, thermal gelation, enzymatic reactions, click chemistry, photo-oxidation, and radiation crosslinking, reversible addition–fragmentation chain transfer polymerization, catechol redox chemistry, crosslinking copolymerization, ring-opening polymerization, etc.

Semi-interpenetrating/interpenetrating networks result from polymerization techniques. Biologically mediated processes occur in the presence of laccases/peroxidases or a whole cell (fungal)-mediated process. The crosslinking grafted lignin procedure uses unsaturated monomers or other functional chemicals to improve its reactivity. Esterification of the phenolic hydroxyl group of lignin resulted in unsaturated grafted lignin that was copolymerized with hydroxyethyl acrylate, resulting in lignin-based hydrogels. The "graft-from strategy" leads to the production of polymers starting from the active sites into the polymer backbone, while the "graft-onto" procedure combines the synthetic polymers with lignin (as the result of creating covalent links between the lignin backbone and the terminal groups of the graft polymers). Both strategies are based on the two procedures used to obtain hydrogels, namely atom transfer radical polymerization (ATRP) and fragmentation chain transfer (RAFT) polymerizations. The obtained networks of interpenetrating lignin/polymer such as hydrogels have the perfect aligned structures and controlled properties [215,223,224].

Compared with the microbial attack point of view, hydrogels with a high crosslinking degree proved to be more resistant than hydrogels with low crosslinking, due to the reduced accessibility of ligninolytic fungi and actinomycetes [225]. It is known that the most ligneous fungi have enzyme systems that attack the phenolic substructures in a direct way; therefore, lowering the hydrogel concentration can protect them from a fungal attack. Controlled biodegradation is still a target with high importance in drug delivery domain [226].

Due to population growth, the use of pesticides has significantly increased, as along with the demand for agricultural products. In the meantime, waters have been also polluted with pesticides, resulting in serious negative effects on human health and on the environment. In order to remove pesticides from the aqueous environment, activated carbons or biobased materials represent important alternatives due to their properties (i.e., bioactivity, biodegradability, and biocompatibility). Sustainable solutions to remove pesticides from aqueous environment consist of using activated carbons or biobased materials due to their complementary functionalities such as bioactivity, biocompatibility, biodegradability, and unique chemistry [210,227–229]. Aerogels, xerogels, and cryogels as mesoporous materials with low density, high porosity, and tunable surface chemistry can be useful for environmental remediation applications. For example, aerogels remove CO_2 and volatile organic

compounds from air as well as ions of heavy metals, oils, and organic pollutants from water.

Applications have been found for lignin hydrogels in agriculture (sustained/controlled water absorption, slow release of pesticides/fertilizers), being superior in terms of mechanical properties (such as tensile strength and compression resistance), environment protection (heavy metal adsorption, dye removal, water treatment), suitability for food packaging and the biomedical sector [230] (wound healing/dressing, anti-microbial coatings on medical implants, oxygen scavenging, tissue engineering, sustained drug release), and preventing spontaneous combustion of coal, biosensors, and electronics (supercapacitors) (Table 3).

Table 3. Characteristics of lignin-containing hydrogels and their applications in various domains (recent studies).

Hydrogel Components	Characteristics and Applications	Refs
Agriculture		
Alkali lignin and -based poly(ethylene glycol) diglycidyl ether	Increased availability and retention of soil water, which is beneficial for plant growth; high efficiency in severe dryness conditions; alleviated drought stress in maize	[231]
Physically crosslinked alkaline and organosolv lignins or lignins/poly(vinyl alcohol) hydrogels	Significant swelling and water holding capacity; addition of lignin enhanced the swelling/water retention ability of hydrogels by 800%	[232]
Lignin/alginate/konjaku flour-based hydrogel	Increased water holding/retention and of the nutrient retention capacity of the soil, increase in the mass of tobacco plant under dryness conditions	[233]
Lignin/polyacrylic acid-based hydrogels	Controlled release of some pesticides (i.e., paraquat, cyfluthrin, and cyhalofop-butyl)	[234]
Wastewater treatment and removal of pollutants		
Black liquor lignin-hydroxyethyl cellulose hydrogel	Super-absorbent hydrogel; removal of dye pollutants	[235]
Polyacrylic acid-g-pretreated alkali lignin porous hydrogel	Removal of Pb^{2+}, Cu^{2+}, and Cd^{2+}	[236]
Lignin functionalized with hexadecyltrimethylammonium-bromide-based spherical particles	Lignin-based biosorbents; removal of vanadium (V) ions from aqueous solution	[237]
Lignosulfonate/lysine hydrogel	Adsorption of heavy metal ions	[238]
Lignin/PVA or LNP/nanocellulose (cryogels); anchoring lignin nanoparticles (LNPs) to the nanocellulose network via electrostatic attraction	Environmental engineering. Adsorbents for pharmaceutical pollutants (e.g., diclofenac, metoprolol, tramadol, carbamazepine) and Bisphenol A	[186,239]
Hydrogel was obtained by free-radical polymerization in the presence of methylenebisacrylamide (MBA), alkali lignin (AL), and potassium persulfate (PPS). Carboxylated cellulose nanofibrils (CCNs) and carbon dots (CDs) as fluorescent probes were prepared via a condensation reaction	Fluorescent hydrogel. Adsorption of Cr (VI), excellent optical properties, biocompatibility, and nontoxicity significant efficiency in adsorption and detection of Cr (VI)	[240]
Biomedical [206]		
Alkaline and organosolv lignins, hydoxymethylated lignins, peroxidated lignins/PVA	Onion peels were valorized for quercetin (natural drug) microwave extraction; controlled drug delivery, and quercetin-controlled delivery applications	[241]

Table 3. *Cont.*

Hydrogel Components	Characteristics and Applications	Refs
Lignin-agarose hydrogel/silk fibroin (SF) embedded zinc chromite nanoparticles	Hemocompatibility and antibacterial activity; complete healing of the wounds in mice treated with the scaffold of crosslinked lignin–agarose/SF/$ZnCr_2O_4$ nano-biocomposite after five days; wound healing application;	[242]
Enzymatic hydrolysis lignin (wheat straw)–alginate cryogels and cryogels obtained from the freezing technique; wet and dry alginate–lignin aerogels	Porous structure; lignin reduced hydrophilicity of alginate; wound healing and tissue repairing/tissue engineering; regenerative medicine	[243]
Lignin-co-gelatin (cryogels) and chemically crosslinking and Ag_2O/CuO NPs	Antioxidant, antibacterial, injectable lignin/gelatin composite cryogels; wound healing and tissue engineering; good mechanical properties and microporous structure; very good free scavenging activity; inhibited growth of both Gram-positive and Gram-negative bacteria	[244]
Lignin/gelatin hydrogels with different concentrations of lignin	Fast-release drug carriers used to deliver Ribavirin in COVID-19 treatment	[245,246]
Organosolv lignin/gelatin composite cryogels obtained by chemically crosslinking at −20 °C. Organosolv lignin and gelatin; multifunctional, bioactive lignin-co-gelatin composite cryogels obtained by chemically crosslinking lignin together with gelatin at −20 °C.	Multifunctional, bioactive cryogel with antimicrobial (reduced *E. coli* and *S. aureus* viability) and antioxidant activities; in vitro cyto-compatibility (after 72 h of incubation, viability of 3T3 cells was 97%); improved mechanical properties and syringe injectability	[219,242]
Ag/lignin NPs/PAA-pectin hydrogel	Good mechanical, antibacterial, and wound healing properties; epidermal growth factor loaded in the Ag-lignin NPs-PAA-pectin hydrogel increases the wound healing activity	[188,247]
Lignin/poly(ethylene) glycol diglycidyl ether hydrogel	Drug delivery; controlled release of paracetamol	[248]
Organosolv lignin extracted from coconut husks/polyethylene glycol (PEG), polypropylene glycol (PPG), polydimethylsiloxane (PDS) nanogel	Thermo-responsive polyurethane-based copolymer nanogel; lignin-incorporated nanogel; acts as an antioxidant biomaterial for wound healing; human L-02 hepatocyte cell viability > 90%; rapid and complete wound healing after 25 days; wound-dressing application	[249]
Lignin-carbohydrate complex/PEG diglycidyl ether	Cell carriers; positive hepatocyte adhesion; biocompatibility	[250]
Alkali lignin/chitosan hydrogels	Wound healing applications; low cytotoxicity, biocompatibility, 99 ± 3% cell viability	[143]
Lignosulfonate/poly(vinyl alcohol)/chitosan composites hydrogel; lignin mixing an aqueous acidic solution of chitosan and solutions of lignin and PVA	Composite hydrogel; 10 wt% lignin had enhanced hydrophilicity, antimicrobial behavior, and antioxidant capability; wound dressing	[220]
Lignosulfonate; in situ reduction of AgNPs then crosslinked in the lignin/PVA hydrogel	Improved antibacterial activity against *Staphylococcus aureus* and *Escherichia coli*, non-cytotoxicity, biocompatibility, wound healing	[251]
Lignin/PVA cryogel; freeze-drying crosslinking and curing methods	"Smart" biomaterial scaffolds elaborated by using a factorial design scaffold fabrication model; 800% water retention capacity; controlled drug loading and delivery; pH and temperature responsiveness; antifungal activity against *Aspergillus niger* strain	[232,252]

Table 3. *Cont.*

Hydrogel Components	Characteristics and Applications	Refs
40–24% lignin-containing alcohol groups/Gantrez S-97 (GAN) (methylvinylether and maleic acid copolymer)/PEG by esterification reaction accelerated by microwave radiation, crosslinking time was reduced from 24 to 1 h	Reductions in *Staphylococcus aureus* and *Proteus mirabilis* adherence (two common pathogens responsible for medical-device-associated infections); curcumin delivery	[222]
Glycinated kraft lignin/hyaluronic acid hydrogels	Non-cytotoxicity (>90% cell viability); positive cell migration and cell growth	[253]
Kraft lignin/PLA/Rose Bengal, gold, silver	pH-responsive hydrogels; antifungal and antimicrobial properties at very low IC50 values (0.1 μg/mL)	[254]
Lignin epoxy-modified resin/xanthan crosslinking with epichlorohydrin	Superabsorbent hydrogel; high swelling rate in aqueous medium; release of hydrophilic bisoprolol fumarate drug for high blood pressure and heart failure treatments	[255]
Low and high lignin content/cellulose nanofiber; ultrasound-assisted	Tissue engineering; cytocompatibility with gingival fibroblast cells	[256]
Methacrylated lignin (lignin-MA)/sulfobetaine methacrylate (SBMA) double network structure consisting of chemical and physical crosslinking between SBMA and lignin-MA	Lignin-MA as hydrogel skeleton and antibacterial agent; 94.8% reduction rate against *E. coli* and 95.7% against *S. aureus;* high hydrophilicity because of zwitterionic SBMA. Antifouling and antimicrobial properties, potential applications in medical devices and as biological material	[257]
	Food packaging	
Lignin (black liquor of bagasse) into PVA/gelatin blends	Antimicrobial and antibiofilm activities against food-borne contaminants as Gram-positive bacteria *Bacillus subtilis* and *Staphylococcus aureus* and Gram-negative bacteria *Escherichia coli* and *Pseudomonas aeruginosa*	[258]

Lignin hydrogels are stimuli-responsive to pH, temperature, ionic strength, etc., being desirable for the development of drug delivery systems [20,215]. Hydrogels with a significant content of lignin are characterized by a high cumulative drug release because they exhibit an improved viscoelastic behavior, adequate structure of pores, and good swellability. Between their significant disadvantages, one can mention their low mechanical properties, fast drug release kinetics, and non-adherent nature (a supplementary dressing being necessary in order to protect them), and it is not always easy to obtain hydrogels of a pure or high lignin content due to the polydispersity and differences in the molecular structure of lignin [230].

Antimicrobial, antioxidant, and anti-inflammatory intrinsic properties of lignin make it a valuable therapeutic agent, and it is beneficial in other medical applications. It enhances the viability, propagation, and the differentiation of Schwann cells and, ultimately, facilitates nerve tissue generation. Antimicrobial activity is explained by the interaction of the hydroxyl group of phenolic compound lignin with the bacterial cell, causing cell membrane disruption, the infiltration of cell components, and ultimately bacterial cell lysis. The antioxidant ability of lignin also has proven to be useful in composite hydrogels for biomedical applications [215] that still are in the lab research stage. However, their commercialization continues to present various difficulties, such as lignin isolation, standardized molecular weight, lignin structural characteristics, and lignin cost. Functionalization of lignin to improve its polymerization with other polymeric materials is an open direction for research, and in vitro and in vivo detailed toxicity studies are required to facilitate the application of lignin-based hydrogels in the food and pharmaceutical industries. Cost-effective technology, scaling, and proof of concept (POC) to attract industrial production are required for lignin-based hydrogel commercialization.

Other applications: Composites of bio-polyamides reinforced with lignin, which also acts as a fire retardant, have been obtained [259]. Sodium lignosulfonate in polypropylene matrix is a surfactant, flame retardant and smoke suppression agent [260]. Practically, lignosulfonate (with a structure of hydrophobic aromatic rings and hydrophilic sulfonate groups) biosurfactants have a wide range of applications, including as a substitute for standard surfactants, as an asphalt emulsifying and wetting agent [261], and solubilization and stabilization of thymol in water [262]. Sulfethylated lignin (similarly, butyric anhydride-modified kraft lignin and PEGylated lignin) can be a surfactant, stabilizer for oil–water emulsions, reinforcement, UV protection additive, and antioxidant, and surfactant activity offers a green and economic route to obtaining strong and transparent polymeric nanocomposites containing ~30 wt% LNPs [263] as well as a *stabilizer/surfactant* for oil–water emulsions [264]. Nanosized lignin using soda lignin from empty fruit bunches of oil palms is nontoxic and superior to the commercial emulsifying agent, and sulfethylated lignin was established to be a good emulsifier for water-in-oil emulsions.

8. Three-Dimensional-Printing-Based Lignin Biomaterials

"Additive manufacturing (AM) or 3D printing is a digital manufacturing computer-aided design process to fabricate layer-by-layer products with customized sizes, shapes, and functionality" [265]. It is performed for medical/pharmaceutical or food purposes using different techniques, such as stereolithography (SLA), digital light processing (DLP), direct ink writing (DIW), fused deposition modeling (FDM), selective laser sintering, selective laser melting, 4D/5D/6D printing, melt electrowriting (MEW), and cryoprinting [266–270]. AM is utilized to address the demand for production of pharmaceuticals with patient-specific dosages [271], customized drug formulations [272], the most desirable geometrics [273], and controllable drug release profiles. AM should be available in hospitals or medical care centers for printing tailored personalized medicine or delivering therapeutic agents [274]. Lignin-based materials meet both printing and medical requirements, such as appropriate printability, mechanical properties, biodegradability, biocompatibility, tissue biomimicry, and non-cytotoxicity [275]. They have been used to design meshes for wound dressing, capsules for pharmaceutical oral drug carriers, and innovative hydrogel bioinks for 3D bioprinting in tissue engineering, microextrusion, and laser-assisted bioprinting techniques [276,277].

AM techniques, such as extrusion printing, direct ink writing, and fused deposition modeling, are suitable for printing pure lignin, lignin derivatives, or a combination with other polymers or monomers as fillers or additives necessary to create lignin-based printable feedstocks [278,279]. For printing lignin-based biomaterials, extrusion and vat photopolymerization are the most commonly used technologies [280–282]. Lignin-coated PLA composite pellets containing drugs printed by fused deposition modeling into various mesh sizes have been obtained [283]. Antimicrobial and antioxidant filaments composed of lignin and polybutylene succinate (PBS) have been studied by Abdullah et al. [267,284], using printing based on fused deposition modeling and coated with silver/zinc oxide (Ag/ZnO), which exhibits a strong inhibitory effect against bacteria to fungi. A Ag-LNP nanocomposite inserted in a methacrylated O-acetyl-galactoglucomannan (GGMMA) network is a good printed antimicrobial hydrogel with strong bactericidal performance [285]. Domínguez-Robles et al. [286] designed a bioactive wound dressing by loading curcumin (an anti-inflammatory and antimicrobial agent) and D-Panthenol onto PCL/lignin for 3D printing. The printed composite displayed sustainable release of bioactives and antioxidant, antimicrobial, and anti-inflammatory properties.

The large-scale utilization of lignin in 3D printing is still a great challenge due to its inherent brittleness and non-thermoplasticity. Thermoplastic polyurethane regulates the rheological properties of lignin for 3D printing [287]. Other examples are given in Table 4.

Table 4. Recent examples of lignin use in 3D printing materials, their properties, and applications.

Components	Characteristics and Applications	Refs
15% by weight modified lignin-containing photoactive resins	These materials generate new products for additive manufacturing applications, with a four-fold increase in ductility. Excellent print quality was obtained with modified lignin resins with a commercial stereolithography system	[288]
Organosolv lignin OSL/hydroxypropyl cellulose (HPC), 40/60 and 50/50 mixtures	Lignin/HPC biobased aqueous inks; direct-write lyotropic blends; high performance	[289]
Lignin–carrageenan/AgNP-$MgCl_2$ one-pot synthesis of AgNPs	Lignin as a reducing agent for AgNP green synthesis and capping agent in the carrageenan matrix crosslinked with divalent cations; wound healing; fast wound dressing	[290]
Spherical colloidal lignin particles/cellulose nanofibril-alginate	Three-dimensional printed cell culture model; soft-tissue engineering	[291]
Keratin/lignin hydrogels	Smooth films and nanoparticles; 4D functional biocomposite materials. Protein complexation by lignin was applied to form copolymers and reinforce keratin crosslinking networks on aqueous and solid state processing 3D and 4D printing	[292]
Kraft lignin/keratin	Fully biodegradable keratin hydrogels through ”greener” processes. Lignin binder to deliver 3D-printability; keratin/lignin biocomposite materials. Lignin as material additive manufacturing technology: 3D and 4D printed responsive materials without the need for synthetic chemical modifications	[293]
Granular dealkaline lignin/corn-derived zein protein by extrusion	3D-printed insoluble lignin granules act as a binder for enhanced printability and degradation in soil. Suitable biocomposites for 3D printing manufacturing biodegradable circuit boards are used, along with inexpensive industrial byproducts lignin and zein as precursors and benign solvents, such as ethanol and water	[294]
Poly(caprolactone)/lignin/loaded curcumin	3D-printed dressings; antioxidant and antimicrobial activities	[286]
Carboxylated lignin/polylactic acid melt mixing;	Suitable biocomposites for 3D printing via fused deposition modeling (FDM); improved interfacial adhesion between the COOH-lignin surface and PLA matrix; reduced cost of printing PLA 3D filaments without changing their thermal and mechanical properties	[295]
Lignin-coated cellulose nanocrystal/methacrylate composites	3D stereolithography printing; mechanical reinforcement and thermal stabilization	[276]

Lignin is physically or chemically mixed with other components, such as cellulose or its derivatives, to take advantages of each component to formulate high-performance 3D bio-feedstocks for 3D products. Several lignin-based compositions of inks used in 3D printing are known as lignin/poly(ethylene oxide) (PEO), 20–40% lignin/acrylonitrile butadiene rubber (NBR41)/acrylonitrile-butadiene-styrene (ABS);/polyacrylonitrile (PAN)-based carbon fiber (CF); lignin modified with nylon 12/acrylonitrile butadiene rubber (NBR41) [275]. Lignin/poly(ethylene oxide) (PEO) blend filaments for 3D printing with a melt-spinning process have been prepared. The filament derived from lignin with 15% PEO had a uniform diameter, smooth surface, adequate mechanical properties, and thermal stability. Bio-feedstocks in the presence of lignin allowed good printability at lower temperatures.

Many existing processes operate at very high temperatures, being expensive and difficult to scale. To address these challenges, researchers from the University of Delaware replaced methanol, a traditional solvent used in lignin deconstruction, with glycerin to enable the process to take place at a normal atmospheric pressure [296]. Replacing methanol with glycerin provided the same chemical functionality but at a much lower vapor pressure, leading to a more cost-effective system.

9. Lignin Use in Green Functional/Complex Materials

Green polymer biocomposites generally consist of a biobased thermoplastic or thermoset matrix with organic (e.g., wood flour, chicken feather) fillers (particulates or fibers) and/or organic matrices (biopolymers) with inorganic additives such as carbon black, clays (montlorillonites, haloysite, glass fibers), or silver nanoparticles (AgNPs).

The possibility of creating lignin-based polymer biocomposites to replace petroleum-based composites has attracted the interest of many researchers worldwide due to the negative environmental impact of traditional composites over time. Their aromatic and crosslinkable functional groups make them suitable for a variety of polymeric matrices with improved wettability, strength of the polymer composites, mechanical properties, and new properties such as fire-retardant and UV-light-blocking characteristics [297,298]. Lignin, with its distinctive chemical structure, can function in lignin-based biomaterials including biocomposites, copolymers, nano-/micro particles, fibers as a stabilizer, compatibilizers, and flame retardants. Lignin's role is very different as an eco-friendly biodegradable and renewable matrix, crosslinking agent, and nano- and micro-filler, being used in building the designed structure and in modifying some properties such as mechanical, thermal, antioxidant, antibacterial, biodegradability, biocompatibility, permeability, porosity, water solubility, and adsorption ability. However, it can only be incorporated in small amounts in other polymers because of its rather poor miscibility.

Stabilized morphology and improved thermal properties with lignin as an additive increased the number of phenolic groups, ketone molecules, and chromophores, this leading to higher UV light barrier properties, as lignin exhibits a strong UV-blocking capacity, as well as antioxidant and radical scavenging characteristics. Lignin has been investigated as an active ingredient to create film materials with reduced hydrophilicity and ultraviolet-blocking qualities.

The differences in characteristics between lignin and conventional polymers led to the incompatibility of the biocomposite. Its highly hydrogen-bonded network through phenolic groups makes it immiscible with many polymers. Solvent casting and extrusion methods are mainly used to incorporate lignin into polymeric matrices. Chemical modification, which depends on lignin origin and on the extraction conditions, was applied to obtain better compatibility of lignin with polymer matrices in bi- and multiphase composites [299–302]. Deconstruction and chemical modifications will increase lignin utilization in complex materials. Modified lignins are useful materials for environmentally friendly polymeric materials. However, chemical modifications require additional investments in the form of solvents, reagents, and energy inputs.

After cellulose, lignin is the most commonly used natural polymer in green and synthetic biomaterials. Introducing lignin into commercial polymers can create green functional/complex materials such as composites or eco-friendly composites, with very interesting properties. Lignin contributes to improving properties, such as dimensional stability, hydrophobicity, porosity, material density, mechanical properties, biodegradability, biocompatibility and non-cytotoxicity; lignin can also possibly impart functionalities of the resulting products, such as antibacterial and antioxidant properties and controlled drug release, at lower production costs. LNPs are also used. Using strategies inspired by nature, different researchers have developed lignin-based nanocomposites that display both the well-known properties of bio/nanocomposites (improved mechanical and gas barrier properties and higher thermal stability) and the remarkable features of either the biological or inorganic (sometimes nanoparticles) moieties, such as biocompatibility,

biodegradability, and, in some cases, functional properties. Lignin can be incorporated into the biocomposites as a nucleating agent, UV absorber [45,303], copolymer, filler material, reinforcement, coupling agent, compatibilizer, etc. Lignin-based biocomposites are applied in drug delivery systems, wound dressing, tissue engineering, and regenerative medicine (e.g., skin, nerve, cartilage, bone, and hard tissues). However, the valorization of lignin for high-value applications in composite materials is low, which could result in large increases in costs. Its use as a reinforcement material in biopolymers is a comparatively new and emerging research field [304].

Although lignin is highly resistant to chemical and biological degradation, it is slowly degraded by ligninolytic microbes [305]. Lignin has been used as the main matrix in a new class of engineering materials based only on renewable resources. For example, the Arboform® composites consist of isolated lignin, natural fibers, and natural additives, while Xylomer™ (made up of lignin/polymer blends) materials are elaborated through conventional thermoplastic processes, such as injection molding [306]. Lignin use in composites manufacturing is limited by its low solubility and reactivity, high polydispersity, glass-transition temperature (Tg), sulfur content, color, etc. Selection of a suitable lignin type and its deconstruction methods, functionalization/modification, and the incorporation of UV stabilizers can be applied [307,308].

Carbonyl and conjugated phenol groups, such as chromophores, inside the lignin structure explain the light absorption in the UV range (200–400 nm), thus showing very good UV shielding and being a promising material to substitute the synthetic UV absorbers in composites, mainly in food packaging, because they help to protect food from UV irradiation. The chromophore groups also impart an undesirable dark color, creating a loss of visible transparency of the polymer film. Visible transparency is an important factor for food packaging because customers generally desire to see the product inside the packaging. The UV-absorbing lignin composite materials can be included in food packaging, healthcare products, and solar panel protection [36]. The UV-shielding properties and color of lignin are modified by selected extraction process, chemical modification method, and size of lignin particles, etc. The synergetic effect between lignin and the other constituents of the complex materials was demonstrated. More efficient lignin dispersion and compatibilization will lead to improvement in the properties of the multicomponent materials.

As mentioned before, other types of materials (LNPs, hydrogels, etc.) have many possible applications in agriculture, biomedicine, and the food and building industries, and different lignin-containing materials such as LNPs as well as 3D-printing can help to reduce the quantity of waste products and decrease environmental pollution [308].

Possible ways to improve the dispersibility and compatibility are lignin esterification [309–311], the use of crosslinkers [312–314], and polymer surface modification using physical or chemical methods [315–318].

The most useful blends/composites containing lignin are those biobased polymers (such as starch, cellulose, epoxy, natural rubber, chitosan, alginate, plant proteins) and synthetic ones (polypropylene (PP), PVA, polylactic acid (PLA), polyhydroxy butyrate (PHB), poly(ethylene glycol) (PEG), poly(vinylpyrrolidone, polyamides, etc.). There is a special interest in obtaining and improving the green composites containing lignin (Table 5). Corn was blended with soda lignin and graphene oxide in a wheat starch matrix. Different combinations have been tested such as corn starch, cassava starch, urea-crosslinked tapioca starch, kraft and acid hydrolyzed lignin in modified corn starch microparticles with crosslinking agents, adipic acid in corn starch and glycerol, and lignin–sago starch blends for novel food packaging film using a solvent casting process. The films with kraft and soda lignin as fillers have an improved water barrier and thermomechanical and seal strength properties and a considerable reduction in permeability (water vapor) and transmission, particularly when films are made from hydrophilic materials, such as alginate and starch, because of the interaction of lignin and the hydrophilic groups of the biopolymer [319–321]. Starch/20% kraft lignin foams obtained by compression molding

showed similar properties to PS. Starch foams are biodegradable alternatives to foamed polystyrene [322]. Lignin incorporation reduces the oxygen and water vapor permeability. Lignin from the lignocellulosic ethanol process is further valorized for sustainability reasons. The obtained LNPs with an average diameter of less than 160 nm were used as reinforcement for green biodegradable starch films. The 20% incorporated lignin improved mechanical properties and stability of the composites. The presence of lignin-rich solid particles with high hydroxyl group content enhanced the hydrophilicity and the surface energy of starch/lignin film [323]. Lignin-starch films exhibit advantageous physical properties, such as low odor, color changes, and a slight decrease in light transmittance in the visible light region (400–800 nm) after the addition of LNPs, while the starch/lignin (SL) composite films exhibit excellent UV shielding properties, nontoxicity, mechanical properties (Figure 4), oxygen permeability, and good antioxidant performance.

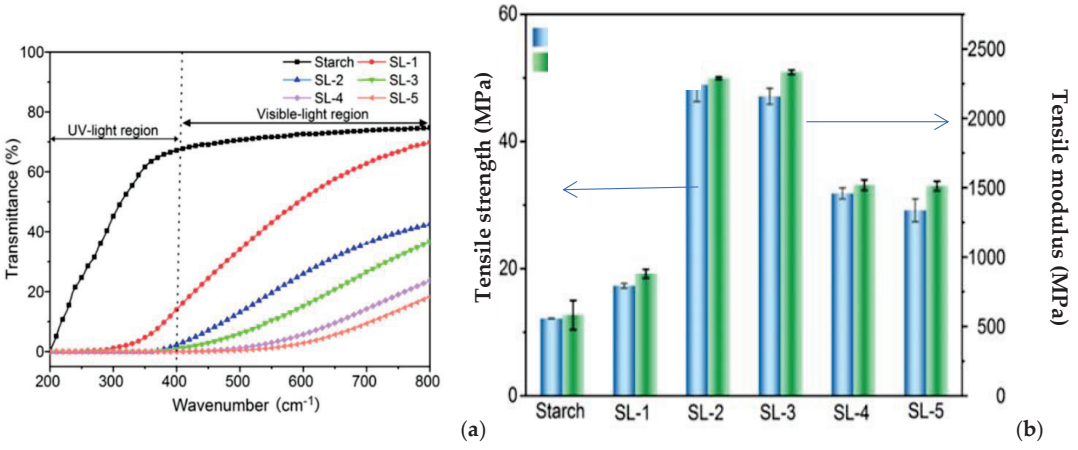

Figure 4. UV–Vis light transmittance spectra (**a**) and mechanical properties of starch film and starch/lignin composite films containing: 1% LNPs (SL-1); 2% LNP (SL-2); 3% LNP (SL-3), 4% LNP (SL-4 and 5% LNPs (SL-5), respectively **[324]**.

Starch/lignin composite film production using an agro-industrial waste byproduct could assist in achieving waste biomass management in a cost-effective and environmentally friendly way. They are promising materials for slowing down the oxidative deterioration of soybean oil, food preservation, and the sustainable packaging industry. Kraft lignin has been blended in soy protein and glycinin, thermoplastic zein, wheat gluten, fish protein-based plastics, the protein matrix of wheat gluten, gelatine, soy protein, formaldehyde, and citronella essential oil to impart antifungal activity, etc.

Lignosulfonate, desulfonated lignosulfonate, and acid-hydrolyzed lignin have been introduced in the PLA matrix, leading to some important improvements in terms of mechanical and thermal stability. Lignin in polyhydroxy butyrate (PHB)-based biocomposites has also been used to improved properties. Lignin/PHB is completely biocompatible, biodegradable, and thermoplastic. The kraft lignin/PHB blend showed excellent biocompatibility and biodegradability.

All these applications of lignin are important reasons to consider lignin valorization in high-performance complex polymeric materials, as an important direction for sustainability and a circular economy. To date, studies on the interaction of lignin with the packaged food, as well as in vivo digestion, are very preliminary and will require additional investigation.

Generally, the compatibility of the lignin with polar components is a challenge; therefore, only small quantities of 10–25 wt% lignin can be used in PP or PE. Lignin can act as stabilizer for polyolefins, but when it is added to PS, the mechanical properties are deteriorated. Satisfactory results are obtained for blends with PET [325] or PVC.

Compostability of the lignin-based materials is an important aspect [326]. It has been mentioned above that lignin is efficiently biodegraded by white-rot fungi and various types of bacteria, but its degradation under composting conditions, commonly used to dispose of food packaging items, is incomplete and inefficient. The improved gas barrier, decreased water permeability, and increased hydrophobicity can be associated with reduction in the material degradability in the composting conditions.

Lignin biocomposites in biomedicine. Nanolignin (NL) and chitin nanofibril (CN) have been assembled into micro-complexes and loaded with bioactive factors, such as the glycyrrhetinic acid (GA) and CN-NL/GA (CLA). Completely biobased and bioactive films and fiber meshes designed for wound healing have been obtained from poly(3-hydroxybutyrate)/poly(3-hydroxyoctanoate-co-3-hydroxydecanoate), surface-modified via electrospraying/electrospinning of CN and NL and tested in vitro with human keratinocytes. The nanoparticles improved the antimicrobial and anti-inflammatory activity of the electrospun fiber meshes, leading to promise for wound healing applications [327].

Table 5. Lignin use in various green blends and composites, its role and applications (recent studies).

Components of Biocomposites	Lignin Role/Application of Product	References
	Agriculture	
Azide-modified cellulose/0.5–2 wt% covalently bonded lignin with UV-blocking properties; propargylated lignin	Biodegradable, flexible, and transparent UV protection films from renewable resources	[297]
Polyvinyl alcohol PVA/lignin, spherical organosolv, lignin particles, LNPs obtained by dialysis with THF or ethanol as solvents	UV-blocking lignin–PVA composite film	[328]
Alkali lignin/carbon nanoparticles (C-NPs) containing lignin nanoparticles (L-NPs)	Agro-nanotechnology - Cost-effective alternative compared to conventional commercial fungicides - Environmentally benign nanopesticides for long-term plant protection - Antifungal nanocomposite - Control agent against *Fusarium verticillioides* in maize	[329]
Alginate/polyvinyl alcohol/calcium chloride and boric as crosslinkers	Three-dimensional (3D) biocomposite adsorbent; multiporous architecture; excellent substitute for a commercial EDTA-Fe micronutrient; eco-friendly, highly efficient	[330]
	Waste treatment	
Hydrophilic sulfonated kraft lignin/polyethersulfone (PES)	Layer-by-layer (LbL) assembly; antifouling coating; oily wastewater treatment	[331]
Lignin-derived adsorption materials	Compounded lignin with other materials; high-value-added lignin adsorbent material wastewater treatment	[332]
	Food Packaging	
Enzymatic hydrolysis of dried solid from alkali treatment of wheat straw/dry corn starch, glycerol, solution casting method	Lignin particles act as reinforcements for green biodegradable starch films	[323]
Technical lignin/cellulose	Cellulose/technical lignin composites; antioxidant and UV barrier Advanced packaging	[333]
Lignosulfonate/alginate	Photoprotective and antioxidant properties; enhanced barrier properties of the blend films and antioxidant activity; active packaging applications	[334]

Table 5. *Cont.*

Components of Biocomposites	Lignin Role/Application of Product	References
Lignin nanoparticles/chitosan/polyvinyl alcohol	Lignin increased mechanical strength and antioxidant and antibacterial activity. Active food packaging	[335]
Low molar mass alkali lignin/PLA	Increased water barrier properties (up to 73%) photodegradability; biocompatibility, antimicrobial activity; very good cellular response and very low cytotoxicity levels; food packaging	[336]
Hydroxypropyl lignin or lignosulfonate or alkaline lignin/soy protein	Enhanced mechanical performance, water resistivity of soy protein plastics and specific functional properties; biomedical uses; food packaging	[337]
Alkaline lignin (AL) and sodium lignosulfonate (LSS)/PEG/thermoplastic zein	Strong H-bonding modifying α-helix, β-sheet, and β-turn secondary structures; improved physical properties; due to the interaction of AL with zein molecules, enhanced strength and water resistivity of soy protein plastics. Food packaging Biomedical uses	[338]
Lignin/tannic acid/biodegradable PBAT composite film: epoxidized soya bean (ESO) oil as plasticizer and encapsulated lignin/tannic acid as filler	Reduced water vapor and oxygen transmission rate; improved properties and degradability. Extended shelf-life and preservation of food, including fresh potato and onion Packaging of dry food products	[339]
Kraft lignin/poly(3-hydroxybutyrate) nano-composite Pickering emulsion and hot compression	Hydrogen bonding interactions; improved mechanical properties, UV resistance/blocking and higher melt viscosity; Food packaging	[340]
Technical soda lignin (ethyl acetate extract/high-density polyethylene. Melt extrusion	Composite for food packaging. Antioxidant and insect repellent activities	[341]
	Biomedical	
Alkali lignin green synthesis of AgNP/carrageenan/calcium chloride, copper chloride magnesium chloride silver	Antibacterial against *Staphylococcus aureus and Escherichia coli*; biocompatible; Wound dressing and healing effect	[190]
Nanolignin (NL) and its composites	Cancer therapy drug and gene delivery, biosensing, bioimaging, and tissue engineering; therapeutic potency of chemotherapeutic drugs by decreasing their dose and reducing their adverse effects	[342]
Lignin as decoration for multi-walled nanotubes/PVA-lignin fiber nanocomposites	Antimicrobial properties Wound healing/tissue engineering	[343]
Lignosulfonate/PVA/chitosan	70% reduction in free radicals; good antibacterial abilities at 10% (*w*/*w*) lignin; wound healing	[220]
Kraft lignin/PVA/poly(glycerol sebacate) (PGS) electrospinning	PVA-PGS-lignin fibers. Lignin incorporation promotes neural cell proliferation and differentiation. Tissue engineering/regeneration	[344]
Kraft lignin/electrospun PCL fibers embedding lignin nanoparticles	Peripheral nerve regeneration	[345]
Alkali lignin/PLA-lignin nanofiber silver-ion-containing lignin nanoparticles/poly(lactide)–lignin nanofibers.	Antioxidant activity; eco-friendly alternative to AgNPs in antimicrobial and antioxidative applications; biomedical application Tissue engineering	[193]

Table 5. *Cont.*

Components of Biocomposites	Lignin Role/Application of Product	References
Lignins extracted from pine residue esterified with succinic anhydride/PLA	Enhanced mechanical and thermal properties of PLA Excellent antimicrobial and biocompatibility.	[346]
Lignosulfonate/polyoxazoline/triazoles (linked silver)	Antimicrobial against many strains such as *Escherichia coli*, *Pseudomonas aeruginosa*, *Salmonella typhi Klebsiella pneumonia*, *Staphylococcus aureus*, *Staphylococcus epidermidis*, *Candida albicans*, and *Candida tropicalis*; Antioxidant, anti-inflammatory, preventing infection; promotion of healing; reduced inflammation on burn wound	[347]
Softwood kraft lignin/poly(butylene succinate) melt-mixing extrusion	Antimicrobial and antioxidant properties; resistance to adherence of the common nosocomial pathogen *Staphylococcus aureus*. Pharmaceutical/biomedical applications	[181]
New High-Performance Materials		
Organosolv lignin/polylactide/PVAc poly(vinyl acetate)/GMAglycidyl methacrylate, reactive extrusion	Super-toughened bio-elastomer PLA composite; improved interfacial adhesion; PVAc and GMA as toughening agents; single glass transition temperature. High elongation at break and impact strength; replaces petroleum-based elastomers such as EPDM elastomer	[348]
Micro- or nano-Soda lignin (NL) as green filler; content between 0.5–5 wt%/PLA masterbatch prepared by solvent casting, then melt mixing.	Biobased and biodegradable PLA films; Interfacial interactions, slightly stronger in the case of NL acting as fillers. Competitive green alternative in the food packaging industry	[201]
Acetylated lignin/thermoplastic polyurethane mixing	Lignin-based thermoplastic polyurethane adhesive. Wood adhesive	[349]
1–10 wt% grape seed lignin/highly crystalline (PHB)/amorphous (PHA). Polyhydroxyalkanoate modification	Improved mechanical and gas-barrier properties, high antioxidant capacity of lignin; biodegradability; active biodegradable packaging films; lignin can change the crystallinity of PHB in compost; nontoxicity of materials and its degradation products; positive effect on white mustard (*Sinapis alba* L.) seed germination	[350]
Methylated lignin, lignin esters, or lignin-containing epoxy groups/poly(butylene adipate-co-terephthalate) (PBAT) coextrusion; PBAT grafted with maleic anhydride as a stabilizer; poly-3-hydroxybutyrate PHB or poly-3-hydroxybutyrate-co-3-hydroxyvalerate	Economically competitive biodegradable PBAT/lignin and PHB/L composites Low-cost filler, 36% price reduction; good properties; degradability	[351]
Lignin-containing microfibrillated cellulose isolated from chemi-thermomechanical pulp or acetylated/PLA	Biocomposites with controlled biodegradation of polylactic acid (PLA). Biotic degradability	[352]
Unfunctionalized lignin and 3-aminopropyltriethoxy silane functionalized lignin/waterborne polyurethane. Chemical reaction	Lignin as natural reinforcing filler	[353]
Lignin/polyfurfuryl alcohol	Thermosets; Eco-friendly composite resins	[354]

Known applications of lignin-based composites are packaging, plant protection, biomedical materials, life sciences, automotive, advanced biocomposites, flame retardants, electroactive materials, energy storage, and others [355]. Synergistic interactions found in lignin-containing systems, mainly in nanocomposites and nanohybrid assemblies, are highly beneficial [356]. Most of the publications related to lignin-containing blends and composites used kraft or alkali lignins; especially kraft lignin in crude form. Higher risks in terms of cytotoxicity compared to lignins stemming from other biorefinery approaches like organosolv processes are possible.

10. Energy Storage and Conversion Technologies

Fossil fuels are increasingly used day-by-day worldwide, which will lead to their eventual depletion. The resulting environmental degradation necessitates the progression of renewable energy sources and energy storage/conversion technologies. Attempts have been made to seek out sustainable different energy sources. Plant biomass, especially wood containing mainly cellulose and lignin with a content of 18–30%, should be a good choice. Polymers and their composites play a vital role in energy storage and conversion technologies. A large volume of lignin is used as biofuels and in energy production. Lignin can partly replace fossil-based materials and allows more environmentally friendly formulations. Renewable lignin could reduce non-renewable coke consumption by approximately 20%.

10.1. Sustainable Fuel from Lignin

Sustainable energy sources and biofuels from renewable sources are very important. Bio-oils are rarely blended with crude oil as a feedstock for refineries. Lignin-derived fuels could reduce greenhouse gas emissions and dependency on fossil fuels. There are two basic methods for converting lignin into fuel: thermochemical and catalytic. Preliminary materials are utilized in hydrotreatment and fluid catalytic cracking (FFC) with zeolites as catalysts. Catalytic hydrogenation converts low-value products (as aromatics) to jet fuel. This coproduction improved the overall economic viability of an integrated biorefinery process [357–360].

10.2. Sustainable Aviation Fuel (SAF)

Sustainable aviation fuel (SAF) is essential to decreasing the carbon footprint of the aviation industry. A team in the USA, the National Renewable Energy Laboratory (NREL), Massachusetts Institute of Technology (MIT), and Washington State University used lignin for the production of the SAF. The two main challenges are finding an effective catalyst and removing the oxygen from the lignin. The lignin oils in existing research projects had an oxygen content of 27 to 34%. For aviation fuel, however, this value has to be lower than 0.5%. To date, catalysts containing expensive precious metals have been used, which, in addition, showed only low efficiency. Carbon dioxide emissions can only be achieved with the massive use of SAFs [361]. A collaboration of US researchers has pioneered a 100% sustainable aviation fuel using lignin [362].

10.3. Electrochemical and Energy Storage Applications

Because of its redox functionalities, lignin has an important role in various energy conservation processes where energy conversion and storage occur through a series of reversible oxidation/reduction reactions such as respiration and photosynthesis. The use of lignin in energy storage devices contributes to obtaining greener energy, improving performance, and also decreasing price and toxicity. Lignosulfonates are preferred for such applications [363]. Most studies deal with the improvement of electrochemical performance, novel lignin sources for this purpose, or structure and surface modifications of obtained materials. A process–structure–properties–performance correlation was associated with lignin valorization from a byproduct of biorefineries to high-performance energy storage materials, with low-cost production.

Lignin shows high potential for use as a renewable precursor for carbon materials, utilized in many energy storage devices. These applications include lignin as an expander for lead–acid batteries, electrodes for primary and rechargeable batteries, electronic double layer capacitors, and electrochemical pseudocapacitors as well as feeding different types of fuel cells, solar cells, etc. [364–367].

10.4. Lignin-Based Organic Flow Batteries

Organic flow battery systems for ships featuring electric propulsion have been developed in the maritime sector. One of the most promising technologies for this purpose is based on lignin developed by the German company CMBlu. Lignin-based organic flow batteries are more secure and stable, less costly, and more sustainable regarding resource use. Finally, the disposal is ecological, the components are easily recycled, and no problematic waste products are generated [368].

11. Conclusions

11.1. Lignin as Promising Renewable Source

The global demand for lignocellulosic biomass and for energy and chemical production has increased, along with the available amount of lignin as waste. Lignin valorization has been mainly focused on production of fine chemicals and biobased high-performance materials. The market size for lignin-based products includes colloidal lignin particles, vanillin, catechol, propyl guaiacol, BTX, PHA, PUR foams as polyols, carbon fibers, eugenol, and jet fuel. At the market level is established that, the selected applications depend on the lignin type. Low-purity lignin is utilized in energy production, bitumen, and biofuel, and with the increase in purity, other uses are envisaged, such as in production of the BTX, phenols, cement additives, activated carbon, and phenolic resins, while high-purity lignin is used to obtain carbon fibers, vanillin, phenol derivatives, materials with applications in medicine, pharmacy, cosmetics, and the food industry, etc. With increased lignin purity, their costs increased and also the value of the obtained products. Thermoset networks via step-growth polymerization from lignin-derivable compounds are also modern fields of research. From this renewable but heterogeneous chemical resource, greater value could be gained by developing higher value pharmaceutical applications which would help to improve integrated biorefinery economics.

A transition from the current petrochemical infrastructure requires either that: (1) regulations accelerate a shift from petroleum or (2) polymers derived from lignocellulosic biomass exhibit superior performance or longer-term (socio) economic advantages. The realization of cost-competitive petrochemical alternatives from biomass may require significant innovations in separation, purification, and polymerization chemistry. Bio-sourced materials are inherently greener than petrochemical-based systems, but the complexities are associated with lignin heterogeneity and modifications. The non-homogeneous, polydisperse nature and varying molecular weight and structure of lignin result from highly biodiverse sources and the lack of standardized extraction procedures, which is important when the lignin biomaterial is used for medical purposes such as in scaffold fabrication. Research interests are focused on the development of lignin nanoparticles/nanofibers, hydrogels, green composites as multicomponent, functional materials, etc., with a complex composition, which assures the good performance of materials through these synergistic interactions. The use of 3D-printable lignin monomers/formulations is particularly beneficial, but a lack of material diversity is considered a major limitation in stereolithographic printing. The high-volume utilization of lignin in 3D printing applications would further broaden its application fields and alleviate the environmental load of lignin. Lignin is one of the prime candidates for various biomaterial applications, such as raw materials, additives, drug and gene delivery, biosensors, bioimaging, 3D printing, tissue engineering, and dietary supplements. In applications related to food and pharmaceutical fields, the toxicity profiles require more in-depth, long-term analyses due to the phenolic nature of lignin biomaterials. Detailed structure/function relationships must be investigated to better understand the

mechanism and behavior of lignin-drug carrier interactions, and also detailed studies on lignin biomaterial sterilization, in vivo biodegradation, and biocompatibility to better assess the role of lignin on cells and tissues are necessary.

The use of bulk lignin in composite materials incorporates renewability, reduces costs, and increases functionality. Novel bio-nanocomposites with improved properties and multifunctionality domain can be envisaged as an emerging, open field of research, with many possibilities because of the great abundance and diversity of biopolymers in nature, synergistic combination with inorganic nanosized solids, lignin graft copolymers, enzymatic grafting, and crosslinked networks.

11.2. Challenges and Future Trends

Lignin, the second-most abundant renewable biopolymer on Earth, is one of the largest natural renewable sources of aromatic structures. Sources of lignin are paper-pulping wastewater and agricultural/forestry residues, including straw, husk, stalks, stover, and cobs as the largest sources of wasted lignin, which are considered highly valuable as bioenergy and biorefinery materials because they are renewable, non-edible, and do not interfere with the food industry. Suitable valorization of lignin waste streams from the pulp and paper industry and biorefinery processes could be a crucial step for the development of a circular sustainable economy. The extraction of lignin is one of the major barriers in the reclamation and reuse of lignin from waste. Eco-friendly isolation of lignin from agricultural wastes is in the development stage and should be further studied [369]. Lignin has multiple impressive physicochemical properties (good mechanical and physicochemical properties, low weight, and excellent thermal stability, and it can undergo a range of modifications to tailor or impart special characteristics, such as improved compatibility and processability) and shows important bioactive effects (antioxidant, antimicrobial, antifungal, anti-inflammatory properties, etc.) being considered a multipurpose/multifunctional raw material with important roles/applications in the various fields. Therefore, lignin possesses huge potential for the production of a variety of materials because of its high carbon content, low cost, and bio-renewability. However, challenges appear because of the large differences found in molecular structure and molecular weight of lignins resulting/extracted from different sources (plant family and species, their culture conditions, part of plant, age, climate, etc.), extraction procedures, and after further treatments. Some technical/processed lignins are less chemically reactive and more cytotoxic compared to native lignin. In such cases, it is important to both evaluate in detail structure, molecular weight, biocompatibility, cytotoxicity, etc. of each type of lignin and to select suitable type for a certain application domain. Better-controlled composition and properties of the obtained products are necessary. The characterization and quantification of functional groups and the ratio of monomeric units are the main characteristics of technical lignins, affect the possibilities and strategies for further processing, and are among the chief obstacles of the utilization of this highly abundant biopolymer. Although several techniques were developed for this purpose, there is still a need for quick, cost-efficient, detailed characterization and reliable quantification methods for the utilization and modification of lignins for high-performance materials.

Because of its large number of hydrogen bonds, lignin has strong intermolecular and intramolecular forces, showing either favorable interactions with some components or a poor incompatibility and dispensability in complex polymer systems. To overcome these difficulties, careful selection of lignin type and modification methods for improving the compatibility have been used. Numerous studies have been conducted to develop natural alternatives, starting from biodegradable, renewable resources, which are safer and cleaner for the environment, including lignin valorization. New materials will be developed by combining green chemistry and engineering technology as a consequence of the demand for development of environmentally friendly and sustainable production/consumption/waste management systems for both plastics and biodegradable materials. This trend has changed in recent years because of modifications in consumer habits; preferences for single-use

products, fresh food, and ready-to-eat packed food; awareness of the need for a healthy life and environment; and the growing need for fabricating packaging, medical devices, healthcare products, and others in a more environmentally friendly way. Lignin-based materials are excellent candidates for greenhouse gas diminution in comparison to many petroleum-based chemicals.

However, the valorization of lignin to high-performance and cost-competitive materials remains a challenge. It better adheres to "green design" principles in comparison to petroleum counterparts, but its properties rank below those of several common petrochemical plastics with respect to environmental impact considering a full life-cycle analysis and economic gains. Moreover, lignin valorization has encountered a series of constraints related to its heterogeneous polymeric nature/composition, intrinsic recalcitrance, strong smell, dark color, some problems encountered in lignocellulose fractionation, recalcitrance to depolymerization/deconstruction, and a complex mixture of aromatic compounds resulting during degradation, etc. Deconstruction and chemical modifications will increase lignin utilization in complex environmentally friendly polymeric materials. However, these procedures require additional investments in the form of solvents, reagents, and energy inputs.

The simulation of biorefinery processes for the design of manufacturing processes to obtain value-added chemicals from lignocellulosic resources has been conducted, but this method must be continuously developed to assess/control all steps of the studied processes. Researchers and the industry should pay attention to life-cycle assessment (LCA) studies and technical–economic assessments. The importance of reactivity and constant quality of lignin as a raw material is also necessary. The developments are necessary in the alternative preparation methods to ensure low cost, biocompatibility, surface modification, sustainability, eco-friendliness and ease of large-scale production of LNPs and hybrid materials, especially those designed for medical applications. Functionalization of lignin to improve its polymerization with other polymeric materials is an open direction for research, and in vitro and in vivo detailed toxicity studies are required to facilitate the application of lignin-based hydrogels, LNPs, biocomposites in the food and pharmaceutical industries, and biomedicine. The large-scale utilization of lignin in 3D printing is still a great challenge due to its inherent brittleness and non-thermoplasticity. Cost-effective technology, scaling, and proof of concept are required to attract industrial production for lignin-based hydrogels/LNPs and green composite commercialization.

Author Contributions: This is written at the beginning. These authors contributed equally to this work. All authors have read and agreed to the published version of the manuscript.

Funding: This research received no external funding.

Institutional Review Board Statement: Not applicable.

Conflicts of Interest: The authors declare no conflict of interest. The authors alone are responsible for the content and writing of the paper.

References

1. Kakkalameli, S.; Daphedar, A.B.; Faniband, B.; Sharma, S.; Nadda, A.K.; Ferreira, L.F.R.; Bilal, M.; Américo-Pinheiro, J.H.P.; Mulla, S.I. Chapter 2 Biopolymers and Environment. In *Biopolymers Recent. Updates, Challenges and Opportunities*; Nadda, K.A., Sharma, S., Bhat, R., Eds.; Springer Series on Polymer and Composite Materials; Springer International Publishing: Cham, Switzerland, 2022; pp. 19–35, ISBN 978-3-030-98391-8.
2. European Bioplastics. Available online: https://www.european-bioplastics.org (accessed on 12 May 2023).
3. Thiruchelvi, R.; Das, A.; Sikdar, E. Bioplastics as better alternative to petro plastic. *Mater. Today Proc.* **2021**, *37*, 1634–1639. [CrossRef]
4. Nilsen-Nygaard, J.; Fernández, E.N.; Radusin, T.; Rotabakk, B.T.; Sarfraz, J.; Sharmin, N.; Sivertsvik, M.; Sone, I.; Kvalvåg-Pettersen, M. Current status of biobased and biodegradable food packaging materials: Impact on food quality and effect of innovative processing technologies. *Compr. Rev. Food Sci. Food Saf.* **2021**, *20*, 1333–1380. [CrossRef] [PubMed]

5. Jafarzadeh, S.; Jafari, S.M.; Salehabadi, A.; Nafchi, A.M.; Uthaya Kumar, U.S.; Abdul Khalil, H.P.S. Biodegradable green packaging with antimicrobial functions based on the bioactive compounds from tropical plants and their by-products. *Trends Food Sci. Technol.* **2020**, *100*, 262–277. [CrossRef]
6. Bar-On, Y.M.; Phillips, R.; Milo, R. The biomass distribution on Earth. *Proc. Natl. Acad. Sci. USA* **2018**, *115*, 6506–6511. [CrossRef] [PubMed]
7. Li, C.; Zhao, X.; Wang, A.; Huber, G.W.; Zhang, T. Catalytic Transformation of Lignin for the Production of Chemicals and Fuels. *Chem. Rev.* **2015**, *115*, 11559–11624. [CrossRef]
8. Amidon, T.E.; Liu, S. Water-based woody biorefinery. *Biotechnol. Adv.* **2009**, *27*, 542–550. [CrossRef]
9. Cao, L.; Yu, I.K.M.; Liu, Y.; Ruan, X.; Tsang, D.C.W.; Hunt, A.J.; Ok, Y.S.; Song, H.; Zhang, S. Review Lignin valorization for the production of renewable chemicals: State-of-the-art review and future prospects. *Bioresour. Technol.* **2018**, *269*, 465–475. [CrossRef] [PubMed]
10. Ncube, L.K.; Ude, A.U.; Ogunmuyiwa, E.N.; Zulkifli, R.; Beas, I.N. Environmental impact of food packaging materials: A review of contemporary development from conventional plastics to polylactic acid based materials. *Materials* **2020**, *13*, 4994. [CrossRef]
11. Renewables. Biofuels. IEA Report. 2021. Available online: https://www.iea.org/reports/renewables-2021/biofuels?mode=transport&region=World&publication=2021&flow=Consumption&product=Ethanol (accessed on 12 May 2023).
12. Ragauskas, A.J.; Beckham, G.T.; Biddy, M.J.; Chandra, R.; Chen, F.; Davis, M.F.; Davison, B.H.; Dixon, R.A.; Gilna, P.; Keller, M.; et al. Lignin valorization: Improving lignin processing in the biorefinery. *Science* **2014**, *344*, 1246843. [CrossRef]
13. Garlapati, V.K.; Chandel, A.K.; Kumar, S.P.J.; Sharma, S.; Sevda, S.; Ingle, A.P.; Pant, D. Circular Economy Aspects of Lignin: Towards a Lignocellulose Biorefinery. *Renew. Sustain. Energy Rev.* **2020**, *130*, 109977. [CrossRef]
14. NILE—New Improvements for Lignocellulosic Ethanol Project. Raporteur Alfred Abächerli. Evaluation by Computer Simulation of the Influence of Lignin Separation on Mass Flow and Cost for Lignocellulosic Bioethanol Plants Contract No.: 019882;/28 May 2010′/Granit Recherche & Dévelopement SA D3-3-11 DelivReport2010-Public V2-1.doc. Available online: https://cordis.europa.eu/project/id/19882 (accessed on 15 May 2023).
15. Li, W.; Sun, N.; Stoner, B.; Jiang, X.; Lu, X.; Rogers, R.D. Rapid dissolution of lignocellulosic biomass in ionic liquids using temperatures above the glass transition of lignin. *Green Chem.* **2011**, *13*, 2038–2047. [CrossRef]
16. Nimz, H. Beech lignin proposal of a constitutional scheme. *Angew. Chem. Int. Ed. Engl.* **1974**, *13*, 313–321. [CrossRef]
17. Beckham, G.T. *Lignin Valorization: Emerging Approaches*; OSTI.GOV United States: Oak Ridge, TN, USA, 2018; ECCC Environmental eBooks 1968–2022 Series: Energy and Environment; Publication date: 29 March 2018; 528p.
18. Agrawal, R.; Kumar, A.; Singh, S.; Sharma, K. Recent advances and future perspectives of lignin biopolymers. *J. Polym. Res.* **2022**, *29*, 222. [CrossRef]
19. Bass, G.F.; Epps, T.H. Recent developments towards performance-enhancing lignin-based polymers. From themed collection: Sustainable Polymers. *Polym. Chem.* **2021**, *12*, 4130–4158. [CrossRef]
20. Sethupathya, S.; Morales, G.M.; Gao, L.; Wang, H.; Yang, B.; Jiang, J.; Sun, J.; Zhu, D. Lignin valorization: Status, challenges and opportunities. Review. *Bioresour. Technol.* **2022**, *347*, 126696. [CrossRef] [PubMed]
21. Wyman, C.E. Potential synergies and challenges in refining cellulosic biomass to fuels, chemicals, and power. *Biotechnol. Prog.* **2003**, *19*, 254–262. [CrossRef]
22. The Global Market for Lignin 2023–2033. Available online: https://www.giiresearch.com/report/fmi1223534-global-market-lignin.html (accessed on 21 July 2023).
23. Shu, F.; Jiang, B.; Yuan, Y.; Li, M.; Wu, W.; Jin, Y.; Xiao, H. Biological Activities and Emerging Roles of Lignin and Lignin-Based Products—A Review. *Biomacromolecules* **2021**, *22*, 4905–4918. [CrossRef]
24. Tao, J.; Li, S.; Ye, F.; Zhou, Y.; Lei, L.; Zhao, G. Lignin—An Underutilized, Renewable and Valuable Material for Food Industry. *Crit. Rev. Food Sci. Nutr.* **2020**, *60*, 2011–2033. [CrossRef]
25. Ariyanta, H.A.; Sari, F.P.; Sohail, A.; Restu, W.K.; Septiyanti, M.; Aryana, N.; Fatriasari, W.; Kumar, A. Current roles of lignin for the agroindustry: Applications, challenges, and opportunities. *Int. J. Biol. Macromol.* **2023**, *240*, 124523. [CrossRef]
26. Zhang, Y.; Naebe, M. Lignin: A Review on Structure, Properties, and Applications as a Light-Colored UV Absorber. *ACS Sustain. Chem. Eng.* **2021**, *9*, 1427–1442. [CrossRef]
27. Hasan, M.S.; Sardar, M.R.; Shafin, A.; Rahman, M.S.; Mahmud, M.; Hossen, M.M. A Brief Review on Applications of Lignin. *J. Chem. Rev.* **2023**, *5*, 56–82. [CrossRef]
28. Zhu, D.; Yang, B.; Wang, H.; Shahnawaz, M. Editorial: Lignin valorization: Recent trends and future perspective. *Front. Bioeng. Biotechnol.* **2023**, *11*, 1190128. [CrossRef]
29. Bajwa, D.S.; Pourhashem, G.; Ullah, A.H.; Bajwa, S.G. A concise review of current lignin production, applications, products and their environmental impact. *Ind. Crop. Prod.* **2019**, *139*, 111526. [CrossRef]
30. Zhang, Z.; Fang, Y.; Yang, J.; Li, X.A. comprehensive review of bio-oil, bio-binder and bio-asphalt materials: Their source, composition, preparation and performance. *J. Traffic Transp. Eng. (Engl. Ed.)* **2022**, *9*, 151–166. [CrossRef]
31. Zheng, T.; Zheng, D.; Qiu, X.; Yang, D.; Fan, L.; Zheng, J. A novel branched claw-shape lignin-based polycarboxylate superplasticizer: Preparation, performance and mechanism. *Cem. Concr. Res.* **2019**, *119*, 89–101. [CrossRef]
32. Iglesias, M.C.; Gomez Maldonado, D.; Davis, V.A.; Peresin, M.S. A review on lignocellulose chemistry, nanostructure, and their impact on interfacial interactions for sustainable products development. *J. Mater. Sci.* **2022**, *58*, 685–706. [CrossRef]
33. Gosselink, R.J.A.; Landa, P. Lignin-Based Bio-Asphalt. Patent WO2019/092278, 13 November 2018.

34. Malik, S.; Khan, A.; Ali, N.; Rahdar, A.; Yasin, G.; Hussain, S.; Bilal, M. Natural polymer-based nanostructures and their applications. In *Smart Polymer Nanocomposites: Design, Synthesis, Functionalization, Properties, and Applications. Part III: Applications of Polymer Nanostructures and Polymer Nanocomposites*; Ali, N., Khan, A., Gupta, R.K., Bilal, M., Nguyen, T.A., Eds.; Elsevier Inc.: Amsterdam, The Netherlands, 2023; Chapter 24; pp. 529–541.
35. Mondal, S.; Jatrana, A.; Maan, S.; Sharma, P. Lignin modification and valorization in medicine, cosmetics, environmental remediation and agriculture: A review. *Environ. Chem. Lett.* **2023**, *21*, 2171–2197. [CrossRef]
36. Boarino, A.; Klok, H.-A. Opportunities and Challenges for Lignin Valorization in Food Packaging, Antimicrobial, and Agricultural Applications. *Biomacromolecules* **2023**, *24*, 1065. [CrossRef] [PubMed]
37. Figueiredo, P.; Lintinen, K.; Hirvonen, J.T.; Kostiainen, M.A.; Santos, H.A. Properties and chemical modifications of lignin: Towards lignin-based nanomaterials for biomedical applications. *Prog. Mater. Sci.* **2018**, *93*, 233–269. [CrossRef]
38. Nan, N.; Hu, W.; Wang, J. Lignin-Based Porous Biomaterials for Medical and Pharmaceutical Applications. *Biomedicines* **2022**, *10*, 747. [CrossRef]
39. Calvo-Flores, F.G.; Dobado, J.A. Lignin as Renewable Raw Material. *ChemSusChem* **2010**, *3*, 1227–1235. [CrossRef] [PubMed]
40. Zakzeski, J.; Bruijnincx, P.C.A.; Jongerius, A.L.; Weckhuysen, B.M. The Catalytic Valorization of Lignin for the Production of Renewable Chemicals. *Chem. Rev.* **2010**, *110*, 3552–3599. [CrossRef] [PubMed]
41. Eswaran, S.c.d.; Subramaniam, S.; Sanyal, U.; Rallo, R.; Zhanget, X. Molecular structural dataset of lignin macromolecule elucidating experimental structural compositions. *Sci. Data* **2022**, *9*, 647. [CrossRef] [PubMed]
42. Thoresen, P.P.; Matsakas, L.; Rova, U.; Christakopoulos, P. Recent advances in organosolv fractionation: Towards biomass fractionation technology of the future. *Bioresour. Technol.* **2020**, *306*, 123189. [CrossRef]
43. International Lignin Institute, Analytical Protocol. Available online: https://www.ili-lignin.com/activities/analytical-protocols.html (accessed on 21 July 2023).
44. Fabbri, F.; Bischof, S.; Mayr, S.; Gritsch, S.; Bartolome, M.J.; Schwaiger, N.; Guebitz, G.M.; Weiss, R. The Biomodified Lignin Platform: A Review. *Polymers* **2023**, *15*, 1694. [CrossRef]
45. Mikame, K.; Ohashi, Y.; Naito, Y.; Nishimura, H.; Katahira, M.; Sugawara, S.; Koike, K.; Watanabe, T. Natural Organic Ultraviolet Absorbers from Lignin. *ACS Sustain. Chem. Eng.* **2021**, *9*, 16651–16658. [CrossRef]
46. Tolbert, A.; Akinosho, H.; Khunsupat, R.; Ragauskas, A.J. Characterization and analysis of the molecular weight of lignin for biorefining studies. *Biofuels Bioprod. Biorefin.* **2014**, *8*, 836–856. [CrossRef]
47. Gao, Q.; You, J.; Liao, X.; Wang, Z. Identification and analysis of ancient ship wood excavated at Nantong hydraulic site. *Bioresources* **2023**, *18*, 5028–5040. [CrossRef]
48. Blindheim, F.H.; Ruwoldt, J. The Effect of Sample Preparation Techniques on Lignin Fourier Transform Infrared Spectroscopy. *Polymers* **2023**, *15*, 2901. [CrossRef]
49. Vasile, C.; Gosselink, R.; Quintus, P.; Koukios, E.G.; Koullas, D.P.; Avgerinos, E.; Abacherli, A. Analytical methods for lignin characterization I. Thermogravimetry. *Cell. Chem. Technol.* **2006**, *40*, 421–429.
50. Pokryshkin, S.; Sypalova, Y.; Ivahnov, A.; Kozhevnikov, A. Optimization of Approaches to Analysis of Lignin by Thermal Decomposition. *Polymers* **2023**, *15*, 2861. [CrossRef] [PubMed]
51. Brebu, M.; Vasile, C. Thermal Degradation of Lignin—A Review. *Cell. Chem.Technol.* **2010**, *44*, 353–363.
52. Tham, D.; Gardner, C.; Haskell, W. Potential health benefits of dietary phytoestrogens: A review of the clinical, epidemiological, and mechanistic evidence. *J. Clin. Endocrinol. Metab.* **1998**, *83*, 2223–2235. [CrossRef] [PubMed]
53. Rodríguez-García, C.; Sánchez-Quesada, C.; Toledo, E.; Delgado-Rodríguez, M.; Gaforio, J.J. Naturally Lignan-Rich Foods: A Dietary Tool for Health Promotion? *Molecules* **2019**, *24*, 917. [CrossRef] [PubMed]
54. Vishtal, A.; Kraslawski, A. Challenges in Industrial Applications of Technical Lignins. Challenges of lignins. *BioResources* **2011**, *6*, 3547–3568. [CrossRef]
55. Services Testing Laboratory, Technical Lignins: Physico-Chemical Characterisations. Specification of Technical and Industrial Lignins. Available online: https://www.webctp.com/en/technical-lignins-physico-chemical-characterisations (accessed on 25 July 2023).
56. Mastrolitti, S.; Borsella, E.; Guliano, A.; Petrone, M.T.; De Bari, I.; Gosselink, R.; van Erven, G.; Annevelik, E.; Triantafyllidi, K.S.; Stichnothe, H. Sustainable-Lignin-Valorization. Technical Lignins, Processes and Market Development. IEA Bioenergy Task 42 & LignoCOST—195p. BBP Biorefinery & Sustainable Value Chains IAEA Bioenergy, LignoCOST Task 42: Biorefining in a Circular Economy. Edited by: IEA Bioenergy Task 42 Biorefining in a Circular Economy & LignoCOST. October 2021. Available online: https://task42.ieabioenergy.com/publications/sustainable-lignin-valorization/ (accessed on 6 June 2023).
57. Jia, W.; Shi, H.; Sheng, X.; Guo, Y.; Fatehi, P.; Niu, M. Correlation between physico-chemical characteristics of lignin deposited on autohydrolyzed wood chips and their cellulase enzymatic hydrolysis. *Bioresour. Technol.* **2022**, *350*, 126941. [CrossRef]
58. Rosado, M.J.; Rencoret, J.; Gutiérrez, A.; del Río, J.C. Structural Characterization of the Milled-Wood Lignin Isolated from Sweet Orange Tree (*Citrus sinensis*) Pruning Residue. *Polymers* **2023**, *15*, 1840. [CrossRef]
59. Gbenebor, O.P.; Olanrewaju, O.A.; Usman, M.A.; Adeosun, S.O. Lignin from Brewers' Spent Grain: Structural and Thermal Evaluations. *Polymers* **2023**, *15*, 2346. [CrossRef]

60. Nasrullah, A.; Bhat, A.H.; Khan, A.S.; Ajab, H. Comprehensive approach on the structure, production, processing, and application of lignin. In Lignocellulosic Fibre and Biomass-Based Composite Materials. Processing, Properties and Applications; Jawaid, M., Tahir, P.M., Saba, N., Eds.; In Composites Science and Engineering. Cambridge Series; Woodhead Publishing: Sawston, UK, 2017; Chapter 9; pp. 165–178.
61. Tribot, A.; Amer, G.; Alio, M.A.; de Baynast, H.; Delattre, C.; Pons, A.; Mathias, J.-D.; Callois, J.-M.; Vial, C.; Michaud, P.; et al. Wood-lignin: Supply, extraction processes and use as bio-based material. *Eur. Polym. J.* **2019**, *112*, 228–240. [CrossRef]
62. Smit, A.T.; Verges, M.; Schulze, P.; van Zomeren, A.; Lorenz, H. Laboratory- to Pilot-Scale Fractionation of Lignocellulosic Biomass Using an Acetone Organosolv Process. *ACS Sustain. Chem. Eng.* **2022**, *10*, 10503–10513. [CrossRef]
63. Wang, H.; Tucker, M.; Ji, Y. Recent Development in Chemical Depolymerization of Lignin: A Review. *J. Appl. Chem.* **2013**, *2013*, 838645. [CrossRef]
64. Mukundan, S.; Boffito, D.; Shrotri, A.; Atanda, L.; Beltramini, J.; Patience, G. Thermocatalytic Hydrodeoxygenation and Depolymerization of Waste Lignin to Oxygenates and Biofuels in a Continuous Flow Reactor at Atmospheric Pressure. *ACS Sustain. Chem. Eng.* **2020**, *8*, 13195–13205. [CrossRef]
65. Shen, D.; Zhao, J.; Xiao, R. Catalytic transformation of lignin to aromatic hydrocarbons over solid-acid catalyst: Effect of lignin sources and catalyst species. *Energy Convers. Manag.* **2016**, *124*, 61–72. [CrossRef]
66. Chio, C.; Sain, M.; Qin, W. Lignin utilization: A review of lignin depolymerization from various aspects. *Renew. Sustain. Energy Rev.* **2019**, *107*, 232–249. [CrossRef]
67. Schutyser, W.; Renders, T.; Van den Bosch, S.; Koelewijn, S.-F.; Beckham, G.T.; Sels, B.F. Chemicals from lignin: An interplay of lignocellulose fractionation, depolymerisation, and upgrading. *Chem. Soc. Rev.* **2018**, *47*, 852–908. [CrossRef]
68. Tabone, M.D.; Cregg, J.J.; Beckman, E.J.; Landis, A.E. Sustainability Metrics: Life Cycle Assessment and Green Design in Polymers. *Environ. Sci. Technol.* **2010**, *44*, 8264–8269. [CrossRef]
69. Montazeri, M.; Zaimes, G.G.; Khanna, V.; Eckelman, M.J. Meta-Analysis of Life Cycle Energy and Greenhouse Gas Emissions for Priority Biobased Chemicals. *ACS Sustain. Chem. Eng.* **2016**, *4*, 6443–6454. [CrossRef]
70. Fadlallah, S.; Sinha Roy, P.; Garnier, G.; Saito, K.; Allais, F. Are lignin-derived monomers and polymers truly sustainable? An in-depth green metrics calculations approach. *Green Chem.* **2021**, *23*, 1495–1535. [CrossRef]
71. Vural Gursel, I.; Dijkstra, J.W.; Huijgen, W.J.J.; Ramirez, A. Techno-economic comparative assessment of novel lignin depolymerization routes to bio-based aromatics. *Biofuels Bioprod. Biorefin.* **2019**, *13*, 1068–1084. [CrossRef]
72. Funkenbusch, L.T.; Mullins, M.E.; Vamling, L.; Belkhieri, T.; Srettiwat, N.; Winjobi, O.; Shonnard, D.R.; Rogers, T.N. Techno-economic assessment of hydrothermal liquefaction oil from lignin with catalytic upgrading for renewable fuel and chemical production, Advanced Review. *WIREs Energy Environ.* **2019**, *8*, e319. [CrossRef]
73. Lappalainen, J.; Baudouin, D.; Hornung, U.; Schuler, J.; Melin, K.; Bjelić, S.; Vogel, F.; Konttinen, J.; Joronen, T. Sub- and Supercritical Water Liquefaction of Kraft Lignin and Black Liquor Derived Lignin. *Energies* **2020**, *13*, 3309. [CrossRef]
74. Fernández-Rodríguez, J.; Erdocia, X.; Gonzalez Alriols, M.; Labidi, J. Techno-economic analysis of different integrated biorefinery scenarios using lignocellulosic waste streams as source for phenolic alcohols production. *J. Clean. Prod.* **2021**, *285*, 124829. [CrossRef]
75. Tey, T.O.; Chen, S.; Cheong, Z.X.; Xian Choong, A.S.; Ng, L.Y.; Chemmangattuvalappil, N.G. Synthesis of a sustainable integrated biorefinery to produce value-added chemicals from palm-based biomass via mathematical optimisation. *Sustain. Prod. Consum.* **2021**, *26*, 288–315. [CrossRef]
76. Serrano, L.; Cecilia, J.A.; García-Sancho, C.; García, A. Lignin Depolymerization to BTXs Review. *Top. Curr. Chem.* **2019**, *377*, 26. [CrossRef]
77. Ramirez Brenes, R.G.; Alhadeff, E.M.; Bojorge, N.; Trales, L.E.M.; Pazos, G.A.D. Review. BTX production by breaking down lignin: Current status and future prospects. *Biofuels Bioprod. Biorefin.* **2023**, *17*, 3664–3681. [CrossRef]
78. Wang, Y.; Wei, L.; Hou, Q.; Mo, Z.; Liu, X.; Li, W. A Review on Catalytic Depolymerization of Lignin towards High-Value Chemicals: Solvent and Catalyst. *Fermentation* **2023**, *9*, 386. [CrossRef]
79. Alcazar-Ruiz, A.; Sanchez-Silva, L.; Dorado, F. Enhancement of BTX production via catalytic fast pyrolysis of almond shell, olive pomace with polyvinyl chloride mixtures. *Process Saf. Environ. Prot.* **2022**, *163*, 218–226. [CrossRef]
80. Nadányi, R.; Ház, A.; Lisý, A.; Jablonský, M.; Šurina, I.; Majová, V.; Baco, A. Lignin Modifications, Applications, and Possible Market Prices. *Energies* **2022**, *15*, 6520. [CrossRef]
81. Liu, X.; Bouxin, F.; Fan, J.; Clark, J.H. Recent Advances in the Catalytic Depolymerization of Lignin towards Phenolic Chemicals: A Review. *ChemSusChem* **2020**, *13*, 4296–4317. [CrossRef]
82. Biswas, B.; Kumar, A.; Kaur, R.; Krishna, B.B.; Bhaskar, T. Catalytic hydrothermal liquefaction of alkali lignin over activated bio-char supported bimetallic catalyst. *Bioresour. Technol.* **2021**, *337*, 125439. [CrossRef]
83. Shu, R.; Long, J.; Yuan, Z.; Zhang, Q.; Wang, T.; Wang, C.; Ma, L. Efficient and product-controlled depolymerization of lignin oriented by metal chloride cooperated with Pd/C. *Bioresour. Technol.* **2015**, *179*, 84–90. [CrossRef]
84. Martinez-Gomez, A.; Caballero, I.; Blanco, C.A. Phenols and Melanoidins as Natural Antioxidants in Beer. Structure, Reactivity and Antioxidant Activity. *Biomolecules* **2020**, *10*, 400. [CrossRef]
85. Borges, A.; Freitas, V.; Mateus, N.; Fernandes, I.; Oliveira, J. Solid Lipid Nanoparticles as Carriers of Natural Phenolic Compounds. *Antioxidants* **2020**, *9*, 998. [CrossRef]

86. Kim, E.; Ban, C.; Kim, S.O.; Lim, S.; Choi, Y.J. Applications and perspectives of polyphenol-loaded solid lipid nanoparticles and nanostructured lipid carriers for foods. *Food Sci. Biotechnol.* **2022**, *31*, 1009–1026. [CrossRef]
87. Kleinert, M.; Barth, T. Phenols from Lignin. *Chem. Eng. Technol. Spec. Issue Chang. Raw Mater.* **2008**, *31*, 736–745. [CrossRef]
88. Bbosa, D.; Mba-Wright, M.; Brown, R.C. Modeling and Analysis. More than ethanol: A techno-economic analysis of a corn stover-ethanol biorefinery integrated with a hydrothermal liquefaction process to convert lignin into biochemicals. *Biofuels Bioprod. Biorefin.* **2018**, *12*, 497–509. [CrossRef]
89. Martinez-Hernandez, E.; Cui, X.; Scown, C.D.; Amezcua-Allieri, M.A.; Aburto, J.; Simmons, B.A. Techno-economic and greenhouse gas analyses of lignin valorization to eugenol and phenolic products in integrated ethanol biorefineries. *Biofuels Bioprod. Biorefin.* **2019**, *13*, 978–993. [CrossRef]
90. Reshmy, R.; Balakumaran, P.A.; Divakar, K.; Philip, E.; Madhavan, A.; Pugazhendhi, A.; Sirohi, R.; Binod, P.; Awasthi, M.K.; Sindhu, R. Microbial valorization of lignin: Prospects and challenges. *Bioresour. Technol. Part A* **2022**, *344*, 126240. [CrossRef]
91. Weng, C.; Peng, X.; Han, Y. Depolymerization and conversion of lignin to value added bioproducts by microbial and enzymatic catalysis. *Biotechnol. Biofuels* **2021**, *14*, 84. [CrossRef]
92. Abdelaziz, O.Y.; Clemmensen, I.; Meier, S.; Costa, C.A.E.; Rodrigues, A.E.; Hulteberg, C.P.; Riisager, A. On the Oxidative Valorization of Lignin to High-Value Chemicals: A Critical Review of Opportunities and Challenges. *ChemSusChem* **2022**, *15*, e202201232. [CrossRef]
93. Costa, C.A.E.; Casimiro, F.M.; Vega-Aguilar, C.; Rodrigues, A.E. Lignin Valorization for Added-Value Chemicals: Kraft Lignin versus Lignin Fractions. *Chem. Eng. Spec. Issue Green. Environ. Sustain. Chem. Process.* **2023**, *7*, 42. [CrossRef]
94. Unlu, S.; Niu, W.; Demirel, Y. Bio-based adipic acid production: Feasibility analysis using a multi-criteria decision matrix. *Biofuels Bioprod. Biorefin.* **2020**, *14*, 794–807. [CrossRef]
95. Xu, Y.; Liu, Y.; Ni, Y. Current overview of carbon fiber: Toward green sustainable raw materials. *Bioresources* **2020**, *15*, 7234–7259. [CrossRef]
96. Poursorkhabi, V.; Abdelwahab, M.A.; Misra, M.; Khalil, H.; Gharabaghi, B.; Mohanty, A.K. Processing, Carbonization, and Characterization of Lignin Based Electrospun Carbon Fibers: A Review. *Energy Res. Sec. Bioenergy Biofuels* **2020**, *8*, 208. [CrossRef]
97. Chatterjee, S.; Saito, T. Lignin-Derived Advanced Carbon Materials. *ChemSusChem* **2015**, *8*, 3941–3958. [CrossRef]
98. Bajpai, P. *Carbon Fibre from Lignin*; Springer Nature Singapore Pte Ltd.: Singapore, 2017; ISBN 978-981-10-4229-4.
99. Xu, C.; Ferdosian, F. Conversion of Lignin into Bio-Based Chemicals and Materials. In *Green Chemistry and Sustainable Technology*; Springer: Berlin, Germany, 2017; pp. 55–79, ISBN 978-3-662-54959-9. Available online: https://link.springer.com/book/10.1007/978-3-662-54959-9 (accessed on 21 July 2023).
100. Porc, O.; Hark, N.; Carus, M.; Carrez, D. (BIC) European Bioeconomy in Figures 2008–2019. Commissioned by Biobased Industries Consortium. Brussel, Belgium. 2022. Available online: www.biconsortium.eu (accessed on 26 May 2023).
101. Naydenova, I.; Radoykova, T.; Petrova, T.; Sandov, O.; Valchev, I. Utilization Perspectives of Lignin Biochar from Industrial Biomass Residue. *Molecules* **2023**, *28*, 4842. [CrossRef]
102. Gul, E.; Al Bkoor Alrawashdeh, K.; Masek, O.; Skreiberg, Ø.; Corona, A.; Zampilli, M.; Wang, L.; Samaras, P.; Yang, Q.; Zhou, H.; et al. Production and use of biochar from lignin and lignin-rich residues (such as digestate and olive stones) for wastewater treatment. *J. Anal. Appl. Pyrolysis* **2021**, *158*, 105263. [CrossRef]
103. Rodrigues, J.S.; de Freitas, A.d.S.M.; Lopes, H.S.M.; Pires, A.A.F.; Lemes, A.P.; Ferreira, M.; Botaro, V.R. Improvement of UV stability of thermoplastic starch matrix by addition of selected lignin fraction—Photooxidative degradation. *Int. J. Biol. Macromol.* **2023**, *230*, 123142. [CrossRef]
104. Kaur, R.; Bhardwaj, S.K.; Chandna, S.; Kim, K.H.; Bhaumik, J. Lignin-based metal oxide nanocomposites for UV protection applications: A review. *J. Clean. Prod.* **2021**, *317*, 128300. [CrossRef]
105. Wang, M.; Leitch, M.; Xu, C. Synthesis of phenol–formaldehyde resol resins using organosolv pine lignins. *Eur. Polym. J.* **2009**, *45*, 3380–3388. [CrossRef]
106. Qiao, W.; Li, S.; Guo, G.; Han, S.; Ren, S.; Ma, Y. Synthesis and characterization of phenol-formaldehyde resin using enzymatic hydrolysis lignin. *J. Ind. Eng. Chem.* **2015**, *21*, 1417–1422. [CrossRef]
107. Pandey, M.; Kim, C.S. Lignin depolymerization and conversion: A review of thermochemical methods. *Chem. Eng. Technol.* **2011**, *34*, 29–41. [CrossRef]
108. Li, H.; Liang, Y.; Li, P.; He, C. Conversion of biomass lignin to high-value polyurethane: A review. *J. Bioresour. Bioprod.* **2020**, *5*, 163–179. [CrossRef]
109. Cinelli, P.; Anguillesi, I.; Lazzeri, A. Green synthesis of flexible polyurethane foams from liquefied lignin. *Eur. Polym. J.* **2013**, *49*, 1174–1184. [CrossRef]
110. Griffini, G.; Passoni, V.; Suriano, R.; Levi, M.; Turri, S. Polyurethane Coatings Based on Chemically Unmodified Fractionated Lignin. *ACS Sustain. Chem. Eng.* **2015**, *3*, 1145–1154. [CrossRef]
111. Vieira, F.R.; Magina, S.; Evtuguin, D.V.; Barros-Timmons, A. Lignin as a Renewable Building Block for Sustainable Polyurethanes. *Materials* **2022**, *15*, 6182. [CrossRef]
112. Lettner, M.; Hesser, F.; Hedeler, B.; Tobias, S. Barriers and incentives for the use of lignin-based resins: Results of a comparative importance performance analysis. *J. Clean. Prod.* **2020**, *256*, 120520. [CrossRef]
113. Fache, M.; Boutevina, B.; Caillol, S. Epoxy thermosets from model mixtures of the lignin-to-vanillin process. Lignin-Based Epoxy Resins. *Green Chem.* **2016**, *18*, 712–725. [CrossRef]

114. Gioia, C.; Colonna, M.; Tagami, A.; Medina, L.; Sevastyanova, O.; Berglund, L.A.; Lawoko, M. Unravelling the Relationship between Structure and Material Properties. *Biomacromolecules* **2020**, *21*, 1920–1928. [CrossRef]
115. Liu, G.; Jin, C.; Huo, S.; Kong, Z.; Chu, F. Preparation and properties of novel bio-based epoxy resin thermosets from lignin oligomers and cardanol. *Int. J. Biol. Macromol.* **2021**, *193*, 1400–1408. [CrossRef]
116. Karagoz, P.; Khiawjan, S.; Marques, M.P.C.; Santzouk, S.; Bugg, T.D.H.; Lye, G.J. Pharmaceutical applications of lignin-derived chemicals and lignin-based materials: Linking lignin source and processing with clinical indication. *Biomass Convers. Biorefinery* **2023**. [CrossRef]
117. Kai, D.; Tan, M.J.; Chee, P.L.; Chua, Y.K.; Yap, Y.L.; Loh, X.J. Towards lignin-based functional materials in a sustainable world. *Green Chem.* **2016**, *18*, 1175–1200. [CrossRef]
118. Shi, K.; Liu, G.; Sun, H.; Weng, Y. Polylactic Acid/Lignin Composites: A Review. *Polymers* **2023**, *15*, 2807. [CrossRef]
119. Raschip, I.E.; Hitruc, E.G.; Vasile, C.; Popescu, M.C. Effect of the lignin type on the morphology and thermal properties of the xanthan/lignin hydrogels. *Int. J. Biol. Macromol.* **2013**, *54*, 230–237. [CrossRef]
120. Athinarayanan, J.; Periasamy, V.S.; Alshatwi, A. Assessment of Osteogenic Differentiation Potential of Cytocompatible Rice Husk-Derived Lignin/Silica Nanohybrids for Bone Tissue Engineering. *Silicon* **2023**. [CrossRef]
121. Qin, Z.; Liu, H.M.; Gu, L.B.; Sun, R.C.; Wang, X.D. Lignin as a Natural Antioxidant: Property-Structure Relationship and Potential Applications. In *Reactive and Functional Polymers Volume One*; Gutiérrez, T.J., Ed.; Springer: Cham, Switzerland, 2020; pp. 65–93. [CrossRef]
122. Lu, X.; Gu, X.; Shi, Y. A review on lignin antioxidants: Their sources, isolations, antioxidant activities and various applications. *Int. J. Biol. Macromol.* **2022**, *210*, 716–741. [CrossRef]
123. Xiao, L.; Liu, W.; Huang, J.; Lou, H.; Qiu, X. Study on the Antioxidant Activity of Lignin and Its Application Performance in SBS Elastomer. *Ind. Eng. Chem. Res.* **2021**, *60*, 790–797. [CrossRef]
124. Piccinino, D.; Capecchi, E.; Tomaino, E.; Gabellone, S.; Gigli, V.; Avitabile, D.; Saladino, R. Nano-Structured Lignin as Green Antioxidant and UV Shielding Ingredient for Sunscreen Applications. *Antioxidants* **2021**, *10*, 274. [CrossRef]
125. Chupka, É.I.; Vershal, V.V.; Burlakov, V.M.; Gvozdev, V.N. A comparison of the antioxidant properties of some natural antioxidants and lignin. *Chem. Nat. Compd.* **1980**, *16*, 513–516. [CrossRef]
126. Dong, X.; Dong, M.; Lu, Y.; Turley, A.; Jin, T.; Wu, C. Antimicrobial and antioxidant activities of lignin from residue of corn stover to ethanol production. *Ind. Crop. Prod.* **2011**, *34*, 1629–1634. [CrossRef]
127. Alzagameem, A.; Klein, S.E.; Bergs, M.; Do, X.T.; Korte, I.; Dohlen, I.S.; Hüwe, C.; Kreyenschmidt, J.; Kamm, B.; Larkins, M.; et al. Antimicrobial Activity of Lignin and Lignin-Derived Cellulose and Chitosan Composites against Selected Pathogenic and Spoilage Microorganisms. *Polymers* **2019**, *11*, 670. [CrossRef]
128. Lourençon, T.V.; de Lima, G.G.; Ribeiro, C.S.P.; Hansel, F.A.; Maciel, G.M.; da Silva, K.; Winnischofer, S.M.B.; de Muniz, G.I.B.; Magalhães, W.L.E. Antioxidant, Antibacterial and Antitumoural Activities of Kraft Lignin from Hardwood Fractionated by Acid Precipitation. *Int. J. Biol. Macromol.* **2021**, *166*, 1535–1542. [CrossRef]
129. Luzi, F.; Yang, W.; Ma, P.; Torre, L.; Puglia, D. *Chapter 9-Lignin-Based Materials with Antioxidant and Antimicrobial Properties Lignin-Based Materials for Biomedical Applications Preparation, Characterization, and Implementation*; Santos, H., Figueiredo, P., Eds.; Elsevier: Amsterdam, The Netherland, 2021; pp. 291–326.
130. Lee, E.; Song, Y.; Lee, S. Crosslinking of Lignin/Poly(Vinyl Alcohol) Nanocomposite Fiber Webs and Their Antimicrobial and Ultraviolet-Protective Properties. *Text. Res. J.* **2019**, *89*, 3–12. [CrossRef]
131. de Melo, C.M.L.; da Cruz Filho, I.J.; de Sousa, G.F.; de Souza Silva, G.A.; do Nascimento Santos, D.K.D.; da Silva, R.S.; de Sousa, B.R.; de Lima Neto, R.G.; de Lima, C.A.M.; de Moraes Rocha, G.J. Lignin Isolated from Caesalpinia Pulcherrima Leaves has Antioxidant, Antifungal and Immunostimulatory Activities. *Int. J. Biol. Macromol.* **2020**, *162*, 1725–1733. [CrossRef]
132. Li, R.; Ouda, R.; Kimura, C.; Narita, R.; Nishimura, H.; Fujita, T.; Watanabe, T. Conversion of Beech Wood into Antiviral Lignin–Carbohydrate Complexes by Microwave Acidolysis. *ACS Sustain. Chem. Eng.* **2021**, *9*, 9248–9256. [CrossRef]
133. Zhao, Y.; Shakeel, U.; Saif Ur Rehman, M.; Li, H.; Xu, X.; Xu, J. Lignin-Carbohydrate Complexes (LCCs) and Its Role in Biorefinery. *J. Clean. Prod.* **2020**, *253*, 120076. [CrossRef]
134. Fukuchi, K.; Koshikawa, T.; Asai, D.; Inomata, M.; Sakagami, H.; Takemura, H.; Kanamoto, T.; Aimi, H.; Kikkawa, Y. Lignosulfonate Rapidly Inactivates Human Immunodeficiency and Herpes Simplex Viruses. *Medicines* **2021**, *8*, 56. [CrossRef]
135. Rico-García, D.; Ruiz-Rubio, L.; Pérez-Alvarez, L.; Hernández-Olmos, S.L.; Guerrero-Ramírez, G.L.; Vilas-Vilela, J.L. Lignin-Based Hydrogels: Synthesis and Applications. *Polymers* **2020**, *12*, 81. [CrossRef]
136. Zongo, L.; Lange, H. Lignins and their potential for use as biopolymers in pharmaceutical engineering—A review. *J. Afr. Technol. Pharm. Biopharm. (JATPB)* **2022**, *1*, 37–62. [CrossRef]
137. .Chandna, S.; Paul, S.; Kaur, R.; Gogde, K.; Bhaumik, J. Photodynamic Lignin Hydrogels: A Versatile Self-Healing Platform for Sustained Release of Photosensitizer Nanoconjugates. *ACS Appl. Polym. Mater.* **2022**, *4*, 8962–8976. [CrossRef]
138. Sugiarto, S.; Leow, Y.; Tan, C.L.; Wang, G.; Kai, D. How far is lignin from being a biomedical material? *Bioact. Mater.* **2022**, *8*, 71–94. [CrossRef]
139. Tortora, M.; Cavalieri, F.; Mosesso, P.; Ciaffardini, F.; Melone, F.; Crestini, C. Ultrasound driven assembly of lignin into microcapsules for storage and delivery of hydrophobic molecules. *Biomacromolecules* **2014**, *15*, 1634–1643. [CrossRef]
140. Yiamsawas, D.; Baier, G.; Thines, E.; Landfester, K.; Wurm, F.R. Biodegradable lignin nanocontainers. *RSC Adv.* **2014**, *4*, 11661–11663. [CrossRef]

141. Jiang, S.; Kai, D.; Dou, Q.Q.; Loh, X.J. Multi-arm carriers composed of an antioxidant lignin core and poly (glycidyl methacrylate-co-poly (ethylene glycol) methacrylate) derivative arms for highly efficient gene delivery. *J. Mater. Chem. B* **2015**, *3*, 6897–6904. [CrossRef]
142. Zheng, Q.; Chai, L.; Du, B.; Li, W.; Fu, L.-H.; Chen, X. A pH-Sensitive Lignin-Based Material for Sustained Release of 8-Hydroxyquinoline. *Polymers* **2023**, *15*, 1867. [CrossRef]
143. Ravishankar, K.; Venkatesan, M.; Desingh, R.P.; Mahalingam, A.; Sadhasivam, B.; Subramaniyam, R.; Dhamodharan, R. Biocompatible hydrogels of chitosan-alkali lignin for potential wound healing applications. *Mater. Sci. Eng. C* **2019**, *102*, 447–457. [CrossRef]
144. Ahmad, U.M.; Ji, N.; Li, H.; Wu, Q.; Song, C.; Liu, Q.; Ma, D.; Lu, X. Can lignin be transformed into agrochemicals? Recent advances in the agricultural applications of lignin. *Ind. Crop. Prod.* **2021**, *170*, 113646. [CrossRef]
145. Abbas, A.; Wang, Z.; Zhang, Y.; Peng, P.; She, D. Lignin-based controlled release fertilizers. A review. *Int. J. Biol. Macromol. Part B* **2022**, *222*, 1801–1817. [CrossRef]
146. Eraghi Kazzaz, A.; Hosseinpour Feizi, Z.; Fatehi, P. Grafting Strategies for Hydroxy Groups of Lignin for Producing Materials. *Green Chem.* **2019**, *21*, 5714–5752. [CrossRef]
147. Lu, J.; Cheng, M.; Zhao, C.; Li, B.; Peng, H.; Zhang, Y.; Shao, Q.; Hassan, M. Application of Lignin in Preparation of Slow-Release Fertilizer: Current Status and Future Perspectives. *Ind. Crop. Prod.* **2022**, *176*, 114267. [CrossRef]
148. Savy, D.; Cozzolino, V. Novel Fertilising Products from Lignin and Its Derivatives to Enhance Plant Development and Increase the Sustainability of Crop Production. *J. Clean. Prod.* **2022**, *366*, 132832. [CrossRef]
149. Chen, J.; Fan, X.; Zhang, L.; Chen, X.; Sun, S.; Sun, R. Research Progress in Lignin-Based Slow/Controlled Release Fertilizer. *ChemSusChem* **2020**, *13*, 4356–4366. [CrossRef]
150. Sutradhar, S.; Fatehi, P. Latest development in the fabrication and use of lignin-derived humic acid. *Biotechnol. Biofuels Bioprod.* **2023**, *16*, 38. [CrossRef]
151. Gazzurelli, C.; Migliori, A.; Mazzeo, P.P.; Carcelli, M.; Pietarinen, S.; Leonardi, G.; Pandolfi, A.; Rogolino, D. Making agriculture more sustainable: An environmentally friendly approach to the synthesis of lignin@Cu pesticides. *ACS Sustain. Chem. Eng.* **2020**, *8*, 14886–14895. [CrossRef]
152. Machado, T.O.; Beckers, S.; Fischer, J.; Müller, B.; Sayer, C.; Araújo, P.H.H.; Landfester, K.; Wurm, F.R. Bio-based Lignin Nanocarriers Loaded with Fungicides as Versatile Platform for Drug Delivery in Plants. *Biomacromolecules* **2020**, *21*, 2755–2763. [CrossRef]
153. Machado, T.O.; Grabow, J.; Sayer, C.; de Araújo, P.H.H.; Ehrenhard, M.L.; Wurm, F.R. Biopolymer-based nanocarriers for sustained release of agrochemicals: A review on materials and social science perspectives for a sustainable future of agri- and horticulture. *Adv. Colloid. Interface Sci.* **2022**, *303*, 102645. [CrossRef]
154. Iravani, S.; Varma, R.S. Greener synthesis of lignin nanoparticles and their applications. *Green Chem.* **2020**, *22*, 612–636. [CrossRef]
155. Fischer, J.; Beckers, S.J.; Yiamsawas, D.; Thines, E.; Landfester, K.; Wurm, F.R. Targeted drug delivery in plants: Enzyme-responsive lignin nanocarriers for the curative treatment of the worldwide grapevine trunk disease esca. *Adv. Sci.* **2019**, *6*, 1802315. [CrossRef]
156. Albornoz-Palma, G.; Ortega-Sanhueza, I.; Teruel-Juanes, R.; Henríquez-Gallegos, S.; Ribes-Greus, A.; Pereira, M. Understanding the effect of lignin on the production process and characteristics of lignocellulose nanofibrils from Eucalyptus nitens. *Cellulose* **2023**, *30*, 6811–6831. [CrossRef]
157. Haldar, D.; Duarah, P.; Purkait, M.K. Chapter 16—Progress in the synthesis and applications of polymeric nanomaterials derived from waste lignocellulosic biomass. In *Advanced Materials for Sustainable Environmental Remediation*; Terrestrial and Aquatic Environments; Giannakoudakis, D., Meili, L., Anastopoulos, I., Eds.; Elsevier Inc.: Amsterdam, The Netherlands, 2022; pp. 419–433.
158. Tang, Q.; Qian, Y.; Yang, D.; Qiu, X.; Qin, Y.; Zhou, M. Lignin-Based Nanoparticles: A Review on Their Preparations and Applications. *Polymers* **2020**, *12*, 2471. [CrossRef]
159. Prasadini Perera, U.; Foo, M.L.; Leng Chew, I.M. Synthesis and characterization of lignin nanoparticles isolated from oil palm empty fruit bunch and application in biocomposites. *Sustain. Chem. Clim. Action.* **2023**, *2*, 100011. [CrossRef]
160. Parot, M.; Rodrigue, D.; Stevanovic, T. Electrospinning of Softwood Organosolv Lignin without Polymer Addition. *ACS Sustain. Chem. Eng.* **2022**, *11*, 607–616. [CrossRef]
161. Jiang, S.; Liu, X.; Wang, Z.; Zhou, L.; Meng, Z.; Wang, X.; Chen, G.; Wang, S.; Jiang, Y. In Situ Lignin Modification Enabling Enhanced Interfibrillar Interactions in Lignocellulosic Nanomaterials toward Structural Applications. *ACS Sustain. Chem. Eng.* **2023**, *11*, 7705–7718. [CrossRef]
162. Zhou, Y.; Han, Y.; Li, G.; Yang, S.; Chu, F. Lignin-Based Hollow Nanoparticles for Controlled Drug Delivery: Grafting Preparation Using β-Cyclodextrin/Enzymatic-Hydrolysis Lignin. *Nanomaterials* **2019**, *9*, 997. [CrossRef]
163. Qian, Y.; Deng, Y.H.; Qiu, X.Q.; Li, H.; Yang, D.J. Formation of uniform colloidal spheres from lignin, a renewable resource recovered from pulping spent liquor. *Green Chem.* **2014**, *16*, 2156–2163. [CrossRef]
164. Yiamsawas, D.; Beckers, S.J.; Lu, H.; Landfester, K.; Wurm, F.R. Morphology-Controlled Synthesis of Lignin Nanocarriers for Drug Delivery and Carbon Materials. *ACS Biomater. Sci. Eng.* **2017**, *3*, 2375–2383. [CrossRef]
165. Figueiredo, P.; Lintinen, K.; Kiriazis, A.; Hynninen, V.; Liu, Z.; Bauleth-Ramos, T.; Rahikkala, A.; Correia, A.; Kohout, T.; Sarmento, B.; et al. In Vitro Evaluation of Biodegradable Lignin-Based Nanoparticles for Drug Delivery and Enhanced Antiproliferation Effect in Cancer Cells. *Biomaterials* **2017**, *121*, 97–108. [CrossRef]

166. Dai, L.; Liu, R.; Hu, L.-Q.; Zou, Z.-F.; Si, C.-L. Lignin Nanoparticle as a Novel Green Carrier for the Efficient Delivery of Resveratrol. *ACS Sustain. Chem. Eng.* **2017**, *5*, 8241–8249. [CrossRef]
167. Zhou, Y.; Han, Y.; Li, G.; Yang, S.; Xiong, F.; Chu, F. Preparation of Targeted Lignin–Based Hollow Nanoparticles for the Delivery of Doxorubicin. *Nanomaterials* **2019**, *9*, 188. [CrossRef]
168. Chen, N.; Dempere, L.A.; Tong, Z. Synthesis of pH-Responsive Lignin-Based Nanocapsules for Controlled Release of Hydrophobic Molecules. *ACS Sustain. Chem. Eng.* **2016**, *4*, 5204–5211. [CrossRef]
169. Frangville, C.; Rutkevicius, M.; Richter, A.P.; Velev, O.D.; Stoyanov, S.D.; Paunov, V.N. Fabrication of Environmentally Biodegradable Lignin Nanoparticles. *Chemphyschem* **2012**, *13*, 4235–4243. [CrossRef] [PubMed]
170. Verdini, F.; Gaudino, E.C.; Canova, E.; Tabasso, S.; Behbahani, P.J.; Cravotto, G. Lignin as a Natural Carrier for the Efficient Delivery of Bioactive Compounds: From Waste to Health. *Molecules* **2022**, *27*, 3598. [CrossRef] [PubMed]
171. Stanisz, M.; Klapiszewski, Ł.; Jesionowski, T. Recent Advances in the Fabrication and Application of Biopolymer-Based Micro and Nanostructures: A Comprehensive Review. *Chem. Eng. J.* **2020**, *397*, 125409. [CrossRef]
172. Li, B.Q.; You, S.P.; Qi, W.; Wang, Y.F.; Su, R.X.; He, Z.M. Structure-tunable assembly of lignin sub-micro spheres by modifying the amphiphilic interfaces of lignin via n-alkane. *Eur. Polym. J.* **2020**, *126*, 109539. [CrossRef]
173. Yan, Z.Y.; Liao, G.F.; Zou, X.X.; Zhao, M.K.; Wu, T.; Chen, Y.H.; Fang, G.G. Size-Controlled and super long-term stable lignin nanospheres through a facile self-assembly strategy from kraft lignin. *J. Agric. Food Chem.* **2020**, *68*, 8341–8349. [CrossRef]
174. Trevisan, H.; Rezende, C.A. Pure, stable and highly antioxidant lignin nanoparticles from elephant grass. *Ind. Crop. Prod.* **2020**, *145*, 112105. [CrossRef]
175. Yadav, K.V.; Gupta, N.; Kumar, P.; Dashti, M.G.; Tirth, V.; Khan, S.H.; Yadav, K.K.; Choudhary, S.I.N.; Algahtani, A.; Bera, S.P.; et al. Recent Advances in Synthesis and Degradation of Lignin and Lignin Nanoparticles and Their Emerging Applications in Nanotechnology. *Materials* **2022**, *15*, 953. [CrossRef]
176. Pathania, K.; Sah, S.P.; Salunke, D.B.; Jain, M.; Yadav, A.K.; Yadav, V.G.; Pawar, S.V. Green synthesis of lignin-based nanoparticles as a bio-carrier for targeted delivery in cancer therapy. *Int. J. Biol. Macromol.* **2023**, *229*, 684–695. [CrossRef]
177. Chen, L.; Zhou, X.; Shi, Y.; Gao, B.; Wu, J.; Kirk, T.B.; Xu, J.; Xue, W. Green synthesis of lignin nanoparticle in aqueous hydrotropic solution toward broadening the window for its processing and application. *Chem. Eng. J.* **2018**, *346*, 217–225. [CrossRef]
178. Figueiredo, P.; Lahtinen, M.H.; Agustin, M.B.; Morais de Carvalho, D.; Hirvonen, S.P.; Penttilä, P.A.; Mikkonen, K.S. Green Fabrication Approaches of Lignin Nanoparticles from Different Technical Lignins: A Comparison Study. *ChemSusChem* **2021**, *14*, 4718–4730. [CrossRef]
179. Chen, L.; Shi, Y.; Gao, B.; Zhao, Y.; Jiang, Y.; Zha, Z.; Xue, W.; Gong, L. Lignin Nanoparticles: Green Synthesis in a γ-Valerolactone/Water Binary Solvent and Application to Enhance Antimicrobial Activity of Essential Oils. *ACS Sustain. Chem. Eng.* **2020**, *8*, 714–722. [CrossRef]
180. Liu, R.; Dai, L.; Xu, C.; Wang, K.; Zheng, C.; Si, C. Lignin-Based Micro- and Nanomaterials and their Composites in Biomedical Applications. *ChemSusChem* **2020**, *13*, 4266–4283. [CrossRef]
181. Domínguez-Robles, J.; Cárcamo-Martínez, Á.; Stewart, S.A.; Donnelly, R.F.; Larrañeta, E.; Borrega, M. Lignin for Pharmaceutical and Biomedical Applications—Could This Become a Reality? *Sustain. Chem. Pharm.* **2020**, *18*, 100320. [CrossRef]
182. Alqahtani, M.S.; Alqahtani, A.; Al-Thabit, A.; Roni, M.; Syed, R. Novel Lignin Nanoparticles for Oral Drug Delivery. *J. Mater. Chem. B* **2019**, *7*, 4461–4473. [CrossRef]
183. Garg, J.; Chiu, M.N.; Krishnan, S.; Tripathi, L.K.; Pandit, S.; Far, B.F.; Jha, N.K.; Kesari, K.K.; Tripathi, V.; Pandey, S. Applications of lignin nanoparticles for cancer drug delivery: An update. *Mater. Lett.* **2022**, *311*, 131573. [CrossRef]
184. Yang, W.; Owczarek, J.S.; Fortunati, E.; Kozanecki, M.; Mazzaglia, A.; Balestra, G.M.; Kenny, J.M.; Torre, L.; Puglia, D. Antioxidant and antibacterial lignin nanoparticles in polyvinyl alcohol /chitosan films for active packaging. *Ind. Crop. Prod.* **2016**, *94*, 800–811. [CrossRef]
185. Far, B.F.; Isfahani, A.A.; Nasiriyan, E.; Pourmolaei, A.; Mahmoudvand, G.; Rouzbahani, A.K.; Amin, M.N.; Jamal, M.R.N. An Updated Review on Advances in Hydrogel-Based Nanoparticles for Liver Cancer Treatment. *Livers* **2023**, *3*, 161–189. [CrossRef]
186. Agustin, M.; Lehtonen, M.; Kemell, M.; Lahtinen, P.; Oliaei, E.; Mikkonen, K.S. Lignin nanoparticle-decorated nanocellulose cryogels as adsorbents for pharmaceutical pollutants. *J. Environ. Manag.* **2023**, *330*, 117210. [CrossRef] [PubMed]
187. Zikeli, F.; Vettraino, A.M.; Biscontri, M.; Bergamasco, S.; Palocci, C.; Humar, M.; Romagnoli, M. Lignin Nanoparticles with Entrapped Thymus spp. Essential Oils for the Control of Wood-Rot Fungi. *Polymers* **2023**, *15*, 2713. [CrossRef]
188. Gan, D.; Xing, W.; Jiang, L.; Fang, J.; Zhao, C.; Ren, F.; Fang, L.; Wang, K.; Lu, X. Plant-inspired adhesive and tough hydrogel based on Ag-Lignin nanoparticles-triggered dynamic redox catechol chemistry. *Nat. Commun.* **2019**, *10*, 1487. [CrossRef]
189. Banpean, A.; Hararak, B.; Winotapun, C.; Kitchaicharoenporn, S.; Naimlang, S. Lignin nanoparticles as sustainable biobased nucleating agents of poly(L-lactic acid): Crystallization behavior and effect of particle sizes. *J. Mater. Sci.* **2023**, *58*, 6823–6838. [CrossRef]
190. Luraghi, A.; Peri, F.; Moroni, L. Electrospinning for drug delivery applications: A review. *J. Control. Release* **2021**, *334*, 463–484. [CrossRef] [PubMed]
191. Pant, B.; Park, M.; Park, S.J. Drug delivery applications of core-sheath nanofibers prepared by coaxial electrospinning: A review. *Pharmaceutics* **2019**, *11*, 305. [CrossRef]
192. Kumar, M.; Hietala, M.; Oksman, K. Lignin-Based Electrospun Carbon Nanofibers Frontiers in Materials: Rising Stars mini review. *Front. Mater.* **2019**, *6*, 62. [CrossRef]

193. Kai, D.; Ren, W.; Tian, L.; Chee, P.L.; Liu, Y.; Ramakrishna, S.; Loh, X.J. Engineering poly (lactide)–lignin nanofibers with antioxidant activity for biomedical application. *ACS Sustain. Chem. Eng.* **2016**, *4*, 5268–5276. [CrossRef]
194. Wang, D.; Jang, J.; Kim, K.; Kim, J.; Park, C.B. Tree to Bone: Lignin/Polycaprolactone Nanofibers for Hydroxyapatite Biomineralization. *Biomacromolecules* **2019**, *20*, 2684–2693. [CrossRef]
195. An, L.; Heo, J.W.; Chen, J.; Kim, Y.S. Water-soluble lignin quaternary ammonium salt for electrospun morphology-controllable antibacterial polyvinyl alcohol/lignin quaternary ammonium salt nanofibers. *J. Clean. Prod.* **2022**, *368*, 133219. [CrossRef]
196. Kai, D.; Chong, H.M.; Chow, L.P.; Jiang, L.; Lin, Q.; Zhang, K.; Zhang, H.; Zhang, Z.; Loh, X.J. Strong and biocompatible lignin/poly (3-hydroxybutyrate) composite nanofibers. *Compos. Sci. Technol.* **2018**, *158*, 26–33. [CrossRef]
197. Abudulah, T.; Gauthaman, K.; Mostafavi, A.; Alshahrie, A.; Salah, N.; Morganti, P.; Chianese, A.; Tamayol, A.; Memic, A. Sustainable Drug Release from Polycaprolactone Coated Chitin-Lignin Gel Fibrous Scaffolds. *Sci. Rep.* **2020**, *10*, 20428. [CrossRef] [PubMed]
198. Liang, R.; Yang, X.; Yew, P.Y.M.; Sugiarto, S.; Zhu, Q.; Zhao, J.; Loh, X.J.; Zheng, L.; Kai, D. PLA-lignin nanofibers as antioxidant biomaterials for cartilage regeneration and osteoarthritis treatment. *J. Nanobiotechnol.* **2022**, *20*, 327. [CrossRef] [PubMed]
199. . Ni, S.; Bian, H.; Zhang, Y.; Fu, Y.; Liu, W.; Qin, M.; Xiao, H. Starch-Based Composite Films with Enhanced Hydrophobicity, Thermal Stability, and UV-Shielding Efficacy Induced by Lignin Nanoparticles. *Biomacromolecules* **2022**, *23*, 829–838. [CrossRef] [PubMed]
200. Qi, G.; Yang, W.; Puglia, D.; Wang, H.; Xu, P.; Dong, W.; Zheng, T.; Ma, P. Hydrophobic, UV resistant and dielectric polyurethane-nanolignin composites with good reprocessability. *Mater. Des.* **2020**, *196*, 109150. [CrossRef]
201. Makri, S.P.; Xanthopoulou, E.; Valera, M.A.; Mangas, A.; Marra, G.; Ruiz, V.; Koltsakidis, S.; Tzetzis, D.; Zoikis Karathanasis, A.; Deligkiozi, I.; et al. Poly(Lactic Acid) Composites with Lignin and Nanolignin Synthesized by In Situ Reactive Processing. *Polymers* **2023**, *15*, 2386. [CrossRef] [PubMed]
202. Cheng, L.; Deng, B.; Luo, W.; Nie, S.; Liu, X.; Yin, Y.; Liu, S.; Wu, Z.; Zhan, P.; Zhang, L.; et al. pH-Responsive Lignin-Based Nanomicelles for Oral Drug Delivery. *J. Agric. Food Chem.* **2020**, *68*, 5249–5258. [CrossRef]
203. Danti, S.; Trombi, L.; Fusco, A.; Azimi, B.; Lazzeri, A.; Morganti, P.; Coltelli, M.-B.; Donnarumma, G. Chitin Nanofibrils and Nanolignin as Functional Agents in Skin Regeneration. *Int. J. Mol. Sci.* **2019**, *20*, 2669. [CrossRef]
204. Wang, J.; Tian, L.; Luo, B.; Ramakrishna, S.; Kai, D.; Loh, J.X.; Yang, I.H.; Deen, G.R.; Mo, X. Engineering PCL/lignin nanofibers as an antioxidant scaffold for the growth of neuron and Schwann cell. *Colloids Surf. B Biointerfaces* **2018**, *169*, 356–365. [CrossRef]
205. Li, B.; Xia, X.; Chen, J.; Xia, D.; Xu, R.; Zou, X.; Wang, H.; Liang, C. Paclitaxel-loaded lignin particle encapsulated into electrospun PVA/PVP composite nanofiber for effective cervical cancer cell inhibition. *Nanotechnology* **2020**, *32*, 015101. [CrossRef] [PubMed]
206. Aadil, K.R.; Mussatto, S.I.; Jha, H. Synthesis and characterization of silver nanoparticles loaded poly(vinyl alcohol)-lignin electrospun nanofibers and their antimicrobial activity. *Int. J. Biol. Macromol.* **2018**, *120*, 763–767. [CrossRef]
207. Elsherbiny, D.A.; Abdelgawad, A.M.; El-Naggar, M.E.; Hemdan, B.A.; Ghazanfari, S.; Jockenhövel, S.; Rojas, O.J. Bioactive tri-component nanofibers from cellulose acetate/lignin//N-vanillidene-phenylthiazole copper-(II) complex for potential diaper dermatitis control. *Int. J. Biol. Macromol.* **2022**, *205*, 703–718. [CrossRef]
208. Tabakoglu, S.; Kołbuk, D.; Sajkiewicz, P. Multifluid electrospinning for multi-drug delivery systems: Pros and cons, challenges, and future directions. *Biomater. Sci.* **2023**, *11*, 37–61. [CrossRef] [PubMed]
209. Yang, D.-L.; Faraz, F.; Wang, J.-X.; Radacsi, N. Combination of 3D Printing and Electrospinning Techniques for Biofabrication. *Adv. Mater. Technol.* **2022**, *7*, 2101309. [CrossRef]
210. Gujjala, L.K.S.; Kim, J.; Won, W. Technical lignin to hydrogels: An Eclectic review on suitability, synthesis, applications, challenges and future prospects. *J. Clean. Prod.* **2022**, *363*, 132585. [CrossRef]
211. Abdullah, T.; Ilyasoglu, G.; Memi, A. Designing Lignin-Based Biomaterials as Carriers of Bioactive Molecules. *Pharmaceutics* **2023**, *15*, 1114. [CrossRef]
212. Hama, R.; Ulziibayar, A.; Reinhardt, J.W.; Watanabe, T.; Kelly, J.; Shinoka, T. Recent Developments in Biopolymer-Based Hydrogels for Tissue Engineering Applications. *Biomolecules* **2023**, *13*, 280. [CrossRef]
213. Altuntas, E.; Özkan, B.; Güngör, S.; Özsoy, Y. Biopolymer-Based Nanogel Approach in Drug Delivery: Basic Concept and Current Developments. *Pharmaceutics* **2023**, *15*, 1644. [CrossRef]
214. Daassi, R.; Durand, K.; Rodrigue, D.; Stevanovic, T. Optimization of the Electrospray Process to Produce Lignin Nanoparticles for PLA-Based Food Packaging. *Polymers* **2023**, *15*, 2973. [CrossRef]
215. Meng, Y.; Lu, J.; Cheng, Y.; Li, Q.; Wang, H. Lignin-based hydrogels: A review of preparation, properties, and application. *Int. J. Biol. Macromol.* **2019**, *135*, 1006–1019. [CrossRef]
216. Eggermont, L.J.; Rogers, Z.J.; Colombani, T.; Memic, A.; Bencherif, S.A. Injectable cryogels for biomedical applications. *Trends Biotechnol.* **2020**, *38*, 418–431. [CrossRef]
217. Memic, A.; Colombani, T.; Eggermont, L.J.; Rezaeeyazdi, M.; Steingold, J.; Rogers, Z.J.; Navare, K.J.; Mohammed, H.S.; Bencherif, S.A. Latest Advances in Cryogel Technology for Biomedical Applications. *Adv. Ther.* **2019**, *2*, 1800114. [CrossRef]
218. Memic, A.; Rezaeeyazdi, M.; Villard, P.; Rogers, Z.J.; Abudulah, T.; Colombani, T.; Bencherif, S.A. Effect of Polymer Concentration on Autoclaved Cryogel Properties. *Macromol. Mater. Eng.* **2020**, *305*, 1900824. [CrossRef]
219. Abdullah, T.; Colombani, T.; Alade, T.; Bencherif, S.A.; Memic, A. Injectable Lignin-co-Gelatin Cryogels with Antioxidant and Antibacterial Properties for Biomedical Applications. *Biomacromolecules* **2021**, *22*, 4110–4121. [CrossRef] [PubMed]

220. Zhang, Y.; Jiang, M.; Zhang, Y.; Cao, Q.; Wang, X.; Han, Y.; Sun, G.; Li, Y.; Zhou, J. Novel lignin–chitosan–PVA composite hydrogel for wound dressing. *Mater. Sci. Eng. C* **2019**, *104*, 110002. [CrossRef]
221. Tian, R.; Liu, Q.; Zhang, W.; Zhang, Y. Preparation of lignin-based hydrogel and its adsorption on Cu^{2+} ions and Co^{2+} ions in wastewaters. *J. Inorg. Organomet. Polym. Mater.* **2018**, *28*, 2545–2553. [CrossRef]
222. Larraneta, E.; Imízcoz, M.; Toh, J.X.; Irwin, N.J.; Ripolin, A.; Perminova, A.; Domínguez-Robles, J.; Rodríguez, A.; Donnelly, R.F. Synthesis and characterization of lignin hydrogels for potential applications as drug eluting antimicrobial coatings for medical materials. *ACS Sustain. Chem. Eng.* **2018**, *6*, 9037–9046. [CrossRef]
223. Ganewatta, M.S.; Lokupitiya, H.N.; Tang, C. Lignin biopolymers in the age of controlled polymerization. *Polymers* **2019**, *11*, 1176. [CrossRef] [PubMed]
224. Liu, Z.; Lu, X.; Xie, J.; Feng, B.; Han, Q. Synthesis of a novel tunable lignin-based star copolymer and its flocculation performance in the treatment of kaolin suspension. *Sep. Purif. Technol.* **2019**, *210*, 355–363. [CrossRef]
225. Liu, C.; Li, Y.; Zhuang, J.; Xiang, Z.; Jiang, W.; He, S.; Xiao, H. Conductive Hydrogels Based on Industrial Lignin: Opportunities and Challenges. *Polymers* **2022**, *14*, 3739. [CrossRef]
226. Savina, I.N.; Zoughaib, M.; Yergeshov, A.A. Design and assessment of biodegradable macroporous cryogels as advanced tissue engineering and drug carrying materials. *Gels* **2021**, *7*, 79. [CrossRef]
227. Álvarez-Torrellas, S.; Sanz-Santos, E.; García, J. Chapter 22—Activated carbons derived from biomass for the removal by adsorption of several pesticides from water. In *Advanced Materials for Sustainable Environmental Remediation. Terrestrial and Aquatic Environments*; e-book; Elsevier: Amsterdam, The Netherlands, 2022; pp. 565–583.
228. Gizli, N.; Çok, S.S.; Koç, F. Chapter 7, Aerogel, xerogel, and cryogel: Synthesis, surface chemistry, and properties—Practical environmental applications and the future developments. In *Advanced Materials for Sustainable Environmental. Remediation Terrestrial and Aquatic Environments*; Giannakoudakis, D., Meili, L., Anastopoulos, I., Eds.; Elsevier: Amsterdam, The Netherlands, 2022; pp. 195–229.
229. .Lyu, Z.; Zheng, Y.; Zhou, H.; Dai, L. Lignin-based Hydrogels for Biological Application. *Pap. Biomater.* **2023**, *8*, 37–52. [CrossRef]
230. Mantha, S.; Pillai, S.; Khayambashi, P.; Upadhyay, A.; Zhang, Y.; Tao, O.; Pham, H.M.; Tran, S.D. Smart hydrogels in tissue engineering and regenerative medicine. *Materials* **2019**, *12*, 3323. [CrossRef]
231. Mazloom, N.; Khorassani, R.; Zohury, G.H.; Emami, H.; Whalen, J. Lignin-based hydrogel alleviates drought stress in maize. *Environ. Exp. Bot.* **2020**, *175*, 104055. [CrossRef]
232. Morales, A.; Labidi, J.; Gullon, P. Assessment of green approaches for the synthesis of physically crosslinked lignin hydrogels. *J. Ind. Eng. Chem.* **2020**, *81*, 475–487. [CrossRef]
233. Song, B.; Liang, H.; Sun, R.; Peng, P.; Jiang, Y.; She, D. Hydrogel synthesis based on lignin/sodium alginate and application in agriculture. *Int. J. Biol. Macromol.* **2020**, *144*, 219–230. [CrossRef] [PubMed]
234. Sun, Y.; Ma, Y.; Fang, G.; Ren, S.; Fu, Y. Controlled pesticides release from porous composite hydrogels based on lignin and polyacrylic acid. *BioResources* **2016**, *11*, 2361–2371. [CrossRef]
235. Huang, S.; Wu, L.; Li, T.; Xu, D.; Lin, X.; Wu, C. Facile preparation of biomass lignin-based hydroxyethyl cellulose super-absorbent hydrogel for dye pollutant removal. *Int. J. Biol. Macromol.* **2019**, *137*, 939–947. [CrossRef]
236. Liu, M.; Liu, Y.; Shen, J.; Zhang, S.; Liu, X.; Chen, X.; Ma, Y.; Ren, S.; Fang, G.; Li, S.; et al. Simultaneous removal of Pb^{2+}, Cu^{2+} and Cd^{2+} ions from wastewater using hierarchical porous polyacrylic acid grafted with lignin. *J. Hazard. Mater.* **2020**, *392*, 122208. [CrossRef]
237. Stanisz, M.; Klapiszewski, Ł.; Kołodynska, D.; Jesionowski, T. Development of functional lignin-based spherical particles for the removal of vanadium (V) from an aqueous system. *Int. J. Biol. Macromol.* **2021**, *186*, 181–193. [CrossRef]
238. Jiang, C.; Wang, X.; Hou, B.; Hao, C.; Li, X.; Wu, J. Construction of a Lignosulfonate-Lysine Hydrogel for the Adsorption of Heavy Metal Ions. *J. Agric. Food Chem.* **2020**, *68*, 3050–3060. [CrossRef]
239. . Ivanov, A.E.; Halthur, T.; Ljunggren, L. Flow permeable composites of lignin and poly(vinyl alcohol): Towards removal of bisphenol A and erythromycin from water. *J. Environ. Chem. Eng.* **2016**, *4*, 1432–1441. [CrossRef]
240. Yuan, H.; Peng, J.; Ren, T.; Luo, Q.; Luo, Y.; Zhang, N.; Huang, Y.; Guo, X.; Wu, Y. Novel fluorescent lignin-based hydrogel with cellulose nanofibers and carbon dots for highly efficient adsorption and detection of Cr(VI). *Sci. Total Environ.* **2021**, *760*, 143395. [CrossRef]
241. Morales, A.; Labidi, J.; Gullón, P. Influence of lignin modifications on physically crosslinked lignin hydrogels for drug delivery applications. *Sustain. Mater. Technol.* **2022**, *33*, e00474. [CrossRef]
242. Eivazzadeh-Keihan, R.; Aliabadi, H.A.M.; Radinekiyan, F.; Sobhani, M.; Khalili, F.; Maleki, A.; Madanchi, H.; Mahdavi, M.; Shalan, A.E. Investigation of the Biological Activity, Mechanical Properties and Wound Healing Application of a Novel Scaffold Based on Lignin–Agarose Hydrogel and Silk Fibroin Embedded Zinc Chromite Nanoparticles. *RSC Adv.* **2021**, *11*, 17914–17923. [CrossRef] [PubMed]
243. Barros, A.; Quraishi, S.; Martins, M.; Gurikov, P.; Subrahmanyam, R.; Smirnova, I.; Duarte, A.R.C.; Reis, R.L. Hybrid Alginate Based Cryogels for Life Science Applications. *Chem. Ing. Tech.* **2016**, *88*, 1770–1778. [CrossRef]
244. Memic, A.; Abudulah, T. Antioxidant, Antibacterial, Injectable Lignin-Gelatin Composite Cryogels for Wound Healing and Tissue Engineering. U.S. Patent US10881760B1, 5 January 2021.
245. Chiani, E.; Beaucamp, A.; Hamzeh, Y.; Azadfallah, M.; Thanusha, A.; Collins, M.N. Synthesis and characterization of gelatin/lignin hydrogels as quick release drug carriers for Ribavirin. *Int. J. Biol. Macromol.* **2023**, *224*, 1196–1205. [CrossRef]

246. Kim, B.; Kim, Y.; Lee, Y.; Oh, J.; Jung, Y.; Koh, W.G.; Chung, J.J. Reactive Oxygen Species Suppressive Kraft Lignin-Gelatin Antioxidant Hydrogels for Chronic Wound Repair. *Macromol Biosci.* **2022**, *22*, 2200234. [CrossRef]
247. . Nunes, D.; Andrade, S.; Ramalho, M.J.; Loureiro, J.A.; Pereira, M.C. Polymeric Nanoparticles-Loaded Hydrogels for Biomedical Applications: A Systematic Review on In Vivo Findings. *Polymers* **2022**, *14*, 1010. [CrossRef]
248. Culebras, M.; Pishnamazi, M.; Walker, G.M.; Collins, M.N. Facile Tailoring of Structures for Controlled Release of Paracetamol from Sustainable Lignin Derived Platforms. *Molecules* **2021**, *26*, 1593. [CrossRef] [PubMed]
249. Xu, J.; Xu, J.J.; Lin, Q.; Jiang, L.; Zhang, D.; Li, Z.; Ma, B.; Zhang, C.; Li, L.; Kai, D.; et al. Lignin-incorporated nanogel serving as an antioxidant biomaterial for wound healing. *ACS Appl. Bio Mater.* **2020**, *4*, 3–13. [CrossRef]
250. Zhao, H.; Feng, Q.; Xie, Y.; Li, J.; Chen, X. Preparation of biocompatible hydrogel from lignin-carbohydrate complex (LCC) as cell carriers. *BioResources* **2017**, *12*, 8490–8504. [CrossRef]
251. Li, M.; Jiang, X.; Wang, D.; Xu, Z.; Yang, M. In situ reduction of silver nanoparticles in the lignin based hydrogel for enhanced antibacterial application. *Colloids Surf. B Biointerfaces* **2019**, *177*, 370–376. [CrossRef]
252. Morales, A.; Labidi, J.; Gullón, P. Effect of the formulation parameters on the absorption capacity of smart lignin-hydrogels. *Eur. Polym. J.* **2020**, *129*, 109631. [CrossRef]
253. Musilová, L.; Mráček, A.; Kovalcik, A.; Smolka, P.; Minařík, A.; Humpolíček, P.; Vícha, R.; Ponížil, P. Hyaluronan hydrogels modified by glycinated Kraft lignin: Morphology, swelling, viscoelastic properties and biocompatibility. *Carbohydr. Polym.* **2018**, *181*, 394–403. [CrossRef]
254. Chandna, S.; Thakur, N.S.; Kaur, R.; Bhaumik, J. Lignin–bimetallic nanoconjugate doped pH-responsive hydrogels for laser-assisted antimicrobial photodynamic therapy. *Biomacromolecules* **2020**, *21*, 3216–3230. [CrossRef]
255. Raschip, I.; Panainte, A.; Daniela, P.; Profire, L.; Vasile, C. In Vitro Testing of Xanthan/Lignin Hydrogels as Carriers for Controlled Delivery of Bisoprolol Fumarate. *Rev. Med. Chir. Soc. Med. Nat. Iasi* **2015**, *119*, 1189–1194. [PubMed]
256. Huerta, R.R.; Silva, E.K.; Ekaette, I.; El-Bialy, T.; Saldana, M.D.A. High-intensity ultrasound-assisted formation of cellulose nanofiber scaffold with low and high lignin content and their cytocompatibility with gingival fibroblast cells. *Ultrason Sonochem.* **2020**, *64*, 104759. [CrossRef] [PubMed]
257. Xu, C.; Liu, L.; Renneckar, S.; Jiang, F. Chemically and physically crosslinked lignin hydrogels with antifouling and antimicrobial properties. *Ind. Crop. Prod.* **2021**, *170*, 113759. [CrossRef]
258. El-Nemr, K.F.; Mohamed, H.R.; Ali, M.A.; Fathy, R.M.; Dhmees, A.S. Polyvinyl alcohol/gelatin irradiated blends filled by lignin as green filler for antimicrobial packaging materials. *Int. J. Environ. Anal. Chem.* **2020**, *100*, 1578–1602. [CrossRef]
259. Mandlekar, N.; Cayla, A.; Rault, F.; Giraud, S.; Salaun, F.; Guan, J. Valorization of industrial lignin as biobased carbon source in fire retardant system for Polyamide 11 blends. *Polymers* **2019**, *11*, 180. [CrossRef]
260. Wu, K.; Xu, S.; Tian, X.-Y.; Zeng, H.-Y.; Hu, J.; Guo, Y.-H.; Jian, J. Renewable lignin-based surfactant modified layered double hydroxide and its application in polypropylene as flame retardant and smoke suppression. *Int. J. Biol. Macromol.* **2021**, *178*, 580–590. [CrossRef]
261. Xu, Q.; Bai, Y.; Zhao, X.; Ren, M.; Wang, S.; Kong, F. Synthesis and characterization of an amphiphilic lignin-based cationic surfactant. *Ind. Crop. Prod.* **2021**, *164*, 113376. [CrossRef]
262. Soares, A.K.; Gatto, D.A.; Magalhaes, W.L.E.; Erdocia, X.; Gutierrez, M.A.U.; Delucis, R.A.; Missio, A.L. Kraft lignin as a partial replacement for a traditional surfactant in thymol-based biocidal suspensions: Physical and chemical features. *J. Wood Chem. Technol.* **2021**, *41*, 199–209. [CrossRef]
263. Moreno, A.; Morsali, M.; Liu, J.; Sipponen, M.H. Access to tough and transparent nanocomposites of PS/PBMA (poly(butylmethacrylate) nanocomposites via Pickering emulsion polymerization using biocatalytic hybrid lignin nanoparticles as functional surfactants. *Green Chem.* **2021**, *23*, 3001–3014. [CrossRef]
264. Ghavidel, N.; Fatehi, P. Interfacial and Emulsion Characteristics of Oil-Water Systems in the Presence of Polymeric Lignin Surfactant. *Langmuir* **2021**, *37*, 3346–3358. [CrossRef] [PubMed]
265. Abdullah, T.; Qurban, R.O.; Bolarinwa, S.O.; Mirza, A.A.; Pasovic, M.; Memic, A. 3D Printing of Metal/Metal Oxide Incorporated Thermoplastic Nanocomposites With Antimicrobial Properties. *Front. Bioeng. Biotechnol.* **2020**, *8*, 568186. [CrossRef]
266. Karakurt, I.; Lin, L. 3D printing technologies: Techniques, materials, and post-processing. *Curr. Opin. Chem. Eng.* **2020**, *28*, 134–143. [CrossRef]
267. Abdullah, T.; Okay, O. 4D Printing of Body Temperature-Responsive Hydrogels Based on Poly (acrylic acid) with Shape-Memory and Self-Healing Abilities. *ACS Appl. Bio Mater.* **2023**, *6*, 703–711. [CrossRef]
268. Sharma, K.S. Artificial Intelligence Assisted Fabrication of 3D, 4D and 5D Printed Formulations or Devices for Drug Delivery. *Curr. Drug Deliv.* **2023**, *20*, 752–769. [CrossRef] [PubMed]
269. Ghazal, A.F.; Zhang, M.; Mujumdar, A.S.; Ghamry, M. Progress in 4D/5D/6D printing of foods: Applications and R&D opportunities. *Crit. Rev. Food Sci. Nutr.* **2022**, 1–24. [CrossRef]
270. Wang, Y.; Zhou, X.; Zhu, S.; Wei, X.; Zhou, N.; Liao, X.; Peng, Y.; Tang, Y.; Zhang, L.; Yang, X. Cryoprinting of nanoparticle enhanced injectable hydrogel with shape-memory properties. *Mater. Des.* **2022**, *223*, 111120. [CrossRef]
271. Awad, A.; Fina, F.; Goyanes, A.; Gaisford, S.; Basit, A.W. 3D printing: Principles and pharmaceutical applications of selective laser sintering. *Int. J. Pharm.* **2020**, *586*, 119594. [CrossRef] [PubMed]
272. Tan, Y.J.N.; Yong, W.P.; Low, H.R.; Kochhar, J.S.; Khanolkar, J.; Lim, T.S.E.; Sun, Y.; Wong, J.Z.E.; Soh, S. Customizable drug tablets with constant release profiles via 3D printing technology. *Int. J. Pharm.* **2021**, *598*, 120370. [CrossRef]

273. Seoane-Viaño, I.; Trenfield, S.J.; Basit, A.W.; Goyanes, A. Translating 3D printed pharmaceuticals: From hype to real-world clinical applications. *Adv. Drug Deliv. Rev.* **2021**, *174*, 553–575. [CrossRef] [PubMed]
274. Samandari, M.; Mostafavi, A.; Quint, J.; Memic, A.; Tamayol, A. In situ bioprinting: Intraoperative implementation of regenerative medicine. *Trends Biotechnol.* **2022**, *40*, 1229–1247. [CrossRef] [PubMed]
275. Yang, J.; An, X.; Liu, L.; Tang, S.; Cao, H.; Xu, Q.; Liu, H. Cellulose, Hemicellulose, Lignin, and Their Derivatives as MultiComponents of Bio-Based Feedstocks for 3D Printing. *Carbohydr. Polym.* **2020**, *250*, 116881. [CrossRef] [PubMed]
276. Feng, X.; Yang, Z.; Chmely, S.; Wang, Q.; Wang, S.; Xie, Y. Lignin-Coated Cellulose Nanocrystal Filled Methacrylate Composites Prepared via 3D Stereolithography Printing: Mechanical Reinforcement and Thermal Stabilization. *Carbohydr. Polym.* **2017**, *169*, 272–281. [CrossRef]
277. Ramiah, P.; du Toit, L.C.; Choonara, Y.E.; Kondiah, P.P.D.; Pillay, V. Hydrogel-Based Bioinks for 3D Bioprinting in Tissue Regeneration. *Front. Mater. Sec. Colloid. Mater. Interfaces* **2020**, *7*, 76. [CrossRef]
278. Azad, M.A.; Olawuni, D.; Kimbell, G.; Badruddoza, A.Z.M.; Hossain, M.S.; Sultana, T. Polymers for extrusion-based 3D printing of pharmaceuticals: A holistic materials–process perspective. *Pharmaceutics* **2020**, *12*, 160–163. [CrossRef]
279. Ngo, T.D.; Kashani, A.; Imbalzano, G.; Nguyen, K.T.Q.; Hui, D. Additive manufacturing (3D printing): A review of materials, methods, applications and challenges. *Compos. Part B Eng.* **2018**, *143*, 172–196. [CrossRef]
280. Ebers, L.S.; Arya, A.; Bowland, C.C.; Glasser, W.G.; Chmely, S.C.; Naskar, A.K.; Laborie, M.P. 3D printing of lignin: Challenges, opportunities and roads onward. *Biopolymers* **2021**, *112*, e23431. [CrossRef]
281. Glasser, W.G. About Making Lignin Great Again. Some Lessons from the Past. *Front. Chem. Sec. Green. Sustain. Chem.* **2019**, *7*, 565. [CrossRef]
282. Sachdeva, I.; Ramesh, S.; Chadha, U.; Punugoti, H.; Selvaraj, S.K. Computational AI models in VAT photopolymerization: A review, current trends, open issues, and future opportunities. *Neural Comput. Appl.* **2022**, *34*, 17207–17229. [CrossRef]
283. Domínguez-Robles, J.; Martin, N.K.; Fong, M.L.; Stewart, S.A.; Irwin, N.J.; Rial-Hermida, M.I.; Donnelly, R.F.; Larrañeta, E. Antioxidant PLA Composites Containing Lignin for 3D Printing Applications: A Potential Material for Healthcare Applications. *Pharmaceutics* **2019**, *11*, 165. [CrossRef]
284. Abdullah, T.; Qurban, R.O.; Abdel-Wahab, M.S.; Salah, N.A.; Melaibari, A.A.; Zamzami, M.A.; Memic, A. Development of Nanocoated Filaments for 3D Fused Deposition Modeling of Antibacterial and Antioxidant Materials. *Polymers* **2022**, *14*, 2645. [CrossRef] [PubMed]
285. Wang, L.; Wang, Q.; Slita, A.; Backman, O.; Gounani, Z.; Rosqvist, E.; Peltonen, J.; Willför, S.; Xu, C.; Rosenholm, J.M.; et al. Digital light processing (DLP) 3D-fabricated antimicrobial hydrogel with a sustainable resin of methacrylated woody polysaccharides and hybrid silver-lignin nanospheres. *Green Chem.* **2022**, *24*, 2129–2145. [CrossRef]
286. Domínguez-Robles, J.; Cuartas-Gómez, E.; Dynes, S.; Utomo, E.; Anjani, Q.K.; Detamornrat, U.; Donnelly, R.F.; MorenoCastellanos, N.; Larrañeta, E. Poly(caprolactone)/lignin-based 3D-printed dressings loaded with a novel combination of bioactive agents for wound-healing applications. *Sustain. Mater. Technol.* **2023**, *35*, e00581. [CrossRef]
287. Zhou, X.; Ren, Z.; Sun, H.; Bi, H.; Gu, T.; Xu, M. 3D printing with high content of lignin enabled by introducing polyurethane. *Int. J. Biol. Macromol.* **2022**, *221*, 1209–1217. [CrossRef]
288. Sutton, J.T.; Rajan, K.; Harper, D.P.; Chmely, S.C. Lignin-Containing Photoactive Resins for 3D Printing by Stereolithography. Available online: https://chemrxiv.org/engage/api-gateway/chemrxiv/assets/orp/resource/item/60c73f19ee301c3697c7882e/original/lignin-containing-photoactive-resins-for-3d-printing-by-stereolithography.pdf (accessed on 19 May 2023).
289. Ebers, L.-S.; Laborie, M.-P. Direct Ink Writing of Fully Bio-Based Liquid Crystalline Lignin/Hydroxypropyl Cellulose Aqueous Inks: Optimization of Formulations and Printing Parameters. *ACS Appl. Bio Mater.* **2020**, *3*, 6897–6907. [CrossRef]
290. Jaiswal, L.; Shankar, S.; Rhim, J.W.; Hahm, D.-H. Lignin-Mediated Green Synthesis of AgNPs in Carrageenan Matrix for Wound Dressing Applications. *Int. J. Biol. Macromol.* **2020**, *159*, 859–869. [CrossRef]
291. Zhang, X.; Morits, M.; Jonkergouw, C.; Ora, A.; Valle-Delgado, J.J.; Farooq, M.; Ajdary, R.; Huan, S.; Linder, M.; Rojas, O.; et al. Three-Dimensional Printed Cell Culture Model Based on Spherical Colloidal Lignin Particles and Cellulose Nanofibril-Alginate Hydrogel. *Biomacromolecules* **2020**, *21*, 1875–1885. [CrossRef]
292. Nuutinen, E.-M.; Valle-Delgado, J.J.; Kellock, M.; Farooq, M.; Österberg, M. Affinity of Keratin Peptides for Cellulose and Lignin: A Fundamental Study toward Advanced Bio-Based Materials. *Langmuir* **2022**, *38*, 9917–9927. [CrossRef]
293. Grigsby, W.J.; Scott, S.M.; Plowman-Holmes, M.I.; Middlewood, P.G.; Recabar, K. Combination and processing keratin with lignin as biocomposite materials for additive manufacturing technology. *Acta Biomater.* **2020**, *104*, 95–103. [CrossRef]
294. Lee, J.G.; Guo, Y.; Belgodere, J.A.; Al Harraq, A.; Hymel, A.A.; Pete, A.J.; Valsaraj, K.T.; Benton, M.G.; Miller, M.G.; Jung, J.P.; et al. Lignin-Zein Composite: Synthesis, Three-Dimensional Printing, and Microbial Degradation. *ACS Sustain. Chem. Eng.* **2021**, *9*, 1781–1789. [CrossRef]
295. Hong, S.H.; Park, J.H.; Kim, O.Y.; Hwang, S.H. Preparation of Chemically Modified Lignin-Reinforced PLA Biocomposites and Their 3D Printing Performance. *Polymers* **2021**, *13*, 667. [CrossRef] [PubMed]
296. Researchers Upcycle Lignin for Sustainable 3D Printing with Economics in Mind Hayley Everett January 21st 2022—2:55pm. Available online: https://3dprintingindustry.com/news/researchers-upcycle-lignin-for-sustainable-3d-printing-with-economics-in-mind-202718/ (accessed on 28 May 2023).
297. Sadeghifar, H.; Ragauskas, A. Lignin as a UV Light Blocker—A Review. *Polymers* **2020**, *12*, 1134. [CrossRef]

298. Solihat, N.N.; Sari, F.P.; Falah, F.; Ismayati, M.; Lubis, M.A.R.; Fatriasari, W. Lignin as an active biomaterial: A review. *J. Sylva Lestari* **2021**, *9*, 1–22. [CrossRef]
299. Polat, Y.; Stojanovska, E.; Negawo, T.A.; Doner, E.; Kilic, A. Lignin as an additive for advanced composites. In *Green Biocomposites: Manufacturing and Properties*; Jawaid, M., Sapuan, S.M., Alothman, O.Y., Eds.; Springer International Publishing: Manhattan, NY, USA, 2017; pp. 71–89.
300. Taleb, F.; Ammar, M.; Mosbah, M.; Salem, R.B.; Moussaoui, Y. Chemical modification of lignin derived from spent coffee grounds for methylene blue adsorption. *Sci. Rep.* **2020**, *10*, 11048. [CrossRef]
301. Komisarz, K.; Majka, T.M.; Pielichowski, K. Chemical and Physical Modification of Lignin for Green Polymeric Composite Materials. *Materials* **2022**, *16*, 16. [CrossRef]
302. Cazacu, G.; Chirilă, O.; Totolin, M.I.; Ciolacu, D.; Niţă, L.; Drobotă, M.; Vasile, C. Chemical Treatment of Lignosulfonates Under DBD Plasma Conditions. I. Spectral Characterization. *J. Polym. Environ.* **2021**, *29*, 900–921. [CrossRef]
303. Tran, M.H.; Phan, D.-P.; Lee, E.Y. Review on Lignin Modifications toward Natural UV Protection Ingredient for Lignin-Based Sunscreens. *Green Chem.* **2021**, *23*, 4633–4646. [CrossRef]
304. Mariana, M.; Alfatah, T.; Abdul Khalil, H.P.S.; Yahya, E.B.; Olaiya, N.G.; Nuryawan, A.; Mistar, E.M.; Abdullah, C.K.; Abdulmadjid, S.N.; Ismail, H. A current advancement on the role of lignin as sustainable reinforcement material in biopolymeric blends. *J. Mater. Resear. Technol.* **2021**, *15*, 2287–2316. [CrossRef]
305. Ruiz-Dueñas, F.J.; Martínez, Á.T. Microbial degradation of lignin: How a bulky recalcitrant polymer is efficiently recycled in nature and how we can take advantage of this: Action mechanisms of ligninolytic peroxidases. *Microb. Biotechnol.* **2009**, *2*, 164–177. [CrossRef]
306. Nägele, H.; Pfitzer, J.; Näegele, E.; Inone, E.R.; Eisenreich, N.; Eckl, W.; Eyerer, P. Arboform: A thermoplastic, processable material from lignin and natural fibers. In *Chemical Modification, Properties, and Usage of Lignin*; Hu, T.Q., Ed.; Kluwer Academic/Plenum: New York, NY, USA, 2002; pp. 101–120.
307. Bertella, S.; Luterbacher, J.S. Lignin Functionalization for the Production of Novel Materials. *Trends Chem.* **2020**, *2*, 440–453. [CrossRef]
308. Vasile, C.; Cazacu, G. Biocomposites and Nanocomposites Containing Lignin. Chapter 23. In *Biopolymer Nanocomposites: Processing, Properties, and Applications*; Dufresne, A., Thomas, S., Pothen, L.A., Eds.; John Wiley & Sons: Hoboken, NJ, USA, 2013. [CrossRef]
309. Guo, J.; Chen, X.; Wang, J.; He, Y.; Xie, H.; Zheng, Q. The Influence of Compatibility on the Structure and Properties of PLA/Lignin Biocomposites by Chemical Modification. *Polymers* **2020**, *12*, 56. [CrossRef]
310. Gao, Y.; Qu, W.; Liu, Y.; Hu, H.; Cochran, E.; Bai, X. Agricultural Residue-derived Lignin as the Filler of Polylactic Acid Composites and the Effect of Lignin Purity on the Composite Performance. *J. Appl. Polym. Sci.* **2019**, *136*, 47915. [CrossRef]
311. Anugwom, I.; Lahtela, V.; Kallioinen, M.; Kärki, T. Lignin as a Functional Additive in a Biocomposite: Influence on Mechanical Properties of Polylactic Acid Composites. *Ind. Crop. Prod.* **2019**, *140*, 111704. [CrossRef]
312. Kumar, A.; Tumu, V.R.; Ray Chowdhury, S.; Ramana Reddy, S.V.S. A Green Physical Approach to Compatibilize a Bio-Based Poly (Lactic Acid)/Lignin Blend for Better Mechanical, Thermal and Degradation Properties. *Int. J. Biol. Macromol.* **2019**, *121*, 588–600. [CrossRef]
313. Ge, X.; Chang, M.; Jiang, W.; Zhang, B.; Xing, R.; Bulin, C. Investigation on Two Modification Strategies for the Reinforcement of Biodegradable Lignin/Poly(Lactic Acid) Blends. *J. Appl. Polym. Sci.* **2020**, *137*, 49354. [CrossRef]
314. Wang, N.; Zhang, C.; Weng, Y. Enhancing Gas Barrier Performance of Polylactic Acid/Lignin Composite Films through Cooperative Effect of Compatibilization and Nucleation. *J. Appl. Polym. Sci.* **2021**, *138*, 50199. [CrossRef]
315. He, X.; Luzi, F.; Hao, X.; Yang, W.; Torre, L.; Xiao, Z.; Xie, Y.; Puglia, D. Thermal, Antioxidant and Swelling Behaviour of Transparent Polyvinyl (Alcohol) Films in Presence of Hydrophobic Citric Acid-Modified Lignin Nanoparticles. *Int. J. Biol. Macromol.* **2019**, *127*, 665–676. [CrossRef]
316. Boarino, A.; Schreier, A.; Leterrier, Y.; Klok, H.-A. Uniformly Dispersed Poly(Lactic Acid)-Grafted Lignin Nanoparticles Enhance Antioxidant Activity and UV-Barrier Properties of Poly (Lactic Acid) Packaging Films. *ACS Appl. Polym. Mater.* **2022**, *4*, 4808–4817. [CrossRef]
317. Sun, Y.; Ma, Z.; Xu, X.; Liu, X.; Liu, L.; Huang, G.; Liu, L.; Wang, H.; Song, P. Grafting Lignin with Bioderived Polyacrylates for Low-Cost, Ductile, and Fully Biobased Poly(Lactic Acid) Composites. *ACS Sustain. Chem. Eng.* **2020**, *8*, 2267–2276. [CrossRef]
318. Ruwoldt, J.; Blindheim, F.H.; Chinga-Carrasco, G. Functional surfaces, films, and coatings with lignin—A critical review. *RSC Adv.* **2023**, *13*, 12529–12553. [CrossRef]
319. Aqlil, M.; Nzenguet, A.M.; Essamlali, Y.; Snik, A.; Larzek, M.; Zahouily, M. Graphene Oxide Filled Lignin/Starch Polymer Bionanocomposite: Structural, Physical, and Mechanical Studies. *J. Agric. Food Chem.* **2017**, *65*, 10571–10581. [CrossRef]
320. Bhat, R.; Abdullah, N.; Din, R.H.; Tay, G.S. Producing novel sago starch based food packaging films by incorporating lignin isolated from oil palm black liquor waste. *J. Food Eng.* **2013**, *119*, 707–713. [CrossRef]
321. Ma, C.; Kim, T.-H.; Liu, K.; Ma, M.-G.; Choi, S.-E.; Si, C. Multifunctional Lignin-Based Composite Materials for Emerging Applications. *Front. Bioeng. Biotechnol.* **2021**, *9*, 708976. [CrossRef]
322. Stevens, E.S. Starch-lignin foams. *Express Polym. Lett.* **2010**, *4*, 311–320. [CrossRef]
323. Roostazadeh, R.; Behzad, T.; Karimi, K. Isolation and characterization of lignin-rich particles as byproducts of bioethanol production from wheat straw to reinforce starch composite films. *Ind. Crop. Prod.* **2022**, *186*, 115175. [CrossRef]

324. Sun, X.; Li, Q.; Wu, H.; Zhou, Z.; Feng, S.; Deng, P.; Zou, H.; Tian, D.; Lu, C. Sustainable Starch/Lignin Nanoparticle Composites Biofilms for Food Packaging Applications. *Polymers* **2023**, *15*, 1959. [CrossRef]
325. Kun, D.; Pukánszky, B. Polymer/lignin blends: Interactions, properties, applications. *Eur. Polym. J.* **2017**, *93*, 618–641. [CrossRef]
326. Cui, L.; Wang, Z.; Zeng, Y.; Yang, N.; Liu, M.; Zhao, Y.; Zheng, Y. Lignin Biodegradation and Its Valorization. *Fermentation* **2022**, *8*, 366. [CrossRef]
327. Azimi, B.; Thomas, L.; Fusco, A.; Kalaoglu-Altan, O.I.; Basnett, P.; Cinelli, P.; De Clerck, K.; Roy, I.; Donnarumma, G.; Coltelli, M.B.; et al. Electrosprayed chitin nanofibril/electrospun polyhydroxyalkanoate fiber mesh as functional nonwoven for skin application. *J. Funct. Biomater.* **2020**, *11*, 62. [CrossRef]
328. Posoknistakul, P.; Tangkrakul, C.; Chaosuanphae, P.; Deepentham, S.; Techasawong, W.; Phonphirunrot, N.; Bairak, S.; Sakdaronnarong, C.; Laosiripojana, N. Fabrication and Characterization of Lignin Particles and Their Ultraviolet Protection Ability in PVA Composite Film. *ACS Omega* **2020**, *5*, 20976–20982. [CrossRef]
329. El-Ganainy, S.M.; Mosa, M.A.; Ismail, A.M.; Khalil, A.E. Lignin-Loaded Carbon Nanoparticles as a Promising Control Agent against *Fusarium verticillioides* in Maize: Physiological and Biochemical Analyses. *Polymers* **2023**, *15*, 193. [CrossRef] [PubMed]
330. Meng, S.; Wang, H.; Yuncong, C.; Li, Y.C.; Li, T.; Liu, G.; Zhang, S.; Tong, Z. Porous 3D-Biocomposite Adsorbent for Iron Reclamation and Use in Agricultural Applications. *ACS Appl. Polym. Mater.* **2022**, *4*, 8277–8289. [CrossRef]
331. Shamaei, L.; Khorshidi, B.; AmirulIslam, M.; Sadrzadeh, M. Industrial waste lignin as an antifouling coating for the treatment of oily wastewater: Creating wealth from waste. *J. Clean. Prod.* **2020**, *256*, 120304. [CrossRef]
332. Wang, T.; Jiang, M.; Yu, X.; Niu, N.; Chen, L. Application of lignin adsorbent in wastewater Treatment: A review. *Sep. Purif. Technol.* **2022**, *302*, 122116. [CrossRef]
333. Guo, Y.; Tian, D.; Shen, F.; Yang, G.; Long, L.; He, J.; Song, C.; Zhang, J.; Zhu, Y.; Huang, C.; et al. Transparent Cellulose/Technical Lignin Composite Films for Advanced Packaging. *Polymers* **2019**, *11*, 1455. [CrossRef]
334. Dumitriu, R.P.; Stoica, I.; Vasilescu, D.S.; Cazacu, G.; Vasile, C. Alginate/Lignosulfonate Blends with Photoprotective and Antioxidant Properties for Active Packaging Applications. *J. Polym. Environ.* **2018**, *26*, 1100–1112. [CrossRef]
335. Ji, M.; Li, J.; Li, F.; Wang, X.; Man, J.; Li, J.; Zhang, C.; Peng, S. A Biodegradable Chitosan-Based Composite Film Reinforced by Ramie Fibre and Lignin for Food Packaging. *Carbohydr. Polym.* **2022**, *281*, 119078. [CrossRef]
336. Buzarovska, A.; Blazevska-Gilev, J.; Perez-Martnez, B.T.; Balahura, L.R.; Pircalabioru, G.G.; Dinescu, S.; Costache, M. Poly(l-lactic acid)/alkali lignin composites: Properties, biocompatibility, cytotoxicity and antimicrobial behavior. *J. Mater. Sci.* **2021**, *56*, 13785–13800. [CrossRef]
337. Wei, M.; Fan, L.; Huang, J.; Chen, Y. Role of star-like hydroxylpropyl lignin in soy-protein plastics. *Macromol. Mater. Eng.* **2006**, *291*, 524–530. [CrossRef]
338. Oliviero, M.; Verdolotti, L.; Nedi, I.; Docimo, F.; Di Maio, E.; Iannance, S. Effect of two kinds of lignins, alkaline lignin and sodium lignosulfonate, on the foamibility of thermoplastic zein-based biocomposites. *J. Cell. Plast.* **2012**, *48*, 516–525. [CrossRef]
339. Olonisakin, K.; Wen, A.; He, S.; Lin, H.; Tao, W.; Chen, S.; Yang, W. The Development of Biodegradable PBAT-Lignin-Tannic Acid Composite Film: Properties, Biodegradability, and Potential Barrier Application in Food Packaging. *Food Bioprocess Technol.* **2023**, *16*, 1525–1540. [CrossRef]
340. Lugoloobi, I.; Li, X.; Zhang, Y.; Mao, Z.; Wang, B.; Sui, X.; Feng, X. Fabrication of lignin/poly(3-hydroxybutyrate) nanocomposites with enhanced properties via a Pickering emulsion approach. *Int. J. Biol. Macromol.* **2020**, *165 Pt B*, 3078–3087. [CrossRef]
341. Vachon, J.; Assad-Alkhateb, D.; Baumberger, S.; van Haveren, J.; Gosselink, R.J.A.; Monedero, M.; Bermudez, J.M. Use of lignin as additive in polyethylene for food protection: Insect repelling effect of an ethyl acetate phenolic extract. *Compos. Part C* **2020**, *2*, 100044. [CrossRef]
342. Sathasivam, T.; Kai, J.; Sugiarto, S.; Yu, Y.; Soo, D.X.Y.; Zhu, Q.; Merzaban, J.; Kai, D. Review. Nano-Strategies for Lignin Biomaterials toward Cancer Therapy. *Adv. Healthc. Mater.* **2023**, 2300024. [CrossRef] [PubMed]
343. Lee, E.-S.; Kim, Y.-O.; Ha, Y.-M.; Lim, D.; Hwang, J.Y.; Kim, J.; Park, M.; Cho, J.W.; Jung, Y.C. Antimicrobial properties of lignin-decorated thin multi-walled carbon nanotubes in poly (vinyl alcohol) nanocomposites. *Eur. Polym. J.* **2018**, *105*, 79–84. [CrossRef]
344. Saudi, A.; Amini, S.; Amirpour, N.; Kazemi, M.; Kharazi, A.Z.; Salehi, H. Promoting neural cell proliferation and differentiation by incorporating lignin into electrospun poly (vinyl alcohol) and poly (glycerol sebacate) fibers. *Mater. Sci. Eng. C.* **2019**, *104*, 110005. [CrossRef]
345. Amini, S.; Saudi, A.; Amirpour, N.; Jahromi, M.; Najafabadi, S.S.; Kazemi, M.; Rafienia, M.; Salehi, H. Application of electrospun poly-caprolactone fibers embedding lignin nanoparticle for peripheral nerve regeneration: In vitro and in vivo study. *Int. J. Biol. Macromol.* **2020**, *159*, 154–173. [CrossRef]
346. Yan, Y.; Zhang, L.; Zhao, X.; Zhang, X. Utilization of lignin upon successive fractionation and esterification in polylactic acid (PLA)/lignin biocomposite. *Int. J. Biol. Macromol.* **2022**, *203*, 49–57. [CrossRef] [PubMed]
347. Mahata, D.; Jana, M.; Jana, A.; Mukherjee, A.; Mondal, N.; Saha, T.; Sen, S.; Nando, G.B.; Mukhopadhyay, C.K.; Chakraborty, R.; et al. Lignin-graft-polyoxazoline conjugated triazole a novel anti-infective ointment to control persistent inflammation. *Sci. Rep.* **2017**, *7*, 46412. [CrossRef] [PubMed]
348. Abdelwahab, M.A.; Jacob, S.; Misra, M.; Mohanty, A.K. Super-tough sustainable biobased composites from polylactide bioplastic and lignin for bio-elastomer application. *Polymer* **2021**, *212*, 123153. [CrossRef]

349. Gouveia, J.R.; de Sousa Júnior, R.R.; Ribeiro, A.O.; Saraiva, S.A.; dos Santos, D.J. Effect of soft segment molecular weight and NCO: OH ratio on thermomechanical properties of lignin-based thermoplastic polyurethane adhesive. *Eur. Polym. J.* **2020**, *131*, 109690. [CrossRef]
350. Vostrejs, P.; Adamcová, D.; Vaverková, M.D.; Enev, V.; Kalina, M.; Machovsky, M.; Šourková, M.; Marova, I.; Kovalcik, A. Active Biodegradable Packaging Films Modified with Grape Seeds Lignin. *RSC Adv.* **2020**, *10*, 29202–29213. [CrossRef] [PubMed]
351. Xiong, S.J.; Pang, B.; Zhou, S.-J.; Li, M.-K.; Yang, S.; Wang, Y.-Y.; Shi, Q.; Wang, S.-F.; Yuan, T.-Q.; Sun, R.-C. Economically competitive biodegradable PBAT/lignin composites: Effect of lignin methylation and compatibilizer. *ACS Sustain. Chem. Eng.* **2020**, *8*, 5338–5346. [CrossRef]
352. Yetiş, F.; Liu, X.; Sampson, W.W.; Gong, R.H. Biodegradation of Composites of Polylactic Acid and Microfibrillated Lignocellulose. *J. Polym. Environ.* **2023**, *31*, 698–708. [CrossRef]
353. Ng, Q.Y.; Low, J.H.; Pang, M.M.; Idumah, C.I. Properties Enhancement of Waterborne Polyurethane Bio-composite Films with 3-aminopropyltriethoxy Silane Functionalized Lignin. *J. Polym. Environ.* **2023**, *31*, 688–697. [CrossRef]
354. Guigo, N.; Mija, A.; Vincent, L.; Sbirrazzuoli, N. Eco-friendly composite resins based on renewable biomass resources: Polyfurfuryl alcohol/lignin thermosets. *Eur. Polym. J.* **2010**, *46*, 1016–1023. [CrossRef]
355. Rasyidur, M.R.; Agustiany, E.A.; Dn, M.R.; Madyaratri, E.W.; Ghozali, M.; Restu, W.K.; Falah, F.; Lubis, M.A.R.; Syamani, F.A.; Nurhamiyah, Y.; et al. Lignin as Green Filler in Polymer Composites: Development Methods, Characteristics, and Potential Applications. *Hindawi Adv. Mater. Sci. Eng.* **2022**, *10*, 1–33. [CrossRef]
356. Lizundia, E.; Sipponen, M.H.; Greca, L.G.; Balakshin, M.; Tardy, B.L.; Rojas, O.J.; Puglia, D. Multifunctional lignin-based nanocomposites and nanohybrids. *Green Chem.* **2021**, *23*, 6698–6760. [CrossRef]
357. Shen, R.; Tao, L.; Yang, B. Modeling and Analysis. Techno-economic analysis of jet-fuel production from biorefinery waste lignin. *Biofuels Bioprod. Biorefin.* **2019**, *13*, 486–501. [CrossRef]
358. Lu, X.; Gu, X. A review on lignin pyrolysis: Pyrolytic behavior, mechanism, and relevant upgrading for improving process efficiency. *Biotechnol. Biofuels* **2022**, *15*, 106. [CrossRef] [PubMed]
359. Kocaturk, E.; Salan, T.; Ozcelik, O.; Alma, M.H.; Candan, Z. Recent Advances in Lignin-Based Biofuel Production. *Energies* **2023**, *16*, 3382. [CrossRef]
360. Bacovsky, D. IEA-Energy a Report to IEA Bioenergy Task 39. Available online: https://www.osti.gov/etdeweb/servlets/purl/22110325 (accessed on 22 July 2023).
361. Stone, M.L.; Webber, M.S.; Mounfield, W.P.; Bell, D.C.; Christensen, E.; Morais, A.R.C.; Li, Y.; Anderson, E.M.; Heyne, J.S.; Beckham, G.T.; et al. Continuous hydrodeoxygenation of lignin to jet-range aromatic hydrocarbons. *Joule* **2022**, *6*, 2324–2337. [CrossRef]
362. 100% Sustainable Aviation Fuel Developed from Lignin. *Energy*. 28 September 2022. Available online: https://www.innovationnewsnetwork.com/100-sustainable-aviation-fuel-developed-from-lignin/25767/ (accessed on 22 July 2023).
363. Mukhopadhyay, A.; Hamel, J.; Katahira, R.; Zhu, H. Metal-Free Aqueous Flow Battery with Novel Ultrafiltered Lignin as Electrolyte. *ACS Sustain. Chem. Eng.* **2018**, *6*, 5394–5400. [CrossRef]
364. Liu, H.; Xu, T.; Liu, K.; Zhang, M.; Liu, W.; Li, H.; Du, H.; Si, C. Lignin-based electrodes for energy storage application. *Ind. Crop. Prod.* **2021**, *165*, 113425. [CrossRef]
365. Wang, H.; Fu, F.; Huang, M.; Feng, Y.; Han, D.; Xi, Y.; Xiong, W.; Yang, D.; Niu, L. Lignin-based materials for electrochemical energy storage devices. *Nano Mater. Sci.* **2023**, *5*, 141–160. [CrossRef]
366. Li, W.; Shi, J. Lignin-derived carbon material for electrochemical energy storage applications: Insight into the process-structure-properties-performance correlations. *Front. Bioeng. Sec. Biomater. Biotechnol.* **2023**, *11*, 21027. [CrossRef]
367. Zhang, W.; Zhang, X.; Ren, S.; Dong, L.; Ai, Y.; Lei, T.; Wu, Q. Lignin containing cellulose nanofiber based nanopapers with ultrahigh optical transmittance and haze. *Cellulose* **2023**, *30*, 5967–5985. [CrossRef]
368. Yeasmin, F.; Masud, R.A.; Chisty, A.H.; Hossain, M.A.; Mallik, A.K.; Rahman, M.M. Lignin-metal oxide composite for photocatalysis and photovoltaics. In *Renewable Polymers and Polymer-Metal. Oxide Composites. Synthesis, Properties, and Applications. A Volume in Metal. Oxides*; Haider, S., Haider, A., Eds.; Elsevier: Amsterdam, The Netherlands, 2022; Chapter 14; pp. 447–476. [CrossRef]
369. Meraj, A.; Singh, S.P.; Jawaid, M.; Nasef, M.M.; Alomar, T.S.; AlMasoud, N. A Review on Eco-friendly Isolation of Lignin by Natural Deep Eutectic Solvents from Agricultural Wastes. *J. Polym. Environ.* **2023**, *31*, 3283–3316. [CrossRef]

MDPI AG
Grosspeteranlage 5
4052 Basel
Switzerland
Tel.: +41 61 683 77 34

Polymers Editorial Office
E-mail: polymers@mdpi.com
www.mdpi.com/journal/polymers

Academic Open
Access Publishing

mdpi.com

ISBN 978-3-7258-1672-9